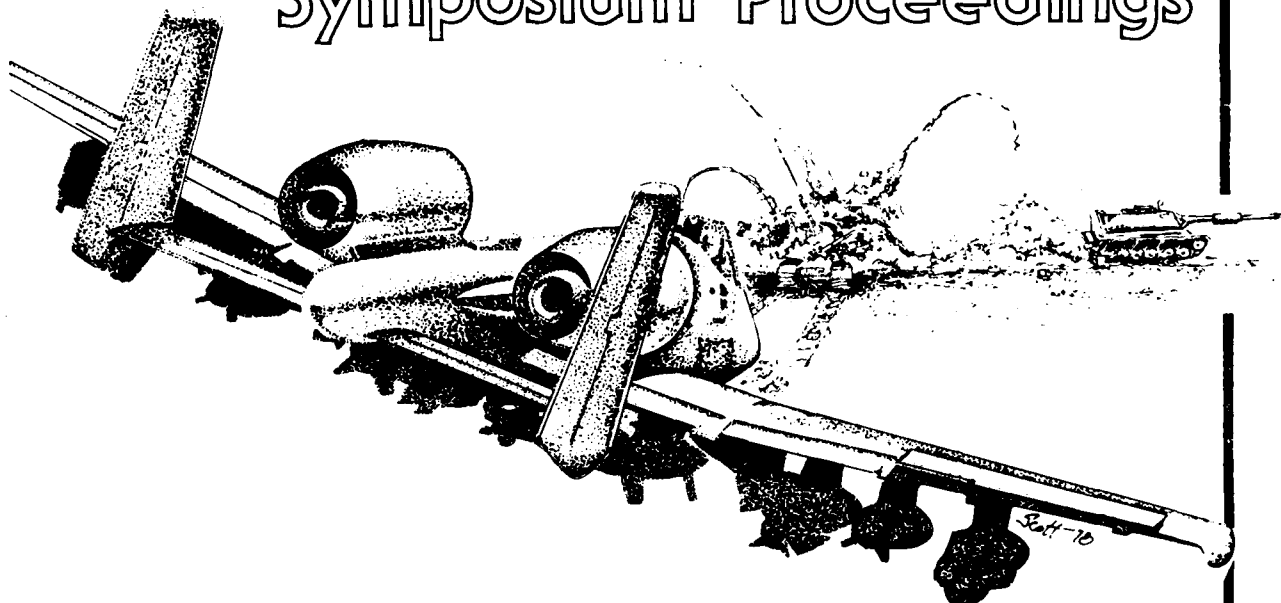LEVEL

DTIC
SELECTE
APR 9 1980
S   D
C

Fourth
Aircraft/Stores Compatibility
Symposium Proceedings

ADA082876

SPONSORED BY:

JOINT TECHNICAL COORDINATING
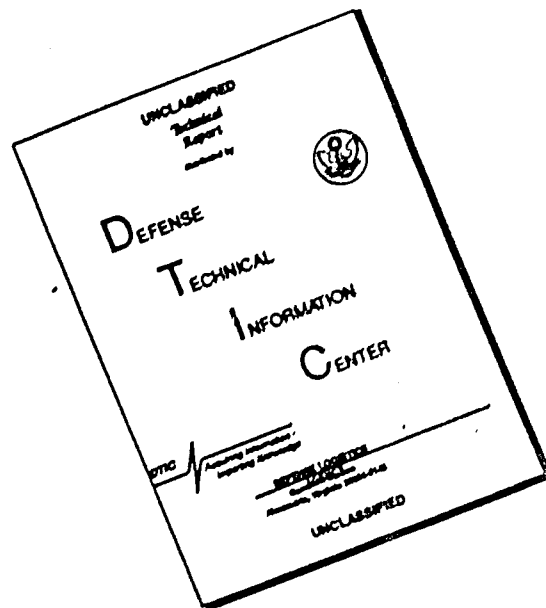GROUP FOR MUNITIONS DEVELOPMENT

HELD AT:

CIVIC AUDITORIUM
FORT WALTON BEACH, FLORIDA
12-14 OCTOBER 1977

DC FILE COPY

80   4   9   003

DISCLAIMER NOTICE
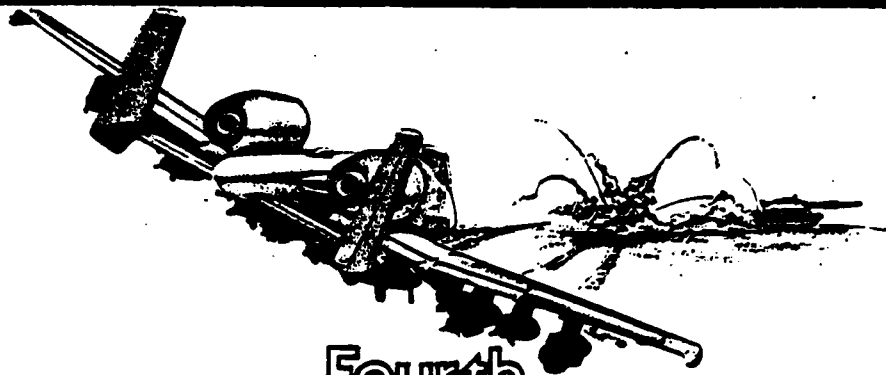
DEFENSE TECHNICAL INFORMATION CENTER

THIS DOCUMENT IS BEST QUALITY AVAILABLE. THE COPY FURNISHED TO DTIC CONTAINED A SIGNIFICANT NUMBER OF PAGES WHICH DO NOT REPRODUCE LEGIBLY.

NOTICE

When Government drawings, specifications, or other data are used for any purpose other than in connection with a definitely related Government procurement operation, the United States Government thereby incurs no responsibility nor any obligation whatsoever; and the fact that the Government may have formulated, furnished, or in any way supplied the said drawings, specifications, or other data, is not to be regarded by implication or otherwise as in any manner licensing the holder or any other person or corporation, or conveying any rights or permission to manufacture, use, or sell any patented invention that may in any way be related thereto.

Fourth Aircraft/Stores Compatibility Symposium Proceedings

12-14 OCTOBER 1977

VOLUME 2

SPONSORED BY
JOINT TECHNICAL COORDINATING GROUP
FOR
MUNITIONS DEVELOPMENT
(JTCG/MD)

PROCEEDINGS COMPILED BY

AIR FORCE ARMAMENT LABORATORY

ARMAMENT DEVELOPMENT AND TEST CENTER

AIR FORCE SYSTEMS COMMAND

REPORT DOCUMENTATION PAGE		READ INSTRUCTIONS BEFORE COMPLETING FORM
1. REPORT NUMBER	2. GOVT ACCESSION NO.	3. RECIPIENT'S CATALOG NUMBER
4. TITLE (and Subtitle) Aircraft/Stores Compatibility Symposium Proceedings (U) Held at Fort Walton Beach, Volume 2 Florida on ... Volume II.		5. TYPE OF REPORT & PERIOD COVERED Final - 12-14 Oct 77
		6. PERFORMING ORG. REPORT NUMBER JTCG/MD WP12
7. AUTHOR(s) Various, described in text.		8. CONTRACT OR GRANT NUMBER(s) 6011
9. PERFORMING ORGANIZATION NAME AND ADDRESS Various, described in text.		10. PROGRAM ELEMENT, PROJECT, TASK AREA & WORK UNIT NUMBERS Oct 77
11. CONTROLLING OFFICE NAME AND ADDRESS Aircraft Compatibility Branch Munitions Division Air Force Armament Laboratory		12. REPORT DATE 12 - 14 October 1977
		13. NUMBER OF PAGES 605
14. MONITORING AGENCY NAME & ADDRESS(If different from Controlling Office) Air Force Armament Laboratory Armament Development and Test Center Eglin AFB FL 32542		15. SECURITY CLASS. (of this report) UNCLASSIFIED
		15a. DECLASSIFICATION/DOWNGRADING SCHEDULE

16. DISTRIBUTION STATEMENT (of this Report)

Approved for public release: distribution unlimited.

JTCG/MD-WP-12-Vol.-2

17. DISTRIBUTION STATEMENT (of the abstract entered in Block 20, if different from Report)

18. SUPPLEMENTARY NOTES
Volumes 1 and 2
Available in DDC

19. KEY WORDS (Continue on reverse side if necessary and identify by block number)

Aircraft	Aeroelastic	Aeroheating	Scaling	Bomb Racks
Store	Wind Tunnel	Electromagnetic	A-10	Lugs
Compatibility	Flight Test	Jettison	F-16	MIL-A-8591
Aerodynamics	Cost Effectiveness	Separation	Airloads	
Structures	Muzzle Blast	Flowfield	Ejector Racks	

20. ABSTRACT (Continue on reverse side if necessary and identify by block number)
These proceedings contain the technical papers presented at the Fourth Aircraft/ Stores Compatibility Symposium held at the Civic Auditorium, Fort Walton Beach, Florida, USA on 12-14 October 1977 which was sponsored by the Joint Technical Coordinating Group for Munitions Development (JTCG/MD). Purpose of this symposium was to bring together world-wide technical expertise to review and discuss air- craft/store compatibility developments and experiences. Technical papers were presented in five different sessions: General, Store Separation, Aero/Structures, Bomb Racks/Interface, and Experimental. Each of the 35 papers (Cont'd on reverse)

DD FORM 1473 EDITION OF 1 NOV 65 IS OBSOLETE
1 JAN 73

in the proceedings has its own abstract, and contains sections including
presentation of data, discussion of findings, and recommendations/conclusions.
The compilation of these papers, each focusing on the compatibility problem,
should prove extremely valuable to aircraft and store designers by making each
aware of the others' technical problems and possible solutions.

FOREWORD

This publication contains the proceedings of and technical papers presented at the Fourth JTCG/MD Aircraft/Stores Compatibility Symposium, held at the Civic Auditorium, Fort Walton Beach, Florida, USA on 12-14 October 1977.

The purpose of the symposium was to bring together the technical expertise within Government and industry throughout the world to review and discuss compatibility developments and experiences. Exchanging methods and ideas is essential in present and future systems development. No one organization holds all the answers to aircraft/stores compatibility problems. Solutions to these problems depend upon coordinated efforts by both aircraft and store designers who are aware of the other's requirements.

The symposium committee wishes to express its appreciation to those persons responding to the call for papers, the authors and the presenters, the session chairmen, and the attendees for their contributions in making the symposium highly successful. Special appreciation is extended to Major General Howard M. Lane, USAF, Commander, Armament Development and Test Center, Air Force Systems Command, for his welcoming remarks in opening the symposium.

Accession For

NTIS GRA&I
DDC TAB
Unannounced
Justification

By

Distribution/

Availability Codes

Dist   Avail and/or
        special

i

Acknowledgement is made to all those people from Eglin AFB who worked long hours so diligently, cheerfully and efficiently to give us such a pleasant, professional success.

Suggestions are welcomed for making our next conference (late 1979) even more productive. Comments may be forwarded to Mr. C. S. Epstein, Air Force Armament Laboratory (DLJCE), Eglin AFB, FL, USA, 32542.

Publication of this report does not constitute Air Force approval of the technical papers' findings or conclusions. It is published only for the exchange and stimulation of ideas.

CHARLES S. EPSTEIN
Chairman, Working Party 12
JTCG/MD

ii

SYMPOSIUM COMMITTEE

Mr. C. S. Epstein	USAF/AFSC
Mr. W. P. Steeper	USN/NAVAIR
Mr. Frank Shifrar	USAF/AFLC
Mr. Larry Doyle	US Army/AVRADCOM

PAPER SELECTION

Mr. W. P. Steeper	USN/NAVAIR
Mr. C. S. Epstein	USAF/AFSC

SESSION CHAIRMEN

GENERAL	Mr. R. V. Frank, Army AVRADCOM
STORE SEPARATION	Mr. B. R. Bowers, USAF AFATL
AERO/STRUCTURES	Mr. W. P. Steeper, USN NAVAIR
BOMB/RACKS INTERFACE	Mr. T. E. Milhous, USN NADC
EXPERIMENTAL	Mr. C. S. Epstein, USAF AFATL

PROCEEDINGS

Mr. C. S. Epstein	USAF/AFSC

HOST ORGANIZATION

The Armament Development and Test Center
Air Force Systems Command

(The reverse of this page is blank)

TABLE OF CONTENTS

AERODYNAMIC INTERACTIONS OF STORES AND AIRFRAMES
(U)
(Article UNCLASSIFIED)

by

Derek H. Peckham
Royal Aircraft Establishment, Farnborough, UK

ABSTRACT. (U) The effectiveness of a military aircraft depends
on its ability to carry weapons efficiently and deliver them accurately,
with a low risk of losing the aircraft, and to be able to repeat
missions after a short turn-round time. It will be argued that the
achievement of high effectiveness requires careful attention being paid
to the aerodynamic design of weapons and their installation externally
on aircraft, that substantial improvements are attainable, and that
future trends in combat aircraft design are likely to increase still
further the importance of the contributions to be made by the designers
of weapons and weapon installations.

The subject is considered under the three main headings of Drag,
Aircraft Flying Qualities, and Store Release Disturbance. A broad
review is given of recent work in the United Kingdom on the aerodynamic
interactions between stores and airframes, covering work at the Royal
Aircraft Establishment, and work under contract in UK Industry and the
Aircraft Research Association. While reduction of drag is seen as the
prime aim for the aerodynamicist, the paths to be followed will have to
be guided by considerations of flying qualities and store release
requirements.

The origins of the high drag of current stores installations are
examined, and recommendations made of ways in which improvements could
be made in the short, medium and long term. A case is made for
improved prediction methods and the importance is stressed of making
comprehensive plans at an early stage in the life of a project to set up
a methodology for treating the complete problem.

LIST OF FIGURES

INTRODUCTION

The effectiveness of a military aircraft depends on its ability to carry weapons efficiently and to deliver them accurately, with a low risk of losing the aircraft, and to be able to repeat missions after a short turn round time. Achievement of high effectiveness requires careful attention being paid to the aerodynamic design of weapons, and the means of carrying them externally on aircraft, coupled with a sound appreciation of engineering and operational requirements.

In particular, good aerodynamic design of the weapon installation can make an essential contribution to achieving:

increased speed at low level to reduce vulnerability to ground fire

increased radius of action or time over target

increased speed, turn rate, rate of climb, acceleration and manoeuvrability in air-to-air combat

improved stability and control for more accurate weapon aiming

improved weapon accuracy stemming from reduced release disturbance

increased safety and higher limiting speeds in release or jettison of stores

reduced aircraft weight and improved structural integrity by reducing carriage loads.

With equal truth, it can be said that lack of attention to the aerodynamic design of weapon installation can result in degradation of aircraft performance and effectiveness. Despite the increased attention paid to the aerodynamic aspects of weapon carriage over the last decade, it still seems to be necessary to warn about the penalties that can be suffered. Fig 1 shows 3 views of a typical combat aircraft. At the top is a view of the clean aircraft, next is a view of the aircraft with a heavy load of weapons. Obviously, these will have an effect on drag but, at first sight, it does not appear that it will be very large. However the third view shows the frontal area of each component scaled in proportion to its drag contribution, and it becomes clear that the stores and their carriers contribute a drag of about the same magnitude as the clean aircraft. The impact of such a
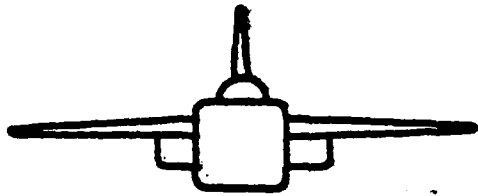
Clean aircraft
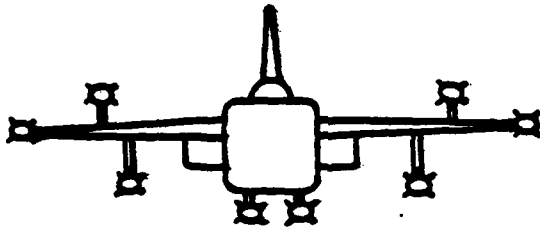
With stores:
geometric
view
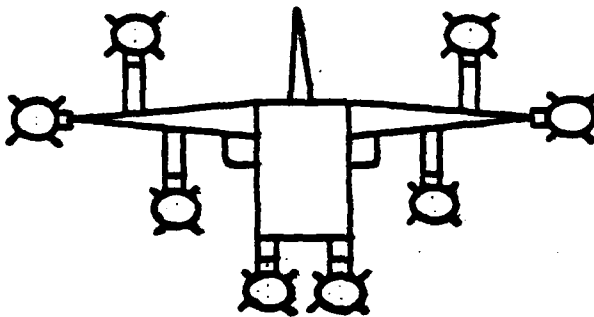
With stores:
aerodynamic drag
view

Fig.1   Three views of a typical combat aircraft

load on aircraft performance is illustrated in Fig 2 which shows diagrammatically – but to scale – the likely effects on a representative mission.

However, rather than dwelling on the negative aspects of the problem, ie of the penalties and what can go wrong, the aim of this paper is to outline some of the positive contributions that aerodynamicists concerned with weapon carriage can make in the short, medium and long term. While the emphasis in this paper is on design for low drag, it will be argued that the paths to be followed will have to be guided by considerations of aircraft flying qualities and store release requirements, particularly in the long term, and that future trends in combat aircraft design are likely to increase still further the importance of the contributions to be made by the designers of weapons and weapon installations. A comprehensive review of the subject is not attempted in this short paper; rather, emphasis is put on the significance of results from recent work in the UK.

THE AERODYNAMIC INTERFERENCE BETWEEN WEAPONS AND THE CARRIER AIRCRAFT

Scarcely any characteristic of an aircraft escapes modification due to the external carriage of stores. The principal effects are that external stores increase inertias, degrade stability, reduce lift and increase drag – usually by far more than the drag of the store itself (Fig 3). Furthermore, just as the presence of a store load modifies the flow field round the aircraft, so the presence of the aircraft can pose difficult problems for the weapon in terms of carriage loads and release disturbance (Fig 4).

The author makes no excuses for stating these elementary facts because when the primary aim is a low-drag weapon installation, it is all too easy to set out on a path leading to problems in other areas which can be expensive and time-consuming to remedy late in the development stage of an aircraft project, or which lead to restrictions on aircraft operating speeds and manoeuvre limits if remedies cannot be found.

Though we may comfort ourselves that we have been getting better in the way in which we install weapons on aircraft, and that the path forward in the short term is fairly clear, the normal evolutionary trends of combat aircraft design (and often weapon design) will mean that designing good weapon installations will become more difficult in the longer term.

Without digressing deeply into the complexities of aircraft design, it is clear that improvements in wing-sections for high speed, high-lift systems for low speeds, new structural materials, engines of lower specific weight and fuel consumption, lower equipment weights etc, will all lead towards aircraft (designed to meet a given performance requirement, say) being lighter and of smaller wing area than they would
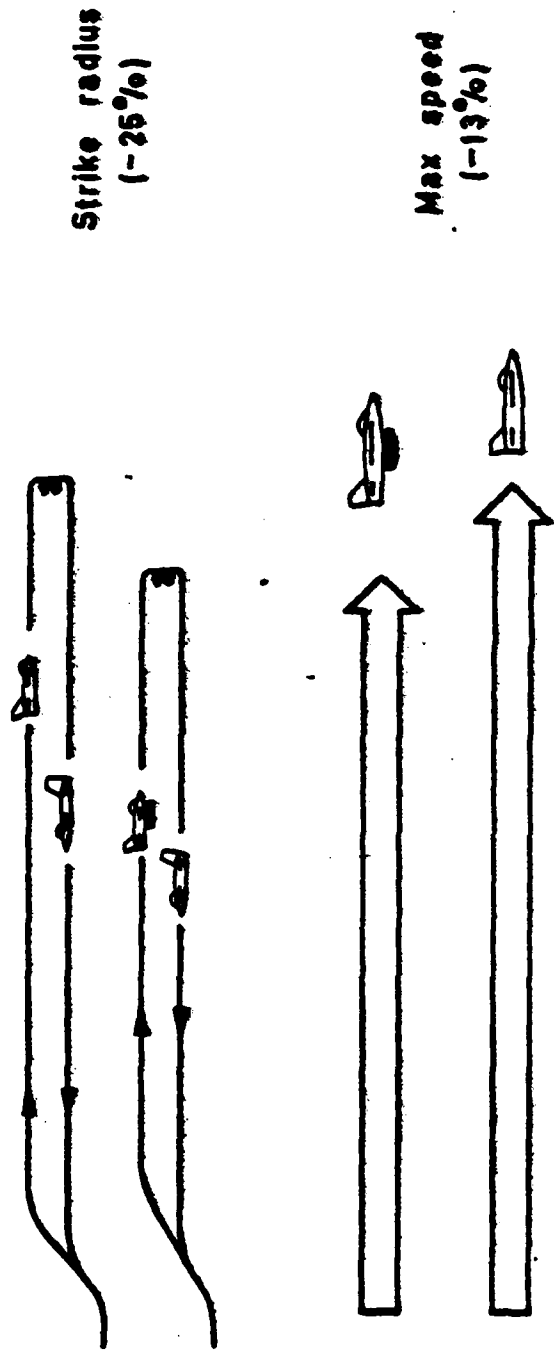
Fig 2   Effect of store drag on typical combat mission
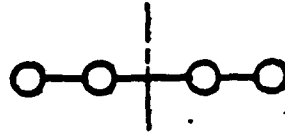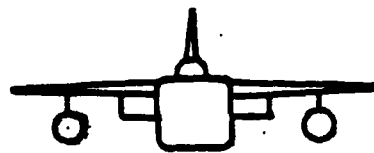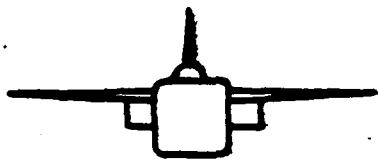
Increase in inertias
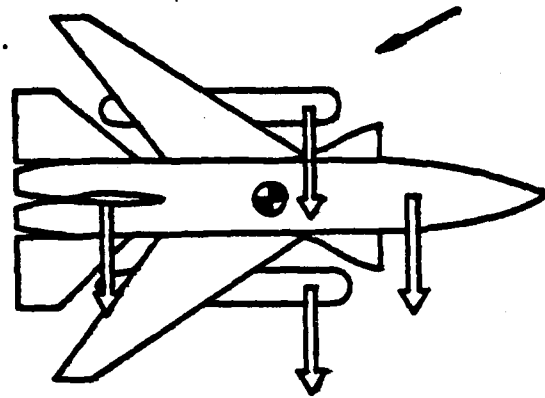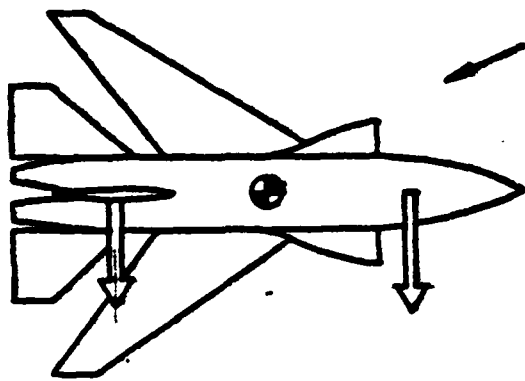
Reduction of stability
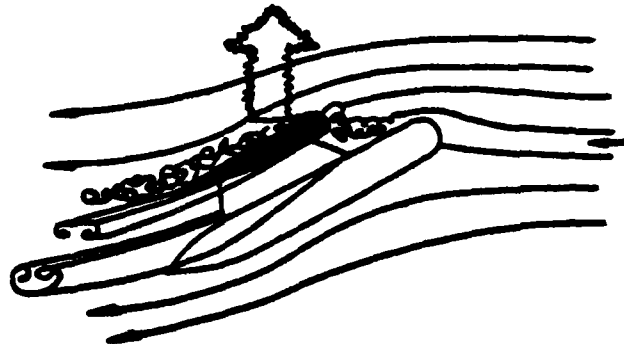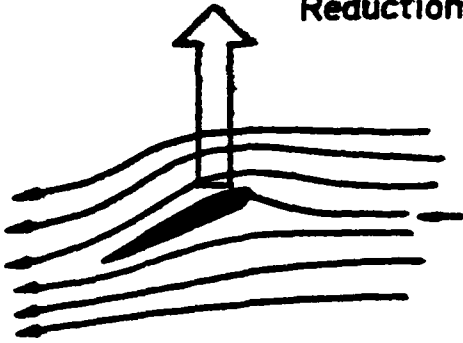
Loss of lift
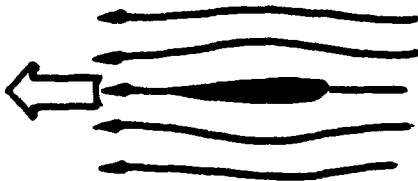
Increase in drag

Fig. 3   Principal   effects   of   external   stores   on   aircraft

501

Aircraft flow field distorted
by presence of store

Weapon flow field distorted
by presence of aircraft
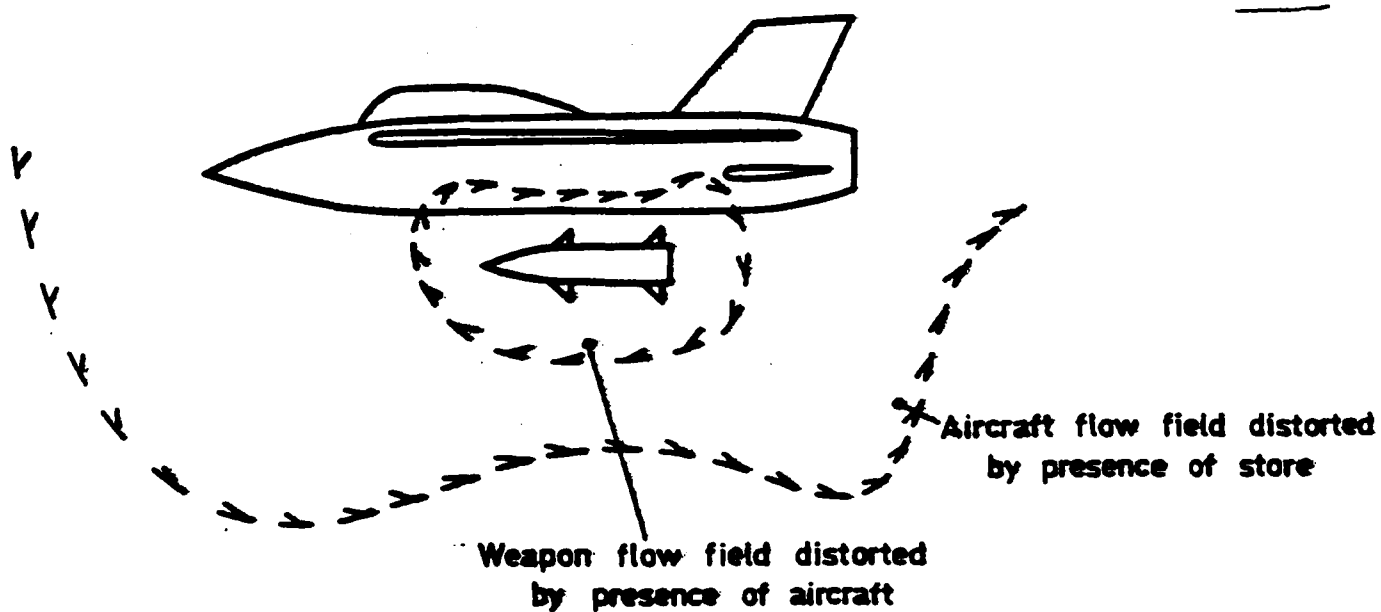
Loads=free-stream loads+(free-stream derivatives x differences
between local flow and free-stream)+loads due to non-uniformity
of aircraft flow field+"close interference" loads

Fig 4   Loads on store   when   store   is   close   to   aircraft

be if designed to current in-service standards. Thus the carrying capability of aircraft in terms of store payload-fraction can be expected to increase, so that the size of the store load relative to the aircraft dimensions will also increase (Fig 5). Furthermore, there is a continuing tendency for new weapon shapes to be less dense than previously (Fig 6), accentuating still further the likely difference in the relative sizes of weapons and airframes in the future. Thus we can expect the ratio of wetted areas of stores to the wetted area of the airframe to increase, and the closer proximity of greater numbers of larger stores on a smaller airframe will increase aerodynamic interference, both these effects leading towards a greater proportion of the total drag being due to the stores installation — unless we improve our methods of weapon carriage. Similar remarks apply to the likely severity of effects on aircraft flying qualities and weapon release disturbance. In addition, it can also be expected that the Air Forces of the world will demand still higher performance for the next generation of combat aircraft, adding further complication to the problem.

Thus there are a number of trends one can foresee in the development of future combat aircraft and weapons, all of which will make the design of weapon installations more difficult. Unless progress is made towards still better ways of understanding and minimising the aerodynamic interactions between stores and airframes, the performance penalties associated with carriage of stores externally will increase, and it is likely that the problem of effects on aircraft flying qualities and store release will become more severe.

THE INSTALLED DRAG OF STORES

Clearly, a primary cause of the high installed drag of stores is that the stores themselves have a high drag in free air. It is easy for the aircraft aerodynamicist, having designed a clean aircraft, to criticise the weapon designer for producing weapons with excessively bluff noses, various excrescenses, far from good surface finish, lap joints, bluff bases etc. On free fall weapons, perhaps we are still suffering from the standard practices of the days when they were carried in bomb bays and drag did not matter. On boosted weapons, perhaps the designer is mesmerised by (thrust-drag), where only modest gains in acceleration would be obtained from a big effort in drag reduction. Whatever the reasons, the message is still not getting across of the need for low drag of the weapon in isolation.

One aspect of this problem has been investigated by a group in the UK, composed of members from industry and research establishments. It has been found that while various estimating methods generally predict the total drag of a store with reasonable accuracy, the methods differ considerably in detail, with the result that there are often wide differences in the estimates of the contributions of the various drag-producing features of a store. This may be a clue to why little progress is being made. Unless we can say with confidence that certain
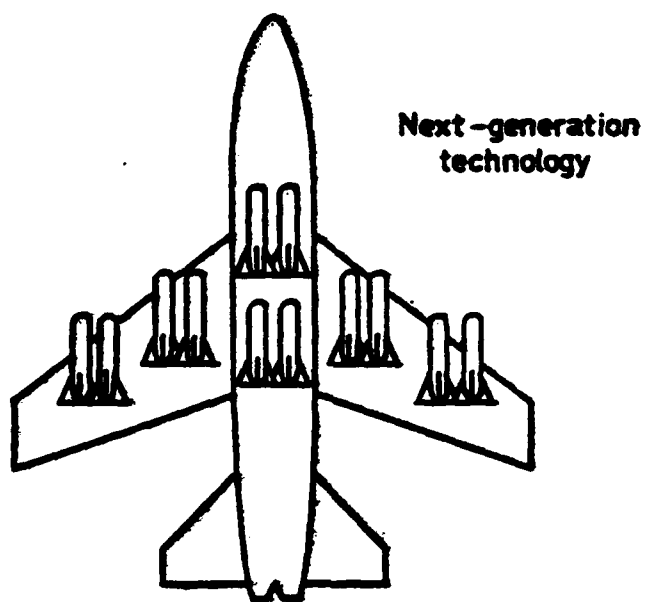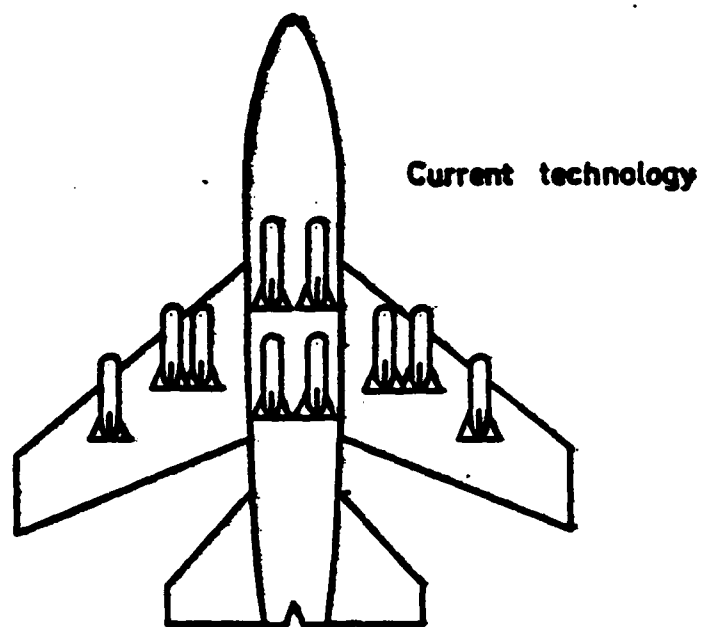
Fig. 5 Effect of improvements in aircraft technology on spacing of store load
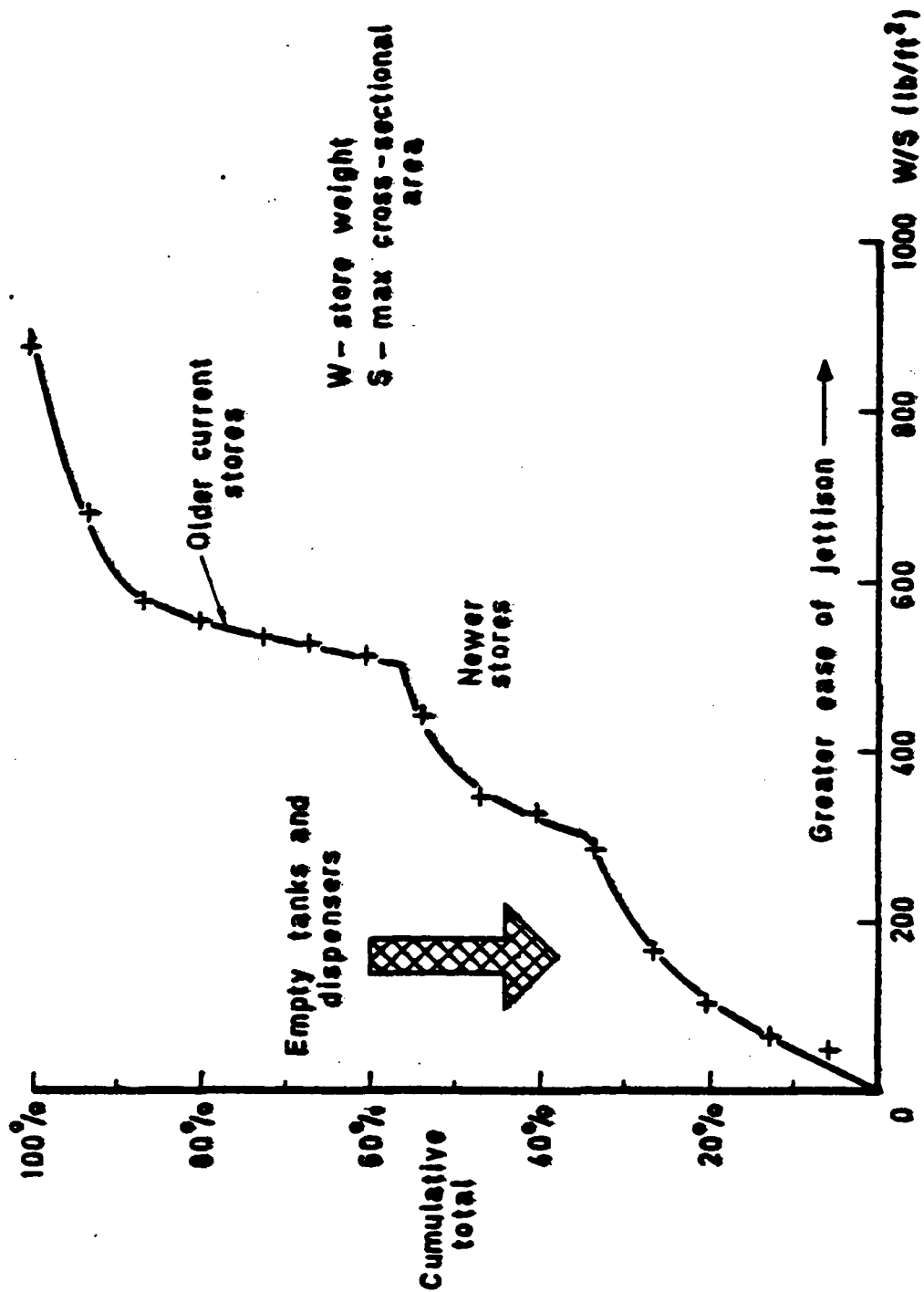
Fig 6   Trend towards lower density stores

features are responsible for drag contributions of particular magnitudes and can point to proven ways of reducing drag (ie experimental results and some theoretical analysis) it is understandable why weapon designers do not respond to general exhortations to improve their drag standards.

Various programmes of work are under way in the UK to improve our knowledge of weapon drag. An extensive series of tests on the drag and pressure fluctuations caused by surface excrescences has been undertaken (1) and increasing use is being made of the isolated store drag rig at ARA (Fig 7). Also, because stores often have a lower drag-rise Mach number and steeper drag rise then a clean aircraft, a series of wind tunnel tests have been made at the RAE (2) on a variety of forebody shapes with varying amounts of blunting to provide both empirical results of direct value to designers and material for validation of theoretical methods of transonic drag prediction (Fig 8).

The next reason for high installed drag is that the free-air drag of a weapon is magnified by the carrier and the ejector release unit to which it is attached. Even after the stores have been released, the carriers and ERU's can give substantial drag penalties, and their effects are especially damaging as they have to be carried back from as well as to the target. The same remarks apply to designator pods, camera pods and gun installations which are also carried   throughout the mission. Thus reducing the drag of such items can give an even greater return than reducing the drag of stores which are released half-way through the mission.

The drag penalties caused by the crutch arms of ejector release units are now well known, and major reductions in drag have been achieved (3) by the development of Minimum Area Crutchless Ejector units (MACE) as shown in Fig 9. An added bonus from this system is that the elimination of flow separations caused by crutch arms gives a smoother flow over the rear of the store, which can reduce the fatigue loading on the weapon and carrier.

Much can be done to reduce the installed drag of multiple store carriers, as was reported (4) by Haines of ARA at the 1975 JTCG Symposium, by application of simple established aerodynamic principles involving relatively minor modifications and re-design of existing store carriers and assemblies. An example was given where it had been found possible to reduce the isolated drag of a loaded triple carrier to a value of only about a third of that of the original "standard" carrier. Research on this theme has continued at the ARA and extended to the investigation of the problems of twin carrier design (Fig 10).

Similar principles can be applied to reduce the drag of groups of stores by exploiting favourable aerodynamic interference. In essence there are two main forms of such beneficial interference, normally referred to as tandem effects and axial stagger.

Skein of electrical
wires and pressure
tubes

Sting clamp

Sting

Balance

Balance adaptor
Pylon (earthed)
Adaptor

62.90 parallel

1000 lb Mk10 bomb
($\frac{1}{4}$ scale)

Dimensions in inches

Strut

5.125

0.06 gap

Support body

Live components

11.50 nose
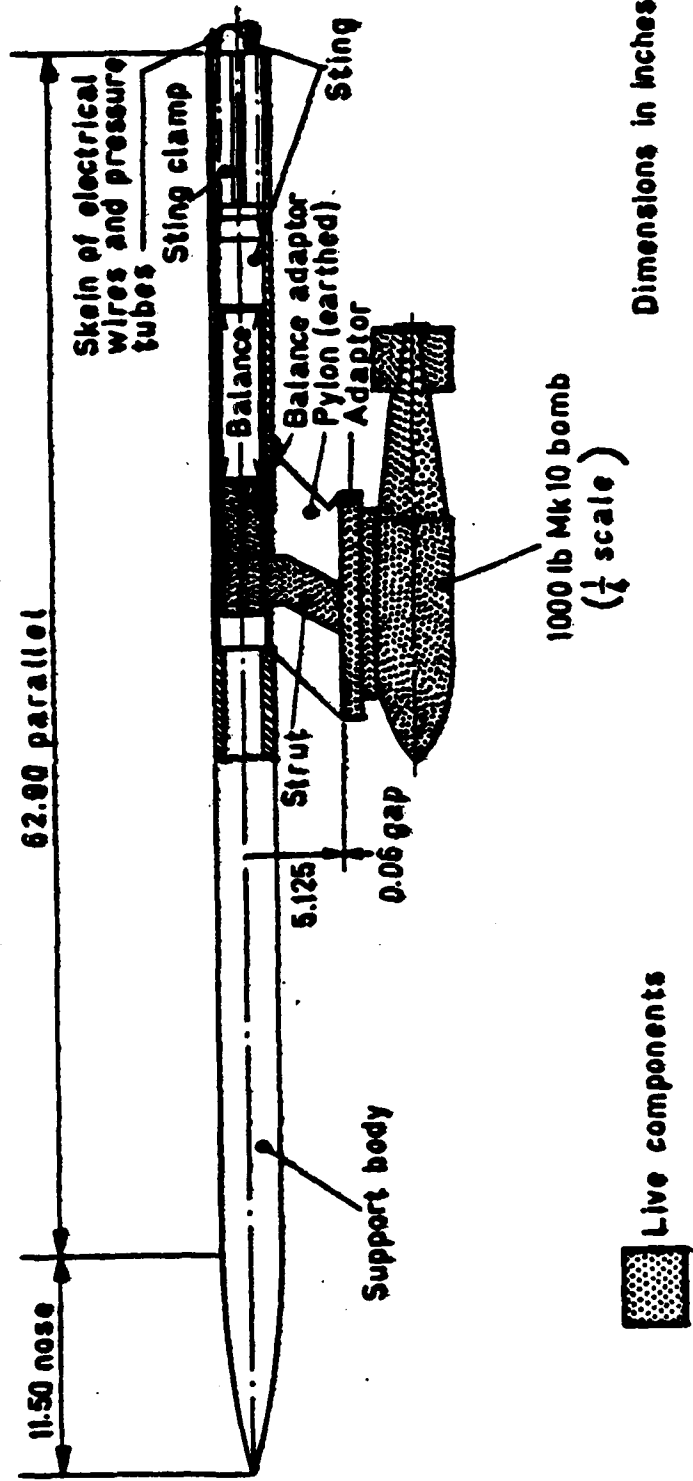
Fig.7 Details of isolated store drag rig (ARA)

507
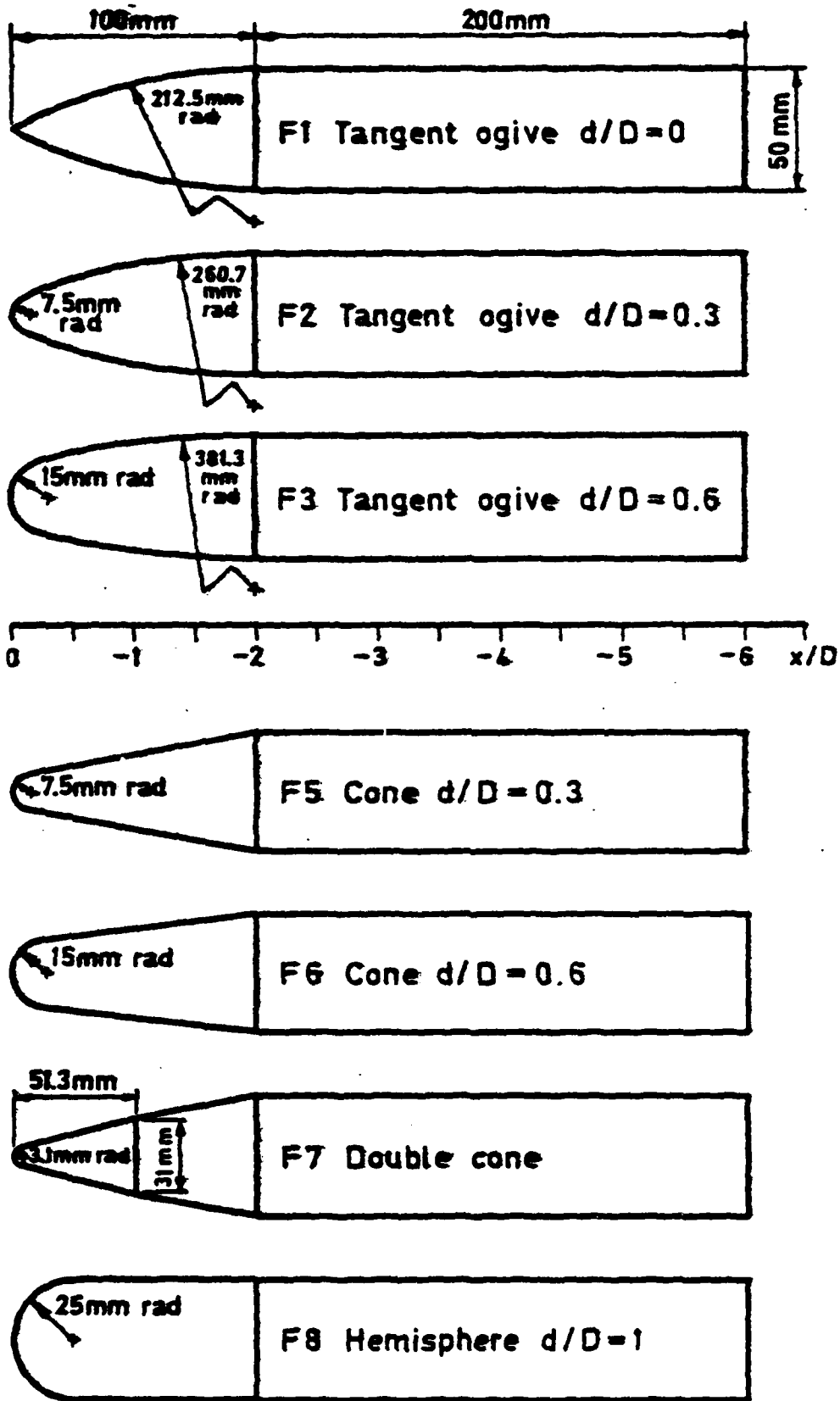
Fig 8   Forebody shapes tested at transonic speeds
(RAE)
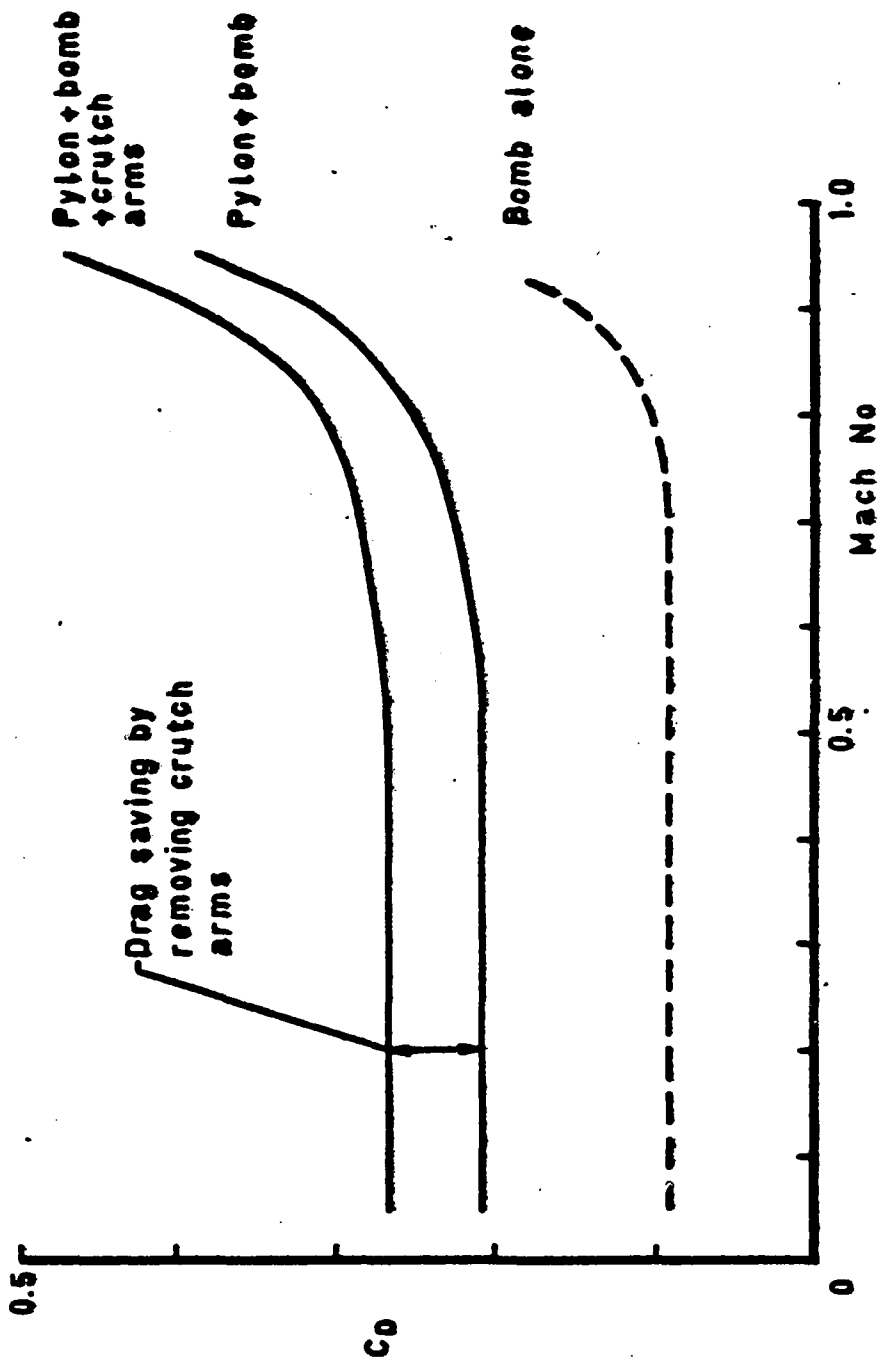
Fig.9   Drag reduction through use of MACE

Triple carrier

Twin carrier

Current
carriers

New
carriers

Current carriers

New carriers

g/q

Drag/q

0   Mach No   1.0

0   Mach No   1.0
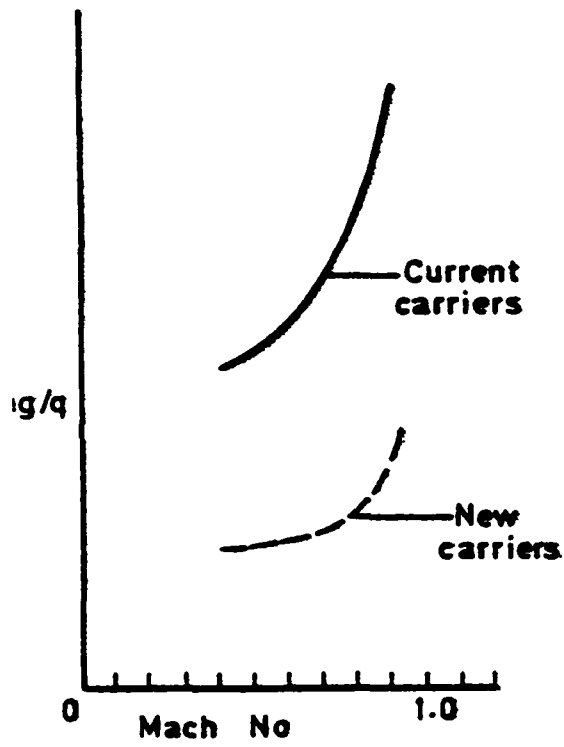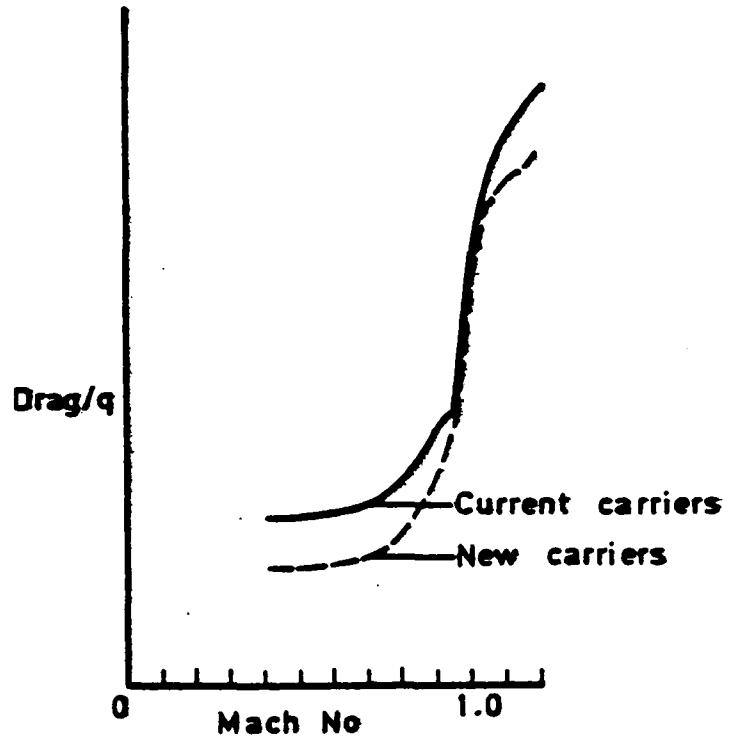
Fig.10 Recent improvements in carrier design

Tandem effects are obtained by placing one store in the wake of another and by shielding it from the full impact of the free stream. Obviously, the maximum beneficial tandem effect is obtained if the stores are closely packed and have large flat bases, or if for any other reason they have high drags and generate wide wakes. It is effective at all speeds, and gives the greatest savings with stores that have basically high drag; if stores are well streamlined they should have relatively small wakes and tandem effects will be small. Many of the various schemes for "conformal" carriage make use of this effect. Axial stagger is a more subtle exercise in which the pressure fields of adjacent stores are so disposed as to promote their mutual cancellation, thereby delaying the onset of shock waves. Its main application is at transonic speeds and to those stores for which wave drag is an important constituent of the total drag. An example of drag reduction for a group of stores by the combined use of tandem effects and axial stagger is given in Fig 11. It was found that the drag of a load of 8 bombs under fuselage carried in 4 pairs on twin carriers could be reduced by about 30% at high subsonic speeds by re-arrangement of the bomb load. This question has been investigated further using an array of stores under a reflection plate (Fig 12), the aim being to identify tandem and axial stagger effects in the absence of an aircraft flow field, otherwise these effects can be obscured by the influence on the area distribution of the weapon/aircraft combination.

All of the preceding methods, reduction of isolated store drag, better carriers and ERU's and better grouping of stores to obtain maximum benefit from tandem effects and axial stagger will all need to be pursued if store installation drag is to be kept within reasonable bounds on future aircraft designs.

Evidently, attention to the ways in which weapons are supported and grouped together can give valuable rewards. While it should not be too difficult to define an optimum arrangement for one type of store load, this is likely, however, to be non-optimum for another weapon fit. Perhaps what is required are carriage systems with scope for easy adjustment of ERU positions, so that near-optimum groupings of a wide variety of store loads can be achieved. Close collaboration between aerodynamicists and weapon installation engineers is obviously needed to achieve this aim, and critical examination is needed of the effects of engineering constraints made on the grounds of low cost and practical simplicity, which can often be the source of excess drag.

EFFECTS OF STORES ON AIRCRAFT FLYING QUALITIES

Most stores have considerable capability to generate lift and hence their presence can change the loads on an aircraft. Typical effects on lateral stability are increases in side force and reductions in yawing and rolling moments due to side slip (n_v and l_v) because of the forward and downward movement of the centre of pressure (Fig 13).
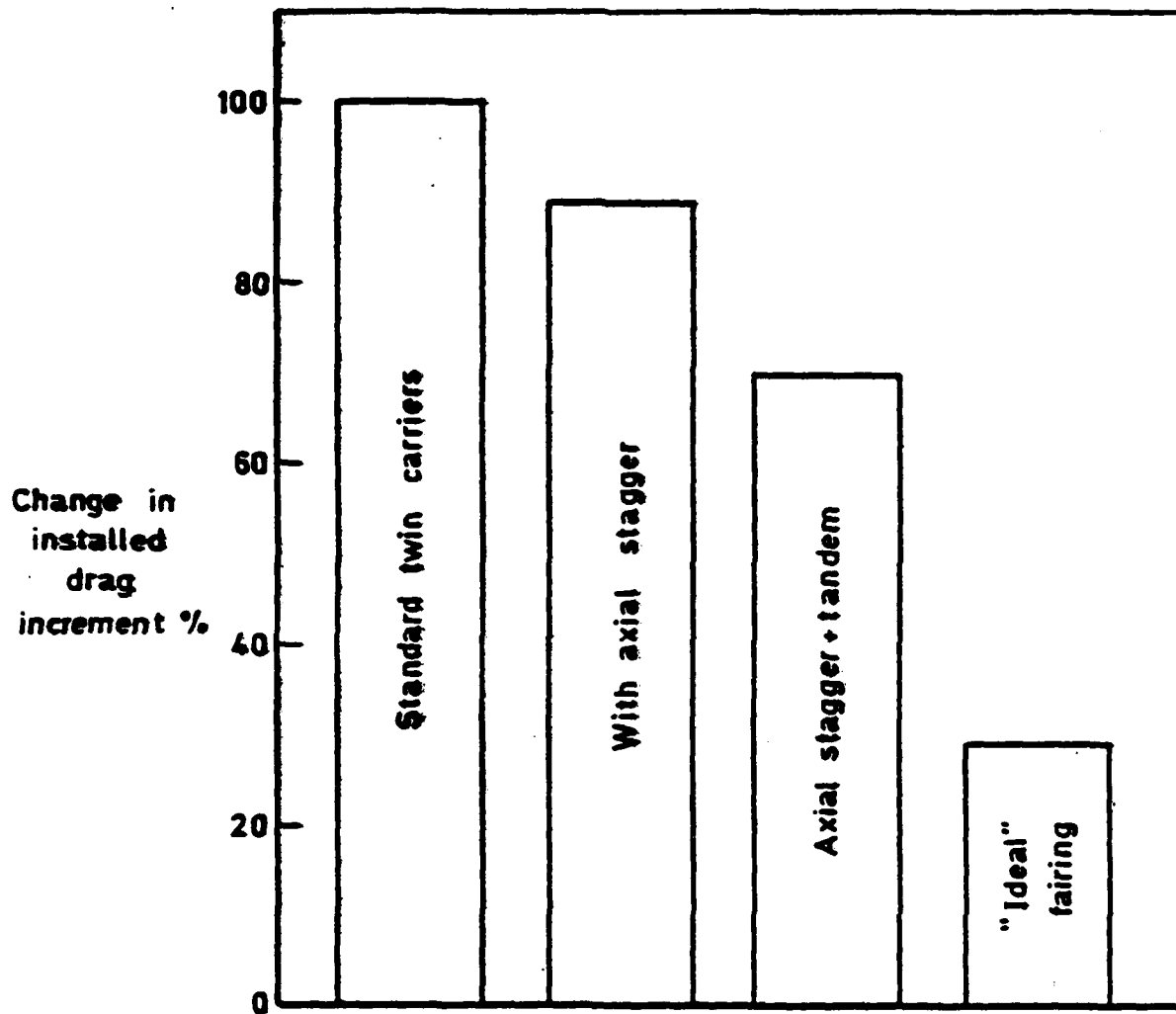
Fig.11 Example of drag reductions obtained from use of axial stagger and tandem effects
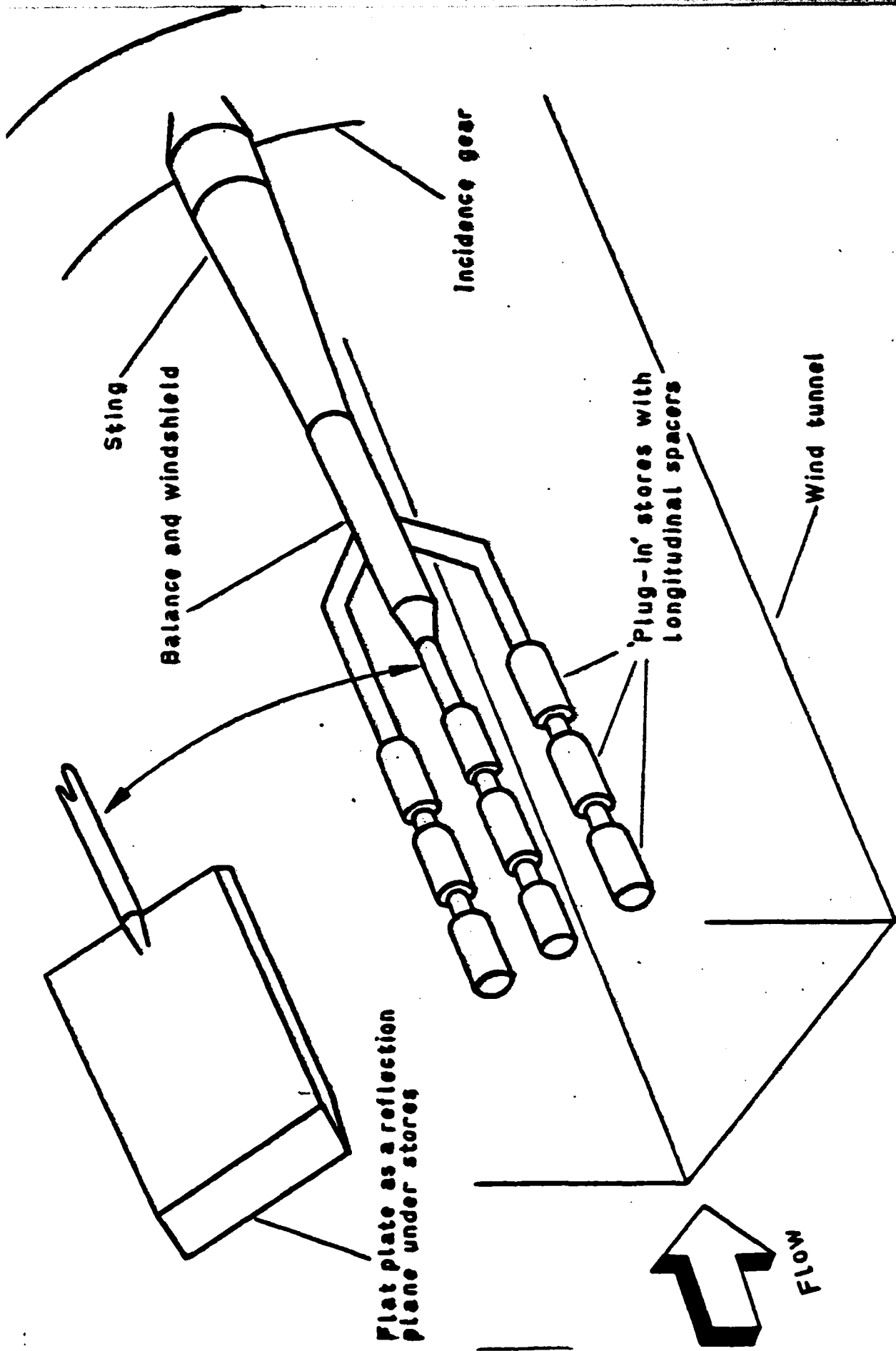
Fig 12 Drag balance rig with stores array (RAE)

Sting

Balance and windshield

Incidence gear

'Plug-in' stores with longitudinal spacers

Wind tunnel

Flat plate as a reflection plane under stores

FLOW

513
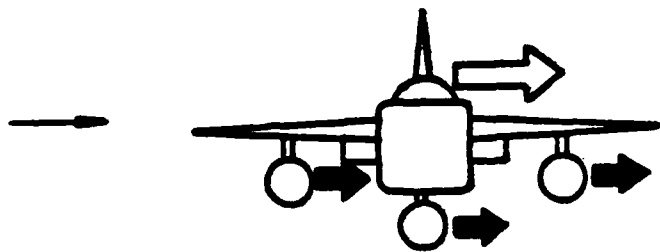
Forces on stores

Force on clean aircraft
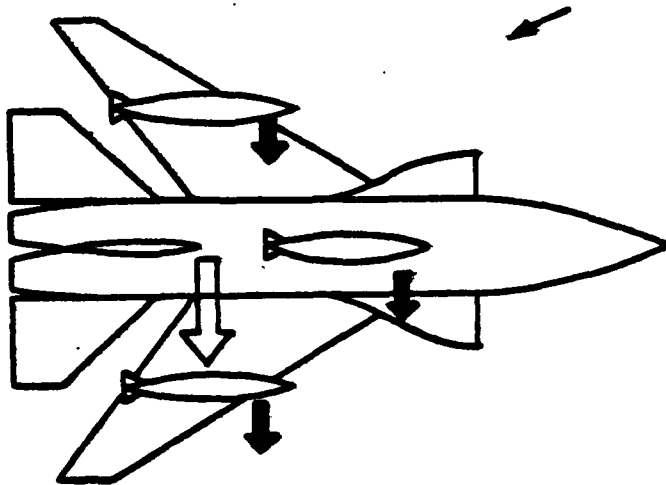
Fig 13 Reduction of lateral stability

Although any loss of static stability in the yaw plane is generally undesirable, the major problem is often encountered at high incidence. A necessary, but not sufficient, condition for stability is a positive value of a "divergence parameter", and a typical variation with incidence is plotted in Fig 14, which illustrates how manoeuvre limitations may be imposed by weapon carriage. Reduction in n_v is the major culprit in this case, but changes in inertias have also had an influence. To minimise such effects, one should endeavour to:

- place the weapons as far aft as possible to reduce the loss of n_v

- minimise the extent to which stores are placed below the aircraft centre of gravity to reduce the loss of l_v

- try to minimise changes in aircraft inertias, which means getting the stores as close as possible to the aircraft centre of gravity.

Such aims are not always compatible with the demands of low installed drag. While possible effects on lateral handling should not inhibit exploration of new ideas concerning weapon carriage, it is necessary that they should be kept in mind. An example of a recent RAE investigation into under fuselage carriage of 8 bombs is given in Fig 15, which charts the variation of yawing moment as schemes were developed for progressive reductions in drag. Eventually, a substantial drag reduction was obtained with a minimal loss of stability, though various intermediate schemes combined smaller drag savings with greater loss of stability.

It is more difficult to give general guidance on the effects of stores on longitudinal stability. Instability can result from stores promoting separation of the flow over a wing, the resulting loss of lift causing pitch up; there can be loss of tailplane effectiveness when this part is bathed in the wake of a store. In such cases, reduced drag from cleaner aerodynamic design is in harmony with improved flying qualities.

The presence of stores can also readily upset the "finely-tuned" aerodynamics of the wing, with the result that maximum lift is reduced, despite the lift generated by the store itself. This problem may become more difficult in the future in that advanced designs may have quite high pressure gradients on the wing lower surfaces which raises the possibility of flow separations (and consequent buffet) being induced by stores at low, as well as at high, lift conditions. Even if stores do not reduce the maximum lift of the wing, their drag still has serious effects on sustained turn rate (Fig 16).

CARRIAGE LOADS AND STORE SEPARATION

The flow field in which a weapon is situated can be significantly
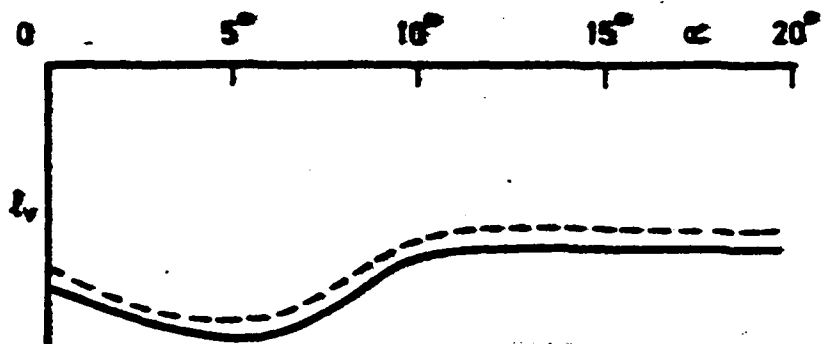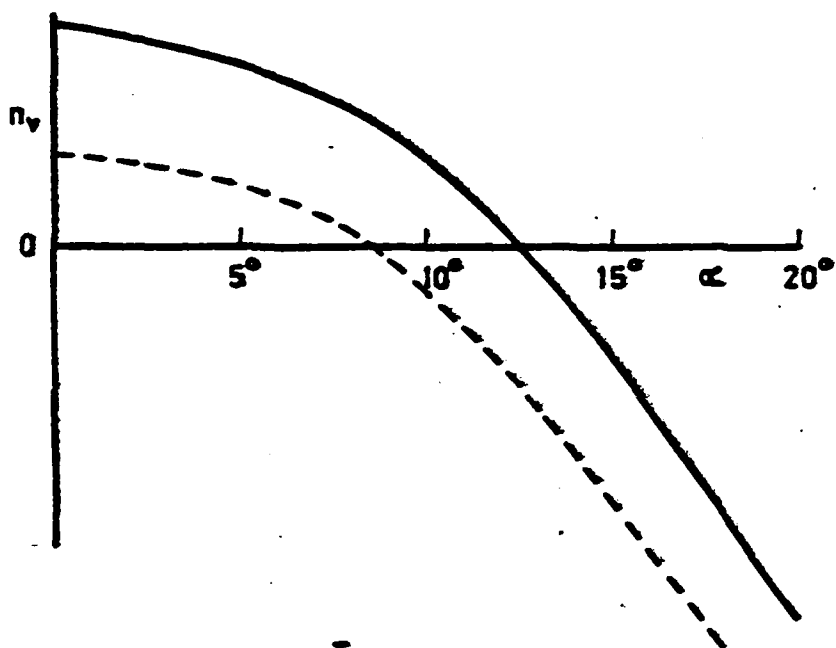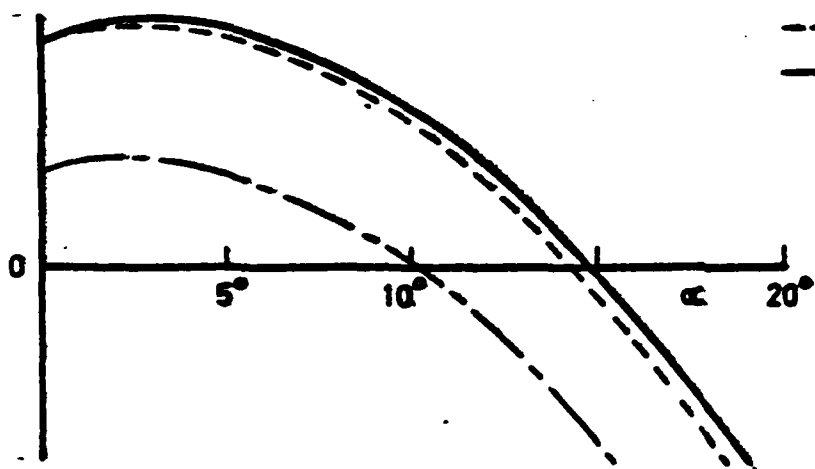
Fig 14 Degredation of lateral stability
at high incidence
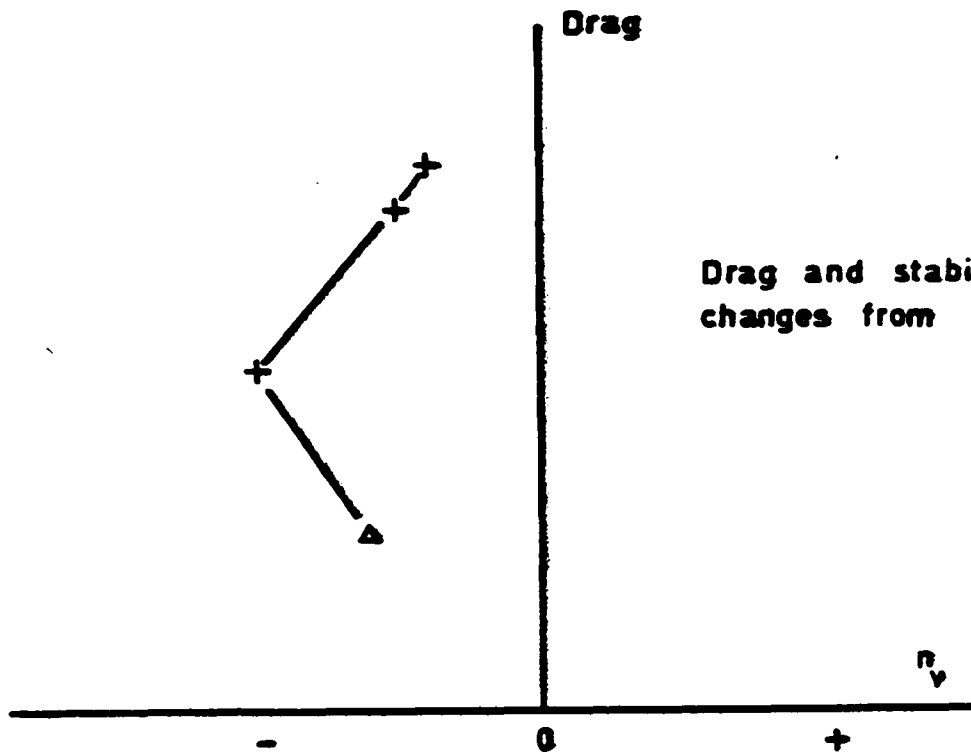
Fig 15 Evolution of lateral stability during
drag reduction exercise
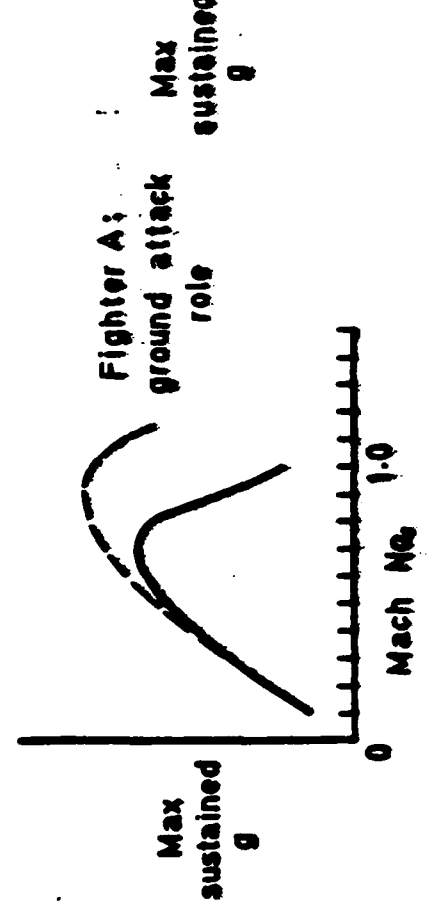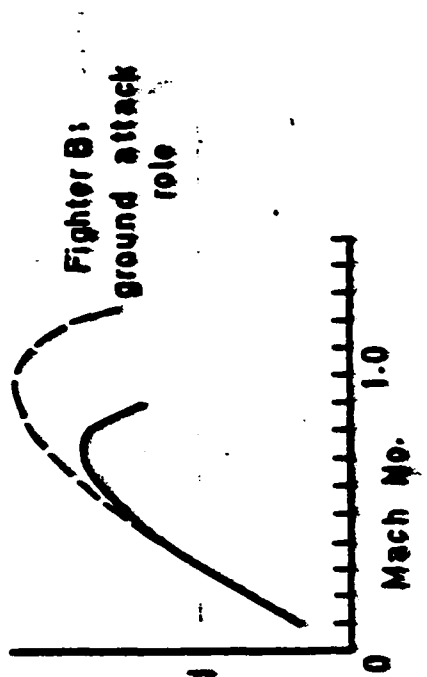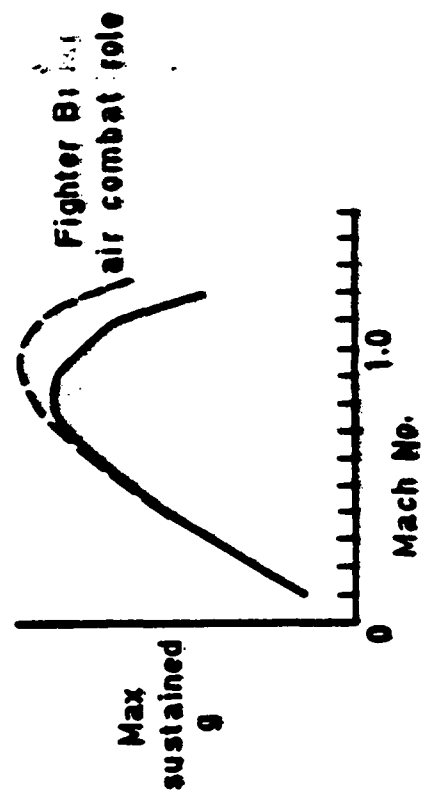
Fig.16 Effect of store carriage on sustained normal acceleration

influenced by local effects, such as the presence of another weapon nearby, and this has already been discussed in the context of installed drag. But in general, local flow conditions in the regions under wings and fuselages where weapons might be mounted vary with location and the attitude of the parent aircraft.

To fix some ideas as to magnitudes, a combat aircraft pulling around 8 g at sea level could have an angle of attack of 17°, which might be accompanied by a yaw of 3°. At typical weapon locations this can lead to local values of incidence and yaw on the fuselage of around 25° and 40°, respectively. Under the wings, the local incidence can vary from 25° at the leading edge to 5° at mid-chord, with the local yaw angles being around 15 to 20°.

The most obvious lesson to the weapon installation engineer is the need for the carriage system and the weapon to be able to withstand large forces, especially side forces. Moreover, the non-uniformity of the flow field means that the distribution of aerodynamic forces over the weapon is likely to be very different during carriage from that in free flight. Thus carriage may pose a completely distinct and demanding design stressing case from both ultimate and fatigue strengths points of view.

Similar remarks apply to store separation characteristics, which are even more difficult to predict than carriage loads. To illustrate the problem, the manner in which the interference between a weapon and aircraft decays as the weapon separates is summarised in Fig 17, and an example is given in Fig 18 of an analysis of the variation of pitching moment on a weapon in a typical underwing flow. This grossly oversimplifies a complex situation, but the aim is to illustrate that the relative sizes of the zones in which the various contributions to the total load on the weapon can vary substantially with the aircraft and weapon configuration.

Difficult as the problems are, it is the author's view that aerodynamicists seeking to design low drag weapon installations must further develop methods to predict carriage loads and store separation characteristics, which can be used in parallel with methods for drag prediction in the early stages of design. Great precision is not required; the main aim is to identify 'bad' features of a weapon installation at an early stage.

More exact predictions of store separation characteristics by experiment and/or calculation are often time-consuming, expensive and have long lead times. Thus it is important that sufficiently comprehensive plans for work on release problems are made at an early stage in the life of a project, as the consequence of not mounting an adequately extensive and timely programme can be expensive and lead to protracted modifications to the project at a late stage in its development. It is also essential at an early stage to set up a methodology

519

Store loads	Characteristic distance	No. of characteristic distances to half amplitude (typical only)
Free-stream	—	—
Derivatives x differences between free-stream and local flows	Aircraft span	$\frac{1}{4}$
Due to non-uniformity of aircraft flow field	Fuselage diameter of wing chord	2
Close interference with aircraft	Store diameter	2
Close interference with other stores	Store diameter	$\frac{1}{2}$

Fig 17   Decay rates of typical store loads

520
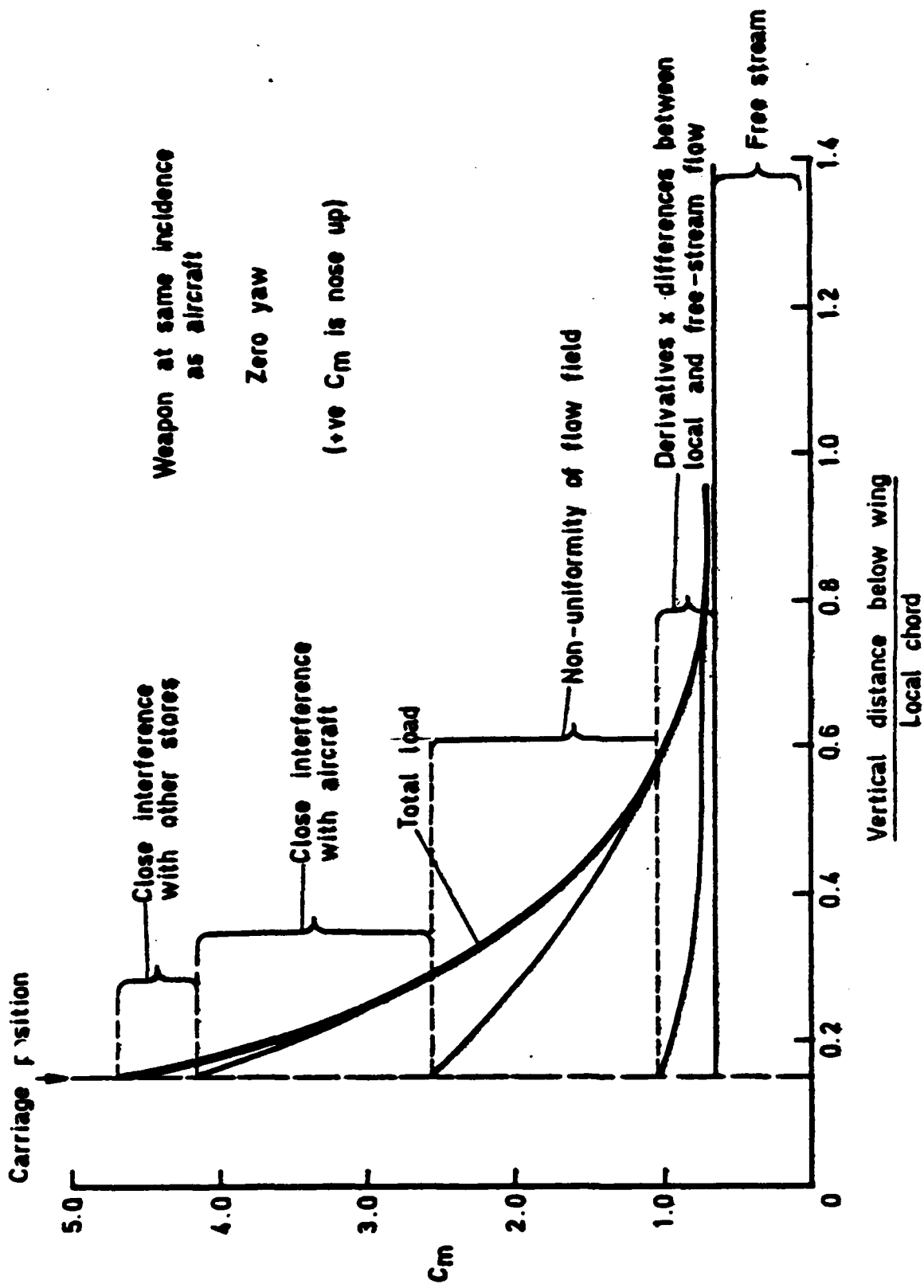
Fig 18 Theoretical analysis of loads on a G.W. in a typical underwing flow: pitching moment.

for treating the complete problem that is sufficiently comprehensive and precise to make full use of all the data that will become available. A flow chart for such a methodology is illustrated in Fig 19.

Probably one of the quickest methods for checking on store trajectories is the light model dropping technique, which is used extensively to establish release conditions which are acceptable from an aircraft safety point of view. Its main drawback is that if the correct Mach number is used, the techniques give conservative answers because the model store trajectory will be closer to the parent aircraft than at full scale. Effectively, the test is done in a gravity deficient environment. To improve the simulation of store drops by this technique, HSA (Brough) have developed a rig which can accelerate a 1/30 scale model vertically upwards at 29 g, thereby compensating for the error in vertical separation distance (Fig 20). This works well, and it has been proved that pyrotechnically-powered ERU's can be fired immediately after the model acceleration starts with precise timing and repeatability. Comparisons between tests with and without acceleration of the model show significant differences in pitch angle and sideways movement of the store due to accelerating the aircraft model. This result is important because it has been the practice to correct for the gravitational deficiency by the addition of an increment in the vertical separation distance. Thus this type of correction is not sufficient, and the sideways movement of the store could not have been predicted by any simple method.

PROSPECTS FOR DRAG REDUCTION

GENERAL

Because the time-scale of weapon and aircraft developments are not usually in phase with each other, and because the development time scales of weapons are usually shorter than those for aircraft, the type of improvements that can be made in weapon installations will vary between the short, medium and long term. A suggested overall strategy is summarised in Fig 21, the main theme being that the passage of time will bring increasing opportunity to realise the large potential benefits of reduced drag due to store carriage, and that in the longer term the weapon installation designer ought to make a major contribution towards the design of new weapon-airframe systems from conception.

SHORT-TERM

Within short time scales, changes are confined to those that can be contrived with existing equipment, but this is not so restricting as might be thought at first sight. The most obvious example is that maximum use should be made of MACE-type carriers, which can reduce the installed drag of single stores by over 25%, and research has shown that similar percentage gains are obtained on multiple carriers. A further example of short-term benefit is the greater use of tandem
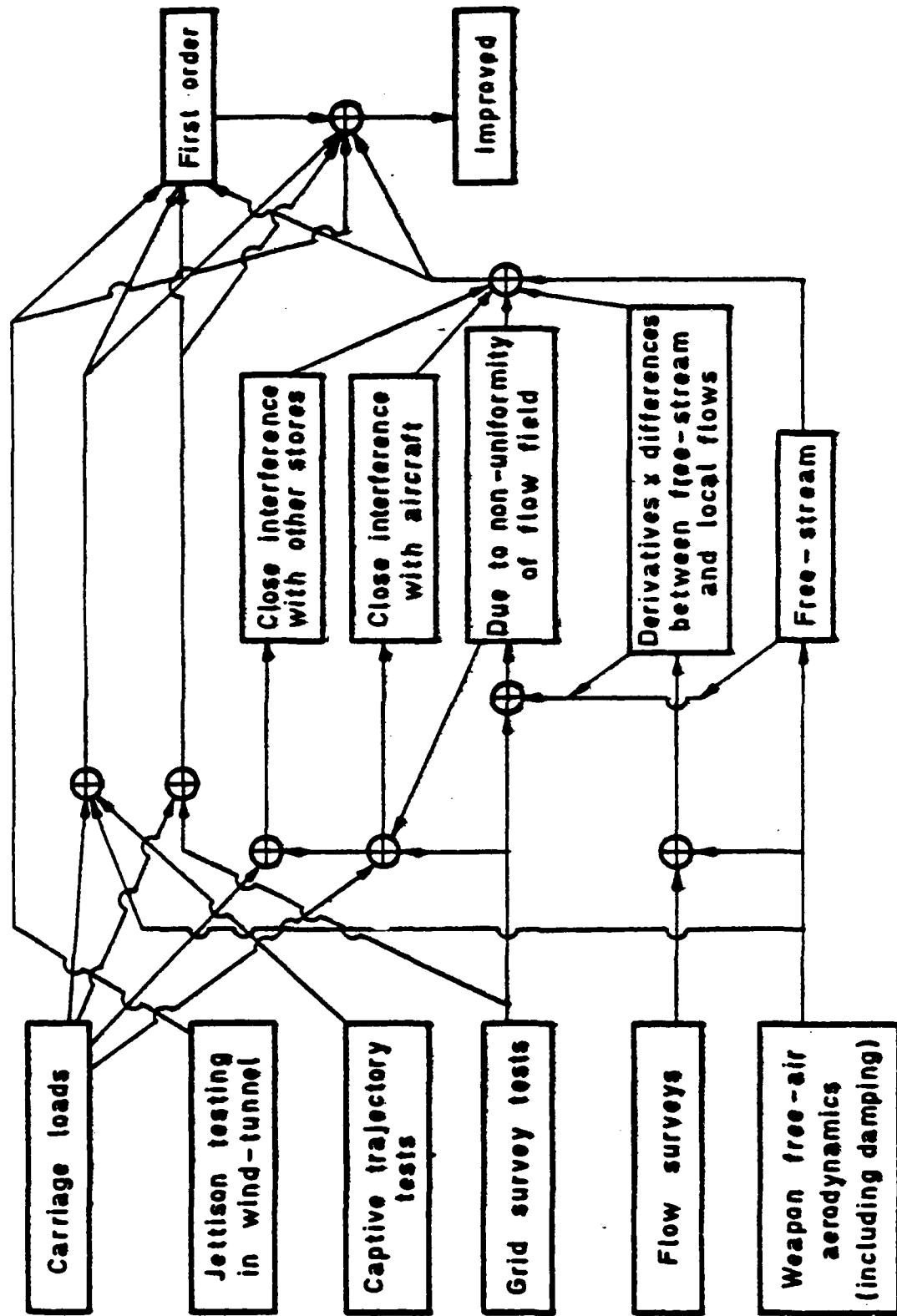
Fig 19 Use of experimental data in studies of release disturbance

Linear acceleration and deceleration unit

29g acceleration

$\frac{1}{30}$ scale model
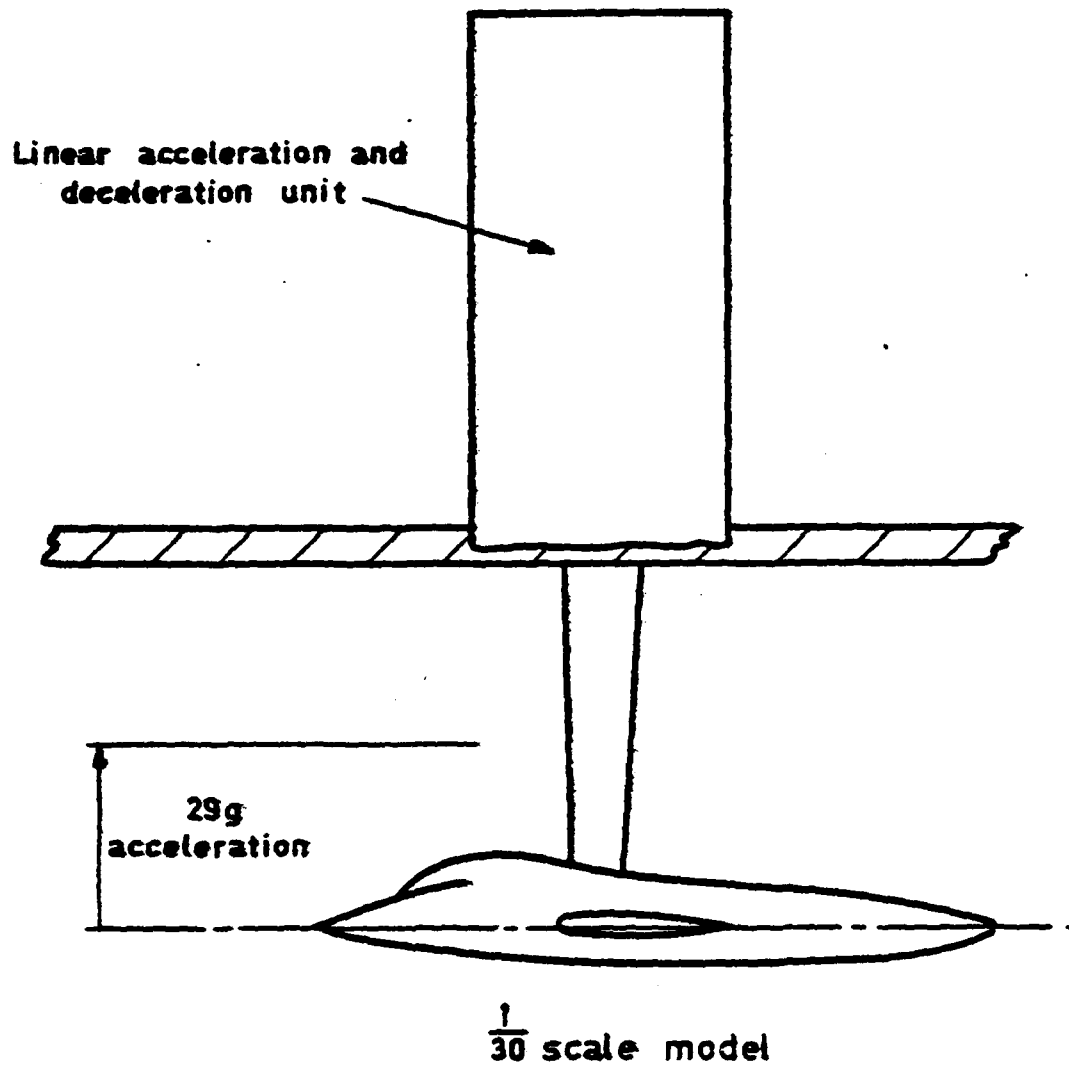
Fig 20   The HSA (Brough) model acceleration rig

	Short-term Existing aircraft Existing weapons	Medium-term Existing aircraft New & improved weapons	Long-term New aircraft New weapons
Overall aim	Make more effective use of existing equipment	Develop cleaner weapons and carriers	Make major contribution to design from conception
Drag	Use MACE-type ERU's Use tandem beams Some re-arrangement of store load	Reduce avoidable drag of stores Engineering realisation of low-drag carriers Re-arrangement of store load	Improved design based on better physical understanding and proven methods
Release disturbance & carriage loads	Establish and validate wind tunnel as cost effective alternative to flight trials	Develop and improve simple prediction methods as aid to good design	Development of prediction techniques which include allowance for mutual interference effects between stores in groups
Flying qualities	Little or no deterioration likely. Possible some improvement from suppression of flow separations	Develop and improve simple prediction methods as aid to good design	Improved design based on better physical understanding and proven methods

Fig 21 Suggested strategy for improvement of weapon installations

carriage, particularly for stores which have relatively high free-air drags. Such stores are often carried side-by-side on twin carriers. Installed drag savings of up to 25% are possible. Tandem carriage can give problems of cg shifts, and flexibility of the beams can cause ejection velocities to be a function of the position of each store in the release sequence. However, underfuselage locations should be free from most, or all, of these problems.

Thus, with some re-arrangement of the store load making greater use of tandem-beam carriage, and low drag ERUs, reductions in overall aircraft drag of up to 25% might be possible. It is difficult to see how equivalent gains in aircraft performance could be achieved by uprating of engine thrust for the same financial outlay.

MEDIUM TERM

For the medium term, the most obvious possibilities for improvement are the development of weapons having lower free-air drags and the engineering realisation of improved carriers. While it is difficult to quantify the aerodynamic improvements that might be achieved without undue cost, it is suggested that a halving of the 'avoidable' drag of weapons by reduction of excrescences, better nose shapes etc is an achievable aim in many cases. Since many stores have an avoidable drag comparable to their basic skin friction drag, it is possible that overall drag reductions up to 20% could be obtained for stores carried underfuselage or underwing at subsonic speeds, though it would appear that the benefits of reduced free-air drag can be almost completely offset by store/aircraft interference for underwing carriage at transonic speeds. On carriers, research in the UK has shown that dramatic improvements in drag are possible while remaining within the obvious engineering constraints of not excessively exacerbating the torques imposed by the action of ERUs, space for ERU fitment, access for loading and arming etc. In addition, there is some evidence that axial stagger, which is an essential feature of these designs, can reduce release disturbances. The drag reductions achieved by means of such designs are around 60% for the triple carrier, and about 30% for the twin carrier at low speeds, reducing to about 10% at high speeds.

In principle, the ultimate step in the aerodynamic design of carriers, would be to bury them in the aircraft or a pallet and thus shield them from the airstream, ie 'tangential carriage'. Unfortunately, such a step undoubtedly increases the problems of access for loading and arming, with the danger that turn-round times would become extended. With the development of MACE, and the potential large improvements in carrier design just described, the penalties for exposing the carriers to the airstream are diminishing and hence eroding the aerodynamic benefits of tangential carriage. The author suspects that there is room for much technical argument on this question in coming years.

In the medium term there will also be greater opportunities for

re-arrangement of stores underfuselage and underwing, along lines
discussed earlier, but care will be needed to avoid degradation of
lateral stability characteristics, as discussed earlier.

LONG TERM

In the longer term, the logical exploitation of tandem effects
leads to various schemes generally referred to as 'conformal carriage'.
The efficacy of conformal carriage in reducing drag is indisputable,
but it has its limitations. One difficulty is that when a variety of
stores of differing length need to be carried in an installation where
the ERU positions are fixed, gaps are left which can considerably
increase the installed drag. Another problem is that stores which
are ideal for conformal carriage, in that they can be packed closely
together, tend to have high free-air drags which makes them unsuitable
for underwing carriage on conventional carriers, say. If the situation
arises where larger store loads have to be installed or smaller
aircraft, as argued in Section 2, then it would appear that space under-
fuselage will not be adequate, and stores will have to be distributed in
an optimum fashion both underwing and underfuselage; thus it may be
undesirable to develop stores which are suitable only for underfuselage
carriage. Perhaps the solution is to have ERU positions under fuselage
which can be varied to suit different store lengths, thereby obtaining
near-optimum layouts for a wide variety of store combinations.

The most important contribution that the designer of weapon
installations can make in the longer term is to have his ideas ready
at the time of conception of a new aircraft design, and to be flexible
in his approach, this flexibility being based on a better physical
understanding of the aerodynamics of weapons installations than we
have today, backed by proven prediction methods.

If the designers of weapon installations take an active part in
the initial aircraft design process, then they will have much more
influence on the sizing of the aircraft, with consequent savings in
initial cost and life-cycle costs. An illustrative example has been
produced using the military version of the RAE multivariate design
synthesis computer program (5). The aircraft was sized for a ground
attack mission with 6 bombs, and the effects of successive reductions
of 10%, 20% and 30% in bomb installation drag were investigated. It
was found that these reduced the aircraft size by 2%, 4% and 7%,
respectively. If these drag reductions were obtained only after the
design had been frozen, there would be little or no savings in
aircraft cost and life-cycle costs (though performance would be some-
what better than required).

IMPROVED PREDICTION METHODS

Throughout this paper, the author has been making a plea for
improved prediction methods covering, and linking, the various aspects

of weapon installation design as it affects aircraft performance and flying qualities and release of stores. What seems to be needed are essentially simple but comprehensive methods, based as far as possible on the underlying physics of the problem, as opposed to empirical correlations, which can be used as a framework to guide future work as well as providing better predictions of drag, stability etc. This is not meant to denigrate the value of existing methods for calculating store trajectories, for example. These give valuable assistance once the aircraft and store flow fields have been modelled, but it is a time-consuming process to set them up, and time-consuming to investigate the effects of changes in aircraft and store geometries (as distinct from the effects of changing store position).

A start has been made at the RAE on improving methods for drag estimation (6), the main aim being to replace the use of empirical 'assembly factors' by methods for estimating mutual interference within a group of stores. Allowance for mutual interference between stores seems to be a notable lack in current methods for calculating store trajectories.

The method has been shown to have adequate accuracy for many purposes during preliminary project work and to give a reliable guide to the relative merits of alternative means of carriage both conventional and unconventional. It is being used as a framework to guide future work, and it has highlighted the need for further understanding of the mutual interactions between stores at transonic speeds, tandem effects between closely spaced bodies and installation effects at supersonic and transonic speeds. Broadly speaking, it can be described as an empirical method structured by theory.

A start has also been made in developing similar methods for estimation of carriage loads, release disturbance and the effects of weapon carriage on aircraft stability. An example of preliminary results from an investigation of methods for predicting release disturbance for a guided weapon is given in Fig 22, where it can be seen that representation of a wing by a simple theory (line vortex + line source + line sink) and calculating yawing moments on the store from flow angles at the moment reference point and near the canard control surfaces, gives results close in general shape to a more-exact theory, both the theoretical estimates being close to experiment. It is suggested that such methods should be very useful to weapon designers, and designers of weapon installations, to guide them towards the best type of weapon installation early in the initial project stage, rather than finding out later or, when more exact calculations have been performed, that problems have to be overcome.

CONCLUDING REMARKS

To sum up, understanding the aerodynamic interactions between stores and airframes has a dominating effect on the design of stores installations for low drag. While the path towards lower drag
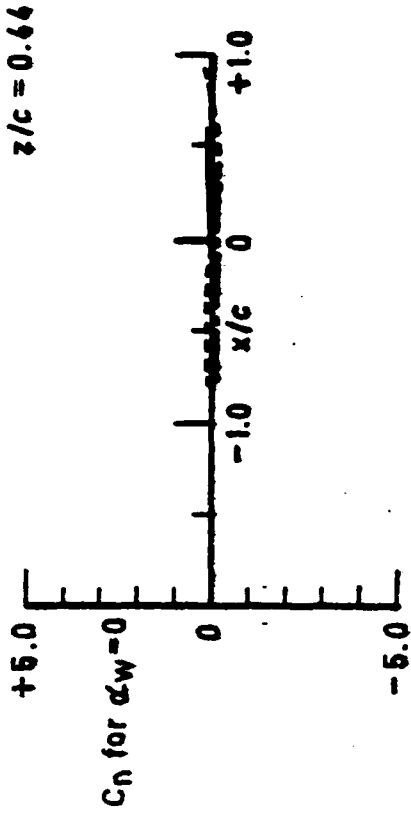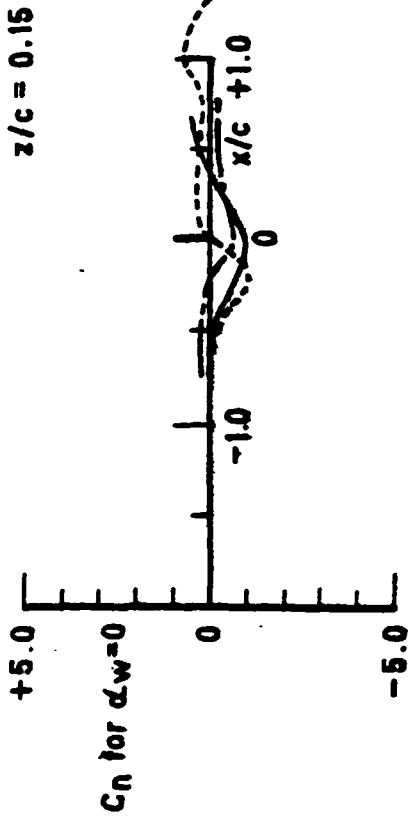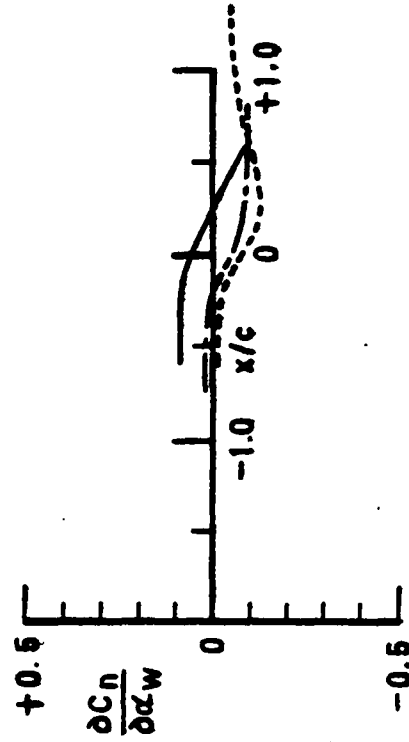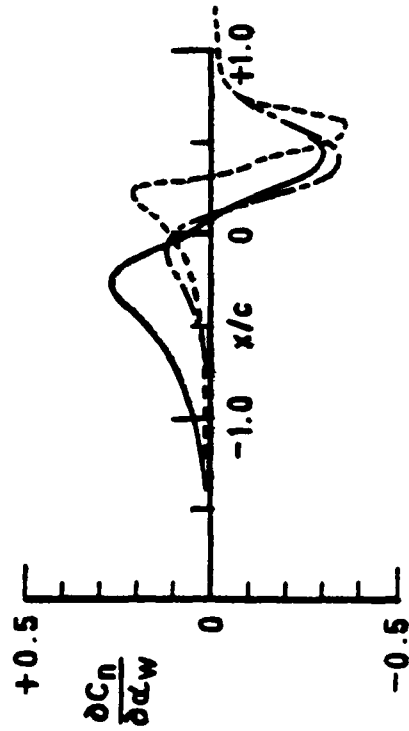
Fig 22 Prediction of yawing moments and comparison with experiment

installations is fairly clear, future trends in aircraft and weapon design are likely to present increasingly difficult problems for the designers of weapon installations, but will also increase the importance of their future contributions to the design of effective combat aircraft.

Achievement of low drag will need to be guided by considerations of weapon installations on aircraft flying qualities, carriage loads and release disturbance, and there is a need for simple prediction methods on all of these subjects to guide the designer towards good installations in the early project stage.

ACKNOWLEDGEMENTS

REFERENCES

1   K. G. Winter   Measurements of the drag of some charac-
    L. Gaudet   teristic aircraft excrescences immersed
                        in turbulent boundary layers.
                        Paper 4, Agard Conference Proceedings 124,
                        April 1977.

2   L. C. Ward   Force measurements at transonic speeds on
                        axisymmetric forebodies to determine the
                        effects of bluntness. (1976)
                        Unpublished RAE Report (Restricted).

3   J. H. Hasquenoph   Advantages and possible developments of
    J. P. L. Lautour   release and ejector units utilising the
                        saddle store suspension system.
                        Proceedings of 3rd JTCG Symposium Sept 1975.

4   A. B. Haines   The reduction of the installed drag of
                        multiple store carriers.
                        Proceedings of 3rd JTCG Symposium
                        Sept 1975.

5   D. L. I. Kirkpatrick   Initial design optimisation on civil and
    M. J. Larcombe   military aircraft.
                            RAE Tech Memo Aero 1539, 1973

6   P. G. Pugh   The estimation of the installed drag of
                        stores (1976).
                        Unpublished RAE Report.

DEREK H. PECKHAM

1946-51	Handley Page Ltd and part-time student at London University studying for BSc in Aeronautical Engineering.
1951-53	Royal Air Force, trainee pilot.
1953-58	Royal Aircraft Establishment (Bedford), 13 ft x 9 ft low speed wind tunnel, working on aerodynamics of slender wing.
1958-60	Ministry of Supply Headquarters, Technical Staff Officer to Chief Scientist.
1960-65	Royal Aircraft Establishment (Farnborough), Hypersonics Division, working on lifting slender bodies and wave-riders.
1965-72	Royal Aircraft Establishment (Farnborough), Aerodynamics Projects Division, working on studies of future transport aircraft and development of computer based methods for design synthesis and optimisation.
1972-75	Procurement Executive, Ministry of Defence Headquarters, Assistant Director Civil Aircraft Development.
1975-date	Royal Aircraft Establishment, Head of Weapon Aerodynamics Division.

Chartered Engineer, Member of Royal Aeronautical Society.

THE AFATL LOADS PROGRAM; MACLIP
(MAXIMUM AIRCRAFT CARRIAGE LOADS AT INSTALLED POSITIONS),
A DISCUSSION OF THE TECHNIQUE
(U)
(Article UNCLASSIFIED)

by

C. Wayne Ingram
William W. Dyess, Jr.
US Air Force Armament Laboratory
Eglin Air Force Base, Florida 32542

ABSTRACT. (U)   In the AFSC Regulation 80-33 "Class II Modification Procedure," the responsibility for clearing stores for flight on AFSC aircraft was relegated to ADTC/DLJC. It thus was incumbent on DLJC to determine some manner of approach to the question of insuring the aircraft structural integrity while carrying stores. This approach should be as accurate as possible, as inexpensive to operate as possible, and as responsive to short suspenses as possible. Obviously there were a number of trade offs to be considered. The result of this trade off study was the technique used in the program MACLIP (Maximum Aircraft Carriage Loads at Installed Positions). MACLIP is used or will be used to determine the structural integrity of the F4C/D, F4E, A10, F16A, and F16B aircraft with stores installed on their various pylons. This paper discusses the primary modules of this program and how they will be used. These modules and a general description of each is as follows:

     a. Executive Module - Controls flow of information and order of execution of all other modules.

     b. Aircraft Modules - Determine the inertial and attitude parameters for each of the candidate aircraft throughout various maneuvers.

     c. Aerodynamic Module - Reads installed aerodynamic coefficients for the stores being evaluated, and transfers this data into a format which may be accessed by the other modules.

     d. Loads Module - Combines aerodynamic and inertial data to determine total loads at a reference point.

     e. Structures Module - Compares previously generated loads to defined maximum allowable loads at various control points on the aircraft.

     f. Output Module - Controls all output options. Data may be printed out in tabular or graphic form in either engineering or managerial format.

LIST OF FIGURES

LIST OF SYMBOLS

$\overline{A}$ Aerodynamic Reference Area

[A]   Least Squares Coefficient Array

{A}   Least Square Constant Column Matrices

C_A Aerodynamic Axial Force Coefficient

C_1 Aerodynamic Rolling Moment Coefficient

C_m Aerodynamic Pitching Moment Coefficient

C_N Aerodynamic Normal Force Coefficient

C_Y Aerodynamic Lateral Force Coefficient

C_η Aerodynamic Yawing Moment Coefficient

DMF   Dynamic Magnification Factor

F_X Total X Direction Force at Store C.G.

F_Y Total Y Direction Force at Store C.G.

F_Z Total Z Direction Force at Store C.G.

F_{A_X} Aerodynamic X Direction Force at Store C.G.

F_{A_Y} Aerodynamic Y Direction Force at Store C.G.

F_{A_Z} Aerodynamic Z Direction Force at Store C.G.

F_{I_X} Inertial X Direction Force at Store C.G.

F_{I_Y} Inertial Y Direction Force at Store C.G.

F_{I_Z} Inertial Z Direction Force at Store C.G.

L   Aerodynamic Reference Length

M   Mach Number

x

M_X	Total Moment about Store X Axis
M_Y	Total Moment about Store Y Axis
M_Z	Total Moment about Store Z Axis
M_{A_X}	Aerodynamic Moment about Store X Axis
M_{A_Y}	Aerodynamic Moment about Store Y Axis
M_{A_Z}	Aerodynamic Moment about Store Z Axis
M_{I_X}	Inertial Moment about Store X Axis
M_{I_Y}	Inertial Moment about Store Y Axis
M_{I_Z}	Inertial Moment about Store Z Axis
$\{N\}$	Least Squares Constant Column Matrix
N_X	Inertial Load Factor in X Direction
N_Y	Inertial Load Factor in Y Direction
N_Z	Inertial Load Factor in Z Direction
P	Roll Rate
$\overset{o}{P}$	Roll Acceleration
Q	Incompressible Dynamic Pressure
SI	Structural Index
T	Aerodynamic Transfer Function
W	Store Weight
Y	Y Coordinate of Store C.G.
$\overline{Y}$	Y Coordinate Axis
$\{Y\}$	Least Squares Constant Column Matrix
Z	Z Coordinate of Store C.G.

Z	Z Coordinate Axis
f_a	Allowable Load
f_c	Calculated Load
g	Acceleration Constant (32.2 ft/sec^2)
$\{1\}$	Least Square Constant Column Matrix
$\{m\}$	Least Square Constant Column Matrix
α	Angle of Attack
β	Angle of Sideslip
$\{n\}$	Least Squares Constant Column Matrix
θ	Angle Formed by Y and Z Store C.G. Coordinates (arctan $\frac{Z}{Y}$)

INTRODUCTION

The analytical approaches currently available to the loads engineer considering the prediction of aircraft flight loads are many and varied.

The loads engineer may, based on experience and previous flight test data, determine by analogy that the aircraft is capable structurally to carry a given store or stores. This analogy approach is by far the least expensive and usually the least time consuming of all approaches. Although the advantages are evident, many clearance requests do not lend themselves to the analogy approach due to a store's singular aerodynamic, geometric, and/or inertial characteristics.

At the other end of the spectrum the maneuver response may be obtained by use of a digital or hybrid simulation program. An advantage of loads prediction by dynamic simulation is the higher degree of accuracy obtainable as compared to other analytical methods. The major disadvantages are the requirements for significant amounts of computer time and manhours. To investigate a flight envelope using a simulation method, an adequate number of mach-altitude points must be considered to cover the full scope of the desired envelope. At each mach-altitude combination, loads critical maneuvers must be modeled. The large number of permutations which arise from consideration of many mach-altitude points and critical maneuvers at each point result in significant usage of computer time by the time dependent simulation method. Also, a simulation program generally requires wind tunnel data consisting of store and aircraft airloads data as well as aircraft stability data.

Due to the type of workload at Eglin AFB (i.e. response to on-going projects) a method of predicting loads was needed which would have the fast turn-around features of the analogy method and yet still be accurate like the simulation method. This approach involves loads analyses independent of the time variable hereafter called the compressed maneuver model (CMM) approach. This approach can be used when critical loading points within a maneuver time interval can be isolated and predicted as functions of aircraft performance and attitude parameters. The aircraft performance and attitude parameters can be obtained by using existing aircraft stability and airloads data for store-aircraft configurations which provide conservative or outer bound values of these parameters. The major advantages of the CMM approach are the reduced requirement for aerodynamic data associated with each new configuration and a reduction of computer time as compared to the time dependent simulation method. Although the CMM method is not as accurate as the simulation method, its conservative base does not generally exclude its usage as an analytical tool for clearance studies on the majority of flight configurations.

A loads prediction computer program, Maximum Airborne Carriage Loads at Installed Positions (MACLIP), based on the latter approach is currently being developed by AFATL/DLJCS, Eglin AFB, FL. This program,

538

described herein, is being written in FORTRAN code for use on the CDC 6600 computer in both batch and interactive modes.

MACLIP OVERVIEW

MACLIP is organized into a modular structure. The modular structure provides for greater clarity in the overall understanding of the program and allows for more efficient computer processing by overlaying of the code.

Figure 1 illustrates the primary level of modularization. Execution of each module below EXECUTIVE is controlled by the EXECUTIVE module. The order of execution of the various modules, as indicated by Figure 1, is controlled by inputing control cards, with at most the EXECUTIVE module and one other module being employed at any particular time. Overlay structuring, possible because of the modular concept, allows for minimum core usage which can be of significant importance since time-sharing interactive terminals may limit core. The current overlayed version of MACLIP requires 62K octal words on the Eglin CDC 6600 computer.

EXECUTIVE MODULE

The EXECUTIVE module performs 5 primary functions. These functions are:

(1) Defines necessary files

(2) Reserves common blocks

(3) Reads all data from the input file

(4) Produces an input data echo on a specified output file

(5) Controls program flow to the various modules

The EXECUTIVE module defines the standard input, output, punch, and plot files. Of special interest are files tape 10 and tape 11 which serve as communication files from one module to another. Input data and values of variables calculated within a particular module are written onto one of the two communication tapes. The following module which is executed will read from the tape, placing the read information and additional calculated values onto the second communication tape. The next module will read from the second communication tape and place the read information plus calculated values back onto the first tape in an overwrite mode. This process of tape flip-flopping will result in a final data tape which contains all initial, intermediate, and final variable information as utilized and developed during program execution. Employment of the tape flip-flop method allows a significant reduction in core usage.
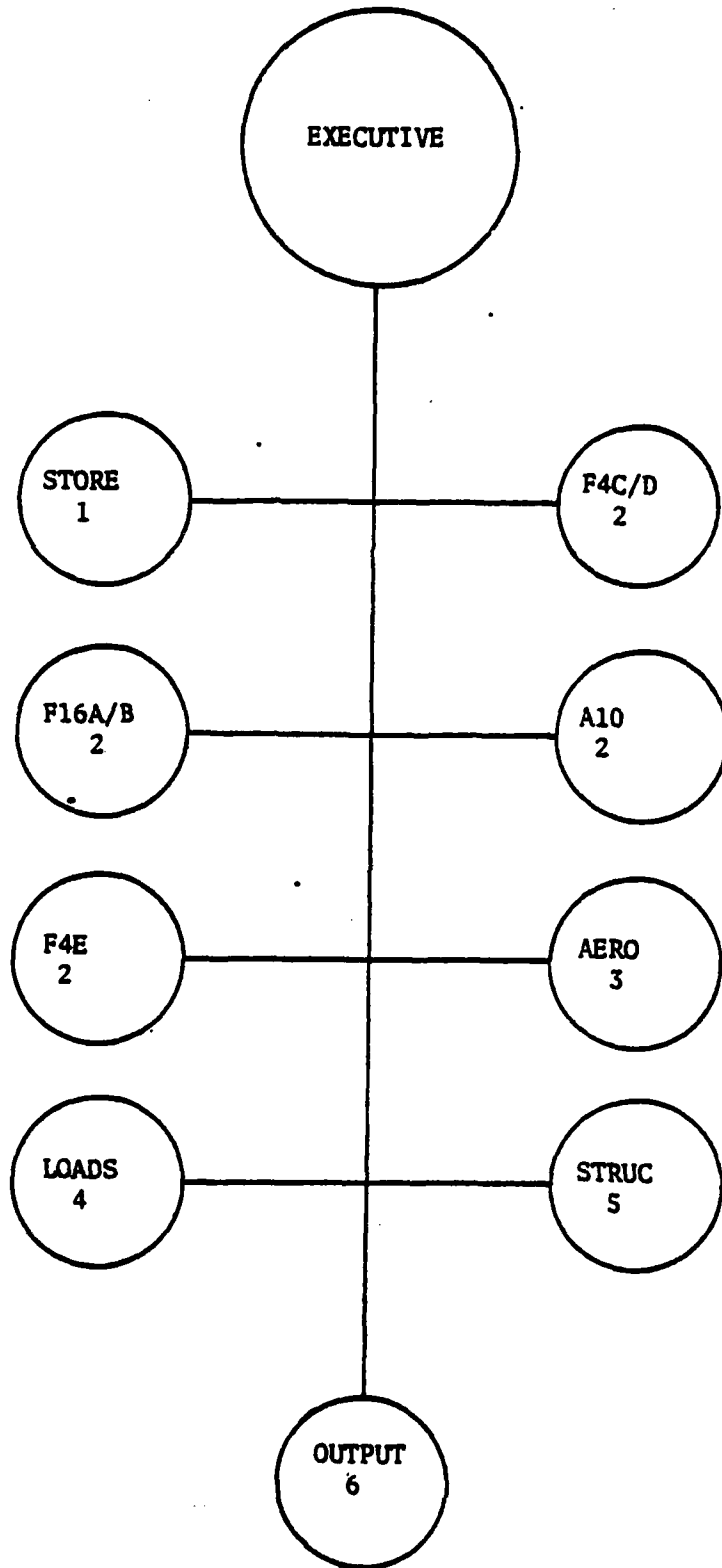
Figure 1. MACLIP Modular Structure

A common block consisting of 1390 words is reserved by the MAIN routine. The majority of the common storage allocated is required for the plotting routines within the OUTPUT module. If plots are not desired, the common size can be reduced significantly.

The MAIN routine reads all data from the input file and echoes the data onto the chosen output file, showing record count and providing a column number reference heading.

Program flow to the different modules is controlled within MAIN by use of code cards. Module execution sequencing is usually 1 to 6, although modules can be executed in any order. The user must be aware of the necessity for a correctly formed communication data tape prior to execution of a module.

STORE MODULE

The purpose of the STORE module is to compute the position of the center of gravity (C.G.) of the composite of all stores, beams and/or adapters of one store station on the aircraft. In addition, the weight, pitch inertia, yaw inertia, and roll inertia of the composite about its C.G. are computed.

The capability to perform C.G., weight and rotational inertia calculations exists for both internally and externally mounted hardware. A maximum of one store can be handled with internal mounting and maximums of 6 stores, 2 beams, and/or 2 adapters with external mounting. The simple case as illustrated in Figure 2 shows sample required geometrical inputs for use in the STORE module.

The STORE module also computes the distances from each store, beam, and adapter C.G. to the composite C.G. and places these values in an array. Subsequently the values may be used to determine the aerodynamic contribution of each piece of equipment to the total aerodynamic coefficients referenced to the composite C.G.

The inertial values obtained by the STORE module may be used to provide inputs for total aircraft inertia calculations and load path equation development.

AIRCRAFT (A/C) MODULES

An aircraft or A/C module exists for each aircraft or significant aircraft model, A-10, F-4C/D, F-4E, and F-16A/B. The function of these modules is to compute those aircraft parameters which influence and describe the dynamic maneuvering capability of the aircraft. These parameters are computed for each chosen maneuver at each chosen mach-altitude point. The computed parameters are based on both analytical flight performance data and, where possible, flight measured performance data.
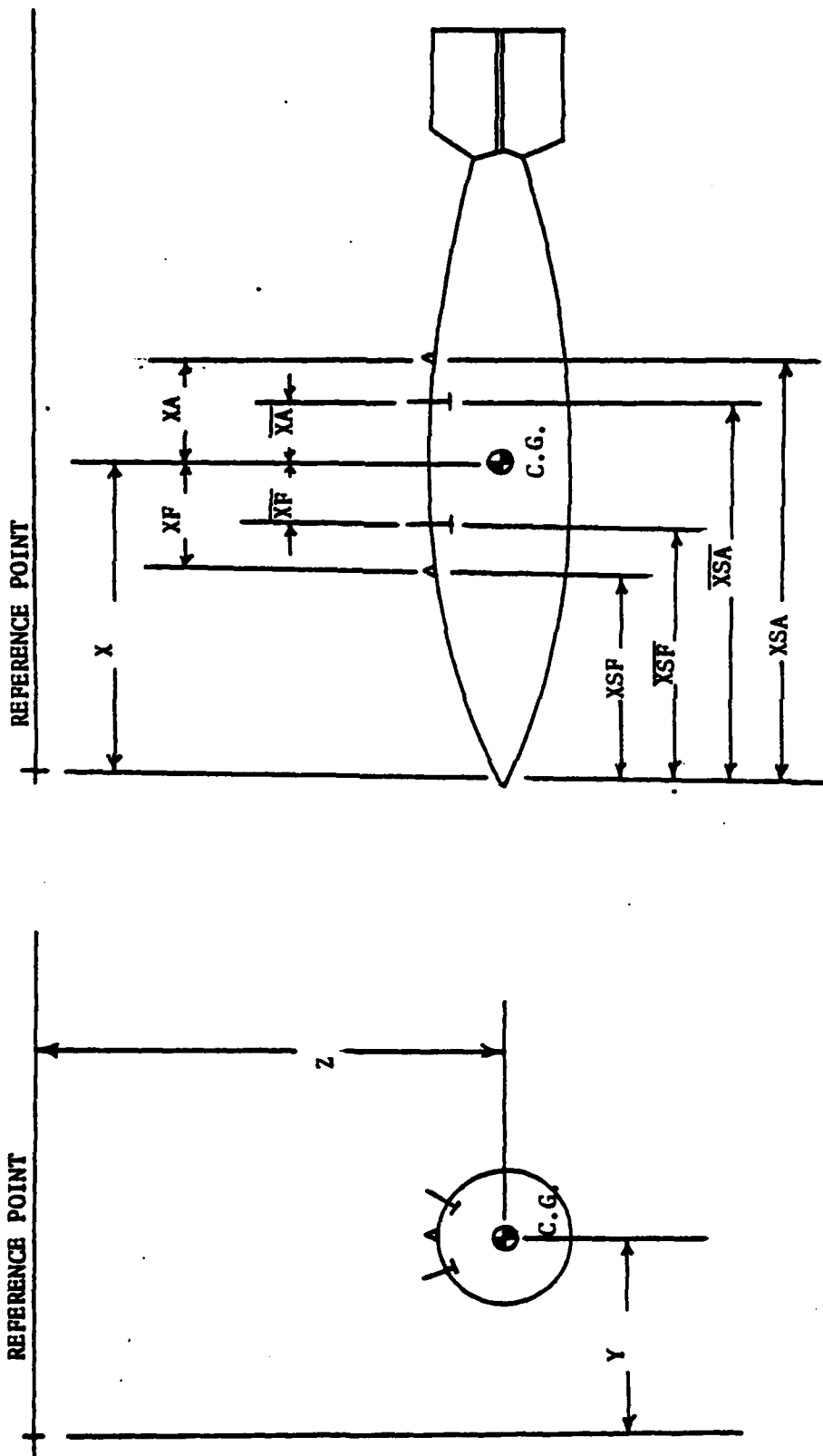
Figure 2. Typical Geometric Inputs

Extensive use of curve fitting techniques has been employed to reduce the core requirements of a table look-up method. The primary functions of the A/C module are:

(1) Define the flight envelope and the specific mach-altitude point within the envelope to be investigated.

(2) Define the maneuvers to be investigated at each mach-altitude point.

(3) Compute aircraft C.G. location, total weight, and rotational inertias for the aircraft including fuel load and store carriage.

(4) Compute aircraft dynamic magnification factor (DMF).

(5) Compute aircraft angle of attack at predetermined points within the maneuver.

(6) Compute aircraft sideslip at predetermined points within the maneuver.

(7) Compute full stick roll rates, pitch rates, and yaw rates at predetermined maneuver points.

(8) Compute full stick roll accelerations, pitch accelerations, and yaw accelerations at predetermined maneuver points.

Figure 3 illustrates the chosen envelope and mach-altitude points investigated during a typical F-4C/D loads analysis. Fifty points, primarily along constant knots calibrated airspeed (KCAS) lines, are chosen. At each point symmetric and unsymmetric g maneuvers are analyzed. Symmetric maneuvers consist of pullups and pushovers for N_z's of -2 to +5 in increments of 1g. Unsymmetric maneuvers consisting of full stick rolling pullups and rolling pushovers from -1 to +5g's are executed in 1g increments.

Aircraft C.G. location, total weight and rotational inertias are computed using weight and balance data for the basic aircraft. Inertial parameter values for the carriage hardware (Ref. STORE module) are added.

The dynamic magnification factor, which is a measure of the effect of the wing's flexibility on dynamic loading, varies for each aircraft. The F-4C/D DMF variations are obtained from Reference 1.

Angle of attack (alpha) and sideslip angle (beta) data for each aircraft has been obtained using specific configurations which produce conservative values of these angles as compared with most other configurations. An F-16 370 gallon fuel tank configuration has been found to produce wide ranging alpha and beta values and will be employed in the F-16A A/C module. Equations for alpha and beta, which are functions of

543
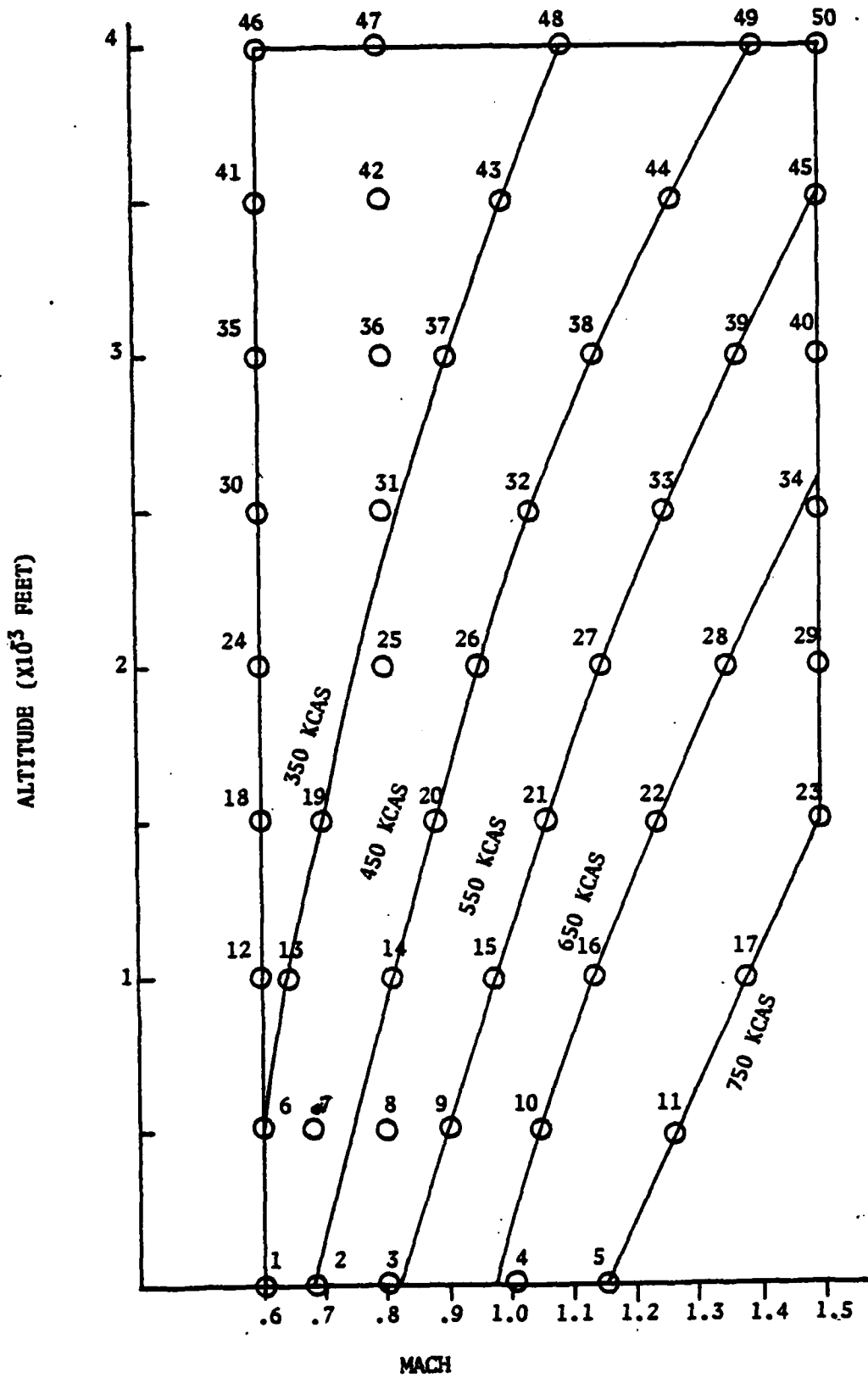
Figure 3. Typical Loads Investigation Envelope

544

altitude, mach, N_Z, and lift, are developed by curve-fitting techniques. Linear interpolation between curves is performed when necessary.

The three axis full stick rotation rates and accelerations are dependent upon mach, altitude, aircraft inertia, and control surface effectiveness, for a particular aircraft. An aircraft configured to provide conservative values of these parameters is utilized.

In general the pitch and yaw motion of an aircraft produces less significant loading than does roll motion. Since loading due to roll motion is more significant, the method used to describe its contribution toward total loads will be presented. In the case of roll motion both rate and acceleration are important. The critical points to be considered during the roll or unsymmetric maneuver are best described by the aircraft's roll response model. Figure 4 shows the model used for the F-16A A/C module. Points 2, 3, and 4 of Figure 4 are investigated as separate load cases in both right and left rolling maneuvers, thus giving six load cases for each unsymmetric maneuver.

The load cases studied for each maneuver at each mach-altitude point become large in number, if an entire envelope is investigated. Although large in number, the computer time required is not large, since integration of time dependent equations is not necessary as is the case for simulation programs. Typical full envelope investigation for the F-4C/D is 1 to 2 minutes depending on output desired.

. In addition the A/C modules provide the user the option of a case by case study, where user generated mach-altitude and maneuver definition data is input. This option is useful for comparison purposes with flight test loads data.

AERO MODULE

The purpose of the AERO module is to calculate the aerodynamic coefficients of the store or composite equipment in the presence of the aircraft. These coefficients may be calculated (depending on input data) for each individual piece of equipment or for the entire composite.

The module uses a least squares technique to compute the aerodynamic coefficients for equipment installed on the aircraft when angle of attack, sideslip angle, and mach number are known. The computation is performed in two phases.

PHASE I

All measured aerodynamic data is input. This data consists of (for each data point, i) M_i, α_i, β_i, C_{N_i}, C_{Y_i}, C_{A_i}, C_{l_i}, C_{m_i}, and C_{n_i}. M_i, α_i, and β_i are independent variables and, depending on the degree of curve fit required, are stored along with their cross terms and multiples in the least squares coefficient array, [A]. The degree of curve fit relating

545
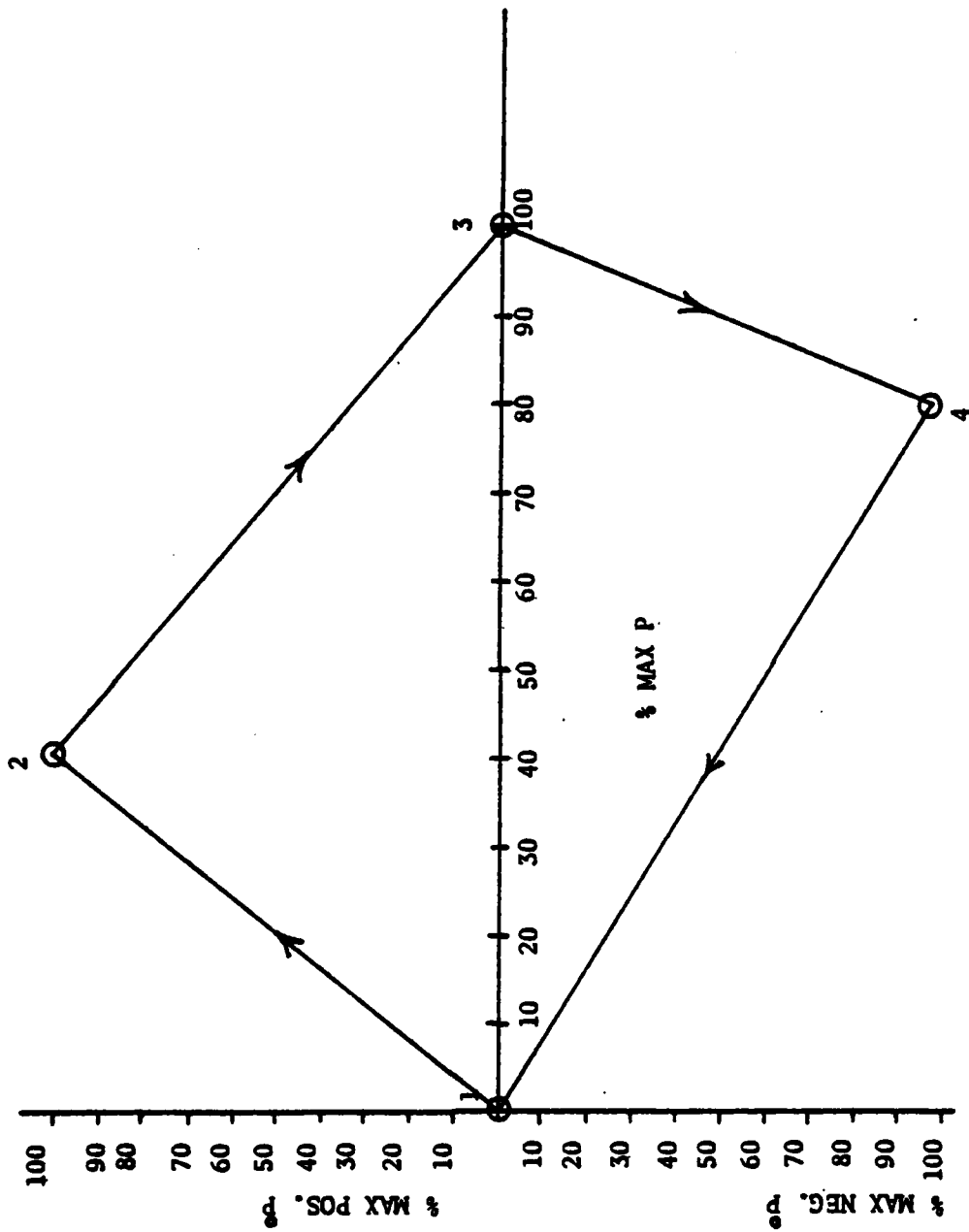
Figure 4. Typical Roll Response Model

each coefficient to each independent variable is chosen by the user based on his knowledge of the particular store aerodynamic characteristics. The elements C_{N_i}, C_{Y_i}, C_{A_i}, C_{1_i}, C_{m_i}, and C_{n_i} are stored in column matrices $\{C_N\}$, $\{C_Y\}$, $\{C_A\}$, $\{C_1\}$, $\{C_m\}$ and $\{C_n\}$ respectively. Thus, using least squares techniques,

$$[A] \{N\} = \{C_N\}$$

$$[A] \{Y\} = \{C_Y\}$$

$$[A] \{A\} = \{C_A\} \qquad\qquad (1) - (6)$$

$$[A] \{1\} = \{C_1\}$$

$$[A] \{m\} = \{C_m\}$$

$$[A] \{n\} = \{C_n\}$$

where the column matrices $\{N\}$, $\{Y\}$, $\{A\}$, $\{1\}$, $\{m\}$, and $\{n\}$ are the least squares constant matrices for the respective equations. Using backward and forward substitution methods, the least squares constant matrices can be obtained.

PHASE 2

The specific flight parameters M, α, and β are input and the corresponding values for C_N, C_Y, C_A, C_1, C_m, and C_n are to be determined. The matrix [A] is reformed with the new values for the independent variables. Thus, considering again Equations (1) to (6) and using the previously obtained least squares constant matrices, only the coefficient matrices remain unknown and therefore can be solved. The Phase 2 procedure is executed for each load case, since changes in M, α, and/or β are occurring.

Additional features of the AERO module include tape handling procedures to allow direct usage of wind tunnel data tapes and plotting routines to assist the user in correctly chosing the degree of curve fit.

LOADS MODULE

The loads module computes the total loads at the center of gravity of the composite. These total loads are then used to determine the reaction loads at the aircraft interface. The primary loading will occur in the Y and Z axis directions and for brevity sake, only the equations of motion for these degrees of freedom will be presented. First, consider an aircraft as viewed from the rear

547

AFT VIEW
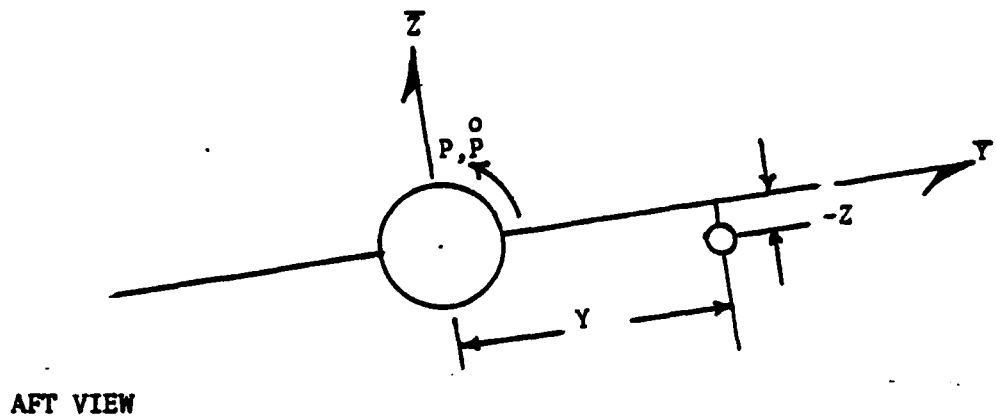
Figure 5.   Aircraft Coordinate System

Now consider free body diagrams
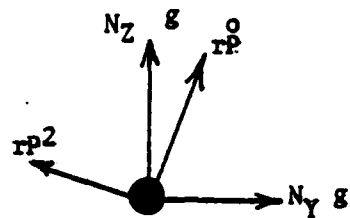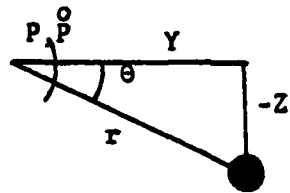
Thus

$$N_Y \, g = -r\overset{o}{P} \sin\theta \; + \; rP^2 \cos\theta \qquad (7)$$

or

$$N_Y \;\; = \frac{Z\overset{o}{P}}{g} \; + \; \frac{YP^2}{g} \qquad (8)$$

and N_Z

$$N_Z \, g \;=\; -r\overset{o}{P} \cos\theta \; - \; rP^2 \sin\theta \qquad (9)$$

or

$$N_Z \;\;\; = \; \frac{-Y\overset{o}{P}}{g} \;\; + \;\; \frac{ZP^2}{g} \qquad (10)$$

548

In addition to the above, one has to consider that when an abrupt roll is initiated by an aircraft, the wings will flex and spring back. This results in a momentary increase in the roll acceleration. A dynamic magnification factor (DMF) has been determined and is applied as a multiple of the roll acceleration term of the above equations,

Thus

$$N_Y \quad = \quad \frac{Z\overset{o}{P}}{g}(DMF) \quad + \quad \frac{YP^2}{g} \qquad (11)$$

and

$$N_Z \quad = \quad \frac{-Y\overset{o}{P}}{g}(DMF) \quad + \quad \frac{ZP^2}{g} \qquad (12)$$

Next consider the possibility that the store is on the left wing (viewed from rear). This would, for the same maneuver, produce a sign change in N_Y and N_Z. Since Y will change sign for this wing, the terms multiplied by Y will have the correct sense. However, those multiplied by Z will be incorrect. This problem may be corrected by either writing different equations for different wings or by some algebraic form. The latter method is used and the result is as follows

$$N_Y \quad = \quad \frac{YZ\overset{o}{P}}{Y\,g}(DMF) \quad + \quad \frac{YP^2}{g} \qquad (13)$$

$$N_Z \quad = \quad \frac{-Y\overset{o}{P}}{g}(DMF) \quad + \quad \frac{YZP^2}{Y\,g} \qquad (14)$$

In addition to this calculated N_Y due to roll there is an empirically determined N_{Y_i} due to aircraft handling problems and a contribution to N_Y due to yawing motion. Since during any given maneuver, this could be in either direction, the worst case is assumed, i.e., this additional N_Y is in the same direction as that calculated above. Also there is an additional N_{Z_i} term that results from the pitch plane portion of the maneuver. This portion is input as positive down. Thus, adding these additional variables into the equations, we have,

$$N_Y \quad = \quad \frac{Y}{Y}N_{Y_i} \quad + \quad \frac{YZ\overset{o}{P}}{Y\,g}(DMF) \quad + \quad \frac{YP^2}{g} \qquad (15)$$

$$N_Z \quad = \quad -N_{Z_i}\,\frac{-Y\overset{o}{P}}{g}(DMF) \quad + \quad \frac{YZP^2}{Y\,g} \qquad (16)$$

Now that the inertia load factors have been determined, the inertial forces and moments acting at the composite C.G. may be determined.

$$F_{I_X} = N_X W \tag{17}$$

$$F_{I_Y} = N_Y W \tag{18}$$

$$F_{I_Z} = N_Z W \tag{19}$$

$$M_{I_X} = M_{I_Y} = M_{I_Z} = 0 \tag{20}$$

where

F_{I_X} is the inertial force in the x-direction

F_{I_Y} is the inertial force in the y-direction

F_{I_Z} is the inertial force in the z-direction

M_{I_X} is the inertial moment about the x-axis

M_{I_Y} is the inertial moment about the y-axis

M_{I_Z} is the inertial moment about the z-axis

W is the total composite weight

Next we must determine the aerodynamic forces and moments. To do this, the input values of the aerodynamic coefficients of axial force (C_A), side force (C_Y), normal force (C_N), rolling moment (C_1), pitching moment (C_m), and yawing moment (C_η); the aerodynamic reference length (L), the aerodynamic reference area ($\overline{A}$), the aerodynamic transfer function (T), and the dynamic pressure (Q) are used. Thus,

$$F_{A_X} = C_A Q \overline{A} \tag{21}$$

$$F_{A_Y} = C_Y Q \overline{A} \tag{22}$$

$$F_{A_Z} = C_N Q \overline{A} \tag{23}$$

$$M_{A_X} = C_1 Q \overline{A} L \tag{24}$$

$$M_{A_Y} = C_m Q \overline{A} L + C_N Q \overline{A} T \tag{25}$$

$$M_{A_Z} = C_\eta Q \overline{A} L + C_Y Q \overline{A} T \tag{26}$$

where F_A and M_A are the forces and moments in the designated directions. Finally to obtain the total loads and moments at the C.G., one has to add the inertial and aerodynamic components. Thus,

$$F_X = F_{I_X} + F_{A_X} \tag{27}$$

$$F_Y = F_{I_Y} + F_{A_Y} \tag{28}$$

$$F_Z = F_{I_Z} + F_{A_Z} \tag{29}$$

$$M_X = M_{I_X} + M_{A_X} \qquad (30)$$

$$M_Y = M_{I_Y} + M_{A_Y} \qquad (31)$$

$$M_Z = M_{I_Z} + M_{A_Z} \qquad (32)$$

The LOADS module uses the method of Reference 2 to determine reactions loads at the aircraft interface. The standard hook and swaybrace arrangement applies to the majority of equipment/aircraft configurations and is the only interfacing technique considered. The assumptions and equations, being sufficiently covered by Reference 2, will not be presented herein.

STRUCTURAL MODULE

The STRUC module utilizes the equipment/aircraft interface loads to determine the structural integrity of the aircraft undergoing flight maneuvers. Structurally critical points within the aircraft are defined for the many different combinational loading cases. The structural integrity of these critical points for a particular maneuver is expressed by structural indices (SI).

The STRUC module is, of course, aircraft dependent. For this reason, the module consists of subroutines which apply to specific aircraft structural characteristics. Dependent upon aircraft and mounting station, critical loading points may vary from the hook and swaybrace points to the vertical tail-fuselage junction. Development of the load path equations which compute loading at critical points has been accomplished using static stress analysis methods. Non-flexure analysis generally results in a conservative stress value, since flexure often allows stress relief through adjacent structure. Once the static stress of a critical point has been defined, the SI is determined relating the computed stress to the allowable.

$$SI = \frac{f_c}{f_a} \times 10 \qquad (33)$$

As can be seen from Equation (33), an SI greater than 10 indicates possible structural failure. An SI is calculated for each critical structural point for each maneuver performed at a mach-altitude point. Maximum SI values provide a summary chart as developed by the OUTPUT module.

OUTPUT MODULE

The OUTPUT module gives the user a quick-look summary of results and also provides options for data output as necessary for in-depth engineering analysis of a loading case. The output options available are:

(1) Configuration Definition

(2) SC4020 Plot OUTPUT

(3) SI Summary Charts

(4) Tabular Output

The OUTPUT module defines the configuration in two ways. First, a narrative output giving equipment type, mounting position, and other pertinent facts is provided. Second, a pictoral head-on display of the aircraft and equipment in symbolic form is given.

The option of plotting up to five curves on an X-Y axis plot is available. A routine which forms X-Y data arrays from any repeatable record binary tape utilizes format specifications supplied by the program user. Performance parameters, aerodynamic data, or loads can be plotted from the binary communication tapes, 10 and 11.

The SI summary charts display the maximum SI obtained for one critical point at one particular N_Z for all mach-altitude points checked. A typical SI chart (see Figure 6) places the SI values on a mach-altitude graph at positions corresponding to the pre-determined mach-altitude check points.

Tabular output consists of communication tape (tape 10 or tape 11) printing. Tabular output may be obtained at the conclusion of each module execution and gives a running history of initial, intermediate and final calculations. This output can be used to provide backup data for justification of SI calculation. Also, should the user suspect program problems, an effective aid in debugging is thus available.

<div align="center">RESULTS</div>

In order to verify the CMM approach, flight test data obtained during F-4D/GBU-15CWW flight loads testing was utilized (Reference 3). A MAU-12 rack on the right inboard wing pylon was instrumented to provide swaybrace and $\bar{Z}$ direction hook loads as a function of time. Normal acceleration, altitude and mach for specific time hacks during a maneuver were used as inputs to MACLIP. Using these parameters, the program calculated the angles of attack, aerodynamic loads at the store C.G., and ultimately the hook and swaybrace reaction loads.

For comparison purposes a 5g symmetric pullup was selected. The maneuver was initiated at .9 mach and 14000 feet altitude. Figure 7 compares forward hook, aft hook and maximum swaybrace loads at one second time intervals. The program load values remain at slightly higher than flight test load values throughout the maneuver. This conservatism can be primarily attributed to the assumptions used by Reference 2. At lower values of the normal acceleration the forward
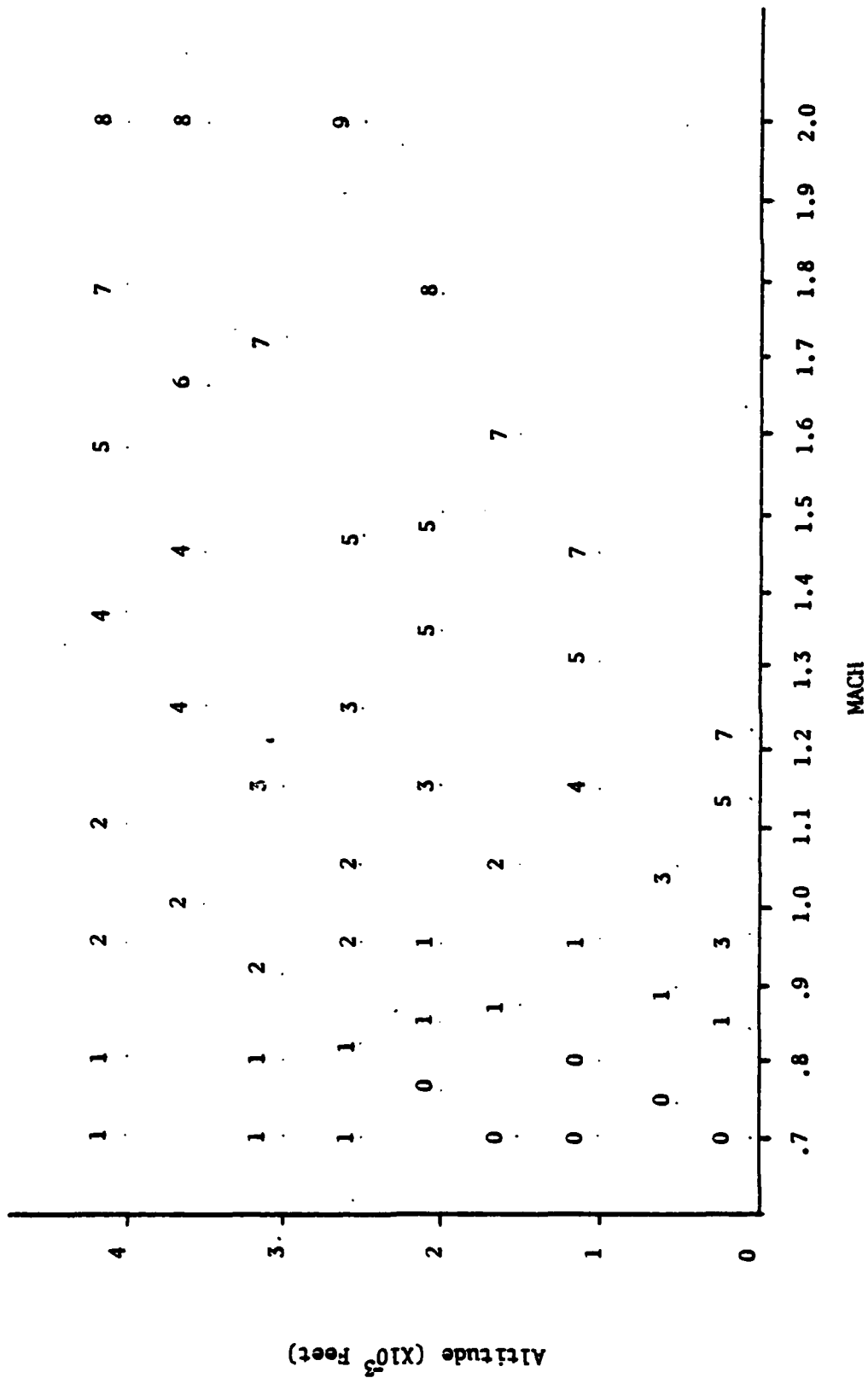
Figure 6. Typical Structural Index (SI) Chart

MACH

Altitude ($\times 10^3$ Feet)
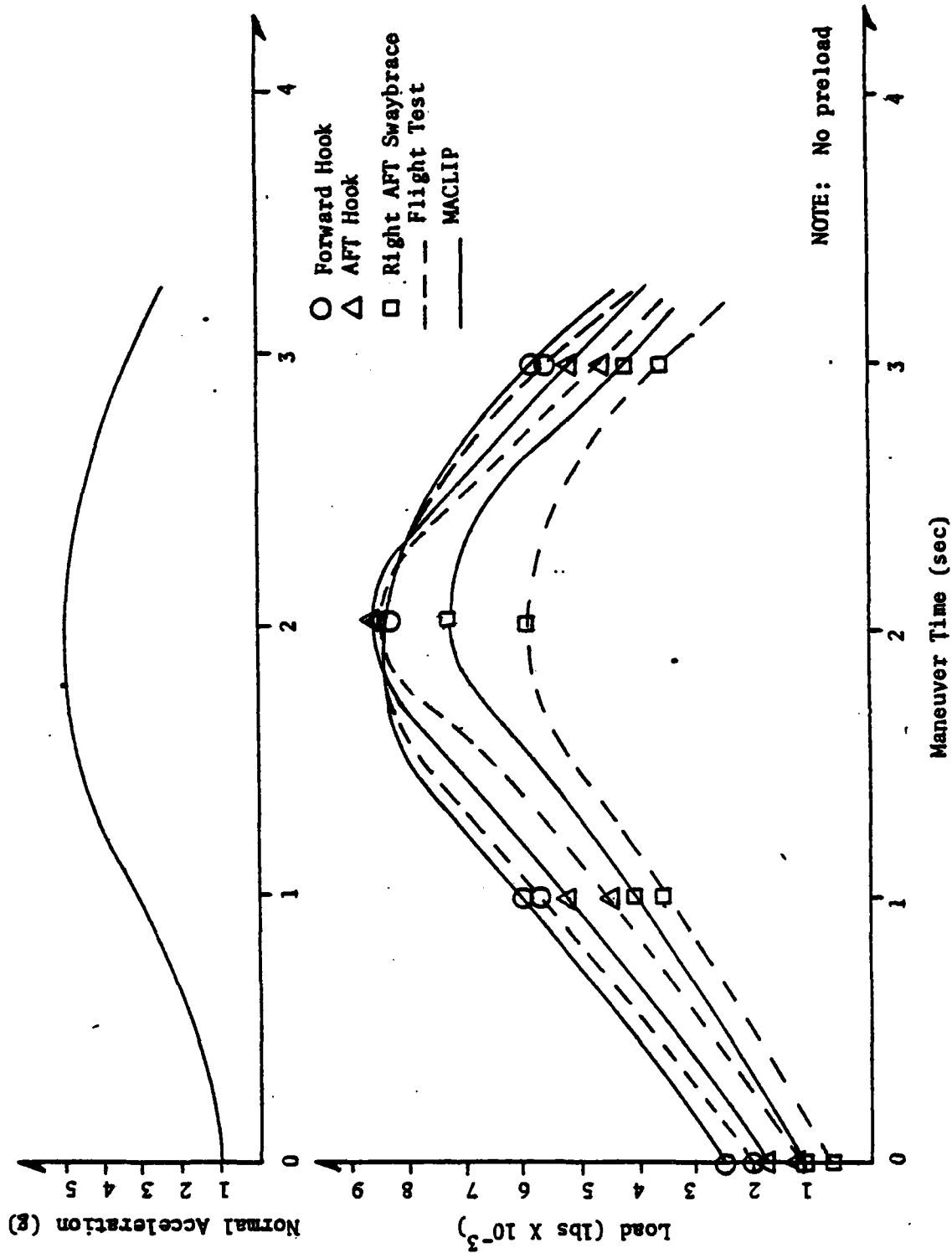
Figure 7. MACLIP - Flight Test Comparison (5g Symmetric Pullup)

554

hook is the most heavily loaded. Even though the store C.G. position is 17 inches aft of forward hook (30 inch suspension), the loading is driven by the pitch down aerodynamic moment. As the normal acceleration increases, maximum hook loading shifts to the aft hook and the maximum loading can be attributed to inertia. The aft right swaybrace is the most heavily loaded swaybrace due to aerodynamic pitch and yaw moments.

CONCLUSION

Loads analysis by the CMM approach is an acceptable means of analysis for the majority of aircraft flight clearance requests involving store carriage. The isolation of critical loading points within a maneuver nullifies the need for a time dependent maneuver model which requires, relatively speaking, large amounts of computer time. Although the CMM approach may produce slightly conservative loading values, the conservatism is not unduly restrictive for most desired aircraft flight limits.

Future development of MACLIP will involve completion of the A-10 and F-16 A/C and STRUC modules. Further correlation of MACLIP produced loads with flight test loads data will be pursued using instrumented A-10 and F-16 aircraft. Correlation work will concentrate on loading produced by unsymmetric flight maneuvers.

REFERENCES

1. Jendras, S.J., _Structural, Flutter, and Aerodynamic Evaluation of the MER/TER-100 Supersonic Multiple Bomb Rack on F-4 Series Aircraft_, Dec 1967, AFATL-TR-67-225.

2. Military Specification-A-8591E, _Airborne Stores, Associated Suspension Lugs and Aircraft-Store Interface (Carriage Phase)_, General Design Criteria for, 12 Jan 1976.

3. Data Package 75-18, _Aircraft/Store Reaction Load Data_, ADTC Project 5613WG08, Oct 1975.

AUTOBIOGRAPHY

C. W. INGRAM
AIR FORCE ARMAMENT LABORATORY
EGLIN AFB, FL 32542

Mr. Ingram received his B.S. and M.S. degrees in Aerospace Engineering from Auburn University in 1970 and 1976 respectively. In 1972 he entered the USAF as an officer stationed at Tinker AFB, Oklahoma. His duty assignments at Tinker AFB involved structural engineering on the A-7D aircraft and AGM-69A SRAM missile. In 1975 he transferred to the Air Force Armament Laboratory and began work in the areas of loads and structures as related to aircraft-store compatibility. In 1977 he separated from the Air Force and continued work in loads and structures as a civilian employee within the Air Force Armament Laboratory. Mr. Ingram is a member of the TAU BETA PI engineering society.

AUTOBIOGRAPHY

W. W. DYESS
AIR FORCE ARMAMENT LABORATORY
EGLIN AFB, FL 32542

Mr. Dyess received his B.S. in Aerospace Engineering from Auburn
University in 1967. He received his M.S. in Aerospace Engineering
(Structures) from Auburn University in 1969. He is currently working
on a Ph.D. degree in Applied Mathematics from University of Florida.
In 1969, Mr. Dyess began work with the USAF at Eglin AFB FL. Since
then he has worked as a structures and loads engineer as a member of
first the Advanced Armament Concepts Branch and then the Aircraft
Compatibility Branch of the Air Force Armament Laboratory. Throughout
this period his area of effort and responsibility has been in deter-
mining the loads on aircraft and store due to the presence of the
other and the effect the loads have on the structural integrity of the
aircraft or store.

THE PROPER USE OF MILITARY SPECIFICATION
MIL-A-8591E FOR DESIGN OF STORES TO BE USED BY
THE UNITED STATES AIR FORCE
(U)
(Article UNCLASSIFIED)

by

William W. Dyess, Jr.
US Air Force Armament Laboratory (DLJC)
Eglin Air Force Base, Florida 32542

ABSTRACT. (U) For years there has been a great deal of discussion among contractors and the Air Force about how to apply the Military Specification MIL-A-8591, about how to obtain waivers from the specification for their design and about the rational behind the specification. ADTC/DLJC has the charter from AFSC Regulation 80-33, "Class II Modification of Aerospace Vehicles" to review and approve for flight all "nonnuclear ordnance and all other types of external stores, except RPVs." Thus DLJC has been in a position to answer these questions from contractors. However, this has always been done on a price-wise basis.

The purpose of this paper is to define to the general stores community what is the acceptable manner of using MIL-A-8591 for store designs. The major topics of concern will be:

    a. What is the purpose of the specification?

    b. What is the relationship of the total loads generated in accordance with the specification to the "real world" loads?

    c. How is the specification used to predict distributed loads?

    d. What are the major problems associated with designing a store using the specification?

    e. What is the future of the specification?

LIST OF FIGURES

1.0 INTRODUCTION

For a number of years now, the compatibility office at Eglin AFB (DLJC) has had the responsibility of certifying stores for flight on ADTC aircraft. Recently this responsibility was extended to all AFSC aircraft by the publication of AFSC Regulation 80-33 (see Reference 1). Part of the evaluation leading to certification is the review of the structural integrity of the store when installed in the desired carriage position. In order to insure sufficient structural strength, stores are supposed to be designed to MIL-A-8591E (see Reference 2).

A careful review of loads analyses of many different external stores shows three basic problems:

      a. Incorrect use of the methods of MIL-A-8591E resulting in incorrect loads being generated

      b. Use of techniques other than those of MIL-A-8591E without obtaining proper authority

      c. Use of a variety of different incorrect methods of distributing loads along the store

2.0 DESIGN OF STORES AND SUSPENSION EQUIPMENT

2.1 Recommended Method for General Design of Stores

The methods of MIL-A-8591E, Procedure II are recommended for use by a store designer in the design of a store for general use throughout the Air Force. The proper use of this technique will result in a set of loads, which if designed to, will insure that the store has sufficient strength for its carriage location.

This recommended method consists of two classes of suspension location, wing and fuselage, and three types of carriage condition; flight, arrested landing, and catapult. Since this paper concerns the Air Force application, and since little confusion seems to exists as to the proper way to employ these last two carriage conditions, this paper will concern itself with the flight condition only. The specification presents the loads calculations in two parts: inertial and aerodynamic.

The inertial loads are computed using one of the design limit load factor (DLLF) envelopes as shown in Figures 1 and 2.

The aerodynamic loads are computed using the equations below where the "corners" referred to are as shown in Figures 1 and 2.

FIGURE 2. CENTERLINE MOUNTED STORE
DESIGN LIMIT LOADS FACTOR
ENVELOPE

FIGURE 1. WING MOUNTED STORE DESIGN LIMIT LOAD
FACTOR ENVELOPE

562

Corners (1) and (2)

$$\alpha_S = 0 \text{ to } \frac{38000}{q} \text{ degrees} \qquad (1)$$

$$\beta_S = \pm \frac{3000}{q} \text{ degrees} \qquad (2)$$

Corners (3) and (4)

$$\alpha_S = 0 \text{ to } -\frac{22800}{q} \text{ degrees} \qquad (3)$$

$$\beta_S = \pm \frac{3000}{q} \text{ degrees} \qquad (4)$$

Corner (5)

$$\alpha_S = \frac{100}{q^{1/2}} \text{ to } \frac{-15200 + 100q^{1/2}}{q} \text{ degrees} \qquad (5)$$

$$\beta_S = \pm \frac{13000}{q} \text{ degrees} \qquad (6)$$

Corner (6)

$$\alpha_S = 0 \text{ to } \frac{30400 + 100q^{1/2}}{q} \text{ degrees} \qquad (7)$$

$$\beta_S = \pm \frac{13000}{q} \text{ degrees} \qquad (8)$$

Corners (7) and (9)

$$\alpha_S = 0 \text{ to } \frac{38000}{q} \text{ degrees} \qquad (9)$$

$$\beta_S = \pm \frac{13000}{q} \text{ degrees} \qquad (10)$$

Corners (8) and (10)

$$\alpha_S = 0 \text{ to } \frac{30400}{q} \text{ degrees} \qquad (11)$$

$$\beta_S = \pm \frac{13000}{q} \text{ degrees} \qquad (12)$$

The method of using this data is relatively simple, certainly much more so than other correct methods of design. One first computes the DLLFs to be used and the α_S and β_S to be used. These are then applied uniformly along the store body as depicted in Figure 3.
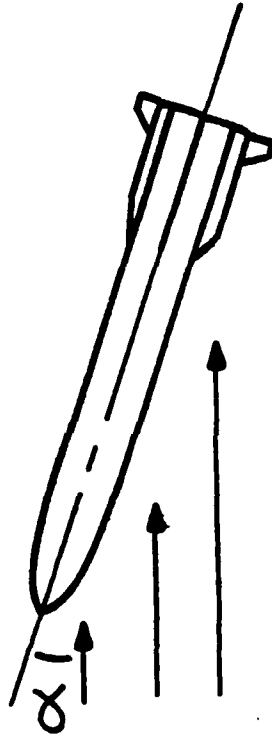
FIGURE 3. AERODYNAMIC DISTRIBUTION AS PER MIL-A-8591E

564

From this data, shear-moment diagrams can be computed which can then be used for the detailed stress analysis. Unless, as is rarely the case, the algebraic summation of all component aerodynamic forces and moments equals those generated by using the total aerodynamic coefficients for the store, then the reactions calculated at the attach points to the carriage aircraft will not be the same for the two methods. Thus if, as has been done, a designer were to start at the nose of a store and work his way back forming the shear-moment diagrams and using the reactions as calculated by using total store aerodynamics, when he got to the other end of the store he would find that his curves did not close. His result might look something like Figure 4.

There are several methods by which the above problem can be reduced to an acceptable level.

   a. The total aerodynamics coefficients used can be those
       which are computed by summing all component aerodynamics.

   b. Start at each end of the store and work toward the attach
       points generating the shear-moment diagrams. When the
       attach points are reached, input the reaction values com-
       puted using total store aerodynamics. Then for the area
       between the attach points force the curves to close by
       connecting the values with a straight line for the shear
       and the corresponding curve for the moment. As an illus-
       tration of the results see Figure 5.

   c. Assume that the measured or calculated total aerodynamic
       coefficients are correct. Compute the shear-moment dia-
       grams starting from each end of the store and attempt to
       close the diagrams using the reaction forces generated by
       the total aerodynamic forces. Adjust the component aero-
       dynamics and try again until a solution which closes and
       is reasonable is reached.

Since in general the specification results in an overdesign of the strongback region of the store, the second method, which is easy to employ, should be sufficient.

Just because only one shear-moment diagram has been discussed above is not to imply, of course, that only one is needed for a design effort. Various loadings and their corresponding shear-moment diagrams must be examined to obtain the critical family of curves for design.

2.2 Some Additional Methods of Design of Stores

2.2.1 Using MIL-A-8591E with Modified DLLF

In some cases where the actual load factors for the various aircraft under consideration can be determined these values may be used instead of

FIGURE 4. AN EXAMPLE OF A TYPICAL SHEAR DIAGRAM WHICH DOES NOT CLOSE
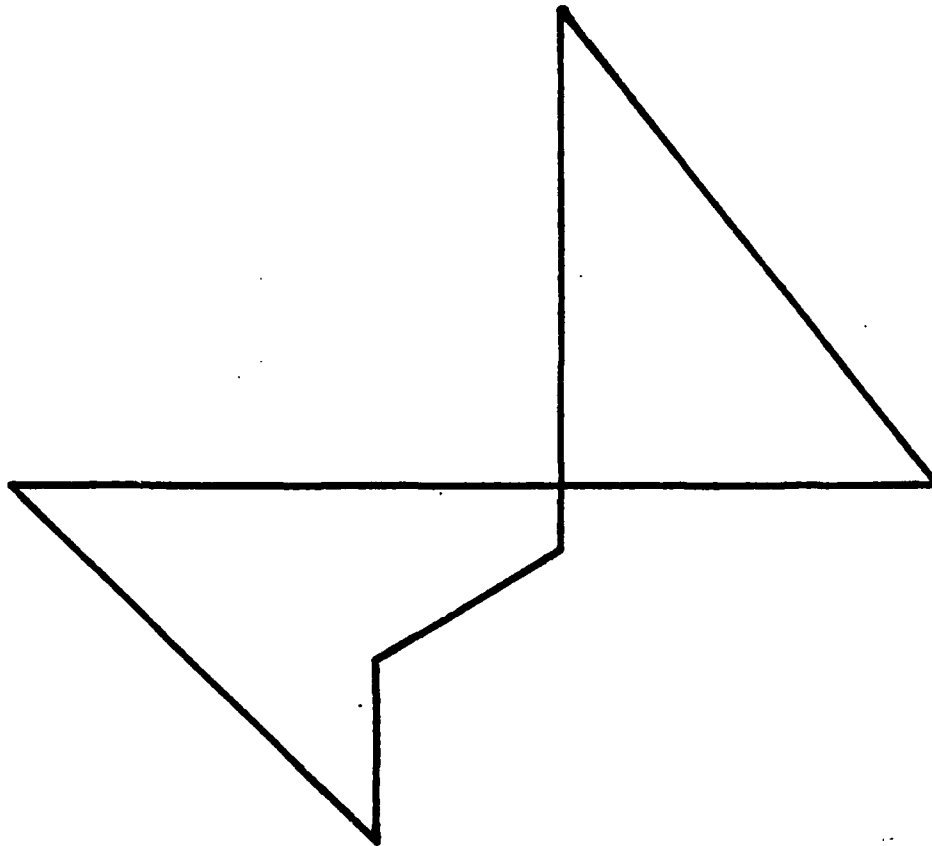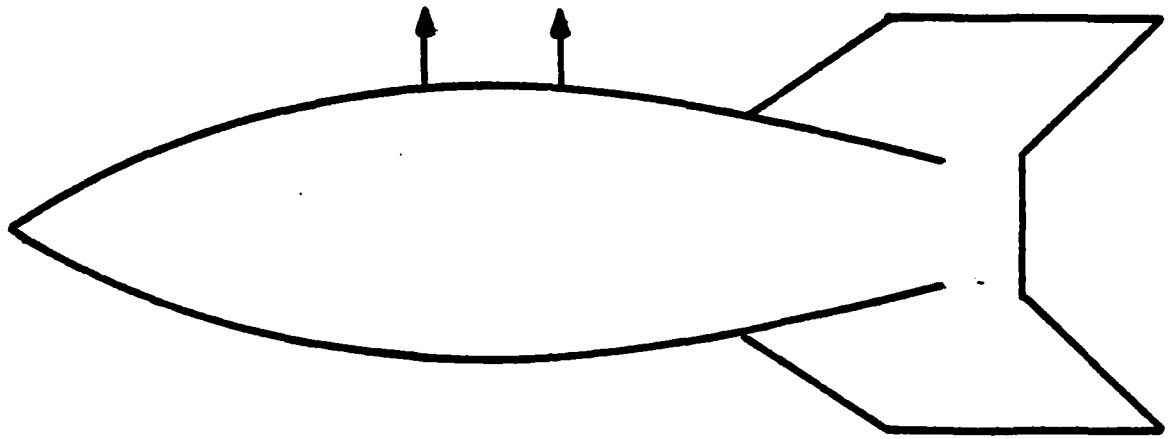
FIGURE 5. RESULTS OF COMPUTING THE SHEAR DIAGRAM FROM EACH END OF THE STORE AND FORCING THE DIAGRAM TO CLOSE BY LINEARIZING THE SECTION BETWEEN THE LUGS

the DLLF's in MIL-A-8591E. Care should be taken, however, to insure that those load factors include such factors as dynamic magnification of wing, or local station and pylon increase in local g on wing or station and pylon due to angular rates and accelerations of the aircraft, gust loads on the aircraft, etc.

2.2.2 Using MIL-A-8591E with Modified Aerodynamics

This technique is used in programs where money is available and the major concerns are lightness of weight, increased performance, and low drag. In this technique the actual aerodynamic coefficients for the components of the store are determined in wind tunnel testing with the store in its carriage position. This procedure has several drawbacks which make it impractical for most design work.

a. The testing involved is very expensive compared to a normal MIL-A-8591E run.

b. Reduction and correlation of data is very time consuming.

c. Methodology needed to distribute loads along the body may be difficult to determine.

d. Due to the high cost of the store model (since it must contain several balances, pressure tapes, and/or strain gages), the aerodynamic design of the store must be essentially fixed before the test can start. This is the reverse of the way a good feedback design loop should work.

e. The future use of the store will be limited to the carriage position on the aircraft for which aerodynamic data was obtained. If it is desired to fly this store at another store position and/or on another aircraft then the wind tunnel test and analyses would probably have to be re-performed.

2.2.3 Using Both Modified DLLF and Aerodynamics

This method combines the modified portions of 2.2.1 and 2.2.2 resulting in using both modified DLLF's and modified aerodynamics.

2.3 Recommended Method for Obtaining Waivers and Invoking Changes to the Recommended General Method of Design for Stores

If for some specific reason it appears that the Air Force could be best served by using something other than the recommended design method for design, then the designer should present his design plan to the procuring agency for approval. If the store is to be tested under the provisions of AFSC Regulation 80-33 then the procuring agency should require from DLJC an evaluation of the design plan. Failure to do this could result in delay or even cancellation of the flight test program.

2.4 Recommended Method for General Design of Suspension Equipment

2.4.1 Background

MIL-A-8591E was not written to cover design of suspension equipment, however there is no specification currently written for this design. Therefore, it is recommended that MIL-A-8591E be used, as follows, for this design effort.

2.4.2 Parent Rack

Consider the case where a store, or store and adaptor, or beam and stores, or whatever, is suspended from parent rack or other suspension equipment which is to be designed. Assume everything below the rack is a "store" or "composite store." Determine the composite center of gravity (c.g.) and the total aerodynamic coefficients for the entire composite. With this data perform a MIL-A-8591E analysis to determine the maximum loads at the composite/parent rack interface. Evaluate the loads to determine the worst cases for design of the suspension equipment. Use these loads along with the DLLF and aerodynamic coefficient for the suspension equipment to design the equipment. This procedure must be repeated for all different composites possible.

2.4.3 Multiple Rack

Consider the case where more than one store or "composite" is suspended from the same piece of suspension equipment (TER, MER, VER, MSER, etc.). Basically the same procedure is followed as in 2.4.2. After the loads at each of the rack-composite interfaces have been determined then the worst case combinations are obtained and used in the design of the rack along with the inertial and aerodynamic properties of the rack itself. This is done by generating a family of shear-moment diagrams of the loaded piece of suspension equipment. Again, as before, this procedure must be followed for all identified stores or "composites."

2.5 Some Additional Methods of Design of Suspension Equipment

Basically the additional methods which could be used for this design follow those of paragraphs 2.2.1, 2.2.2, and 2.2.3. An additional problem is related to 2.2.1 in that the flexibility of the suspension equipment itself must be considered. This may, in fact, add somewhat to the aircraft dynamic magnification factor. Application of 2.2.2 to this case is actually easier than to the store. This is since the aerodynamic coefficient need be determined only at the store-suspension system interface.

2.6 Recommended Method for Obtaining Waivers and Invoking Changes to the Recommended General Method for Design of Suspension Equipment

The designer should present his design method or plan to the procuring agency for review and approval prior to employing it. DLJC will

be available for support to the procuring agency during this review.
It is strongly recommended that this support be taken advantage of since
if the suspension equipment is to be tested under the provisions of AFSC
Regulation 80-33 there is a possibility of delays or cancellation of the
flight test program if the method is found to be unacceptable at a
later date.

3.0 GENERAL DISCUSSIONS OF THE CURRENT MIL-A-8591E

3.1 Comparison of Aerodynamic Data "Real World" to MIL-A-8591E

In order to comprehend this comparison, let us first examine
Figure 6. This figure shows some of the maximum angles of attack which
a typical aircraft may attain during flight with maneuvers and the
corresponding maximum angle of attack as generated by MIL-A-8591E for
this same condition. Now let us examine a symmetric pull-up maneuver,
corner (1) or (2), on the DLLF envelope of Figure 1. For this con-
dition, equation (1) applies for α. Thus for a nominal q of 1200 psf
we have

$$\alpha_S \quad = \quad 0 \text{ to } 32^{\circ}$$

This would give us the loading as shown in Figure 7(b). But suppose the
worst condition involving all symmetric maneuvers of the aircraft in the
"real world" condition results in the flow as shown in Figure 7(a).
These are obviously not the same. Now examine Figure 7(c). This is the
results of computing the α_S based on equation (3).

$$\alpha_S \quad = \quad 0 \text{ to } -19^{\circ}$$

Now recalling the procedure outlined in paragraph 2.1 for obtaining the
shear-moment diagrams it can be easily seen that if the angles shown in
Figure 7(a) do not exceed in magnitude those of Figures 7(b) and 7(c)
then the actual shear-moment will be covered by the analyses using
MIL-A-8591E. Now how reasonable are the actual angles used? Again,
since the primary purpose of the spec. is to design the entire store,
let's examine a nose component. MIL-A-8591E has predicted a maximum α
of 32°. Let us examine the real world values. Consider Figure 6 again.
For a q of 1200 psf at SL the Mach is .9. Thus the aircraft angle is 12°.
If we add an interference angle of attack from 10° to 15° (reasonable
values), the total angle is then between 22° and 27°. The total on the
store is then near the 32° shown on the figure as the upper curve. Thus
the angles being used are reasonable for nose and tail work. However
this discussion illustrates one bad point of MIL-A-8591E. That is, it
predicts centerbody (that area near and including the lugs and swaybraces)
loads and moments which are totally incorrect.

As an extreme example, consider the case where the aerodynamic lift
of the tail and nose cancel each other so that no total lift exists but a
large pitching moment about the store c.g. does exist. The store would
attempt to assume the shape of Figure 8(a). However computing the loads
and moment using MIL-A-8591E the results are as shown in Figures 8(b) and
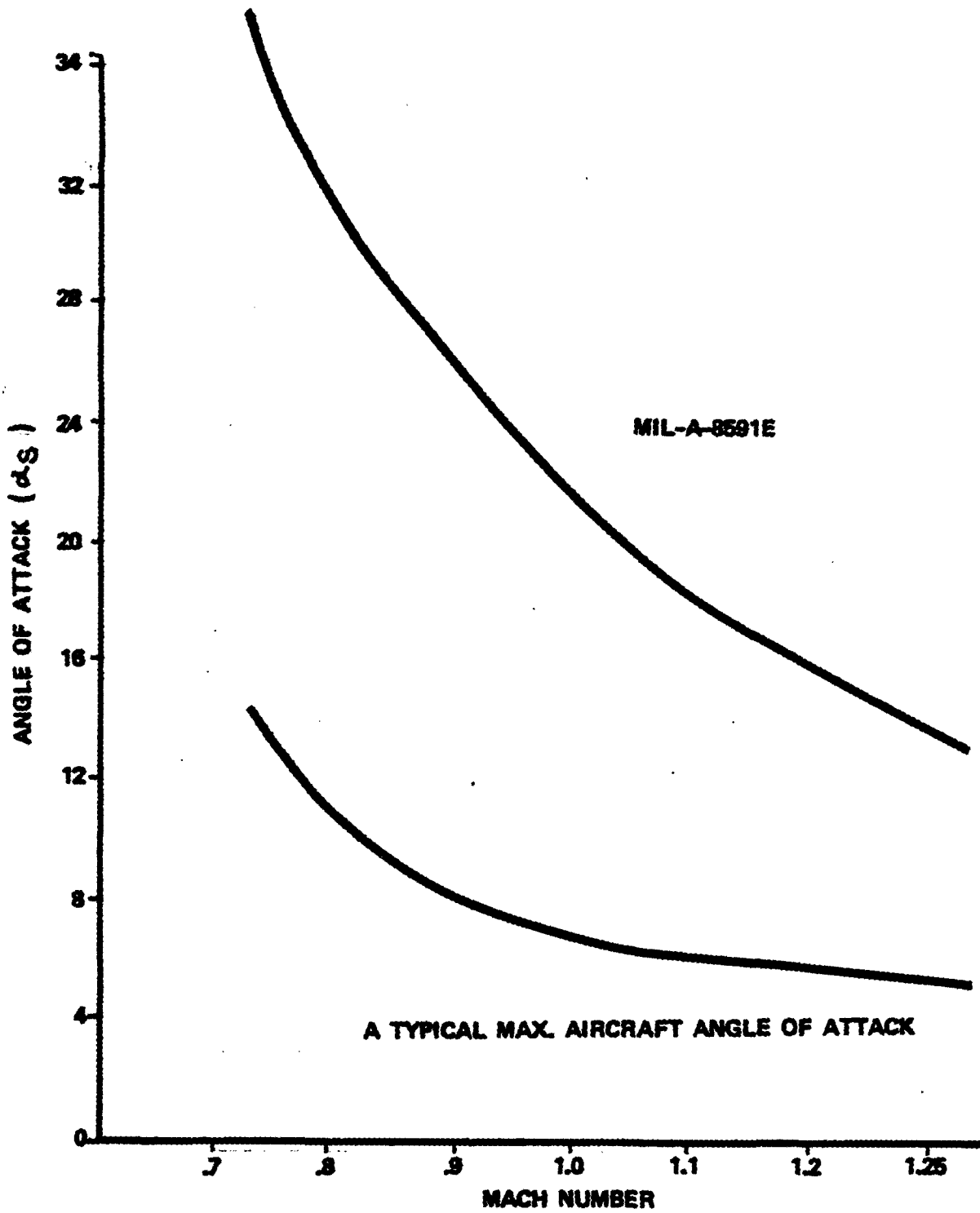
FIGURE 6. COMPARISON OF STORE ANGLE AS PREDICTED BY MIL-A-8591E VS
TYPICAL AIRCRAFT ANGLE OF ATTACK

571
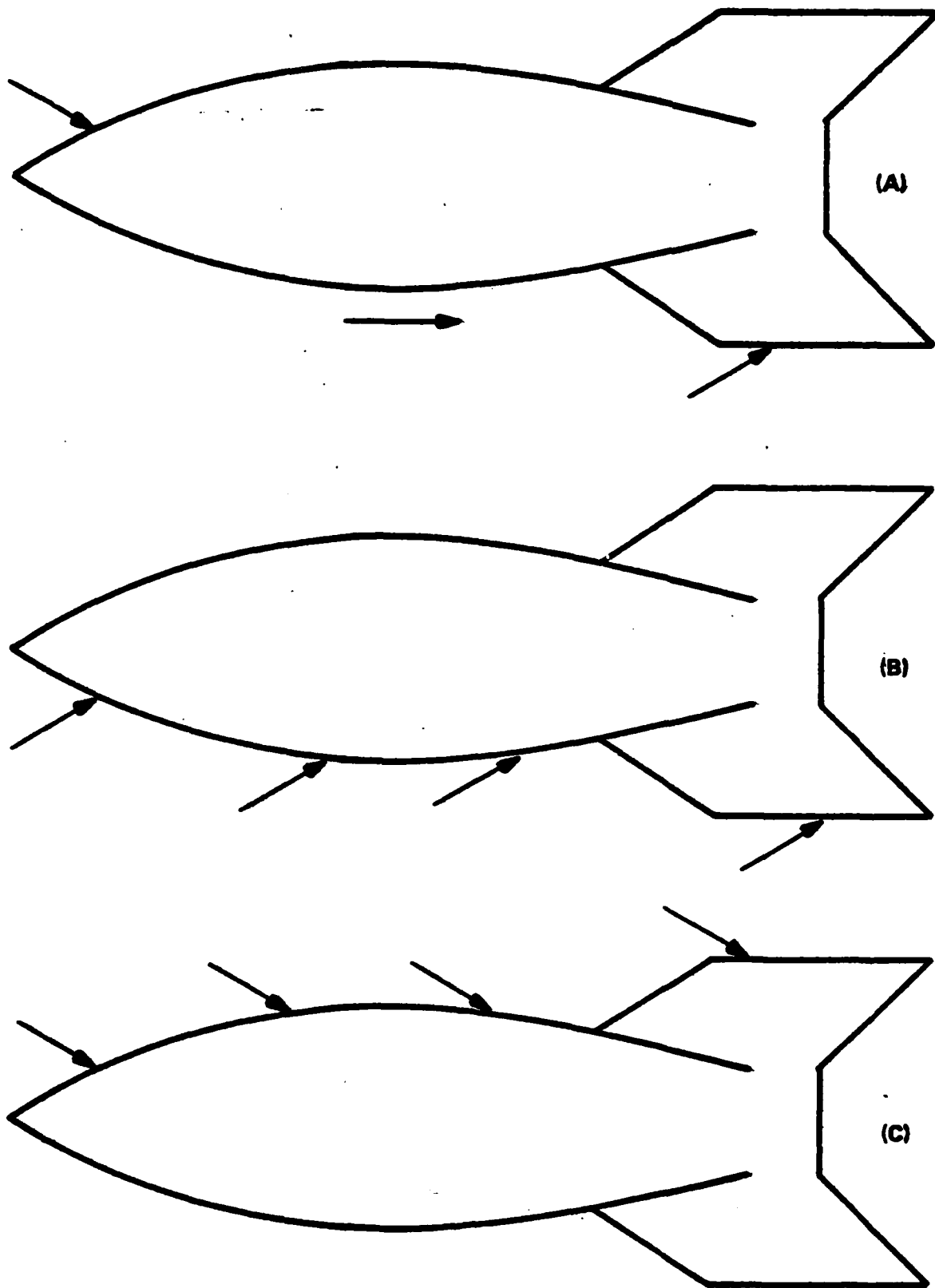
FIGURE 7. THE AERODYNAMIC FLOW FIELD AROUND A STORE FOR
(A) INSTALLED POSITION, (B) MIL-A-8591E, AND (C) MIL-A-8591E

(A)

(B)

(C)
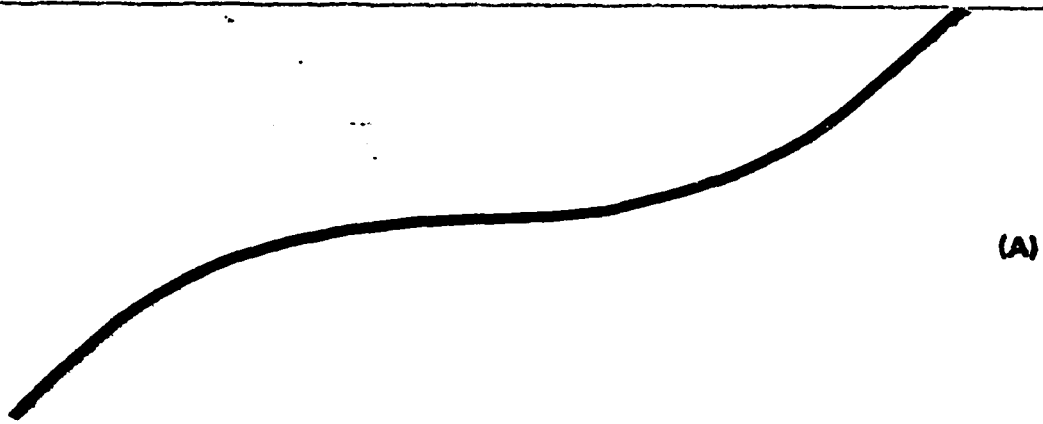
FIGURE 8. THE SHAPE WHICH THE STORE ATTEMPTS TO TAKE
WHEN EXPOSED TO THE CORRESPONDING LOADINGS
OF FIGURE 7

8(c). Obviously the "real world" and MIL-A-8591E do not match in this strongback area.

As can be seen a relatively simple case has been reviewed. A longer store may cause even more complications because of reverses in flow on just one end of the store. The advent of speed brakes, adjacent stores, etc. all may affect the aerodynamic properties of a store. However, even for this simple case one major advantage of using MIL-A-8591E should be readily apparent. The distribution of the aerodynamics along the store for purposes of design when using actual measured aerodynamics is an expensive, time consuming, and difficult problem to solve, whereas with the methods of MIL-A-8591E the effort is much more reasonable for early design purposes.

3.2 Comparison of Inertial Factors "Real World" to MIL-A-8591E

The DLLF envelopes as shown in Figures 1 and 2 were originally designed to incorporate all aircraft capabilities. In reality this is no longer the case. Comparison of the DLLF of Figures 9 and 10 with Figure 1 shows that for the new aircraft, the DLLF envelopes of MIL-A-8591E are not sufficient to insure correct design. These envelopes are for the clean aircraft configuration, but for the F-16 this means a missile configuration. Currently missiles are not being designed to withstand this captive environment. Thus care should be taken on the part of the procuring agency to insure that any store being designed for these aircraft are designed to the proper inertial envelope.

This same problem exists on the centerline station. For a comparison see Figures 2 and 11. For the first time we have a case of a significant side load being introduced on the centerline station due to aircraft roll. This is caused by the roll axis of the aircraft being a significant distance from the store station.

4.0 FUTURE APPLICATION AND CHANGES OF MIL-A-8591

4.1 General

As the Air Force continues its policy of clearing stores on all available aircraft it becomes more and more important, because of increasing time and cost, to design stores so that they will have sufficient strength for carriage on any aircraft in the inventory. MIL-A-8591 has always given the store designer a quick and cheap way to determine his initial design loads. This is critical! The specification must continue to be one that can be applied quickly and cheaply.

4.2 Inertial DLLF Envelopes

These envelopes need to be updated to reflect not only the supermaneuverable new fighters but also the slow aircraft such as FAC's. The

574
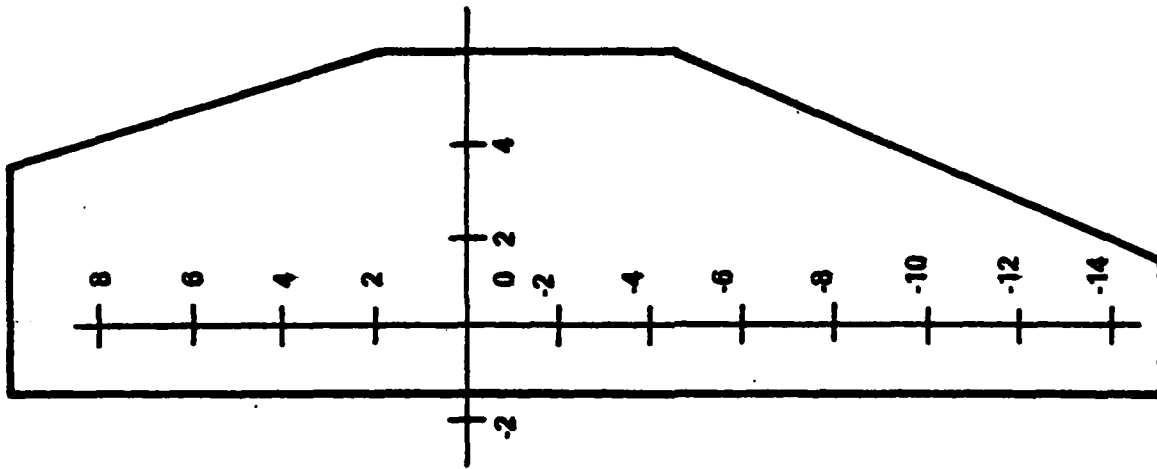
FIGURE 9. THE MAXIMUM DESIGN LIMIT LOAD FACTOR ENVELOPE FOR THE F-111 AIRCRAFT, OUTBOARD PIVOT PYLON
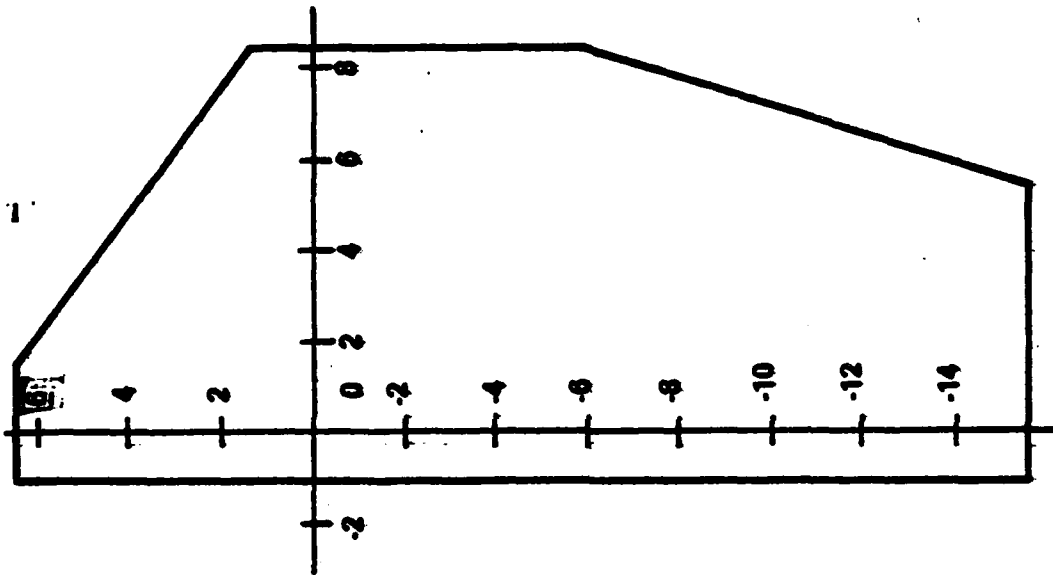
FIGURE 10. THE MAXIMUM DESIGN LIMIT LOAD FACTOR ENVELOPE FOR THE F-18 AIRCRAFT, WING STATIONS
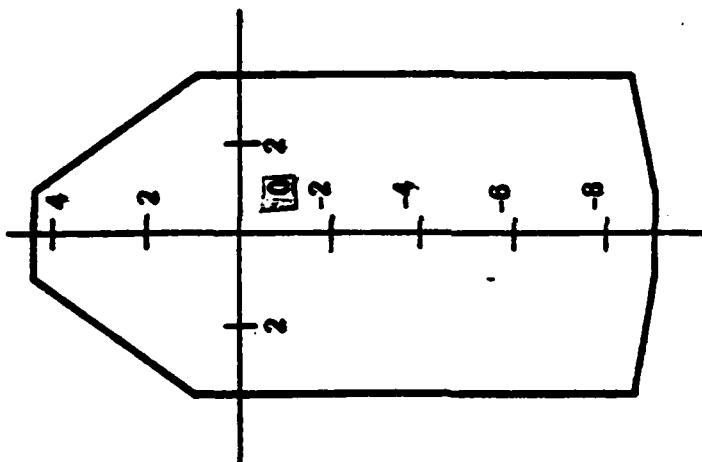
FIGURE 11. THE MAXIMUM DESIGN LIMIT LOAD FACTOR ENVELOPE FOR THE
F-16 AIRCRAFT, CENTERLINE STATION

latter of these needs has already been met by the incorporation of a low speed DLLF curve into MIL-A-8591F currently in draft. As for the supermaneuverable aircraft this fix would be fairly simple to make and probably should be accomplished in the same manner as the slow speed aircraft above. However it will probably be some time before this is accomplished due to the time required to generate a new revision.

4.3 Aerodynamic Coefficients

The only possible area of hope for this problem to be solved and still maintain the basic premise of a cheap and fast design aid is the use of flow-field-emersion technique. This concept is to measure the flow at every pylon which is of interest, then "emerse" the store's free stream data in this flow field. This technique still needs R&D before it can be proposed for incorporation into the MIL-A-8591.

5.0 SUMMATION

There are a number of valid criticisms of the present specification. However, the theoretical ones are being corrected and the philosophical ones are being studied. Further, there is not now any cheaper, quicker and better method to design stores for general use, and this must remain the most important factor of the spec.

This paper has presented the methodology by which MIL-A-8591E should be used for design of stores. However the designer should be cautioned that this is only one part of total design of the store. Other factors such as vibration environment, fatigue, etc. must be considered. But at least MIL-A-8591E gives the designer a good basis with which to start his design.

6.0 REFERENCES

AFSC Regulation 80-33, Class II Modification of Aerospace Vehicles, 1 July 1975.

MIL-A-8591E, Airborne Stores, Associated Suspension Lugs, and Aircraft-Store Interface (Carriage Phase); General Design Criteria for, 12 January 1976.

AUTOBIOGRAPHY

Mr. Dyess received his B.S. in Aerospace Engineering from Auburn University in 1967. He received his M.S. in Aerospace Engineering (Structures) from Auburn University in 1969. He is currently working on a Ph.D. degree in Applied Mathematics from University of Florida. In 1969, Mr. Dyess began work with the USAF at Eglin AFB FL. Since then he has worked as a structures and loads engineer as a member of first the Advanced Armament Concepts Branch and then the Aircraft Compatibility Branch of the Air Force Armament Laboratory. Throughout this period his area of effort and responsibility has been in determining the loads on aircraft and store due to the presence of the other and the effect the loads have on the structural integrity of the aircraft or store.

(The reverse of this page is blank)

THE PREDICTION OF EJECTOR RELEASE UNIT (ERU) PERFORMANCE

(Article Unclassified)

by

M J Twigger

Royal Aircraft Establishment
Farnborough
Hampshire, England

ABSTRACT. (U) A mathematical model of a store ejector release unit (ERU) is useful as a design tool and as an aid to release disturbance prediction. The model described has been constructed with these two purposes in mind. It has already been used for both applications.

The model uses the basic thermodynamic equations and conservation laws and it has been found unnecessary as yet to introduce real gas refinements. Essentially, the system is modelled as a number of chambers interconnected by orifices, some chambers being designated breeches or rams. Cartridges are burned assuming a power law burning rate. Heat losses are accounted for by empirical data. The ERU ram forces are reacted by a flexible structure, with one degree of linear freedom vertically and one degree of rotational freedom about the pitch axis. Steady aircraft acceleration is modelled, as are friction in rams and store aerodynamic forces and moments. In the application for which it was intended the model adequately predicts the ERU ejection velocity.

The method used in the model is very simple and could easily be incorporated in larger simulation models.

LIST OF TABLES AND FIGURES

1. INTRODUCTION

Military aircraft frequently carry their weapons externally, mounted under the fuselage or attached to wing pylons. Store release ideally should be possible at all points in the aircraft flight envelope, and should be free of any risk of the released store hitting the aircraft as well as being repeatable for aiming accuracy.

A device known as an Ejector Release Unit (ERU) is usually used. This holds the store to the aircraft by means of hooks until store release is commanded. It then releases the hooks and pushes the store away from the aircraft. Power cartridges are the normal energy source. These pressurise one or two rams.

A mathematical model of an ERU can usefully be used in design and development to predict performance of designs off the drawing board, to investigate sensitivity to changes in volumes and orifices, or to assess the effect of aerodynamic loads. However, its potential lies in reducing the amount of test flying necessary to clear weapons for release. Up to now this activity has involved a great deal of test flying to establish the edges of the release envelope. It is hoped to use an ERU model in conjunction with a twin-sting wind tunnel rig to determine the parts of the flight envelope that may cause difficulties, thus allowing test flying to concentrate on these areas.

2. SYSTEM BEING MODELLED

The features of the ejection system which significantly affect performance (ie ejection velocities) are:-

(a) ERU gas system
(b) aircraft flexibility and motion
(c) store aerodynamic loads.

The model was originally intended for investigation of bomb release disturbance, so a rigid store has been assumed. A store would have to be very flexible to affect ejection velocity significantly.

The gas system of an ERU is generally simple. A solid propellant cartridge is burned to produce gas, which passes through an orifice to a ram. The orifice is used to regulate the ejection velocity, and is pre-set on the ground. Some ERUs have two rams, fed from the same power source. There is a valve to release the hooks holding the store to the ERU when the pressure has built up; this valve sometimes also blocks gas from the rams until release occurs. An ERU may also have telescopic rams to give a longer stroke. At the end of stroke, when the store is clear, the pressure in the ram is usually vented. Non-return valves can be used in complex ERUs.

Aircraft flexibility can have a significant effect on the achieved ejection velocity. It is common practice to carry stores side by side

on an underwing pylon - this arrangement provides a very flexible mounting for each store. A large proportion of the ERU effort goes into moving the structure in such a case.

The presence of aerodynamic loads on the store alters the demand on the ram. The ejection history is thus changed, with an effect on velocity. Aerodynamic moments can be expected to cause large differences in pitch performance.

All of these factors are modelled, although the mounting flexibility is dealt with only in a very simple manner which may eventually prove to be too simple.

3. MODEL DESCRIPTION

The flow diagram of the model is shown in Figure 7. A brief program description is given in Appendix 2.

The ERU is assumed to be attached to a structure having one vertical and one rotational degree of freedom, which simulate in the simplest way a flexible mounting. The system can include damping. Such a simple system will not represent all types of flexible structure. This flexible mounting can be accelerated at a constant value to simulate an aircraft manoeuvre (see Appendix 1, section 2).

The store is assumed to be rigid, with mass and pitch inertia. Aerodynamic normal force and pitch moment can be applied, varying with store cg distance from rest (see Appendix 1, section 2).

The gas system is modelled as a network of chambers, linked by orifices. Non-return valves at orifices can be specified. A release valve, which senses the pressure in a nominated chamber, releases the store when the specified pressure is reached. It can also be used to blank off any orifice until release occurs. It can have one or two rams, which may be telescopic (2 part). Friction can be applied to the rams, varying with ram stroke. At the end of ram stroke, the ram is vented. Leakage is dealt with by adding an orifice and a large chamber. Figure 6 shows a typical idealisation. It may have up to 5 breeches, each with a different cartridge with definable ignition times. Each cartridge is specified by its propellant density, burning law, force constant, and a table of burning area variation with distance burned. The gases produced by all cartridges are assumed to have the same properties, defined by constant specific heat and specific heat ratios. A power burning law is used (see Appendix 1, section 1.3.1). The process of calculation within the gas system is determination of energy liberated by the propellant, energy transferred through an orifice from chamber to chamber, energy lost through heat transfer, and work done on the store. Heat losses are dealt with semi-empirically by assuming a loss rate proportional to temperature difference and pressure (see Appendix 1, 1.3.2). This loss rate applies to chamber walls, and to cartridge cases. Basic thermodynamic equations and conservation laws

584

are used, with a compressibility correction; it has not been found necessary to introduce real gas refinements. The gas system is calibrated by adjusting discharge coefficient, orifices representing pipe losses, and the heat loss coefficients (see Appendix 2, section 4).

The gas system modelling is simple enough to permit it to be incorporated into a larger system model, which could have for instance realistic representation of structure and simulation of store trajectory until clear of aircraft.

The program is written in Fortran IV, using a simple incremental technique with a 5th order integration method.

4. RESULTS

Three ERU types have been modelled and tested in all. Of these, type 1 and type 2 are similar in design, one being larger than the other. Type 3 is a single ram test rig, quite different in all respects from 1 and 2.

Type 1 and 2 consist of 2 rams, with changeable orifices at each ram inlet, served by 2 identical cartridges fired simultaneously in interconnected breeches. A release mechanism holds the store until the breech pressure overcomes a spring. Both were mounted on a flexible ground rig, that for type 1 being less flexible than for type 2. Measurements were made of rig flexibility during the firings of type 2 - flexibility and damping were expressed in terms of a single degree of freedom vertically and this has been used in the model. In the case of type 1 no measurement was made. Thus in both cases any torsional (pitch) flexibility, and vertical flexibility in the case of type 1, have not been modelled. The cartridges for both types comprise many small pellets, some with multiple holes through the middle; burning surface geometry is complex.

Type 3 has a single telescopic ram, with 2 breeches each with a different cartridge, and a reservoir filled via a non-return valve. No measurements of rig flexibility were made. Cartridges consist of large tubular blocks of propellant simple in form.

The test firings of types 1 and 2 were chosen as being representative. In each case the ejection velocity and pressure-time curve shapes are typical. There is only one firing result for type 3 available. On all firings measurements of breech and ram pressures, final ejection velocity and pitch rate were made with respect to time.

Velocity measurements were made via 2 metal strips with spaced holes, a pulse being seen by a PE cell as each hole passes a light. Maximum error of the analysed velocity is quoted as $\pm$ 0.15 m/s, and 0.1 rad/s for pitch rate.

The model runs were all made with the same heat loss coefficients and discharge coefficient. The model was calibrated against type 2 ERU ejection velocities (see Appendix 2, section 4). All other data was measured from drawings or obtained from the cartridge supplier.

The configurations and velocities measured and predicted are shown in Table I. Figures 1 to 5 show the pressure-time history, measured and predicted, for rams and breech for each case. Also shown in Figures 1 and 5 are the idealised configuration.

In comparing results, it should be borne in mind that the rig flexibility affects results, and has not been modelled in most cases.

Looking first at Table I, it will be seen the ERU type 2 linear velocity predictions are close to measured values. The model was calibrated for this ERU because the rig vertical flexibility was known. At first sight pitch rate does not appear to be well matched; however the error between predicted and observed pitch rates is of the same order as the measurement error (0.1 rad/s). Repeated test firings indicate that pitch rate can vary significantly between nominally identical firings.

Model runs predict that for type 2, case A, a 1.8% increase in front orifice diameter together with a similar reduction on the rear orifice gives a pitch rate of 0.063 rad/s. It is therefore probable that such ERUs are pitch sensitive and the apparent prediction errors are due to tolerances. The model would be useful in the investigation of such sensitivity to tolerances.

The velocity predictions for ERU type 1 are not as good as those for type 2. The general design of each case is very similar and the propellant used is identical. One might expect then that the calibration factors should be the same for both and the predictions should be equally good, but they are not. Were it not for type 1, case B (-8.9% on linear velocity), the rig flexibility could be cited as cause. There was rig flexibility, which would reduce the error shown by cases A, C, D, but the error of case B would increase. Comparison of cases A and B show an inconsistency in measured velocity; for the same store mass as case A but one orifice smaller the velocity in case B apparently rises. This result (case B) is therefore suspect. The only case with a non-zero pitch rate shows a prediction error magnitude similar to those for ERU type 2.

For ERU type 3, the velocity prediction is a little worse than for type 2. It was difficult to model this ERU because of the complex geometry and the existence of unmeasured friction. Although the design is completely different from types 1 and 2, the same calibration factors were used. The calibration factors could be changed to better the prediction, but it must be remembered that there is only one firing result.

Figures 1-4 show the match of the pressure-time histories for types 1 and 2. The predicted breech curve shows in all cases a tendency to peak sharply. It appears that there is some tailing off of burning rate occurring in practice which rounds off the peak. This is possibly due to the small propellant pellet geometry being incorrectly modelled. However, the discrepancy does not appear to have an overall effect. These breech curves may be compared with those for type 3; here the fit is much better, indicating that the charge geometry is correct.

The predicted ram pressure curves for type 1 exhibit a tendency to rise more rapidly than that measured, while the reverse is true for type 2. No explanation has been found for this. The orifice size is similar in both types.

The overall operation time in each case matches reasonably, the worst error being for type 2, case D, 9% low on prediction.

Figure 5, for ERU type 3, shows the good match obtained for the breeches and just downstream of the breech orifices. The ram curve is not as good. This may be due to friction varying significantly from that input to the model. There is also some doubt over the exact configuration tested, so that the volume of the ram etc may be in error.

Overall, the predicted velocity is close in engineering terms to measured values. Pitch rate prediction may not be as good, but there is evidence that the twin-ram ERUs may be sensitive to geometric tolerances, thus throwing doubt on any conclusion on pitch rate prediction error.

DISCUSSION

The comparison of predicted and measured result indicate that the model predicts ejection velocity to within about 5%, a level which should be sufficiently low for most purposes. The action time error is 9% maximum. These results were obtained using the calibration factors adjusted against type 2 ERU, suggesting that the modelling is basically correct since the 3 ERU types covered 2 very different designs.

There are however deviations in the pressure-time prediction that would bear investigation. A better heat loss method for the cartridge burning phase might be worth consideration, although the method used gives quite reasonable results in the type 3 application (there is a possibility that the modelling of the cartridge form used in Types 1 and 2 is not good enough, and this may have caused the discrepancy). However, a sound theoretical treatment would be useful.

Other possible areas for improvement are discharge coefficient (incorporate dependence of form and flow characteristics) and variation of gas properties with temperature and pressure.

587

The pitch rate prediction does not match the measured result as well as the linear velocities match. Reasons for this could lie in the measuring accuracy, the prediction method, or ERU geometrical tolerances. The errors ranged from -21% to +15%. It is hoped to obtain more firing results of pitching configurations for comparison purposes.

The model has already been used as follows:-

(a) in-house, in the understanding of store release in the dynamic situation.

(b) by industry in setting up small scale tunnel trials for store release clearance.

(c) by industry in design/development of a new ERU.

It is proposed to incorporate it in a system model which would, in conjunction with a wind tunnel trial, predict store trajectory until clear of the aircraft.

5. CONCLUSIONS AND RECOMMENDATIONS

It is believed that the model of the gas system represents a reasonable compromise between practicality and exactness. However, should improvement be required, areas of the model which could benefit are heat losses and orifice/pipe flow. The heat loss method assumed can probably be improved, particularly during cartridge burning. The present method allows the same coefficient to be used on 3 different ERU types, but nevertheless the breech pressure history is not satisfactory. Improvement would increase confidence in modelling systems off the drawing board. An improvement in predicting flow through orifices, possibly using a discharge coefficient based on orifice geometry and flow state, may help to better the ram pressure history. Repeat firings sometimes show inconsistent ram pressure histories.

As well as the above, there is of course scope for better representation of the flexible mounting structure, and simulation of store flexibility.

The gas system model stands on its own and as such could be incorporated into a larger system model. As pointed out already, flight clearance is expensive and modelling is a way of cutting down the cost. A comprehensive model could be built which would include structural flexibility, gas system, store flexibility and control forces, and full aerodynamics. It would be used after validation to explore all parts of the flight envelope in order to select marginal areas where flight testing should be concentrated.

Another use is in conjunction with wind tunnel tests, designed to measure aerodynamic forces on the store as it is being ejected. The

forces depend on attitude and motion, which in turn depend on the ERU response to the forces. Thus the aerodynamics of a store during ejection cannot be accurately determined without bringing the ERU into the loop. A software and tunnel combination would provide a way of doing this.

Use of the model on its own is useful in the investigation of release disturbance, and in the design of ERUs. In the former, store response to different orifice settings and aerodynamic forces can easily be seen. For the latter, the effect of cartridge changes, changes in volume etc can readily be obtained at little cost, enabling the designer to come to the test site with high confidence in his design, resulting in shorter development programmes.

1. GAS SYSTEM

1.1 GENERAL PRINCIPLE OF THE METHOD

The gas system is idealised into a network of chambers inter-connected by orifices, with one or two chambers being designated as rams, and at least one chamber identified as a breech. Burning of a cartridge pressurises the rams, which apply forces simultaneously to a store and to a flexible structure. See Fig 6 for a typical idealisation.

The gas flows are calculated by consideration of energy transfer, which is easy to handle by computer.

CALCULATION OF GAS CHANGES

1.2 PRESSURE CHANGE IN A CHAMBER DUE TO ENERGY INPUT

Energy can be gained (or lost) by the gas in a chamber by direct input from a cartridge, heat loss, flow through an orifice either in or out, or work done.

The total energy in a chamber, assuming static conditions, is

$$H = m\,c_V\,T + pV$$

where m = mass of gas

c_V = specific heat at constant volume

T = static temperature

p = pressure

V = volume

from which the effect on pressure of an incremental change in energy δH is found by

$$P_2 = P_1 \frac{V_1}{V_2} + \frac{\delta H}{V_2 \left(\frac{c_V}{R} + 1 \right)}$$

where suffices 1 and 2 refer to before and after addition of δH.

At high pressures a correction must be made for the volume occupied by the molecules - volume must be reduced to corrected volume $= V - m\eta$

where η = covolume coefficient

The temperature of the gas is found from $pV = mRT$.

A perfect gas was assumed initially as a convenient starting point since specific heats were not expected to vary much over the expected gas temperature range. This assumption has not been changed during development; introducing varying specific heats would give a minor improvement only. It has further been assumed that the gas properties do not vary as the cartridge burns.

The use of ideal or real gas assumptions and gas properties varying with cartridge status could easily be incorporated in the model if desired.

1.3 ENERGY TRANSFERS

Gas energy is gained by burning propellant, lost through heat losses, transferred through orifices, and does work.

1.3.1 Cartridge burning

When a propellant is burned ideally in a closed vessel, the pressure reached is

$$P_{max} = \frac{m}{V} \frac{R_o T_v}{M}$$

where m = propellant mass burned

V = volume of vessel

R_o = universal gas constant

T_v = flame temperature at constant volume

M = average molecular weight of gases

The expression $\frac{R_o T_v}{M}$ is subsequently referred to as λ, the Force Constant (or Impetus). λ is a measure of the cartridge energy. Thus

$$P_{max} = \frac{m \lambda}{V}$$

$$\text{or } p_2 = p_1 + \frac{\delta m \lambda}{V}$$

Hence the increment of total energy obtained from the cartridge is

$$\delta H_c = \left(\frac{c_v}{R} + 1\right) \delta m \lambda$$

where δm is an increment of propellant mass.

A burning law of $B = a p_c^n$ is used.

591

c_v, R and γ for the gases produced are constant (R = specific gas constant, γ = ratio of specific heats).

1.3.2 Heat losses

The complex internal geometry and the turbulence caused by the cartridge burning makes an analytical approach of doubtful value even if possible.

Inspection of the test record for a blank orifice firing (ie closed vessel) shows that the heat loss during burning is an order greater than after burnout. Possible causes of this are:-

(a) the emissivity of the burning gases is higher than that of the burned gas.

(b) during burning the turbulence must be greater than after burnout, thus the pre-burnout heat transfer mechanism will be dominantly forced convection, while past-burnout it will tend towards free convection.

It is readily shown that radiation alone cannot account for all the heat loss required, or the difference before and after burnout. It makes in fact a relatively small contribution to the losses during burning. However, the emissivity is higher for flames than quiescent gas, so it is probable that it does decrease after burnout.

In an ERU gas system, there is undoubtedly great turbulence during burning. After burnout, however, the turbulence in a blanked off breech probably dies away quickly, and quicker than in a system with orifices. A difference may therefore be seen between ERUs with different orifices.

A simplified system has been used with forced convection and radiation.

Heat loss rate $\qquad q = h(T_g - T_w) + \epsilon\sigma(T_g^4 - T_w^4)$

$$\text{where} \quad h = \text{heat transfer coefficient}$$
$$T_g = \text{gas static temperature}$$
$$T_w = \text{wall temperature}$$
$$\epsilon = \text{emissivity}$$
$$\sigma = \text{Stefan-Boltzmann constant}$$

The heat transfer coefficient is usually based on Nusselt number, which suggests a dependence on pressure. A reasonable fit is obtained by using a coefficient proportional to pressure. Thus the following are used:

592

$$\text{Breeches} \atop \text{pre-burnout} \quad \left\{ \begin{array}{l} h = h_1 \, p_c \\[1em] \epsilon = 1 \end{array} \right.$$

$$\text{Breeches post-burnout} \atop \text{and all other chambers} \quad \begin{array}{l} h = h_2 \, p \\[1em] \epsilon = \epsilon_2 \end{array}$$

Re-radiation by the wall has been ignored.

This heat loss rate is applied to all chambers reached by the gas. In breeches there is also a cartridge holder to be considered. Being small, this will reach a higher temperature than the wall and since it can hold a significant amount of heat it must be accounted for separately.

The heat transferred from the gas is assumed to heat the chamber wall to a specified depth ie a single layer. This simple approach is justified by the low wall temperature relative to the gas temperature. (In fact, it is probable that an acceptable answer would obtain by simply losing the heat and not transferring it to the wall). In the case of a cartridge, the total mass is assumed to be heated without any temperature gradient occurring. Cartridge holders are usually of light construction, making this a reasonable assumption.

_Thus for each chamber the rise in wall temperature is calculated as

$$T_w = \frac{S_w \Delta h}{C \, M_w} (T_g - T_w) + \epsilon \sigma (T_g^4 - T_w^4)$$

where S_w = surface area of chamber

Δ = time increment

M_w = mass of wall heated

$\quad = d_w \, S_w \, \rho_w,$ d_w = depth to which it is heated

$\qquad\qquad\qquad \rho_w$ = density

C = specific heat

h, ϵ previously defined as

$\quad h = h_1 \, p_c,$ $\epsilon = 1$ pre-burnout, breeches only

$\quad h = h_2 \, p,$ $\epsilon = \epsilon_2$ post-burnout

$\quad h_1, h_2, \epsilon_2$ are constant

Additionally, for each cartridge,

$$T_c = \frac{S_c \Delta h}{C \, M_c} (T_g - T_c) + \epsilon \sigma (T_g^4 - T_c^4)$$

where subscript c refers to cartridge values.

593

1.3.3 Flow through an orifice

The standard isentropic flow equations for nozzle flow give

$$N_{Ma} = \sqrt{\left(\frac{T_1}{T_t} - 1\right)\frac{2}{(\gamma-1)}}$$

$$T_t = T_1 \left(\frac{p_t}{p_1}\right)^{\gamma-1/\gamma}$$

$$p_t = p_2 \qquad \text{subsonic}$$

$$\text{or} \quad p_t = p_1 \left(\frac{2}{\gamma+1}\right)^{\gamma/\gamma-1} \qquad \text{sonic}$$

and mass flow rate through the orifice is

$$\dot{m}_t = C_D \rho_t v_t A_t = C_D A_t \frac{p_t}{R T_t} \sqrt{\gamma R T_t}$$

where C_D = discharge coefficient

A = nozzle geometrical area

p = pressure

γ = ratio of specific heats

R = characteristic gas constant

T = static temperature

v = velocity

subscript t = throat conditions
subscript 1 = upstream conditions
subscript 2 = downstream conditions

The discharge coefficient has been assumed constant.

The energy flow rate is

$$\dot{E} = c_v \dot{m}_t T_t + p_t v_t A_t + \tfrac{1}{2} v_t^2 \dot{m}_t$$

1.3.4 Work done by the rams

The energy transferred to the store and wing is $\delta W = p.\delta V$

where δV = volume increment

The program deals with a special case where a free volume is suddenly exposed when the ram reaches a certain point. At this point the

594

pressure ratio is inversely proportional to the volume ratio, ie if state 1 is before and state 2 after the sudden increase,

$$P_2 = P_1 \frac{V_1}{V_2}$$

Note that the usually quoted constant pV^γ does not apply since no work has been done during this expansion. Note also that the equation given for dealing with energy addition in paragraph 1 can be used here, by putting the added energy to zero.

2. STRUCTURAL FLEXIBILITY AND STORE

2.1 MOUNTING STRUCTURE REPRESENTATION

The model represents the linear upward motion of a wing and its twist (about the flexural axis) at the ERU station. A two degree of freedom model has been used. The assumption behind this was that the operation time of the ERU was short enough to allow the complicated wing response to be represented by a single degree of freedom, thus:-
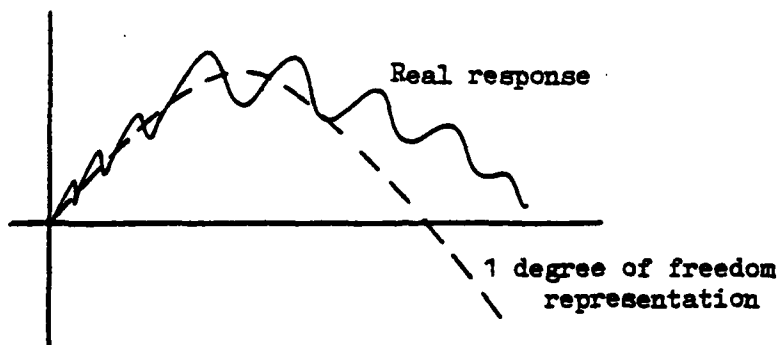
There is no reason why the ERU gas system model could not be used with a more realistic structural model.

The store is assumed rigid; this too could be correctly modelled if required.

2.2 WING AND STORE EQUATIONS OF MOTION

The aircraft fuselage is assumed to be unaffected by the ejection, and assumed to follow a constant upward linear acceleration path $\ddot{a}$ (straight and level, $\dddot{a} = 0$). The wing is pushed by the ERU and oscillates. The store is pushed downwards. Before ERU operation, the wing is deflected by the steady linear acceleration and gravity acting on the store mass; deflections due to wing mass are the same before and after ejection and can be ignored. On ejection, the wing is relieved of these store loads.

595
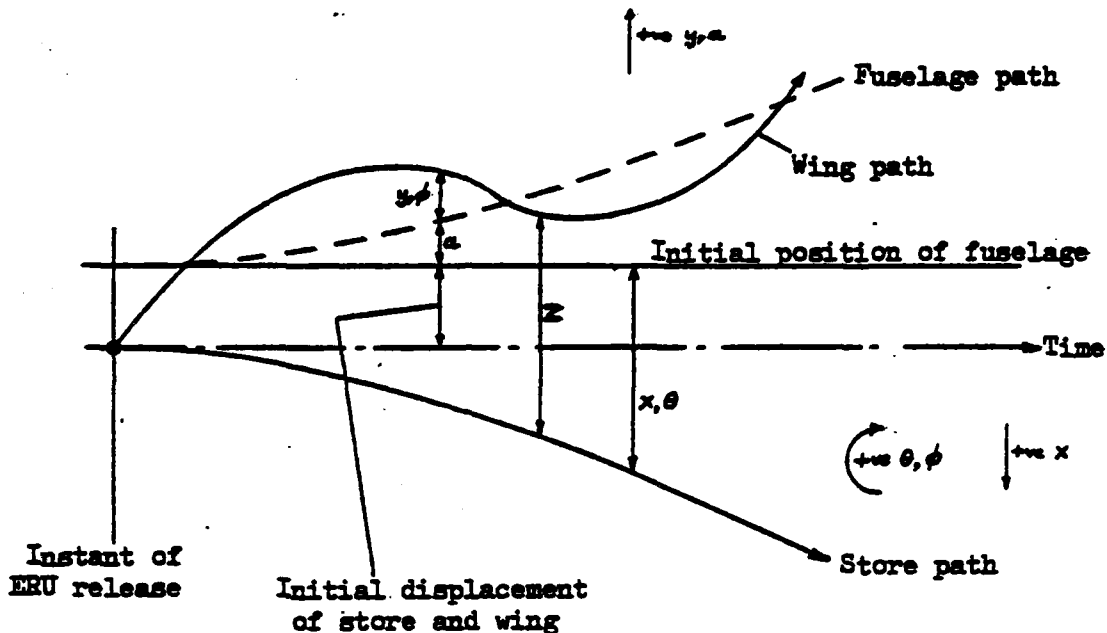
The distance of the fuselage (and wing with no store load) above the initial position is a (positive $\ddot{a}$ upwards). The wing oscillates about the path described by a, hence the wing poisition relative to a is y and has an initial position y_0. The store displacement is measured from the initial fuselage position, with an initial value equal and opposite to y_0. The ram extension z is the distance between wing and store, $z = y + a + x$ if the flexural centre and both centres of gravity are coincident.

All of the above applies also to the wing twist ϕ and store pitch θ, except that there is no angular acceleration of the fuselage and hence the fuselage path is horizontal. Note however that there will be initial angles $\theta_0 = \phi_0$ due to the flexural centre of the wing not coinciding with the wing and store cg, and due to the aerodynamic moment.

2.3 EQUATIONS OF MOTION

Wing system –

596
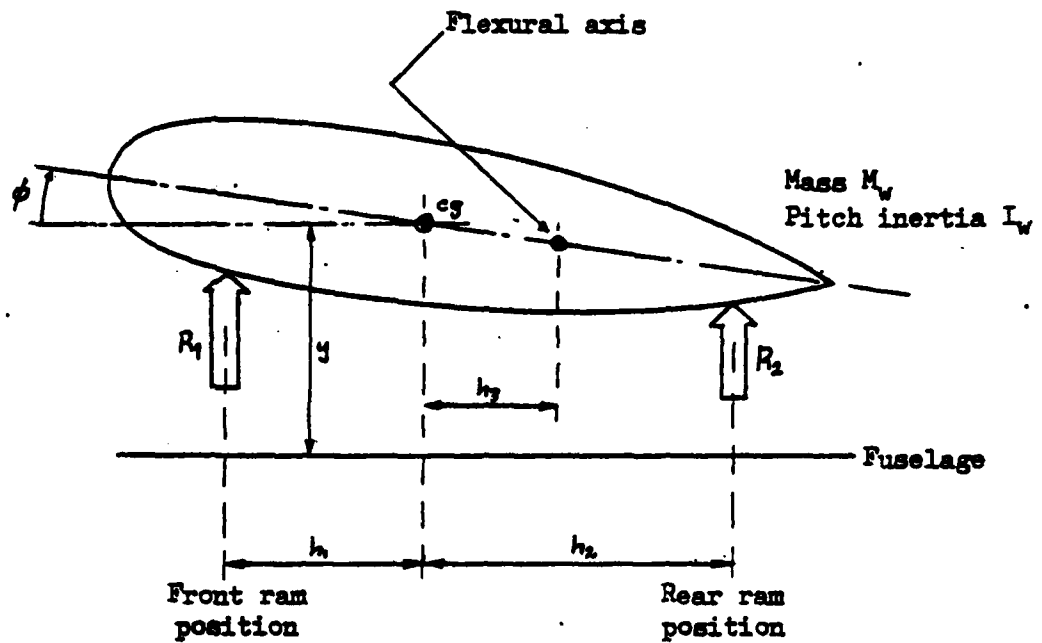
For the wing:-

$$\ddot{y} = \frac{1}{M_w} \left[R_1 + R_2 - \frac{1}{F}(y - \phi\, h_y) - C_F(\dot{y} - \dot{\phi}\, h_y) \right]$$

$$\ddot{\phi} = \frac{1}{I_w} \left[R_1 h_1 - R_2 h_2 - \frac{\phi}{T} - C_T \dot{\phi} + \frac{h_y}{F}(y - \phi\, h_y) \right.$$

$$\left. + h_y C_F (\dot{y} - \dot{\phi}\, h_y) \right]$$

where R_1, R_2 are ram forces

C_F, C_T are damping terms

y is wing cg displacement

ϕ is wing twist

F is wing flexural flexibility

T is wing torsional flexibility

597

Store system -
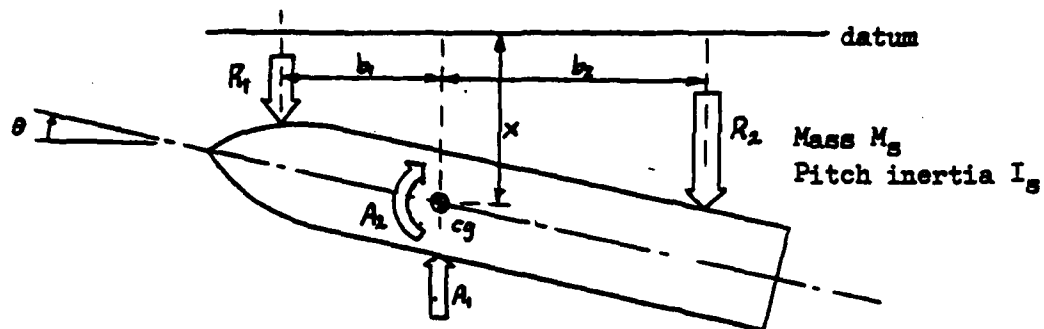
$$\ddot{x} = \frac{1}{M_s} \left[R_1 + R_2 - A_1 + M_s g \right]$$

$$\ddot{\theta} = \frac{1}{I_s} \left[R_2 b_2 - R_1 b_1 + A_2 \right]$$

where A_1 = aerodynamic normal force (+ve upward)

  A_2 = aerodynamic moment (+ve nose up)

Note that these 4 equations of motion do not apply to a case where A_1, A_2 or $\ddot{a}$ are such as to override the ERU forces and thus hold the store against the wing. To avoid the use of the correct equations of motion for these cases (pivoting about front or rear ram position), the artifice of augmenting the appropriate ram force by an amount which increases rapidly with negative stroke is used. This does produce high accelerations and allows small negative strokes but does not corrupt the resulting velocity. The actual form used is

$$\delta R = 10^{17} \left(|z| \right)^3$$

where z = stroke of ram

The ram strokes z_1 and z_2 are

$$z_1 = a + y_1 + x_1$$
$$z_2 = a + y_2 + x_2$$

where $x_1 = x - b_1 \theta$

  $x_2 = x + b_2 \theta$

  $y_1 = y + h_1 \phi$

  $y_2 = y - h_2 \phi$

598

2.4 INITIAL CONDITIONS
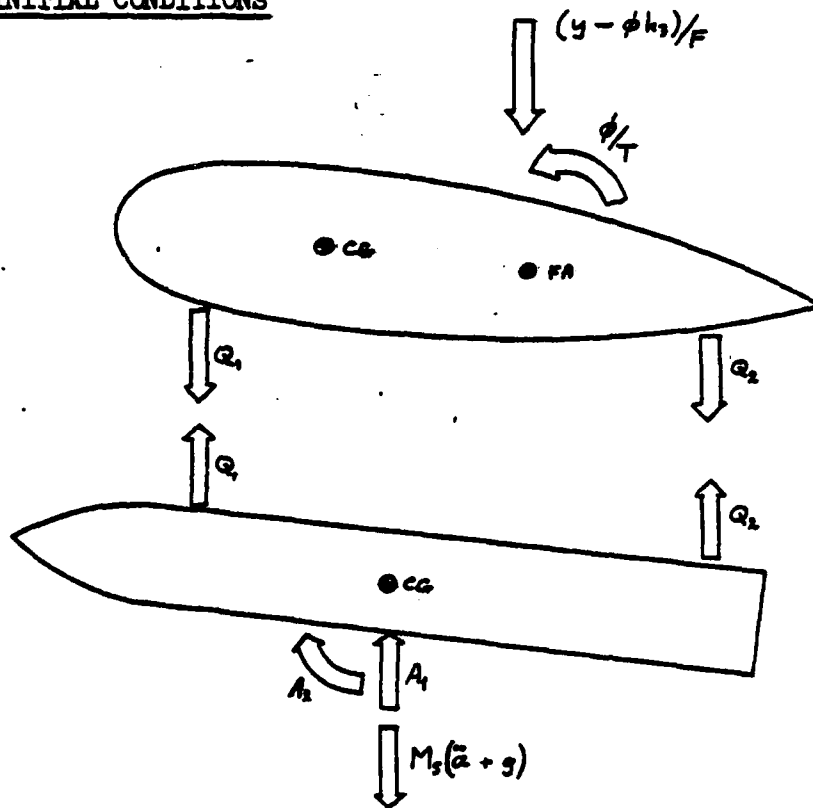
The wing is deflected downwards due to the store loads Q_1 and Q_2
(corresponding to the front and aft ram positions).

$$Q_2 = \frac{1}{(b_1 + b_2)} \left[M_s (\ddot{a} + g) b_1 - A_1 b_1 + A_2 \right]$$

$$Q_1 = M_s \left[\ddot{a} + g \right] - A_1 - Q_2$$

$$\phi_0 = T \left[Q_2 (h_2 - h_3) - Q_1 (h_1 + h_3) \right]$$

$$y_0 = -F \left[M_s (\ddot{a} + g) - A_1 \right] + h_3 \phi_0$$

599

$$X_0 = \phi_0 (b_1 - h_1) - y_0$$

$$\Theta_0 = -\phi_0$$

where y_0 = initial wing cg displacement
ϕ_0 = initial wing twist
X_0 = initial store cg displacement
Θ_0 = initial store pitch angle

APPENDIX 2 - PROGRAM DESCRIPTION

1. GENERAL DESCRIPTION

The program organisation and input has been kept as general as possible so as to apply to most types of ERUs. Separate subroutines are used for calculation of structure motion, store motion and ERU ram forces. The basic calculation method is to systematically work through the idealised ERU, computing the energy exchange between chambers over a small time increment; the ram forces are then applied to the store and structure. Figure 7 shows the overall flow diagram.

2. IDEALISATION TECHNIQUE

2.1 STRUCTURE

So far only a very simple representation of a flexible structure has been used. On the assumption that the mounting structure has a low natural frequency, such that the operation of an ERU will be finished within about a $\frac{1}{4}$ cycle of the fundamental, single degrees of freedom vertically and in pitch are used. If the assumption is correct, the flexibility and mass can be chosen such that the simple system will give a good match to the real system. It would, however, not be difficult to increase the number of degrees of freedom to improve the representation.

Thus the mounting structure is idealised into a mass or inertia, stiffness and damping term for vertical and pitch motion.

2.2 STORE

The store is treated as a rigid mass. However, flexible stores could be modelled if necessary.

2.3 GAS SYSTEM

This is idealised into a network of chambers connected by orifices. Certain chambers are designated breeches or rams. The volumes, internal surface area and specific heat of the wall define each chamber. Orifice diameter, with information on chamber connection and what valving arrangements complete the overall system description. Remaining items are ram areas and stroke, and discharge coefficient.

One cartridge type per breech is assumed, although there can be any number of that type. Each type of cartridge has its own burning law coefficients, force constant, propellant density and charge geometry. The gas constants are assumed to apply throughout the gas system.

Heat loss coefficients and cartridge case heat loss parameters complete the system description.

601

3. PROGRAM METHOD

As all other parts are straightforward, only the gas system is described. The input defines the system. Each chamber volume is read in turn, together with an identification (breech, ram or neither). Following this, each orifice diameter is input, identifying for each the nominally upstream and downstream chamber, and specifying any special valve arrangements. The specification of a chamber as 'upstream' is nominal only and does not restrict the gas flow to that direction. For a time increment, each orifice is dealt with in turn until all have been done. The order in which they are done cycles through a set of 4 orderings. This reduces bias if each ordering is carefully chosen.

For each orifice, the pressure, mass and volume (PMV) are first adjusted to account for energy received from a burning cartridge if the chamber nominally upstream is a breech. Then the energy flowing through the orifice is calculated and the PMV adjusted in both up and downstream chambers. The direction of flow depends on the pressure differential. Should one of the chambers be a ram, the work done in moving the store is calculated and the PMV adjusted. The heat loss surface area and olum of a ram are also adjusted to allow for piston movement.

When all orifices are done, the heat loss in each chamber is calculated and the pressure adjusted accordingly.

The resulting ram pressure is then converted into ram pressure force, from which friction is subtracted or added depending on the direction of movement of the ram.

When the applied aerodynamic forces are such as to overcome the ram forces when the ram has not yet moved from rest (ie keeping it in its carriage position), the ram force is artificially increased to a level that keeps the negative stroke to a low value. This artifice is adopted to avoid using additional equations of motion.

The resulting overall ram forces are then fed into the equations of motion to give ram extension, and the cycle repeated.

4. CALIBRATION OF THE MODEL

The model is calibrated by adjusting the discharge coefficient and the heat loss parameters.

An overall discharge coefficient applying to all orifices is used on the assumption that all orifices will be of the same type. This may not be true; in this case the orifice size must be altered on input. The discharge coefficient will generally lie between 0.4 and 0.8 depending on the form of orifice used. Initially a typical value should be used, adjusting it and possibly the actual orifice size if necessary until a satisfactory fit is obtained. A discharge coefficient of 0.8 has been used in model runs reported here.

Pressure drops along pipes or around bends can be dealt with by introducing artificial orifices or heat losses - the idealisation should be made with this in mind.

The 3 heat loss coefficients are chosen to give the correct slope before and after burnout. A value of 0.3 has been used for emissivity - its value is relatively unimportant since radiation is small compared with convection. The convection coefficients may differ with propellant type. Values of 5×10^{-4} pre-burnout and 10^{-4} post burnout have been found to give a reasonable fit on all types of ERU investigated.

TABLE I - MEASURED AND PREDICTED RESULTS

ERU type	Case	Store max (kg)	cg position (mm)	Store Orifices Front	Store Orifices Rear	Firing Results Linear velocity m/s	Firing Results Pitch rate rad/s	Model runs Linear velocity m/s	Model runs Pitch rate rad/s	% age error of model result Linear velocity	% age error of model result Pitch rate	Remarks
1	A	454	C/L	L	L	3.21	0	3.42	0	+6.5	0	
	B	454	Aft of C/L	S	L	3.26	0	2.97	-0.096	-8.9	-	Twin ram
	C	286	C/L	S	S	3.08	0	3.21	0	+4.2	0	
	D	286	Fwd of C/L	L	L	4.22	+0.495	4.29	+0.565	+1.7	+14.1	
2	A	454	C/L	M	M	4.86	0	4.93	0	+1.4	-	
	B	472	Aft of C/L	S	M	4.75	-0.308	4.68	-0.262	-1.5	-14.9	Twin ram
	C	472	Aft of C/L	M	M	4.74	-0.76	4.82	-0.602	+1.7	-20.8	
	D	692	C/L	M	M	3.93	0	3.90	0	-0.8	0	
3						13.09	0	12.34	0	-5.7	0	Single ram

Pitch rate positive nose up

L = large, M = medium, S = small, C/L centreline
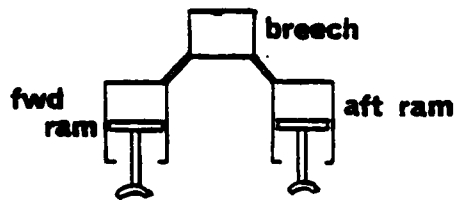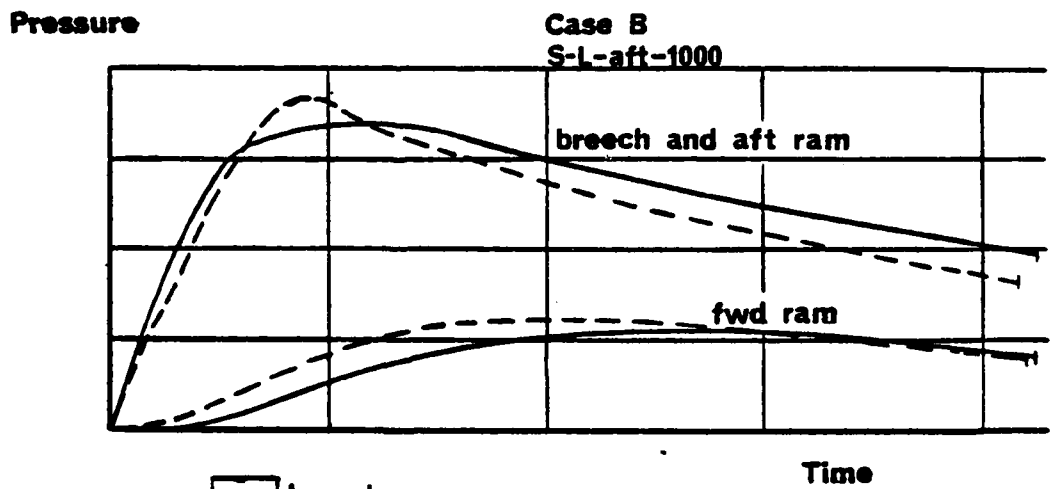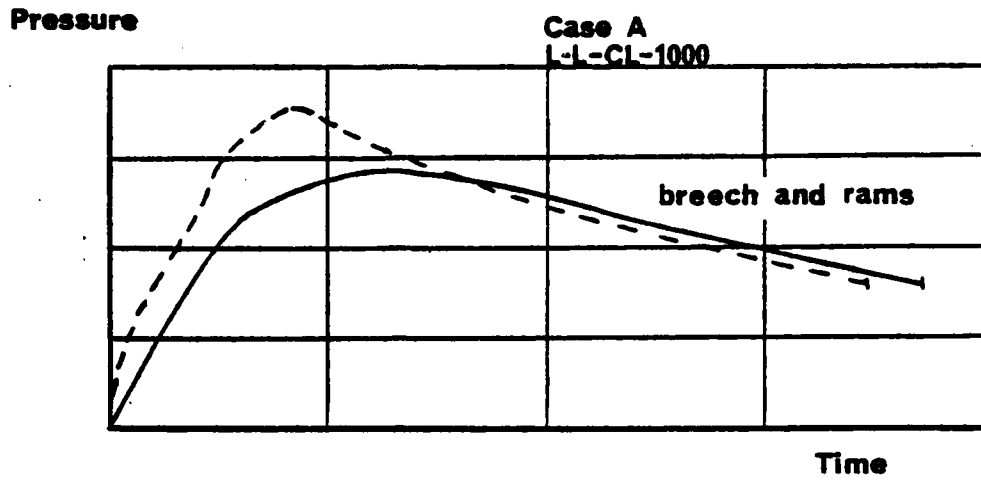
FIGURE 1.   ERU TYPE 1, CASES A-B
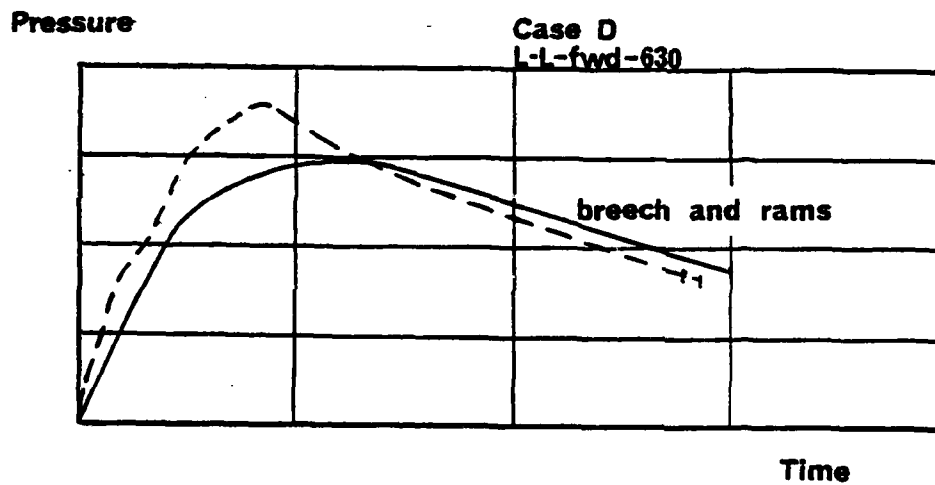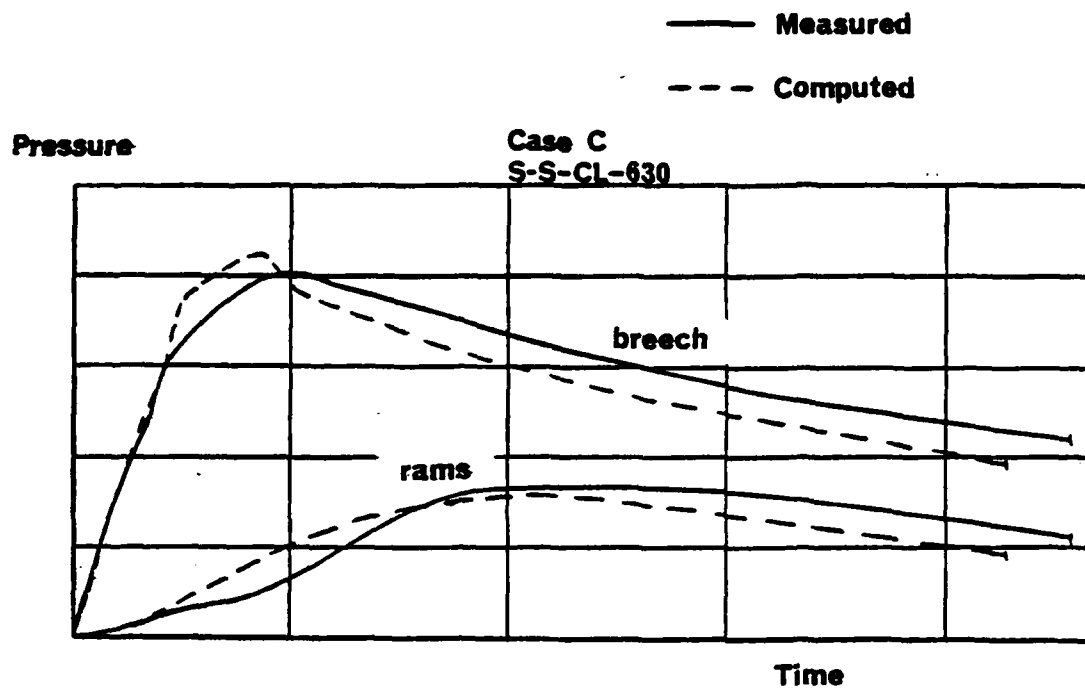
FIGURE 2. ERU TYPE 1, CASES C-D

606

Measured
Computed

Pressure — Case A M-M-CL-1000

breech

rams

Time

Pressure — Case B S-M-aft-1040

breech

aft ram

fwd ram

Time

breech

fwd ram   aft ram
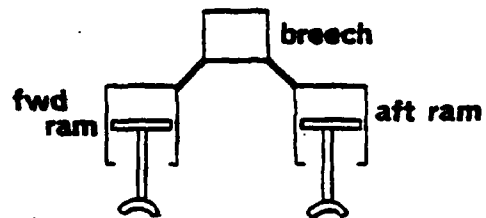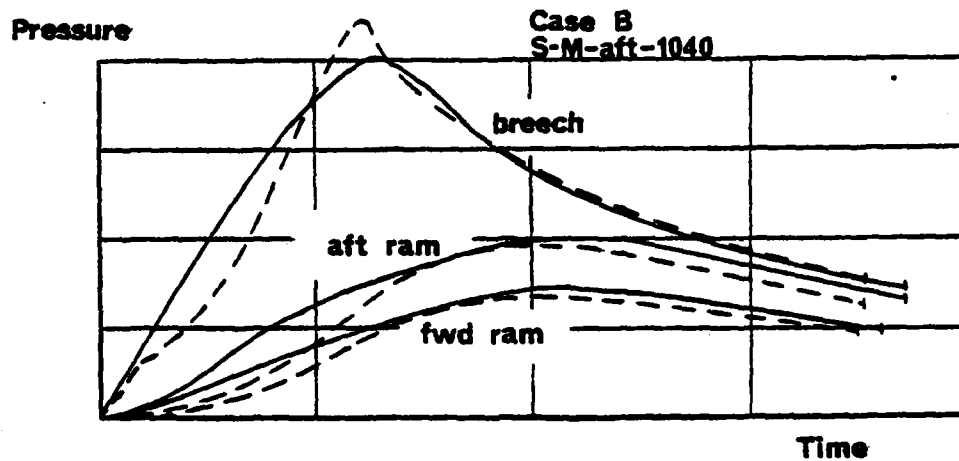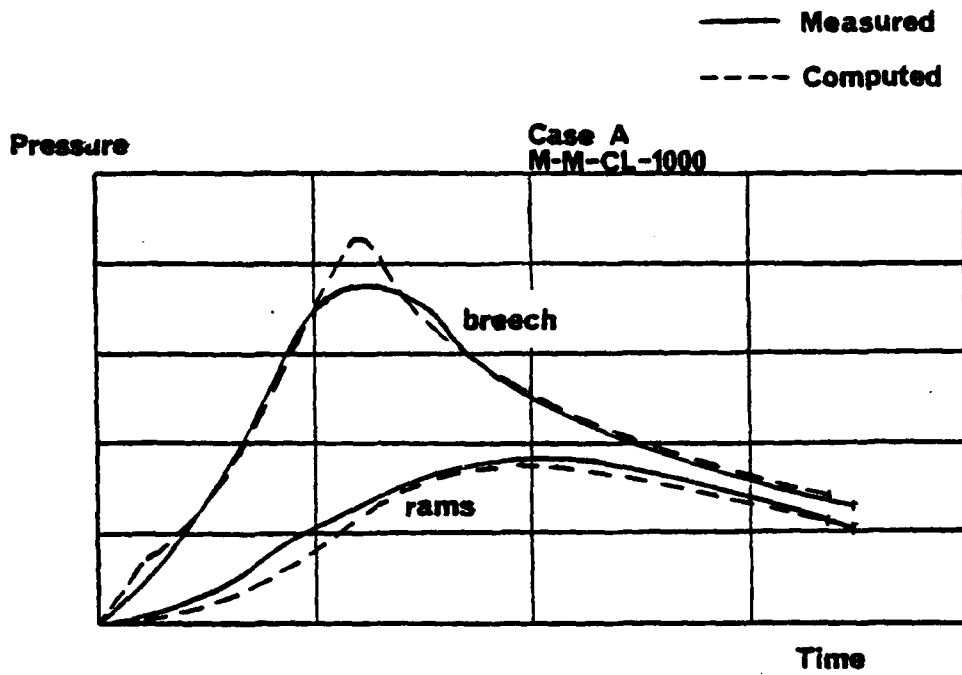
FIGURE 3. ERU TYPE 2, CASES A-B
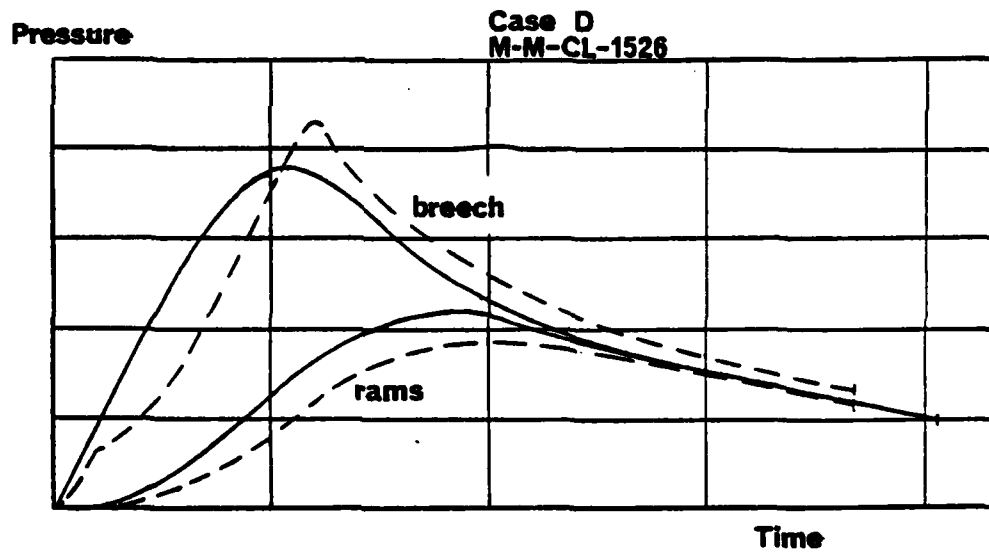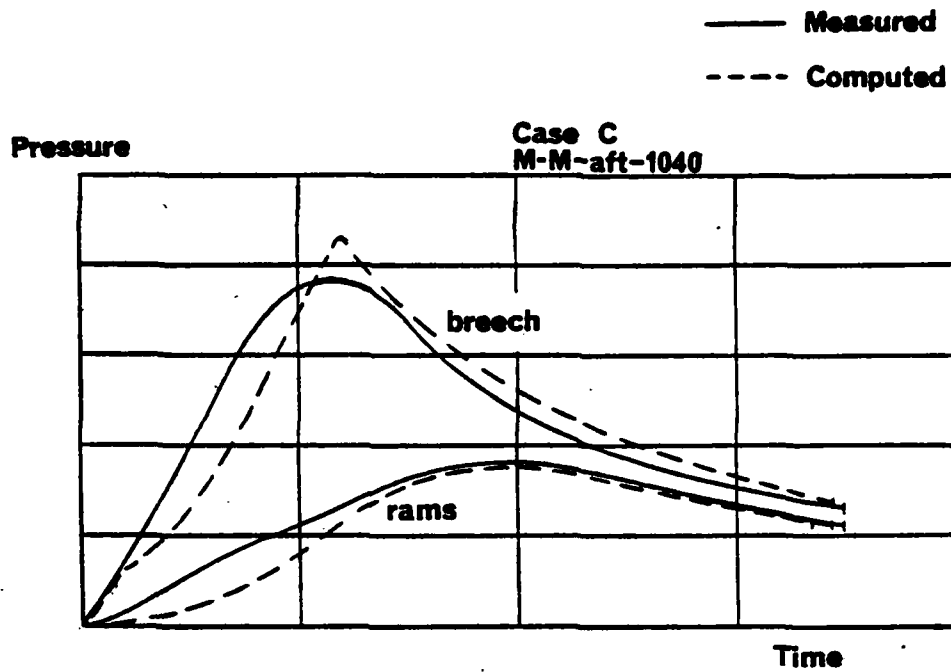
FIGURE 4.   ERU TYPE 2 , CASES C - D

FIGURE 5. ERU TYPE 3

609
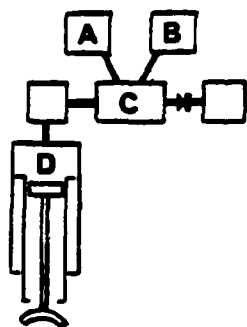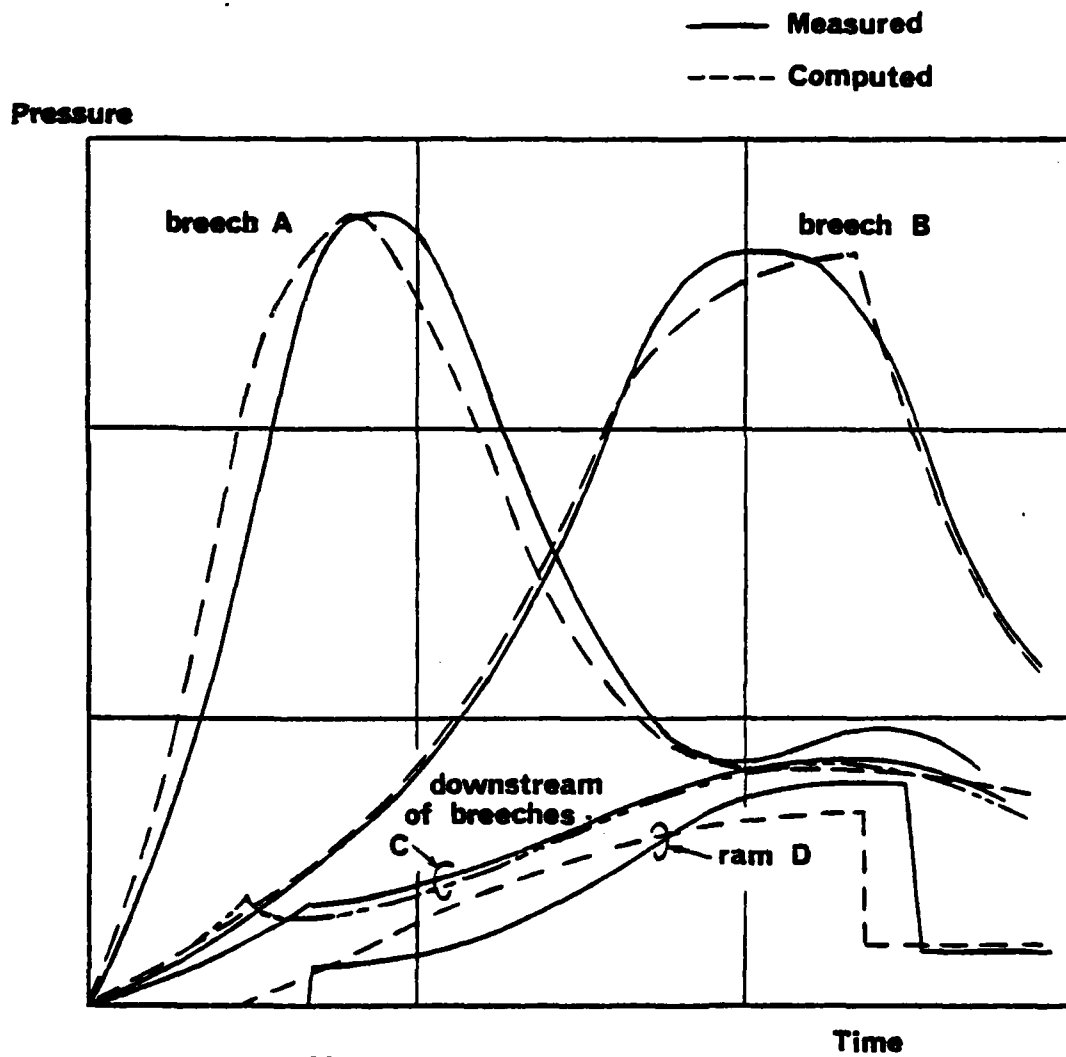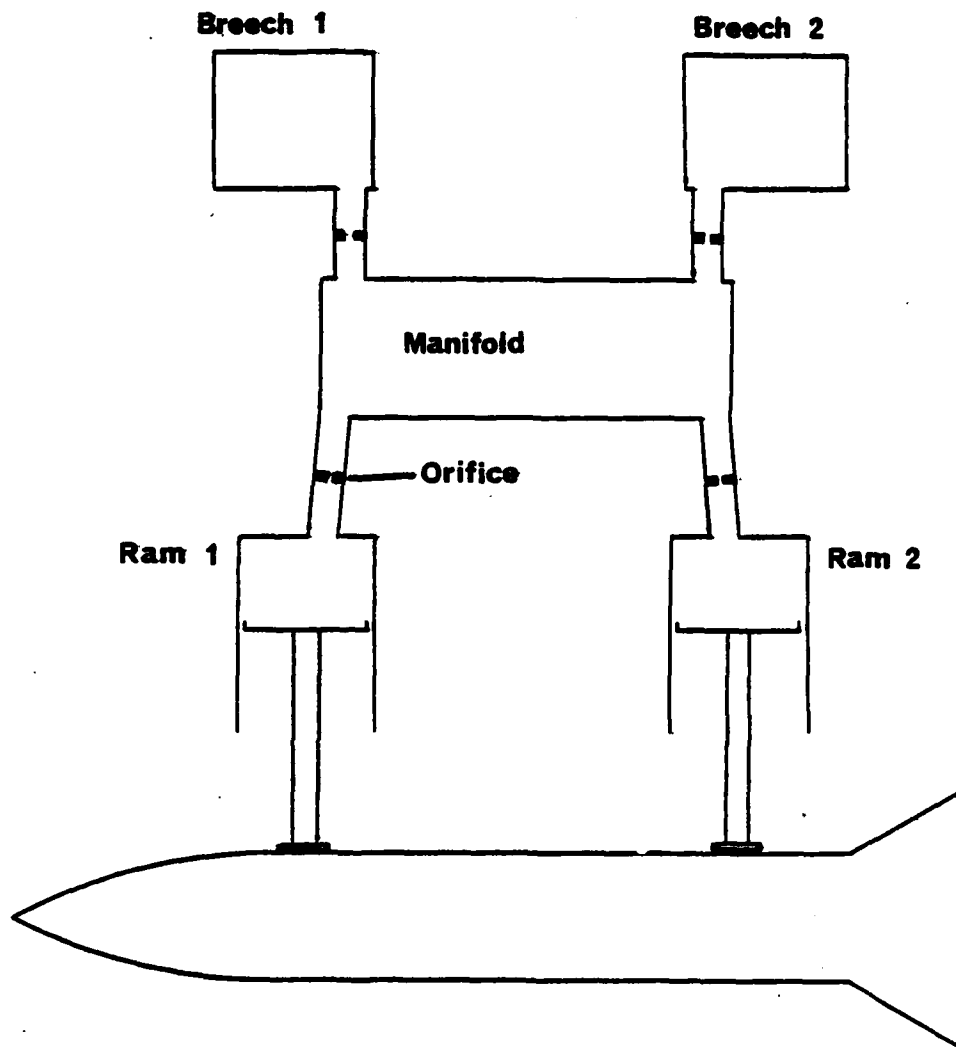
FIGURE 6. TYPICAL IDEALISATION OF AN ERU
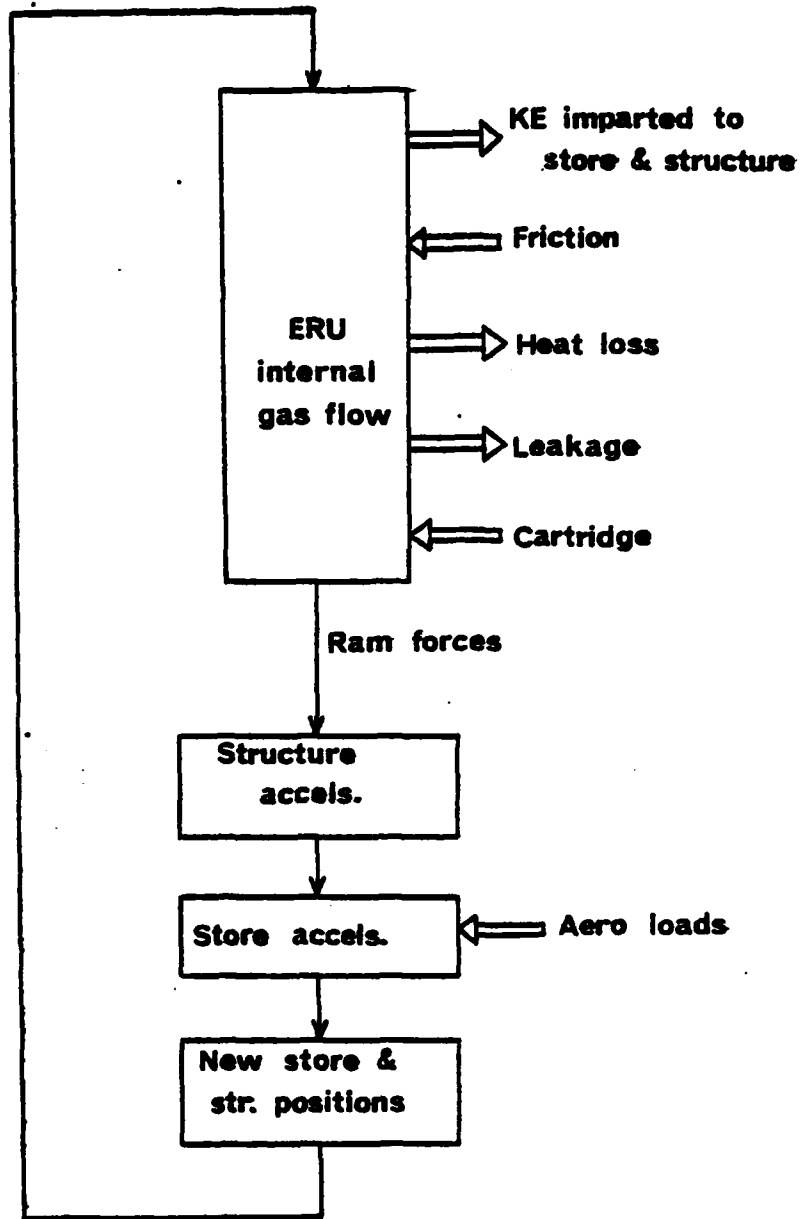
FIGURE 7. PROGRAM FLOW DIAGRAM

AUTOBIOGRAPHY

MICHAEL J TWIGGER

The Author was born in Coventry, England, and after leaving school in 1952 joined Hawker Siddeley Dynamics to serve an apprenticeship. He attended Cranfield Institute of Technology from 1958-1960 and was awarded an MSc for his aircraft design studies. He returned to Hawker Siddeley Dynamics, as a Structural Analyst until 1964, when he joined a Swiss firm, Contraves, in Zurich. He worked on missile, sounding rocket and satellite projects on a wide range of problems including dynamics, kinetic heating, vibration, and structural design. He joined the Royal Aircraft Establishment in 1969. He is a member of the Royal Aeronautical Society.

TEST COMPARISON OF THE SADDLE LUG AND BAIL LUG STORE SUSPENSION AND RELEASE SYSTEMS
(U)
ARTICLE UNCLASSIFIED

by

DENNIS R. McGIVERN
Honeywell Radiation Center

THOMAS E. MILHOUS
Naval Air Development Center

ROBERT V. FRANK
Army Aviation Systems Command

ABSTRACT

The Naval Air Development Center (NAVAIRDEVCEN) is in the process of drafting a detailed bomb rack design specification for future Army AH-1/AAH helicopter weapon system application. Requirements for the rack include automatic store boresighting during rearming and carriage throughout helicopter service environments as well as rapid rearming under various field conditions.

Current-use lug suspension systems with manual swaybracing have proven deficient in these capacities during actual field use.

Recent advances in store suspension technology have resulted in the production and use of racks with capabilities approaching those which would fulfill these requirements.

NAVAIRDEVCEN authorized laboratory testing under critical helicopter environments of five such bomb racks comparing the saddle lug and bail lug suspension systems. These racks were tested specifically regarding their store boresight retention capabilities and to identify from actual comparative testing those characteristics and design approaches which would provide an optimum design to meet all Army requirements.

ABSTRACT
(Cont.)

The purpose of this paper will be to define saddle lug and bail
lug operations, outline the details of the laboratory tests
performed at Dayton T. Brown, Inc. and to present the recom-
mendations for the bomb rack design approach for Army weapon
system application based on these tests and other data sources.

LIST OF FIGURES

INTRODUCTION

STATEMENT OF PROBLEM

In the United States the standard airborne store suspension technique is accomplished by bail type lug bomb racks. Recent U.S. Army investigations of bail type lug suspension systems used on helicopters have revealed various unsatisfactory operational characteristics which should be eliminated. These characteristics include instability of store in flight and difficulty in loading of the store. Furthermore, these characteristics are incompatible with the Required Operational Capability (ROC) for the Light-weight Rocket Launcher (LWL) which requires a bomb rack that automatically achieves and retains store boresight during rearming and accommodates rapid store rearming under various field conditions. Based on the above findings, it is appropriate to evaluate other suspension techniques in search for improvement.

Continued investigations indicate that the saddle type lug bomb racks used on some NATO fixed wing aircraft exhibit features compatible with the LWL ROC. Three of these features are in-flight store stability, automatic boresighting at store engagement and the capability of rapid rearming under various field conditions.

PROGRAM OBJECTIVES

The intent of this investigation was to establish the current state of bomb rack technology for helicopter application and assess the feasibility of meeting LWL ROC requirements. To establish the state-of-art of bomb racks in light of the LWL ROC one bomb rack from each of the four known saddle type lug rack manufacturers and one bail type lug rack exhibiting the required capabilities were subjected to laboratory testing.

In addition, suspension lug and bomb rack test and evaluation data from references (a) and (b) were analyzed. This data served as the basis for recommendations to the Army for directions to take in the development of helicopter weapon systems.

EQUIPMENT DESCRIPTION

SADDLE/BAIL LUG SPECIFICATIONS

The detailed definition of the saddle type lug is controlled by NATO Standardization Agreement (STANAG) 3727, entitled "Saddle Lugs for the Suepension of Airborne Stores." An envelope drawing

of the STANAG 3727 - Saddle Lug for Stores in the 1000-Lb Weight Class is seen in Figure 1. It is noted that a lower profile 1000-lb capacity saddle lug for helicopter application, was at the time proposed for inclusion in STANAG 3727. Of the four saddle type lug racks tested, three conformed to the STANAG 3727 configuration and one with the proposed STANAG 3727 helicopter configuration. NATO aircraft utilizing the saddle type lug system are the MRCA, LYNX, WASP, WESSEX, NIMROD and SEA KING. NATO countries that have ratified STANAG 3727 are Belgium, Canada, Denmark, the Federal Republic of Germany, Netherlands, Norway, Portugal, Turkey, and the United Kingdom. Countries not ratifying STANAG 3727 are France and the United States.

The detailed definition of the bail type lug is controlled by MS-3314, entitled "Lug, Bomb 1000 Pound Class." An envelope drawing of the MS-3314 lug is seen in Figure 2. One of the five racks tested was compatible with the bail type lug but required nonstandard precision tolerancing to meet the LWL ROC boresight requirement. The bail type lug is utilized in all United States store suspension applications.

SADDLE/BAIL LUG OPERATION

The saddle and bail type lugs can be physically installed in any store having threaded lug wells conforming to STANAG 3441 or MIL-A-8591E. The bail type lug is used in conjunction with external swaybracing whereas the saddle type lug accommodates internal swaybracing at a standard surface. Figure 3 shows a schematic representation of a typical load distribution due to store side loads for the two lug concepts. Vertical loads are carried as tension in the lug threads for both concepts. Side loads in the bail type lug configuration are reacted by tension forces in the lug threads and compressive forces in the sway-brace pads. The saddle type lug reacts side loads by tension in the threads and compression on one leg of the saddle. It may be generalized that the saddle type lug system is a more efficient aerodynamic installation in that it does not require external swaybracing.

BOMB RACK OPERATION

The saddle type lug racks use a pair of hooks with nibs or spigots that engage the recesses in the standard saddle and two pairs of chocking wedges to automatically swaybrace and take up clearance between the lugs and rack. Vertical store alignment is achieved through a common bearing plane provided by the saddle's common, rigid mounting surface. Horizontal store alignment is maintained by close toleranced fit between spigots and lugs. The rack hooks and chocking wedges are coupled and manually operated at one point. Refer to Figure 4 for rack principles of operation.
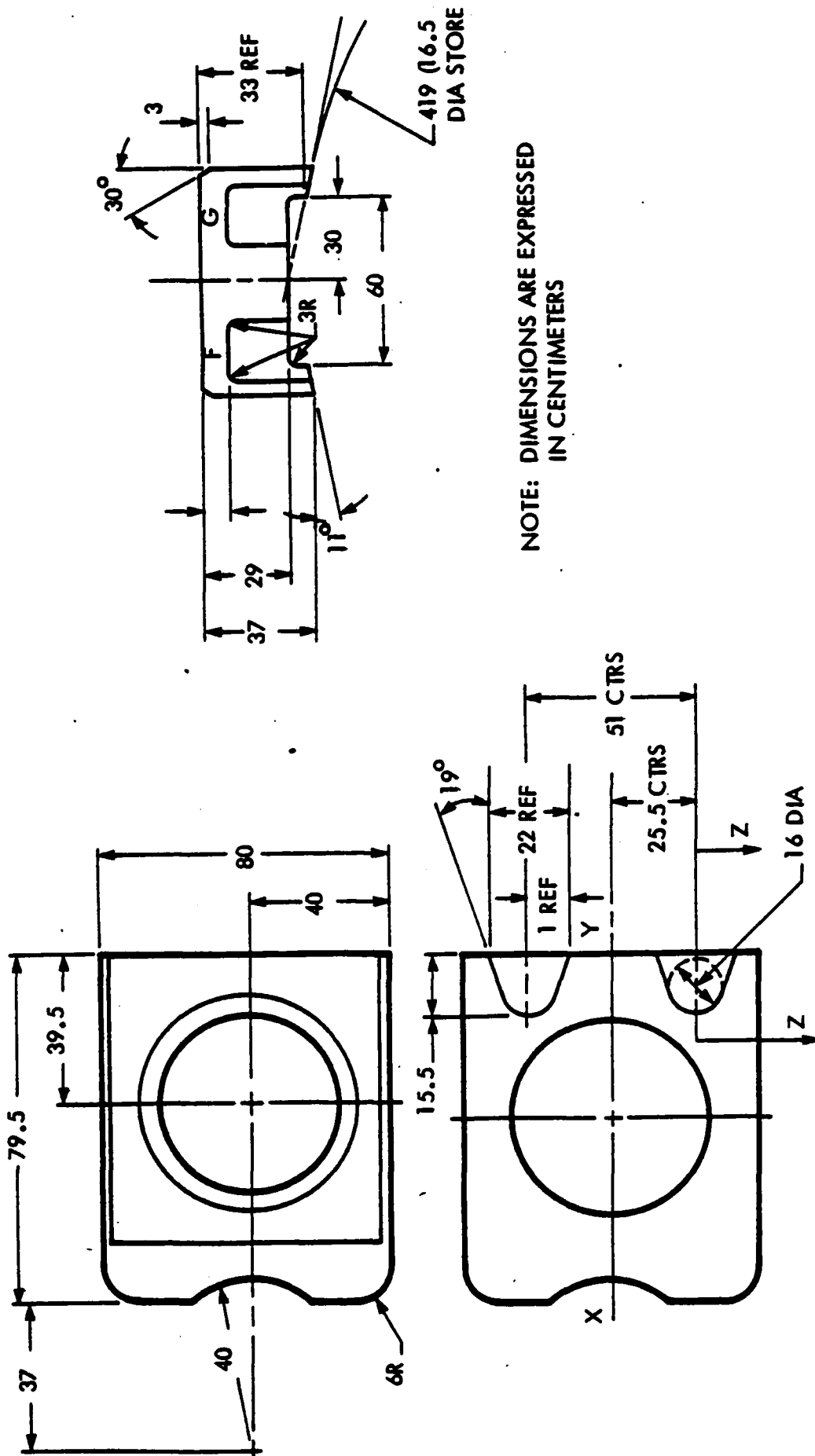
NOTE: DIMENSIONS ARE EXPRESSED
IN CENTIMETERS

Figure 1 SADDLE LUG FOR 1000 LB CLASS STORES

THREAD 1.750 12 UN 3A A PITCH DIA

0.72 +0.03 -0.00

0.620 + 0.030 R

0.12 RAD MIN TYP

0.48 MIN FLAT

2.375 MIN

0.062 x 60°

C

C

0.14 MIN FLAT

0.25

RAD 1.012 +0.030 -0.000

0.250 RAD

SECTION CC

5°

1.000 MIN 1.102 MAX

125

1.00 +0.03 -0.00

58° +2° -

UPPER SURFACE OF STORE (REFERENCE)
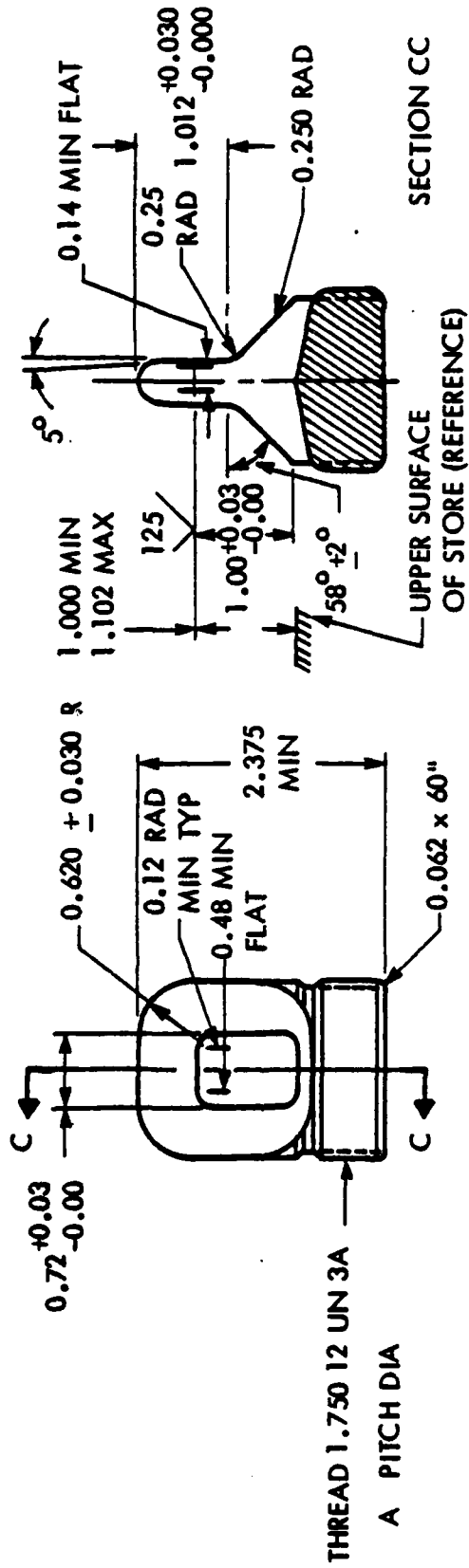
NOTE: DIMENSIONS ARE EXPRESSED IN INCHES

Figure 2 BAIL LUG FOR 1000 LB CLASS STORES
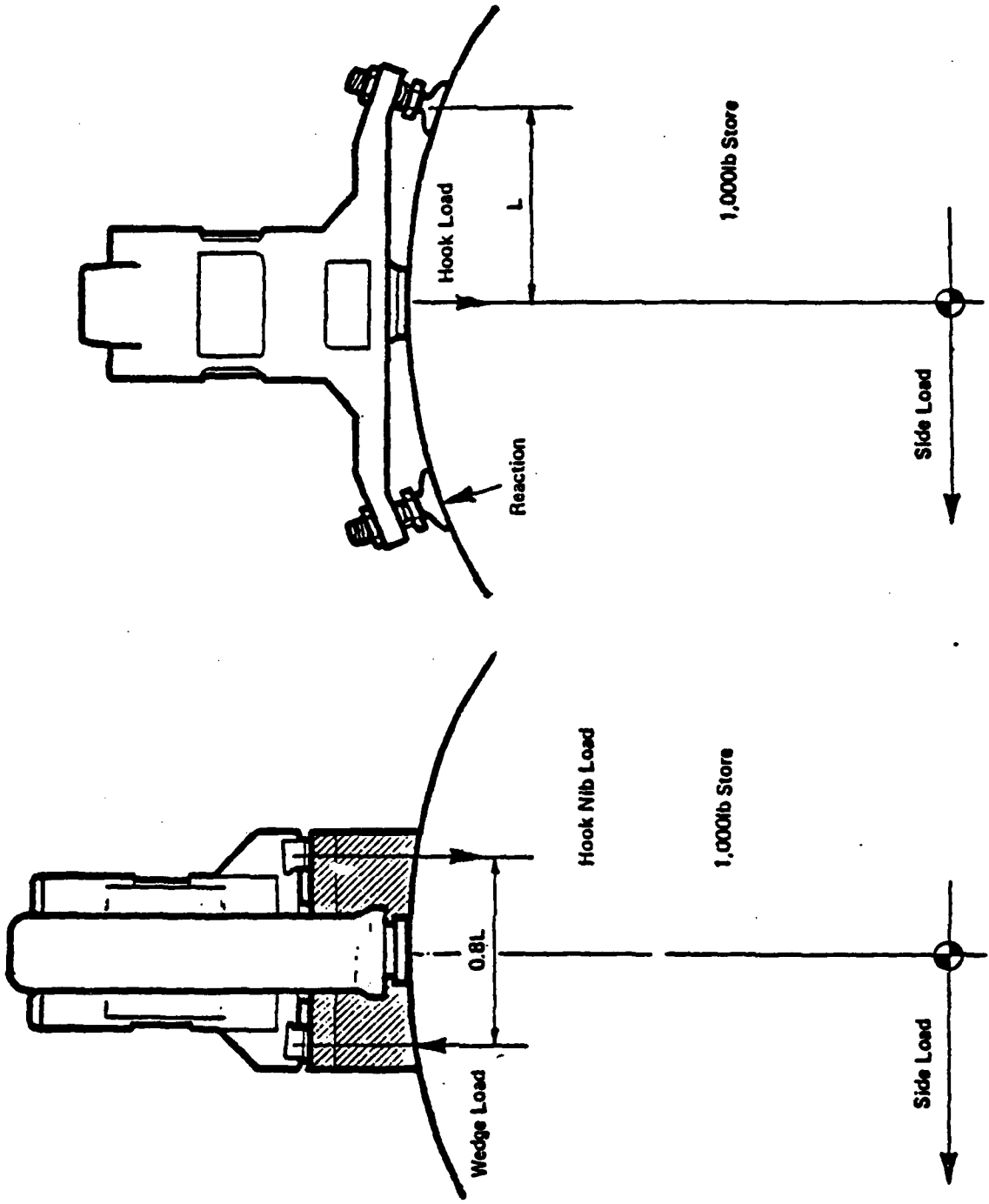
Figure 3   APPLIED LOAD RESULTING FROM A SIDE LOAD
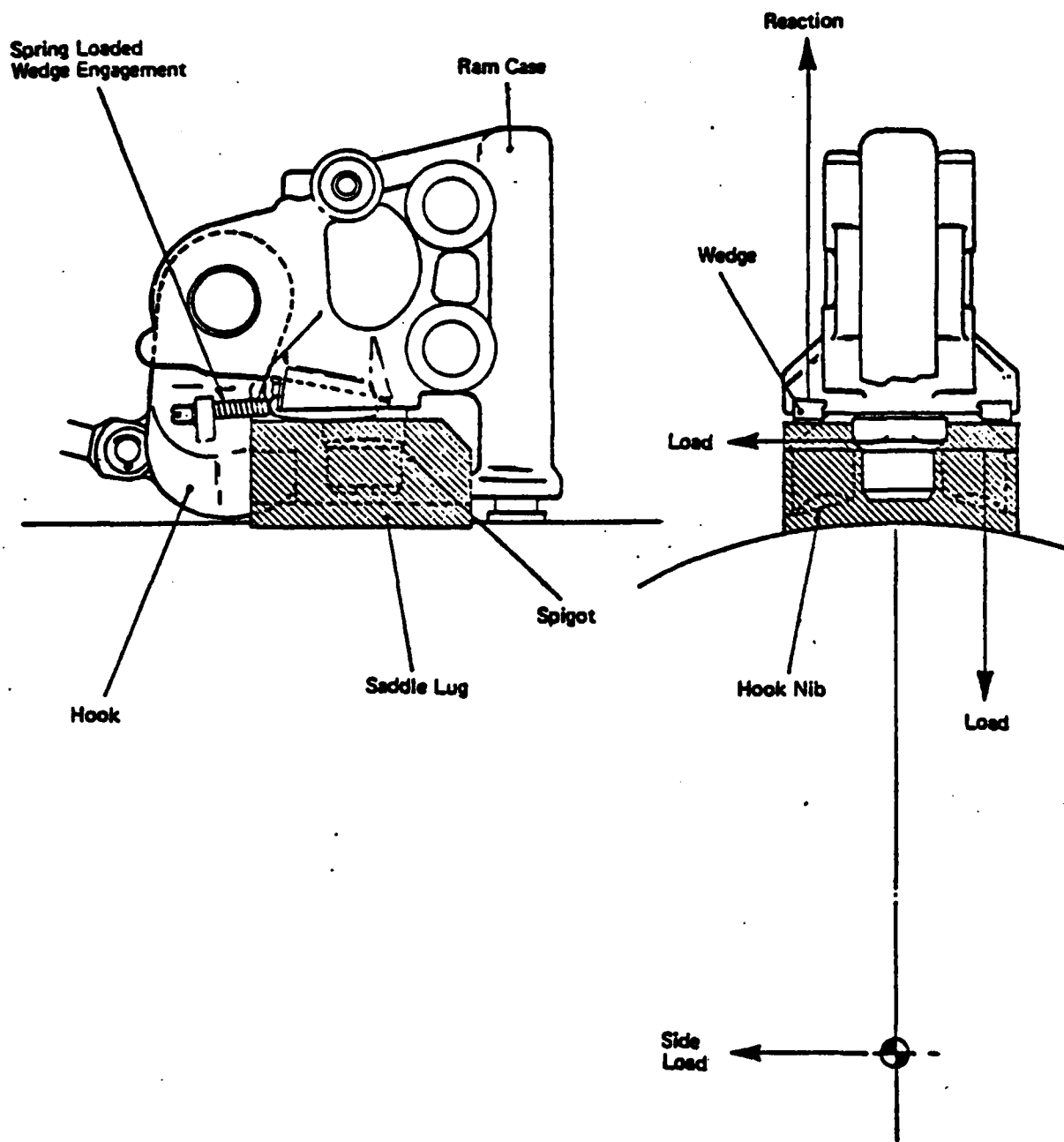
Figure 4   SADDLE TYPE LUG RACK - PRINCIPLE OF OPERATION

621

The bail type rack uses a pair of hooks and self-adjusting sway-braces to engage and restrain the specially design store. The swaybraces are automatically engaged when the independent/self-latching store hooks are engaged. Vertical store alignment is achieved through a common bearing plane provided by a matched set of special lugs threaded and welded to the store lug well. Horizontal store alignment is maintained by closed toleranced fit between specially machined lugs and the rack cheek plates. Refer to Figure 5 for rack principles of operation.

LABORATORY TEST PROGRAM

TEST OVERVIEW

To properly approach the development of the Army's bomb rack design specification, NAVAIRDEVCEN required rack performance data applicable to the helicopter service environment. Due to the recent developments in lightweight, high-strength bomb racks using both saddle lug and bail lug store suspension systems, the Dayton T. Brown Inc. Test Laboratory was approached to evaluate these state-of-the-art developments in light of the Army requirements. The results of this evaluation would help to answer a number of questions:

- Is current technology capable of meeting the Army requirements for boresight stability, rapid in-field servicing, ease of maintenance and commonality?

- What direction should the design take to meet the requirements based upon the approaches already taken by current manufacturers? and

- Based upon the "hands-on" experience, what features would be desirable in the rack from a field operators point of view?

To aid NAVAIRDEVCEN in answering these questions, a test program was developed with Dayton T. Brown Inc. to simulate helicopter environments in which five selected bomb racks could be evaluated with respect to the Army requirements.

PREPARATIONS

Given the variety of tests (shock, vibration, overload and environmental) and fixtures which would be required in the program outlined, a fixture system was devised to give each bomb rack a common frame of reference in which to measure the motion of a store suspended by the bomb rack. The system was composed of the following elements (see Figure 6):
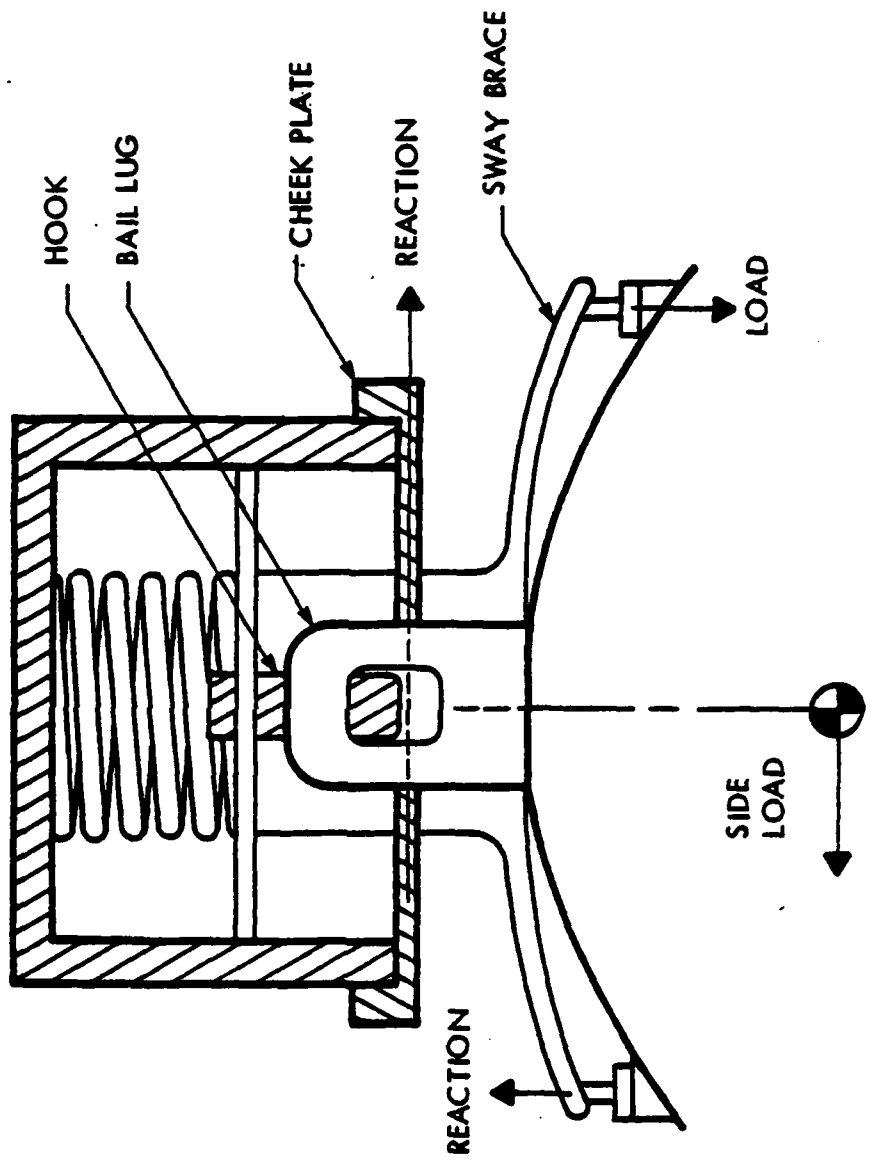
Figure 5 BAIL TYPE LUG RACK - PRINCIPLE OF OPERATION
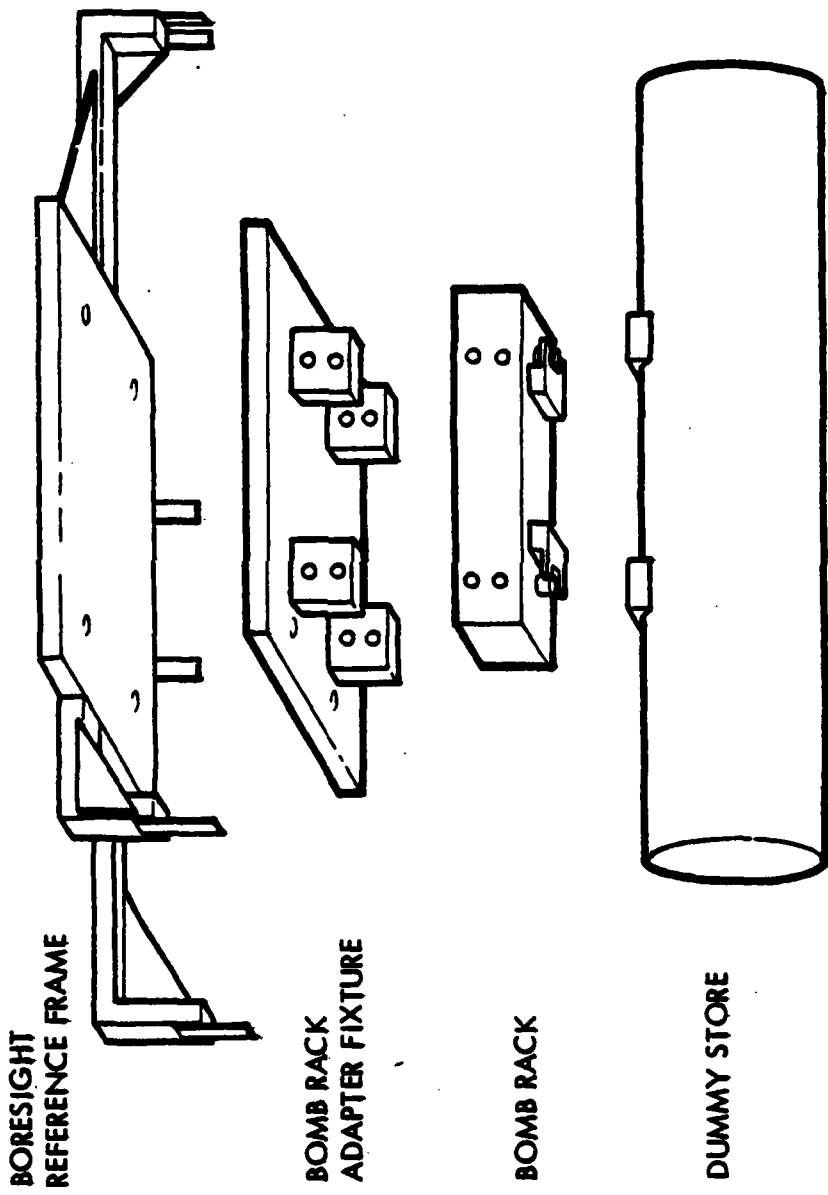
BORESIGHT
REFERENCE FRAME

BOMB RACK
ADAPTER FIXTURE

BOMB RACK

DUMMY STORE

Figure 6   TYPICAL TEST ASSEMBLY FOR BORESIGHT MEASUREMENTS

624

- The bomb rack, mated to a rigid, plate-metal structure giving each rack a common hole pattern for further mounting.

- An external framework of reference measuring surfaces. To this framework all of the racks could be mated. This framework was considered rigid and a valid frame of reference in that, under static conditions, the positions of one reference point on the frame would remain constant relative to any other point of reference on the frame. Measurements would not be made with the system dynamically excited.

- A common store with reference surfaces to which measure ments were made. (The four racks representing the saddle lug system used a common 500 pound dummy store with saddle lugs replacing the bail lugs. The rack representing the bail lug store suspension system uti- lized a 600 pound store with welded in bail lugs and machined sway-brace pads provided by the manufacturer).

It was assumed and verified throughout the tests that motion of the bomb rack in its mated frame was negligible and motion of the rack relative to the external reference framework was like- wise negligible. All motion measured was motion of the dummy store relative to the bomb rack and this data could be compared from rack to rack.

Linear motions measured were resolved into linear and angular components. It was recognized that motions of the store along the three primary axes and store roll would not affect boresight- ing. Store pitch and store yaw were the motion components which determined if the rack could hold the store to the Army require- ments.

To put the Army boresight requirement into perspective, an angular displacement in pitch or yaw of ± 1 milliradian (.001 radian) corresponds to a target size of 1 square meter (3.28 ft on a side) at 500 m (547 yds) and at 6 km (6564 yds) the target would measure 12 m (39.36 ft) on a side (see Figure 7). Motion of the store relative to the rack should not cause an error in arms delivery in excess of these values.

TEST ITEMS

The following bomb racks were selected for evaluation based on availability and advertised capability to meet LWL ROC perform- ance requirements:
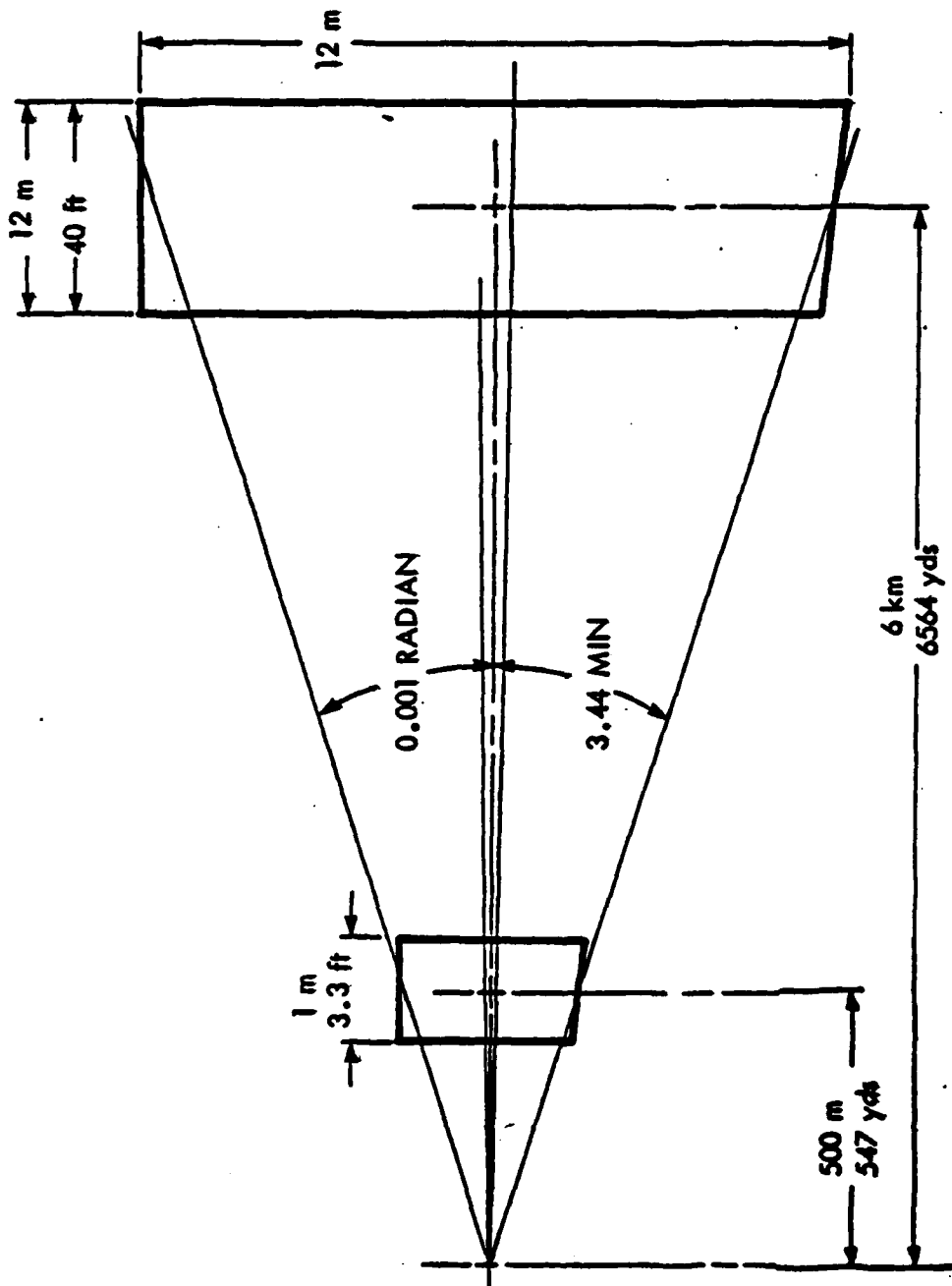
Figure 7 ARMY BORESIGHT REQUIREMENTS

ALKAN - TYPE 220B RELEASE UNIT

- Electro-mechanical gravity release unit; saddle lugs

M. L. AVIATION - ERU 123

- Dual gas cartridge ejector rack; saddle lugs

HUNTING HIVOLT - EMRU NO. 22 MK-1

- Electro-mechanical gravity release unit; saddle lugs

WESTLAND/FRAZER-NASH - ERU

- Dual gas cartridge ejector rack; saddle lugs

EDO CORP. - 14 INCH LIGHTWEIGHT EJECTOR UNIT

- Dual gas cartridge ejector rack; bail lugs

Since most of these racks were developed for fixed-wing aircraft application, they were noted to be too heavy for immediate helicopter application and also exhibited features not required by LWL ROC.

TESTS

The following tests were conducted with each rack:

Manual Load and Release (Ambient Temperature)

Each rack was loaded and released repeatedly and evaluated for operation and boresight repeatability. Efforts were made to simulate rough and hurried ground handling.

Load and Release (Extreme Temperatures)

The above tests were repeated with the racks' temperature stabilized at either -54°C (-65°F) or 65°C (150°F).

Static Overload

Following initial measurements, static loads were simultaneously applied to the C.G. of the dummy store mounted to each rack, in accordance with MIL-A-8591E (Figure 10).

Final store position was measured after the loads were released.

Shock

Shock loads in accordance with MIL-A-8591E (Figure 10) were applied to each rack with store position measured prior to and following each shock.

Sand and Dust

Each unloaded rack was exposed to a sand and dust environment for six hours. Without cleaning, each rack was then loaded with the dummy store and evaluated for operation and boresight repeatability..

Icing

Each unloaded rack was iced at -54°C (-65°F) then repeatedly loaded and released.

This test was repeated with the rack loaded with the dummy store when iced.

Shim Test

1.5 cm (0.060 inch) shims (a randomly selected dimension) were placed in combinations under the chocking wedges or swaybraces of the racks. The effects of a known interference at these critical locations was studied.

Vibration

Each rack was vibrated in accordance with the requirements for helicopter equipment of MIL-T-7743E (loaded and unloaded). Boresight measurements were made throughout the test period especially following resonant dwells.

In addition, each rack was loaded while being vibrated vertically at 11 Hz at 1/2 g, simulating re-armament of an operating helicopter. Boresight repeatability was determined.

TEST RESULTS AND OBSERVATIONS

Boresight Retention and Repeatability

Based upon the repeated data taken under the various helicopter environments, it was concluded that present technology is capable of producing a bomb rack with boresight retention properties meeting the LWL ROC. As a point of interest, two racks with conventional bail lugs and swaybracing (an AH-IJ rack and an AERO 7) were tested for boresight repeatability in the test fixtures. Neither rack could repeat its original boresight configuration or approach the Army boresight requirement.

Operation

From a field operator's point of view, a number of observations were made:

- Manual release of the electro-mechanical release units imparted no direct force to the internal linkage. In case of jamming, forcing the hooks open required improvisation of tools to develop leverage;

- Confirmation of a secure loading of the store varied from rack to rack between audibles, visual indications, safety pins and luck;

- The post holes of the saddle lugs tended to collect ice or dirt which would interfere with loading;

- Internal access and required maintenance was often impaired by requiring specialized tools and working with complex linkaging with springs and cables;

- Of the racks tested, only the rack with bail lugs was provided with automatic latching of the hooks when loaded.

Saddle Lugs

- The springs downloading the chocking wedges often seemed to be too light;

- The chocking wedges tended to freeze into one position when iced and were rendered ineffective for swaybracing (they could be loosened upon impact);

- The chocking wedges moved into position when the hooks were closed but operated independently of each other;

- The saddle lug was adaptable to any store using bail lugs and, as the geometry of the lugs alone determined interfacing dimensions, boresight repeatability from store to store was assured.

Bail Lugs

- When the positive locking mechanism holding the sway-braces in position jammed or froze, there was no rapid access to loosen it, rendering the rack incapable of being reloaded or of moving the swaybraces;

629

- The swaybraces were independent fore and aft, locked immediately upon loading and did not interfere with store release. Recocking was required prior to reloading;

- Repeatable boresighting from store to store depends upon maintaining tight dimensional tolerances between the load bearing surface of a threaded bail lug and the swaybrace pads on each individual store. Boresight repeatability with currently available stores and this variable geometry could not be easily assured.

RECOMMENDATIONS

Based upon these tests, the following recommendations were offered by Dayton T. Brown Inc. as representing desirable characteristics for incorporation in a future Army helicopter weapon system:

a. Minimum Area Crutchless Ejector Support System (Saddle Lugs) - This system can provide boresight repeatability within the specified requirements without incurring the costs of specialized manufacturing processes required of stores utilizing bail lugs.

   The size of the supporting strongback is also minimized by elimination of outboard swaybrace pads.

b. Independent, Spring Loaded Swaybrace Wedges - To maintain four point contact on the saddle lug surfaces. The wedges should engage as the hooks move to close and not restrain the linkage when the hooks are opened.

c. Lock Indicators - A positive physical feedback, flags and safety pin clearance; an audible.

d. Manual Release - Must introduce a driving force directly to the release linkage. The release torque should be independent of the load on the hooks.

e. Operation Based on a Single, Multi-function Tool - All operations of the rack must be deliberate by the operator. For example, the safety pin must be removed and used as the tool to manually release the back.

f. Ease of Maintenance - Access to the linkage and wiring should not required complete disassembly when trouble-shooting nor should specialized tools be required for disassembly.

REVIEW OF REPORTS

Experience in present weapon systems provided further information on the advantages and disadvantages of the bail lug store suspension system. Due to the relatively recent development of the saddle lug system, reference (a) and (b) were reviewed for additional data. A compendium of system advantages and disadvantages based on the review follows:

Advantages

a. The lug can be installed on any store having threaded lug walls conforming to STANAG 3441 or MIL-A-8591E;

b. The system eliminates the requirement for external swaybraces; thus reducing overall aerodynamic drag, eliminating manual swaybrace adjustment and decreasing store loading time;

c. The system improves store alignment accuracy upon loading and inflight.

d. The lug provides adequate strength to meet MIL-A-8591E requirements for 1000-pound class stores, and

e. The system provides increased store rigidity in-flight, thus reducing store misalignment approximately 20% from bail type lug racks.

Disadvantages

a. Lug installation in the store requires a special tool and alignment fixture;

b. The lug is larger and heavier than bail type lug;

c. The lug is approximately four times more expensive than bail type lugs; and

d. The system is not directly compatible with existing U.S. bomb racks.

The above data was utilized during the system evaluation phase of this program.

CONCLUSIONS AND RECOMMENDATIONS

CONCLUSIONS

The following conclusions were formulated based upon the laboratory test results and the review of references (a) and (b):

a. Maintaining repeatable ± 1.0 milliradian boresight at the store/rack interface and rapid store rearming is within the current technology of bomb racks.

b. In-service bomb racks, all having manual swaybrace adjustment, cannot meet the boresight and rapid rearming requirements.

c. Bomb racks exhibiting boresight and rapid rearming capability do not adversely affect overall system maintenance or operation.

d. Although certain desirable bomb rack features were identified during testing, a detailed bomb rack design specification should be prepared prior to RFP solicitation. This specification would optimize all desirable features and preclude known problem areas.

RECOMMENDATIONS

To technically assess the bomb rack design approach for Army weapon system application, a list of critical system factors is identified in Figure 8. These factors were prioritized and weighted, based on relative importance and system impact. Figure 9 presents a decision analysis comparing manual bail, automatic bail and saddle type lug racks to the prioritized factors. Comparison of racks to factors was based on data contained herein and qualitative assessments based on experience in weapon systems. The manual bail type rack was eliminated from consideration due to its inability to meet boresight requirements. Based on its ability to currently meet the decision factors with 79% effectivity, the saddle type lug rack is recommended for Army weapon system development with special regard to the LWL ROC for helicopter use.

DECISION FACTORS   WTS

- ± 1 MILLIRADIAN BORESIGHT RETENTION   8

- LUG LOGISTICS IMPACT   7

- ADAPTABILITY TO U.S./NATO STORES   7

- RACK WEIGHT   6

- LAUNCHER LOGISTICS IMPACT   6

- IMPACT OF BORESIGHT TECHNIQUE ON STORE PRODUCTION COST   4

- INTEGRATED BORESIGHT ADJUSTMENT   3

- IN-SERVICE RACK QUALIFICATION   1

- AUTOMATIC STORE LATCHING   1

Figure 8   SADDLE/BAIL LUGGED RACK PRIORITIES

633

EVALUATE BY COMPARISON — Criteria:

1. +1 MILLIRADIAN BORESIGHT RETENTION
2. INTEGRATED BORESIGHT ADJUSTMENT
3. RACK WEIGHT
4. IMPACT OF BORESIGHT TECHNIQUE ON STORE PRODUCTION
5. LUG LOGISTICS IMPACT COST
6. IN-SERVICE RACK QUALIFICATION
7. ADAPTABILITY TO U.S./NATO STORES
8. LAUNCHER LOGISTICS IMPACT
9. AUTOMATIC STORE LATCHING

CREATIVE IDEAS	1	2	3	4	5	6	7	8	9	TOTAL	FINAL ACTION
WEIGHING FACTORS	8	3	6	4	7	1	7	6	1	43	
1. MANUAL BAIL TYPE LUG RACK	0										ELIM FROM CONSIDERATION
2. AUTOMATIC BAIL TYPE LUG RACK	8 / 64	1 / 3	4 / 24	2 / 8	4 / 28	0 / 0	10 / 70	2 / 12	10 / 10	219 (51%)	
3. SADDLE TYPE LUG RACK	10 / 80	8 / 24	6 / 36	9 / 36	4 / 28	10 / 10	10 / 70	9 / 54	0 / 0	338 (79%)	RECOMMEND FOR DEVELOPMENT

Figure 9   RACK DECISION MATRIX

REFERENCES

(a) AFATL-TR-76-49, "Comparative Ground Test and Analysis of the Saddle Lug, Bail Lug and Tee Lug Suspension Concepts of Weapon System", May 1976

(b) DTB02R76-0516, "Suspension Saddle and the Alkan 220 Release Unit, Special Investigation of", NAVAIRSYSCOM sponsored, 18 May 1976

(c) NADC-76354-30, "Test Comparison of the Saddle Lug and Bail Lug Store Suspension and Release Systems", 15 April 1977

(d) Hiscock, B. "The Development of a Compact High Strength Ejector Release Unit for MRCA", Proceedings of the 3rd Bi-Annual Aircraft/Stores Compatibility Symposium, 1975

(e) Hasquenoph, Jean H. "Advantages and Possible Developments of Release and Ejector Units Using the Saddle Suspension System", Proceedings of the 3rd Bi-Annual Aircraft/Stores Compatibility Symposium, 1975

(f) STANAG No. 3727; MS-3314, STANAG 3441; MIL-A-8591E; MIL-T-7743E.

AUTOBIOGRAPHY

DENNIS R. McGIVERN

Mr. McGivern received his Bachelor's Degree in Aeronautical
Engineering from Rensselaer Polytechnic Institute in 1974. He
was first employed with Grumman Aerospace Corporation as a test
engineer in a low speed wind tunnel facility and was involved
in programs with V/STOL aircraft and high lift induction on
performance aircraft. ·

During the course of this program he was employed as a Project
Engineer with Dayton T. Brown, Inc. and was responsible for
evaluation and testing of mechanical armament equipment and
was involved in special evaluation programs for the U.S. Navy
and the Air Force.

Mr. McGivern is currently employed at the Honeywell Radiation
Center, Lexington, Massachusetts, as a Development Engineer
with the Engineering Design and Analysis group, and he is a
member of the American Society for Non-Destructive Testing.

AUTOBIOGRAPHY

THOMAS E. MILHOUS

Mr. T. E. Milhous received his B.S. degree in Mechanical Engin-
eering from Widener College in 1968. Upon graduation, he joined
the Naval Ordinance Laboratory under the work-study program and
received his M.S. degree in Mechanical Engineering from the
University of Maryland in 1971. His work assignments at NOL
included environmental testing of conventional weapon fuzing
systems and Navy membership on JTCG Working Party for Fuzes.
For the past six years he has been employed by the Weapon Sus-
pension Design Branch at the Naval Air Development Center. At
NADC, areas of responsibility have included system and subsystem
research and development of suspension equipment, program manage-
ment of aircraft armament systems, and committee memberships
as follows:

    a. JTCG/MD Working Party for Racks and Ejection Cartridges
       - Principal Navy member;

    b. JTCG/MD Working Party for Aircraft/Stores Compatibility
       - Chairman, Armament Systems Study Group;

THOMAS E. MILHOUS

c. NATO Air Armament Working Party - Navy technical
    representative;

d. ASCC Conventional Aircraft Armament Working Party -
    Navy representative.

Mr. Milhous is a member of the Tau Beta Pi engineering society.

AUTOBIOGRAPHY

ROBERT V. FRANK

Mr. Frank received his B.S. degree in Industrial Engineering from
the University of Missouri in 1968 and has worked for AVSCOM
(Army Aviation Systems Command) now for nine years. For five
years he was responsible for product improvement, component quali-
fication and integration of special mission systems for Southeast
Asia for the UH-1 engineering office. For the past four years
he has been responsible for development and integration of 2.75
inch rocket components and external store carriage systems.

Mr. Frank has been the Army representative to NATO and ASCC for
aircraft armament for three years and he is the former chairman
of the JTCG Working Party for racks and ejection cartridges.

Mr. Frank is the recipient of an Army Commendation in 1974 for
his work in aircraft weaponization and is the author of six
international standardization agreements for helicopter weaponi-
zation and a member of the American Defense Preparedness Associa-
tion.

IMPULSE CARTRIDGES AS THE POWER SOURCE FOR STORES SEPARATION EQUIPMENT
(Article UNCLASSIFIED)

by

William P. Peck
Naval Ordnance Station
Indian Head, Maryland

ABSTRACT: (U) The first stores separation impulse cartridges were developed in the early 1940's for Navy use and were designated as Mk 1 and Mk 2. In spite of their early development, the basic designs have remained in the cartridge inventory. Other improved impulse cartridges for conventional Navy stores applications which have joined the inventory include the second generation Mk 8, Mk 9, and Mk 10 and third generation Mk 124 and Mk 125. The Air Force over the same time period introduced into service the ARD 446 and ARD 863 impulse cartridges for their applications.

The basic requirements for impulse cartridges for stores ejection use are not only a suitable pressure-time power cycle, but include specific electrical ignition and safety characteristics, low exhaust residue/contamination, and low unit cost with high volume producibility. A tri-service family of cartridges, used interchangeably between Navy and Air Force, is being pursued in a CCU-43, CCU-44, and CCU-45 series of cartridges.

Future stores separation ejectors will require a higher degree of cleanliness, exposure/functioning in higher temperature environments, and higher levels of RADHAZ protection. New materials, propellants, ignition elements, and exhaust product encapsulation are under investigation to provide cartridges which will meet these requirements.

639

x

LIST OF ILLUSTRATIONS

LIST OF TABLES

A BRIEF HISTORY

A stores separation impulse cartridge is typically an electrically ignited solid propellant cartridge designed to produce high ballistic gas power for a short duration. The theoretical energy of propellants used in such cartridges is in the neighborhood of 400,000 foot-pounds per pound of propellant and this energy is packaged in a compact cartridge envelope. For this reason, the cartridge has remained popular as a power source for stores separation equipment. Cartridges which have been developed over the past years for the majority of conventional stores ejection equipment are shown in Figure 1.

FIGURE 1. IMPULSE CARTRIDGES FOR STORES SEPARATION

The first use of impulse cartridges began in the 1940's when it became apparent that a forceful ejection from high-speed aircraft was necessary. Air turbulence exists near the body and wings of aircraft, and stores must be forcibly ejected through the turbulence for clean and safe separation from the aircraft. The consequences of an ineffective ejection are store tumbling, random motion, and possible impact with the aircraft.

The first ejection device used was the Aero 1A bomb rack (Figure 2). The Mk 1 cartridge was designed to power the bomb rack and was developed from an engine starting cartridge design used at that time. Later, a Mk 2 cartridge of similar design was developed with less power to be used with lighter stores weights.
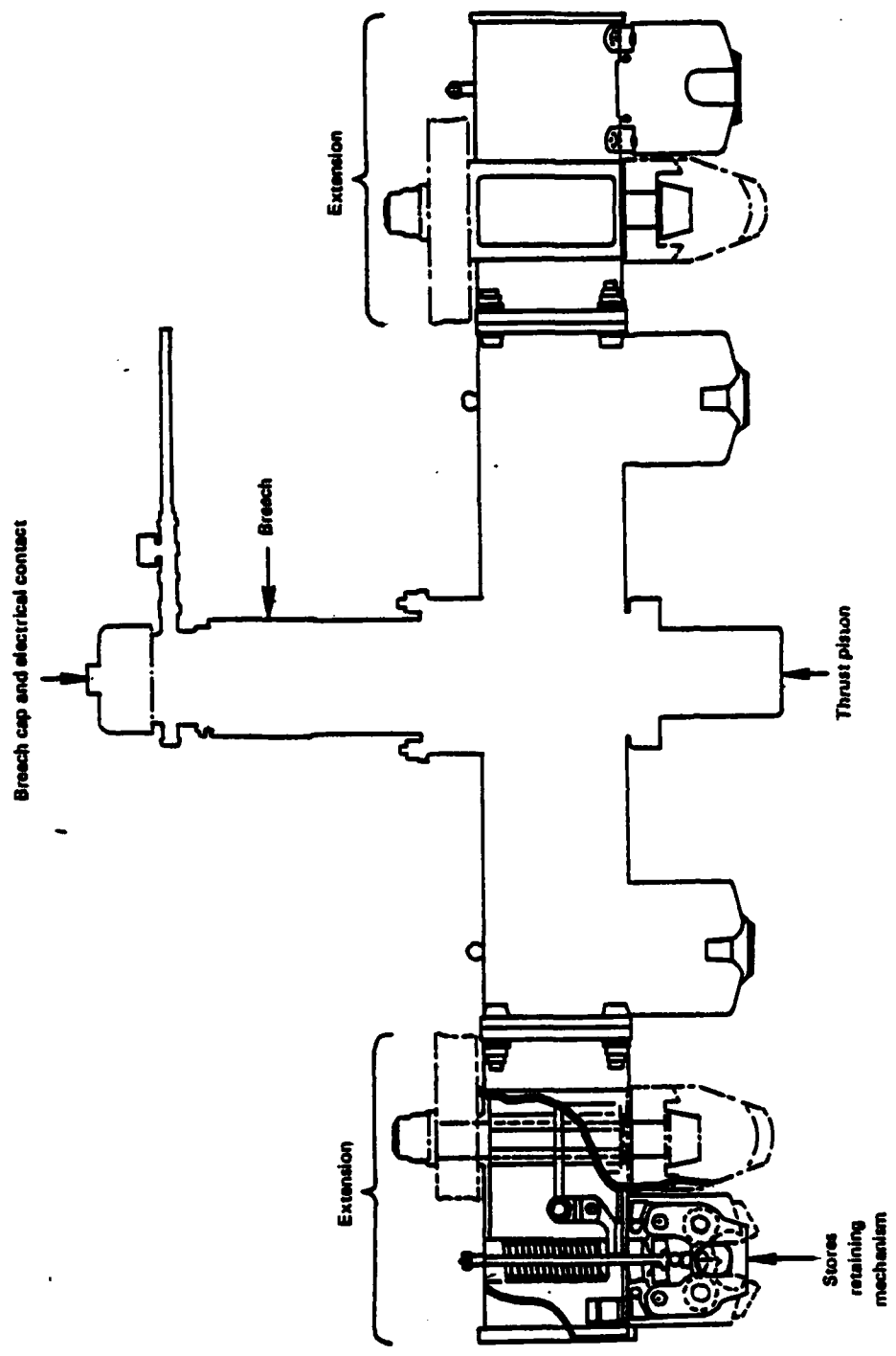
Breech cap and electrical contact

Breech

Thrust piston

Extension

Extension

Stores retaining mechanism

FIGURE 2. AERO 1A BOMB RACK

Since the 1940's and the development of the Mk 1 and Mk 2 cartridges, the number of stores separation applications has increased and new requirements have evolved. Additional cartridges have been added to fleet use to meet the new requirements. The history of this development is illustrated in Figure 3. The ARD 446 cartridge was developed in 1956 for Air Force use. Improved cleanliness was obtained by eliminating the black powder used in the Mk 1 and Mk 2 designs. The ballistic power performance profile was changed to obtain higher efficiency by substituting a progressive burning grain design in place of the solid grains previously used; also, improved resistance to various environments (altitude, moisture, and temperature) was obtained by cartridge case design modifications. Soon after a smaller version, designated as ARD 863, was developed with a lower power level to provide greater flexibility of stores ejectors performance.
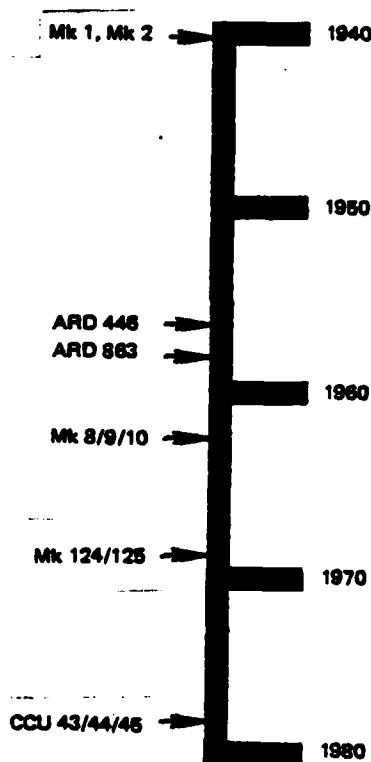

FIGURE 3. CARTRIDGE
DEVELOPMENT HISTORY

In the early 1960's the Navy developed another series of cartridges with the designations Mk 8, Mk 9, and Mk 10. Design work was conducted to improve temperature and humidity resistance of the cartridge and to provide a cleaner burning cartridge. The Navy has continued work to improve the impulse cartridge

design and, in the late 1960's, developed a Mk 124 and a Mk 125 cartridge. The design objectives included a 1-amp/1-watt no-fire requirement for 5 minutes to minimize the hazards of electromagnetic radiation (radar induced currents). Attempts to obtain cleaner burning characteristics were made to reduce maintenance requirements. Physical interchangeability with existing stores cartridges and comparable performance were also goals. These impulse cartridges represent the current "work horse" for Navy and Air Force conventional stores ejection applications. The average use rate of these cartridges over the past 3 years is given in Table I; as indicated, some of these designs have very high use rates.

Table I

3-YEAR (1974-1976) AVERAGE USE RATE

Cartridge	Quantity used/year	Comments
Mk 1	300	Hose guillotine only
Mk 2	–	See Mk 125
ARD 446	21,500	
ARD 863	460,800	
Mk 8	0	
Mk 9	2,500	Standard ARM launcher
Mk 10	0	
Mk 124	125,000	
Mk 125	980,000	The Mk 2 has replaced the Mk 125 in some applications; this is the combined use rate of both cartridges.

There are some special purpose impulse cartridges developed for limited applications because of unique requirements. A series of high temperature cartridges suitable for exposure to 325° F for limited duration was developed by Frankford Arsenal. These are designated as the CCU-1/B, CCU-9, and CCU-10 cartridges. The CCU-1/B is in use for special ordnance applications while the CCU-9 and CCU-10 have not been utilized because of the high cost of such a design and the need being demonstrated in only one application. All of the cartridges are of a center pole electrode, case grounded configuration.

Another stores cartridge utilized in a few Navy F-14 applications and in B-1 applications is the Mk 107. This cartridge has a multipin connector, a machined cartridge case, and a very high energy output of 20,000 foot-pounds.

The Navy has attempted to utilize the Mk 124 and Mk 125 cartridges as much as possible in order to reduce the number of different cartridges in fleet inventory; however, the Mk 124 and Mk 125 cartridges have shown some design deficiencies and system compatibility problems.

IGNITER INTEGRITY

The details of the Mk 124 and Mk 125 cartridge construction are illustrated in Figure 4. It is noted that the igniter unit rests on a narrow shoulder which must take all the forces generated by the internal pressures acting on the igniter as well as provide a gas seal. In some applications, the pressures approach 20,000 psi (JAU-1B initiator for sonobuoy deployment), and these high pressures have been found to cause gas leakage around the igniter components. Also the igniter retention ring stake around the top circumference of the igniter is another weak design area. In some instances, the electric contact in cartridge actuated devices has pushed against the igniter unit with sufficient force to fail the ring stake.
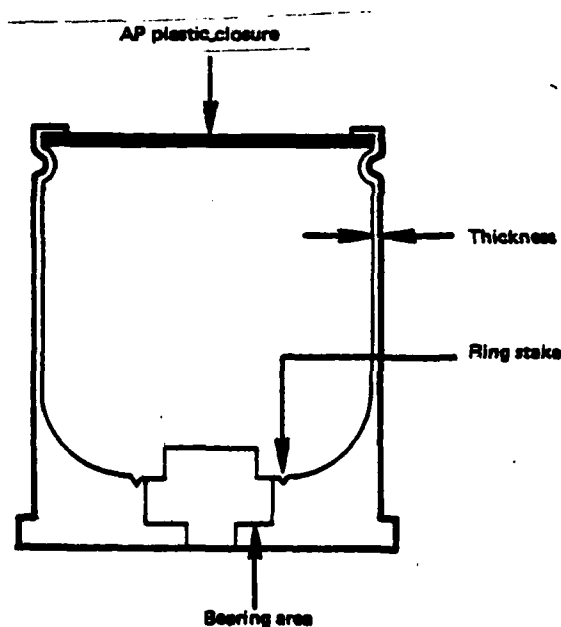

FIGURE 4.   MK 124/125 CARTRIDGES

CORROSION/EROSION

The closure disk material used on the Mk 124 and Mk 125 cartridges is a type of propellant made from a pressed mixture of ammonium perchlorate and plastic (methyl methacroylate). One of the products of combustion of this mixture is hydrochloric acid which readily initiates corrosion of any metal parts. The igniter, designated Mk 14, also contains compounds which generate hot and erosive particles upon combustion and produce effects of erosion on exposed metal parts. Proper selection of closure, propellant, and igniter materials can substantially reduce the required maintenance and provide higher utilization of available stores ejection equipment.

OPTIMUM PRESSURE CYCLE

The main charge propellant used in the Mk 124 and Mk 125 cartridges is a 7-perforated cylindrical shape which provides progressive burning. This provides an increasing operating pressure for good ballistic efficiency for ejecting heavy stores. Light stores, especially practice bombs, have evidenced release problems because such configurations require a fast initial pressure rise to unlatch the holding mechanism. Optimizing the ballistic cycle therefore should include the total pressure cycle with an initial fast pressure rise and a continuously increasing pressure thereafter.

CASE WALL

The Mk 124 and Mk 125 cartridge cases were designed with thin walls to facilitate sympathetic ignition of multiple cartridge configurations including applications where case wall blowthrough is required. However, the thin wall case was found to be a cause of case tearing during cartridge operation resulting in abrasive metal oxides and causing excessive wear and metal debris in the breech chambers. It was subsequently determined that such a thin walled cartridge was not required for sympathetic ignition.

CURRENT CARTRIDGE LIMITATIONS—AIR FORCE

The Air Force has used principally the ARD 446 and ARD 863 cartridges for stores ejection.

HIGH PRESSURE OPERATION

The igniter for the ARD 446 and ARD 863 cartridges is an externally pressed-in-place unit. Under high pressure operation, the igniter unit tends to be mechanically disengaged and to be forced out the rear of the cartridge. Possible results include hot gas leakage and burning of breech hardware.

TEMPERATURE AND HUMIDITY ENVIRONMENTS

The closure disk is made of nitrocellulose. Such a cartridge seal does not withstand extended temperature and humidity environments as required in 28-day temperature/humdity cycle testing. The temperature and humidity environment breaks the hermetic seal between the closure disk and cartridge case permitting moisture to enter the cartridge. The moisture will degrade cartridge performance.

ELECTROMAGNETIC RADIATION

Currently the ARD 446 and ARD 863 cartridges do not achieve a 1-amp/1-watt rating, which today is considered a minimum requirement for safety in radiation environments. The 1-amp/1-watt capability can be engineered into the design of an igniter by proper bridgewire construction and with a bridgewire ignition mixture containing the proper heat dissipation properties.

IMPROVING THE IMPULSE CARTRIDGE

The common need of the Navy and Air Force to eliminate deficiencies and upgrade performance of impulse cartridges, as well as to provide standardization for cross-service usage, has prompted interagency cooperation in a tri-service working agreement for product improvement. Cooperative efforts have resulted in a new cartridge series: the CCU-43, CCU-44, and CCU-45. Details of this cartridge are shown in Figure 5.
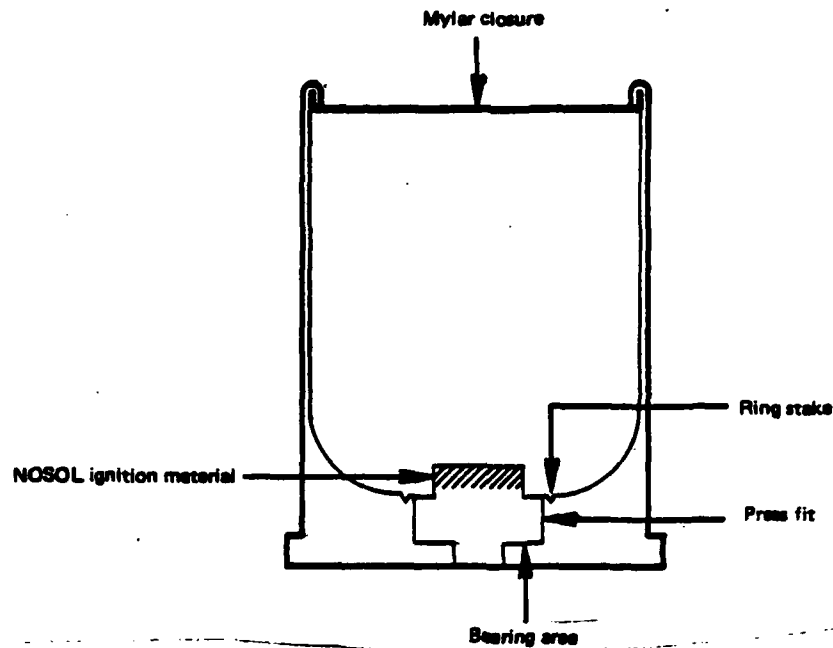
Mylar closure

Ring stake

NOSOL ignition material

Press fit

Bearing area

FIGURE 5. CCU-43/44/45 CARTRIDGES

CARTRIDGE CLOSURE MATERIAL

New materials were investigated to provide a cartridge end closure which will pass the standard 28-day temperature/humidity environment tests, will provide a hermetic seal, and will leave minimal residue after cartridge functioning. A Mylar plastic film, formed to a cup configuration and sealed in place under a case crimp joint, has been found to meet both the environmental exposure and minimal residue requirements.

IGNITER DESIGN

The case to igniter interface has proven to be a weak point in high pressure applications. A new igniter design has been developed and is being tested which incorporates a more substantial thrust bearing surface area as well as eliminates potential gas leakage by using glass-metal seal components and a self-sealing joint feature. The igniter/case joint press fit alone is designed to resist electrical contact forces in excess of 300 pounds. An additional case ring stake is used around the top of the igniter to provide a further safety margin.

The ignition chemicals also have been changed to eliminate acidic residues and erosive particles. The igniter booster charge is NOSOL-318 propellant formulation adapted from a gun propellant. NOSOL-318 propellant is very clean

648

burning with good thermal stability characteristics. The combustion products from the entire cartridge have been tested for acidity in aqueous solutions and a pH level of 8 has been measured, indicating that acid residues are not present in these improved cartridges.

CASE DESIGN

In order to obtain a standardized cartridge for Navy and Air Force use, a standard diameter cartridge of 1.075 ± 0.005 inches was selected. Navy breeches will require modifications in several applications to accomodate this cartridge. A straight bore breech dimension of 1.082 + 0.002, - 0.001, was selected and existing breeches were modified to this diameter, and substantial numbers of firings were performed at Dayton T. Brown test laboratories with the improved design CCU cartridges. No breech compatibility problems were experienced in this and other test series. Some minor adjustments were made as a result of these tests to alter the cartridge case wall thickness and crimp configuration for improved case integrity upon cartridge firing.

CARTRIDGE RESIDUE

Testing at Dayton T. Brown and at Indian Head with the improved cartridges, where residue collection was obtained, indicates substantial reductions in residue, particularly over the Mk 2 and Mk 124/125 cartridges, and to a lesser degree, the ARD 863/446 cartridge series. Rack functioning at Dayton T. Brown was accomplished with cleaning intervals in excess of 50 firings per test series.

FUTURE DEVELOPMENTS

New approaches to improving application of cartridge power to stores ejection equipment are being investigated. There remains a need to further reduce or eliminate cartridge residue for minimal maintenance of stores release equipment. Other improvements include igniter immunity to electromagnetic radiation and improved cartridge materials.

PLASTIC CASES

In an attempt to increase the cleanliness of cartridge operation, the formation of metal oxides can be avoided by replaing much of the metallic cartridge with plastic materials. An investigation of the use of polyethylene in impulse

cartridge construction, as shown in Figure 6, has been accomplished. A molded-in-place base and heat-sealed thin plastic closure are features which should make a "clean" cartridge design and should be cost-effective in mass production quantities. Numerous vendors exist in the plastics industry which would avoid the current limited sources of impact extruded aluminum cases.
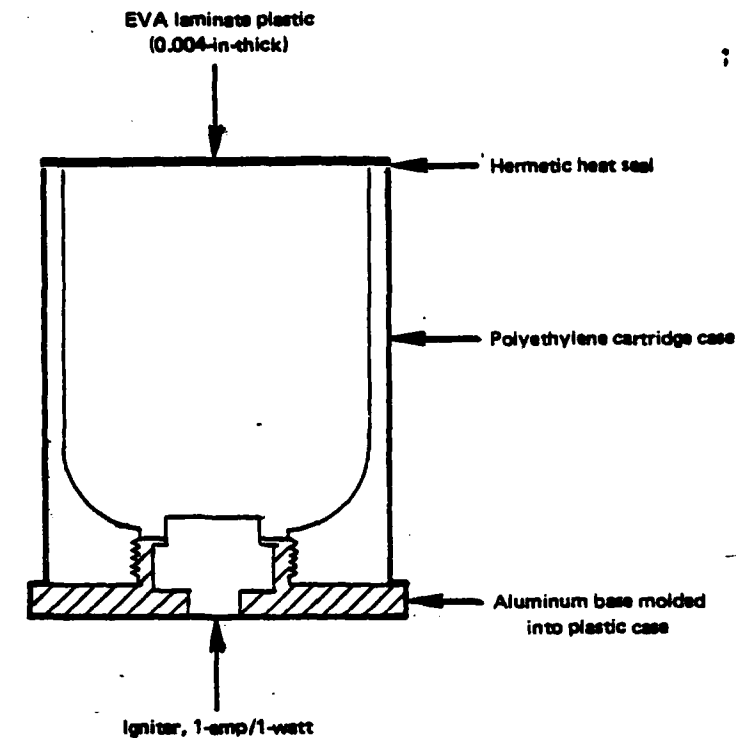
EVA laminate plastic
(0.004-in-thick)

Hermetic heat seal

Polyethylene cartridge case

Aluminum base molded
into plastic case

Igniter, 1-amp/1-watt

FIGURE 6. PLASTIC CARTRIDGE CASE

IGNITER DESIGN

New concepts for igniter designs which will address increased protection against electromagnetic radiation environments and more cost-effective designs are being pursued. One concept being investigated is a printed circuit which could be formed into a flat geometric shape (planar ignition element). Flexibility in designing the shape of the igniter will permit more freedom in obtaining desired operating characteristics such as 1-amp/1-watt rating and increased resistance to electromagnetic radiation. Another igniter concept is to use an induction coupling to transfer electric power to the cartridge igniter. The coupling can be made insensitive to electromagnetic radiation and can also be made to respond only to a certain type of power pulse.

650

FILTERED BALLISTIC GAS

Filters to remove solid residues from the cartridge exhaust have been investigated. In general, chemical filters must be large in comparison to the cartridge to obtain good removal efficiency. Downstream breech filters also have been evaluated but possess the disadvantage of restricting flow and also resulting in a substantial maintenance area. The method permits the use of propellant formulations normally considered too dirty for such an application.

TELESCOPING CARTRIDGE

A telescoping cartridge case has been proven feasible in concept from earlier testing. Such a design, showing that the cartridge is folded back into the interior of the case and forms a sealed system to contain the combustion products, is shown in Figure 7. Such a concept has application in a piston driven, mechanically linked ejector design. Upon ignition, high pressure combustion gases expand and drive a piston to accomplish ejection. Since the combustion gases and their by-products are fully contained, the cartridge represents a clean source of power even if "dirty" propellants are used; therefore, alternate propellant formulations can be considered even though they were previously unsuitable. After cartridge operation the trapped gas pressure will be reduced by the cooling of the exhaust products and utilizing special propellants which have high percentages of condensible products such as water vapor, condensible salts, or condensible oxides.
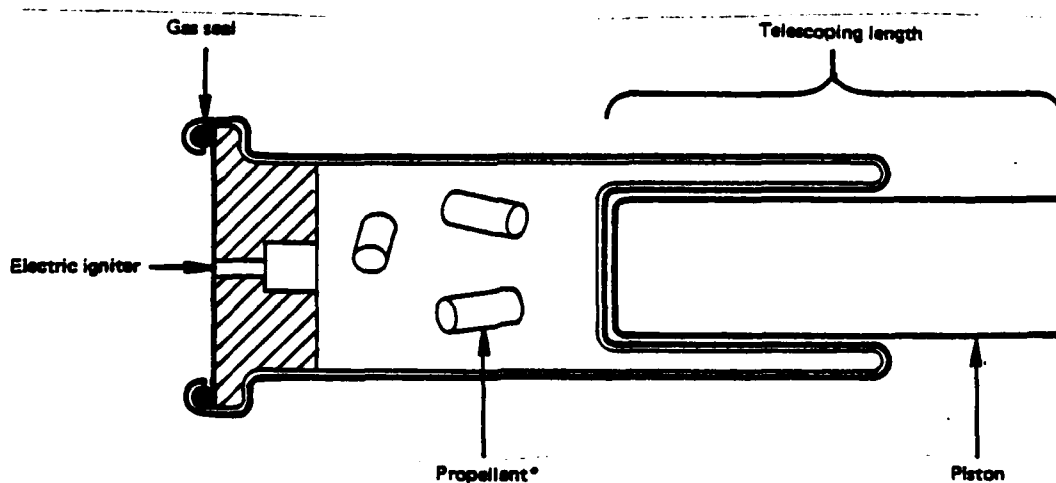
*Formulated for environmental resistance and condensible products.

FIGURE 7.   TELESCOPING CARTRIDGE CONCEPT

Definition of other unique cartridge concepts will be pursued in the future as new application requirements develop.

AUTOBIOGRAPHY

WILLIAM P. PECK

Mr. Peck is a native of Buffalo, New York. In 1959 he received his B.S. in Chemical Engineering from Syracuse University. His first two years of work were at the Naval Weapons Laboratory (now known as Naval Surface Weapons Center) at Dahlgren, Virginia. At NWC he worked in the former Cartridge Actuated Device (CAD) Division. The work concerned both stores ejection equipment and pilot ejection seats. CAD performances were analyzed using analog and digital computers. The next ten years were spent at NASA, Langley Research Center, Hampton, Virginia. The first five years at NASA were spent as Propellant Processing Engineer and involved propellant formulation and processing methods. The last five years at NASA were spent as a Technical Project Manager and included evaluation of a lithium/fluorine/hydrogen propulsion system, construction of a hydrogen peroxide/plexiglass propulsion system, and investigation of teflon combustion in cyrogenic oxygen. Mr. Peck also spent one year working in Submarine Propulsion with the Newport News Ship Building and Dry Dock Company in Newport News, Virginia. In 1973 he came to the Naval Ordnance Station at Indian Head, Maryland, again to work as a Chemical Engineer with the CAD development group. He is currently associated with development efforts in both the stores ejection and escape system areas.

MEASUREMENT OF SUSPENSION LOADS AND DETERMINATION OF SUSPENSION RELIABILITY FOR A STORE IN THE F-111 WEAPONS BAY [1]
(U)

(Article Unclassified)

by

S. D. MEYER
T. L. PAEZ

Sandia Laboratories
Albuquerque, New Mexico   87115

ABSTRACT. (U) The dynamic store suspension environment in an open bay of the F-111 aircraft is under investigation. This experimental study was prompted by the uncertainties relative to the loads on the store suspension system which result from the severe aerodynamic environment in the open bay. Because of the complex flow field which exists, the loads on the swaybraces, vertical chocks, horizontal chocks, and lugs are not amenable to accurate analytical predictions. In an effort to verify that a store is capable of withstanding the loads experienced during carriage to the performance limits of the aircraft, an experimental buildup program was undertaken and is currently in progress. This paper discusses the design of the unit which is being used to measure the random loads on the suspension system during open-door carriage and the methods used to establish the reliability of the store suspension system. A numerical example shows that the suspension system of the store under consideration is highly reliable.

ACKNOWLEDGEMENTS

LIST OF FIGURES

Figures (cont'd)

INTRODUCTION

During open-door carriage in an aircraft weapons bay, a complex flow field exists which results in a random excitation being imposed on a carried store. Therefore, the usual quasistatic approaches to predicting lug and swaybrace loads cannot be used. One solution to the problem might be to measure store pressure distributions in a wind tunnel and then apply this information to a dynamic model of the store-suspension system interface. This approach appears impractical both from the experimental and analytical standpoints because of the difficulty of making adequate pressure measurements on a wind tunnel model and the complexity of the dynamic model required to adequately represent the store-rack interaction. The most direct approach to the problem of determining suspension loads (and associated store suspension system reliability) during carriage in a weapons bay appears to be the instrumentation of a full-scale store so that lug, swaybrace, horizontal-chock, and vertical-chock loads can be measured during bay-door open flights. The measured loads data can then be used to determine the structural reliability of the individual suspension system components.

Based on the above arguments, we decided to establish a full scale test program to determine suspension loads. We planned a build up program which included straight and level flights at various speeds and altitudes as well as 4g pull ups at 6,000 ft MSL. From the first four flights we planned to acquire data under flight conditions which were known to be acceptable from the standpoint of component reliability for the purpose of investigating the influence of bay configuration on loads. We selected the speeds and altitudes on later flights on the basis of analysis of previously acquired data coupled with acceptably high component reliability for the loads predicted on these subsequent flights.

657

The first flight in this test program was conducted on October 1, 1976. To date four missions have been completed. The instrumented unit (Lug Loads Unit or LLU) is being carried in the left bay of an F-111 on all missions. Testing is being done at Eglin Air Force Base, Florida by ADTC, Directorate of Test Engineering.

This paper discusses the instrumentation being used, the test results to date, and the statistical analysis approach employed in attempting to verify the structural integrity of the hardware under investigation. It also discusses future test and evaluation plans.

DESCRIPTION OF SYSTEM OPERATION

Sixteen load cells are used in the Lug Loads Unit (LLU) and associated rack instrumentation. Of these, six are of a commercial variety and ten are Sandia designed. One accelerometer was also monitored during the tests. All of the LLU data were telemetered to ground and recorded on magnetic tape. Also recorded were IRIG B time and conversations between the test director and pilot which define the conditions being flown. A block diagram of the instrumentation is shown in Figure 1. The transducers used to measure swaybrace and vertical chock loads actually replaced the normally used swaybrace and vertical chock pads. These transducers were 20 Series Sensotec load cells which were modified to adapt to the ball on the end of the swaybrace and vertical chock adjusting screws. The swaybrace load cells were 2.0 inches in diameter and had a capacity of 20,000 pounds. The vertical chock load cells were 1.5 inches in diameter with a 5,000 pound capacity.

Horizontal chock forces were measured by instrumenting the actual structure with semiconductor strain gauges. These transducers were calibrated to 10,000 pounds. Vertical and horizontal chock positions are illustrated in Figure 2.
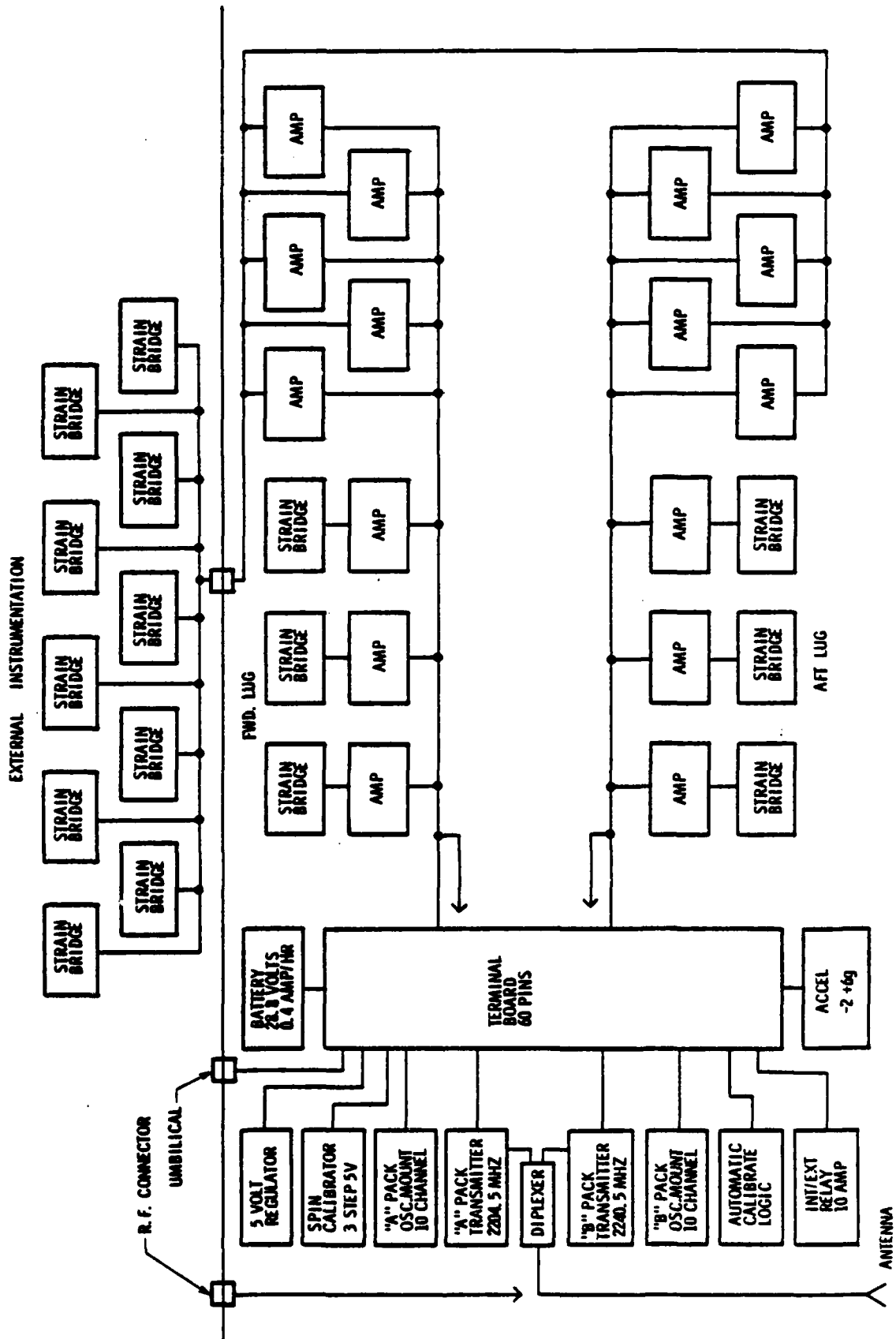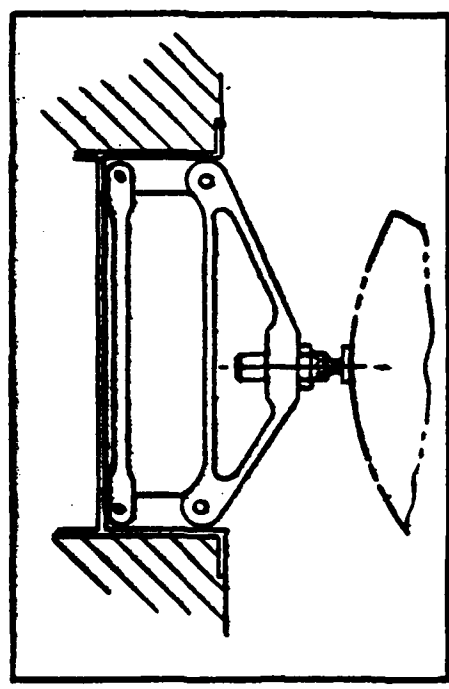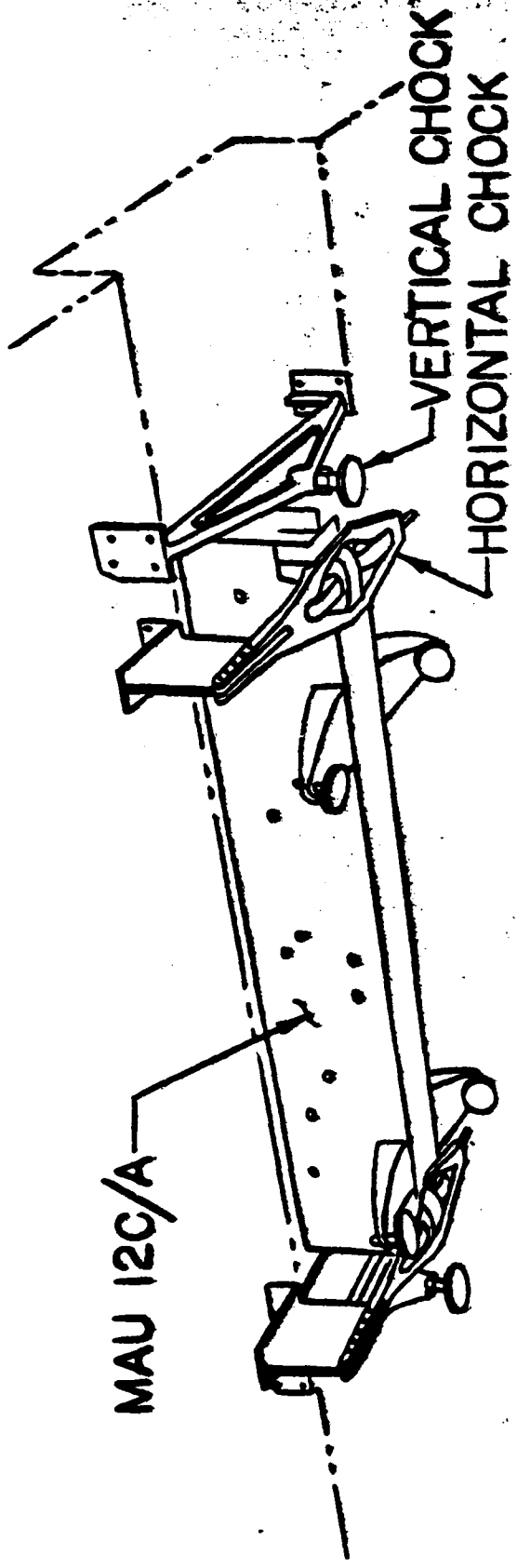
FIGURE 1. LLU INSTRUMENTATION BLOCK DIAGRAM.

VERTICAL CHOCK

HORIZONTAL CHOCK

MAU 12C/A

VERTICAL CHOCK–TYPICAL
EACH END OF BOMB RACK

FIGURE 2–BAY MOUNTED AUXILIARY WEAPON CHOCKS

660

Lug loads were measured using the lug adapter shown in Figure 3. This structure was machined from hand-forged Republic HP 9-4-20 steel and was designed to have a strength exceeding that of the lug. In designing this adapter an attempt was made to match the stiffness of the original lug-case interaction so that response frequency of the system would not be significantly altered.

Axial, lateral, and vertical lug loads were measured through the use of semiconductor strain bridges which were located and connected as shown in Figure 4. The bridges which indicated axial and lateral lug loads were sensitive to bending but insensitive to tensile and compressive loads. The bridge which measured vertical loads was relatively insensitive to bending. Thus, an attempt was made to minimize cross coupling. The lug-load transducer was calibrated for +3,500 pounds axial, +7,500 pounds lateral, and 20,000 pounds vertical loads.

The MAU-12 bomb rack hooks used during these tests were modified to incorporate a circular rather than the original rectangular cross section in the area where the hook transmits side and vertical loads to the lug. This assures consistency in the contact location between the hook and lug thereby precluding the unknown effect of a load path which differs from that experienced during calibration.

Although an effort was made to uncouple the effects of the three components of lug load relative to the force transducer, some coupling still exists. This was handled by applying a calibration matrix to the output voltage vector to obtain the three components of force as indicated below.

$$\{F\} = [C]^{-1}\{V\} \qquad (1)$$

where:

F_1 = axial force on lug

F_2 = lateral force on lug

F_3 = vertical force on lug

C_{11} = voltage output from axial strain bridge due to unit axial load on lug
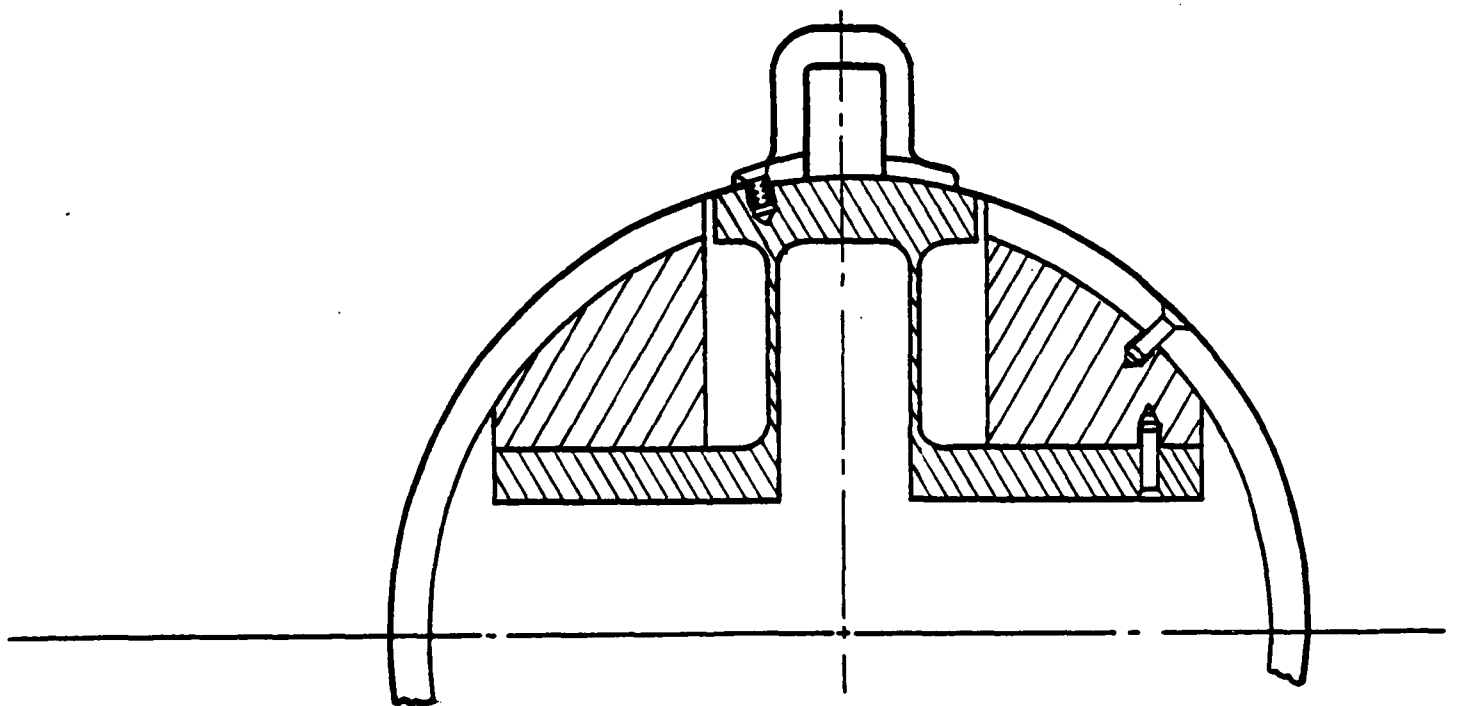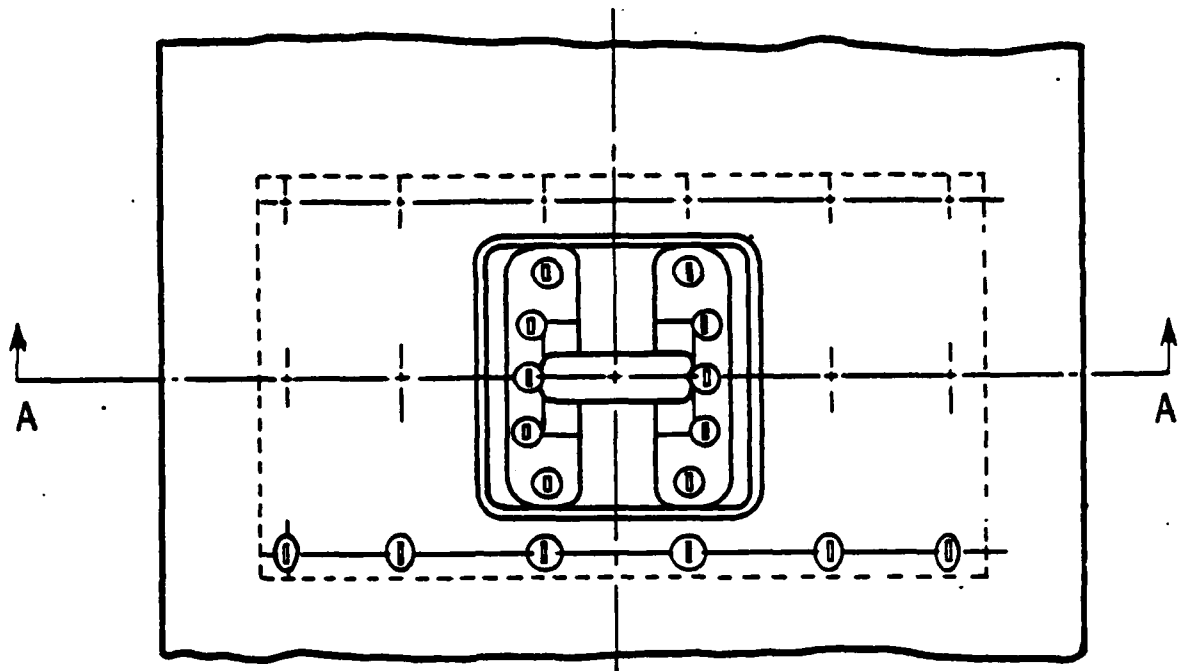
SECTION A-A

FIGURE 3. LUG ADAPTER.

662
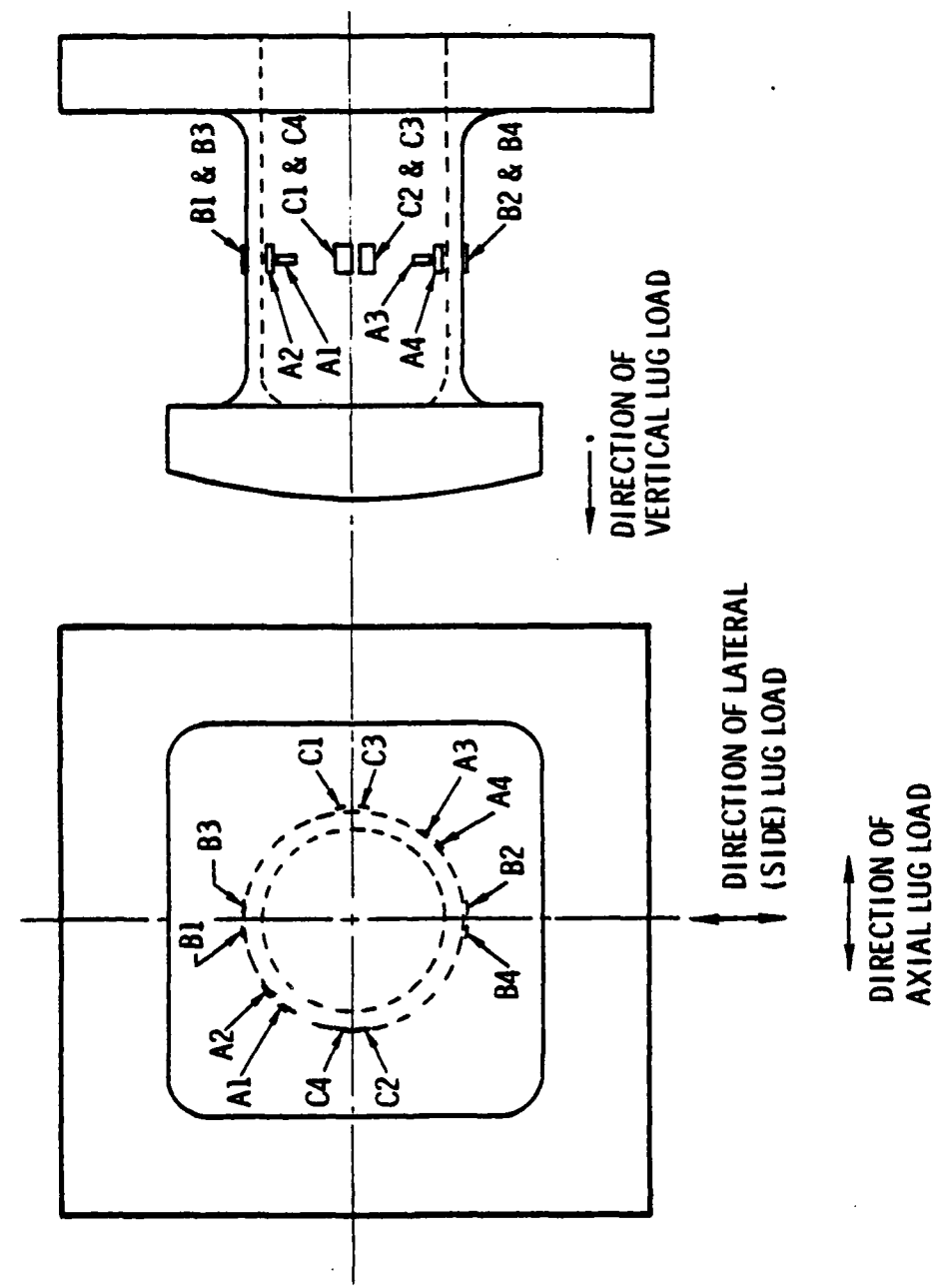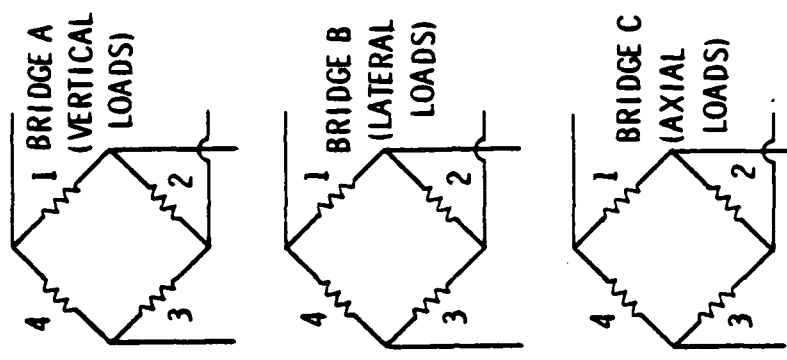
FIGURE 4. LUG LOAD TRANSDUCER STRAIN BRIDGE LOCATIONS AND CONNECTIONS

C_{12} = voltage output from axial strain bridge due to unit lateral load on lug

C_{13} = voltage output from axial strain bridge due to unit vertical load on lug.

.

.

C_{33} = voltage output from vertical strain bridge due to unit vertical load on lug.

V_1 = voltage output from axial strain bridge

V_2 = voltage output from lateral strain bridge

V_3 = voltage output from vertical strain bridge

The $[C]^{-1}$ matrices for the forward and aft lugs are given below. These are presented to show the degree to which cross coupling exists.

$$\text{Forward Lug} \quad [C]^{-1} = \begin{bmatrix} 1485.4 & 128.5 & 0 \\ 42.6 & -3173.6 & 79.8 \\ -46.1 & -700.5 & 3704.4 \end{bmatrix} \quad (2)$$

$$\text{Aft Lug} \quad [C]^{-1} = \begin{bmatrix} -1551.2 & -105.2 & 62.5 \\ 75.9 & 3192.5 & 78.4 \\ -36.0 & 837.2 & 3904.7 \end{bmatrix} \quad (3)$$

Coupling is generally weak as indicated by the relative magnitudes of the diagonal compared to off diagonal terms.

TEST CONDITIONS ON FIRST FOUR FLIGHTS

The primary objective of the test program was to
determine suspension system loads at Mach-altitude
conditions up to the performance limits of the aircraft.
Three bay configurations were of interest:

(1)   LLU in left bay with right bay empty,
(2)   LLU in left bay with gun in right bay,
(3)   LLU in left bay with similar store (BDU) in
      right bay.

To determine the influence of altitude on loads,
altitudes of 6,000 ft., 20,000 ft., and 40,000 ft.
were chosen for initial flights. The minimum altitude
of 6,000 ft. was dictated by a telemetry limitation.

The first four flights were performed at speeds
of 590 KCAS and 660 KCAS, speeds which were known not
to produce excessive loads in the store under
consideration. The objectives of these early flights
were (1) to generate baseline data which could be
extrapolated to determine satisfactory conditions for
subsequent flights and (2) to determine the most
severe bay configuration so that future flights at
higher speeds need only be concerned with one
geometry, thus minimizing cost of the test program.

The data points are being flown with bay doors
full open for approximately 15 seconds. The majority
of data is being measured at constant speed in
straight and level flight. Four g pull-ups are being
performed at the 6,000 foot altitude only.

RESULTS TO DATE

Ten seconds of data recorded on magnetic tape
from each Mach-altitude condition was later digitized
at a rate of 5,000 samples per second. An example of
a force vs. time plot from the aft vertical lug load
transducer is shown in Figure 5. Spectral density
plots were also generated from 10 Hz to 500 Hz using a
band-width of 5 Hz. The spectral density information
corresponding to the time history of Figure 5 is shown
in Figure 6. It should be noted that the

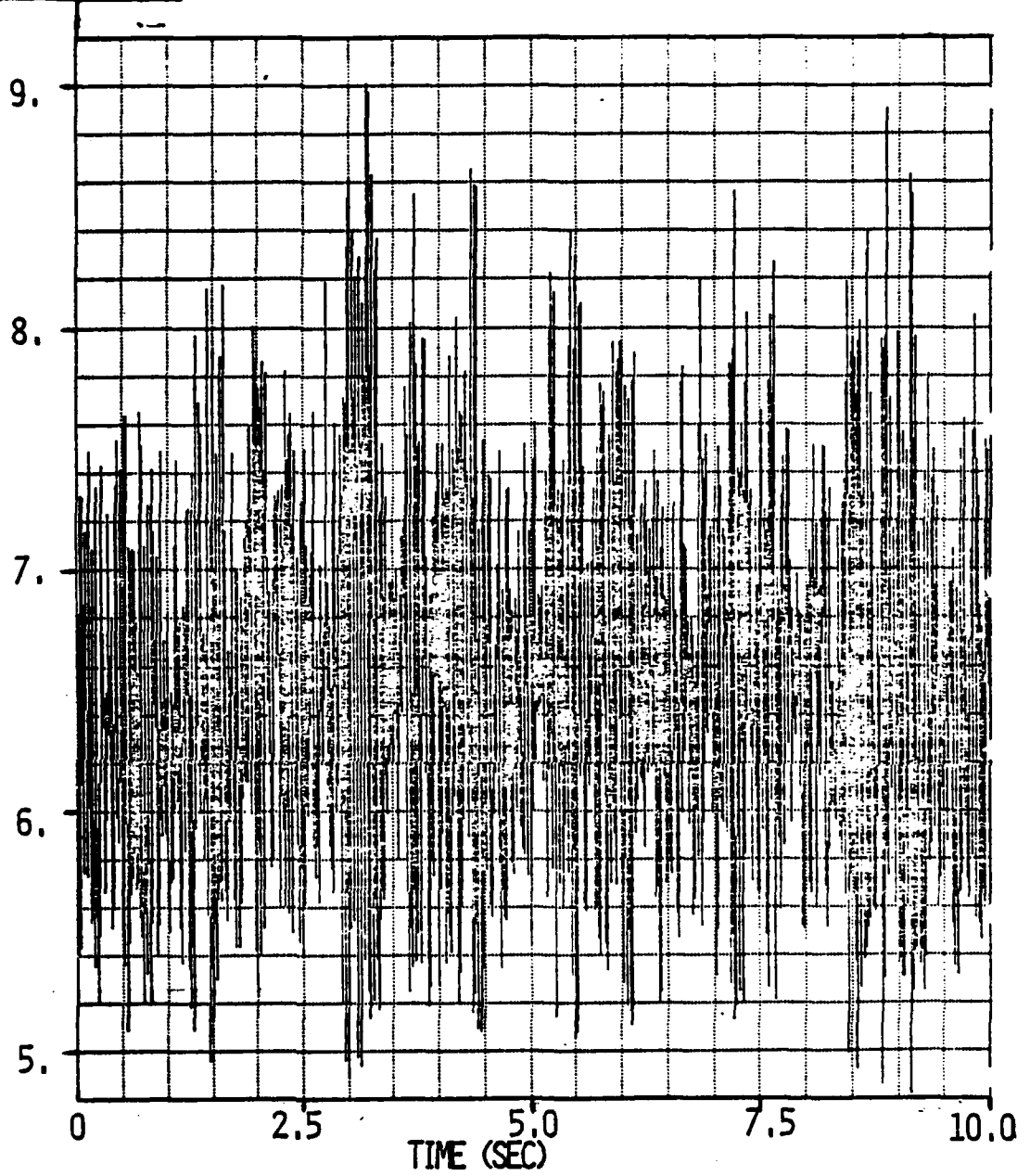FIGURE 5. EXAMPLE OF FORCE VS. TIME HISTORY FROM VERTICAL LUG LOAD TRANSDUCER

FORCE
SPECTRAL
DENSITY
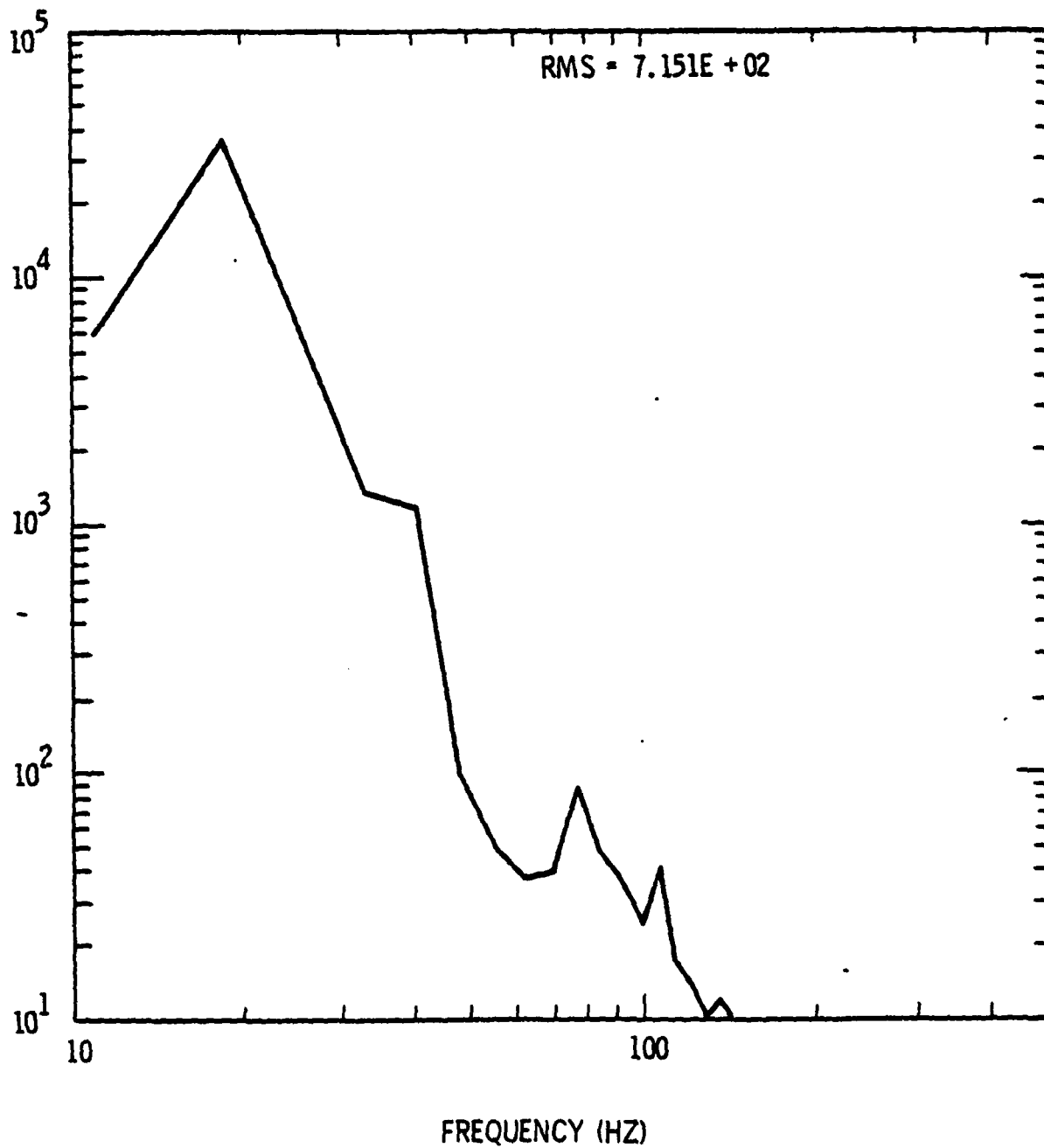(LB^2/HZ)

RMS = 7.151E + 02

FREQUENCY (HZ)

FIGURE 6.   EXAMPLE OF SPECTRAL DENSITY PLOT FROM VERTICAL LUG
LOAD TRANSDUCER.

mean load (which essentially represents preload from tightening the store in the rack) has been subtracted out prior to generating the spectral density plots. These plots, therefore, represent response of the unit due to bay turbulence and other transient forces.

The modal frequencies of the cavity may be predicted by the modified Rossiter equation (Reference 1) which is given by

$$f_m = \frac{V}{L} \ \frac{m - 0.25}{\frac{M}{(1 + 0.2M^2)^{1/2}} + 1.75} \qquad (4)$$

where, V is freestream velocity, L is cavity length, m is mode number, and M is freestream Mach number. Using the flight conditions corresponding to the spectral density shown in Figure 6 results in predicted first four modal frequencies of 20 Hz, 47 Hz, 74 Hz, and 100 Hz. Unfortunately, the fundamental mode of the suspended store is near 20 Hz thus resulting in the peak in the force spectrum seen in Figure 6.

The store suspension components of major concern are the lugs because their failure would necessarily constitute a system demise. Therefore, from the standpoint of damage potential, lug loads are considered to be the most serious problem. Furthermore, the torquing procedure used plus the weight of the store results in static vertical lug loads ranging from 4700 pounds to 7000 pounds with the lateral preload being less than 500 pounds. Thus, this static preload is reasonably consistent and represents less than 15% of the static load carrying capacity of the lugs. Also, this static load does not change significantly during flights in the bay. Thus, it is the deviation from this mean or steady state value which has damage potential. The selection of worst bay configuration and most severe speed-altitude conditions was, therefore, based on the rms values of vertical and lateral lug loads which were obtained from the spectral density plots.

668

The ranges of rms force in the vertical direction on the forward and aft lugs are shown in Figures 7 and 8 as a function of altitude. Similar data for lateral lug loads are shown in Figures 9 and 10. The highest vertical loads on the forward lug correspond to a configuration with a similar store (BDU) in the right bay. This appears to be true at all altitudes. The most severe vertical load variations on the aft lug occur for this same configuration at 6,000 ft. MSL. At 20,000 ft. and 40,000 ft. altitudes, however, the configuration with the right bay empty appears to produce equally severe load variations. The configuration with the gun in the right bay results in the lowest vertical load variations on both lugs. In general, the rms values of vertical load are seen to diminish with increased altitude as expected because the forcing function is Q dependent (1).

The lateral lug loads data (Figures 9 and 10) indicate that in general, the configuration with the LLU in the left bay and the BDU in the right bay produces the most severe environment. These same data indicate that at 660 KCAS higher lateral loads are experienced at the 20,000 ft. than at the 6,000 ft. altitude. No explanation is presently available for this anomaly.

Based on the data of Figures 7 through 10 it has been decided to perform all future tests with the LLU in the left bay and a similar store (BDU) in the right bay. Furthermore, future missions will be flown at altitudes of 20,000 feet and below.

Having acquired loads data the difficult question of store suspension system integrity must next be answered. To estimate reliability, we characterize the system failure mode and use the statistics collected in the field to find the probability that the system will survive a particular environment for a specified length of time. Finally, we combine the probabilities for the individual environments to find the chance that the system will survive a given sequence of environments which is judged to be typical.

669

RMS Force (lb.)

NOTE: TWO IDENTICAL SYMBOLS AT ONE ALTITUDE SIGNIFY A RANGE

BDU in Rt. Bay, 590 KCAS ⊡
BDU in Rt. Bay, 660 KCAS ■
Rt. Bay Empty, 590 KCAS ⊙
Rt. Bay Empty, 660 KCAS ●
Gun in Rt. Bay, 590 KCAS △
Gun in Rt. Bay, 660 KCAS ▲
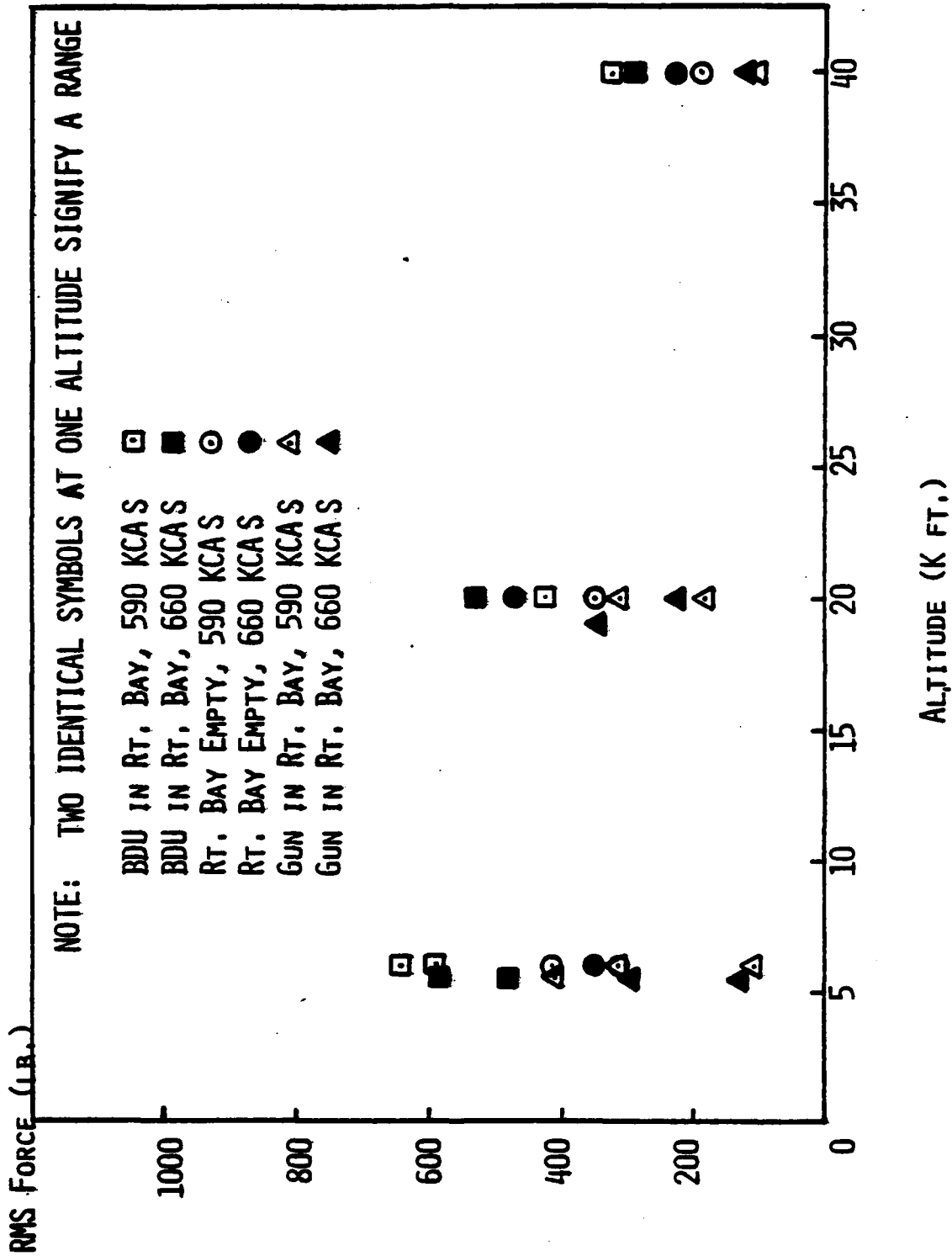
Altitude (K Ft.)

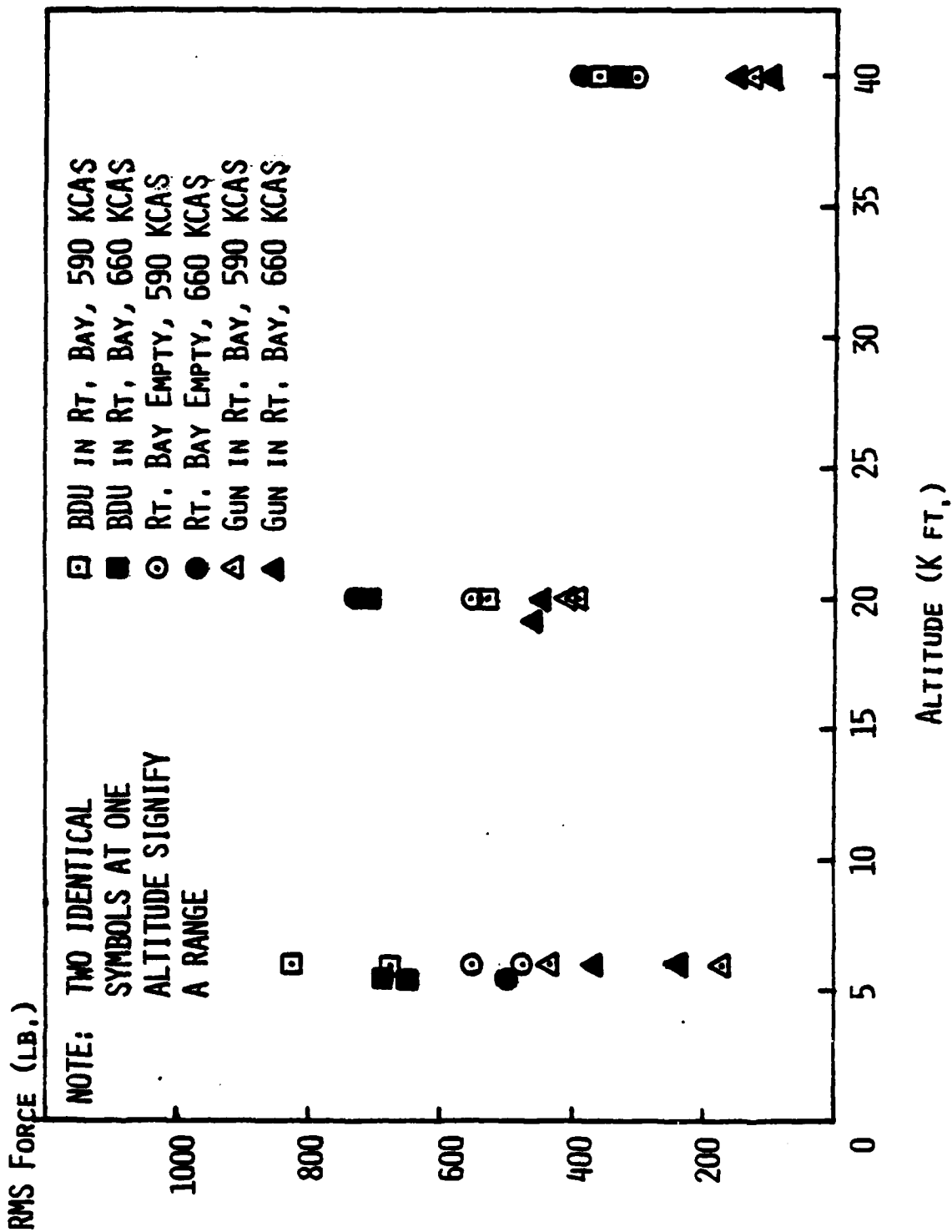FIGURE 7. RMS FORCE VS ALTITUDE IN VERTICAL DIRECTION ON FORWARD LUG

670

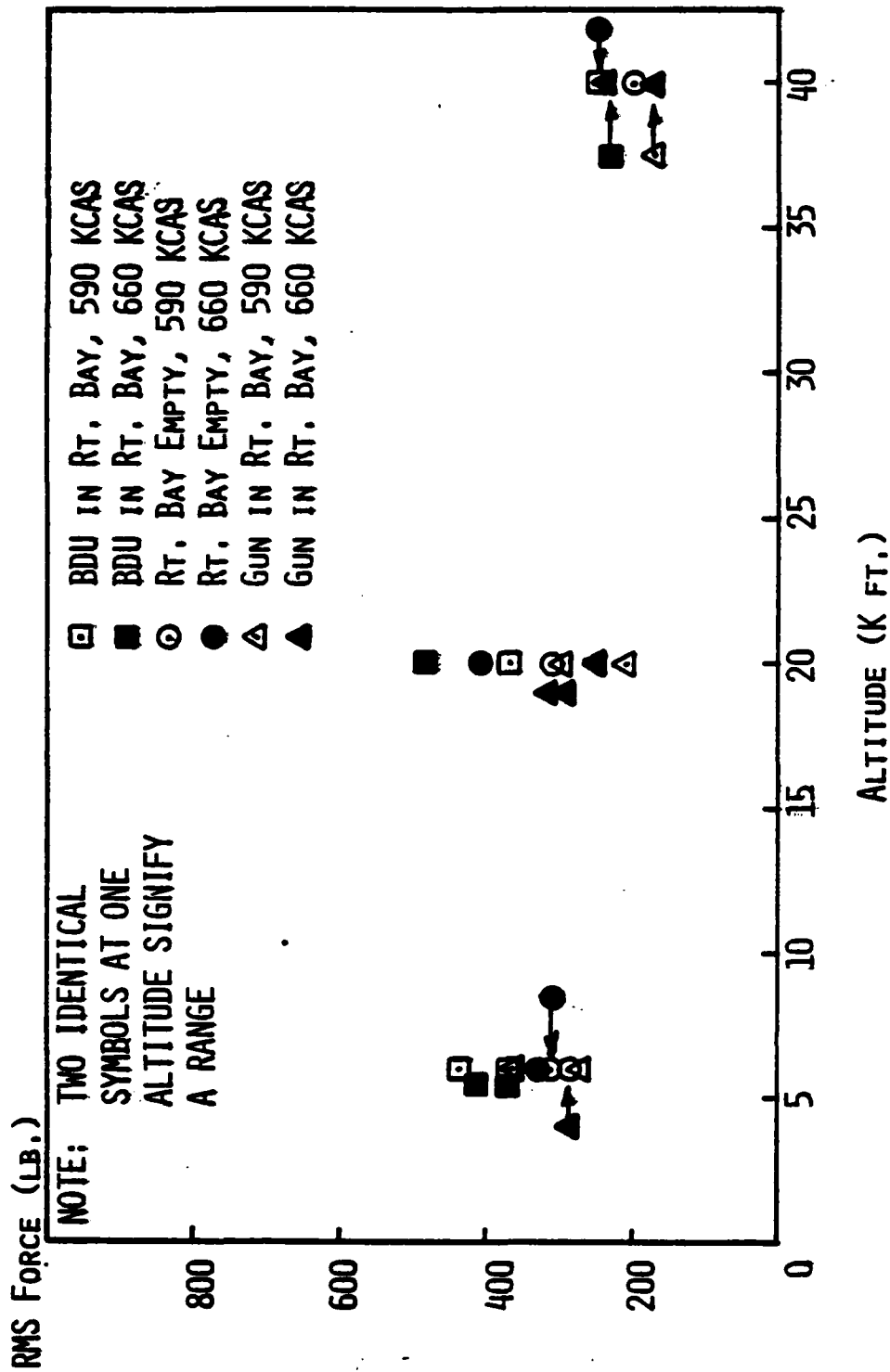FIGURE 8. RMS FORCE VS ALTITUDE IN VERTICAL DIRECTION ON AFT LUG

FIGURE: 9, RMS FORCE VS ALTITUDE IN LATERAL DIRECTION ON FORWARD LUG
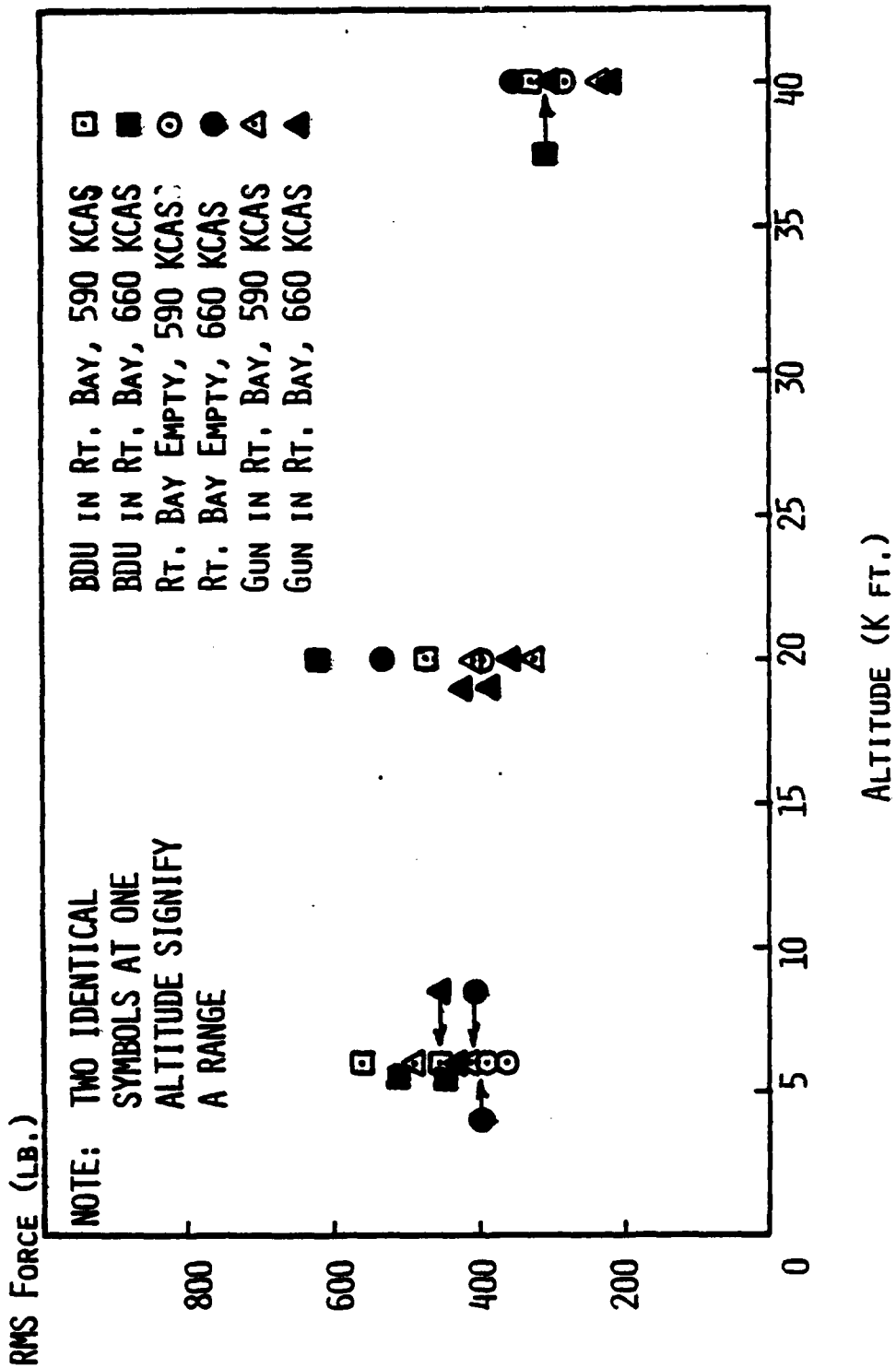
FIGURE 10. RMS FORCE VS ALTITUDE IN LATERAL DIRECTION ON AFT LUG

FIRST PASSAGE AND PEAK PROBABILITY DISTRIBUTIONS

In this section we derive the approximate first passage probability distribution and the probability distribution of the highest peak realized in a finite time duration for a stationary normal random process. We also obtain the first two moments of the latter probability distribution. To derive these probability distributions, we describe the barrier crossing phenomenon as a Poisson random process. This description simplifies the analytical development and provides a satisfactory degree of accuracy. Let $X(t)$, $-\infty < t < \infty$, be a stationary, mean zero, normal random process with joint probability density function (pdf) of the variate and its first derivatives given by

$$p_{X\dot{X}}(x,v) = \frac{1}{2\pi\sigma_x\sigma_{\dot{x}}} \exp\left[-\frac{1}{2}\left(\frac{x^2}{\sigma_x^2} + \frac{v^2}{\sigma_{\dot{x}}^2}\right)\right]$$

$$-\infty < x, v < \infty \qquad (5)$$

where σ_x^2 and $\sigma_{\dot{x}}^2$ are the variances of the random process and its first derivative, respectively. The standard deviations, σ_x and $\sigma_{\dot{x}}$, are root mean square (rms) values of the random process and its first derivative. Let $S_X(f)$, $f > 0$, be the one-sided spectral density of the random process; we have the following relations.

$$\sigma_x^2 = \int_0^\infty S_X(f)\,df$$

$$\sigma_{\dot{x}}^2 = (2\pi)^2 \int_0^\infty f^2 S_X(f)\,df \qquad (6)$$

Rice (2) showed that the average rate at which the above random process crosses the barrier level $x = a$, with positive slope, is given by

$$\nu_a^+ = \int_0^\infty v\, p_{X\dot{X}}(a,v)\,dv \quad . \qquad (7)$$

674

Using Equation 5 in Equation 7 and integrating leads
to

$$v_a^+ = \frac{1}{2\pi} \frac{\sigma_{\dot{x}}}{\sigma_x} \exp\left(-\frac{a^2}{2\sigma_x^2}\right). \qquad (8)$$

This is the average number of positive slope crossings
per-unit-time of the barrier x = a, by the random
process X(t).

To find the probability distribution of the
number of times that the random process X(t) crosses
the barrier x = a during the time period t, we use the
following procedure. Divide the time duration of
interest, t, into n equal intervals of length Δt such
that Δt<<t. We first assume that the crossing event
is a binominal type event, i.e., the random signal
either crosses or does not cross the barrier during
Δt, and second, we assume that the barrier crossings
are independent events. If we denote the probability
of a positive slope barrier crossing during any time
interval Δt, by p, then the number of barrier
crossings occurring during t is governed by a binomial
probability law. Let P_k (t) be the probability that k

barrier crossings with positive slope occur during
time t; then we have

$$P_k(t) = \binom{n}{k} p^k (1-p)^{n-k} \qquad \begin{array}{l} t > 0 \\ k = 0, 1, \ldots n \end{array}$$

where $n = \frac{t}{\Delta t}$. $\qquad\qquad\qquad\qquad (9)$

This expression is the binomial probability mass
function (pmf). When the probability, p, that a
crossing occurs during Δt is small, i.e., when the
barrier level is high, then the binomial pmf can be
approximated by a Poisson pmf. (See, for example, Feller
(3).) Use of this fact yields

$$P_k(t) = \frac{(v_a^+ t)^k}{k!} \exp(-v_a^+ t), \ t > 0 \quad ,$$

$$(10)$$

where $\nu_a^+ t$ is the average number of positive slope barrier crossings occurring during time t, and the right side expression is the Poisson pmf. The probability that the random process does not cross the barrier x = a during time t (i.e., k = 0) is

$$P_o(t) = \exp(-\nu_a^+ t), \quad t > 0 \quad . \qquad (11)$$

The probability of the complementary event, that one or more crossings occurs during time t is

$$P_a(t) = 1 - \exp(-\nu_a^+ t)$$

$$= 1 - \exp\left(-\frac{t}{2\pi} \frac{\sigma_{\dot{x}}}{\sigma_x} \exp\left(-\frac{a^2}{2\sigma_x^2}\right)\right) \quad ,$$

$$t > 0 \quad . \qquad (12)$$

This is known as the first passage probability distribution for the random process X(t) for barrier height a.

The probability of Equation 11 can be thought of in another way. If no crossing of the barrier level a occurs during time t, then this implies that the highest peak realized during time t is equal to or lower than the level a. Let A be the random variable denoting the height of the highest peak in the random process which occurs in a time duration, t. The cumulative distribution function (cdf) of A is

$$P_A(a) = \exp\left(\frac{-t}{2\pi} \frac{\sigma_{\dot{x}}}{\sigma_x} \exp\left(-\frac{a^2}{2\sigma_x^2}\right)\right), \quad a \geq 0 \quad .$$
$$t > 0$$

$$(13)$$

676

This is the chance that the highest peak over a signal duration t, in a zero mean, stationary, normal random signal is equal to or lower than a. This cdf is similar to a Type I extreme value distribution of the largest value and differs only in the square on the variate a. As a becomes large, $P_A(a)$ approaches unity. As a approaches zero, $P_A(a)$ becomes small when t is large. The variate a must be taken greater than or equal to zero because of the square on this quantity in the exponential term. Since a cdf must be nondecreasing we must assume that a cannot take negative values. This results in a small but finite chance that A can assume the value zero. In practical application of the formula, this causes no problems. The pdf of the random variable A is found by differentiating Equation 13 with respect to a.

$$p_A(a) = \frac{t}{2\pi} \frac{\sigma_{\dot{x}}}{\sigma_x^3} a \exp\left(-\frac{t}{2\pi} \frac{\sigma_{\dot{x}}}{\sigma_x} \exp\left(-\frac{a^2}{2\sigma_x^2}\right) - \frac{a^2}{2\sigma_x^2}\right) \quad (14)$$

$$a \geq 0$$

To simplify the notation, we define

$$n = \frac{t}{\pi} \frac{\sigma_{\dot{x}}}{\sigma_x} \quad . \quad (15)$$

When the random process, X(t), is narrow band (i.e., the spectral density and, thus, process energy is concentrated in a narrow band of frequencies), n is the expected number of extrema occurring during time t. When the random process, X(t), is not narrow band, n can be thought of as a weighted average number of extrema over time duration t.

We now find the mode of the pdf for the random variable A by differentiating Equation 14 and setting the resulting expression equal to zero. This yields

$$\frac{n}{2} = \left[1 - \left(\frac{\sigma_x}{a}\right)^2\right] \exp\left[\frac{1}{2}\left(\frac{a}{\sigma_x}\right)^2\right] . \quad (16)$$

When a/σ_x is large, σ_x/a is small and we can neglect the first $(\sigma_x/a)^2$ term to obtain, approximately,

$$\text{Mode}\left[A\right] = \left[2 \ln\left(\frac{n}{2}\right)\right]^{1/2} \sigma_x , \quad (17)$$

and this expression is most accurate for large n. The mode of A corresponds to the amplitude where its pdf peaks; therefore, it is the most likely value that A can assume.

The expected value of A is by definition

$$E\left[A\right] = \int_0^\infty \frac{n}{2}\left(\frac{a}{\sigma_x}\right)^2 \tag{18}$$
$$\cdot \exp\left\{-\frac{n}{2}\exp\left[-\frac{1}{2}\left(\frac{a'}{\sigma_x}\right)^2\right] - \frac{1}{2}\left(\frac{a}{\sigma_x}\right)^2\right\}da \quad.$$

Upon performing a change of variables using the substitution

$$s = \exp\left\{-\frac{1}{2}n\exp\left[-\frac{1}{2}(a/\sigma_x)^2\right]\right\}$$

we obtain

$$E\left[A\right] = \sqrt{2\ln n}\;\sigma_x \int_{e^{-n/2}}^1 \left[1 - \frac{\ln(\ln s^{-2})}{\ln n}\right]^{1/2} ds. \tag{19}$$

But as n becomes large, the integral approaches unity. Therefore, we have approximately,

$$E\left[A\right] \cong \sqrt{2\ln n}\;\sigma_x \quad. \tag{20}$$

It will be seen later that the approximation of Equation 20 is approached from below as n becomes large. Moreover, the approximation becomes a good one quite rapidly. A numerical analysis shows that the integral in Equation 19 equals (0.936, 0.978) at n equal (10., 100.). This result is in agreement with other results found in the literature where other approaches to the same problem have been taken (4,5). The variance of A can be written, by definition,

$$\text{Var}\left[A\right] = \int_0^\infty \frac{n}{2}\left(\frac{a^3}{\sigma_x^2}\right)\exp\left\{-\frac{n}{2}\exp\left[-\frac{1}{2}\left(\frac{a}{\sigma_x}\right)^2\right] - \frac{1}{2}\left(\frac{a}{\sigma_x}\right)^2\right\}da$$
$$- \left\{\int_0^\infty \frac{n}{2}\left(\frac{a}{\sigma_x}\right)^2 \exp\left\{-\frac{n}{2}\exp\left[-\frac{1}{2}\left(\frac{a}{\sigma_x}\right)^2\right] - \frac{1}{2}\left(\frac{a}{\sigma_x}\right)^2\right\}da\right\}^2 \tag{21}$$

When we perform a change of variables using the substitution

$$s = \exp\left\{-\frac{1}{2}n\exp\left[-\frac{1}{2}(a/\sigma_x)^2\right]\right\},$$

678

we obtain

$$\text{Var}\left[A\right] = 2\sigma_x^2 \ln n \left\{ \int_{e^{-n/2}}^{1} \left[1 - \frac{\ln(\ln s^{-2})}{\ln n}\right] ds \right.$$

$$\left. - \left[\int_{e^{-n/2}}^{1} \sqrt{1 - \frac{\ln(\ln s^{-2})}{\ln n}} \ ds\right]^2 \right\}. \tag{22}$$

Each of the integrals within the braces tends to unity as n grows, so that the variance of A tends to zero as n goes to infinity. We approximate the variance of A as follows. First, we find an approximation for the first expression on the right side of Equation 22. Integrating the first term we can write

$$\int_{e^{-n/2}}^{1} \left[1 - \frac{\ln(\ln s^{-2})}{\ln n}\right] ds = 1 - e^{-n/2}$$

$$- \frac{1}{\ln n} \int_{e^{-n/2}}^{1} \ln(\ln s^{-2}) \ ds. \tag{23}$$

We then perform a change of variables using the substitution

$$u = \frac{1}{2} \ln s^{-2}$$

to obtain

$$\int_{e^{-n/2}}^{1} \left[1 - \frac{\ln(\ln s^{-2})}{\ln n}\right] ds = (1 - e^{-n/2})$$

$$- \frac{1}{\ln n}\left[\ln 2(1 - e^{-n/2}) - \gamma + \int_{n/2}^{\infty} e^{-u}\ln u \ du\right].$$

$$\tag{24}$$

where use has been made of the fact that $\int_{0}^{\infty} e^{-u} \ln u \ du = -\gamma.$ As n becomes large we have approximately

$$\int_{e^{-n/2}}^{1} \left[1 - \frac{\ln(\ln s^{-2})}{\ln n}\right] ds \cong 1 - \frac{\ln 2 - \gamma}{\ln n}. \tag{25}$$

679

Now we find an approximation for the second integral on the right side of Equation 22. First we note that

$$\sqrt{1-a} \cong 1 - \frac{a}{2} - \frac{a^2}{8} \ . \qquad (26)$$

We now use this in the integrand to obtain

$$\int_{e^{-n/2}}^{1} \sqrt{1 - \frac{\ln(\ln s^{-2})}{\ln n}} \ ds \cong \int_{e^{-n/2}}^{1} \left\{ 1 - \frac{\ln(\ln s^{-2})}{2 \ln n} \right.$$

$$\left. - \frac{1}{8} \left[\frac{\ln(\ln s^{-2})}{\ln n} \right]^2 \right\} ds \ . \qquad (27)$$

Because of the similarity of the first two terms in the integrand to the integrand in Equation 23, this part is easily approximated. The last term remains to be integrated. Using the substitution $u = 1/2 \ln s^{-2}$ we obtain

$$\int_{e^{-n/2}}^{1} \left[\ln(\ln s^{-2}) \right]^2 ds = \int_{0}^{n/2} e^{-u} (\ln 2 + \ln u)^2 \ du$$

$$= -(\ln 2 - \gamma)^2 + \frac{\pi^2}{6} - \int_{n/2}^{\infty} e^{-u} (\ln 2 + \ln u)^2 \ du \ .$$

$$(28)$$

But when n is large, this is accurately approximated by

$$\int_{e^{-n/2}}^{1} \left[\ln(\ln s^{-2}) \right]^2 ds \cong (\ln 2 - \gamma)^2 + \frac{\pi^2}{6} \ .$$

Equation 27 can now be approximated by

$$\int_{e^{-n/2}}^{1} \sqrt{1 - \frac{\ln(\ln s^{-2})}{\ln n}} \ ds \cong 1 - \frac{\ln 2 - \gamma}{2 \ln n}$$

$$- \frac{(\ln 2 - \gamma)^2 + \pi^2/6}{8 \ (\ln n)^2}$$

$$(29)$$

In terms of the approximations of Equations 25 and 29, the variance of A can now be written

$$
\text{var } [A] \cong 2\sigma_x^2 \ln n \left\{ \frac{\pi^2/6 + 2(\ln 2 - \gamma)^2}{4(\ln n)^2} - \frac{[(\ln 2 - \gamma)^2 + \pi^2/6](\ln 2 - \gamma)}{8(\ln n)^3} \right.
$$

$$
\left. - \frac{[(\ln 2 - \gamma)^2 + \pi^2/6]^2}{64(\ln n)^4} \right\} . \tag{30}
$$

If we approximate this expression by its leading term, we get

$$
\text{Var } [A] \cong \frac{\pi^2}{12 \ln n} \sigma_x^2 . \tag{31}
$$

This is the variance of the highest peak in a random signal which comes from a zero mean, stationary, normal random source. The standard deviation of A is

$$
\sigma_A = \frac{\pi}{\sqrt{12 \ln n}} \sigma_x . \tag{32}
$$

As mentioned previously, the variance of A tends toward zero as n goes to infinity. Also, Equation 29 shows that the mean approximation of Equation 20 is approached from below.

RELIABILITY OF A STORE SUSPENSION SYSTEM

We now demonstrate a means for applying the results of the previous section to the problem of the mechanical reliability of a store suspension system. The store is assumed to be suspended by lugs at forward and aft locations. In the strictest sense, failure can only occur when one or both lugs fracture. But in a more conservative sense we can assume that failure occurs when some load limit is surpassed on a component. Particularly, we analyze the lug which is most severely loaded in the mean square sense, and assuming complete dependence in a probabilistic sense, we state that the less severely loaded lug will certainly survive if the more severely loaded one does.

In this analysis, we assumed that for the lug under consideration there exists an experimentally obtained, two dimensional, static failure load curve. This curve defines the combinations of vertical and lateral static force which will cause lug failure on the first application. Because of the factors of safety used in the design of a lug, it is very unlikely that the static failure envelope could be reached in normal operation. In practice, failure would occur due to a fatigue phenomenon. The lug load would go through many cycles. A crack would be initiated at a point of high stress and then would propagate, causing fracture. However, there exists an endurance limit for the lug such that the lug can be subjected to more than 10^7 load cycles, and as long as the load does not surpass this limit, failure will not occur. In fact, a large number of load cycles surpassing the endurance limit must be realized before failure can occur. In view of the above, it is quite conservative to state that failure of the lug occurs upon the first excursion of the lug force beyond the endurance limit. Because the failure statement is conservative, we can form a lower bound estimate of the suspension system reliability by finding the probability that no excursions past the endurance limit occur when the store-lug system is subjected to a specific sequence of dynamic environments. A lower bound reliability so computed is strictly identified with the sequence of dynamic environments.

682

To simplify this problem we reduce it from a two dimensional one, in which we consider both vertical and lateral force random processes, to a one dimensional problem in which a composite random process is considered. This is done conservatively in the following way. Let $S_V(f)$ and $S_L(f)$ be the

spectral densities of the vertical and lateral lug force random processes, respectively. We can compute the variances, σ_V^2 and σ_L^2, of these force random processes using the first of Equations 6. We define a root-mean-square (rms) force radius for the two-dimensional random process in the vertical force versus lateral force plane as

$$\nu(\theta) = \sigma_L \cos^2\theta + \sigma_V \sin^2\theta \ , \ 0 \leq \theta \leq \frac{\pi}{2} \ , \qquad (33)$$

where θ is the angle between the rms force radius and the right abscissa, and the origin is taken as the intersection of the zero-lateral force with average-vertical force point. We plot this curve on the set of axes showing the lug static failure load curve. Next, we define the lug failure force radius, $\rho(\theta)$, as the distance from the origin (the zero lateral force versus average vertical force point) to the lug static-failure load-envelope. We note that the rms force radius approaches nearest the failure envelope at the angle $\theta = \theta_m$ where $\nu(\theta)/\rho(\theta)$ is a maximum. We

call θ_m the critical angle of the rms forces radius.

Finally, we define a composite one-dimensional force random process, $F(t)$, $-\infty < t < \infty$, as a stationary, mean zero, normal random process with spectral density,

$$S_F(f) = S_L(f) \cos^2\theta_m + S_V(f) \sin^2\theta_m, \qquad f \geq 0 \ .$$

$$(34)$$

683

The variances, σ_F and $\sigma_{\dot{F}}$ of this random process and

its first derivative are found using Equation 6. We take this random process to represent the worst aspects of the joint vertical-horizontal lug force random process. We say that failure occurs, in the conservative sense described previously, when the random force process, $F(t)$, makes its first excursion beyond the level $\alpha\rho(\theta_m)$. Here $\rho(\theta_m)$ is the lug

failure force radius for the composite random process, and α is a fraction which denotes the ratio of the endurance limit to the ultimate strength for the lug material.

Let us now state that the ith environment to which the store-lug system will be subjected is characterized by the composite random force process $F_i(t)$,

$-\infty < t < \infty$ with spectral density $S_{F_i}(t)$, and let this

environment be applied for a duration t. Further, let us state that critical angle of the rms force radius is θ_i . Then the lower-bound reliability, R_i, of the

store-lug system is the probability that the force does not exceed the level $\alpha\rho(\theta_i)$. Using Equation 11 we have

$$R_i = \exp\left[-\frac{t_i}{2\pi} \frac{\sigma_{\dot{F}_i}}{\sigma_{F_i}} \exp-\left(\frac{\alpha^2\rho^2(\theta_i)}{2\sigma_{F_i}^2}\right)\right] , \quad t \geq 0 ,$$

(35)

where σ_{F_i} and $\sigma_{\dot{F}_i}$ are the standard deviations of the

composite random process and are obtained using Equation 6. If the store-lug system is subjected to a sequence of m environments and these environments are independent of one another, then the overall reliability of the system, R, is given by

$$R = \prod_{i=1}^{m} R_i .$$

(36)

684

This is a lower bound on the probability that the system will survive the sequence of m environments.

The expected peak force which will occur in the lug because of the application of the ith environment is

$$E\left[F_{i,max}\right] = \sqrt{2 \ln n_i} \ \sigma_{F_i} \qquad (37)$$

where n_i is obtained using equation 15. The standard deviation of the peak force due to the ith environment is obtained using Equation 32.

$$\sigma\left[F_{i,max}\right] = \frac{\pi}{\sqrt{12 \ln n_i}} \ \sigma_{F_i} \qquad (38)$$

We can find the time at which the expected peak force reaches the failure level by equating Equation 37 to $\alpha\rho(\theta_i)$, using the expression for n_i and solving for t_i

We obtain

$$t_i = \pi \frac{\sigma_{F_i}}{\sigma_{\dot{F}_i}} \exp\left[\frac{1}{2}\left(\frac{\alpha\rho(\theta_i)}{\sigma_{F_i}}\right)^2 \right]. \qquad (39)$$

It should be noted that the lower-bound reliability of Equation 36 is conditioned on the successful operation of all other suspension equipment besides the lugs and the successful operation of the airplane itself if the data used in obtaining the spectral density estimates were recorded during a flight in which all equipment functioned properly. To obtain an unconditional reliability estimate for the store suspension system, we would need to know all the joint probabilities of successful and unsuccessful operation of the lugs, the other suspension equipment and the airplane itself.

NUMERICAL EXAMPLE

In this section, we compute reliabilities of the
store suspension system. Figures 11a and 11b show the
spectral densities of the vertical and lateral lug
load random processes for a store carried in an F111
weapons bay, with doors closed, at 590 KCAS and 6000
ft. altitude during a 4G pullup. Figures 12a and 12b
show the spectral densities of the vertical and
lateral lug-load random processes for the same store
carried in the weapons bay, doors open, at 590 KCAS
and 6000 ft. during straight and level flight. We
wish to find the suspension system reliability as a
function of time for the case in which the store is
carried for an indefinite length of time with the
doors closed and then is carried for eight minutes
with the doors open. We first find the critical angle
of the rms force radius for each of the pairs of
random processes in Figure 11a through 12b. Figure 13
shows the rms force radius on a vertical force versus
lateral force graph for the spectral densities of
Figures 11a and 11b. Along with this we plotted the
static-failure envelope for the lug; we determined
this experimentally. It is clear that rms force
radius is closest to the static failure envelope in
the approximate range $0.35 \pi < \theta < \pi/2$. For simplicity
we take $\theta_m = \pi/2$. Therefore, $S_F(f) = S(f)$. A graph

of the rms force radius for the random processes whose
vertical and lateral force spectral densities are
shown in Figures 12a and 12b reveals that in that case
also, we can take $\theta_m = \pi/2$.

Figures 11a and 12a give the variance of each
random process and its derivative. For the lugs under
consideration we take the ratio of endurance limit to
ultimate strength to be 0.30. Since, in this
particular example, the lower-bound reliability is
very near unity for reasonable times, t, we plotted
the upper bound on probability of system failure, or
1-R. In order to write the reliability as a function
of time, we say that the system reliability is the
product of the reliability of the system for the
eight-minute open-door environment times the
reliability of the system over t-8 minutes of
closed-door environment, where t is the total number
of minutes into flight. Equation 35 uses the
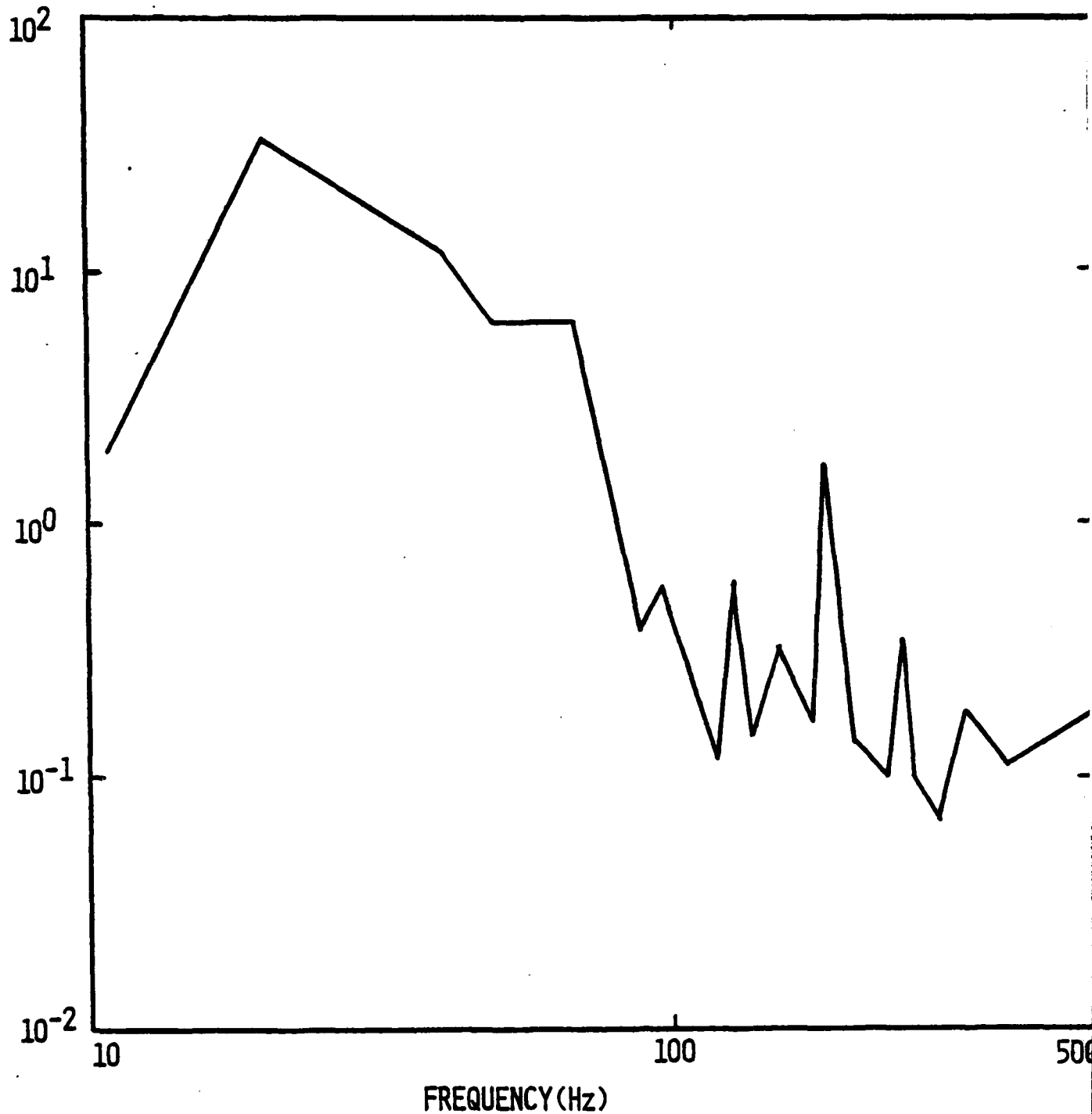parameters listed above and Figures 11a and 12a to

686

FIGURE 11A. SPECTRAL DENSITY OF VERTICAL FORCE RANDOM PROCESS FOR CARRIAGE IN F-111. AT 590 KCAS AND 6000 FT. DURING 4G PULLUP WITH DOORS CLOSED.

$$\sigma_F = 55.42 \text{ lb.}, \quad \sigma_{\dot{F}} = 31,336 \text{ lb/sec}$$
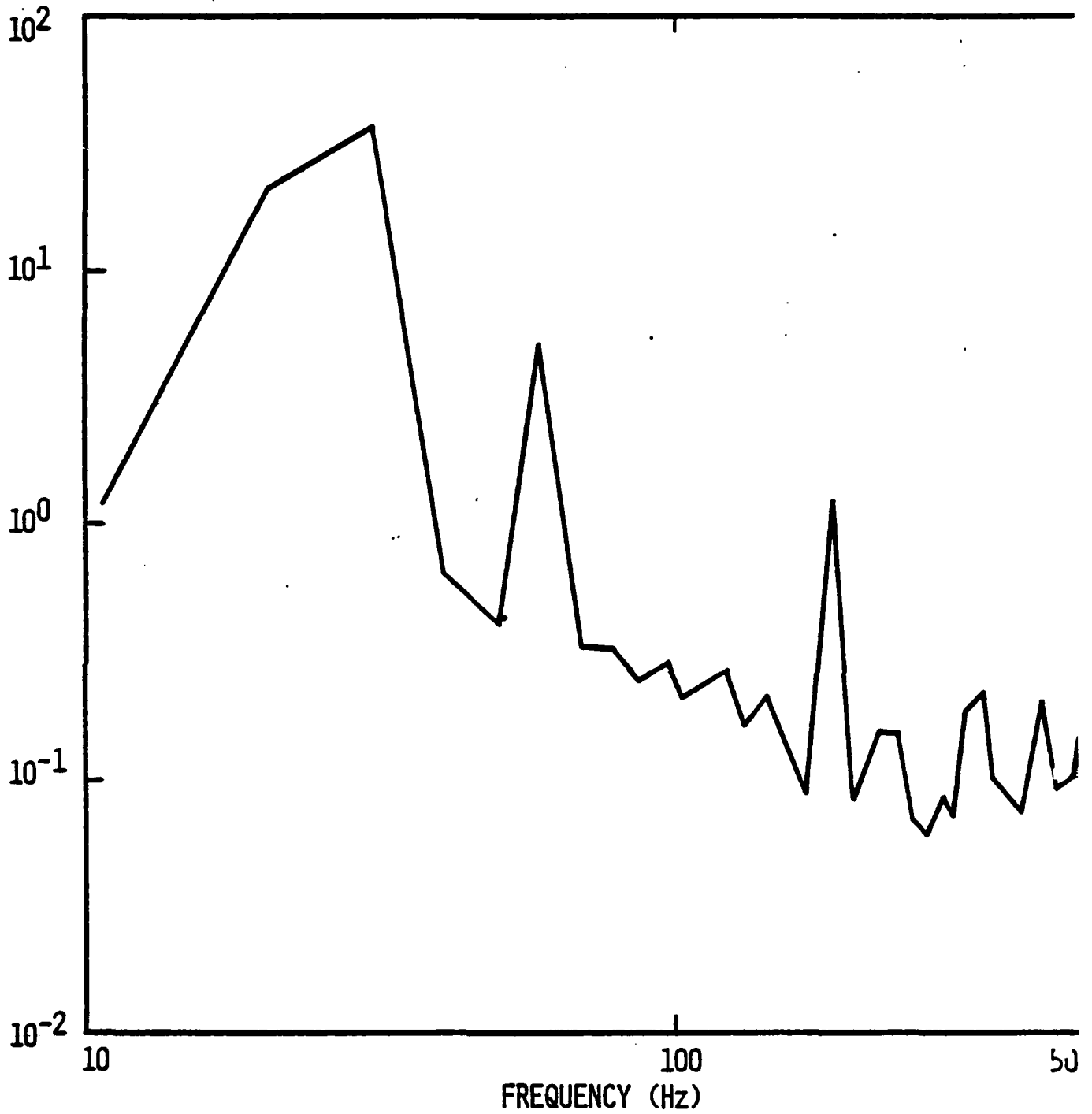
FIGURE 11B. SPECTRAL DENSITY OF LATERAL LUG FORCE RANDOM PROCESS FOR CARRIAGE IN F-111 BAY AT 590 KCAS AND 6,000 FT DURING 4G PULLUP WITH DOORS CLOSED.
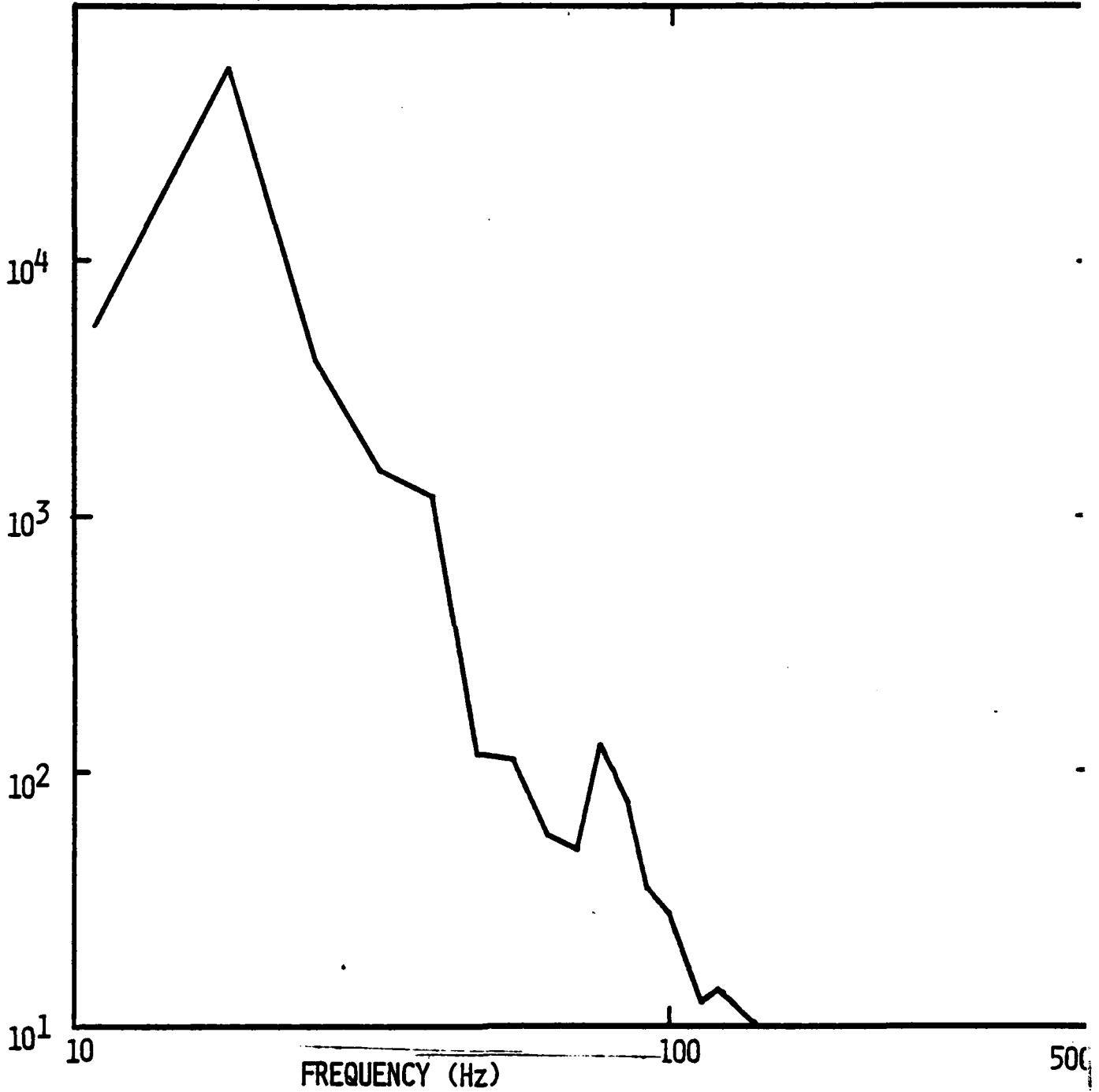
FIGURE 12A.   SPECTRAL DENSITY OF VERTICAL LUG FORCE RANDOM
PROCESS FOR CARRIAGE IN F-111 BAY AT 590 KCAS AND
6,000 FT DURING STRAIGHT AND LEVEL FLIGHT WITH
DOORS OPEN

$$\sigma_F = 822.5 \text{ lb.}, \quad \sigma_{\dot{F}} = 17,785 \text{ lb/sec}$$
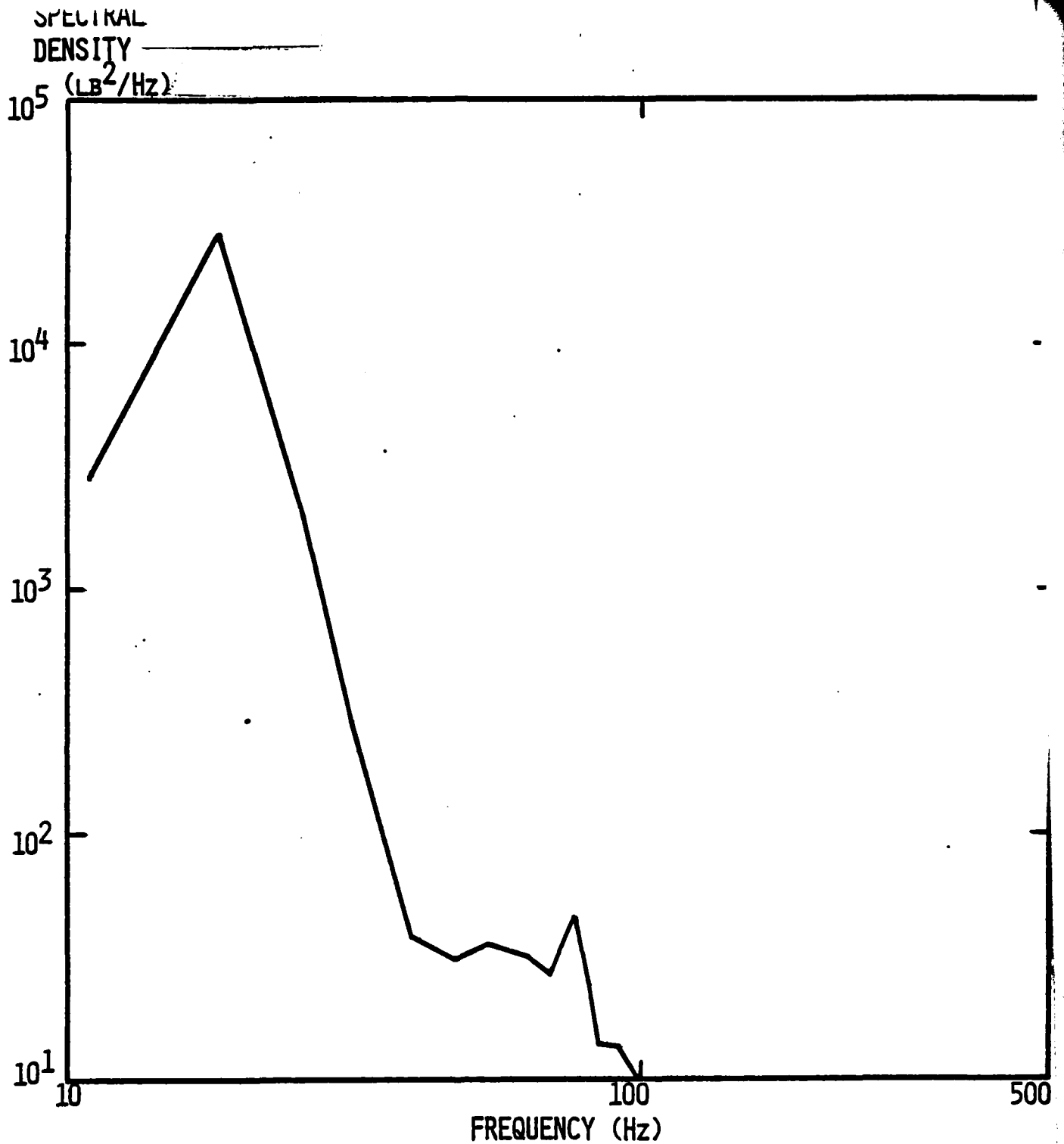
689

FIGURE 12B. SPECTRAL DENSITY OF LATERAL LUG FORCE RANDOM PROCESS FOR CARRIAGE IN F-111 BAY AT 590 KCAS AND 6,000 FT. ALTITUDE DURING STRAIGHT AND LEVEL FLIGHT WITH DOORS OPEN.

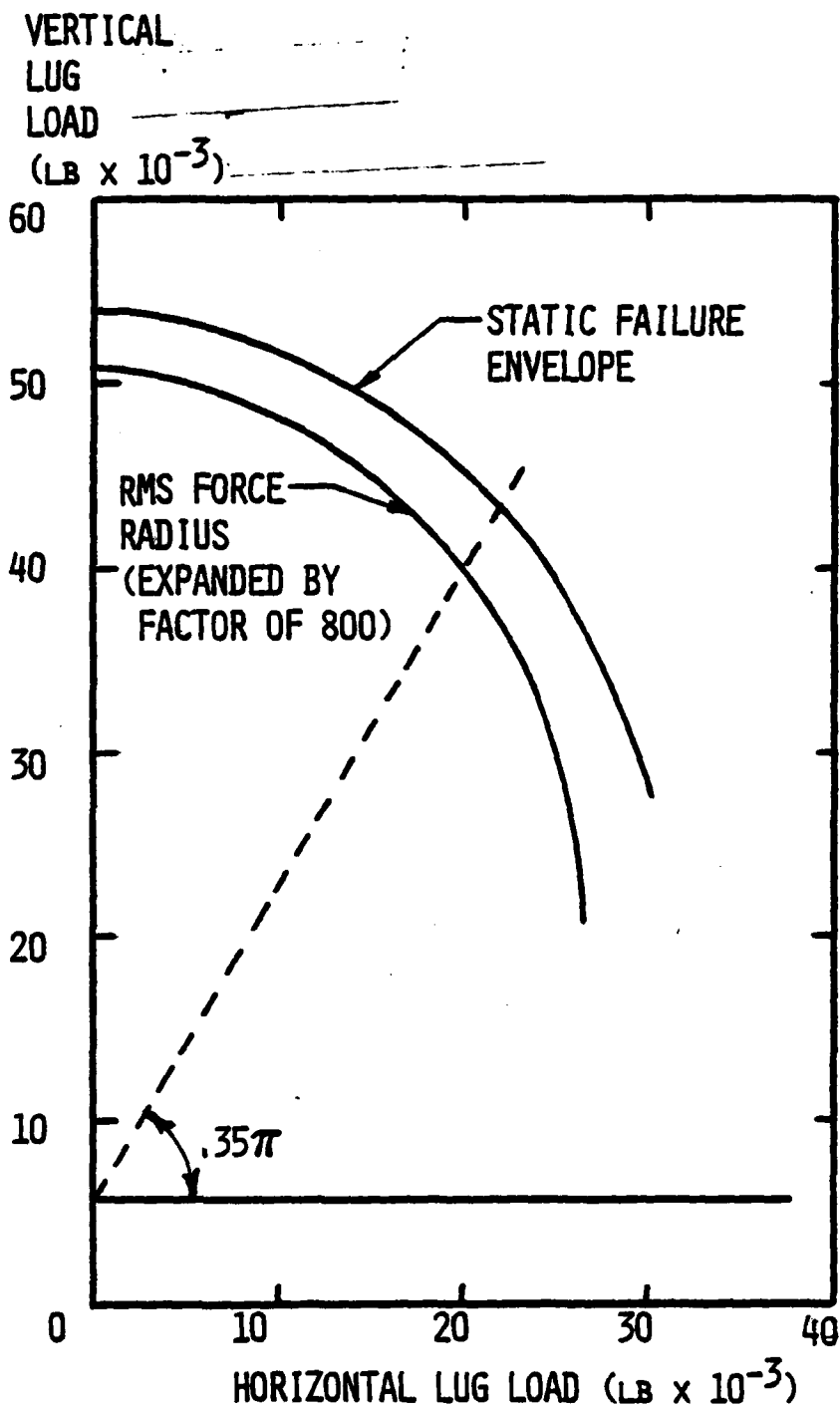690

VERTICAL
LUG
LOAD
($LB \times 10^{-3}$)

FIGURE 13. STATIC FAILURE ENVELOPE FOR LUG AND RMS FORCE RADIUS (EXPANDED BY FACTOR OF 800 FOR CLARITY).

691

obtain the system lower-bound reliability, graphed in
Figure 14. Apparently, the system is quite reliable
up to very long times t. The reason that the
probability of failure curve (1-R) is nearly
horizontal beyond the eight-minute point is that the
barrier height is extremely high in comparison to the
standard deviation of the doors-closed force-random-
process. During the open-door portion of the flight,
the failure barrier is about 13 times as great as the
standard deviation of the force random process;
therefore, this is called a first passage problem with
a 13 sigma barrier. The closed-door portion of the
flight has a 195 sigma barrier. Here sigma refers to
the rms, or standard deviation of the force random
process. The expression for reliability at t greater
than eight minutes is

$$R = (1 - 4.24 \times 10^{-32}) \left\{ \exp \left[- (t - 480)(563.3)e^{-17948} \right] \right\},$$

$$t \geq 480,$$

where t is in seconds. The second part of the
right-hand expression is extremely close to unity.
The entire reliability expression is so close to
unity, in fact, that there is no practical possibility
that failure could occur in this lug, given that the
strength and endurance limit assumptions are correct.

Figure 15 is a graph of Equation 37 versus time
for the more severe open-door environment. Equation
15 is used to relate n to time. The plus and minus
three-standard-deviation bounds on the peak forces are
shown in Figure 15; we obtained these using Equation
38. We consider the preceding calculation to be
reasonably conservative.

Calculations have been performed to determine how
much more severe the environments would be if the
speed were increased from 590 KCAS to 760 KCAS. It
has been conservatively estimated that the spectral
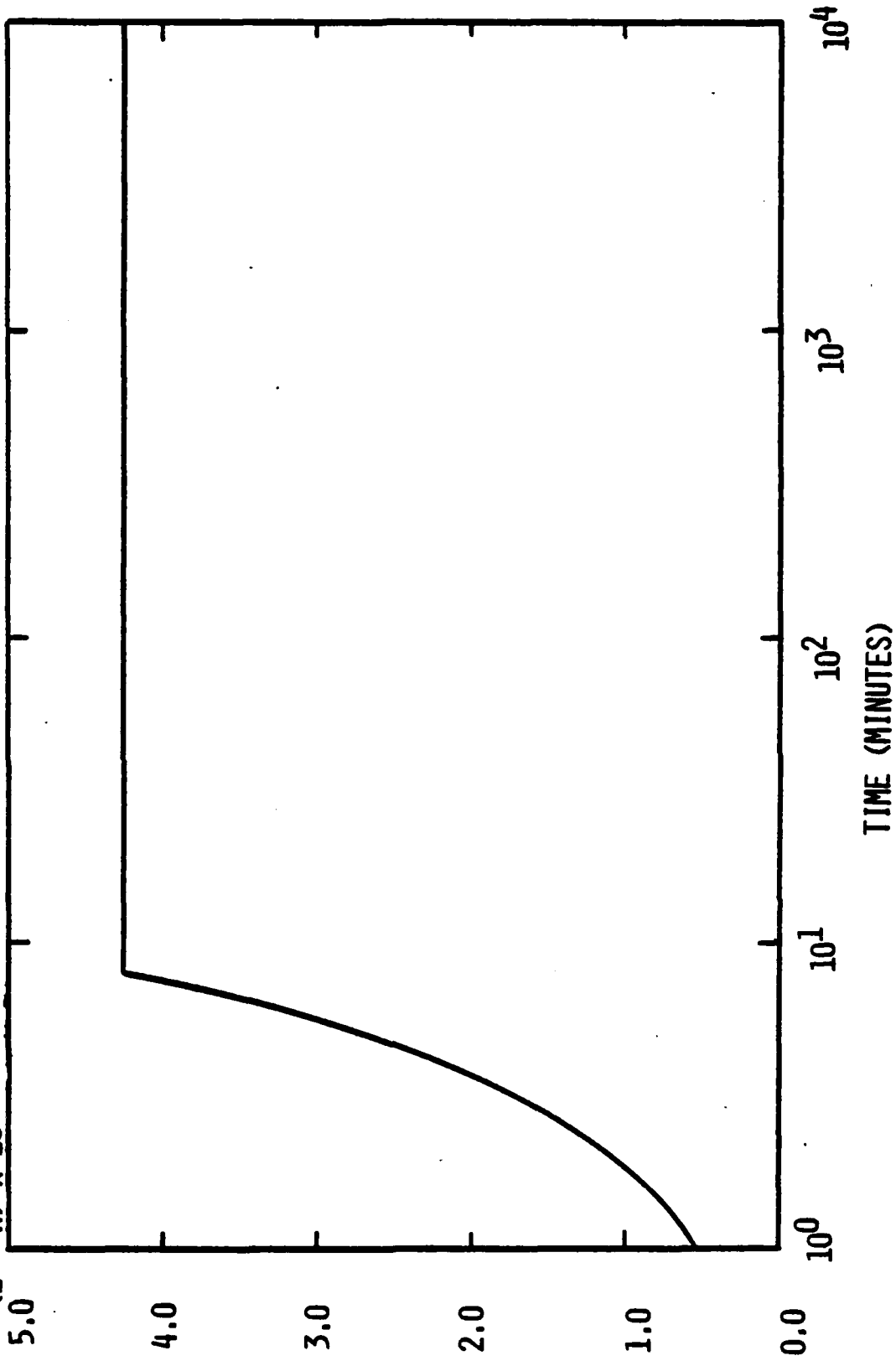densities of Figures 11a through 12b would be

692

FIGURE 14. UPPER BOUND ON PROBABILITY OF FAILURE FOR EIGHT MINUTES OF OPEN DOOR FLIGHT FOLLOWED BY CLOSED DOOR FLIGHT. MEASURED ENVIRONMENT.
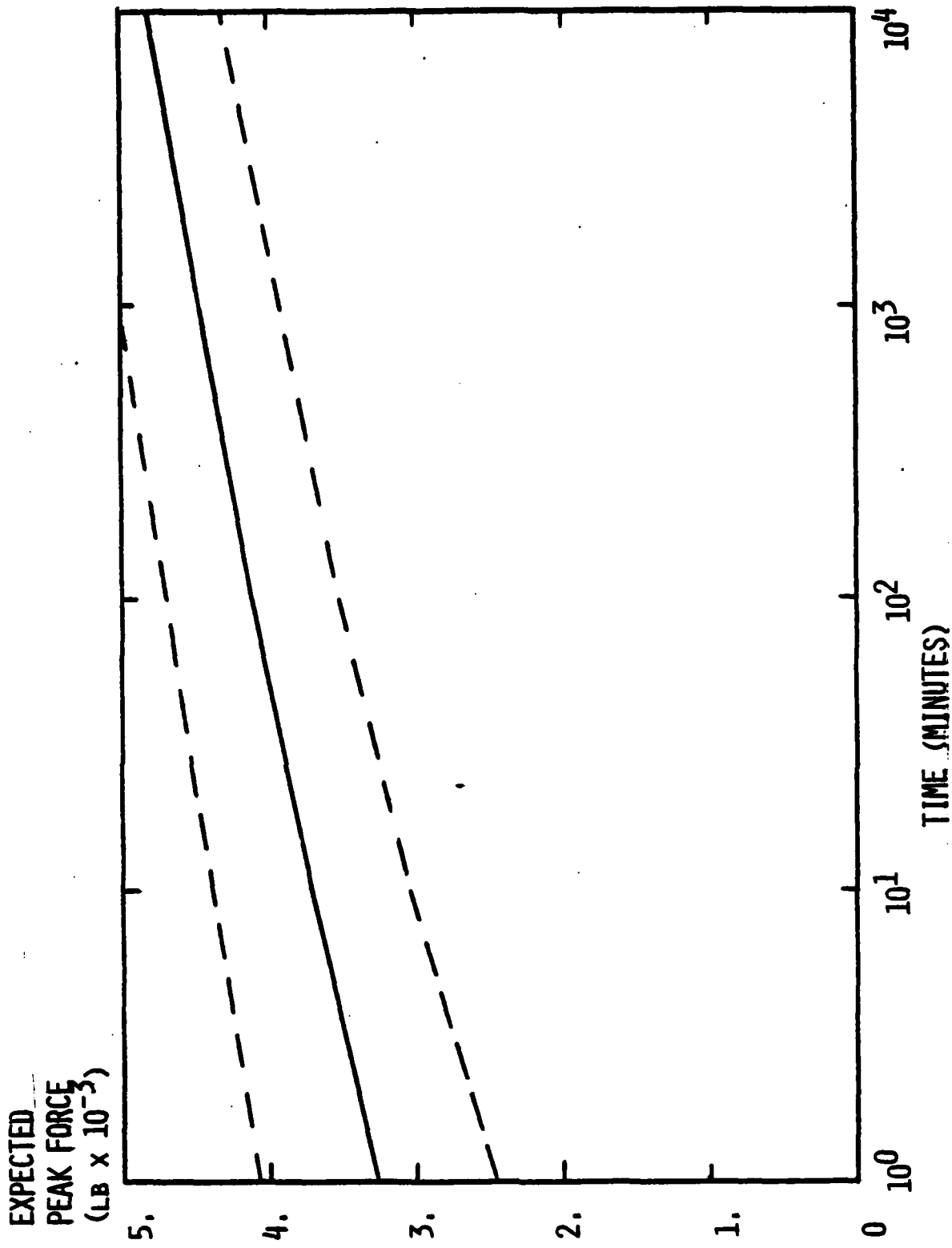
FIGURE 15. EXPECTED PEAK FORCE vs. TIME FOR OPEN DOOR ENVIRONMENT AND THREE STANDARD DEVIATION BOUNDS. MEASURED ENVIRONMENT.

694

increased by a factor of about 2.56. This corresponds
to an rms increase of 1.6. This extrapolation uses
the ratio of dynamic pressures as a criterion. When
we apply the increase, we find that in the closed
door, 760 KCAS, 6000 ft. case, we obtain
σ_F = 89 lb and $\sigma_{\dot{F}}$ = 50138 lb/sec and in the open-

door, 760 KCAS, 6000 ft case we obtain
σ_F = 1316 lb and $\sigma_{\dot{F}}$ = 28457 lb/sec. To be even more

conservative than before, we assume that α = 0.25.
Figure 16 is the upper-bound probability of failure
curve for this case. As before, eight minutes of
open-door flight are contained with an arbitrary
duration of closed-door flight. Again the reliability
is high, but not nearly so high as before. The
barrier during the open-door portion of flight is a
6.1 sigma barrier; during the closed-door portion of
flight, it is a 90 sigma barrier. The structural
reliability estimate past eight minutes is

$$R = (1.0 - 7.6 \times 10^{-5}) \left\{ \exp \left[-563.3(t - 480)e^{-4091} \right] \right\} ,$$

$$t \geq 480,$$

where t is in seconds. As before, the closed-door
portion of flight contributes very little to the
probability of failure of the suspension system
structure. Figure 17 is a graph of the expected peak
force in the lug versus time, obtained using Equation
37. The three-standard-deviation bounds are also
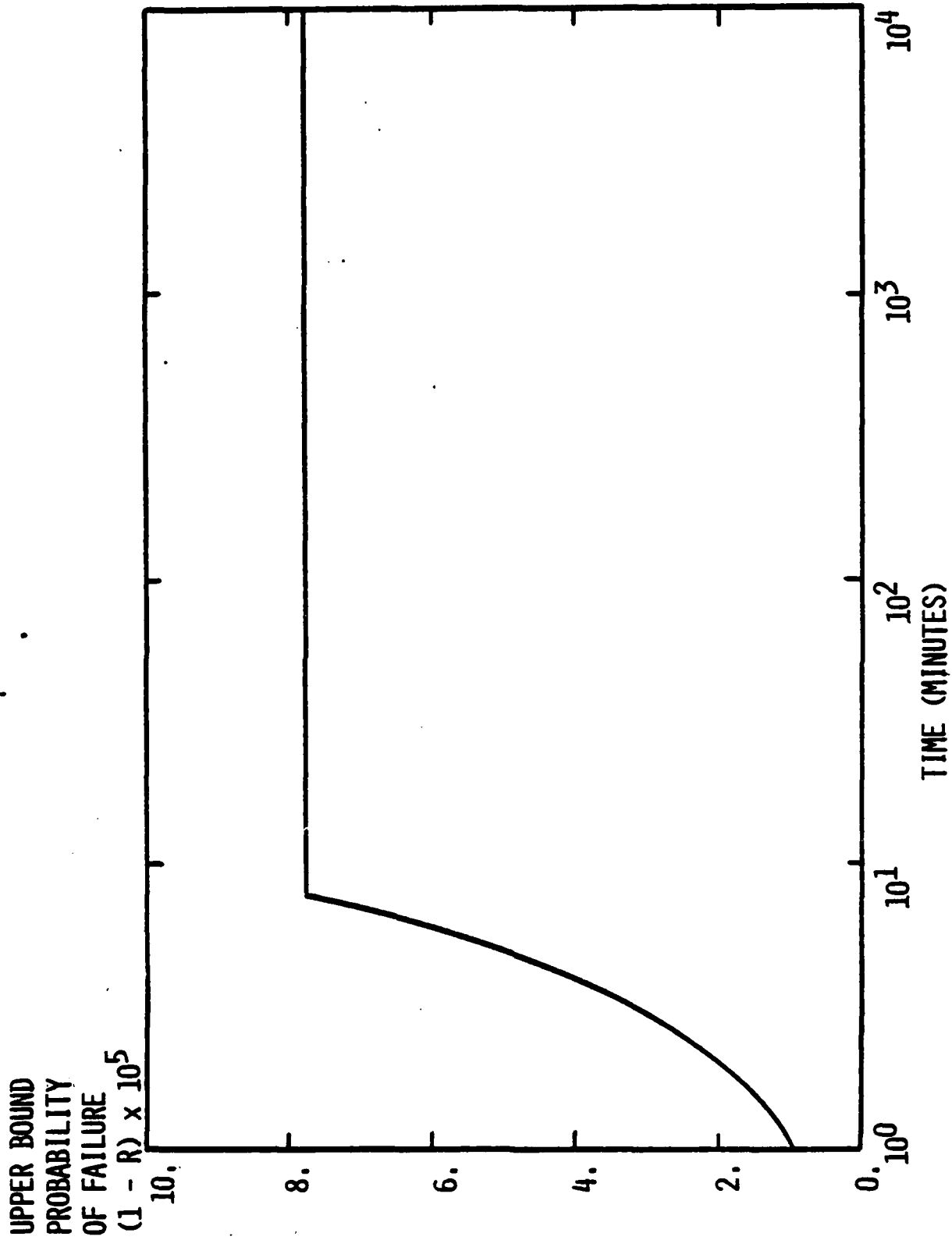included from Equation 38 in Figure 17.

695

Figure 16. UPPER BOUND PROBABILITY OF FAILURE FOR EIGHT MINUTES OF OPEN DOOR FLIGHT FOLLOWED BY CLOSED DOOR FLIGHT. EXTRAPOLATED ENVIRONMENT.
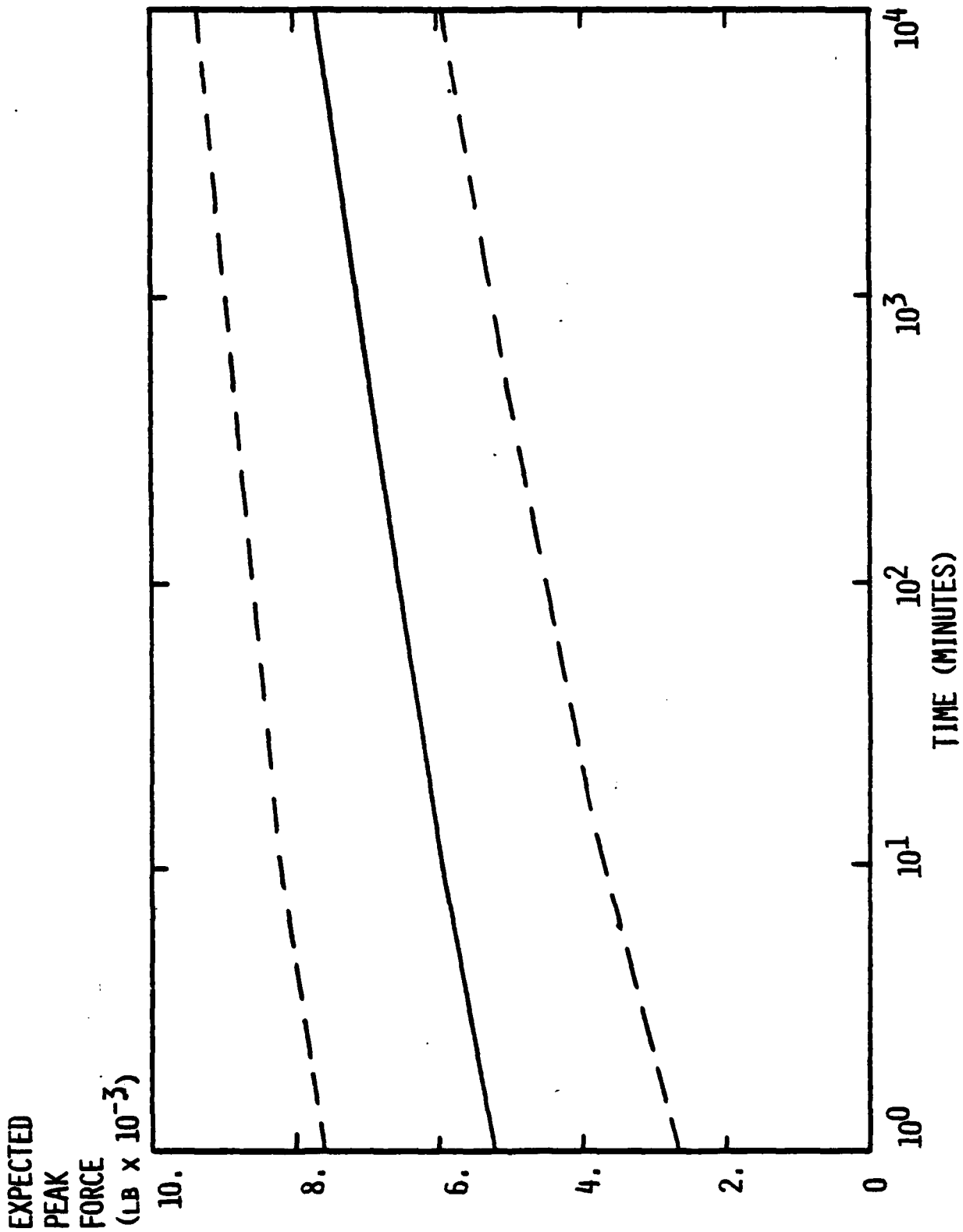
696

FIGURE 17. EXPECTED PEAK FORCE vs. TIME FOR OPEN DOOR ENVIRONMENT AND THREE STANDARD DEVIATION BOUNDS, EXTRAPOLATED ENVIRONMENT.

697

CONCLUSIONS AND RECOMMENDATIONS

Based on the work which has been completed to date, we conclude that a full scale instrumented test unit is an excellent way of determining suspension system loads during store carriage in an F-111 weapons bay. We are satisfied that both the commercially available and the Sandia designed load transducers are producing good results.

The data which have been reduced indicate an anticipated random loading which is Q dependent. Furthermore, for the particular store under study, the most critical loading conditions occur with similar shapes in the left and right bays rather than with one bay empty or a gun in the adjacent bay.

The four flights which have been completed have surveyed altitudes up to 40,000 ft. Results indicate that future flights should be performed at altitudes of 20,000 ft. and below to generate the most severe loading conditions. Further testing at increased speeds is recommended and is currently being planned.

Application of statistical analysis to the measured flight data and a failure envelope of the lug shows that even though the formulation used results in a lower-bound estimate on reliability, it can be useful in many cases. As long as the lower-bound reliability is near unity, safety is guaranteed if the assumptions used in the analysis are satisfied. Equation 31 and the second numerical example show that for a linear system with modal frequencies in the range 20-2000 hz, reliability begins to diminish rapidly when the ratio of barrier height to standard deviation of the force random process is in the range of five to seven and when environmental durations on the order of one hour are considered. Since we use a lower-bound formulation for reliability, when our estimate becomes small this does not necessarily imply that the probability of failure is high; this only implies that an upper bound on the probability of failure is high.

698

To make this method of structural reliability analysis more accurate, there are some important factors that we could consider. Particularly, the material strength and the endurance limit are random variables, and the environmental durations could be considered random variables. Incorporation of these factors into the analysis would yield a lower-bound reliability in which the probabilistic structure of the entire problem has been considered.

As the margin of safety in design of lugs diminishes, the lower bound approach to reliability estimation loses its usefulness since the lower-bound reliability tends to become small. In this case, refinement in treatment of the problem becomes necessary, and the fatigue problem must be considered. This can be done as follows. The random force in a lug must be related to the accumulation of fatigue damage. Then the random process governing force in the lug can be used to describe the random process governing damage accumulation. This is a Markov type random process since the damage accumulation at any given time depends on the damage at previous times. The probability that the accumulated damage surpasses a failure limit during a specified time duration must be computed where the failure limit itself is a random variable.

We recommend that fatigue tests be performed on the critical suspension hardware so that the analytical refinements summarized above can be applied to the data generated in order to more accurately predict the system reliability.

REFERENCES

1. Shaw, L. L., Smith, D. L., and Plzak, G. A.,
    "Aeroacoustic Environment of a Store in an
    Aircraft Weapons Bay," AFFDL-TR-77-18, March 1977.

2. Rice, S. O., "The Mathematical Analysis of Random
    Noise," Bell System Technical Journal, V23, 24,
    1944-45.

3. Feller, W., An Introduction to Probability Theory
    and Its Application, John Wiley & Sons, Inc.,
    1950.

4. Longuet-Higgins, M. S., "On the Statistical
    Distribution of the Heights of Sea Waves," Journal
    of Marine Research, V.11, n.3, 1952.

5. Cartwright, D. E., and Longuet-Higgins, M. S.,
    "The Statistical Distribution of the Maxima of a
    Random Function," Proceedings: ROYAL SOCIETY OF
    LONDON, Ser. A., Vol. 237, 1956.

AUTOBIOGRAPHY

Mr. S. D. Meyer received his BS degree in Mechanical Engineering from the University of Toledo in 1957. After four years in the glass container industry, he returned to school and received an MSME degree from the University of Toledo in 1962. After teaching for one year in the Department of Mechanical Engineering, he jointed Sandia Laboratories. His initial assignment at Sandia was in the area of environmental testing. The past 10 years have been spent working in engineering analysis. Areas of responsibility have included both loads and structural analyses. Mr. Meyer is a member of the American Society of Mechanical Engineers and Tau Beta Pi Engineering Honorary.

AUTOBIOGRAPHY

Thomas Paez is a member of the technical staff at Sandia Laboratories in the Applied Mechanics Department. At Sandia, he has been engaged in the mechanical analysis and testing of structural systems and components, particularly, random vibration analysis and testing. He previously held the position of research scientist at Kaman Sciences Corporation. Mr. Paez was awarded a BS with distinction in General Studies and Civil Engineering and an MS degree from the University of New Mexico in 1971. He then transferred to the School of Civil Engineering at Purdue University where he studied structural analysis, random processes and structural reliability, and was awarded a Ph.D degree in 1973. Mr. Paez is a member of the American Society of Civil Engineers, the Society of Sigma Xi, Phi Kappa Phi, Chi Epsilon, and other honorary Societies.

AN INVESTIGATION OF THE EFFECTS
OF EXTERNAL STORES ON THE
DYNAMIC STABILITY OF AIRCRAFT
(U)
(Article UNCLASSIFIED)

by

LT THOMAS E. SPEER
Air Force Armament Laboratory
Eglin Air Force Base, Florida 32542

ABSTRACT. (U) Recent trends in external store design, particularly in guided weapons, have led to stores which have a significant effect upon the stability characteristics of the parent aircraft. To date, no predictive technique has been adequate to analyze the static stability effects of external stores and little is known about the effects of stores on the aerodynamic damping derivatives. However, recent trends in the use of automatic flight control systems to provide acceptable handling qualities have made it necessary to accurately predict the flight dynamics of a store-laden aircraft.

A technique is presented to assess the effects of external stores on the dynamic stability of aircraft. This technique involves static and forced oscillation wind tunnel tests with and without external stores to provide data for use in three-degree and five-degree-of-freedom simulations. Present progress on the construction of a 1/20 scale F-16 force model and a 1/9 scale F-16 forced oscillation model is also presented.

LIST OF FIGURES

LIST OF TABLES

LIST OF SYMBOLS

b	wing span
c	mean aerodynamic chord
C_l	rolling moment coefficient
C_m	pitching moment coefficient
C_n	yawing moment coefficient
$C_X (-C_A)$	axial force coefficient
C_Y	side force coefficient
$C_Z (-C_N)$	normal force coefficient
d	model reference length
D	damping coefficient
F_X, F_Y, F_Z	forces along X, Y, Z axes
I_{XX}, I_{YY}, I_{ZZ}	moments of inertia about X, Y, Z axes
I_{XY}, I_{YZ}, I_{ZX}	products of inertia
K	balance stiffness
L	rolling moment
M	pitching moment
M	applied moment or general moment coefficient
N	yawing moment
N	general moment coefficient
p	body axis roll rate
P	perturbation roll rate
Q	body axis pitch rate
q	perturbation pitch rate

R	body axis yaw rate
r	perturbation yaw rate
S	wing area
t	time
U, V, W	velocity along X, Y, Z axes
u, v, w	perturbation velocities along X, Y, Z axes
V_T	magnitude of total velocity
X, Y, Z	body axes
α	angle of attack
β	angle of sideslip
ϵ	balance angular deflection
γ	phase angle
θ	pitch angle or model angular displacement
ρ	free stream density
ϕ	roll angle
ψ	yaw angle
ω	angular circular frequency

Subscripts

A	aerodynamic
T	tare
1	initial or steady state value
o	initial or maximum value
V	vacuum

INTRODUCTION

It has long been recognized that external stores can have a significant effect upon the performance and handling qualities of the parent aircraft. To date, most of the attention has been focused upon the static effects of store carriage. Generally, when external stores are added to an aircraft, there is a large increase in drag and, for wing mounted stores, a degradation of the longitudinal static margin. Additionally, speed stability and dutch roll behavior may also be affected adversely. Today's trends in both store and fighter aircraft design are tending to accentuate these degradations. Guided weapons are being designed to be very aerodynamically active by the addition of large fins and canards. New aircraft are using advanced control technology coupled with reduced static stability to tailor the handling qualities and improve performance. As a result, the effects of external stores on aircraft flight dynamics are being felt much more strongly. For example, the addition of some stores to the F-16 can cause neutral point shifts an order of magnitude higher than they would on its predecessor, the F-4.

Whether or not these decrements cause a serious degradation of the handling qualities of the aircraft depends upon the static stability, aerodynamic damping characteristics, mass and inertias, and control system of the given aircraft/store configuration. Nearly all of the work done concerning performance and stability effects of store carriage has been concerned solely with drag and static longitudinal stability. The possible changes to the dynamic stability derivatives and the interaction of active control systems with the affected aerodynamics have been largely ignored. The reason for this past emphasis on static effects is due in part to the difficulty in predicting and measuring dynamic derivatives and in the added complexity of analysis. In addition, experience has shown that satisfactory static stability was sufficient to insure adequate handling qualities in store-laden aircraft. It would seem unlikely that the same approach will be adequate for aircraft that rely on active controls, especially aircraft with large negative static margins, and aircraft which experience exceptionally large static stability degradations when stores are added.

PROGRESS

The inadequacy of the static stability approach was brought sharply into focus by the F-16, with its fly-by-wire control system and large negative static margin. Static tests also showed that external stores have a significant influence on the static aerodynamics. Recognizing the need for a more complete look at aircraft dynamics, the Air Force Armament Laboratory (AFATL) and Arnold Engineering Center (AEDC) entered into a joint project to develop the capability to predict the dynamic effects of store carriage.

Because most of the techniques used to predict the aerodynamic effects of stores rely heavily on wind tunnel data, AFATL has made extensive use of the AEDC wind tunnels and the two agencies have developed a close working relationship. In order to complement their extensive testing capabilities AEDC has developed a capability to provide various types of analysis of experimental data. At approximately the same time that AFATL was recognizing the need to develop a dynamic stability analysis capability, AEDC had begun the first steps toward developing a similar capability. In order to avoid a great deal of duplication of effort and speed the progress in both programs a joint project involving both AEDC and AFATL was initiated. Each agency concentrated their work in different areas.

AEDC began work on three and five-degree-of-freedom linear analysis computer programs, and AFATL initiated work on a nonlinear simulation program. These programs are needed to analyze and simulate the motion of the aircraft based on force and moment information derived from wind tunnel testing. AFATL sponsored the design and fabrication of a 1/9th scale F-16 model to be used in measuring dynamic stability derivatives using the forced oscillation technique and a 5% scale F-16 model to be used in static force testing. The F-16 was selected as the subject for the initial analysis capability and wind tunnel investigation because it is the product of advanced control and aerodynamic technology and, as such, is the ideal test bed for this development in compatibility technology.

Presently, the 5% scale model has been delivered and the first wind tunnel test has been completed. Comparisons are now being made between the 5% scale data and the data from tests of General Dynamics' 1/9 scale model. The dynamic model is nearly completed and the first test is scheduled during February 1978.

TEST TECHNIQUE

In Table I, the six-degree-of-freedom aerodynamic forces and moments are presented. It is assumed that the forces and moments are linear functions of small changes from a steady state condition, and there is no coupling between the longitudinal and lateral directional motions for the range of the small perturbations. The derivatives with respect to α, β, and u determine the static stability of the aircraft and can be determined from conventional wind tunnel techniques. As may be seen from Table II, most of the important derivatives dealing with longitudinal motion (derivatives of C_X, C_Z, and C_m) may be determined from static testing techniques. For lateral directional motion, however, such is not the case. The derivatives dealing with $\dot{\alpha}$, $\dot{\beta}$, p, q, and r are due to the motion of the aircraft. These derivatives may only be determined by allowing some type of motion of the model. In dynamic testing, the model is forced to oscillate within a constant maximum amplitude about one of its axes.

709

The dynamic derivatives mentioned above are generally functions of the frequency of the oscillation. This frequency dependence is due to the lag induced as aerodynamic disturbances influence different parts of the aircraft and to local flow separation effects. Consequently, it is desirable to oscillate the model at a frequency which will simulate the frequencies expected to be produced by the aircraft in flight. The scaling of model frequencies to reflect aircraft frequencies is determined by the reduced frequency factor:

$$\frac{\omega d}{2V_T}$$

where ω is the frequency, d is a characteristic dimension and V_T is the magnitude of the velocity. In order for the model to behave similarly to the full scale aircraft,

$$\left(\frac{\omega d}{2V_T}\right)_{model} = \left(\frac{\omega d}{2V_T}\right)_{aircraft}$$

For a reduced scale model, the resultant frequency is much higher than the aircraft frequency. As will be seen in the section on the theory of forced oscillation testing, there is a natural frequency which is determined by the stiffness of the support system and the moments of inertia of the model. If the desired testing frequency and this natural frequency may be made to coincide, a great simplification in data reduction occurs and the most accurate data is obtained. Testing at frequencies other than this natural resonant frequency is possible, but it is desirable not to stray too far from it.

In order to assess the effects of store carriage on the aircraft, the model is tested with and without external stores. Since, ideally, the aerodynamics are basically linear in nature, the derivatives evaluated for the model without stores are subtracted from those for the model with stores to obtain the effects of the stores. Build-up configurations are generally done to determine the incremental effects due to the addition of pylons, racks, and stores. These increments are then added to the best available full scale data in order to predict the characteristics of the full scale aircraft.

This approach has proven to be very successful in the past when applied to the static derivatives. It is hoped that it will prove equally successful in the case of the dynamic derivatives.

DYNAMIC MODEL

As mentioned above, the natural frequency of the oscillating model is determined by the moments of inertia of the model, and the stiffness of the support system. This relationship coupled with the need to operate at comparatively high frequencies and to reduce the

balance stiffness in order to minimize the tare damping, leads to the desire to have a lightweight model with low moments of inertia. In order to achieve the lightest weight consistent with the strength requirements for testing at high angles of attack and transonic Mach numbers, AEDC conceived a model design which was a novel combination of steel, aluminum, and fiberglass construction.

To speed and simplify construction, General Dynamics' steel 1/9 scale model was borrowed and used as a pattern. Aluminum wings and tail surfaces were machined by tracing the steel flying surfaces. The force model fuselage was used as a plug to cast a female mold. Fiberglass shells were then laid up in the molds.

The aluminum wings and tail surfaces bolt to a hollow steel member along the fuselage centerline. This tubular steel hardback carries all of the structural loads and transfers them to the balance adaptor, which is located inside the hardback. The fiberglass shells are fastened around the assembled metal components. The fiberglass shell carries no structural loads, but is only used to fair the fuselage to the proper shape. The relationship of these components is schetched in Figure 1, and various steps in their construction is shown in Figures 2 through 5. The 5% scale static model is shown for comparison in Figure 6.

The forward end of hardback contains provisions for ballasting the model to obtain the proper moment of inertia and center of gravity position. The central structure design precluded the use of ducting the inlet flow through the model. Consequently, a fairing will be installed to simulate the streamlines at the inlet lip. Lightweight store models are also being constructed. The 370 gallon fuel tank models will have provisions for ballasting the model to adjust for the wide range of configurations to be tested.

THEORY

The following are the kinematic equations of motion for a rigid aircraft having a vertical plane of symmetry. Axes definitions are shown in Figure 7.

$$F_X = m\,(\dot{U} - VR + WQ) \tag{1a}$$

$$F_Y = m\,(\dot{V} + UR - WP) \tag{2a}$$

$$F_Z = m\,(\dot{W} - UQ + VP) \tag{3a}$$

$$L = I_{XX}\,\dot{P} - I_{XZ}\,\dot{R} - I_{XZ}\,PQ + (I_{ZZ} - I_{YY})\,QR \tag{4a}$$

$$M = I_{YY}\,\dot{Q} + (I_{XX} - I_{ZZ})\,PR + I_{XZ}\,(P^2 - R^2) \tag{5a}$$

$$N = I_{ZZ}\,\dot{R} - I_{XZ}\,\dot{P} + (I_{YY} - I_{XX})\,PQ + I_{XZ}\,QR \tag{6a}$$

ALUMINUM FLYING SURFACES

BALANCE CENTER

FIBERGLASS SHELL
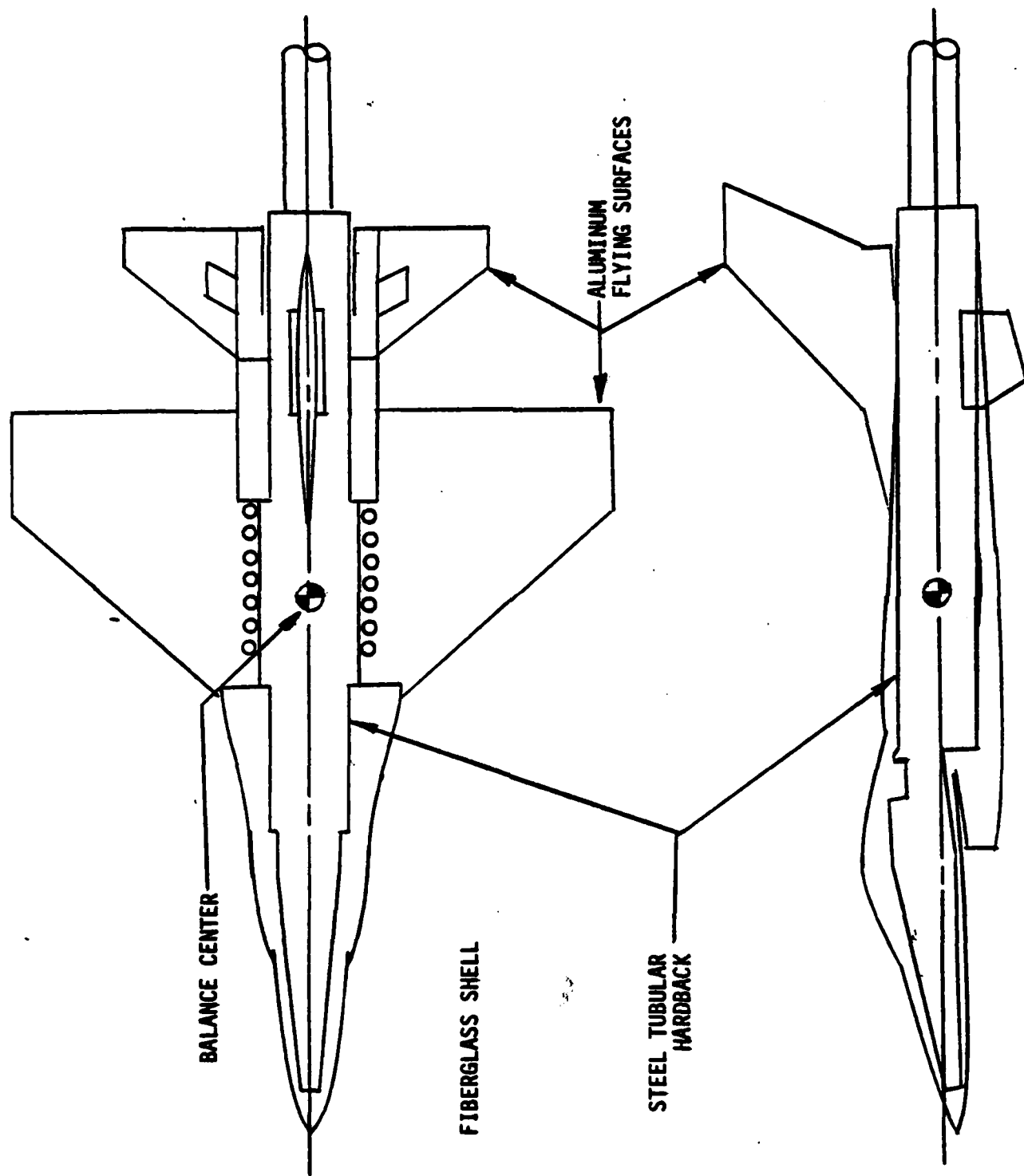
STEEL TUBULAR HARDBACK
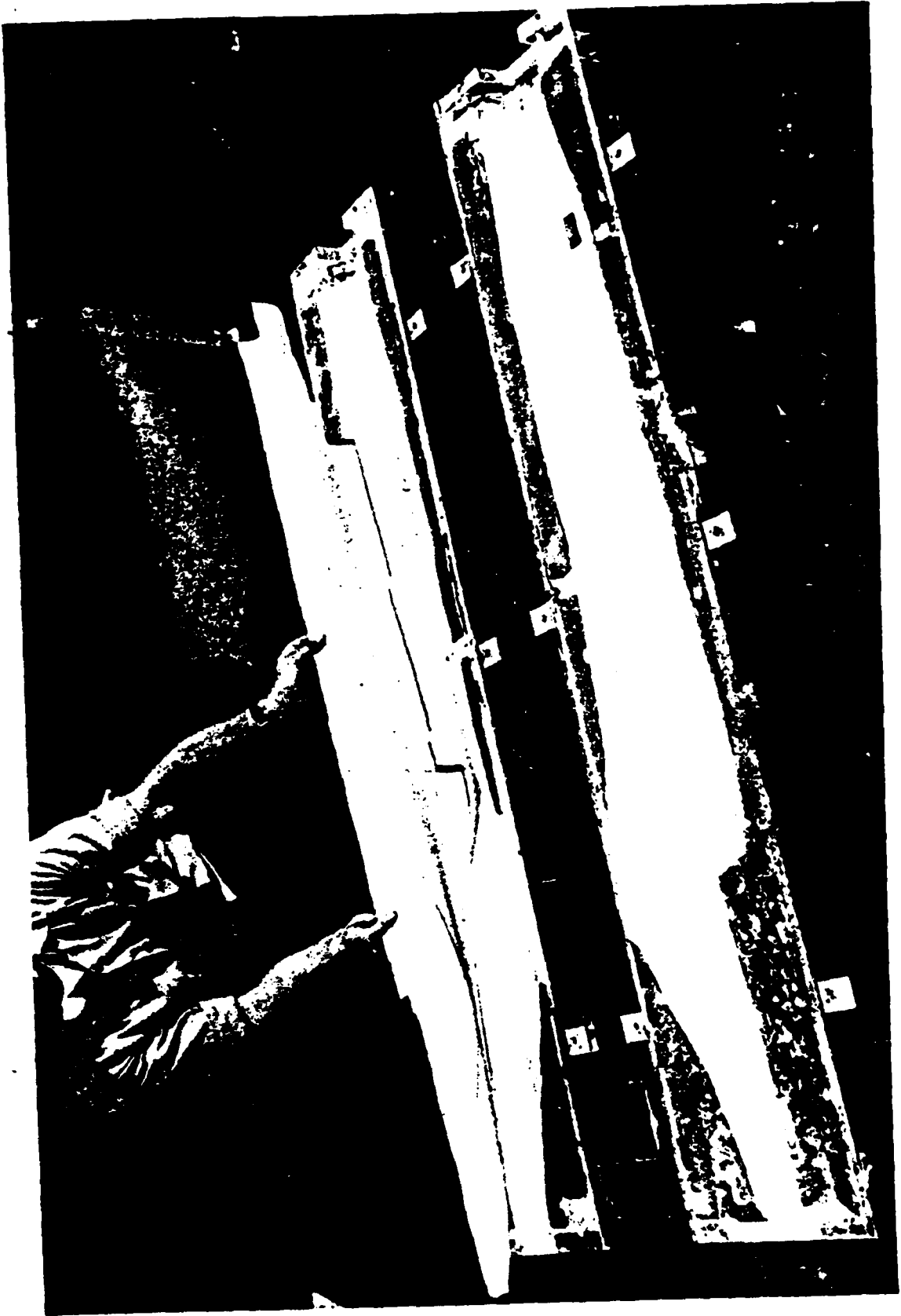
Figure 1.   Lightweight Model

712

Figure 2. Removal of Fiberglass Fuselage Shells

Figure 3. Machining of Fuselage Centerline

714

Figure 4. Lightweight Store Models

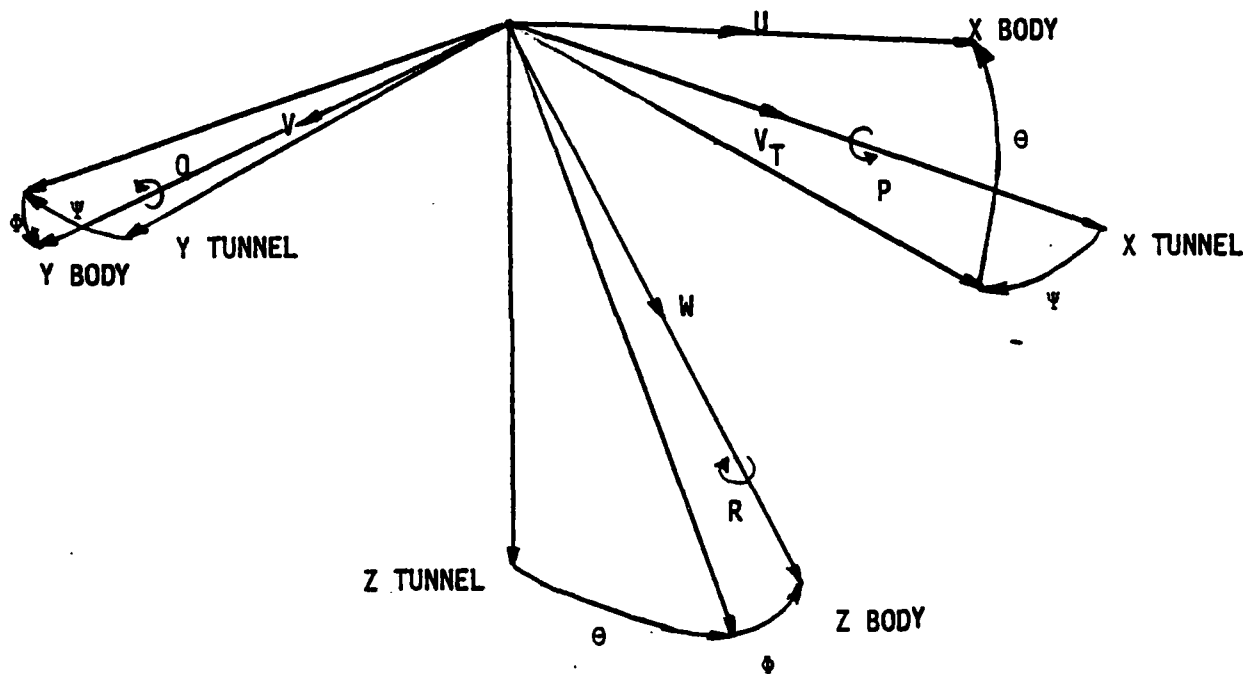Figure 5. Dynamic Model Components

Figure 6. 5% Scale Static Model

717

Figure 7. Axes Definitions

718

TABLE I. AERODYNAMIC STABILITY DERIVATIVES

$$F_X = C_X \ (1/2\rho V_T^2 S) \qquad L = C_l \ (1/2\rho V_T^2 Sb)$$

$$F_Y = C_Y \ (1/2\rho V_T^2 S) \qquad M = C_m \ (1/2\rho V_T^2 S\bar{c})$$

$$F_Z = C_Z \ (1/2\rho V_T^2 S) \qquad N = C_n \ (1/2\rho V_T^2 Sb)$$

$$C_{X_\alpha} = \frac{\partial C_X}{\partial \alpha} \qquad\qquad C_{l_\beta} = \frac{\partial C_l}{\partial \beta} \qquad\qquad C_{Z_q} = \frac{\partial C_Z}{\partial \frac{q\bar{c}}{2V_T}}$$

$$C_{X_{\dot\alpha}} = \frac{\partial C_X}{\partial \frac{\dot\alpha\bar{c}}{2V_T}} \qquad\qquad C_{l_{\dot\beta}} = \frac{\partial C_l}{\partial \frac{\dot\beta b}{2V_T}} \qquad\qquad C_{Z_u} = \frac{\partial C_Z}{\partial \frac{u\bar{c}}{2V_T}}$$

$$C_{X_q} = \frac{\partial C_X}{\partial \frac{q\bar{c}}{2V_T}} \qquad\qquad C_{l_p} = \frac{\partial C_l}{\partial \frac{pb}{2V_T}} \qquad\qquad C_{n_p} = \frac{\partial C_n}{\partial \frac{pb}{2V_T}}$$

$$C_{X_u} = \frac{\partial C_X}{\partial \frac{u}{V_T}} \qquad\qquad C_{l_r} = \frac{\partial C_l}{\partial \frac{rb}{V_T}} \qquad\qquad C_{n_r} = \frac{\partial C_n}{\partial \frac{rb}{2V_T}}$$

$$C_{Y_\beta} = \frac{\partial C_Y}{\partial \beta} \qquad\qquad C_{m_\alpha} = \frac{\partial C_m}{\partial \alpha}$$

$$C_{Y_{\dot\beta}} = \frac{\partial C_Y}{\partial \frac{\dot\beta b}{2V_T}} \qquad\qquad C_{m_{\dot\alpha}} = \frac{\partial C_m}{\partial \frac{\dot\alpha\bar{c}}{2V_T}}$$

$$C_{Y_p} = \frac{\partial C_Y}{\partial \frac{pb}{2V_T}} \qquad\qquad C_{m_q} = \frac{\partial C_m}{\partial \frac{q\bar{c}}{2V_T}}$$

$$C_{Y_r} = \frac{\partial C_Y}{\partial \frac{rb}{2V_T}} \qquad\qquad C_{m_u} = \frac{\partial C_m}{\partial \frac{u}{u_o}}$$

$$C_{Z_\alpha} = \frac{\partial C_Z}{\partial \alpha} \qquad\qquad C_{n_\beta} = \frac{\partial C_n}{\partial \beta}$$

$$C_{Z_{\dot\alpha}} = \frac{\partial C_Z}{\partial \frac{\dot\alpha\bar{c}}{2V_T}} \qquad\qquad C_{n_{\dot\beta}} = \frac{\partial C_n}{\partial \frac{\dot\beta b}{2V_T}}$$

TABLE I. AERODYNAMIC STABILITY DERIVATIVES (Continued)

$$\alpha = \alpha_A - \alpha_1 \qquad\qquad u = U - U_1 \qquad\qquad q = Q - Q_1$$

$$\beta = \beta_A - \beta_1 \qquad\qquad p = P - P_1 \qquad\qquad r = R - R_1$$

$$C_X = C_{X_1} + C_{X_\alpha} \alpha + C_{X_\alpha} \frac{\dot{\alpha}\bar{c}}{2V_T} + C_{X_q} q\bar{c} + C_{X_u} \frac{u}{V_T}$$

$$C_Y = C_{Y_1} + C_{Y_\beta} \beta + C_{Y_{\dot{\beta}}} \frac{\dot{\beta}b}{2V_T} + C_{Y_p} \frac{pb}{2V_T} + C_{Y_r}$$

$$C_Z = C_{Z_1} + C_{Z_\alpha} \alpha + C_{Z_\alpha} \frac{\dot{\alpha}\bar{c}}{2V_T} + C_{Z_q} \frac{qc}{2V_T} + C_{Z_u} \frac{u}{V_T}$$

$$C_1 = C_{1_1} + C_{1_\beta} \beta + C_{1_{\dot{\beta}}} \frac{\beta b}{2V_T} + C_{1_p} \frac{pb}{2V_T} + C_{1_r} \frac{rb}{2V_T}$$

$$C_m = C_{m_1} + C_{m_\alpha} \alpha + C_{m_{\dot{\alpha}}} \frac{\dot{\alpha}\bar{c}}{2V_T} + C_{m_q} \frac{q\bar{c}}{2V_T} + C_{m_u} \frac{u}{V_T}$$

$$C_n = C_{n_1} + C_{n_\beta} \beta + C_{n_\beta} \frac{\dot{\beta}b}{2V_T} + C_{r_p} \frac{pb}{2V_T} + C_{n_r} \frac{rb}{2V_T}$$

TABLE II.   RELATIVE IMPORTANCE OF DERIVATIVES[**]

DERIVATIVE	RELATIVE[*] IMPORTANCE	DERIVATIVE	RELATIVE IMPORTANCE
C_{Z_α}	10	C_{Y_β}	7
C_{m_α}	10	C_{l_β}	10
C_{X_α}	5	C_{n_β}	10
$C_{Z_{\dot\alpha}}$	4	$C_{Y_{\dot\beta}}$	2
$C_{m_{\dot\alpha}}$	7	$C_{l_{\dot\beta}}$	2
$C_{X_{\dot\alpha}}$	1	$C_{n_{\dot\beta}}$	4
C_{Z_u}	5	C_{Y_p}	4
C_{m_u}	8	C_{l_p}	10
C_{X_u}	6	C_{n_p}	8
C_{Z_q}	3	C_{Y_r}	4
C_{m_q}	9	C_{l_r}	7
C_{X_q}	1	C_{n_r}	9

[*] 10 = Major   5 = Minor   0 = Negligible

[**]From Roskam, Jan, <u>Flight Dynamics of Rigid and Elastic Airplanes</u>, published by the Author, 1972

TABLE III.   TEST PLAN

Configuration	1	2	3	4	5	6	7	8	9
1	AIM-9	-	-	-	-	-	-	-	AIM-9
2	AIM-9	-	(3) AGM-65	370 TANK	ECM	370 TANK	(3) AGM-65	-	AIM-9
3	AIM-9	-	ECM	GBU-10	300 TANK	GBU-10	-	-	AIM-9

Mach Numbers .6   .9   .95   1.1

Angles of Attack

   Configuration 1

      -2.5, 2.5, 0, 2.5, 5.0, 7.5, 10.0, 12.5, 15.0, 17.5

   Configuration 2, 3

      0, 2.5, 5.0, 7.5, 10.0, 12.5, 15.0

When the aircraft is restrained, as is a model in a wind tunnel, to a single rotational degree of freedom, these equations reduce to the following:

For rotation about the X axis:

$$Q = R = \dot{U} = \dot{Q} = \dot{R} = 0$$

$$F_X = F_Y = F_Z = 0$$

$$L = I_{XX} \dot{P} \tag{1b}$$

$$M = I_{XZ} P^2 \tag{2b}$$

$$N = I_{XZ} \dot{P} \tag{3b}$$

For rotation about the Y axis

$$P = R = \dot{P} = \dot{R} = \dot{V} = 0$$

$$F_X = F_Y = F_Z = 0$$

$$L = 0 \tag{1c}$$

$$M = I_{YY} \dot{Q} \tag{2c}$$

$$N = 0 \tag{3c}$$

For rotation about the Z axis

$$P = Q = \dot{P} = \dot{Q} = \dot{W} = 0$$

$$F_X = F_Y = F_Z = 0$$

$$L = -I_{XZ} \dot{R} \tag{1d}$$

$$M = -I_{XZ} R^2 \tag{2d}$$

$$N = I_{ZZ} \dot{R} \tag{3d}$$

The reaction forces and moments associated with the above equations consist of an aerodynamic term, terms due to the deflection and damping of the support system, and a forcing function. These forces and moments are represented by the following equations:

$$F_X = F_{A_X} + D_X \dot{x} + K_X x + F_{F_X}(t) \tag{1f}$$

$$F_Y = F_{A_Y} + D_y \dot{y} + K_y y + F_{F_y}(t) \tag{2f}$$

$$F_Z = F_{A_Z} + D_Z \dot{z} + K_Z z + F_{F_Z}(t) \qquad (3f)$$

$$L = L_A + D_1 P + K_1 (\phi) + L_F (t) \qquad (4f)$$

$$M = M_A + D_m Q + K_m (\theta \cos \phi) + M_F (t) \qquad (5f)$$

$$N = N_A + D_N R + K_n (\psi \cos \theta \cos \phi) + N_F (t) \qquad (6f)$$

The aerodynamic forces and moments can be expressed a: the addition of forces and moments in a steady state condition and the forces and moments due to changes from the steady state. These perturbation forces may be assumed to be linear functions of the perturbation for small changes. These aerodynamic forces are nondimensionalized and the resulting coefficients differentiated with respect to the pertinent perturbations. It is assumed that there is no coupling between the lateral directional and longitudinal perturbations. The resulting aerodynamic derivatives are given in Table I. The lower case variables are the perturbation from steady state, e.g., $U = U_1 + u$, etc. Table II gives an approximate indication of the relative importance of each of the derivatives to the aircraft dynamics.

As may be seen in Table I, many of the stability derivatives are functions of the aerodynamic angles, α and β. These angles defined by the following relationships:

$$\alpha = \arctan \left(\frac{W}{U}\right) \qquad (7a)$$

$$\beta = \arcsin \left(\frac{V}{V_T}\right) \qquad (7b)$$

When these relationships are expressed in terms of the Euler angles for a body in a wind tunnel,

$$\alpha = \arctan \left(\frac{\cos \phi \sin \theta \cos \psi + \sin \phi \sin \psi}{\cos \theta \cos \psi}\right) \qquad (7c)$$

$$\beta = \arcsin (-\cos \phi \sin \psi + \sin \phi \cos \psi \sin \phi) \qquad (7d)$$

These equations may be differentiated and the transfer equations for the Euler rates in terms of the body rates. No such derivation will be attempted here. The majority of conditions of interest are those at some large angle of attack and zero sideslip and small oscillations of the model. These assumptions allow for considerable simplification and linearization of α and β.

$$\alpha = \arctan (\tan \theta + \phi \psi \sec \theta) \qquad (7e)$$

$$\beta = -\psi + \phi \sin \theta \qquad (7f)$$

Differentiating:

$$\dot{\alpha} = [\frac{\cos \theta}{1 + 2 \sin (\theta) \phi\Psi + \phi^2\Psi^2}] [(1 + \phi\Psi)(\sec \theta) \dot{\theta} + \tag{7g}$$

$$\Psi\dot{\phi} + \phi\dot{\Psi}]$$

$$\beta = -\Psi + (\sin \theta) \phi + (\phi \cos \theta) \dot{\theta} \tag{7h}$$

The last new equations needed are the body axis rates in terms of the Euler rates.

$$P = \dot{\phi} - \dot{\Psi} \sin \theta \tag{8a}$$

$$Q = \dot{\theta} \cos \phi + \dot{\Psi} \cos \theta \sin \tag{8b}$$

$$R = \dot{\Psi} \cos \theta \cos \phi - \dot{\theta} \sin \phi \tag{8c}$$

Finally, it is possible to write the significant moment equations for three types of model motion in the wind tunnel.

For rotation about the X axis at a large angle of attack, no yaw, small angles of roll, and no initial roll:

$$I_{XX} \ddot{\phi} - (\frac{\bar{q} Sb}{2U_T} (C_{l_{\dot{\beta}}} \sin \theta + C_{l_p}) + D_l) \dot{\phi} \tag{9a}$$

$$- (\bar{q} Sb C_{l_\beta} \sin \theta + K_l) \phi = L_F (t)$$

$$I_{XZ} \ddot{\phi} + (\bar{q} Sb^2 (C_{n_{\dot{\beta}}} \sin \theta + C_{n_p})) \dot{\phi} \tag{9b}$$

$$+ (\frac{\bar{q} Sb}{2U_T} C_{n_\beta} \sin) \phi = - N_F (t)$$

For rotation about the Y axis at a large angle of attack, no roll, and no yaw:

$$I_{YY} \ddot{\theta} - (\frac{\bar{q} S\bar{c}^2}{2U_T} (C_{m_{\dot{\alpha}}} + C_{m_q}) + D_m) \theta \tag{10}$$

$$- (\bar{q} S\bar{c} C_{m_\alpha} + K_m) (\theta - \theta_0) = M_F (t)$$

For rotation about the Z axis at a large angle of attack, no roll, small yaw angles, and no initial yaw:

$$I_{XZ} \ddot{\Psi} + \left(\frac{\bar{q} \, Sb^2}{2V_T} \left(-C_{1_{\dot{\beta}}} + C_{1_r}\right) + D_1\right) \dot{\Psi} \tag{11a}$$

$$+ \left(\dot{q} \, Sb \, C_{1_{\beta}} + K_1\right) \Psi = -L_F \, (t)$$

$$I_{ZZ} \ddot{\Psi} - \left(\frac{q \, Sb^2}{2V_T} \left(-C_{n_{\dot{\beta}}} + C_{n_r}\right)\right) \dot{\Psi} \tag{11b}$$

$$- \left(\bar{q} \, Sb \, \left(-C_{n_{\beta}}\right)\right) \Psi = N_F \, (t)$$

Each of the above equations consist of an inertial term, a damping term which includes aerodynamic and support damping, and a stiffness term, which includes aerodynamic and sting restoring moments. The forcing function is sinusoidal in nature. The general form of the equations becomes:

$$I\ddot{\theta} + D\dot{\theta} + K\theta = M \cos \omega t \tag{12}$$

The solution is assumed to be of the form

$$\theta = \theta_0 \cos (\omega t - \phi) \tag{13a}$$

The velocity and acceleration then become

$$\dot{\theta} = \theta_0 \, \omega \, (- \sin \omega t \cos \phi + \cos \omega t \sin \phi) \tag{13b}$$

$$\ddot{\theta} = -\theta_0 \, \omega^2 \, (\cos \omega t \cos \phi + \sin \omega t \sin \phi) \tag{13c}$$

When equations 13a - 13c are substituted into equation 12 the following relationships result:

$$\tan \phi = \frac{D\omega}{K - I\omega^2} \tag{14a}$$

$$M = \theta_0 \, ((K - I\omega^2) \cos \phi + D\omega \sin \phi) \tag{14b}$$

If either the stiffness of the system, K, or the moment of inertia, I, can be adjusted so that the natural frequency corresponds to the desired testing frequency, the system will be in resonance and the following relationships will result:

$$\phi = 90° \tag{15a}$$

$$K = I\omega^2 \tag{15b}$$

$$D = \frac{M}{\theta_0 \, \omega} \tag{15c}$$

The damping and stiffness terms are composed of an aerodynamic and a support term expressed as:

$$D = M_{\dot{\theta}_A} + M_{\dot{\theta}_T} \tag{16a}$$

$$K = M_{\theta_A} + M_{\theta_T} \tag{16b}$$

Equations 16 are substituted into equations 15 to solve for the aerodynamic damping when the system is operated at resonance. The aerodynamic terms go to zero when the system is operated in a vacuum. The resulting terms are then due only to tare damping and stiffness. These terms are indicated with a subscript "V".

$$M_{\theta_A} = I \ (\omega^2 - \omega_V^2) \tag{17a}$$

$$M_{\dot{\theta}_A} = [\frac{1}{\omega} \ (\frac{M}{\theta_0})] - [\frac{1}{\omega} \ (\frac{M}{\theta_0})] \tag{17b}$$

There is an implicit assumption in the above equations that the tare damping does not change with frequency.

In the case of forced oscillation at frequencies other than at resonance, equation 14a is substituted into 14b and the following relationships result:

$$D = \frac{M \sin \phi}{\omega \theta_0} \tag{18a}$$

$$K = I_\gamma \omega^2 + \frac{M \cos \phi}{\theta_0} \tag{18b}$$

Applying equations 18

$$M_{\theta_A} = [I_\gamma \omega^2 + \frac{M \cos \phi}{\theta_0}] - [I_\gamma \ \omega^2 + \frac{M \cos}{0}]_V \tag{19a}$$

$$M_{\theta_A} = [\frac{M \sin \phi}{\omega \theta_0}] - [\frac{M \sin \phi}{\omega \theta_0}]_V \tag{19b}$$

The phase angle, ϕ, is determined by using electronic resolvers with the displacement signal as the reference and the moment signal as the input.

TEST PLAN

As presented above, the method of evaluating the effects of store carriage on aircraft handling qualities depends upon the use of static and dynamic wind tunnel testing techniques to gather data to be analyzed by computer simulations. The use of simulation and static testing is well established in the state of the art of aircraft design and aircraft/store integration. The accuracy and validity of testing large-scale complex models to determine the store carriage-related dynamic effects remains to be determined by the initial testing of the new model.

The test plan for this first test was driven by four primary considerations: Air Force operational priorities, correlation with previous estimates and testing, a desire to indicate trends due to large finned guided weapons, and, above all, severe budgetary constraints. Considering the test time available, it was decided that three configurations could be tested for a limited set of Mach numbers and angles of attack.

The clean aircraft (with AIM-9 missiles on the wing tips) was selected to provide a baseline for correlation with other tests. The next configuration will have tip missiles, six AGM-65 missiles, ALQ-119-12, and two 370 gallon tanks. This configuration was selected since a large amount of analysis has already been performed by General Dynamics and because it may show large dynamic stability degradations. The last configuration to be tested will include tip missiles, an ALQ-119-12 ECM pod, two GBU-10 laser guided bombs, and a 300 gallon fuel tank. This configuration was selected because of the large, aerodynamically active fins and cannards on the GBU-10, and since static testing had shown the possibility of marked mutual interference between the 300 gallon fuel tank and any large stores carried on the inboard pylons. A summary of the test conditions is given in Table 3. Each condition will be tested with separate oscillations about the three body axes.

CONCLUSION

Forced oscillation wind tunnel testing is a logical extension of the present state of the art in determination of the effects of external store carriage upon the handling qualities of the parent aircraft. Model construction of an advanced fighter configuration is nearly completed. The validity of this application of dynamic stability testing will be investigated in a joint project between the Air Force Armament Laboratory and Arnold Engineering Development Center. It is hoped that we will be able to present the results of our investigations at the next Aircraft Compatibility Symposium.

BIBLIOGRAPHY

1. Beam, Benjamin H., <u>A Wind Tunnel Test Technique for Measuring the Dynamic Rotary Stability Derivatives at Subsonic and Supersonic Speeds</u>, NACA Report 1258, 1956

2. Braslow, Albert L.; Wiley, Harleth G.; Lee, Cullen Q., <u>A Rigidly Forced Oscillation System for Measuring Dynamic - Stability Parameters in Transonic and Supersonic Wind Tunnels</u>, NASA TN D-1231, March 1962

3. Etkin, Bernard, <u>Dynamics of Flight</u>, John Wiley and Sound, 1959

4. Epstein, C. S., <u>Aircraft/Stores Compatibility and Flight Testing</u>, Aircraft/Stores Compatibility Symposium Procedings, September 1975

5. Roskam, Jan, <u>Flight Dynamics of Rigid and Elastic Airplanes</u>, published by the Author, 1972

6. Rutan, Elbert L., <u>The Effects of Stores on High Angle of Attack Flying Qualities</u>, Aircraft/Compatibility Symposium Procedings, August 1972

7. Schueler, C. J.; Ward, L. K.; Hodap, H. E. Jr., <u>Techniques for measurement of Dynamic Stability Derivatives in Ground Test Facilities</u>, AGARD-ograph 121, October 1967

8. Uselton, James C., <u>Dynamic-Stability Measurement Capabilities in the AEDC Wind Tunnels</u>, AEDC/B-2, March 1973

AUTOBIOGRAPHY

Thomas E. Speer received his BS degree in Aeronautical Engineering from Iowa State University in 1975. Since then, he has served as Aeronautical Engineer, Aircraft Compatibility Branch, Air Force Armament Laboratory, Eglin AFB, Florida. He is an associate member of the American Institute of Aeronautics and Astronautics.

SIMULATION OF SWAY BRACES AND MOUNTING
GAPS ON SMALL-SCALE MODELS
FOR WIND TUNNEL TESTS
(U)
(Article UNCLASSIFIED)

by

R. E. DIX
ARO, Inc.
AEDC Division
A Sverdrup Corporation Company
Arnold Air Force Station, Tennessee

ABSTRACT. (U) As the scale factor applied in the design of wind tunnel models is reduced, many details of the configuration being simulated are omitted. A series of tests was conducted in a four-foot transonic wind tunnel to evaluate the effect on captive store loading and store separation trajectories of model details such as sway braces and the mounting gaps existing between store and aircraft components. Six components of aerodynamic loads acting on both pylon-mounted and rack-mounted stable stores in the captive position were measured, and a few separation trajectories were predicted with a captive trajectory system to determine the effects of the model details. A brief comparison of wind tunnel and in-flight measurements of captive loads was made. It was determined that the effects of mounting gaps were negligible, but that sway braces can significantly influence both captive loads and separation trajectories.

ILLUSTRATIONS

NOMENCLATURE

C_A Axial-force coefficient for a store, axial force/$q_\infty S$

C_ℓ Rolling-moment coefficient for a store (referred to the axis of symmetry of the store), rolling moment/$q_\infty SD$

C_m Pitching-moment coefficient for a store (referred to the center of gravity of the store), pitching moment/$q_\infty SD$

C_N Normal-force coefficient for a store, normal force/$q_\infty S$

C_n Yawing-moment coefficient for a store (referred to the center of gravity of the store), yawing moment/$q_\infty SD$

C_Y Side-force coefficient for a store, side force/$q_\infty S$

D Maximum diameter of a store

LIB   Left inboard

M_∞ Free-stream Mach number

p_∞ Free-stream static pressure

q_∞ Free-stream dynamic pressure, $0.7 p_\infty M_\infty^2$

S Reference area of a store, $\pi D^2/4$

TER   Triple ejector rack

Z_p Travel of the center of gravity of a store in the pylon-axis system Z_p direction; ft, full scale, measured from the captive position

α_s Gravimetric angle of attack of a store, degrees

ΔC_x Increment of a force or moment coefficient attributable to an effect, (coefficient with effect) − (coefficient without effect)

θ Angle between the longitudinal axis of a store and the projection of the longitudinal axis in the X_p-Y_p plane; positive when the nose of the store is elevated as seen by the pilot, degrees

733

$\Delta\theta$ Difference in the value of the angle θ at a point in the trajectory of a store and the value of θ in the captive position, degrees

PYLON-AXIS SYSTEM COORDINATES

Directions

X_p Parallel to the longitudinal axis of the store in the captive position; positive direction forward as seen by the pilot

Y_p Perpendicular to the X_p axis and parallel to the lateral, or Y, axis of the aircraft; positive direction is to the right as seen by the pilot

Z_p Perpendicular to both the X_p and Y_p axes; positive direction is downward as seen by the pilot

INTRODUCTION

When designing models for use in wind tunnel experiments, faithful geometric similitude (beyond a fundamental degree of detail that is set, like as not, subjectively) is often sacrificed to the twin tyrants of time and money. The compulsion to simplify the model becomes intense indeed for models of small finished size, say one-twentieth of full size. A typical physical feature of one inch, for example, would be represented in a one-twentieth-size simulation by a model feature of only 0.050 inch. Intuitively, features of such a small size many times seem to be insignificant, and are consequently regarded as dispensable.

A recent series of experiments, conducted in the Propulsion Wind Tunnel (PWT) facility of the Arnold Engineering Development Center (AEDC), was designed to investigate the validity of the above reasoning for certain cases. Specifically, the investigation was limited to two details of store-to-aircraft installations, viz. sway braces, and flow passages between closely-spaced features on the full-size items, such as the stand-off gap between stores and pylons or racks, and the gap existing between ejector racks and the body of multiple suspension devices. An evaluation was made of the effects of simulating these relatively small features on the static aerodynamic loading of an external store. Both pylon-mounted and rack-mounted stores were included. Typical contemporary aircraft and store configurations were used, rather than simplified shapes, to place the results in immediate context.

TEST PROGRAM

WIND TUNNEL

Experiments were conducted in the Aerodynamic Wind Tunnel (4T) of the PWT facility, a closed-circuit wind tunnel in which continuous flow can be maintained at various density settings. Mach number in the free stream can be set at any value from 0.2 to 1.3. Nozzle blocks can be installed to provide discrete Mach numbers of 1.6 and 2.0. Stagnation pressure can be established from 300 to 3700 psfa. The test section is 4 ft square, 12.5 ft long, and is equipped with perforated walls that can be adjusted by remote control to provide a porosity in the nominal range of from 0- to 10-percent open area. A desired fraction of the flow through the test section can be evacuated through the porous walls into a plenum chamber in which the test section is completely enclosed.

Models are supported in the test section with a conventional strut-sting system. A model can be pitched from approximately -12 to 28 deg with respect to the centerline of the tunnel. A capability of rolling a model from -180 to 180 deg about the centerline of the sting is also available. A schematic illustration of a typical model installed for testing is presented in Fig. 1. Tunnel 4T is also equipped with an auxiliary sting support system, the captive trajectory system (CTS), depicted schematically in Fig. 2. The CTS is used frequently to predict store separation trajectories, and is well documented in the literature.

AIRCRAFT

A typical contemporary fighter aircraft was selected because of the availability of both a one-twentieth-size model and a large quantity of data from previous tests, including flow field and store separation data. Throughout the experiments discussed herein, all pylons were installed, but only one was occupied (the left wing inboard). All pylons were of USAF design. For configurations in which a triple ejector rack (TER) was required, a USAF TER was simulated. To allow for sting support of the aircraft model, tail surfaces were not installed. Engine exhaust nozzles were simulated, and airflow was allowed into the engine inlets, through the internal ducting, and out the exhaust nozzles.

STORES

Two classes of stores were considered: large pylon-mounted stores, and smaller rack-mounted stores. The store configurations selected in each category included a stable, low-drag bomb shape.

VENTS

In the interior of the store model, a strain-gage balance was mounted. The store model was attached to one end of the balance, and a supporting bracket to the other end. The bracket protruded through the upper surface of the store model, and was attached to the pylon or rack. In previous tests[1], the bracket appeared to be an extension of the pylon, since it was on the order of 20 percent as long

---

[1]Dix, R. E. "Comparison of Two Methods Used to Measure Aerodynamic Loads Acting on Captive Store Models in Wind Tunnel Tests." AEDC-TR-76-122, September 1976.

DIMENSIONS AND TUNNEL STATIONS IN INCHES
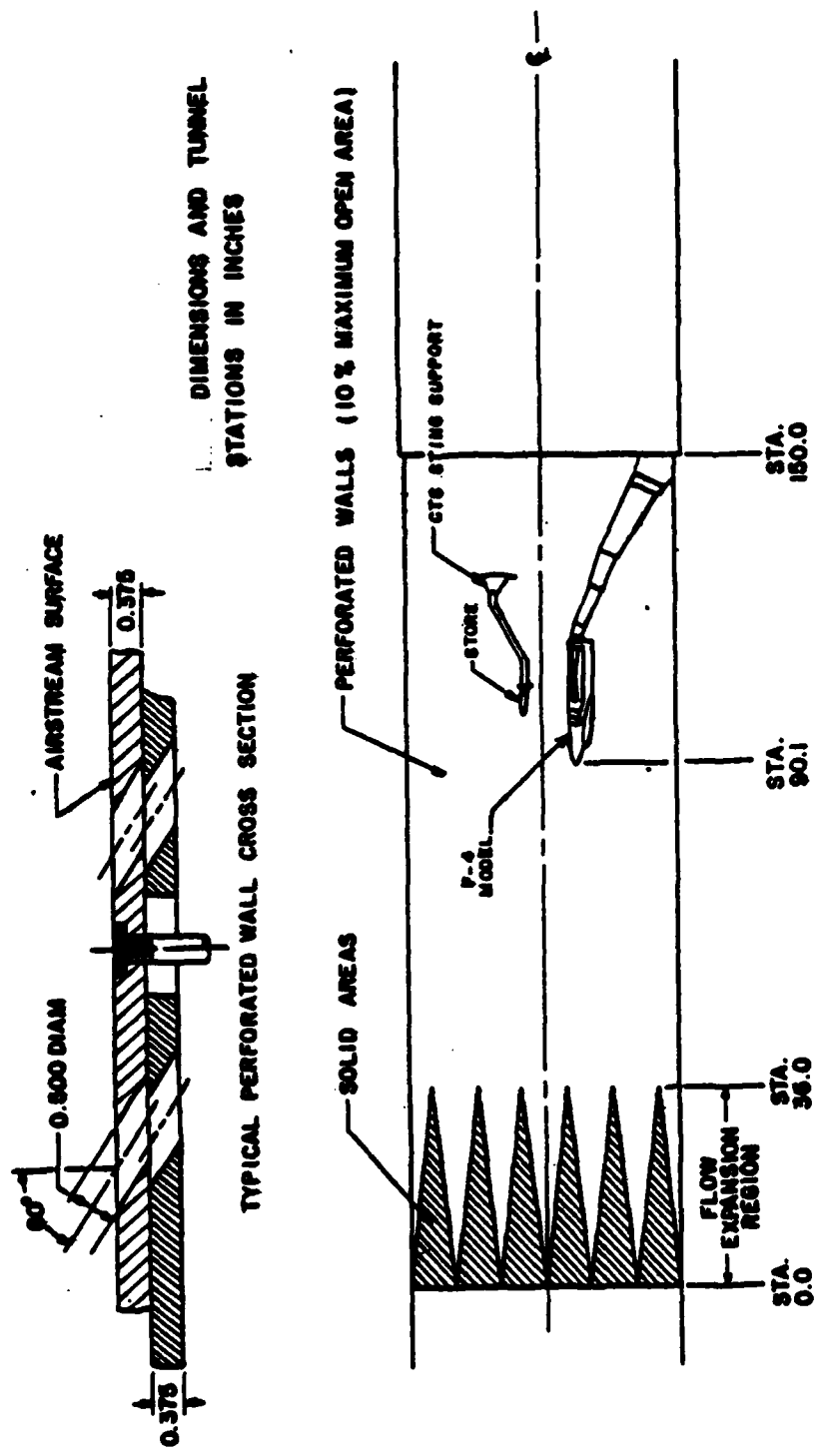
Figure 1   Schematic Illustration of a Typical Model Installation in Tunnel 4T
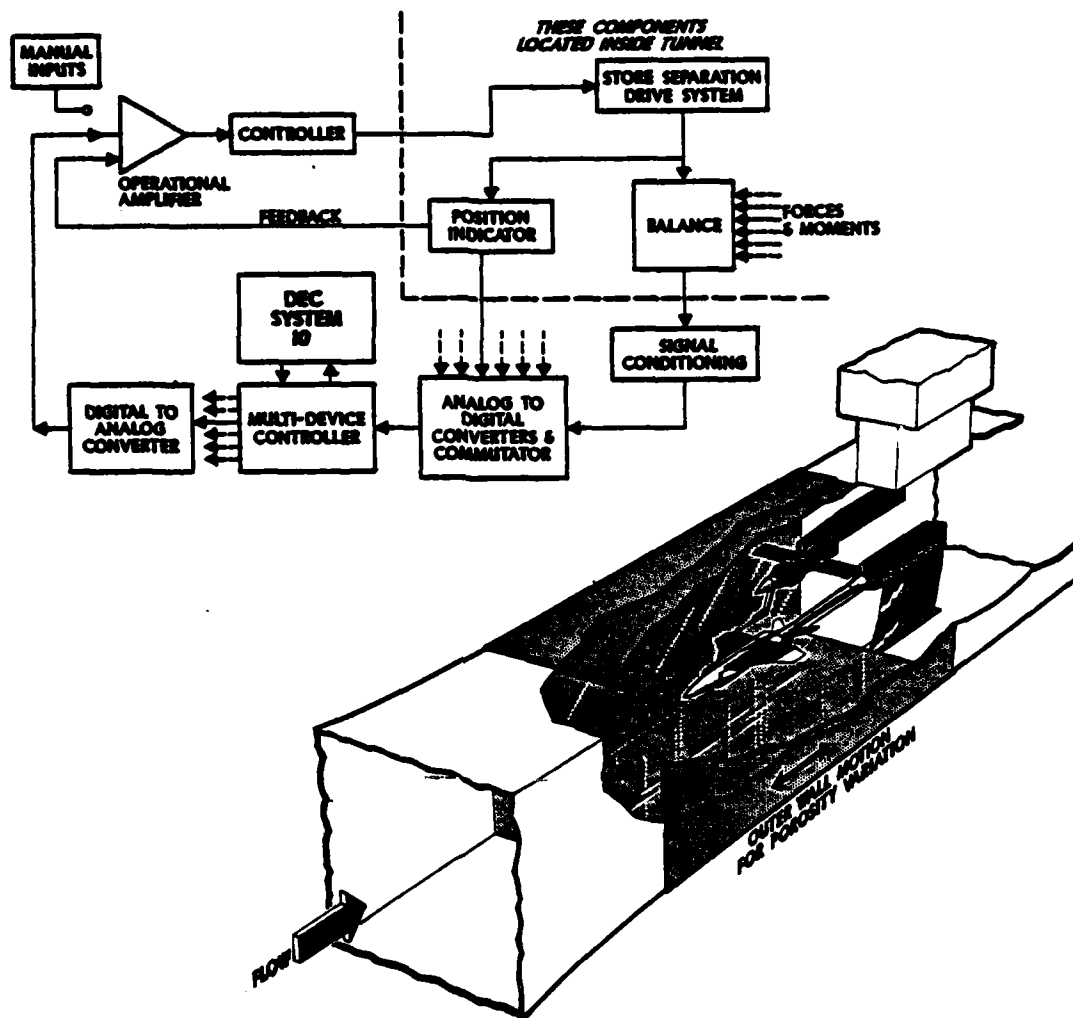
Figure 2   Schematic Illustration of the Captive Trajectory
System (CTS)

738

as the store, and as thick as the pylon. Hence, a venti-
lating slot, or vent, was cut through the bracket, tangent
to both the upper surface of the store and the lower surface
of the pylon, and extending along the length of the bracket
as far as structurally feasible. The remaining bracket
material crudely simulated the lug suspension system for the
store. A photograph of a typical pylon-mounted store with
vented bracket is presented in Fig. 3.

Vents were included in the design of the TER, also. At
full scale, gaps exist between all ejector racks and the
body of the ejector rack assembly. A drawing of the TER
with vents is presented in Fig. 4.

SWAY BRACES

At the scale of these experiments, i.e., one-twentieth
of full size, sway braces for both pylon and rack models
were small, but feasible. For instance, the span of the
model braces for the pylon was approximately 0.4 in., and
the cross section of a sway brace arm was approximately 0.10
by 0.04 in. (see Fig. 5 for a drawing of the pylon). The
sway braces for the TER were even smaller, approximately
0.3-in. span, with a cross section of approximately 0.06 by
0.02 in. Conventional practice has been to ignore model
features of such size. All stations of the TER were equipped
with the braces. On TER station 1, the station on which the
store/balance was installed, the braces were slightly larger,
0.43-in. span, simulating the braces used in an independent
flight test with which those data were to be compared. All
sway braces were removable, to provide a basis for determ-
ination of incremental effects. The essential features of
the TER sway braces are also visible in Fig. 6, with a
simple (undetailed) TER shown alongside for comparison.

INSTRUMENTATION

The strain-gage balances mounted inside the store
models, as discussed above, were of conventional design, and
capable of sensing six components of static aerodynamic
loads acting on the store model. Appropriately-shaped areas
were cut out of the upper surface of each store model to
provide sufficient clearance around the balance-supporting
bracket to prevent fouling of the balance outputs through
physical contact. Angle of attack of the aircraft model was
sensed with a strain-gaged pendulum device. In all cases,
the output of the pendulum was used in data reduction;
hence, the angle of attack reported must be identified as a
gravimetric angle of attack. No adjustments of the data
were made to correct for flow angularity, though corrections
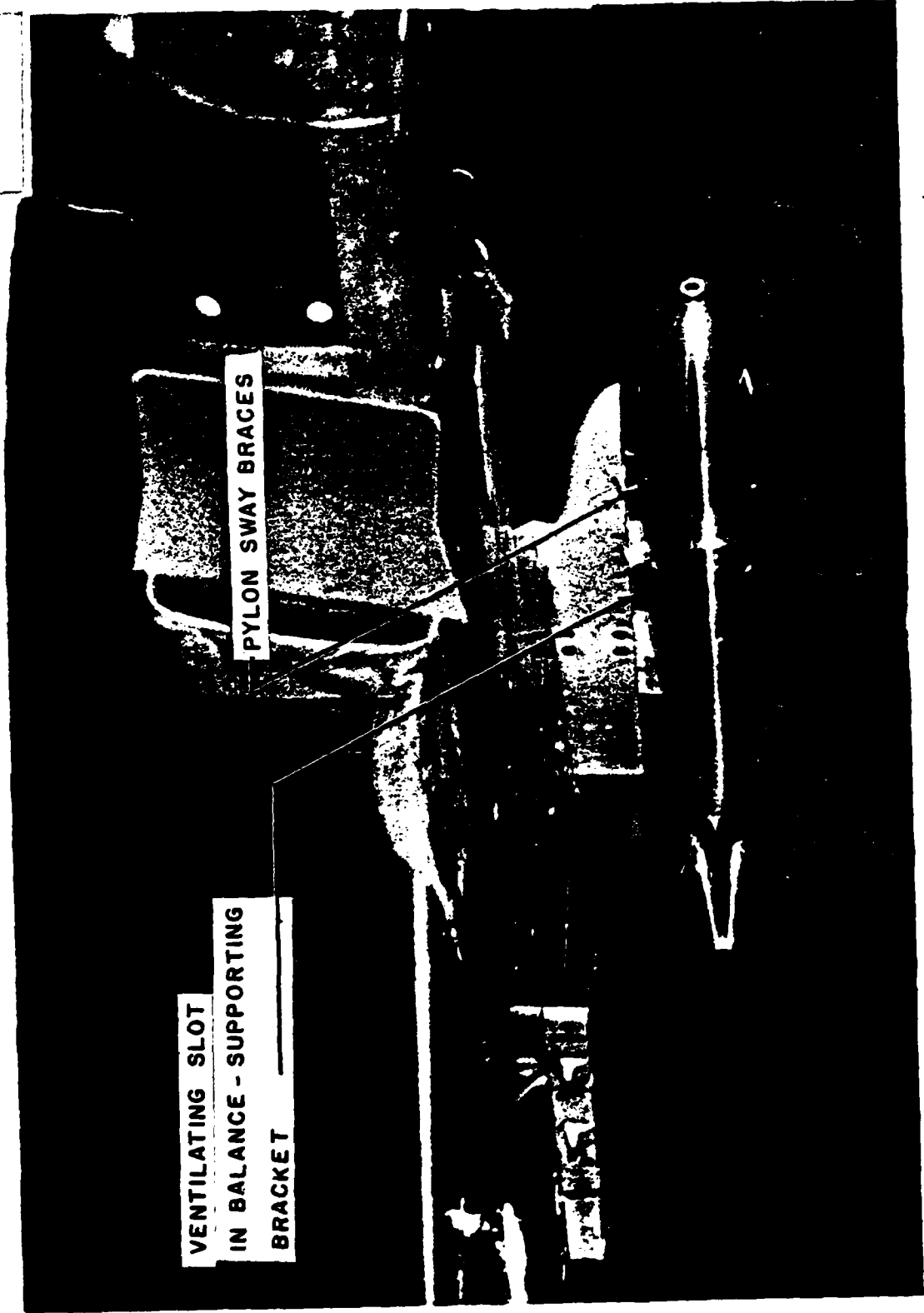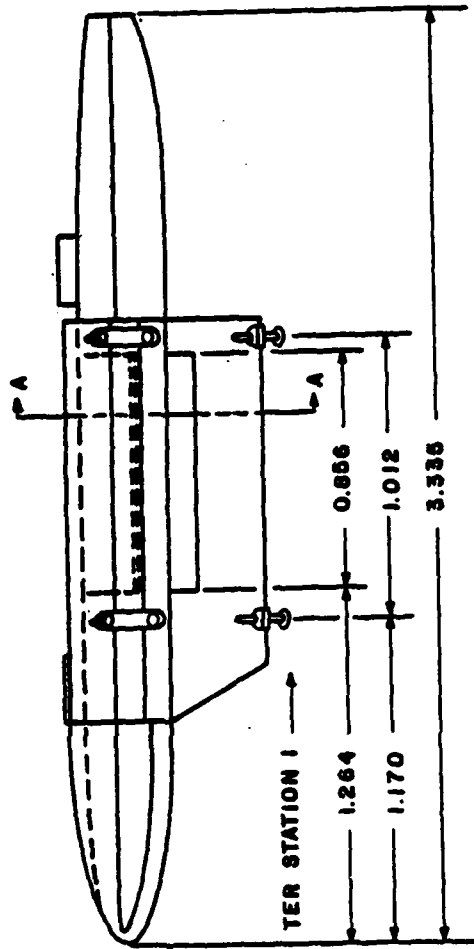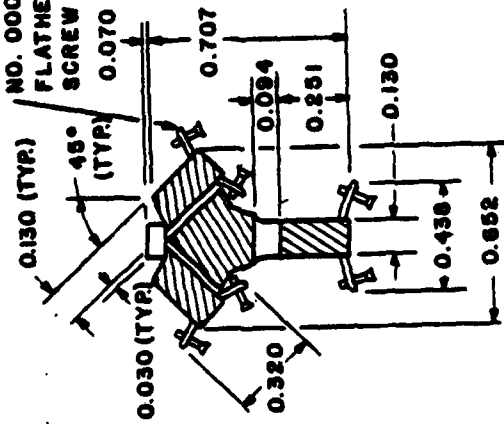for model sting deflections were included in model posi-
tioning.

Figure 3 Pylon-Mounted Store Model in the Wind Tunnel, Showing Ventilating Slots and Sway Braces

PYLON SWAY BRACES

VENTILATING SLOT IN BALANCE - SUPPORTING BRACKET

DIMENSIONS IN INCHES

NO. 000-120 UNF
FLATHEAD MACHINE
SCREW (TYP.)

Figure 4   Ventilating Slot and Sway Brace Details for the
Triple Ejector Rack (TER) Model
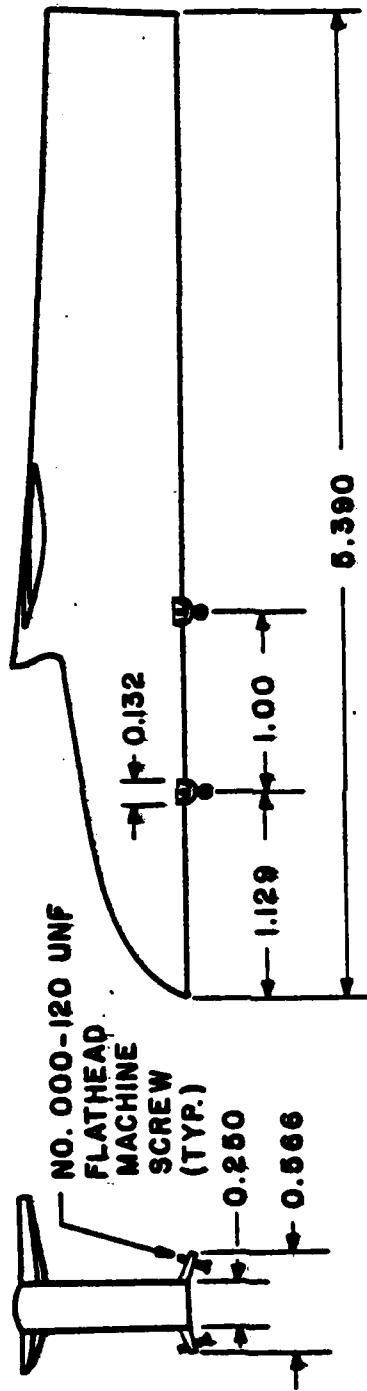
DIMENSIONS IN INCHES

Figure 5 Sway Brace Details for the Left Inboard Pylon (LIB)

Figure 6 Comparison of Detailed and Simple TER Models

TEST PROCEDURE

Data were recorded at Mach numbers 0.6, 0.8, 0.9, 1.1, and 1.2 for the pylon-mounted store, and at 0.7 as well for the rack-mounted store. Reynolds number was maintained at approximately 3.5×10^6 per foot. Dynamic pressure varied over the range of from 450 to 700 psf since the pressure and temperature of the airflow were changed as necessary to maintain the Reynolds number. With flow conditions set, the angle of attack of the aircraft was set in a sequence of two-deg increments from -4 to 12 deg in a pitch-pause mode, with neither roll nor yaw.

As mentioned above, the aircraft model was installed in the tunnel with pylons on all wing stations, including a weapons adapter on the aircraft centerline station. Store models were installed on the left inboard pylon only, not necessarily the pylon on which the store is usually carried, simply to gain information about the effects of interest. The experiments were designed to provide relative measurements instead of absolute values.

DISCUSSION OF TEST RESULTS

PYLON-MOUNTED STORES

A 3000-lb class bomb configuration was selected as the stable, pylon-mounted store. In Fig. 7, data plots are presented to indicate two effects on the static aerodynamic loading of the captive store: the effect of the ventilating slot in the balance-to-pylon supporting bracket, and the effect of both the ventilating slot and the sway braces. The effects are presented for two Mach numbers, 0.6 and 0.9. Bands, denoted by dashed lines and shading, indicate the precision of the data; i.e., only points outside the bands can be considered to represent valid estimates of the effects. Points within the bands are beyond the resolution of the measurements, and cannot be consistently separated from instrument bias and/or random signal errors.

From Fig. 7, it is immediately apparent that both axial force and rolling moment acting on the store are unaffected by the presence of either sway braces or vents. Only at angles of attack above approximately eight deg does the effect of ventilation exceed the uncertainty of the data, and then by only a small amount.
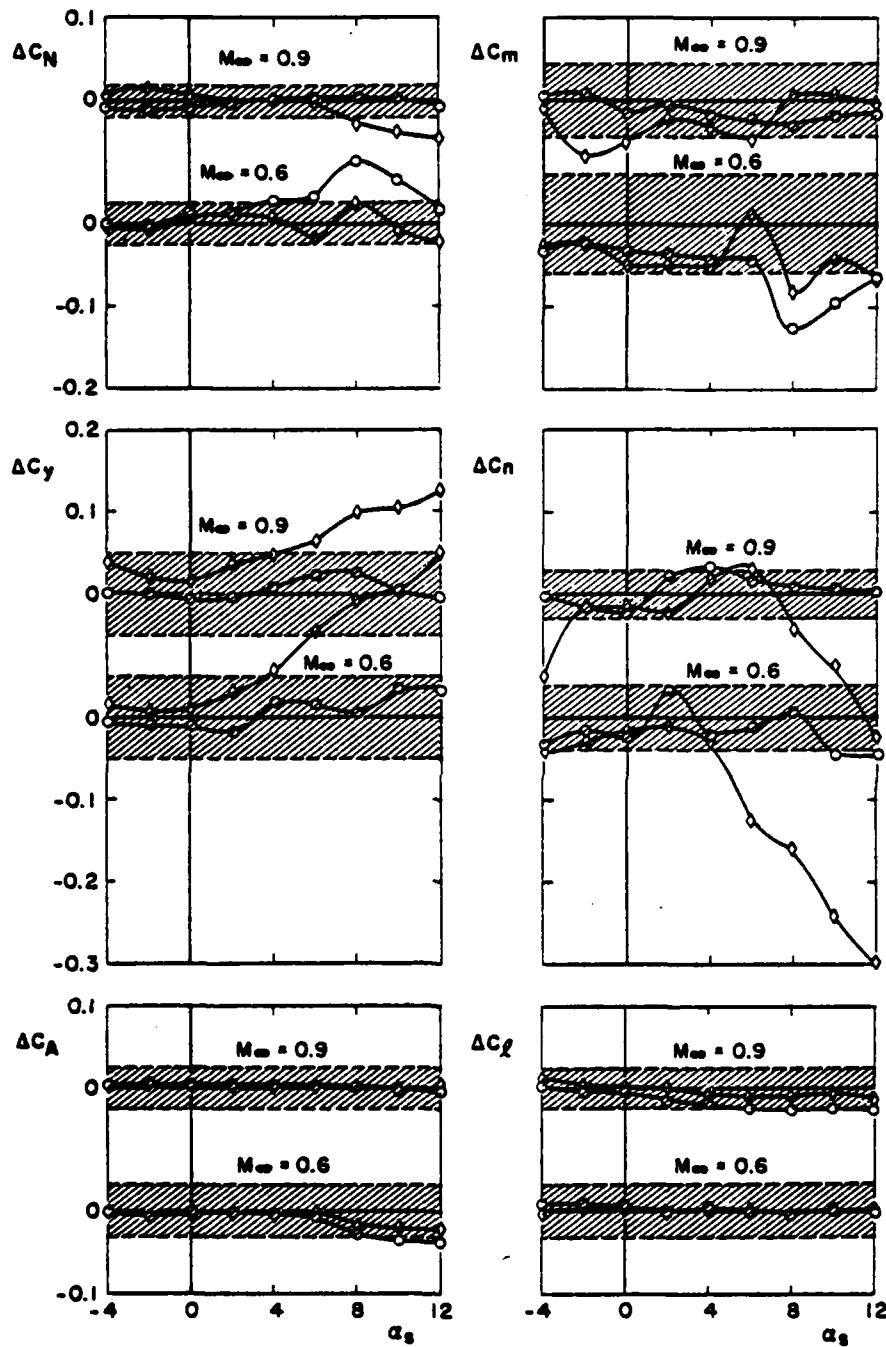
744

Figure 7 Increments in Captive-Position Store Load
Coefficients Attributable to Ventilation
Slots and Sway Braces for a Stable Pylon-
Mounted Store, Left Inboard Pylon

It is also clear that the primary effect of sway braces is to alter the magnitude of the lateral forces acting on the store at positive angles of attack. A concomitant and consistent effect on yawing moment is also apparent. On the other hand, ventilation alone has little effect at any angle of attack in the subsonic regime.

For pylon-mounted stores, the primary effect of ventilation is observed as an influence on the normal force. The pressure distribution over the upper surface of the store is clearly affected by the presence of the vent, probably because pressure cannot be exerted asymmetrically across the upper surface of the store without the solid bracket. At the higher Mach number, the effect of sway braces is strong for lower angles of attack, indicating that regimes of critical flow may exist, but are negated perhaps by separation as the angle of attack is increased. Additional data on the effects of ventilation for other stores are available in the literature.[2]

RACK-MOUNTED STORES

A 1000-lb class low-drag bomb configuration was selected for the rack-mounted store. In Fig. 8, the effects of ventilation and sway braces are presented, as in the case of pylon-mounted stores. However, in the rack-mounted case, ventilation included not only a slot in the balance-to-rack supporting bracket, but also slots in the rack (see Figs. 4 and 6). Again, data are presented for two Mach numbers, 0.6 and 0.9, with data uncertainty bands shown with light dashed lines and shading.

From Fig. 8, it is clear that, just as for pylon-mounted stores, the effects of ventilation and sway braces on axial force and rolling moment acting on the store are negligible. This observation holds throughout the angle-of-attack range investigated for the subsonic regime.

Side force is essentially unaffected, although sway braces do exert some influence at some angles of attack. Yawing moment is disproportionately affected, indicating a change in pressure distribution (center of pressure) when sway braces are simulated. The effects observed for the store on TER station 1 cannot be assumed to apply for other rack stations because of the "shielding" effect of the adjacent dummy stores on TER stations 2 and 3.

---

[2]Dix, R. E. "Evaluation of an Internal Balance-Supporting Bracket Simulating Lug Suspension for Captive Stores in Wind Tunnel Tests." AEDC-TR-76-117, October 1976.
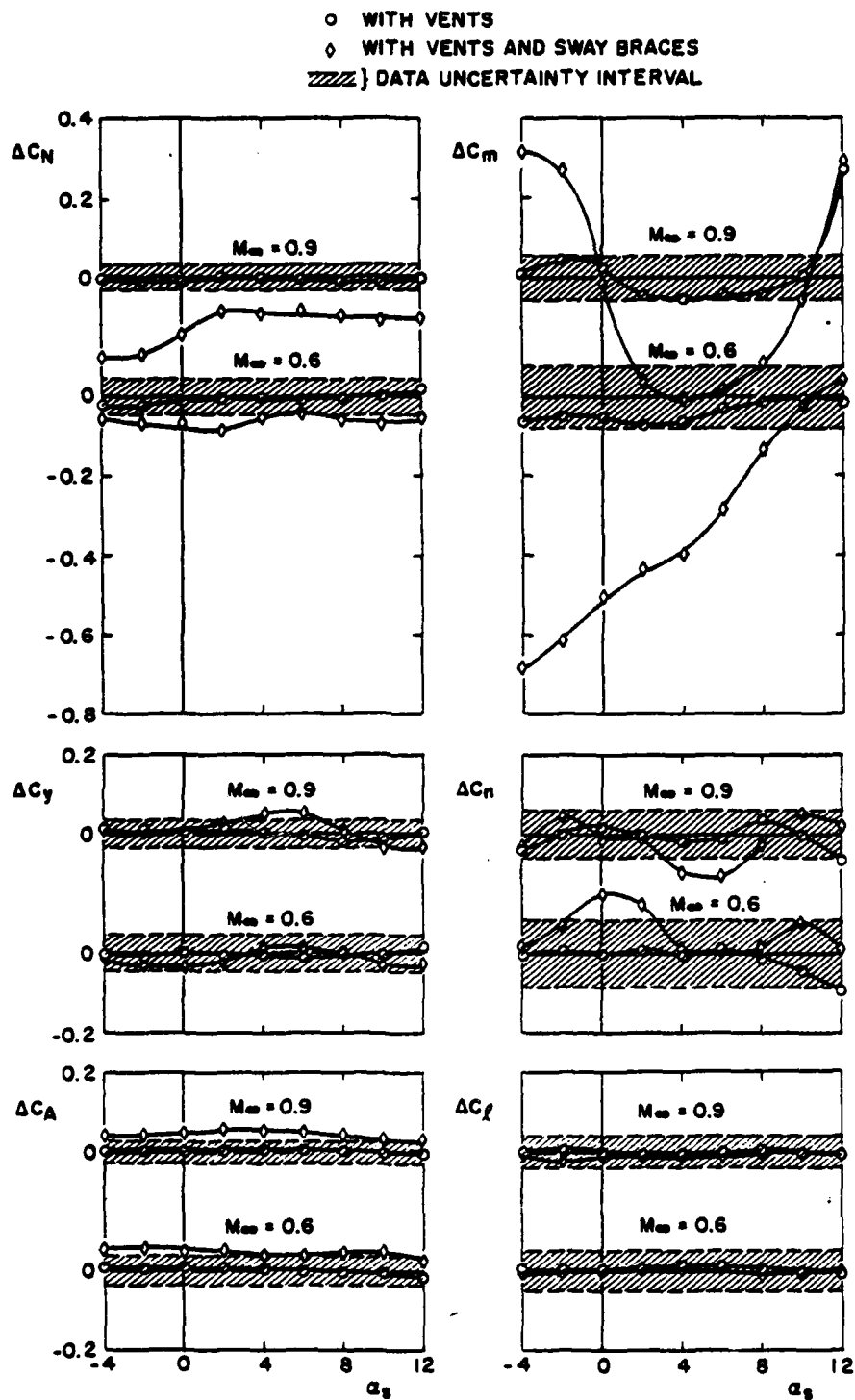
Figure 8   Increments in Captive-Position Store Load Coefficients Attributable to Ventilation Slots and Sway Braces for a Stable Rack-Mounted Store, Left Inboard Pylon, TER Station 1

Normal force acting on the store is virtually unaffected by ventilation, as is pitching moment. The addition of sway braces, however, results in remarkable changes in both normal force and pitching moment, especially at the higher Mach number. Flow stagnation at the sway braces apparently causes considerable change in the location of the center of pressure, with regions of critical flow also probably contributing to the effect at the higher Mach number.

SEPARATION TRAJECTORIES

Figures 9 and 10 reveal the effects of simulating sway braces from another point of view, i.e., the effects on the separation trajectory of a store. Even though the sway braces remain with the aircraft as the store separates, it is the initial force system acting on the store in the captive position that strongly affects the subsequent trajectory.

No ejector force was used for the pylon-mounted store, but a 1200-lb force was impressed for the rack-mounted store. Trimmed flight attitudes were assumed and a release altitude of 5000 ft was simulated using the CTS. Because of inertias, the trajectory of the smaller, lighter, rack-mounted store is affected more than that of the heavy, pylon-mounted store. Even though the trajectory of the rack-mounted store at Mach number 0.9 was aborted early because of the extreme pitch rate (Fig. 10), a comparison of trajectories at a given separation from the aircraft (Z_D) reveals a large difference in pitch of the store ($\Delta\theta$) that could lead to greatly different ultimate trajectories and clearance envelopes.

COMPARISON WITH FLIGHT TEST RESULTS

A final indication of the advisability of simulating sway braces can be seen in Fig. 11, a comparison of wind tunnel and flight test results. For a Mach number of 0.6, both wind tunnel and flight test measurements of the normal force and pitching moment acting on the low-drag bomb mounted on TER station 1 on the left inboard pylon are presented. Data uncertainty bars are shown on each point of in-flight data.

While the addition of sway braces to the wind tunnel model did not significantly alter the slopes of the normal force and pitching moment curves between -4 and 4 deg, a translation of the curves toward better agreement with the
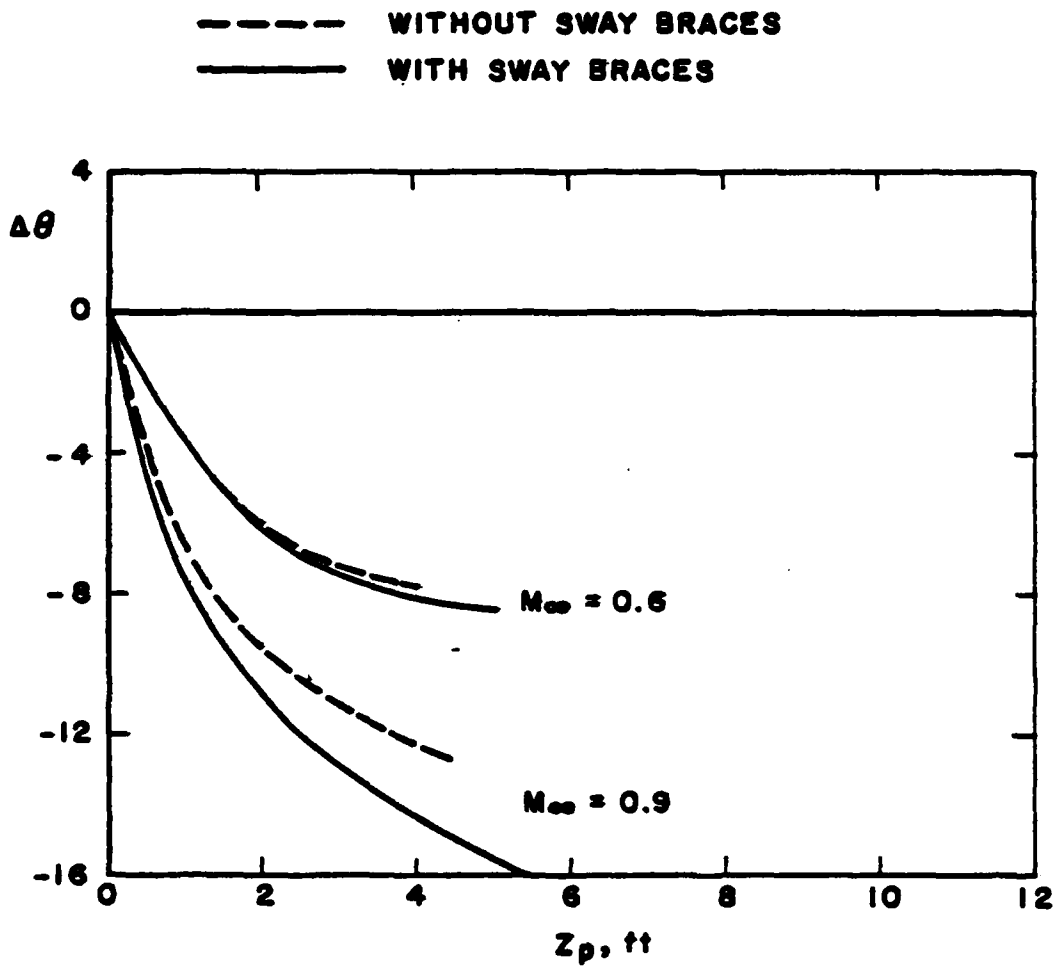
Figure 9 Effect of Sway Braces on the Separation
Trajectory of a Stable Pylon-Mounted Store,
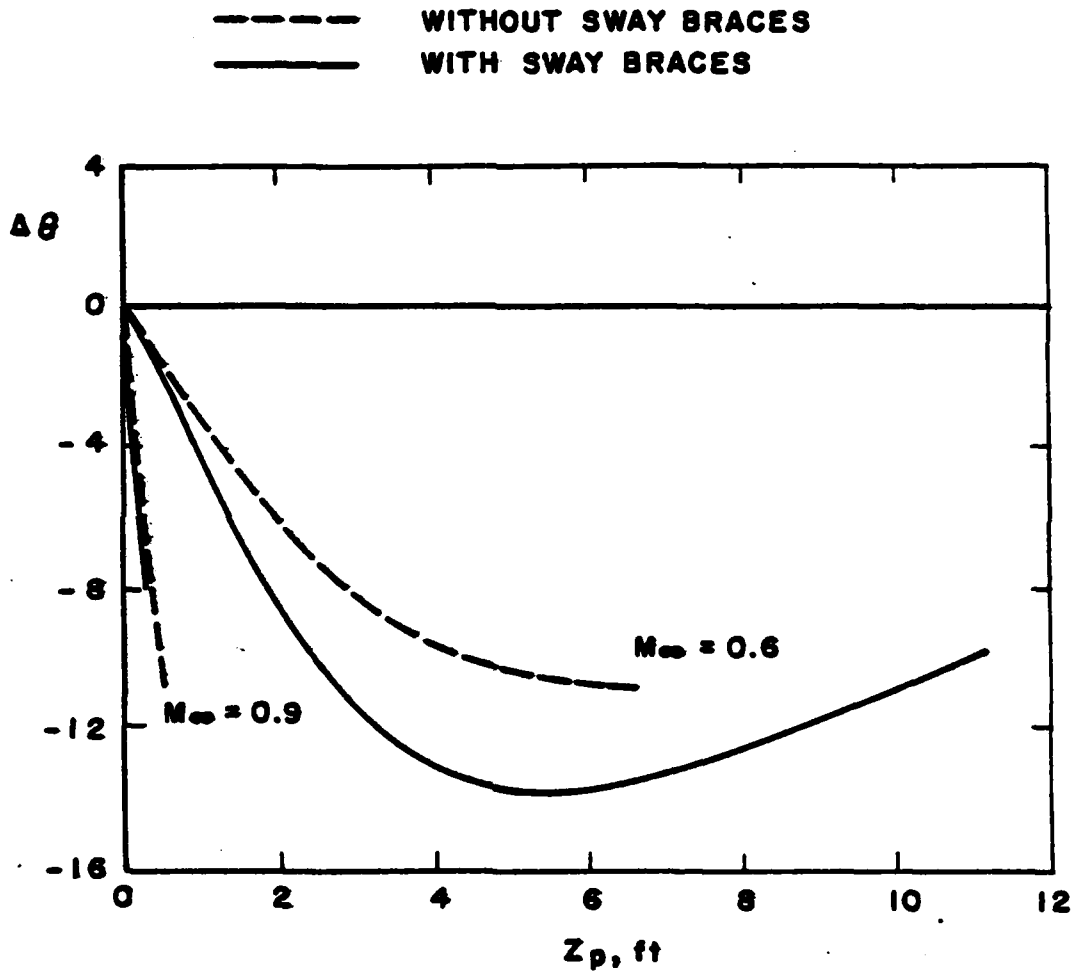Left Inboard Pylon, Level Flight, Zero
Ejector Force

749

Figure 10   Effect of Sway Braces on the Separation Tra-
            jectory of a Stable Rack-Mounted Store,
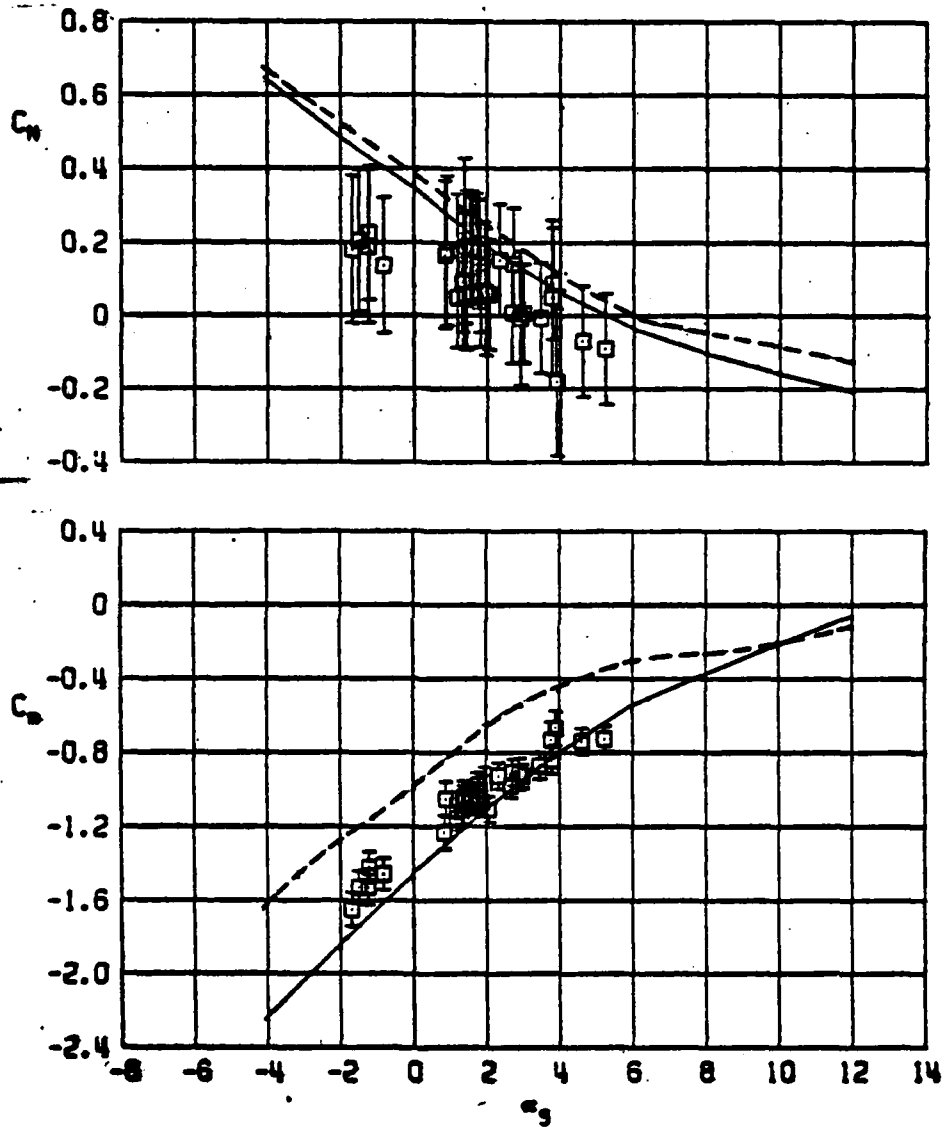   Left Inboard Pylon, TER Station 1, Level
            Flight, 1200-lb. Ejector Force

Figure 11 Effect of Sway Braces on the Comparison of
Wind Tunnel and In-Flight Measurements of
Captive-Position Store Loads for a Stable
Rack-Mounted Store, Left Inboard Pylon,
TER Station 1, $M_\infty = 0.6$

in-flight data is apparent. (It is beyond the scope of this paper to discuss further the flight test. A joint paper by the Author, G. R. Mattasits of AEDC/PWT, and Dr. A. R. Maddox of NWC treats the flight test more thoroughly, and will be published later.)

CONCLUSIONS

An experiment was conducted in the Aerodynamic Wind Tunnel (4T) of the PWT facility at the AEDC to assess the feasibility of simulating, at small model size, two features of full-size store/aircraft installations that are not normally simulated: (1) pressure-relief, or ventilating slots between store and aircraft, and between adjacent bodies on a TER, and (2) sway braces. It was determined from the experiments that:

1. The effects on captive store loading of simulating sway braces in wind tunnel experiments are much more significant than the effects of simulating pressure-relief, or ventilating, slots between adjacent components.

2. For both pylon-mounted and rack-mounted stores, the effects of sway braces and vents on axial force and rolling moment acting on the store in the captive position are negligible.

3. Side force and yawing moment acting on a pylon-mounted store are more seriously affected by the presence of sway braces than for a rack-mounted store on TER station 1 with dummy stores on TER stations 2 and 3.

4. The most severe effect of simulating sway braces for a rack-mounted store on TER station 1 is on the normal force and pitching moment. Forces and moments in the lateral plane are not affected as strongly as in the case of pylon-mounted stores, probably because of the shielding effect of the adjacent stores mounted on the shoulder stations.

5. Significant changes in the separation trajectory of a store as predicted by the CTS can result from inclusion of sway braces on the model.

6. Better agreement between wind tunnel data and flight test data resulted when sway braces were included on the wind tunnel model.

752

AUTOBIOGRAPHY

Richard E. Dix earned the BAE degree from Georgia Tech in June 1959, and the MS degree in June 1961. He joined Lockheed at Marietta in June 1959 and participated in performance studies for the Jet Star and C-141 aircraft until June 1961, when he was employed by ARO, Inc. Through June 1970, he contributed to the development of a low-density high-enthalpy wind tunnel, involving high vacuum, cryogenic, and non-equilibrium nozzle flow technologies. He served as project engineer for the development of a cryogen-ically-pumped sampling probe for in situ identification by mass spectrometer of non-equilibrium flow species. Since June 1970, Mr. Dix has served as research project engineer in the Propulsion Wind Tunnel Facility, concentrating from November 1971 on improving techniques of measuring aero-dynamic loads acting on captive stores in wind tunnel tests. He is a member of the AIAA.

(The reverse of this page is blank)

IN-FLIGHT MEASUREMENT OF AERODYNAMIC LOADS ON CAPTIVE STORES.
DESCRIPTION OF THE MEASUREMENT EQUIPMENT AND COMPARISON OF
RESULTS WITH DATA FROM OTHER SOURCES.
(U)
(Article UNCLASSIFIED)

by

G.J. Alders
National Aerospace Laboratory NLR,
Amsterdam, The Netherlands

ABSTRACT. (U) For store separation analysis the availability of
reliable aerodynamic interference data is of prime importance. Pres-
ently a number of sources is used to obtain these data, such as wind
tunnel measurements, panel method calculations and calculations based
on measured store separation trajectories. To gain more insight into
the limitations of the various sources as well as to obtain a tool
which can be used for the certification of new stores for existing
aircraft an aerodynamic load measuring store was developed. It con-
sists of a support structure to be mounted from 14 or 30 inch bomb
racks, a load measuring balance, and a shape representing the store to
be analysed. The shape is replaceable.

A flight test program has been carried out in August 1977 with a
store resembling a BLU 1/B, on an NF-5A aircraft in various configura-
tions. The results are compared with wind tunnel data from various
sources, panel method calculation results and data obtained from in-
flight separation tests. It is shown that in-flight measurement of
aerodynamic loads will allow a reduction in the number of flight tests
required to demonstrate safe separation.

LIST OF FIGURES

LIST OF TABLES

LIST OF SYMBOLS

a_y	acceleration along the lateral axis of the store
a_z	acceleration along the top axis of the store
C_{l_o}	$\dfrac{L_o}{qSd}$
C_{m_o}	$\dfrac{M_o}{qS\ell}$
C_{n_o}	$\dfrac{N_o}{qS\ell}$
C_{y_o}	$\dfrac{Y_o}{qS}$
C_{z_o}	$\dfrac{Z_o}{qS}$
d	store diameter
KAES	equivalent airspeed in kts
L_o	rolling moment on a captive store
ℓ	store length
M_o	pitching moment on a captive store
M	Mach number
N_o	yawing moment on a captive store
n_z	aircraft normal load factor
p_s	static pressure
q	dynamic pressure
S	$\dfrac{\pi}{4} d^2$
S_1 thru S_5	balance strain gage output signals
Y_o	lateral force on a captive store
Z_o	normal force on a captive store

LIST OF SYMBOLS
(continued)

α angle of attack of aircraft

β angle of sideslip of aircraft

δ_a aileron deflection angle

INTRODUCTION

In the last decade NLR has carried out airworthiness demonstration programs for new aircraft configurations for the Royal Netherlands Air Force (RNLAF). In this period the tools required for this work have been subject to constant improvement. A large part of the research underlying these improvements, including the work described in this paper, has been carried out under contract with the RNLAF.

Store separation prediction at NLR is carried out using the computer model shown in figure 1. The results obtained with this model differ from the store behaviour measured in flight. Trials have shown that the submodels labelled ejection system and wing response are adequate. The differences thus must be attributed to an incorrect representation of the aerodynamic forcing function. This may have two causes:

- incorrect aerodynamic input data, possibly due to differences between wind tunnel measurements or calculations and the full scale situation

- instationnary aerodynamic effects that are not accounted for in the calculations.

Due to this uncertain basis of the predictions, critical store separation cases have to be cleared in a stepwise manner. A typical program set-up is shown in figure 2. At each stage of this program one or two stores per configuration have to be dropped in flight.

The aerodynamic load measuring store was developed to gain more insight in the limitations of the various sources of aerodynamic interference data and in the cause of the differences between predicted and measured store motion.

Furthermore it was expected that in-flight measurements could be used with future projects to reduce the number of stores required for safe separation demonstration and would improve the confidence that can be put in the final result.

A BLU-1/B-like store shape was selected for the flight test program, to evaluate the aerodynamic load measuring store. The tests were carried out with an NF-5 aircraft. This selection was made because for this aircraft-store combination measured and calculated information on interference aerodynamics as well as on store motion was available from various sources.

Flight tests started in August 1977. Five configurations, with the store in the normal captive position, have been tested to date. Tests with the store mounted .15 m below the pylon are planned.
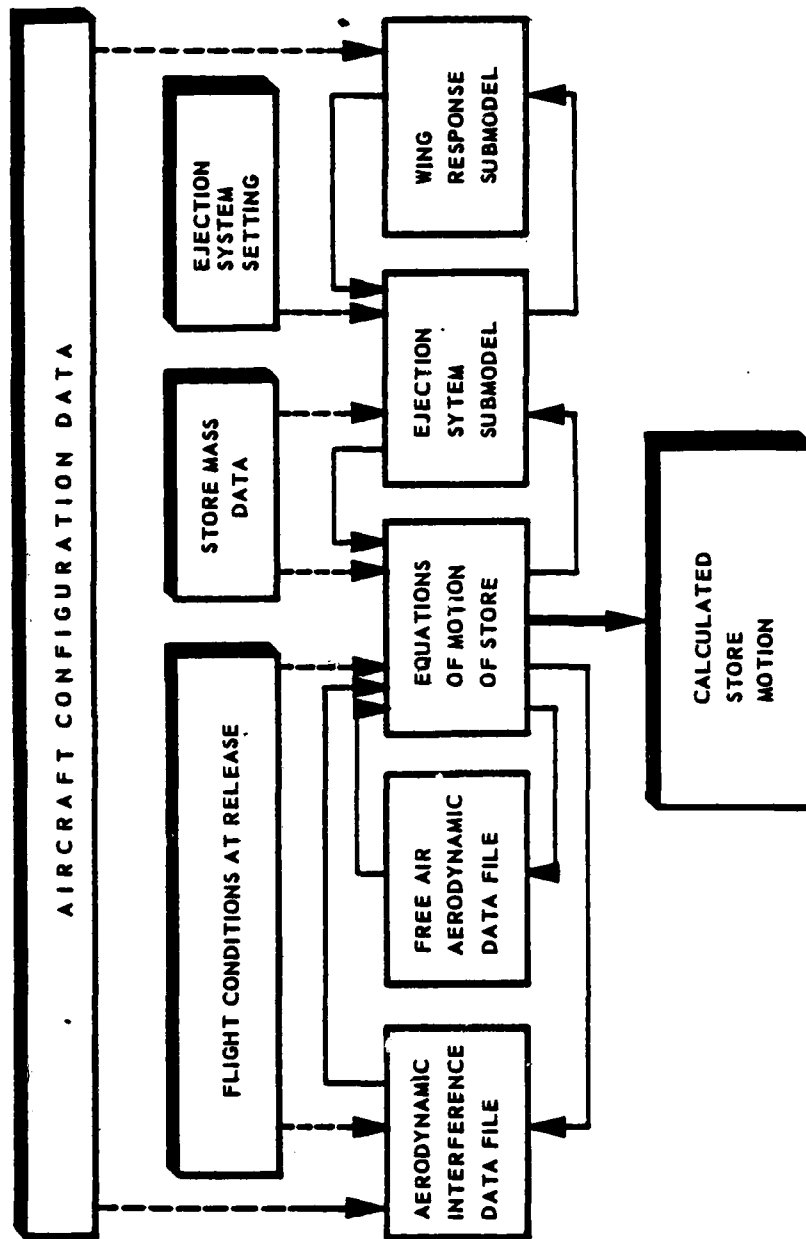
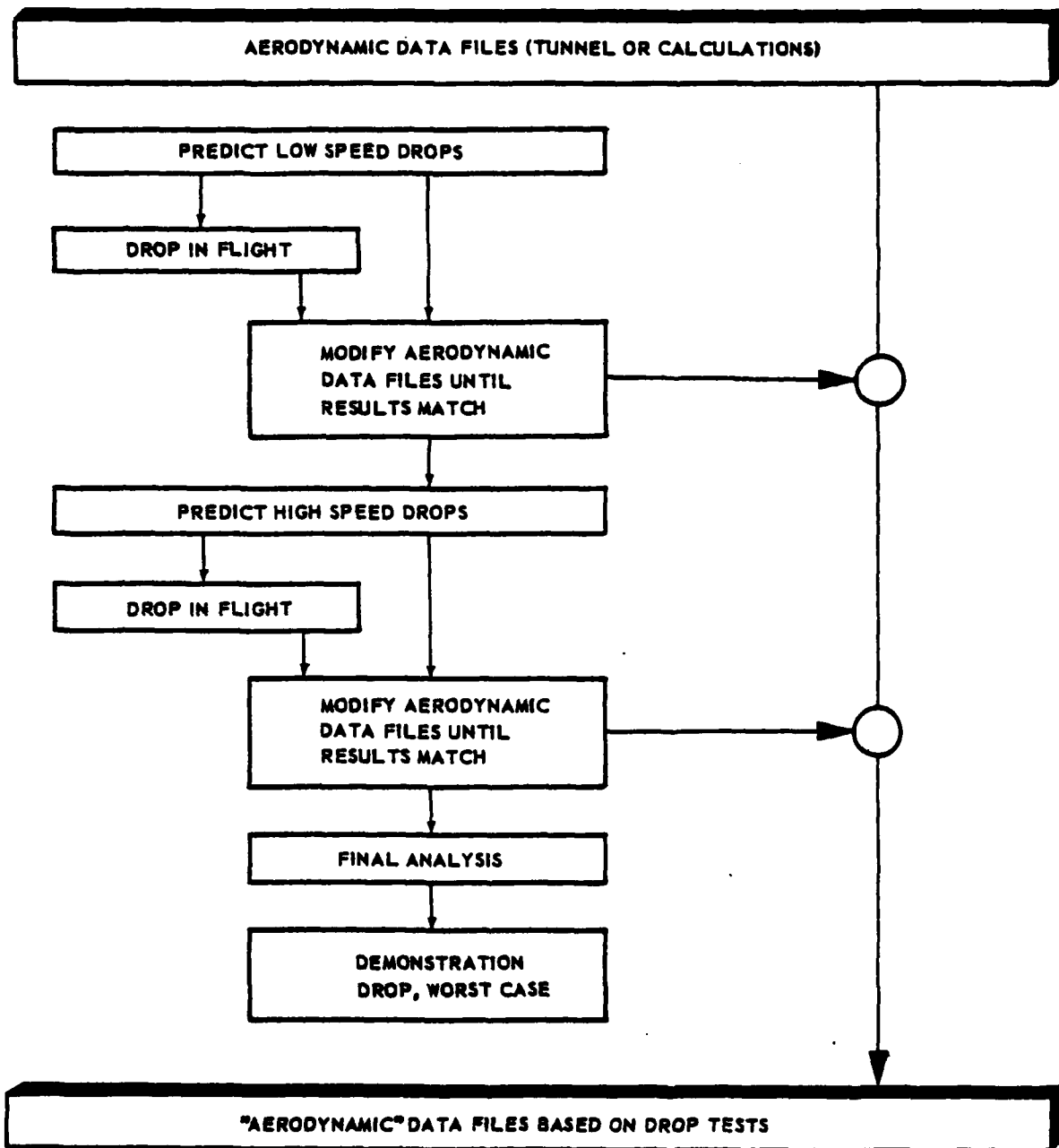Figure 1   Store separation prediction model

761

Figure 2   Evaluation procedure to determine the safe store separation envelope

THE FIVE COMPONENT AERODYNAMIC LOAD MEASURING STORE

The store is shown schematically in figure 3. It consists of four parts:

a. A support beam, provided with bomb lugs and sway brace reaction areas. The beam serves as a mounting base for the load measuring balance and for the instrumentation. The bomb lugs can be replaced by two pillars of up to .15 m length. The pillars are mounted on a bracket that replaces a bomb rack. Thus air loads can be measured with the store .15 m below its normal captive position.

b. A five component balance (Fig. 4) to measure normal and side force as well as the moments in pitch, yaw and roll. The measuring ranges are ±4000 N and ±2000 Nm. The balance is designed to withstand five times its measuring range. The design speed limit is 650 KEAS/Mach 2.0. The balance can be shifted in a forward/aft sense in the store, to obtain an optimum position of its moment centre. Measurement of the axial force has been omitted to improve the ruggedness of the construction. This could be done as axial forces need not be known accurately for store separation analysis.
The space around the balance is sealed off with a thermal insulation material. Heaters are provided to maintain a constant balance temperature.

c. A shell, representing the store to be measured: in the present case a BLU-1/B type weapon (Fig. 5). The shell has to be kept as light as possible to minimize the effect of mass forces, to make optimum use of the measuring range of the balance. The more complicated parts (nose and tail) have been taken from a real store. The cylindrical center section has been specially built, and is provided with a bulkhead to mount the balance. Holes are made in the skin to allow lugs and sway braces to pass. The remaining openings are sealed by means of rubber bellows.

d. Instrumentation (Fig. 6). For the first evaluation of the store use was made of an instrumented aircraft. The instrumentation in the store was limited to two accelerometers and the power supply and signal conditioning for the strain gages, but space is available for a small but complete data acquisition system. This offers the possibility to use the store on any 14 inch weapon station on any aircraft where 28 VDC and 115 VAC are available.
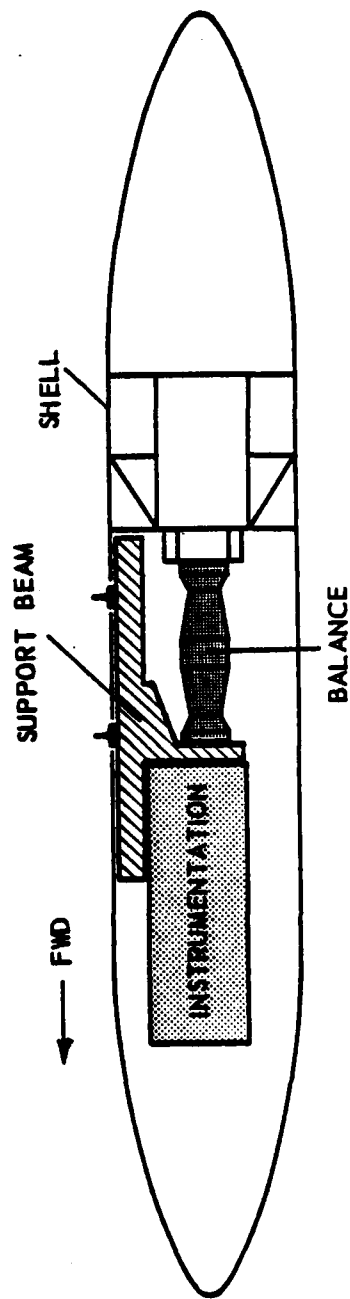
Figure 3   Five component aerodynamic load measuring store

Figure 4   Store balance

765

Figure 5   Store installed at the inboard pylon of the RNLAF NF-5A
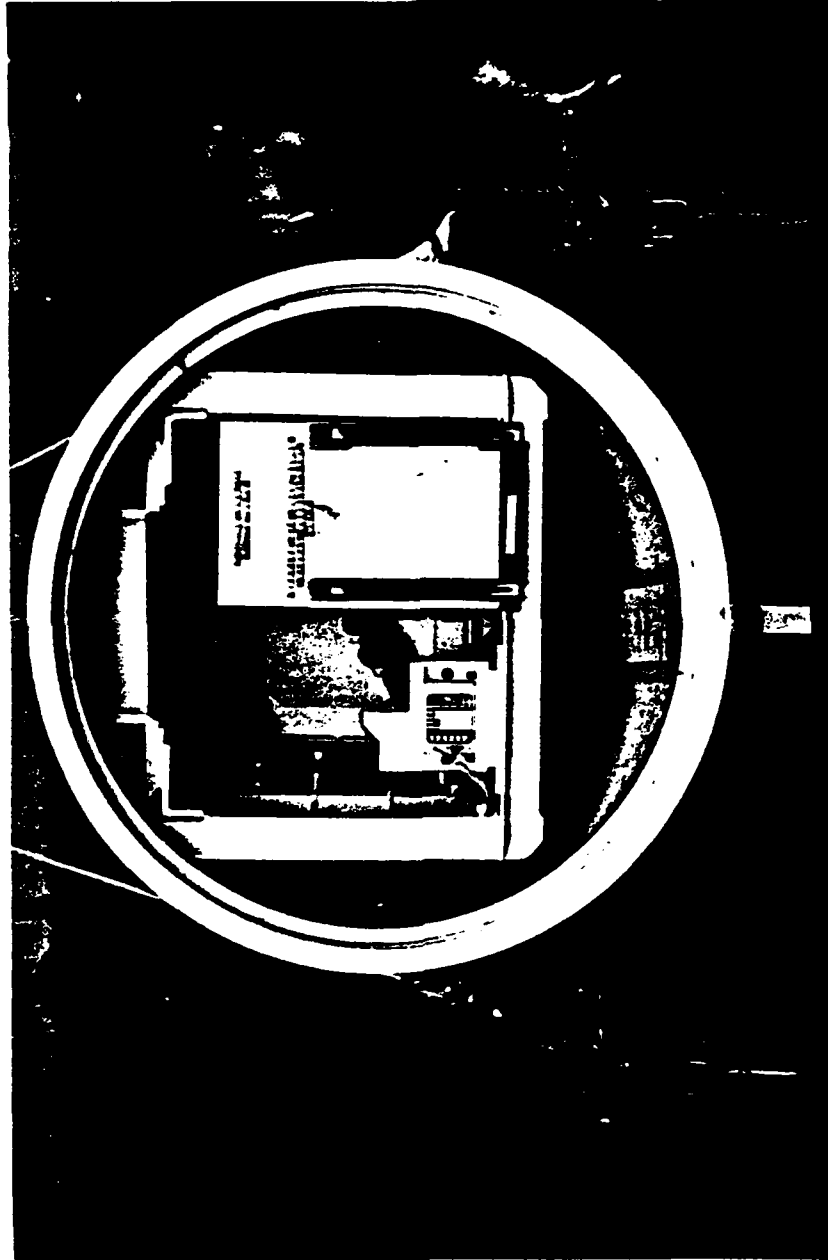test aircraft

Figure 6   Instrumentation space in the store

The total store mass is 165 kg. The weighed part is 90 kg. When mounting the store from a wing pylon store mass properties may be of importance. The present store has the mass properties of a LAU-3/A. By adding mass to the support beam other mass-inertia combinations can be made to satisfy peculiar flutter requirements.

The store was designed to make a change in shape as simple as possible. When other stores are to be measured only the shell needs modification. Balance, support beam and instrumentation remain un-changed. Stores with a diameter down to 14 inch can be accomodated.

DATA ACQUISITION AND PROCESSING

For the present trials the existing NF-5A K-3001 PCM-10 instrumentation system has been used for data acquisition. The most important parameters that have been recorded are shown in the schematic representation of data acquisition and processing in figure 7. Other parameters have been recorded during this first evaluation as a check on the validity of the information that has been obtained, but these are not essential to obtain the aerodynamic coefficients.

The PCM-10 system operates with 138 samples per second and records data with a resolution of one per mill. All signal conditioning used has a cut-off frequency of 5 Hz. The transfer functions of the strain gage and accelerometer channels were made identical, to minimize errors due to dynamic store behaviour.

Standard data selection, reduction and calibration routines are used to convert the raw data on the flight tape into computer compatible data files.

The processing consists of two parts. First force and moment coefficients are calculated, then a sorting and selection process is carried out to yield aerodynamic coefficients as a function of flight parameters. The loads acting on the balance are calculated using the strain gage outputs. The aerodynamic contributions are derived by subtracting the effect of store mass, as measured by the accelerometers. Using Mach number and static pressure the captive aerodynamic coefficients are calculated.

During flight tests it is difficult, if not impossible, to vary one flight parameter at a time. To arrive at an acceptable data presentation some sorting procedure has to be used. Sorting is done in an array consisting of specified intervals of Mach number and one other parameter (either α, β or δ_a). For the two remaining parameters intervals are set before the sorting process takes place. Only data within those intervals is admitted. The data loaded in the array consists of means and standard deviations of the five aerodynamic coefficients and the mean of the second array variable. Prints and plots are available as output. Print-out samples are provided in tables I and II.

When a self-contained instrumentation system is used in the store, a slightly different data acquisition scheme will be used. Static pressure and Mach number will be derived from a small pitot-static system, mounted in the store. Angle of attack and angle of side slip will be calculated from normal and lateral accelerations as measured in the store. For this purpose the pilot will have to record aircraft gross weight as a function of time and time will be recorded in the store as well. Difficulties will be encountered in measuring aileron deflection angle.
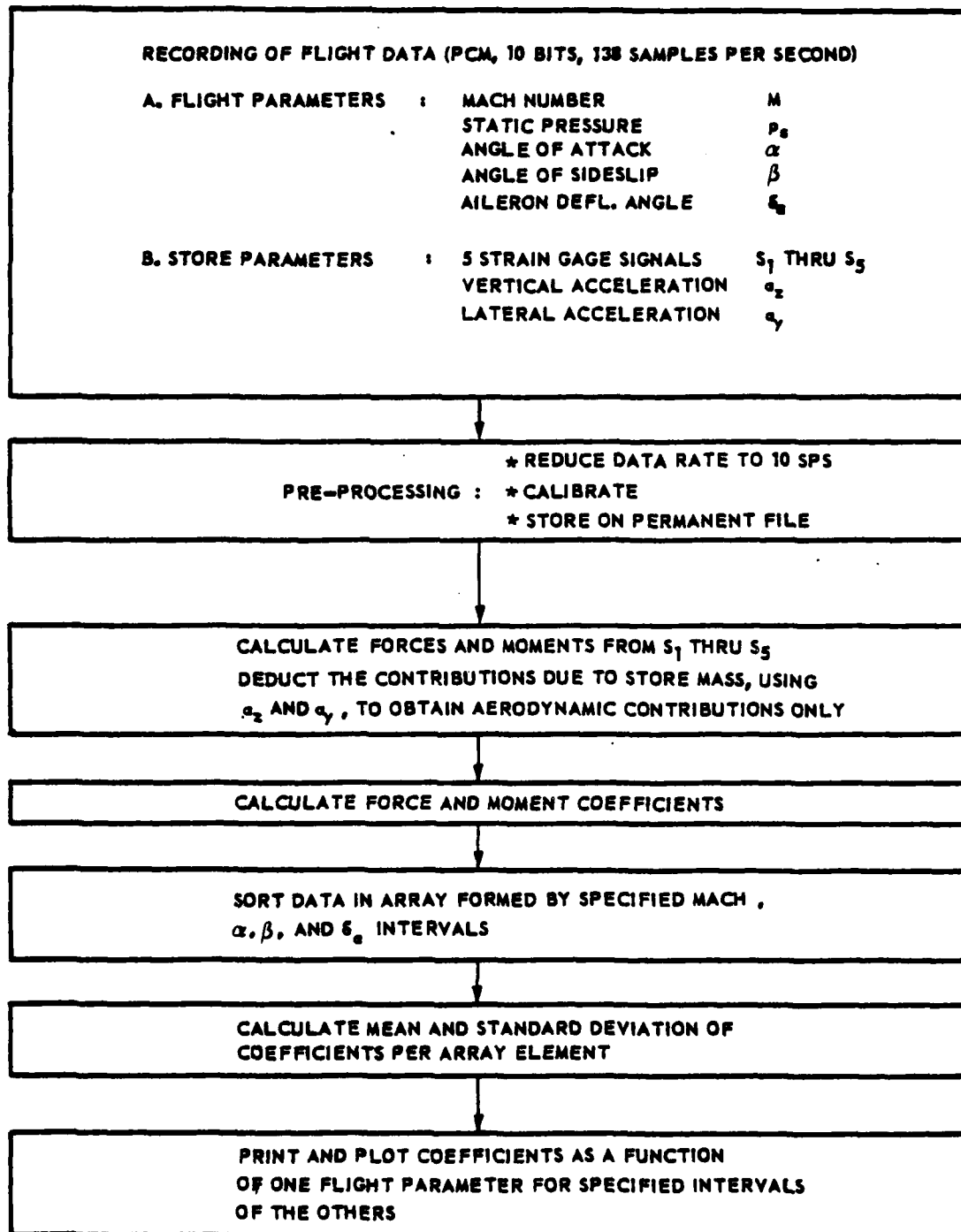
RECORDING OF FLIGHT DATA (PCM, 10 BITS, 138 SAMPLES PER SECOND)

A. FLIGHT PARAMETERS :
- MACH NUMBER .... M
- STATIC PRESSURE .... P_s
- ANGLE OF ATTACK .... α
- ANGLE OF SIDESLIP .... β
- AILERON DEFL. ANGLE ..... ξ_a

B. STORE PARAMETERS :
- 5 STRAIN GAGE SIGNALS .... S_1 THRU S_5
- VERTICAL ACCELERATION .... a_z
- LATERAL ACCELERATION ..... a_y

PRE-PROCESSING :
★ REDUCE DATA RATE TO 10 SPS
★ CALIBRATE
★ STORE ON PERMANENT FILE

CALCULATE FORCES AND MOMENTS FROM S_1 THRU S_5
DEDUCT THE CONTRIBUTIONS DUE TO STORE MASS, USING
a_z AND a_y, TO OBTAIN AERODYNAMIC CONTRIBUTIONS ONLY

CALCULATE FORCE AND MOMENT COEFFICIENTS

SORT DATA IN ARRAY FORMED BY SPECIFIED MACH,
α, β, AND ξ_a INTERVALS

CALCULATE MEAN AND STANDARD DEVIATION OF
COEFFICIENTS PER ARRAY ELEMENT

PRINT AND PLOT COEFFICIENTS AS A FUNCTION
OF ONE FLIGHT PARAMETER FOR SPECIFIED INTERVALS
OF THE OTHERS

Figure 7   Data acquisition and processing scheme

AVERAGES AND STANDARD DEVIATIONS OVER MACH INTERVAL .750 - .850 $(-0.5° < \beta < 0.5° -1° < \delta_e < 1°)$

	α	C_{z_o}		C_{y_o}		$C\ell_o$		C_{m_o}		C_{n_o}		NUMBER OF MEASUREMENTS
1	0.000	0.	0.	0.	0.	0.	0.	0.	0.	0.	0.	0.
2	0.000	0.	0.	0.	0.	0.	0.	0.	0.	0.	0.	0.
3	0.000	0.	0.	0.	0.	0.	0.	0.	0.	0.	0.	0.
4	0.000	0.	0.	0.	0.	0.	0.	0.	0.	0.	0.	0.
5	0.000	0.	0.	0.	0.	0.	0.	0.	0.	0.	0.	0.
6	.101	.123E-02	.674E-02	.625E-01	.570E-02	.190E-02	.202E-02	.090E-01	.499E-02	.677E-02	.120E-02	73.
7	.654	.428E-02	.658E-02	.630E-01	.477E-02	.101E-02	.140E-02	.044E-01	.469E-02	.990E-02	.178E-02	92.
8	.865	.137E-01	.541E-02	.408E-01	.405E-02	.009E-01	.116E-02	.015E-01	.399E-02	.111E-01	.142E-02	185.
9	1.124	.264E-01	.576E-02	.577E-01	.471E-02	.902E-03	.130E-02	.755E-01	.402E-02	.174E-01	.107E-02	66.
10	1.381	.369E-01	.691E-02	.544E-01	.479E-02	.360E-03	.140E-02	.702E-01	.385E-02	.213E-01	.109E-02	72.
11	1.621	.447E-01	.621E-02	.527E-01	.407E-02	.228E-03	.146E-02	.657E-01	.383E-02	.255E-01	.173E-02	57.
12	1.677	.651E-01	.101E-01	.515E-01	.442E-02	.499E-03	.124E-02	.610E-01	.246E-02	.299E-01	.243E-02	56.
13	2.107	.853E-01	.106E-01	.173E-01	.435E-02	.755E-03	.906E-03	.378E-01	.375E-02	.383E-01	.240E-02	182.
14	2.340	.762E-01	.886E-02	.430E-01	.472E-02	.744E-03	.138E-02	.508E-01	.354E-02	.372E-01	.283E-02	91.
15	2.624	.113E+00	.870E-02	.901E-01	.669E-02	.144E-02	.111E-02	.155E-01	.325E-02	.407E-01	.266E-02	79.
16	2.883	.130E+00	.120E-01	.367E-01	.645E-02	.197E-02	.995E-03	.890E-01	.306E-02	.440E-01	.302E-02	76.
17	3.141	.144E+00	.911E-02	.384E-01	.624E-02	.206E-02	.108E-02	.362E-01	.209E-02	.565E-01	.246E-02	197.
18	3.357	.156E+00	.120E-01	.384E-01	.714E-02	.260E-02	.150E-02	.317E-01	.301E-02	.590E-01	.322E-02	172.
19	3.618	.174E+00	.154E-01	.317E-01	.719E-02	.363E-02	.144E-02	.252E-01	.316E-02	.620E-01	.294E-02	115.
20	3.887	.194E+00	.113E-01	.291E-01	.751E-02	.326E-02	.115E-02	.206E-01	.340E-02	.635E-01	.352E-02	90.
21	4.122	.200E+00	.124E-01	.277E-01	.779E-02	.409E-02	.150E-02	.165E-01	.341E-02	.590E-01	.316E-02	115.
22	4.356	.223E+00	.122E-01	.288E-01	.765E-02	.859E-02	.153E-02	.119E-01	.357E-02	.620E-01	.294E-02	71.
23	4.535	.230E+00	.142E-01	.236E-01	.866E-02	.615E-02	.117E-02	.737E-02	.375E-02	.646E-01	.341E-02	107.
24	4.879	.255E+00	.172E-01	.294E-01	.812E-02	.666E-02	.141E-02	.396E-02	.341E-02	.675E-01	.348E-02	67.
25	5.119	.274E+00	.212E-01	.216E-01	.113E-01	.718E-02	.174E-02	.178E-03	.387E-02	.700E-01	.449E-02	82.
26	5.367	.287E+00	.180E-01	.225E-01	.956E-02	.791E-02	.142E-02	.374E-02	.400E-02	.729E-01	.415E-02	63.
27	5.643	.302E+00	.192E-01	.214E-01	.119E-01	.025E-02	.154E-02	.077E-02	.538E-02	.765E-01	.446E-02	79.
28	5.855	.322E+00	.178E-01	.167E-01	.120E-01	.913E-02	.167E-02	.133E-02	.515E-02	.793E-01	.433E-02	76.
29	6.119	.326E+00	.194E-01	.266E-01	.914E-02	.003E-02	.180E-02	.124E-01	.400E-02	.777E-01	.326E-02	36.
30	6.340	.345E+00	.216E-01	.237E-01	.160E-01	.997E-02	.225E-02	.176E-01	.656E-02	.818E-01	.446E-02	39.
31	6.616	.353E+00	.164E-01	.276E-01	.138E-01	.564E-02	.256E-02	.205E-01	.420E-02	.819E-01	.828E-02	34.
32	6.892	.372E+00	.221E-01	.226E-01	.160E-01	.993E-02	.357E-02	.235E-01	.444E-02	.843E-01	.412E-02	42.
33	7.110	.380E+00	.305E-01	.291E-01	.154E-01	.112E-01	.252E-02	.259E-01	.460E-02	.848E-01	.276E-02	21.
34	7.347	.412E+00	.284E-01	.395E-01	.251E-01	.134E-01	.491E-02	.270E-01	.728E-02	.697E-01	.615E-02	21.
35	7.598	.422E+00	.544E-01	.113E-01	.248E-01	.109E-01	.422E-02	.321E-01	.731E-02	.094E-01	.388E-02	19.
36	7.873	.444E+00	.207E-01	.659E-01	.248E-01	.133E-01	.432E-02	.342E-01	.794E-02	.083E-01	.436E-02	10.
37	8.103	.454E+00	.140E-01	.541E-01	.150E-01	.120E-01	.234E-02	.355E-01	.742E-02	.897E-01	.246E-02	4.
38	8.356	.457E+00	.192E-01	.612E-01	.320E-01	.081E-01	.040E-02	.356E-01	.803E-02	.902E-01	.406E-02	6.
39	8.672	.468E+00	.202E-01	.363E-01	.165E-01	.130E-01	.551E-02	.447E-01	.762E-02	.921E-01	.102E-02	6.
40	8.846	.493E+00	.252E-01	.360E-01	.274E-01	.970E-02	.334E-02	.438E-01	.783E-02	.920E-01	.206E-02	4.
41	9.128	.472E+00	.101E-01	.438E-01	.930E-02	.164E-01	.946E-02	.479E-01	.115E-02	.935E-01	.317E-03	2.
42	9.388	.560E+00	.901E-01	.794E-01	.573E-02	.126E-01	.404E-02	.463E-01	.222E-02	.530E-01	.294E-02	2.
43	9.632	.513E+00	.106E-01	.520E-01	.304E-01	.171E-01	.546E-02	.515E-01	.850E-02	.816E-01	.206E-02	6.
44	9.869	.524E+00	.165E-01	.730E-01	.292E-01	.155E-01	.566E-02	.403E-01	.638E-02	.569E-01	.314E-02	10.
45	10.124	.535E+00	.158E-01	.765E-01	.490E-01	.192E-01	.280E-02	.519E-01	.109E-01	.983E-01	.313E-02	7.
46	10.358	.548E+00	.317E-01	.643E-01	.272E-01	.100E-01	.504E-02	.484E-01	.222E-02	.361E-01	.303E-02	7.
47	10.603	.559E+00	.378E-01	.775E-01	.207E-01	.189E-01	.495E-02	.548E-01	.644E-02	.548E+00	.206E-02	24.
48	10.851	.003E+00	.519E-01	.507E-01	.186E-01	.191E-01	.220E-02	.629E-01	.419E-02	.104E+00	.314E-02	5.
49	11.081	.600E+00	0.	.923E-01	0.	.160E-01	0.	.565E-01	0.	.101E+00	.457E-02	1.
50	11.400	.625E+00	.401E+00	.620E-01	.267E-01	.167E-01	.694E-02	.714E-01	.560E-02	.102E+00	.372E-02	14.

Table I   Print-out sample with angle of attack as a variable

AVERAGES AND STANDARD DEVIATIONS OVER MACH INTERVAL   0.600 - .600 $(3°<\alpha<4°\ -4°<\delta<4°)$

β	C_{z_0}		C_{Y_0}	C_{l_0}	C_{m_0}		C_{n_0}	NUMBER OF MEASUREMENTS
-5.564	.536E+00	0.	.954E-01	0.	-.217E-01	0.	.131E+00	1.
-5.195	.516E+00	0.	.792E-01	0.	-.197E-01	0.	.130E+00	1.
0.000	0.	0.	0.	0.	0.	0.	0.	0.
-4.210	.393E+00	.775E-01	.394E-01	.262E-01	.127E-01	.803E-02	.108E+00	5.
0.000	0.	0.	0.	0.	0.	0.	0.	0.
-3.064	.319E+00	.329E-01	.145E-01	.540E-02	.101E-01	.149E-01	.971E-01	2.
-2.802	.264E+00	.302E-01	.129E-02	.433E-02	-.600E-03	.313E-02	.760E-01	2.
-2.006	.227E+00	.564E-02	.564E-02	0.	.227E-02	.709E-02	.620E-01	2.
-1.714	.101E+00	.677E-01	.102E-01	.255E-01	.380E-02	.786E-02	.623E-01	2.
-1.105	.147E+00	.411E-01	.318E-01	.133E-01	.253E-01	.125E-01	.452E-01	2.
-.532	.125E+00	.921E-02	.272E-01	.400E-02	-.298E-02	.314E-02	.392E-01	2.
-.320	.134E+00	.234E-01	-.263E-01	.535E-02	-.364E-02	.427E-02	.445E-01	2.
-.115	.597E-01	.107E-01	-.283E-01	.401E-02	-.430E-02	.192E-02	.322E-01	2.
.775	.390E-01	.250E-01	-.272E-01	.944E-02	.184E-02	.212E-02	.128E-01	19.
1.344	.344E-01		-.237E-01	.842E-02	.341E-02		.130E-01	5.
1.721	.200E-01	.437E-01	-.221E-01	-.873E-03	-.995E-02	.130E-02	.668E-02	2.
0.000	0.	0.	0.	0.	0.	0.	0.	0.
2.659	-.179E-01	.162E-01	-.224E-01	.215E-02	.874E-02	.152E-02	-.219E-01	4.
3.234	-.944E-01	.156E-02	-.239E-01	.242E-02	-.278E-02	.463E-02	-.357E-01	3.
3.732	-.358E-01	0.	-.164E-01	0.	-.234E-02	0.	-.418E-01	1.
4.354	-.795E-01	.130E-01	-.197E-01	.855E-02	-.124E-01	.192E-02	-.576E-01	3.
4.727	-.103E+00	0.	-.821E-02	0.	-.143E-01	0.	-.733E-01	1.
0.000	0.	0.	0.	0.	0.	0.	0.	0.
0.000	0.	0.	0.	0.	0.	0.	0.	0.

Table II   Print-out sample with angle of side slip as a vairable

A summary of the configurations tested to date is provided in table III (M indicates the position of the measuring store). In configuration A the structural integrity of the store was demonstrated. On configurations B and C the largest body of measured and calculated aerodynamic and store motion data is available. Configuration C was selected to evaluate repeatability of the measurements, D to evaluate the effect of the presence or absence of an inboard store.

As a follow-on to this program measurements will be carried out with the store mounted 0.15 m below the pylon. In this way the variation of aerodynamic interference with vertical position relative to the pylon can be evaluated.

To obtain adequate coverage of the Mach number-angle of attack data array a slow symmetrical flight manoeuvre was prescribed. The pilot had to start this manoeuvre at Mach number intervals of approximate 0.025. A number of actual measurement runs is shown in figure 8. Normal load factor was limited to 3, as a precaution not to overload the balance. In the figure it is shown how a typical data sorting array element will be filled. See also table I for the number of measurement points per array element. Variation in aerodynamic coefficients as a function of angle of side slip or aileron deflection angle is measured by means of rudder pulses (β) and aileron oscillations (δ_a) during nominal straight and level flight.

FLIGHT   TEST   SUMMARY   (ONE FLIGHT PER CONFIGURATION)

NF – 5 A CONFIGURATIONS	MACH RANGE
A	0 ⟶ 1.0
B	
C	0 ⟶ 0.85
D	
E	

FLIGHT   CONDITIONS :

0	TO	30.000	FEET
200	TO	600	Kts
0	TO	12	DEGREES ANGLE OF ATTACK
–5	TO	5	DEGREES SIDESLIP ANGLE
–20	TO	20	DEGREES AILERON ANGLE
–0.5	TO	3.0	NORMAL LOAD FACTOR

Table III   Flight test summary
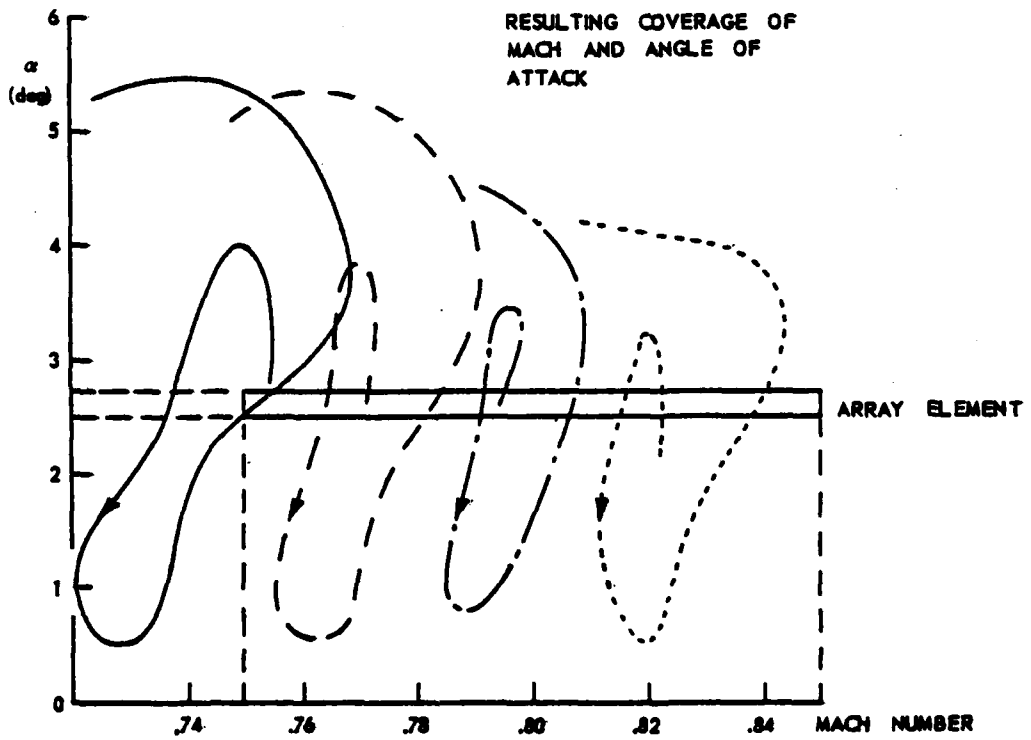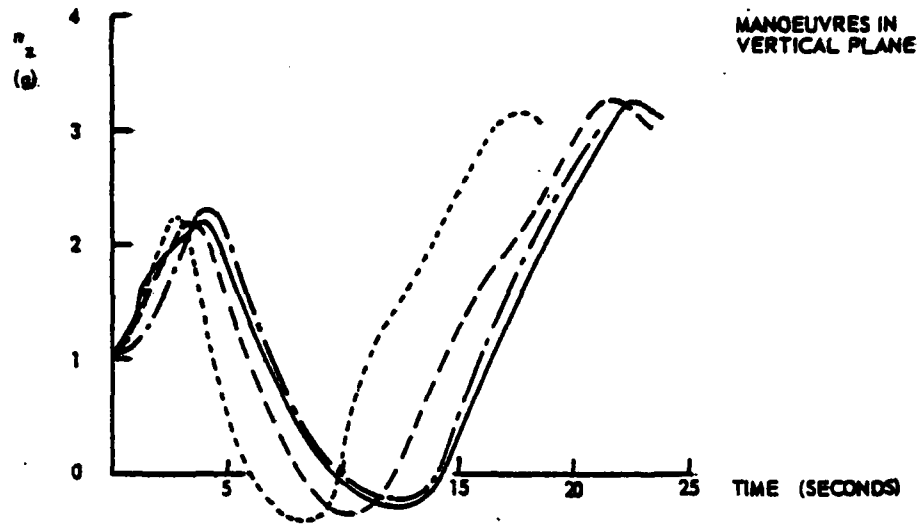
Figure 8   Typical data acquisition manoeuvres

PROPERTIES OF THE MEASURED DATA

From static and dynamic ground trials the accuracy of the aero-dynamic load measuring store has been estimated. The accuracy of the mean value of the measurements in case a large number of measurements is taken and of the standard deviation in that case is shown in table IV.

Parameter	Accuracy of force/moment		Accuracy of coefficients at:					
			200 kts		300 kts		400 kts	
	mean	SD	mean	SD	mean	SD	mean	SD
Z, C_z Y, C_y	±45 N	±70 N	.045	.070	.015	.025	.011	.015
L, C_ℓ	± 3 Nm	± 5 Nm	.003	.010	.002	.005	.001	.003
M, C_m N, C_n	±20 Nm	±40 Nm	.005	.010	.002	.004	.001	.002

Table IV Measurement accuracy data

The standard deviations of the flight test data that have been obtained under low to moderate turbulence conditions match the table IV values. Repeatability checks, where the data obtained in one configuration was processed in batches did confirm the accuracy estimate for the mean value.

In the configuration with the store at the outboard pylon two flights have been carried out, one with the store of the left hand station, and one with the store at the right hand station. Comparison of the results of both flights show a definite difference in captive yawing moment data. The difference appears as a pure shift of ∿.006. As the free air moment coefficient derivative about the vertical store axis is .016 per degree, the difference can be caused by:
- a relative misalignment of left hand and right hand store of 0.4 degree or
- an average aircraft angle of side slip of 0.2 degree.
Either of these conditions may have existed without being noticed.

The measurement runs have been repeated at various altitudes (5,000; 10,000; 20,000; and 30,000 feet). Data has been processed per altitude to evaluate whether any Reynolds-effect was present. No significant differences were noted.

DATA SOURCE/CONFIGURATION	SCALE	REYNOLDS NUMBER[1]	BOUNDARY LAYER TRANSITION STRIP	GAP BETWEEN STORE AND PYLON	METHOD, PARTICULARS
Wind tunnel Ref.1	1/7	$\sim2 \cdot 10^6$	on store nose	partly blocked by balance support	Force/moment measurements full model
Wind tunnel Ref.2	1/45	$5 \cdot 10^6$ to $10 \cdot 10^6$	.05 m from store nose	no gap	Integration of pressure measurements;pressure holes in 11 cross sections, 8 holes per cross-section. Half-wing model, no inboard pylon
Calculations Ref.3	-	-	-	with gap	Assuming potential flow, partly corrected for viscosity effects
Flight tests	1/1	$8 \cdot 10^6$ to $5 \cdot 10^7$	none	with gap	Separation trials. Coefficients calculated according to Fig.2.
Flight tests	1/1	$8 \cdot 10^6$ to $5 \cdot 10^7$	none	with gap	Force/moment measurements

1) Based on wing mean aerodynamic chord.

Table V   Leading particulars on the data sources for aerodynamic coefficients of captive stores.

COMPARISON WITH DATA FROM OTHER SOURCES .

The configuration labelled B in table III has been used in the past to evaluate accuracy of store separation measurement techniques as well as to demonstrate the prediction possibilities of the model shown in figure 1. Thus a large and varied body of information is available. The part that is used is summarized in table V.

The data is compared with the results of the measuring store in figures 9 (pitching moment), 10 (yawing moment) and 11 (normal and lateral forces). Furthermore store motion during separation has been calculated for a flight condition at 450 KEAS, $M = 0.7$, $\alpha = 2.5$, using the M 0,7 wind tunnel data (Ref. 1) as well as the data measured in flight. Note that only the pitching moment coefficient differs in this particular case. The result, shown in figure 12 is indicative of the significance of the differences in the various data sets in figures 9 and 10.

Wind tunnel and calculated force coefficients agree reasonably with the values measured with the store. A notable exception is the C_{z_0} value obtained from reference 2, possibly due to the absence of the gap. The moment coefficients from these sources agree less well. No effort will be made yet to identify the cause of these differences. Candidate causes are listed in table V.

Moment coefficients, calculated by modifying captive aerodynamic coefficient sets based on wind tunnel measurement according to the scheme of figure 2, agree very well with the data measured with the store. In this particular case the prediction model was operating using captive aerodynamic data as the basis for the calculation of interference aerodynamics. The variation of aerodynamic interference with vertical position was based on panel method calculations (Ref. 3).

Difference between measured and recalculated captive aerodynamic data may originate from errors due to the quasi-steady treatment of an non-steady process as is done in the model of figure 1, or from wrong modelling of the variation in interference with vertical position. As the moment coefficients agree well, it is likely that both the quasi-steady treatment and the calculated variation in interference are sufficiently accurate. This will be verified by carrying out measurements in flight with the store 0.15 m below its normal position at the pylon.

Inversely it indicates that, when using aerodynamic coefficients measured in-flight for prediction of store separation, the result will be very reliable, especially when the aerodynamic coefficients are measured at one (or more) positions below the pylon. This possibility will be of prime importance in case separations from multiple ejector racks are concerned.

778
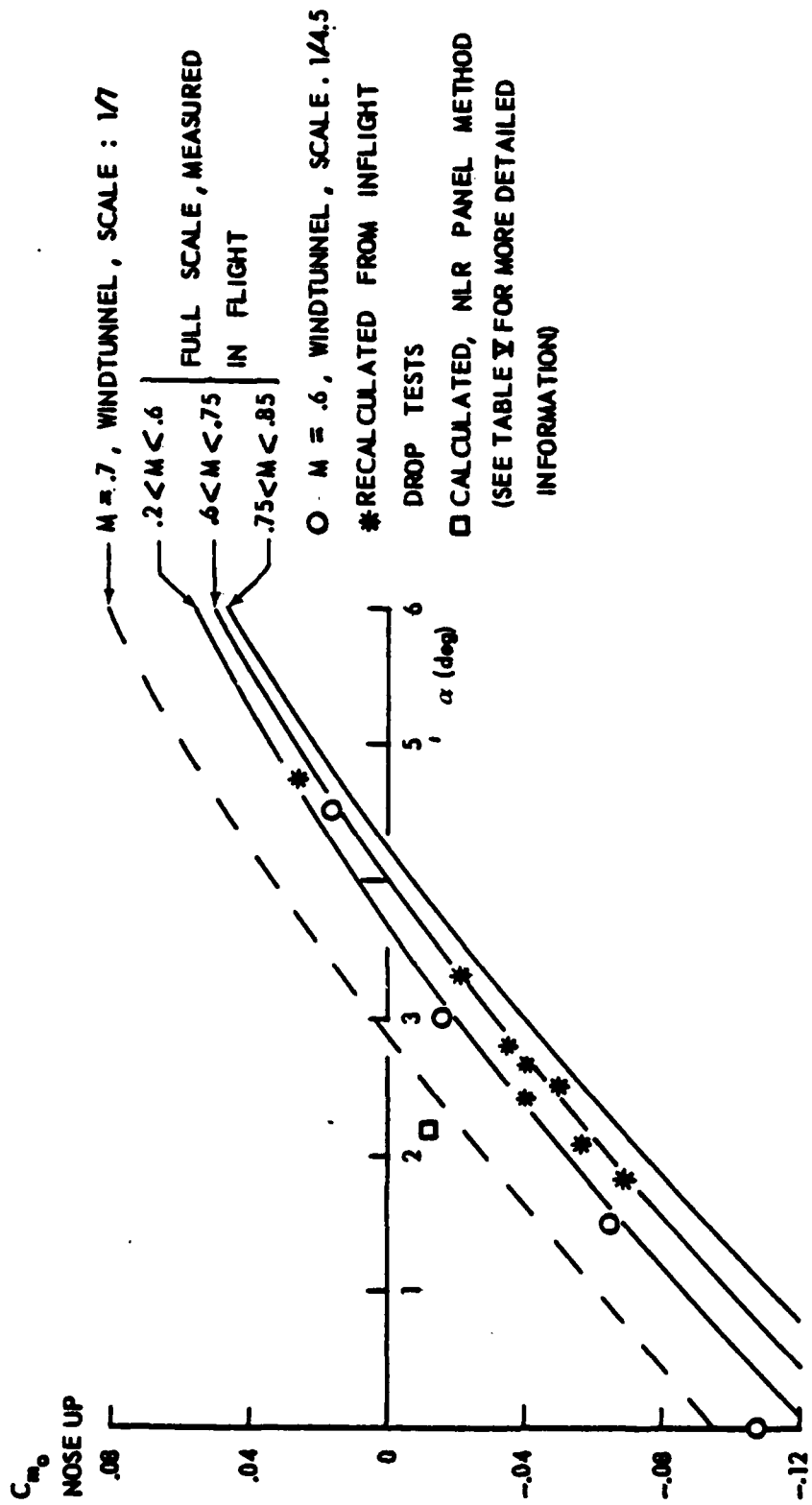
Figure 9   Captive pitching moment coefficient
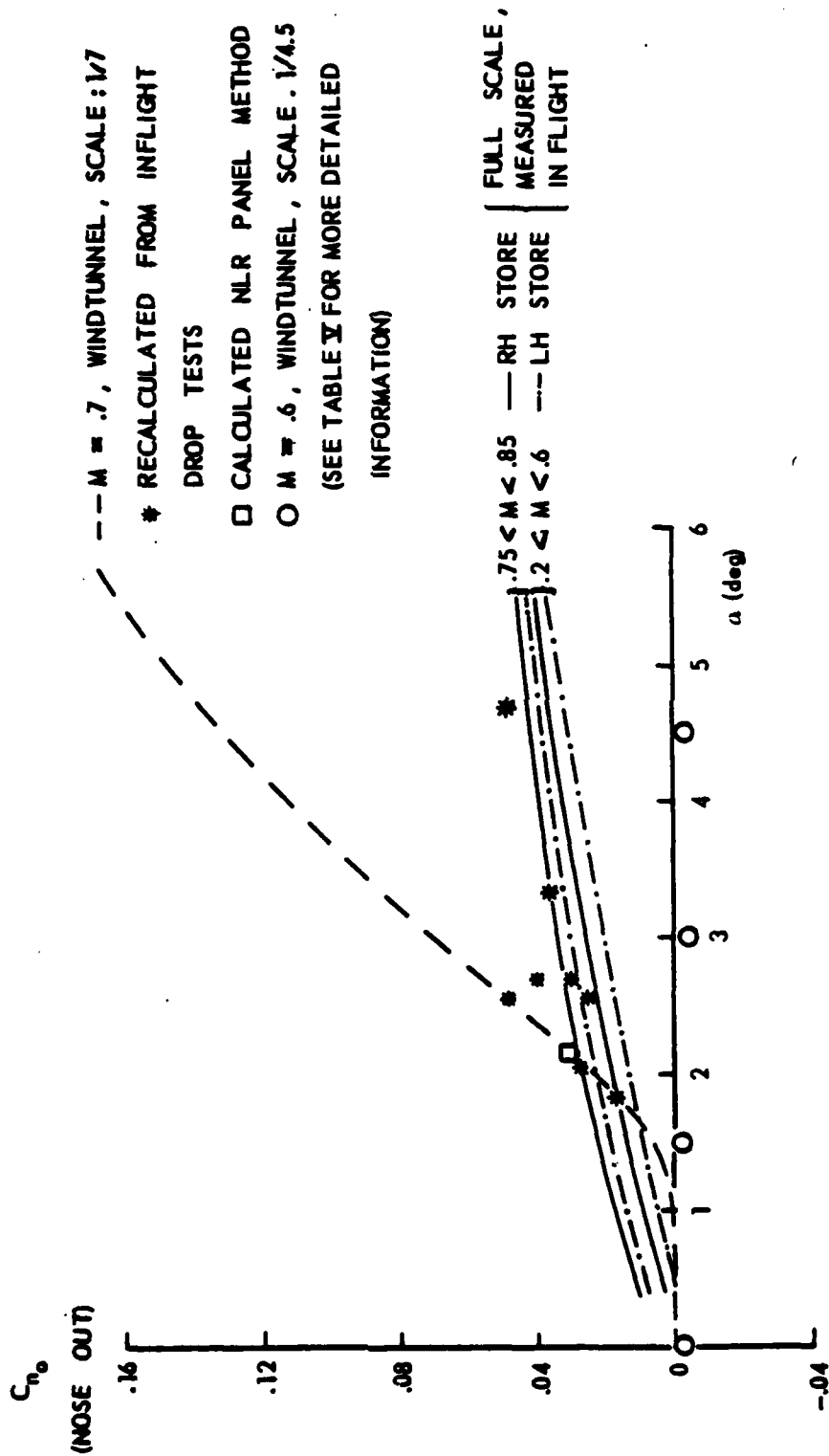
Figure 10   Captive yawing moment coefficient
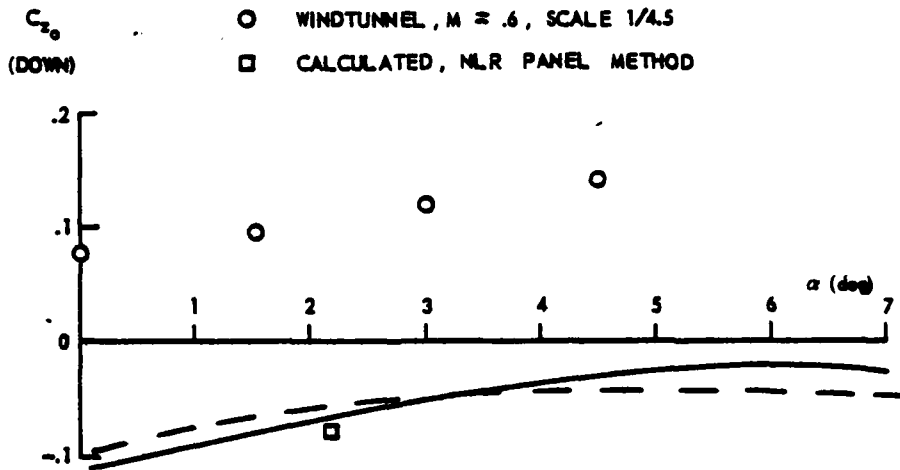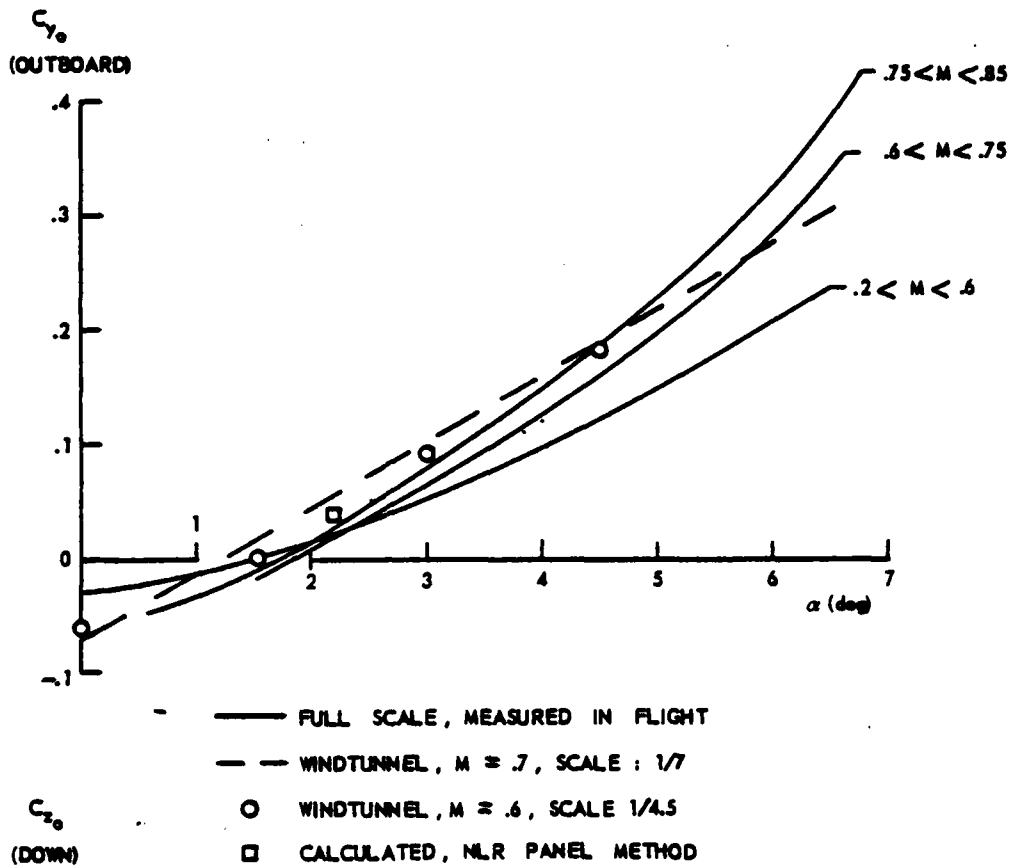
Figure 11   Captive force coefficients
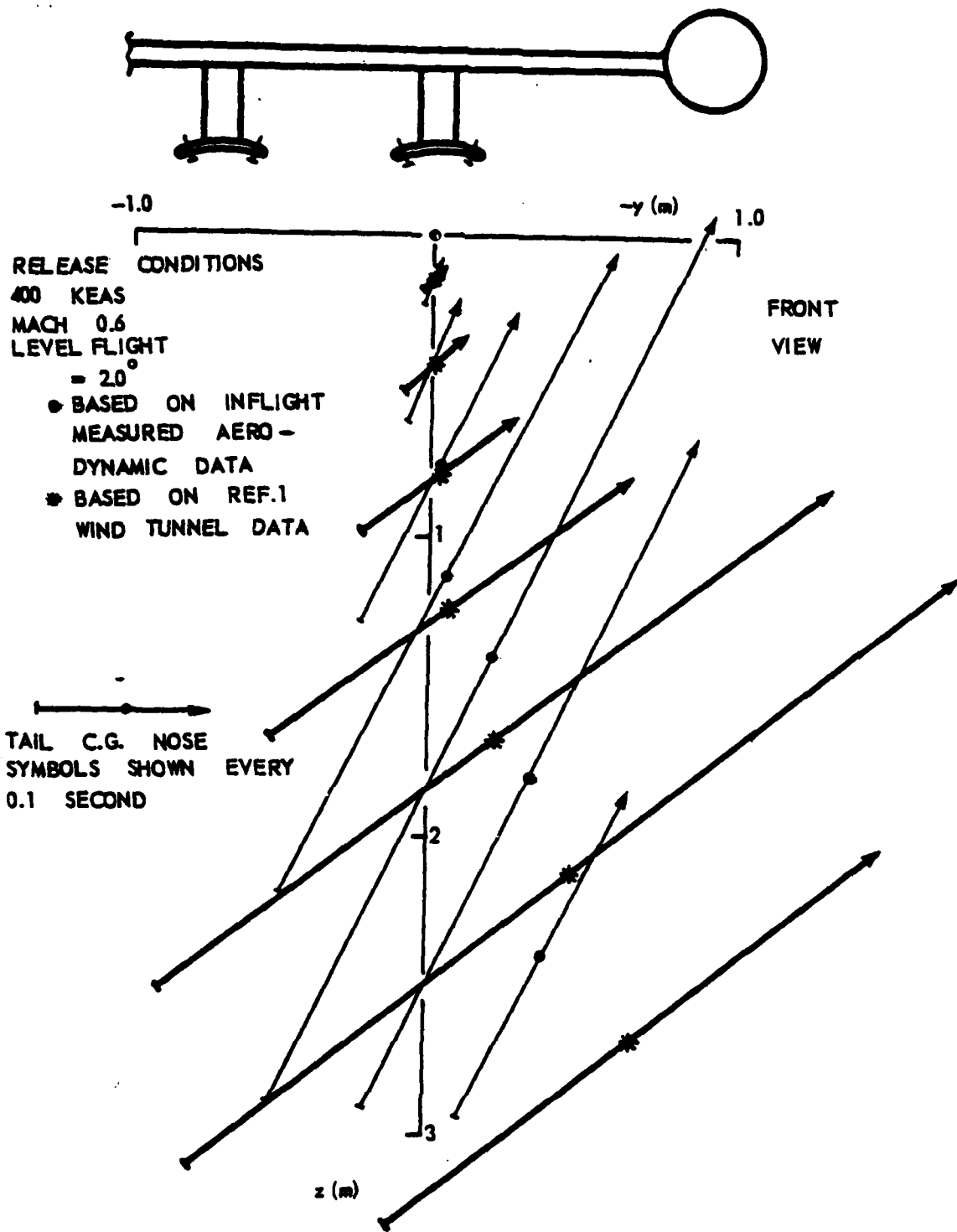
Figure 12   Differences in captive pitching moment coefficient, translated in differences in store motion

CONCLUDING REMARKS

The tests have demonstrated the feasibility of in-flight measurement of aerodynamic coefficients in an accurate manner.

Such measurements, when used in combination with an adequate store separation prediction program, will make store separation analysis more thrustworthy. Subsequently the number of drops required to demonstrate safe separation may be reduced.

It is expected that the use of an aerodynamic load measuring store will pay off primarily in cases where separation might be critical. Light and large stores, unstable stores, and the transonic flight regime are examples of such cases.

REFERENCES

1. Anon. Transonic wind tunnel tests of a 1/7 scale model of the Norair F-5A airplane with external stores. Cornell Aeronautical Laboratory, Inc. CAL-AA-1343-W-15 Oct. 1964.

2. Renirie, L. Steady pressure measurement on a wing with stores in subsonic flow. NLR TR 71095 C 1971.

3. Sytsma, H.A., Slooff, J.W., Janssen, Th., Nyhuis, G.H. Theoretical determination of aerodynamic aircraft-store interference for the Northrop NF-5A aircraft with N-container. NLR TR 73068 C Dec. 1973.

4. Alders, G.J. Investigation into the applicability of the NLR store separation model. NLR TR 73052 C May 1973.

AUTOBIOGRAPHY

The author graduated from the Delft University of Technology in 1966 as an aeronautical "ingenieur", with a specialization in the field of flying qualities.

The years 1966 thru 1968 he spent with the Royal Netherlands Air Force, where he was a project officer in the Bureau for Operations Research and Evaluations.

From 1968 on he is employed by the National Aerospace Laboratory NLR in Amsterdam as a project manager and flight test engineer, mainly in the field of airworthiness demonstration and systems evaluation projects with military aircraft. His activities in the field of store separation analysis include the development of a store separation prediction programme, and of a method to determine actual store motion with on-board film cameras.

(The reverse of this page is blank)

GENERATION OF AERODYNAMIC INFLUENCE COEFFICIENTS FROM AIRCRAFT-STORE SEPARATION KINEMATICS
(U)
(Article UNCLASSIFIED)

by

Guy F. Cooper and Jon Gnagy
Pacific Missile Test Center
Point Mugu, California 93042

ABSTRACT. (U) A method of determining influence coefficients to describe the interference of a parent aircraft on a separating store is being developed at the Pacific Missile Test Center. It involves comparing, segment-by-segment, an experimental separation trajectory with a theoretical free stream trajectory. The differences at the end of each segment are explained as static influence coefficients. Each theoretical trajectory segment is initialized with conditions identical to its corresponding experimental segment. A six-degree-of-freedom computer program is used to develop the coefficients by iterative techniques; it then "closes the loop" by recreating the original separation trajectory using the coefficients. This paper describes the basic concept for estimating the influence coefficient and several techniques for evaluating the basic math and the computer program. Results of these techniques are given as well as results of using the program to analyze two flight-test separations of a typical large store from the bomb bay of a typical large bomber. Factors affecting the accuracy of the results are discussed. Future variations of the computer program for coping with more violent separations will be discussed.

TABLE

Table 1. Coefficients Generated by the "Railroad Track" Trajectory

FIGURES

SYMBOLS

C	Aerodynamic coefficient
$\overrightarrow{C_F}$	Total free stream aerodynamic force coefficient vector
$\overrightarrow{\Delta C_F}$	Influence force coefficient vector
$\overrightarrow{C_M}$	Total free stream aerodynamic moment coefficient vector
$\overrightarrow{\Delta C_M}$	Influence moment coefficient vector
$\overrightarrow{F}$	Air load force vector
1_{ref}	Reference length of store
m	Store mass
$\overrightarrow{M}$	Air load moment vector
q	Free stream dynamic pressure
$\overrightarrow{r}$	Position vector of store CG on a trajectory segment relative to beginning of that segment
$\overrightarrow{\Delta r}$	Position difference vector between theoretical and experimental trajectory segment ends
$\overrightarrow{R}$	Position vector relative to origin of a coordinate system
$\overrightarrow{\Delta R}$	Change in position vector
$\overrightarrow{R_q^m}$	Position vector of store CG in aircraft coordinate system
$\overrightarrow{R_1^a}$	Position vector of aircraft in local geocentric system
S_{ref}	Reference area of store
t	Time
Δt	Time from beginning of a trajectory segment to end
θ	Pitch Euler angle
ϕ	Roll Euler angle
ψ	Yaw Euler angle
$\Delta \Omega$	Vector representation of small angular difference between store body axes at end of theoretical and end of experimental trajectory segments

789

I	Moment of inertia of store about a body axis
x, y, $\bar{z}$, X, Y, Z	Coordinate system axes (see figure 1)

Superscripts:

a	Aircraft
m	Missile or store
$\rightarrow$	Vector value
,	Theoretical or free stream value
$\cdot$	First-time derivative
$\cdot\cdot$	Second-time derivative

Prescripts:

Δ	Incremental value, as with influence coefficient; or, difference value, as with position or time difference

Subscripts:

a	Aircraft coordinate system
F	Force due to air loads
M	Moment due to air loads
m	Missile or store coordinate system
l	Local geocentric, or earth, coordinate system

INTRODUCTION

Various efforts at determining the aerodynamic coefficients of bodies from their free stream trajectory kinematics have been made for many years. Use of these coefficients in math models has allowed estimation of their general flight characteristics. More accurate estimates have become possible with both increased accuracy in trajectory data and with more accurate and comprehensive math models. Determination of aerodynamic influences between two bodies is closely related to determining free stream aerodynamic coefficients; this, in turn, is a special category of parameter estimation. The potential accuracy in six-degree-of-freedom reduction of onboard separation movies possible with PACMIS-TESTCEN's Photo Data Analysis System (PDAS) should allow a minutely accurate analysis of the influence, or interference, of a parent aircraft upon a separating store.

The difference between single-body free stream aerodynamic coefficients and influence coefficients is that the former remain constant, or approximately so, during a portion of a trajectory where the body state does not change much. The latter often change drastically with position relative to the launch aircraft so that they constitute an air loads field. Normally the launch aircraft is assumed to affect the store, but not conversely.

A notable attempt at determination of free stream aerodynamic coefficients is that by Chapman and Kirk (reference 1). This technique has been adapted to estimating influence coefficients for a separating store by the University of Florida (reference 2); software for performing this is included in the reference. The present paper discusses the computerization of a technique described at the 1973 JTCG Aircraft/Stores Compatability Symposium (reference 3). A purely statistical approach is covered in reference 4. A general survey of the state of the art of parameter estimation is given in reference 5, a 1973 symposium on applications to aircraft flight testing.

Many of the techniques involve a comparison of an experimental trajectory (the separation trajectory) with a theoretical trajectory produced by a free stream math model. Corrections are added to the free stream math model coefficients until the two trajectories agree. The Chapman and Kirk method determines a set of partial derivatives that express the sensitivity of the theoretical math model to the coefficients in question. The theoretical math model is then adjusted so that the sum of the squares of the differences, or residuals, between the experimental and the theoretical trajectories is minimized over the entire length of trajectory to be studied. Determination of the partial derivatives is quite complex, but in many cases the resultant corrected theoretical trajectories have agreed very closely with the experimental trajectories.

BASIC APPROACH

The technique described in this paper is analytically much simpler than that of Chapman and Kirk. The experimental trajectory is divided into small segments, as shown in figure 2. Each segment is compared with its corresponding theoretical trajectory of the same duration, Δt, and initialized with the same initial conditions. The translational and rotational differences at the end of Δt, or at the termination of the two trajectory segments, are used in a very simple physical model to estimate the influence air loads.
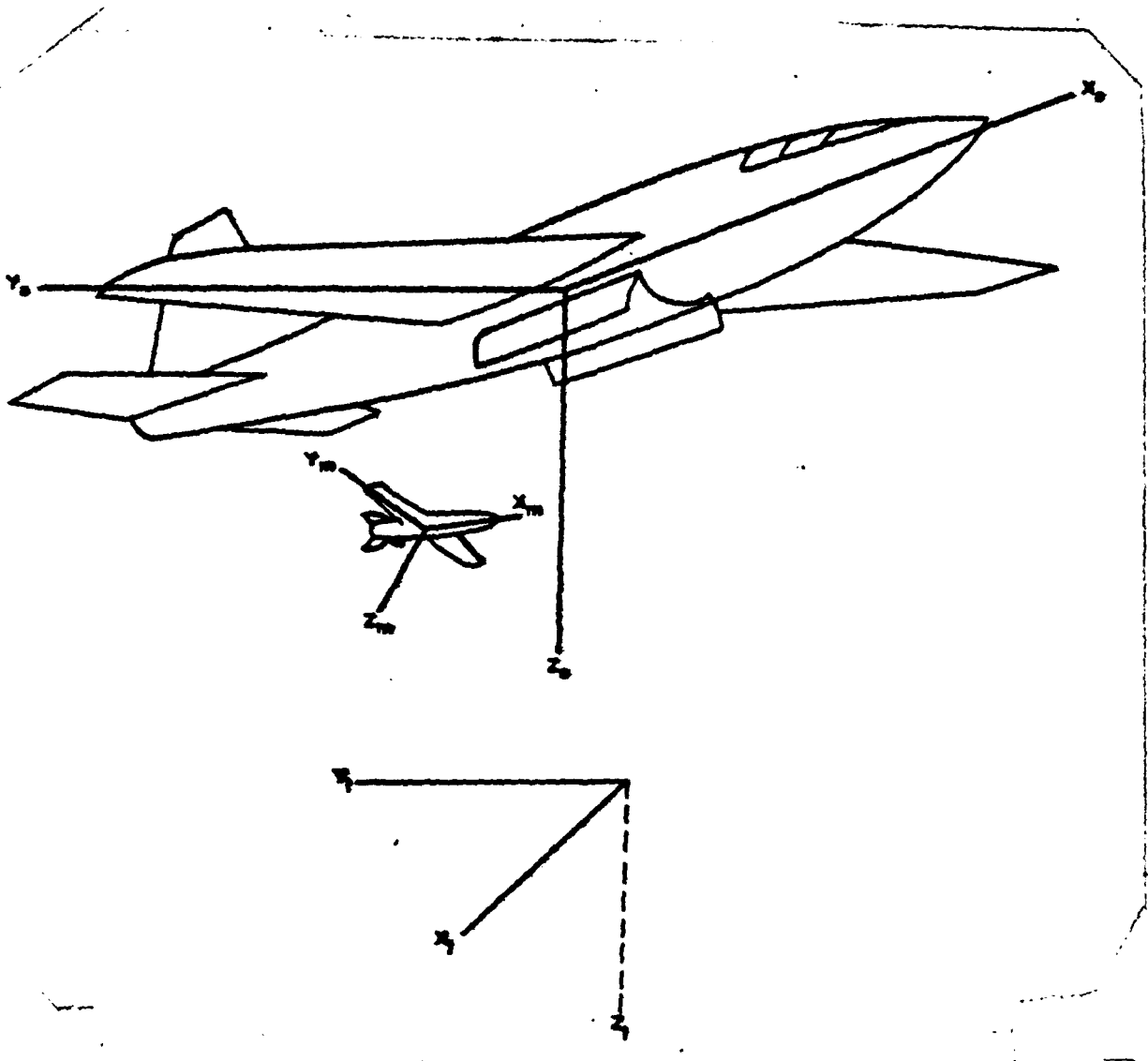
Figure 1. Coordinate Systems Involved in Store Separation.
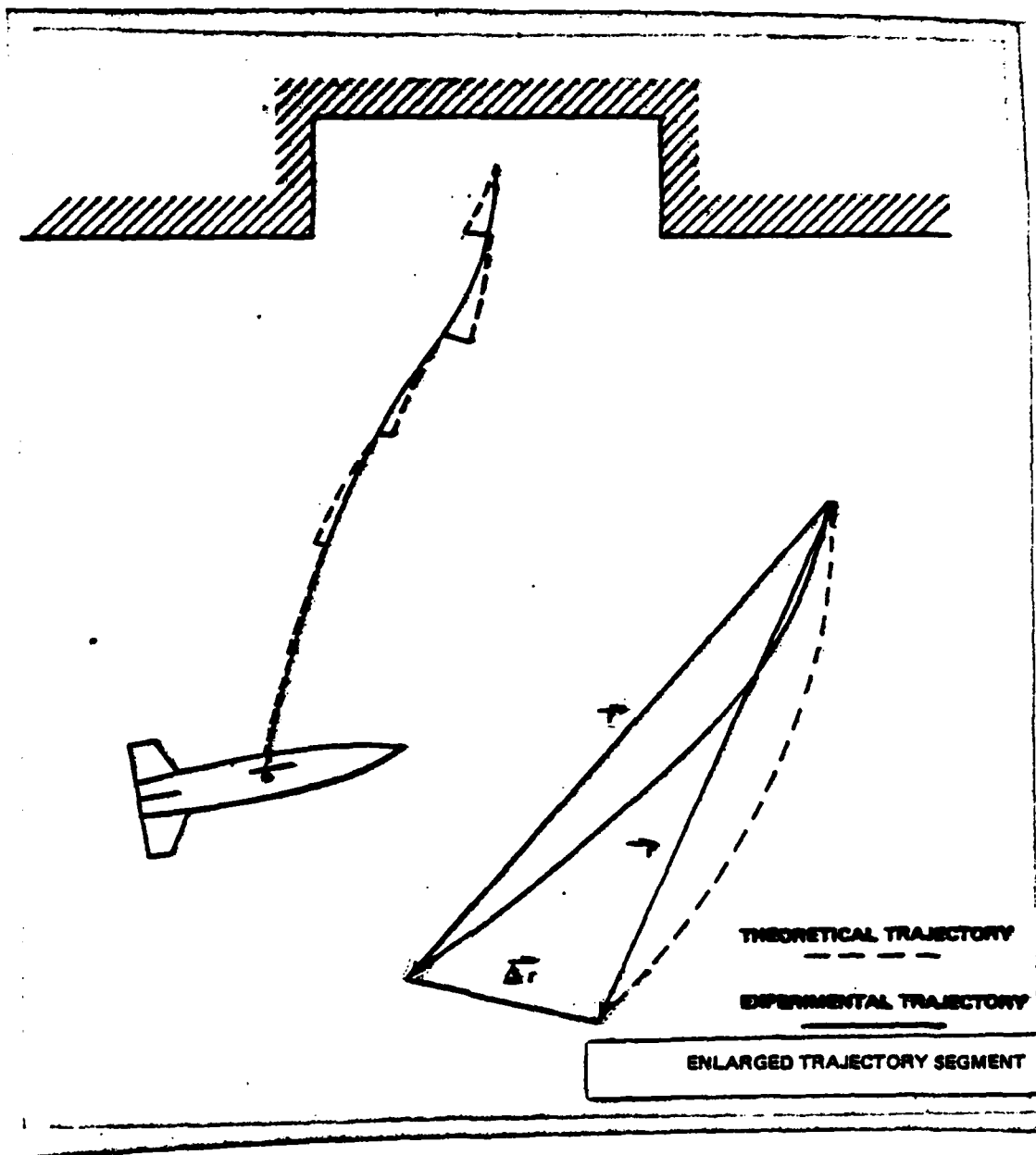
Figure 2. Experimental and Free Stream Theoretical Trajectory Segments Compared.

THEORETICAL TRAJECTORY
– – – – –

EXPERIMENTAL TRAJECTORY

ENLARGED TRAJECTORY SEGMENT

The physical model employed is Galileo's expression for a falling body: displacement varies as acceleration and as time squared. The acceleration is due to air loads acting on the store mass. The acceleration is assumed to be constant. Substituting the free stream dynamic pressure, the store reference dimensions and the coefficients, the physical model in scalar form becomes, for translation:

$$r = \frac{1}{2}\, \ddot{r}\, (\Delta t)^2 = \frac{1}{2}\, \frac{F}{m}\, (\Delta t)^2 = \frac{1}{2}\, q\, \frac{S_{ref}}{m}\, C_F\, (\Delta t)^2 \tag{1}$$

and for rotation:

$$\Omega = \frac{1}{2}\, \ddot{\Omega}(\Delta t)^2 = \frac{1}{2}\, \frac{M}{I}\, (\Delta t)^2 = \frac{1}{2}\, q\, \frac{S_{ref}\, l_{ref}}{I}\, C_M\, (\Delta t)^2 \tag{2}$$

It is assumed that the air loads are constant over the period Δt.

Because we are looking only for the influence coefficients that are added to the free stream coefficients, equations (1) and (2) are developed in vector form below to eliminate the latter.

If the trajectory segments are short enough, the distance traversed in translation, or the angular displacement experienced, is small enough so that one may assume the total air loads are constant during that time interval, and, correspondingly, act constantly over the distance traversed or over the angular change. Then, assuming the law of superposition applies, the free stream air loads and the influence field air loads are summed to give the total air loads. The air loads experienced by the store in moving along the free stream trajectory segment in figure 2 are given by:

$$\ddot{\vec{r}}' = q\, \frac{S_{ref}}{m}\, \vec{C_F} \tag{3}$$

The air loads experienced in moving along the local flow field trajectory segment in figure 2 are given by:

$$\ddot{\vec{r}} = q\, \frac{S_{ref}}{m}\, \left(\vec{C_F} + \Delta\vec{C_F}\right) \tag{4}$$

Integrating equations (3) and (4) respectively to obtain the translation distances:

$$\vec{r}' = \frac{1}{2}\, q\, \frac{S_{ref}}{m}\, \vec{C_F}\, (\Delta t)^2 \tag{5}$$

$$\vec{r} = \frac{1}{2}\, q\, \frac{S_{ref}}{m}\, \left(\vec{C_F} + \Delta\vec{C_F}\right) (\Delta t)^2 \tag{6}$$

The difference between the two trajectory end points is given by subtracting (5) from (6):

$$\vec{\Delta r} = \frac{1}{2}\, q\, \frac{S_{ref}}{m}\, \Delta\vec{C_F}\, (\Delta t)^2 \tag{7}$$

794

The same may be done with the small angular change from beginning to end of trajectory segment resulting in:

$$\overline{\Delta\Omega} = \frac{1}{2} \ \frac{q \ S_{ref} \ l_{ref}}{I} \ \overrightarrow{\Delta C_M} \ (\Delta t)^2 \tag{8}$$

It is assumed that the trajectory segment is short enough, or, the time of the segment is short enough so that the axis of rotation of the store remains approximately in the same direction. It is seen that the free stream coefficients drop out and only the incremental influence coefficient remains to cause the incremental position and angle. Ideally, the system becomes linear. Actually it is not completely linearized, even with a very short trajectory segment.

Equations (7) and (8) are solved for the estimated influence coefficients $\overrightarrow{\Delta C_F}$ and $\overrightarrow{\Delta C_M}$. They are assumed to act at a point midway between the beginning and end of the trajectory segment. $\overrightarrow{\Delta C_F}$ and $\overrightarrow{\Delta C_M}$ are transformed into influence vectors in the aircraft's coordinate system (which is why they are treated as vectors) and are located within the aircraft's coordinate system as shown in figure 3. In this manner, the local flow field influence of the parent aircraft is mapped out along the separation corridors as a result of flight-test separations. When a new separation is to be calculated, the influence coefficient vectors are interpolated as a function of position of the store and transformed into the store coordinate system after which their components are added to the total free stream aerodynamic coefficients.

This process requires a sufficient number of flight-test separation trajectories to bracket the expected trajectory of the store separation trajectory to be predicted. Various means of interpolation and extrapolation using polynomial curve fits of calculated influence coefficient data can be used for positions between locations of known coefficients. This may even apply where there are regions of flow discontinuity since a large store would normally straddle such discontinuities thus evening out their effects.

In developing a set of influence coefficients for the trajectory segment in figure 2, increasingly refined influence coefficients can be obtained by repeated calculations of the theoretical trajectory segment and comparison with the flight-test trajectory segment; each time the calculated influence coefficients obtained from the preceding comparison are used. With each pass the differences, $\overrightarrow{\Delta r}$ and $\overrightarrow{\Delta\Omega}$, should become less and less as the system converges. An alternate approach is to make two passes using equations (7) and (8). A numerical iteration scheme then takes over to correlate the rate of change in $\overrightarrow{\Delta C_F}$ and $\overrightarrow{\Delta C_M}$ to the rates of change in $\overrightarrow{\Delta r}$ and $\overrightarrow{\Delta\Omega}$ from pass to pass and thereby estimate succeeding influence coefficients. The Newton-Raphson technique of doing this is described in the section on computerization.

COMPUTERIZATION

The computer program developed thus far to estimate influence coefficients and to predict trajectories can function in two basic modes. It can generate a trajectory using influence field data, and this includes a free stream trajectory wherein the influence field is zero; and it can dissect a trajectory through a local flow field and estimate the static influence coefficients that must be acting along the trajectory. A number of flight-test separations thus allow mapping out the influence field volume through which the trajectories have passed.

NOTE: ONLY DRAG INFLUENCE COEFFICIENT VECTORS SHOWN.
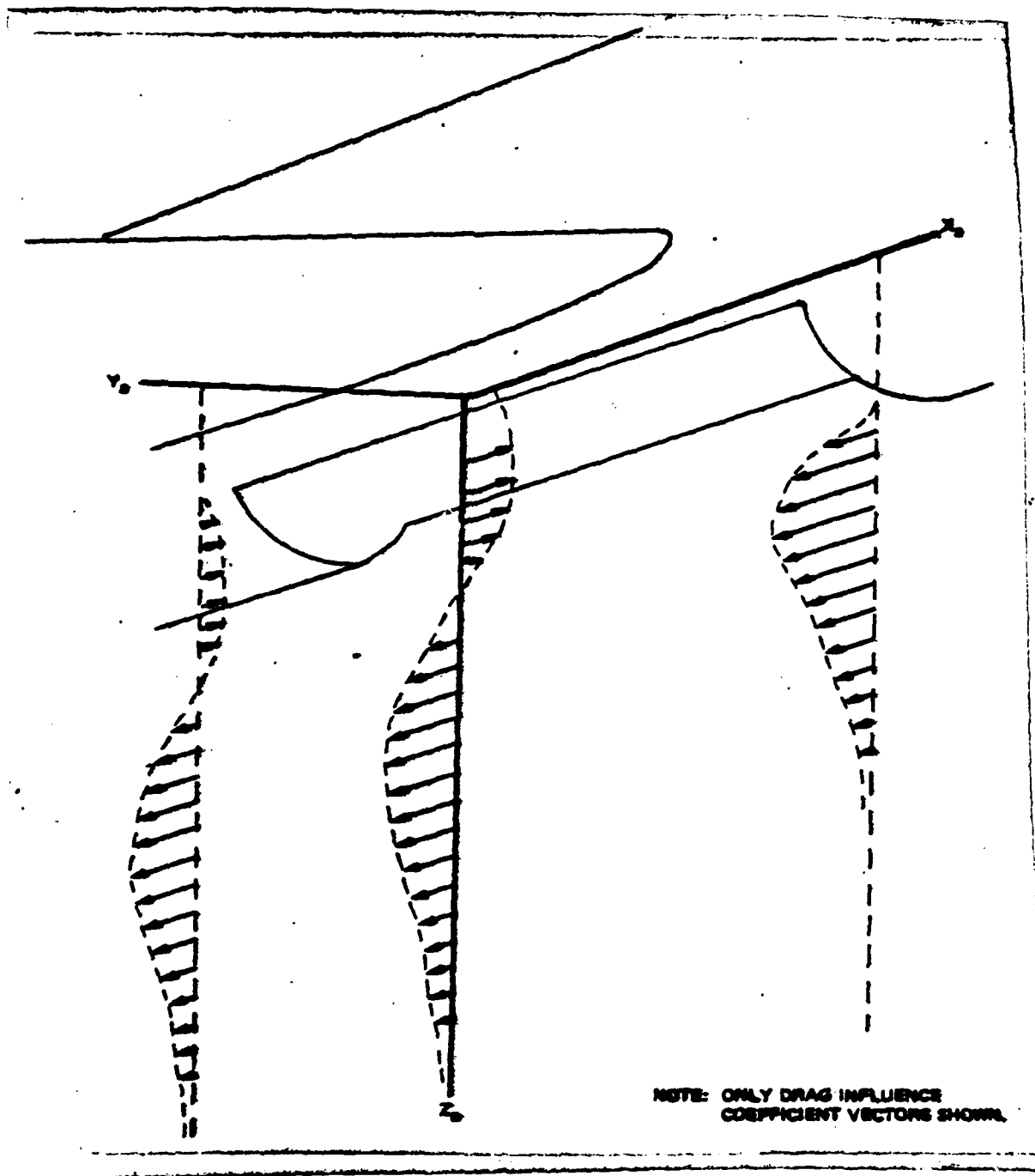
Figure 3. Location of Influence Coefficient Vector Components
in the Aircraft Coordinate System.

796

Figure 4 maps out the primary logical steps taken by the program in estimating the influence coefficients. It is necessary, of course, that the free stream aerodynamic characteristics of the store be as fully described as possible and that the real separation trajectory be described as accurately as possible. Any errors in these pieces of information will simply be reflected in the influence coefficients.

A "RAILROAD TRACK" TRAJECTORY

To evaluate the computer program for extracting influence coefficients, it was felt that an idealized trajectory should be given to the program to see if it could recreate that trajectory. The equations describing this trajectory, which will be called a "railroad track," are as follows:

$$x = -1.61 \, t^2$$

$$y = 8.05 \, t^2$$

$$z = 8.05 \, t^2 \tag{9}$$

$$\psi = 5.0 \, t$$

$$\theta = 5.0 \, t$$

$$\phi = -5.0 \, t$$

The above equations describe the position and attitude of the missile as seen from the aircraft, just as would data reduced from an onboard movie. The Euler angles, ψ, θ, and ϕ, are read in the yaw (ψ) - pitch (θ) - roll (ϕ) sequence to conform with the missile model mount gimbal hierarchy (yaw is outer-most, etc.) of the Photo Data Analysis System (PDAS) at Point Mugu.

Because of the suspected importance of the size of segment of separation trajectory analyzed in each step in the case where a missile moves rapidly relative to the aircraft, the two-trajectory segment durations of 0.05 second and 0.20 second were used. The resultant best estimated influence coefficients were stored as a function of vertical position, Z_a^m, only. In general, it was felt that the smaller the trajectory segment, the more accurately the influence coefficients would be determined until computer round-off errors begin to appear.

Results of the "Railroad Track" Trajectory Study

Figure 5 shows the x and y translation and the yaw (ψ), pitch (θ), and roll (ϕ) as a function of the vertical translation, z. This is because the calculated influence coefficients are stored as a function of z only. The calculated influence coefficients are shown with their corresponding translation or rotation for the two-trajectory segment durations studied — 0.05 second and 0.20 second.

Significant differences will be noticed between translational influence coefficients for the different segment durations while there is little difference for the rotational influence coefficients. It will be noticed that the free stream translations are considerably different from those imposed by the "railroad track" separation trajectory while the free stream rotations are quite similar to the "railroad" rotations, with the exception of roll.

B

READ SEGMENT OF EXPERIMENTAL TRAJECTORY
OF DURATION ΔL

INITIALIZE FREE STREAM THEORETICAL MODEL WITH INITIAL
CONDITIONS IDENTICAL TO THOSE OF EXPERIMENTAL TRAJECTORY
AND COMPUTE A FREE STREAM TRAJECTORY OF DURATION ΔL

COMPARE THEORETICAL AND EXPERIMENTAL TRAJECTORY SEGMENT
END POINTS IN 3-AXIS POSITION AND ATTITUDE DIFFERENCES
(Δx, Δy, Δz, Δφ, Δθ, Δψ).

TEMPORARILY RECORD DIFFERENCES IN FILE D-I.

USE DIFFERENCES TO COMPUTE FIRST ESTIMATED INFLUENCE
COEFFICIENTS USING EQUATIONS (7) AND (8).

TEMPORARILY RECORD COEFFICIENTS IN FILE C-I.

RECOMPUTE THEORETICAL TRAJECTORY WITH FIRST ESTIMATED
INFLUENCE COEFFICIENTS ADDED TO TOTAL FREE STREAM
COEFFICIENTS.

COMPARE NEW THEORETICAL AND EXPERIMENTAL TRAJECTORY
SEGMENT END POINTS IN 3-AXIS POSITION AND ATTITUDE
DIFFERENCES.

TEMPORARILY RECORD DIFFERENCES IN FILE D-II.

USE NEW DIFFERENCES TO COMPUTE SECOND ESTIMATED INFLUENCE
COEFFICIENTS USING EQUATIONS (7) AND (8).

TEMPORARILY RECORD COEFFICIENTS IN FILE C-II.

USE THE NEWTON-RAPHSON ITERATION TECHNIQUE AND DATA
IN FILES C AND D TO REFINE SUCCESSIVE INFLUENCE COEF-
FICIENTS.

COMPUTE THEORETICAL TRAJECTORY WITH REFINED
INFLUENCE COEFFICIENTS.

ALL THE
3-AXIS DIFFERENCES BETWEEN
EXP. AND THEO. TRAJECTORY SEGMENT
END POINTS ARE LESS THAN PRESET
ERROR MAGNITUDES?
NO   YES

PERMANENTLY STORE FINAL REFINED INFLUENCE COEFFICIENTS
IN FILE P ALONG WITH CORRESPONDING MID-SEGMENT POSITION
IN AIRCRAFT COORDINATE SYSTEM

HAVE ALL
THE EXPERIMENTAL
TRAJECTORY SEGMENTS
BEEN ANALYZED?
NO   YES

RERUN THE ENTIRE THEORETICAL TRAJECTORY USING THE IN-
FLUENCE COEFFICIENT VALUES AND POSITIONS FROM FILE P.

PLOT THEORETICAL TRAJECTORY WITH EXPERIMENTAL TRAJECTORY
FOR COMPARISON.

PLOT INFLUENCE COEFFICIENTS AGAINST POSITION IN
AIRCRAFT COORDINATE SYSTEM.

*Figure 4. Primary Logical Steps in Analyzing a Separation
Trajectory for Influence Coefficients.*

Figure 5(a). "Railroad Track" Trajectory Results.

Figure 5(b). "Railroad Track" Trajectory Results.

Figures 5(a) and 5(b) show the resultant recreated trajectory values compared with the original "railroad track" trajectory for both the 0.05-second and 0.20-second trajectory segment lengths. It is curious to note that both result in trajectories very close to the original, even though there are significant differences in the computed influence.coefficients. Table 1 shows estimated influence coefficients and total coefficients at various trajectory points for the short (0.05-second) and the long (0.20-second) segment approach. The total coefficients include missile axis components of the influence coefficients. The latter are in the aircraft axis system; however, the missile angles at the end of the trajectory have changed only a small amount from the stow position so that the arithmetic differences between the total and the influence coefficients are the free stream coefficients. The negative X-axis and negative Z-axis coefficients indicate strong drag and lift influence forces imposed by the "railroad" trajectory. The ability of the simulation to recreate the separation trajectory using X-axis influence coefficients for either 0.05 second or 0.20 second despite their differences indicates an apparent insensitivity of the simulation to that component of influence air loads.

Further studies with a "railroad track" trajectory will shed light on some of the questions raised above. These studies would include (1) a reduction in trajectory segment times and the noting of the probable leveling-off of calculated influence coefficients; and (2) addition of a constant factor to one influence coefficient at a time to determine system sensitivity to particular coefficients, while noting the number of steps required to achieve convergence. The calculated influence coefficients would then be stored as functions of X, Y, and Z positions relative to the aircraft. Also, more violent "railroad track" trajectories can be tried along selective axes to determine an envelope outside of which the program will fail to converge on estimated influence coefficients.

AN ARTIFICIAL INFLUENCE FIELD

The next series of runs to evaluate the program involved creating a separation trajectory using a typical missile with known free stream characteristics and very idealized local flow field coefficients which varied linearly from the stow position to zero at a distance of 15 feet below the aircraft. Below are the artificial influence coefficients used:

$$\Delta C_x = 0.1$$

$$\Delta C_y = 0.2$$

$$\Delta C_z = 0.3$$

$$\Delta C_l = 0.01$$

$$\Delta C_m = 0.02$$

$$\Delta C_n = 0.05$$

At stow position. Linear decay to 0.0 for all influence coefficients at $Z_z^m = 15.0$ feet below aircraft.

The resultant trajectory is then fed back into the program which is set to recreate the influence coefficients as well as the original trajectory. Because of the inconvenience in obtaining accurate influence field data from wind tunnels (the only way in which actual fields can be mapped to date), it is felt that the artificial influence field study performed here is the best means of evaluating the capabilities of the computer program. These efforts have begun at PACMISTESTCEN and the results are given in the following section.

Table 1. Coefficients Generated by the "Railroad Track" Trajectory

Time (Second)	Trajectory Segment Duration (Second)	Coefficients					
		X-axis Infl. Total	Y-axis Infl. Total	Z-axis Infl. Total	Yaw Infl. Total	Pitch Infl. Total	Roll Infl. Total
0.1	0.05	-1.228	1.822	-1.725	-0.028	0.015	-0.004
		-1.047	1.779	-1.817	0.014	0.007	0.001
	0.20	-0.190	1.796	-1.691	-0.018	0.020	-0.004
		-0.343	1.779	-1.785	0.013	0.007	0.001
0.3	0.05	-3.818	2.071	-1.794	-0.116	-0.010	-0.007
		-3.719	1.869	-1.882	0.011	0.004	0.000
	0.20	-0.765	1.913	-1.600	-0.104	-0.014	-0.007
		-0.974	1.827	-1.779	0.014	0.006	0.000
0.5	0.05	-6.248	2.462	-2.024	-0.164	-0.002	-0.003
		-6.248	2.032	-2.042	0.007	-0.004	-0.000
	0.20	-1.301	2.038	-1.545	-0.158	-0.004	-0.003
		-1.568	1.900	-1.798	0.007	-0.003	-0.001
0.7	0.05	-8.495	3.002	-2.411	-0.212	0.024	0.002
		-8.628	2.262	-2.321	0.008	-0.004	-0.000
	0.20	-1.795	2.196	-1.525	-0.206	0.021	0.001
		-2.126	1.983	-1.840	0.008	-0.004	-0.000

Notes:

1. The influence coefficients are in the aircraft coordinate system and oriented with it.

2. The influence coefficients given are the average of values calculated before and after the trajectory times given.

3. The total coefficients are in the missile body axis system and include the influence coefficients rotated into the missile body axis system.

4. "Trajectory segment duration" is the size of segment, in seconds, into which input trajectory is broken down.

Results of the Artificial Influence Field Study

Figures 6(a) and 6(b) show the results of the artificial influence field study. As with the "railroad track" study, the recreation of the body rotations is considerably more accurate than that of the translations. Also, the corresponding influence moment coefficients are recreated far more accurately than the influence force coefficients. The artificial influence coefficient tables were complete down to a distance of 15 feet below the aircraft and the resultant trajectory was run out for 0.5 second. However, large angular rates, particularly in roll, were developing so that the program would not converge when attempting to recreate the influence coefficients and the trajectory after 0.5 second. Thus, the recreated coefficients and trajectory are only given for the first few feet of drop.

FLIGHT-TEST SEPARATION DATA

Using the same typical large store used in the preceding "railroad track" and artificial influence field studies, two real flight-test separation trajectories are shown for a typical bomber bay moving in level flight at Mach 0.6 at 10,000 feet. Figures 7(a) and 7(b) show the match between photo-instrumented trajectory and the computer-recreated trajectory for the first separation. Figures 8(a) and 8(b) show the same for the second separation. The actual trajectories were reduced from on-board movie cameras that had been surveyed in. Reduction was done by the PACMISTESTCEN Photo-Data Analysis System (PDAS) and the resultant six-degree-of-freedom kinematic data represented by polynomial curve fits which both tended to smooth the data and allow for compact storage of the trajectory data in the coefficients estimation program. To determine first- and second-time derivative data, derivatives were simply taken of the polynomials representing the position and attitude of the store with time. The origin of the aircraft coordinate system is at the stow position of the store. Because the cameras could not see the stores in their stow positions, the influence coefficients start approximately 1 foot down. The recreated trajectory also starts at the same point and uses the kinematics of the store at that point as an initial condition.

Figures 7(a) and 7(b) also show the corresponding estimated influence coefficients for the first separation and figures 8(a) and 8(b) show them for the second separation.

CONCLUDING REMARKS

The current stage of development of the computer program has demonstrated its versatility in creating, analyzing, and recreating separation trajectories. While improvement is desired in influence coefficients, the accuracy with which trajectories are recreated has been good. It is felt that the method of comparing the experimental trajectory with that of a theoretical model a small segment at a time is basically sound and warrants further development. Furthur development and testing of the program is needed to allow convergence in more violent cases and to increase accuracy in estimating influence coefficients. Also, it is likely that the technique can be adapted to analyzing other forms of experimental data besides optical-kinematic data. The following discussions cover some of the sources of error and also planned future modifications and applications of the technique.

SOURCES OF ERROR

The work to date has assumed perfect trajectory data. In reality, it is both distorted and noisy. It is presently presented to the computer program in the form of a polynomial curve fit. This removes the noise but can introduce some biases at the beginning and end points. The program doesn't know this and simply creates influence coefficients to explain the fallacious trajectory; the influences of data
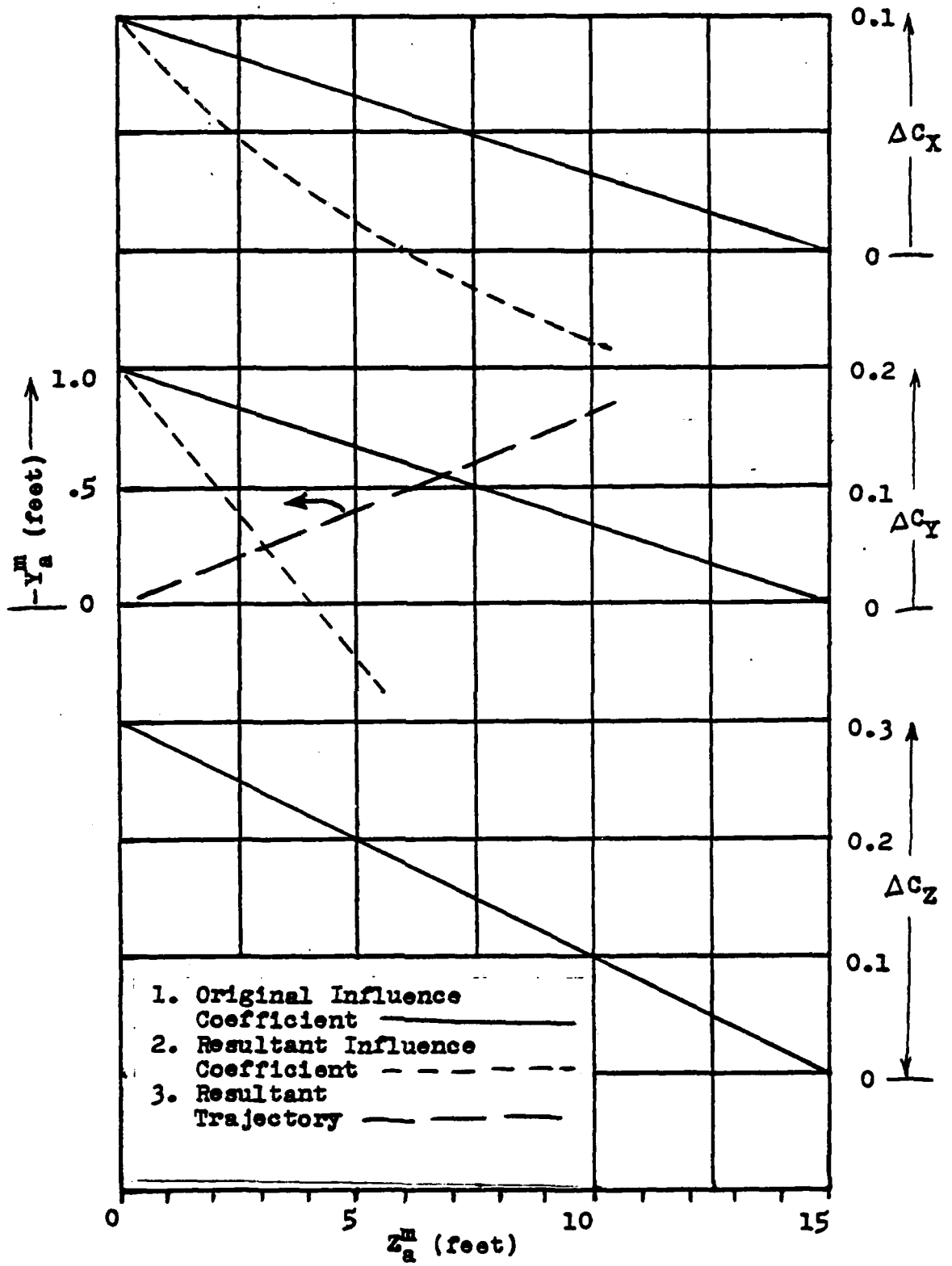
Figure 6(a). Artificial Influence Field Trajectory Results.
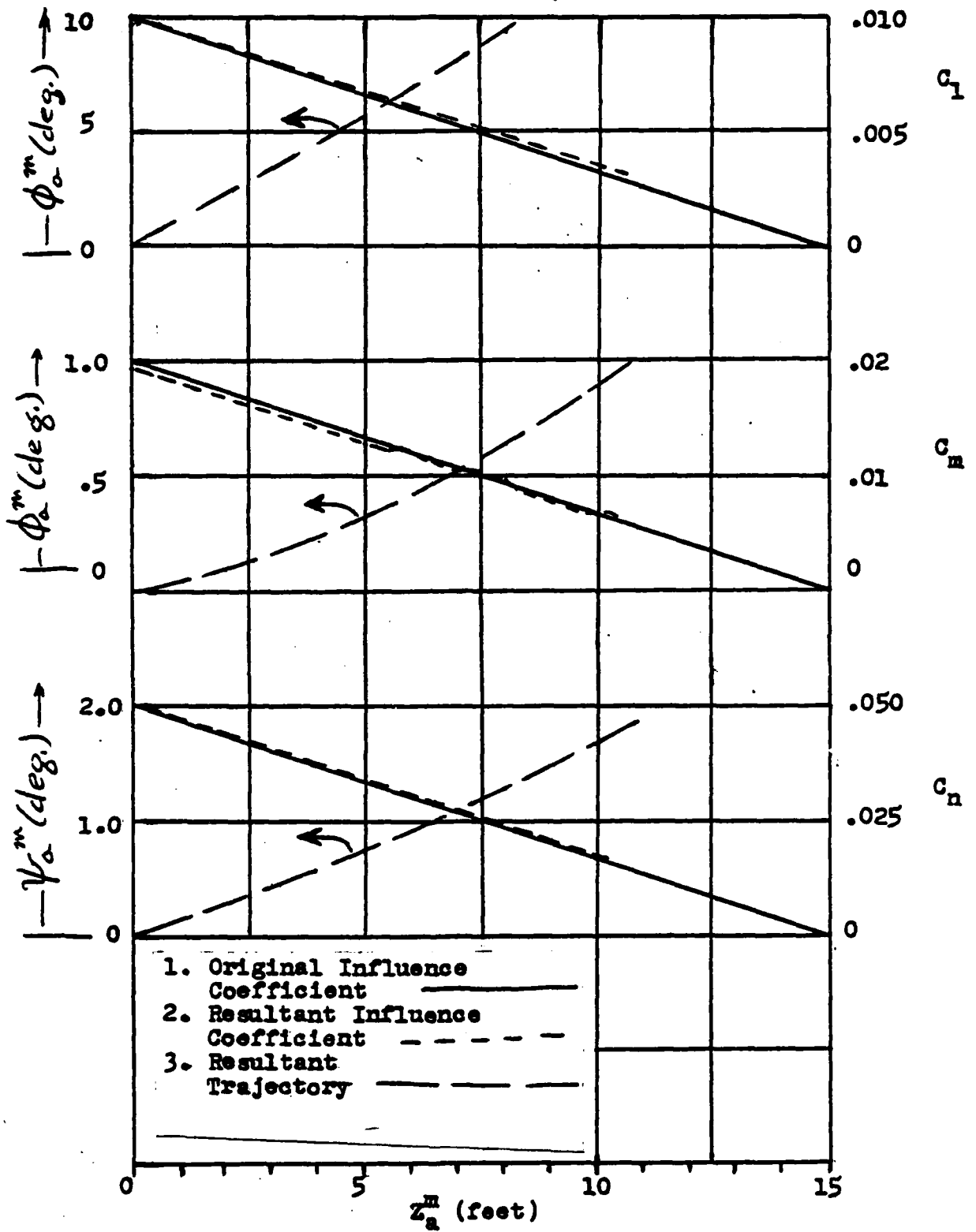
Figure 6(b). Artificial Influence Field Trajectory Results.
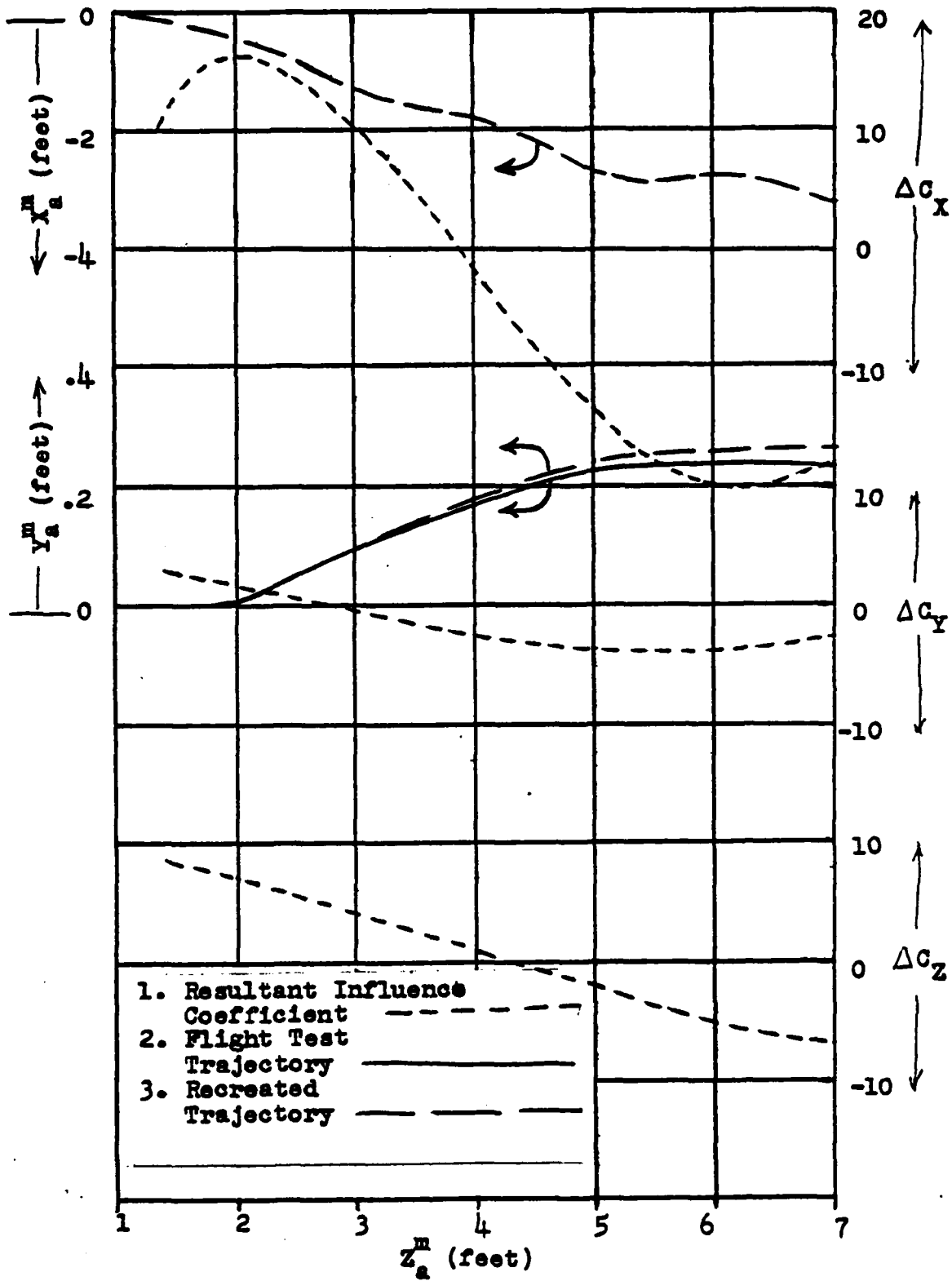
Figure 7(a). Results of Flight Test Separation No. 1.
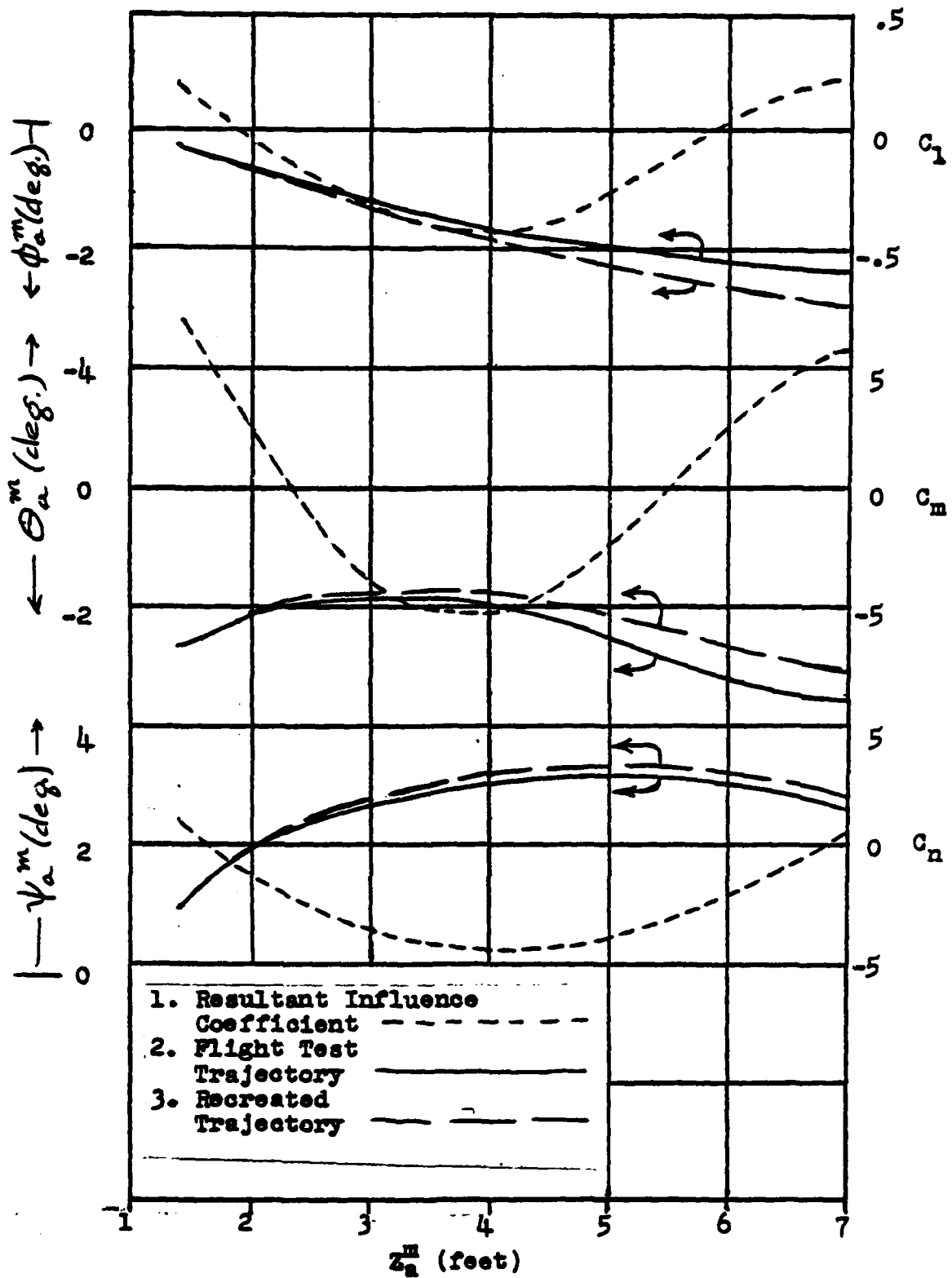
Figure 7(b). Results of Flight Test Separation No. 1.
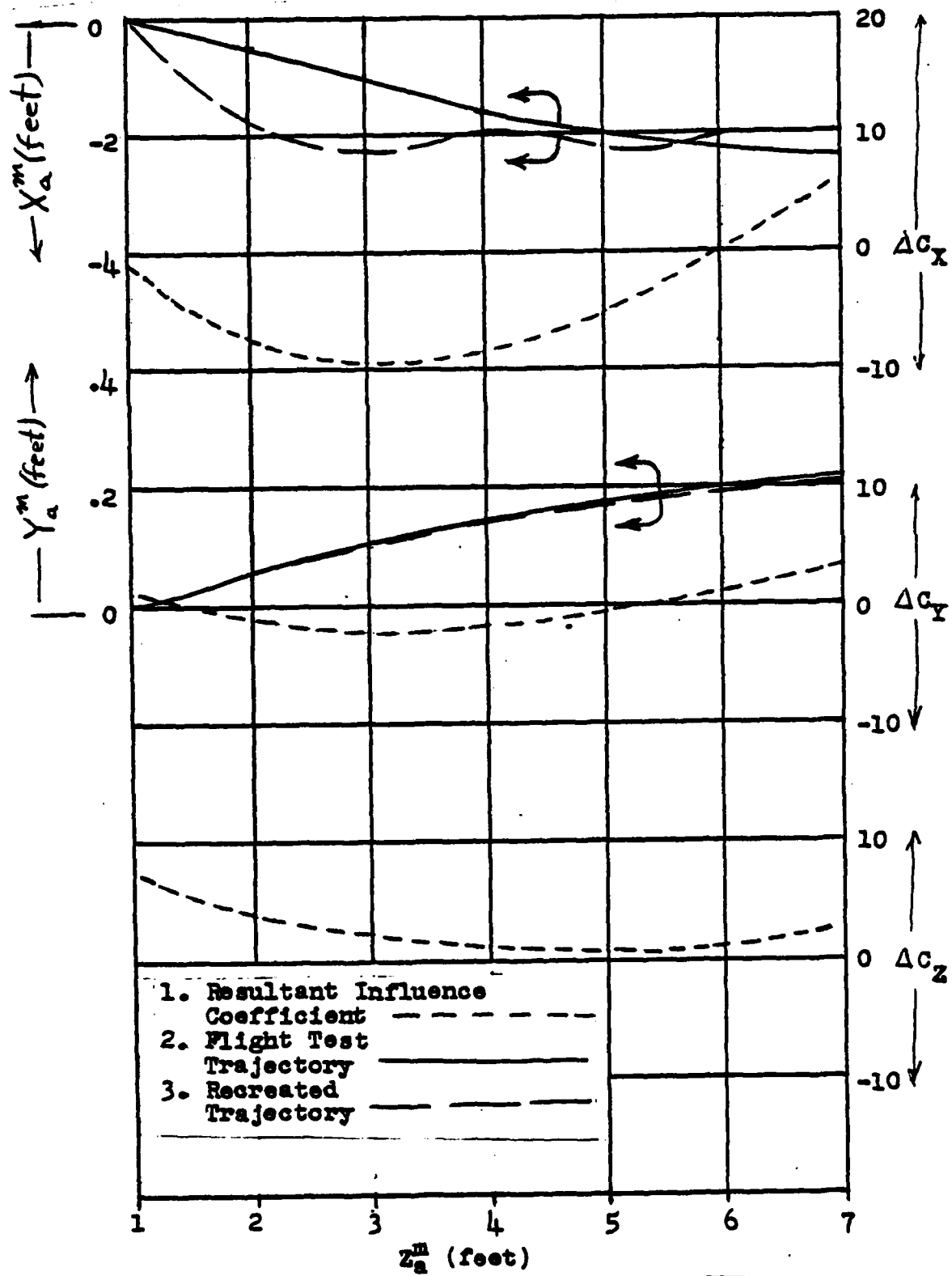
Figure 8(a). Results of Flight Test Separation No. 2.
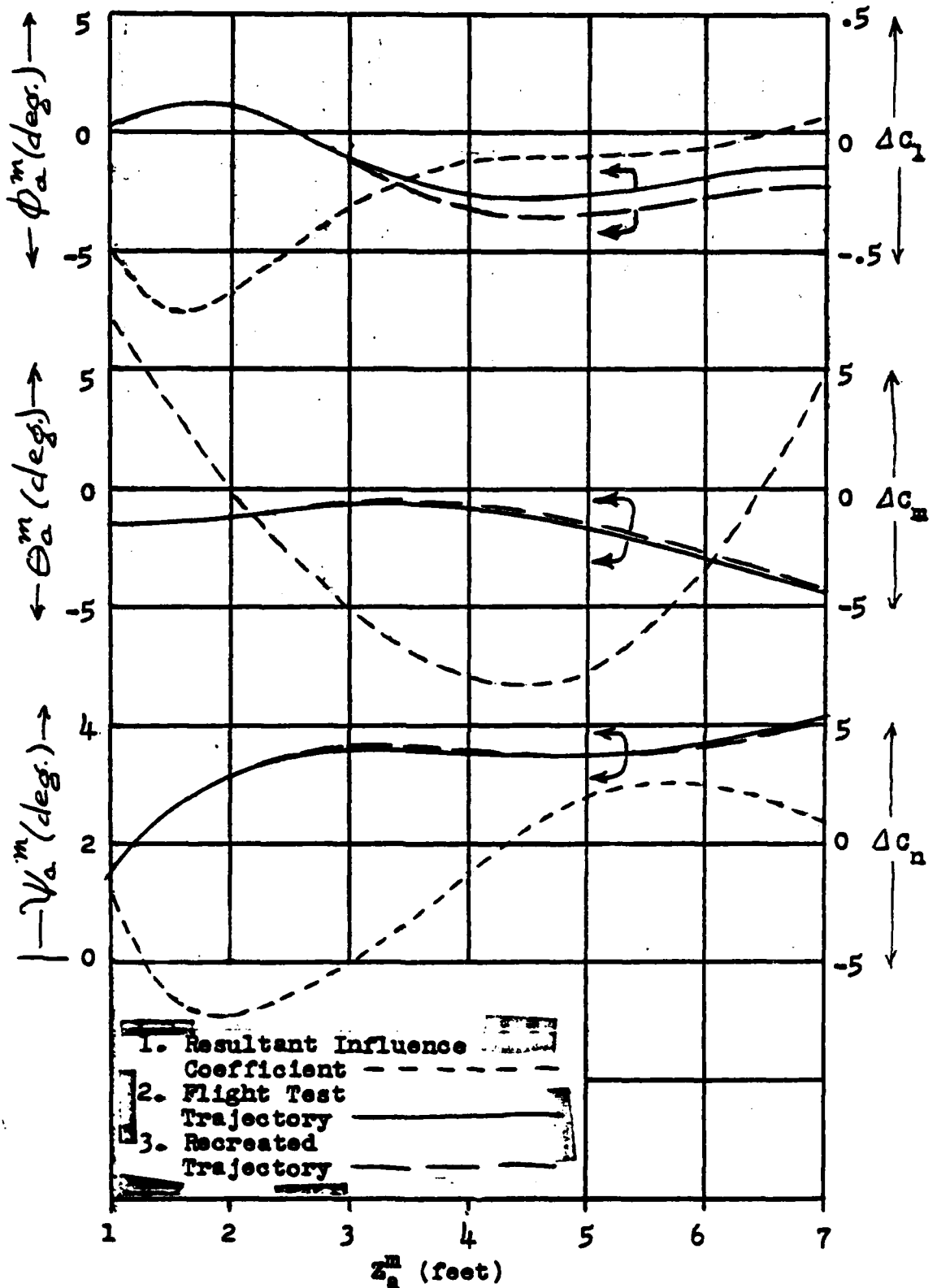
Figure 8(b). Results of Flight Test Separation No. 2.

distortion and bias are accounted for. This fact might allow an adaptation of the program to estimate onboard camera positional errors or unknown lens distortions if the influence field is already thoroughly known.

Slight differences between the initialization of the theoretical trajectory and the starting point of the corresponding experimental trajectory segment will lead to increasingly large errors as the segment duration decreases. As seen in figure 2, a positional or angular error between the starting points of the two segments will reflect itself in equations (7) and (8) as a proportionate error in estimated influence coefficients.

Determination of the six static influence coefficients assumes no coupling between missile body axes. In cases of rapid rotation there will be dynamic cross coupling which will involve more complex equations than (7) and (8) in estimating coefficients. In addition, there will be aerodynamic damping and cross coupling terms. It is suspected that when a store is immersed in a strong vortex, as when in or near an open cavity such as a bomb bay, there is likely to be an angular rate damping influence coefficient. This would be in addition to any free stream angular rate damping and would be a function of both position relative to the launch aircraft, and, hence, the vortex, and the body angular rate about an axis parallel to the vortex filament. Because of cross coupling, reducing the segment duration so that translation and rotation changes become vanishingly small would not necessarily allow one to use the simple expressions (7) and (8) where rapid rotation is involved. To do so would probably result in a set of influence coefficients that would allow convergence and approximate recreation of the experimental trajectory and yet not be the correct set of influence coefficients.

In the work so far the influence coefficients have been stored in the aircraft coordinate system only as a function of vertical distance, Z_a^m. This was done to simplify the program during the development phase. While this is an obvious oversimplification when a store experiences much translation in X_a^m and Y_a^m from its stow position, surprisingly good results have been obtained in simulating the trajectories. It would be interesting to examine the sensitivity of results obtainable with this type of simplification.

FUTURE MODIFICATIONS AND APPLICATIONS

The immediate future will see an examination of the various error-causing mechanisms and the sensitivities of results to these. One object of this study will be to establish envelopes of acceptable utility in analyzing progressively more active separations.

Instead of equations (7) and (8), more sophisticated physical models involving the rigid body equations of motion, angular rate damping, and aerodynamic cross coupling will be employed in estimating influence coefficients. Also, theory versus experiment comparison criteria involving velocity or acceleration differences, rather than position, as done with equations (7) and (8), will be tried. Other criteria involving momentum, work, and Hamilton's Principle will also be examined.

A number of future applications of the program may be evaluated. These include using inertial data rather than photo-kinematic separation data. The experimental trajectory could be defined by telemetered accelerometer and rate gyro information from both the store and the parent aircraft, particularly if the latter responds strongly to releasing a large store. Other events involving spacially fixed influence forces and moments can be evaluated. These include vehicle water entry and departure and the motion of surface vehicles over irregular terrain of varying consistency.

REFERENCES

1. Chapman, Gary T. and Donn B. Kirk. "A Method for Extracting Aerodynamic Coefficients From Free-Flight Data," published in AIAA Journal, Vol. 8, No. 4, Apr 1970, pp. 753-758.

2. Bullick, T. E., M. H. Clarkson, and D. C. Daniel. Preliminary Report on Extracting Aerodynamic Coefficients From Dynamic Data. (University of Flordia). Air Force Armament Laboratory, Mar 1972.

3. Cooper, G. F. and R. W. Kingery. "Naval Missile Center Photo Data Analysis of Store-Separation Films," published in Aircraft/Stores Compatibility Proceedings, Vol. 2, Sep 1973, pp. 51-106.

4. Sekellick, Michael A. "Prediction of Store Launch Characteristics Through Statistical Methods," presented at 8th Navy Symposium on Aeroballistics, May 1969, David Taylor Naval Ship Research and Development Center.

5. NASA. "Parameter Estimation Techniques and Applications in Aircraft Flight Testing," presented at Symposium held at Flight Research Center, Edwards AFB, Calif., Apr 1973. Also published as NASA TN D-7647, Apr 1974.

AUTOBIOGRAPHY

GUY F. COOPER

Presently employed as a systems engineer at the Pacific Missile Test
Center. Work includes coordination of development of a ground control
station for a drone version of the T-38 airplane, evaluation of aircraft
modifications for range relay purposes, and studies of external store
captive loads and launch dynamics. Prior work includes: simulating
missile structural dynamics and preliminary design studies in heat
transfer at General Dynamics, evaluation of advanced propulsion concepts
at Ryan Aircraft, and underwater sound instrumentation at Scripps Institu-
tion of Oceanography. Education includes a Bachelor of Electrical Engineer-
ing Degree earned from Union College and graduate work in aerospace engineer-
ing at the University of Arizona. Presently Chairman of the Navy Aero-
ballistics Committee (NAC) Panel on Launch Dynamics.

JON GNAGY

Prior to employment at Point Mugu, Mr. Gnagy received a B.S. degree in
Aeronautical Engineering from the University of Kansas in 1959. He is
presently a member of the Simulation and Analysis Branch, Weapons Systems
Division of the Systems Technology Dept. at Pacific Missile Test Center.
His experience in the field of aeronautical engineering includes extensive
work in internal aerodynamics, aerodynamic heating prediction and analysis,
and missile trajectory simulation. He is a past member of the Navy Aero-
ballistics Committee (NAC) Panel on Heat Transfer, and presently a member of
the NAC Launch Dynamics Panel.

A COMPARISON OF FLIGHT TEST RESULTS AND 6-DOF CALCULATIONS

USING THE INCREMENTAL COEFFICIENT METHOD FOR STORE

RELEASES FROM THE F-111 WEAPONS BAY

(Article Unclassified)

by

Roger N. Everett*

Sandia Laboratories

Livermore, California

ABSTRACT. (U) Wind tunnel incremental coefficient data has been used to
calculate the six degree of freedom motion of a 2400 pound store being
released from the weapons bay of the F-111 aircraft. Subsequent flight test
results have been compared with these calculations to show an excellent
agreement over an airspeed range of 300 to 500 KCAS. Additional flights will
provide comparisons up to approximately 650 KCAS.

The comparisons to date indicate that the simplified grid simulation method
gives a very reasonable prediction of the motion for weapon bay releases of
low static margin stores. Of special interest is the method for obtaining the
incremental aerodynamic coefficients inside the weapons bay which is detailed
herein.

* Member of the Technical Staff, System Development Department

LIST OF FIGURES AND TABLES

LIST OF SYMBOLS

C_A = Axial force coefficient, positive rearward

C_l = Rolling moment coefficient, positive clockwise when viewed from rear

C_m = Pitching moment coefficient, positive when trying to move store nose upward

C_n = Yawing moment coefficient, positive when trying to move store nose to right

C_N = Normal force coefficient, positive when trying to move store upward

C_Y = Side force coefficient, postive when trying to move store to right

d = Reference length, maximum diameter of store = 1.5 ft

S = Reference area, maximum cross sectional area of store body = 1.7671 ft^2

Z = Distance the store has moved vertically from its original position below the aircraft, positive downward

α = Store angle of attack in pitch plane, positive nose up

θ = Store attitude angle in pitch plane, relative to initial position, positive nose up

ψ = Store attitude angle in yaw plane, relative to initial position, positive nose right

Prefixes

Δ = Contribution to total coefficient due to aircraft flow field

Postfixes

(Z) = Denotes function of Z only

Subscript

FS = Free-stream values at large distances from the aircraft

815

A COMPARISON OF FLIGHT TEST RESULTS AND 6-DOF CALCULATIONS

USING THE INCREMENTAL COEFFICIENT METHOD FOR STORE

RELEASES FROM THE F-111 WEAPONS BAY

INTRODUCTION

A 2400 pound store being developed by Sandia Laboratory is presently undergoing flight drop tests from a number of Air Force and Navy aircraft. This store is to be capable of external carriage and release from the A-4, A-6, A-7, F-4, F-111, and FB-111 aircraft and internal carriage and release from the B-52, F-111 and FB-111 aircraft. Due to a combination of aircraft geometry and performance capability, the most severe release environment is expected to be that of the F-111 and FB-111. A release condition of Mach 1.2 at sea level from both the weapons bay and inboard pylon at full wing sweep is desired. For these reasons Sandia (with some USAF support) has conducted a number of wind tunnel tests[1-5] on 5% scale models to investigate the carriage and release of this store from the F-111. The prime purpose for this investigation has been to secure USAF approval for the development drop tests.

External releases at wing sweeps of 50, 60, and 72.5 degrees were investigated using the Captive Trajectory Simulation[6] (CTS) method for pivot pylon positions. Since this method was not adaptable to the weapons bay positions, it was decided to use a simplified grid simulation method. This decision was made because of the demonstrated success [7-9] of this approach and to preclude the large number of wind tunnel runs required for a full grid mapping approach.

This paper then deals with a simplified grid simulation method for determining the necessary incremental aerodynamic coefficients both inside and below the weapons bay. A six degree of freedom trajectory simulation program which utilized the incremental aerodynamic coefficients, free stream aerodynamic coefficients and calculated rack ejection rates was employed to calculate the separation trajectory. Data from subsequent flight tests provides a means of verifying the procedure.

Store Configuration

This 2400 pound store is 145 inches long and has a maximum diameter of 18 inches. A requirement for high density internal carriage imposed a very small fin geometry. Tee fins were utilized to meet this geometric constraint and still provide the maximum static margin. With a center of gravity at 38 percent of body length the static margin varies from 5 to 10 percent of length. High aspect ratio canted flip fins are deployed from the tee fins shortly after release. This improves the static margin to well over 20 percent which is adequate for good dispersion characteristics in the high altitude free fall mode. The axial and transverse moments of inertia are approximately 25.5 and 660 slug-ft^2 respectively.

816

ANALYTICAL TECHNIQUE

Simplified Grid Simulation Method

The grid simulation method [10] uses a computer to generate store separation trajectories using a matrix of incremental force and moment coefficients which are combined with the free-stream force and moment coefficients for the store. Calculated rack ejection rates are used for initial conditions. Unfortunately, a large number of wind-tunnel runs are usually required to measure these interference coefficients at different pitch and yaw angles at many points in the three-dimensional space below the aircraft carriage position.

References 8 and 9 have shown how a simplified grid method could be used for three-degree-of-freedom store separation trajectories of stores released from centerline aircraft carriage positions when the center of gravity motion of the separated store is close to that of the traverse used to measure the incremental coefficients. The simplified grid method uses interference force and moment coefficients which, for each flight condition and store carriage position, are functions only of the displacement along the traverse below the carriage position. This simplified grid method has been extended[7] to include the yaw plane and implemented using the SIXDOF trajectory simulation computer program[11]. This computer program simulates the complete six-degree-of-freedom trajectory (from release to impact) for stores separated from any aircraft station.

Wind Tunnel Tests

Wind tunnel tests to obtain the incremental aerodynamic coefficients were conducted in the Vought 4x4 foot High Speed Wind Tunnel. The size of the tunnel dictated a 5 percent model scale. An existing Sandia F-111 airplane model was modified to include bay doors and the proper bay geometry along with provisions to internally carry an instrumented store model. The airplane model used had the large inlet ducts representative of the D, E, or F model F-111. Although the duct geometry would make some difference in pylon drops it should not have much if any influence on the bay flow field data. The bay configuration in the model lacked at least one feature known to be in the FB-111 weapons bay. As a result data obtained on this test may be milder than if the FB-111 weapons bay configuration had been used. All data was obtained for the store in the left bay position. A simple sign reversal on the yaw plane data is all that is required in order to use the data for a release from the right side.

The incremental coefficients were obtained using two different techniques. For positions in and near the carriage position, the store was mounted on a 5-component balance attached to the ceiling of the weapons bay. Streamlined pylon spacers were used to locate the store in positions representing the carriage position plus four subsequent positions with a vertical increment of 10 inches full scale. Figure 1 shows the details of the location of the unit in the bay carriage position. Figure 2 is a sketch that shows the store in each of the five positions. Figure 3 is a photograph showing the store in the 40 inch (lowest) position. Note that the store is carried with a nose down altitude of 2.74 degrees and an inboard yaw of .73 degrees.
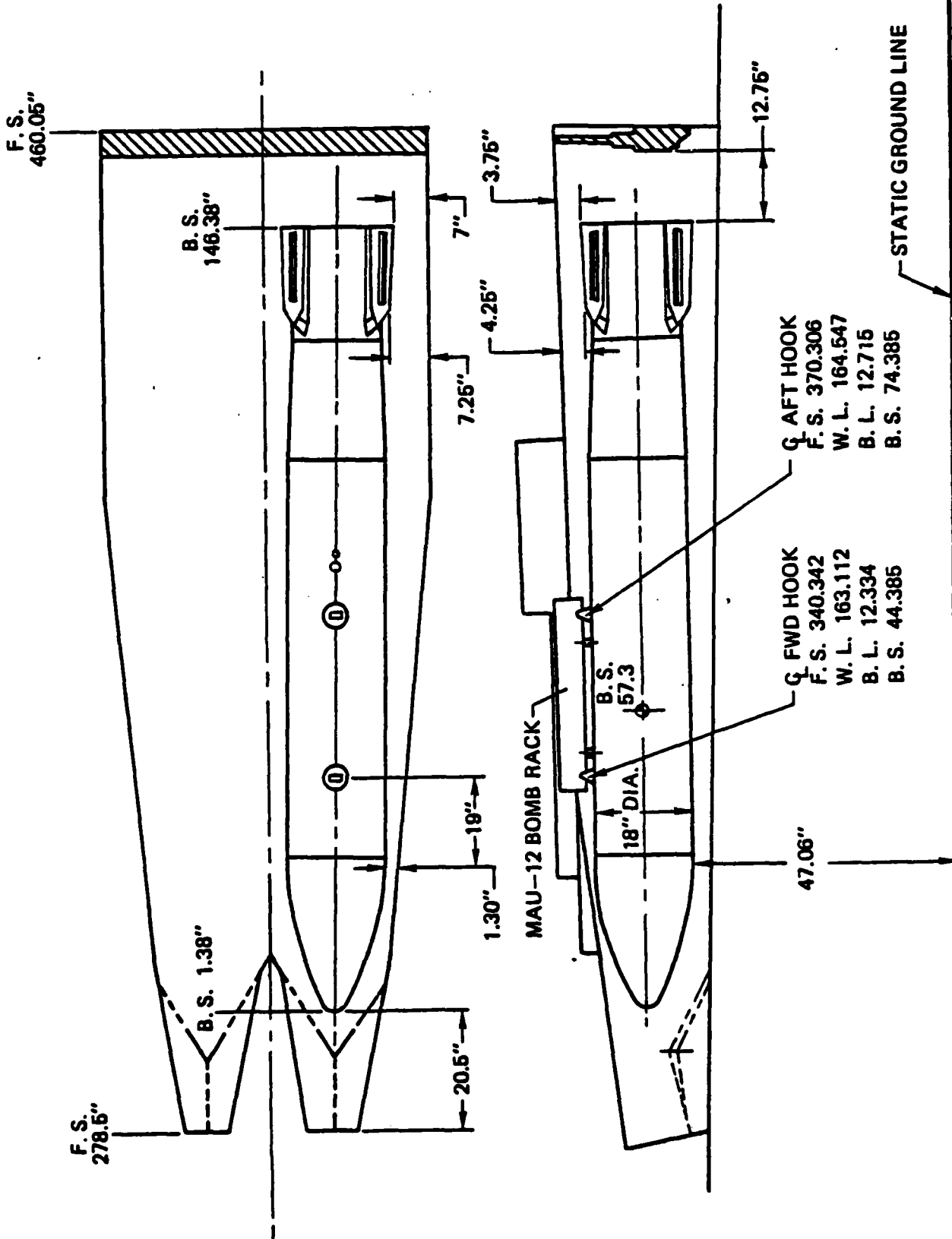
FIGURE 1 — INSTALLATION DETAILS IN F-111 WEAPONS BAY

F. S. 460.05"

B. S. 146.38"

12.76"

3.75"

7"

4.25"

7.26"

STATIC GROUND LINE

Ç AFT HOOK
F. S. 370.306
W. L. 164.547
B. L. 12.715
B. S. 74.385

Ç FWD HOOK
F. S. 340.342
W. L. 163.112
B. L. 12.334
B. S. 44.385

B. S. 57.3

MAU–12 BOMB RACK

18" DIA.

47.06"

19"

1.30"

B. S. 1.38"

20.5"

F. S. 278.5"

818

MAU–12 B/A OR
MAU–12 C/A HOOK POINTS

W. L. 171.173

F. S. 460.06

F. S. 274.87

W. L. 155.10

W. L. 139.10

W. L. 133.90

F. S. 278.50

0
10
20
30
40

DISTANCE
BELOW
CARRIAGE
POSITION
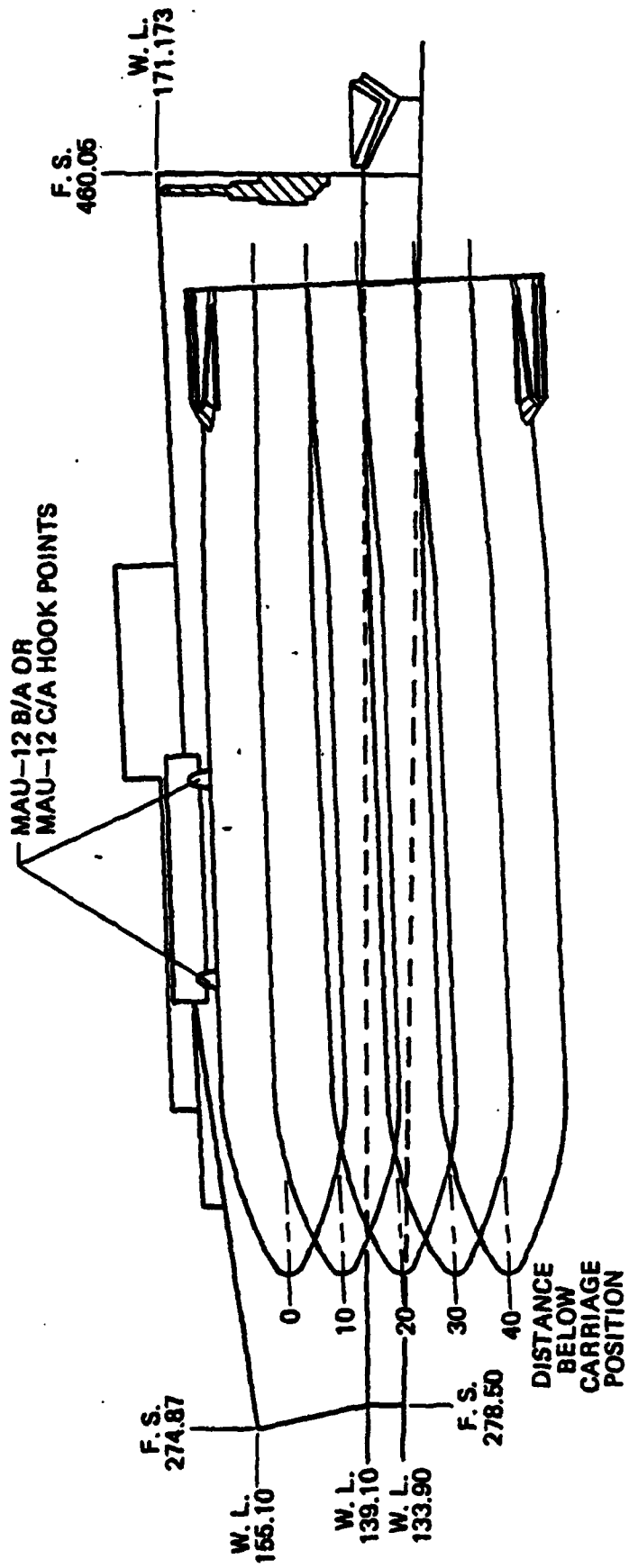
F-111 & FB-111 WEAPONS BAY
SIDE VIEW   1/16 SCALE

FIGURE 2 – SKETCH SHOWING FIVE IN-THE-BAY LOCATIONS FOR OBTAINING INCREMENTAL DATA

FIGURE 3 - F-111 AIRCRAFT MODEL WITH INTERNALLY CARRIED STORE MODEL IN THE 40-INCH POSITION

The airplane model (with store inside) was pitched through an angle of attack range of -10 to +18 degrees with the store in each of five positions at Mach numbers of .8, .95, 1.05, 1.2, 1.5 and 1.8. A five component internal strain gage balance recorded five aerodynamic forces and moments (axial force was not measured). A sample of the recorded data (C_m vs α at Mach .8) is shown in Figure 4. Only the coefficient value with the airplane waterline at α = 2.74 degrees (store α = 0 degrees) was of interest from this phase of the testing.

The same store model was then used with a six component internal strain gage balance on the CTS rig to determine the incremental coefficients below the weapons bay where the other method left off. With the store directly below its carriage position (the store is carried 12.5 inches outboard of the aircraft centerline) vertical traverses were made at angles of attack of +10, 0, and -10 degrees. Sufficient overlap between the two methods occurred so that a match of data from the two techniques could be determined.

Figure 5 presents a sample of the data obtained from these vertical transverses (C_m vs Z at Mach .8). Data from the three vertical transverses at each Mach number were graphically averaged and data points obtained from the five positions inside the bay were added to define the incremental coefficient starting at Z=0. This complete curve which was a function of distance below the carriage position (Z) was used in the six degree of freedom (DOF) trajectory analysis. Although only the pitching moment data has been presented, the same technique was used for the other aerodynamic coefficients. The incremental coefficient data obtained by the above method at all six Mach numbers is presented in Figures 6-9. In general the data seems quite consistent from one Mach number to the next. Note that the perturbation effect distance is largest in the transonic regime as would be expected.

Calculations

The F-111 and FB-111 use the MAU-12 rack and two CCU-1B cartridges for all pivot pylon and weapons bay stations. Knowing the orifice combination as well as the weight, center of gravity and pitch moment of inertia of the store, it is possible to calculate the ejection velocity and pitch rate. Based on F-111 experience with other stores of this size and the wind tunnel data which shows large pitch up moments at all Mach numbers, an orifice combination of -7(.156") forward and -4(.081") aft is used. This combination, an attempt to counteract the tendancy to pitch nose up, results in 73.8 percent of the ejection force on the forward ejector. The calculated ejection rates are 9.5 feet per second and approximately -0.2 radians per second (nose down) pitch rate at the end of the ejector stroke.

The aerodynamic force and moment coefficient equations in the 6 DOF trajectory program were modified as follows:

$$C_A = C_{A_{FS}} \qquad (1)$$

$$C_\ell = C_{\ell_{FS}} \qquad (2)$$
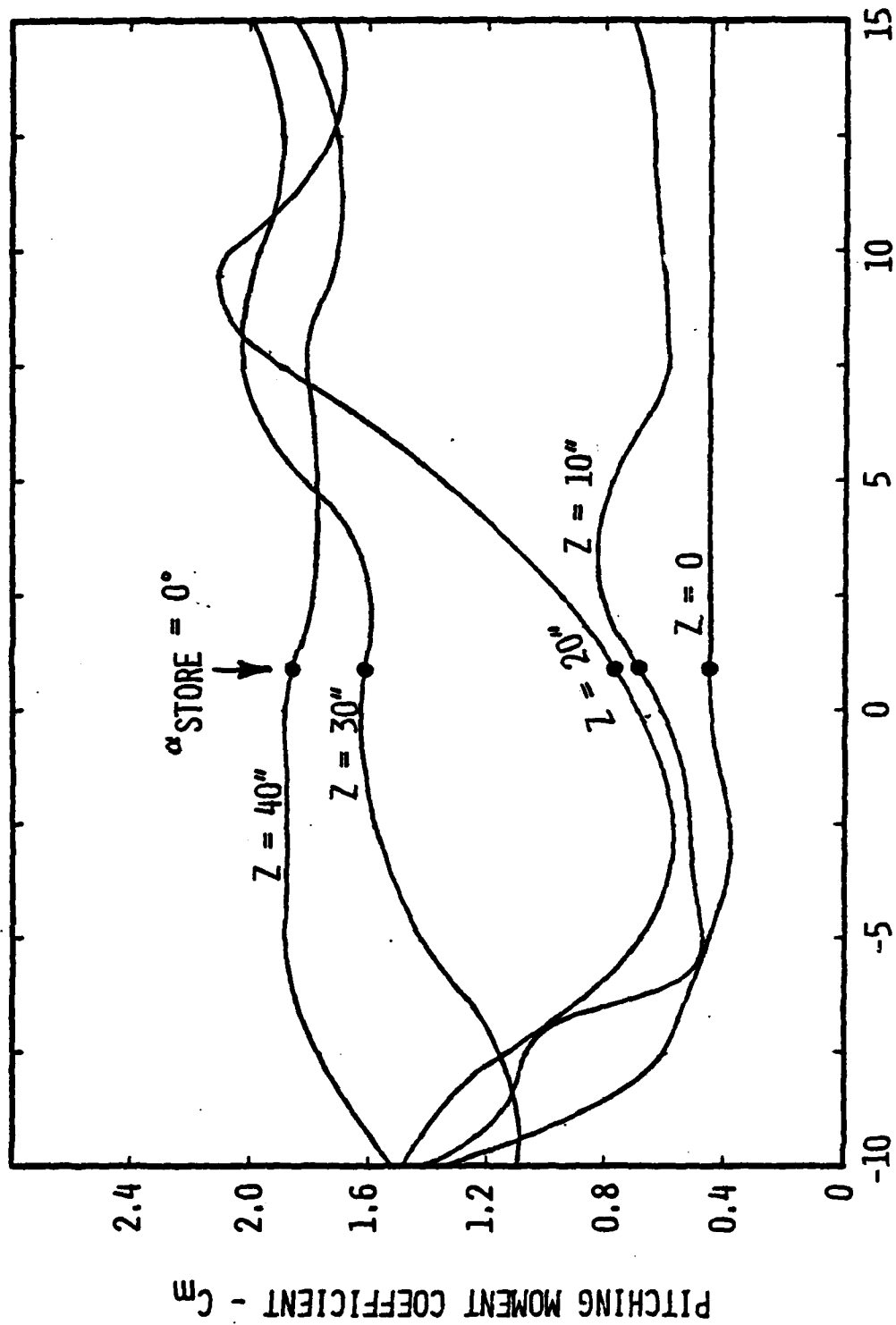
FIGURE 4 – PITCHING MOMENT FOR FIVE POSITIONS IN THE F-111 WEAPONS BAY AT MACH = 0.8

822
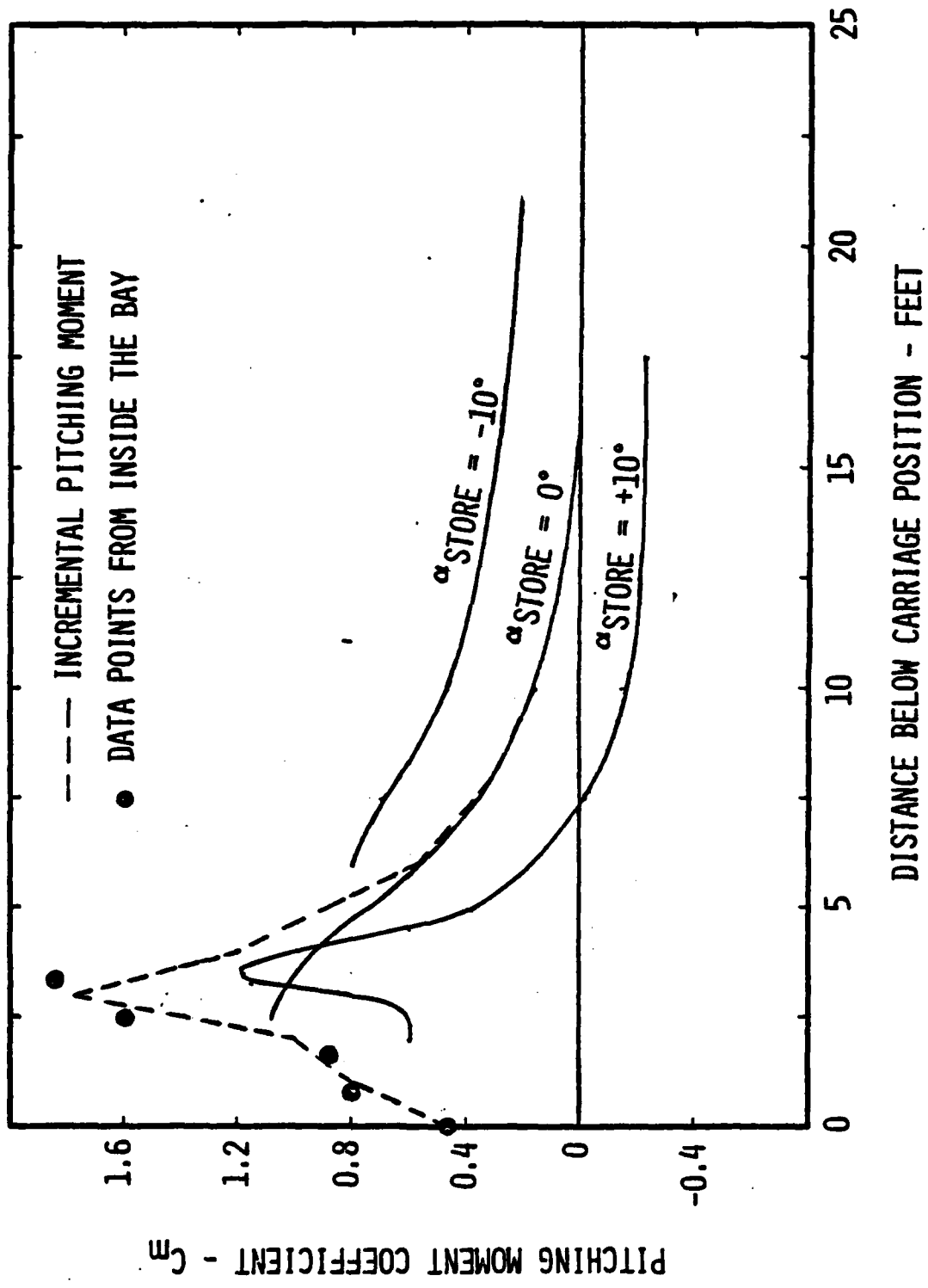
FIGURE 5 - PITCHING MOMENT DETERMINED FROM VERTICAL TRAVERSES
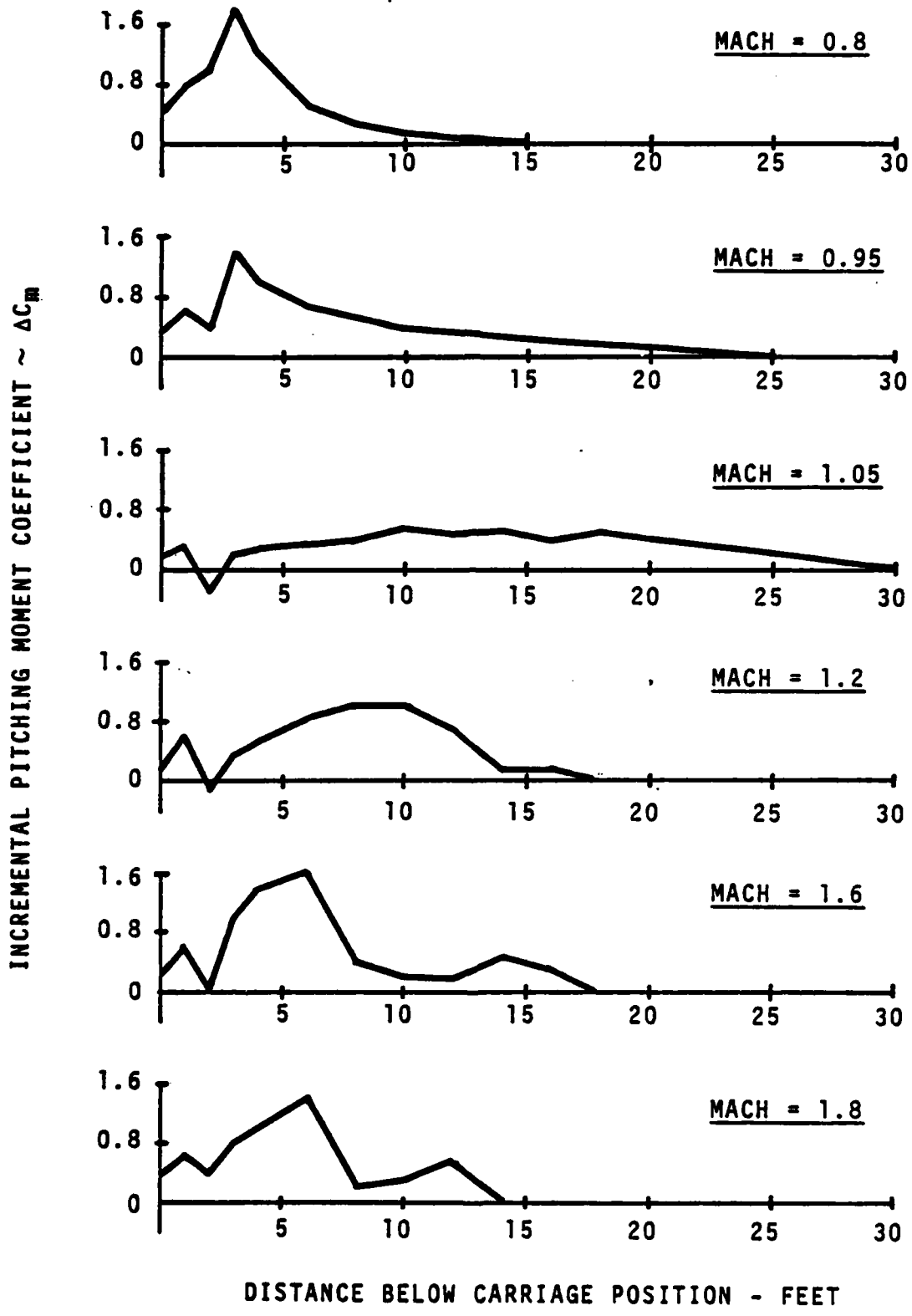
FIGURE 6 - INCREMENTAL PITCHING MOMENT COEFFICIENT

824
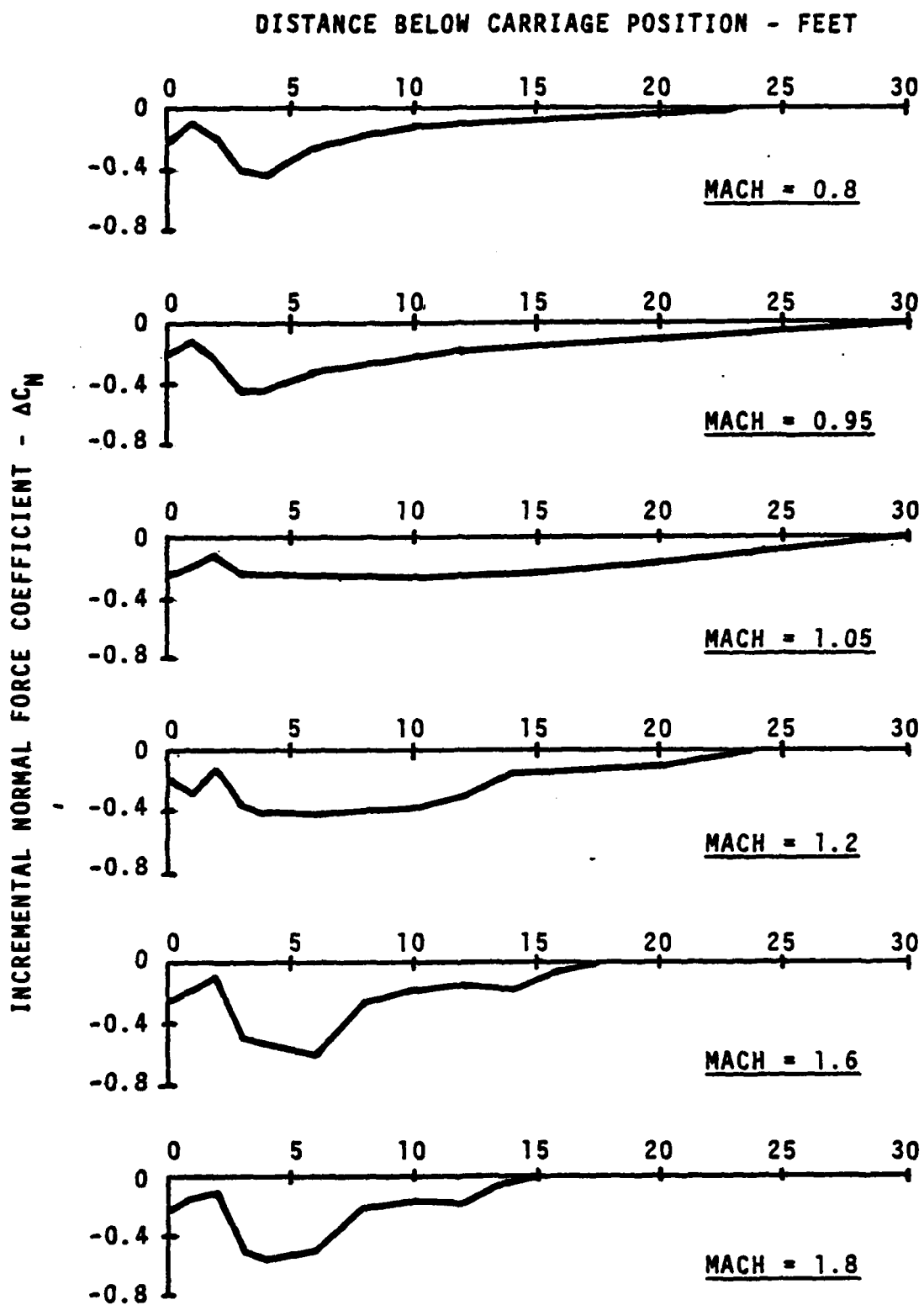
FIGURE 7 - INCREMENTAL NORMAL FORCE COEFFICIENT
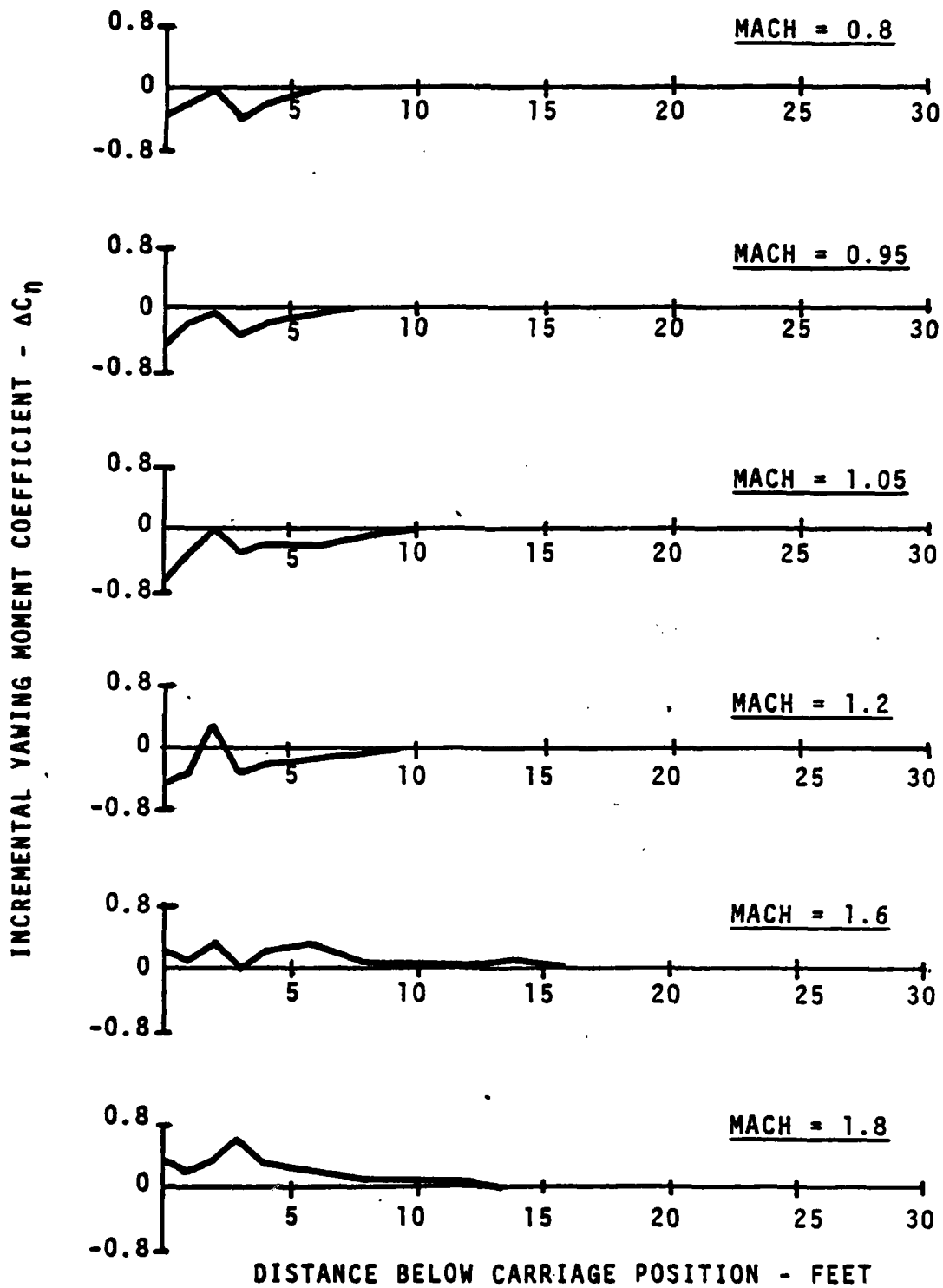
FIGURE 8 - INCREMENTAL YAWING MOMENT COEFFICIENT
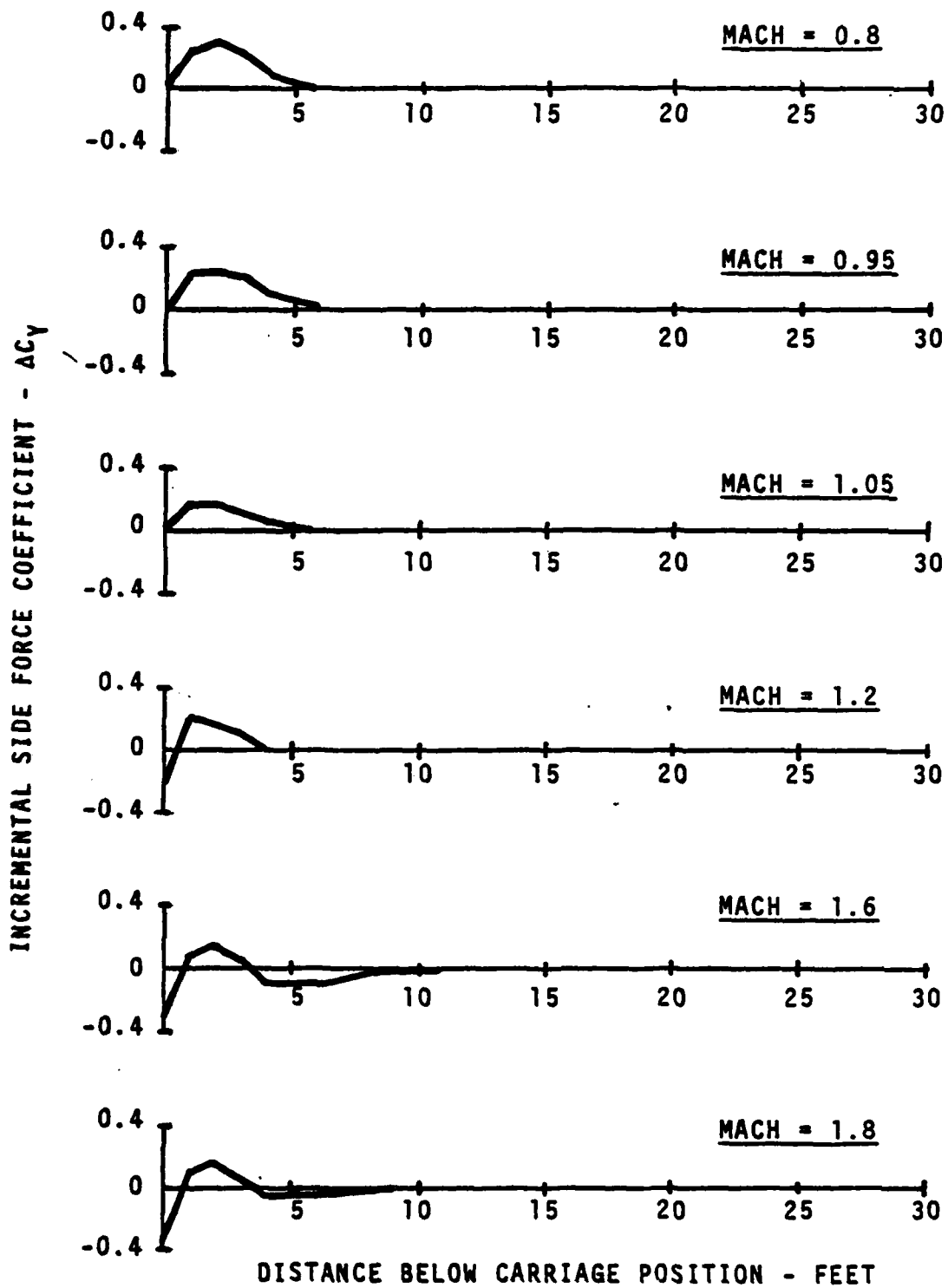
FIGURE 9 - INCREMENTAL SIDE FORCE COEFFICIENT

827

$$C_m = C_{m_{FS}} + \Delta C_m (Z) \qquad (3)$$

$$C_n = C_{n_{FS}} + \Delta C_n (Z) \qquad (4)$$

$$C_N = C_{N_{FS}} + \Delta C_N (Z) \qquad (5)$$

$$C_Y = C_{Y_{FS}} + \Delta C_Y (Z) \qquad (6)$$

Note that the free-stream rolling moment is used directly in the simulation. This was done because the very small scale models typically required for store separation wind tunnel tests make it difficult to determine small incremental rolling moment coefficients accurately, since the rolling moment coefficient may be dominated by fin misalignment rather than the nonuniform flow field effects. Also, the free-stream axial force is used directly because it usually is more accurate, being obtained with larger scale models, and the interference flow field contribution is typically small.

Although incremental coefficients were not obtained with the flip fins extended, this omission is not judged serious since it involves only the high altitude free fall drops. As mentioned earlier, canted flip fins are deployed at about 0.7 seconds after release on the ballistic free fall drops in order to improve inflight stability and maintain the roll rate. When this event occurs the store is about 14.6 feet below its carriage position and most of the flow-field effects have disipated by this time. In addition the canted fins start to roll the store which would introduce complications in the analysis if this effect were included.

COMPARISONS WITH FLIGHT DATA

An extensive full-scale flight drop test program is underway to define the separation characteristics, the ballistic dispersion and system performance of the store. These drop tests are conducted at the Sandia Laboratories Tonopah Test Range in Nevada.

Each full-scale drop test typically includes photographic coverage from movie cameras on the drop aircraft, in the chase aircraft, and on ground-based photo-theodolites and tracking telescopes. In addition, ground-based radars track the drop aircraft prior to release and thus define the initial conditions at release. Meteorological data are obtained from a meteorological balloon launched just before the drop time.

Each instrumented store contains an extensive motion sensor package and a telemetry system to transmit pertinent information to the ground station. The motion sensor package includes a gyro-stablized platform to measure the body angular orientation, rate gyros to measure the body angular rates, three-axis accelerometers to measure body accelerations, and discrete event data channels.

Table I presents a summary of all the F-111 weapon bay drops scheduled for the development test program. Store separation calculations using the 6 DOF analysis have been performed for each of the units and data from five of the seven scheduled drops are available for comparison. Although velocity and position data are obtained from the calculations, this data is not very

interesting, is not available from the flight tests for comparison and will not be presented. The only case where the translational data is of interest is at dynamic pressures exceeding 1700 psf. Calculations at these conditions predict a reversal in the vertical velocity indicating a tendency to float, a situation that has actually been experienced on a similar store.

Table I

F-111 WEAPONS BAY DROP SUMMARY

High Altitude Ballistic Free Fall Drops

	Mach	KCAS	$Q\left(\frac{LB}{FT^2}\right)$	ALTITUDE (FT-MSL)	DATE
DTU-91*	.80	300	282	30000	12/7/76
DTU-23**	.96	345	346	33000	12/9/76
DTU-15**	1.21	424	483	35000	2/24/77

Low Altitude Parachute Retarded Drops

	Mach	KCAS	$Q\left(\frac{LB}{FT^2}\right)$	ALTITUDE (FT-MSL)	DATE
PTU-40**	.49	289	281	6400 (1000AGL)	7/14/77
PTU-94*	.80	478	750	6400 (1000AGL)	2/24/77
PTU-95*	.95	570	1060	6400 (1000AGL)	6/78
PTU-61**	1.05	640	1340	5450 (100AGL)	6/78

* Uninstrumented units
** Fully instrumented units

829

In general the calculations indicate that all of the units will pitch nose up after release even though a nose down ejection force was applied. This pitch up increases as the Mach number and dynamic pressure increase. A pitch up angle in excess of 35 degrees would be predicted at a release velocity of 730 KCAS.

The calculations for PTU-40 at Mach 0.49 utilized the incremental coefficient data obtained at Mach 0.80. The pitch motion of PTU-40 is presented in Figure 10. The correlation is reasonably good except that it underestimates by approximately 50%. Comparison of the yaw motion in Figure 11 indicates an underestimation by the prediction. Both show an outboard yaw of small magnitude. PTU-40 was the only unit released from the right side of the bay.

Figure 12 presents pitch angle data from the two uninstrumented units at Mach 0.80. Pitch angle was read from the chase aircraft films for DTU-91 and from the ground films for PTU-94. PTU-94 experienced a large pitch up after release and this was predicted very well by the calculation.

The pitch motion for DTU-23 is shown in Figure 13. The calculation slightly underpredicts the pitch motion. In the case of the yaw motion shown in Figure 14 the calculation indicates the proper magnitude but the wrong direction. Note the effect of cross coupling on the pitch and yaw rates once the vehicle begins to spin.

The pitch motion from DTU-15 is shown in Figure 15. Again the calculation does a reasonable job but underestimates the magnitude of the pitch up. The yaw motion shown in Figure 16 shows similar magnitudes but the prediction is in the wrong direction. Again note the effects of spin on the pitch and yaw rates.

CONCLUDING REMARKS

The simplified grid simulation method has been especially useful at Sandia since it provides the only way of predicting store separations out of the F-111 weapons bay. These calculations and the correlation shown here provide an excellent basis for requesting USAF drop approvals.

This method has been shown to provide reasonable predictions of the pitch motion of a store exiting the F-111 weapons bay. Even though in some cases the magnitude is underpredicted; it does correctly model the nose up pitch attitude. The prediction of the yaw plane motion is of questionable value. In most cases the magnitude was about right, but the direction was reversed.

The major advantage of the simplified grid simulation method is that a large number of store separation trajectories can be generated over the complete Mach range at a minimum of time and cost. Thus, this method is ideally suited for including the effect of store separation in impact point dispersion and parametric studies investigating the effects of different store mass properties or ejection conditions. Additional comparisons at the two remaining drop conditions will extend the validity of the method.
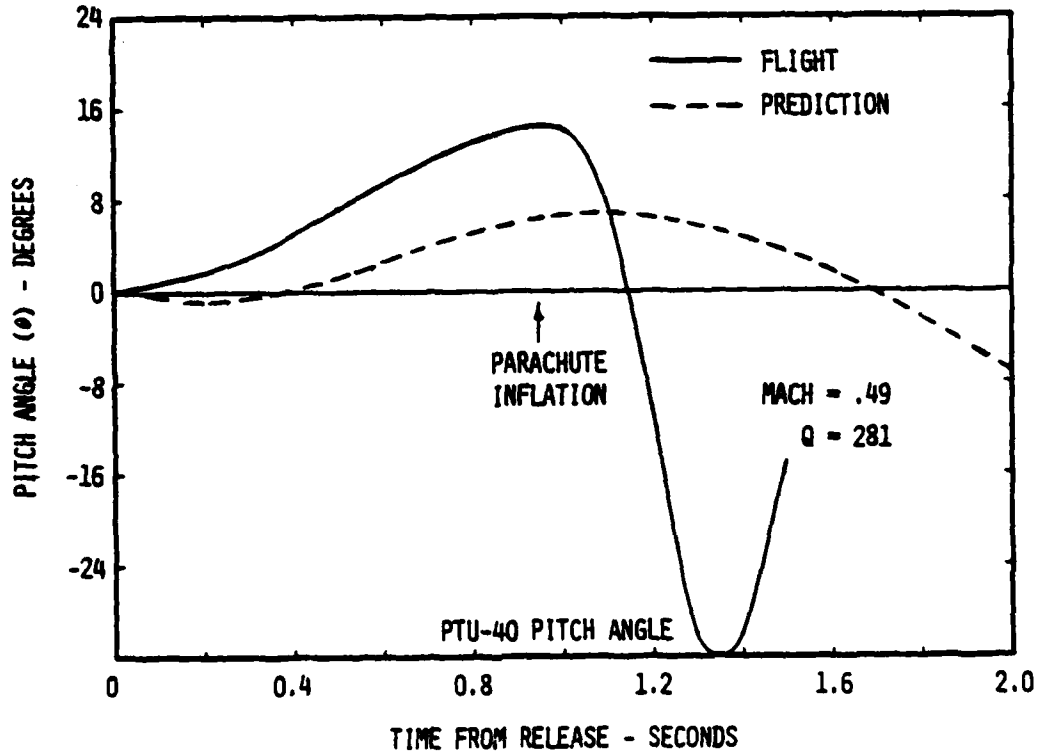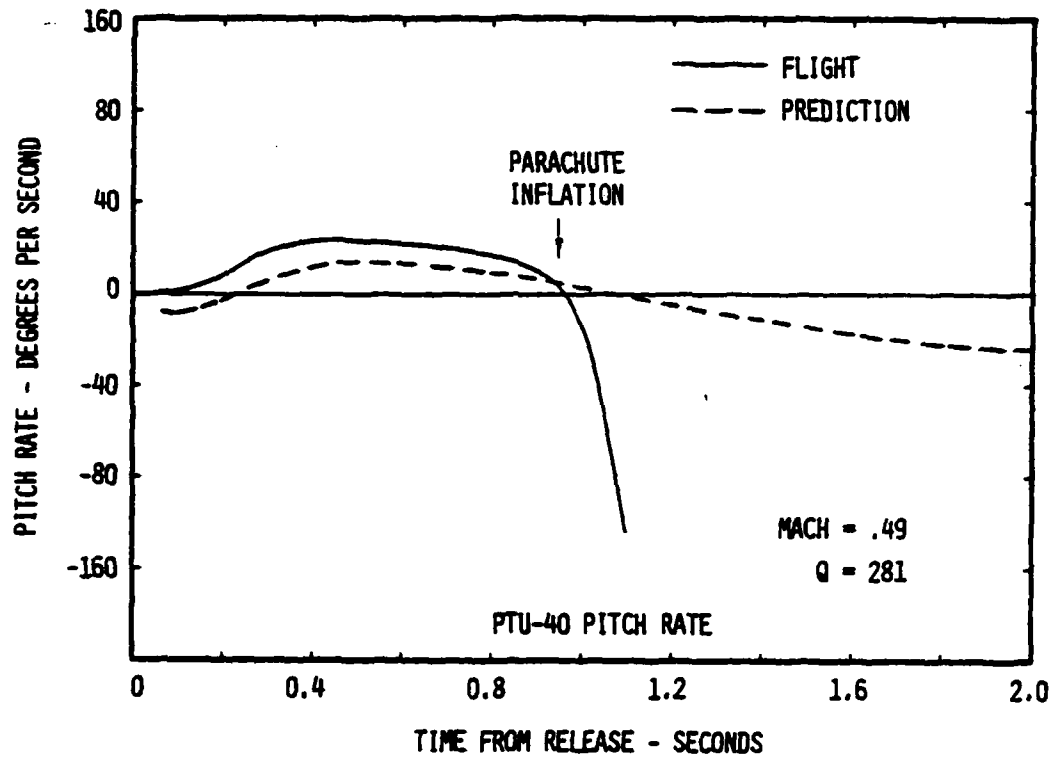
FIGURE 10   PTU-40 PITCH MOTION
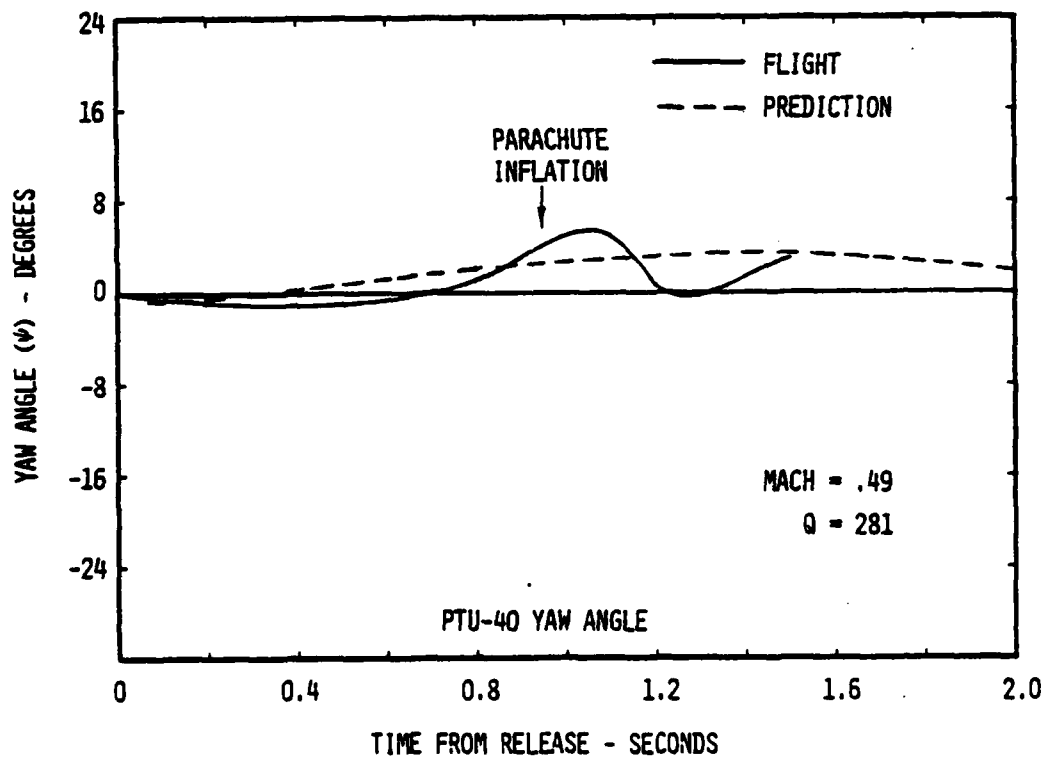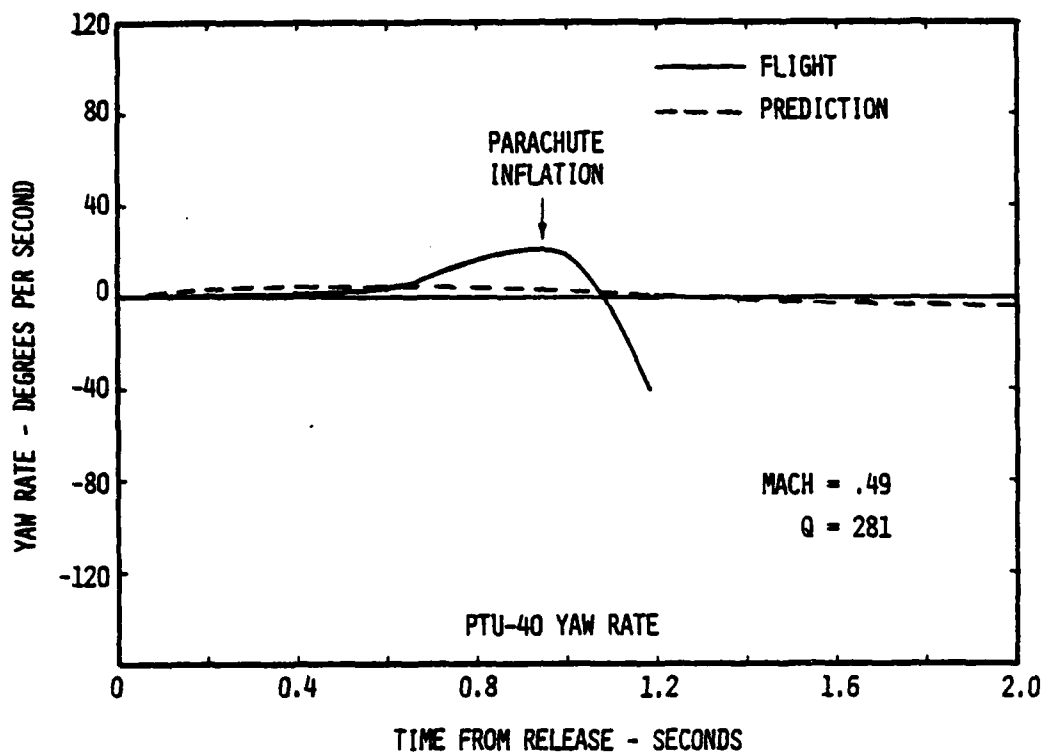
FIGURE 11   PTU-40 YAW MOTION
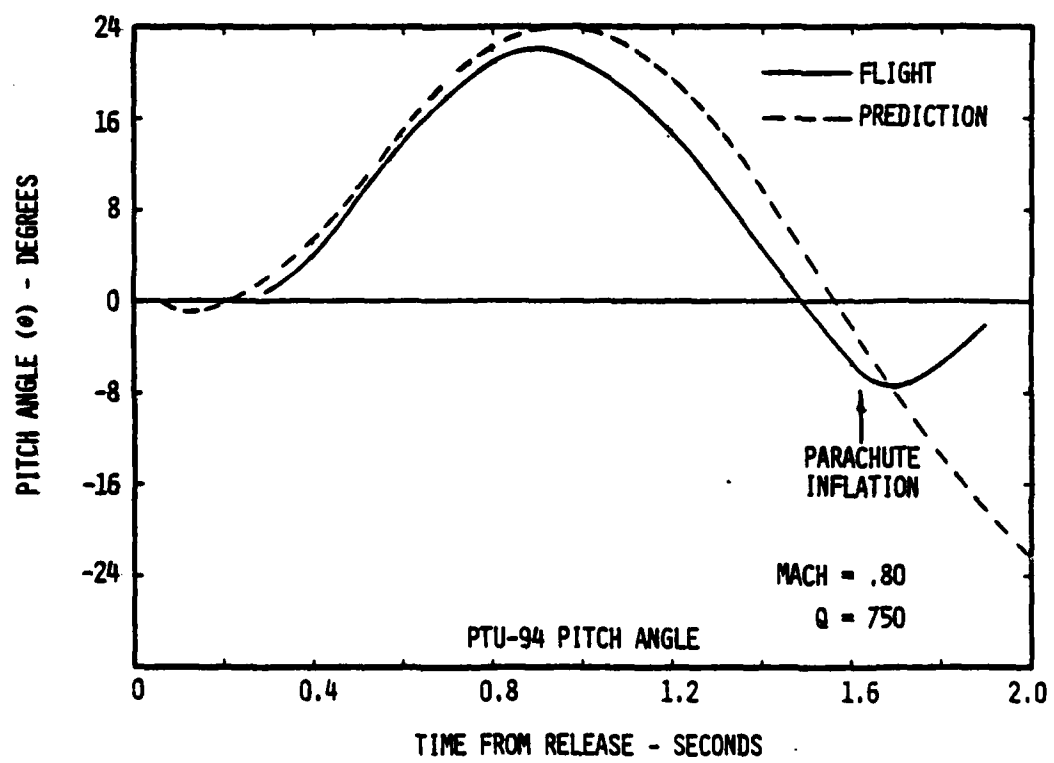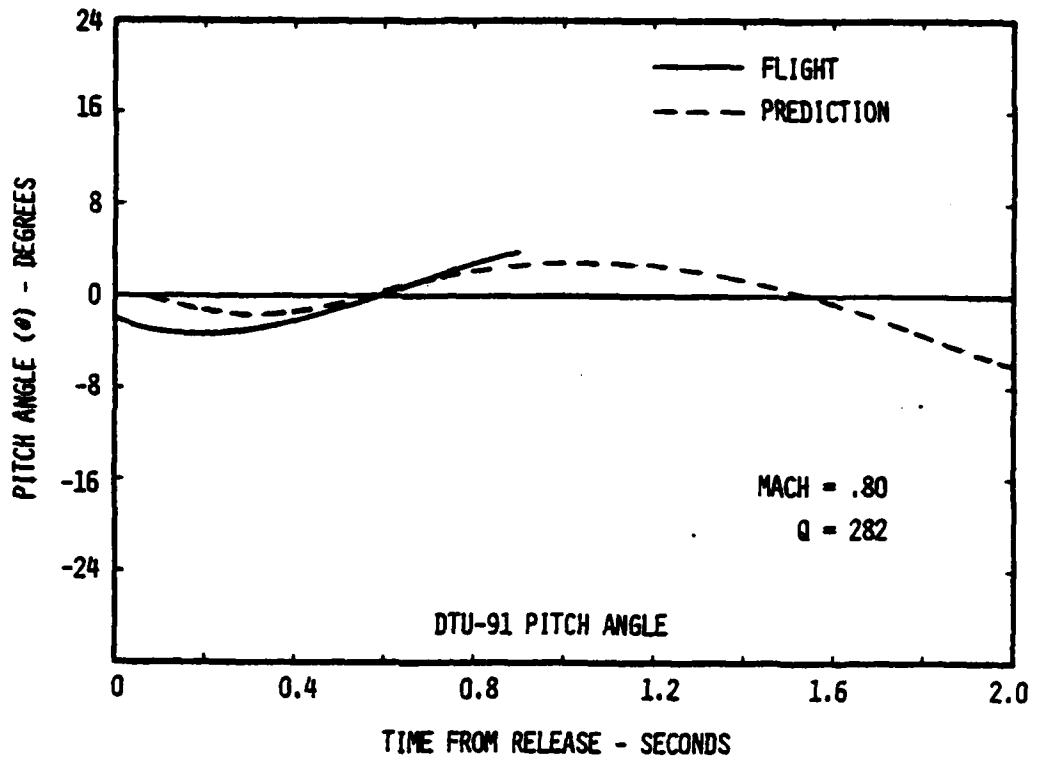
FIGURE 12   PTU-91 AND PTU-94 PITCH ANGLE
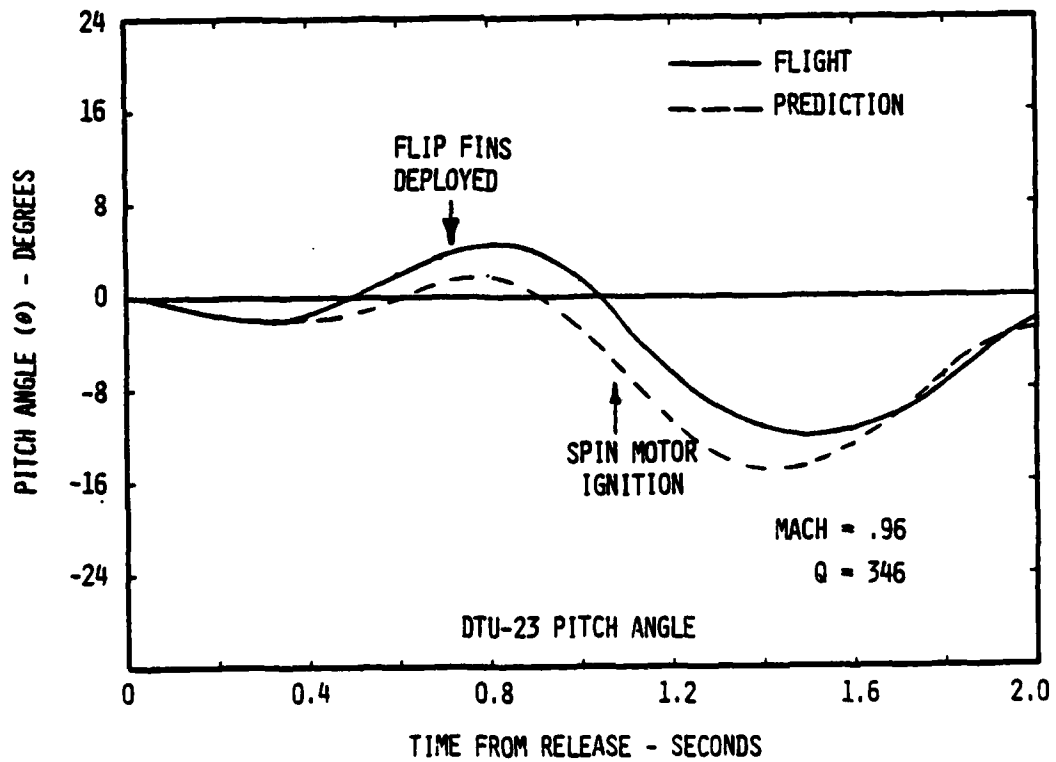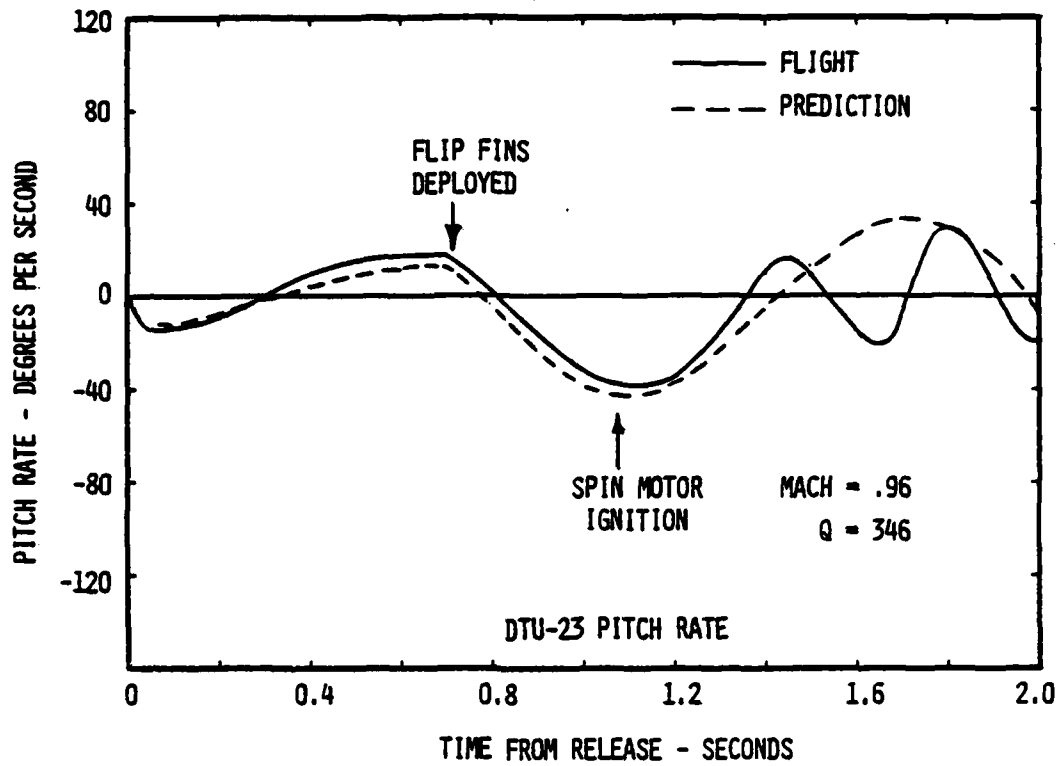
FIGURE 13 - DTU-23 PITCH ANGLE
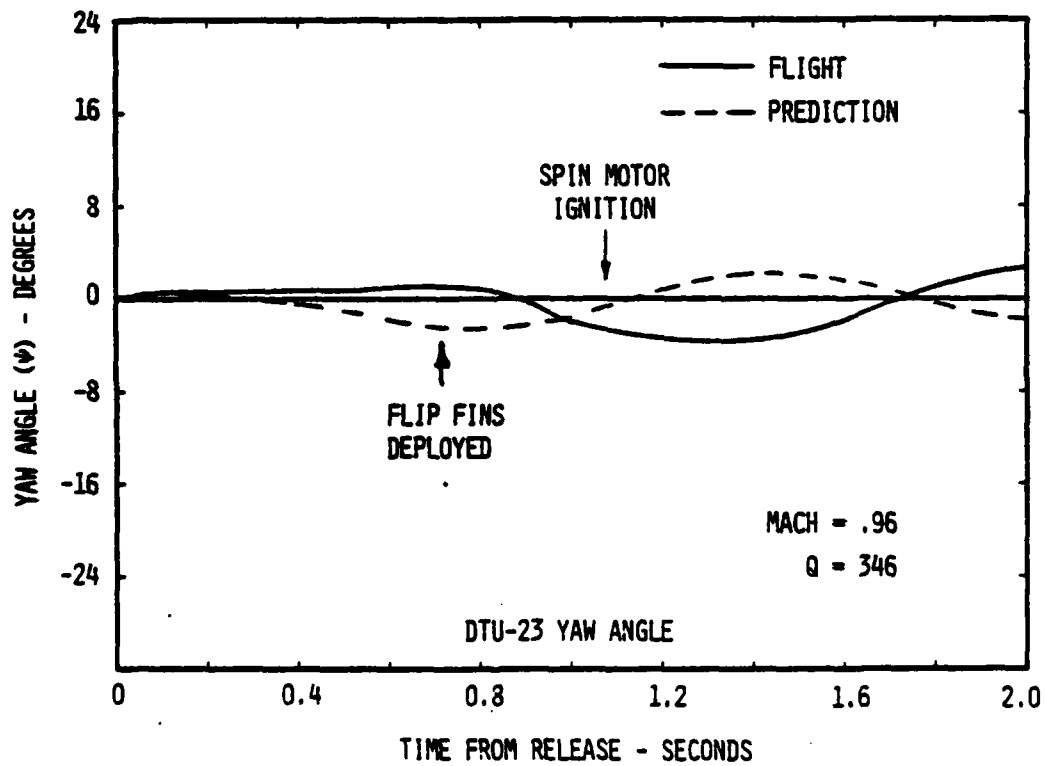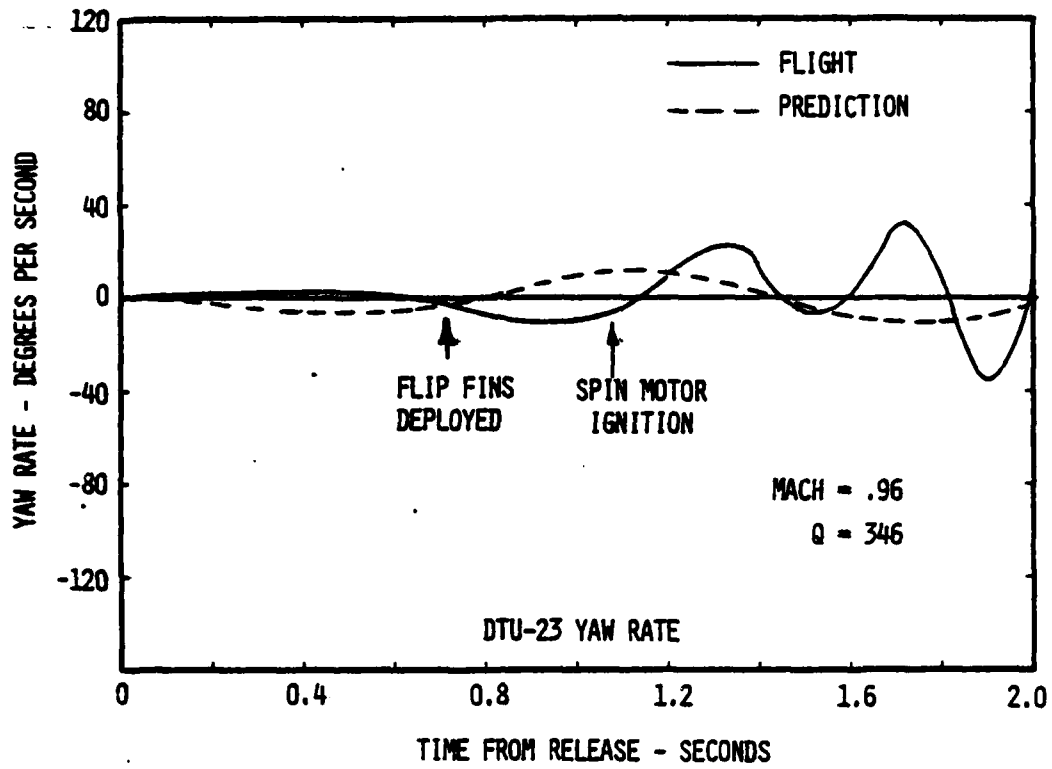
FIGURE 14 - DTU-23 YAW MOTION

835
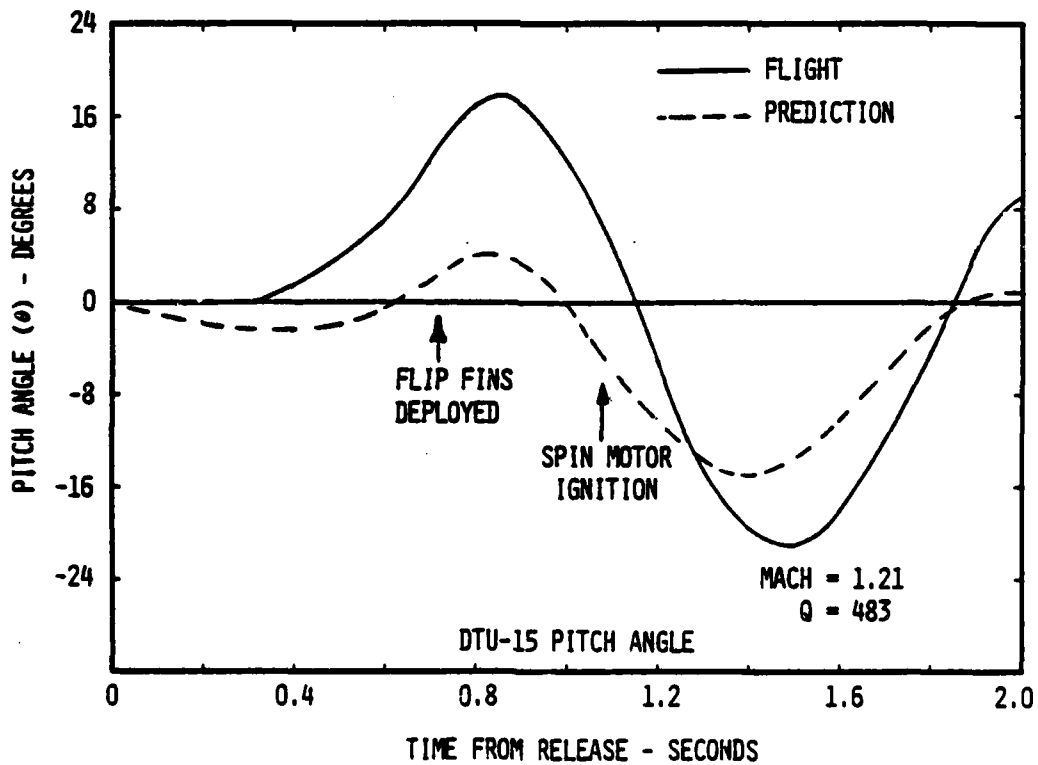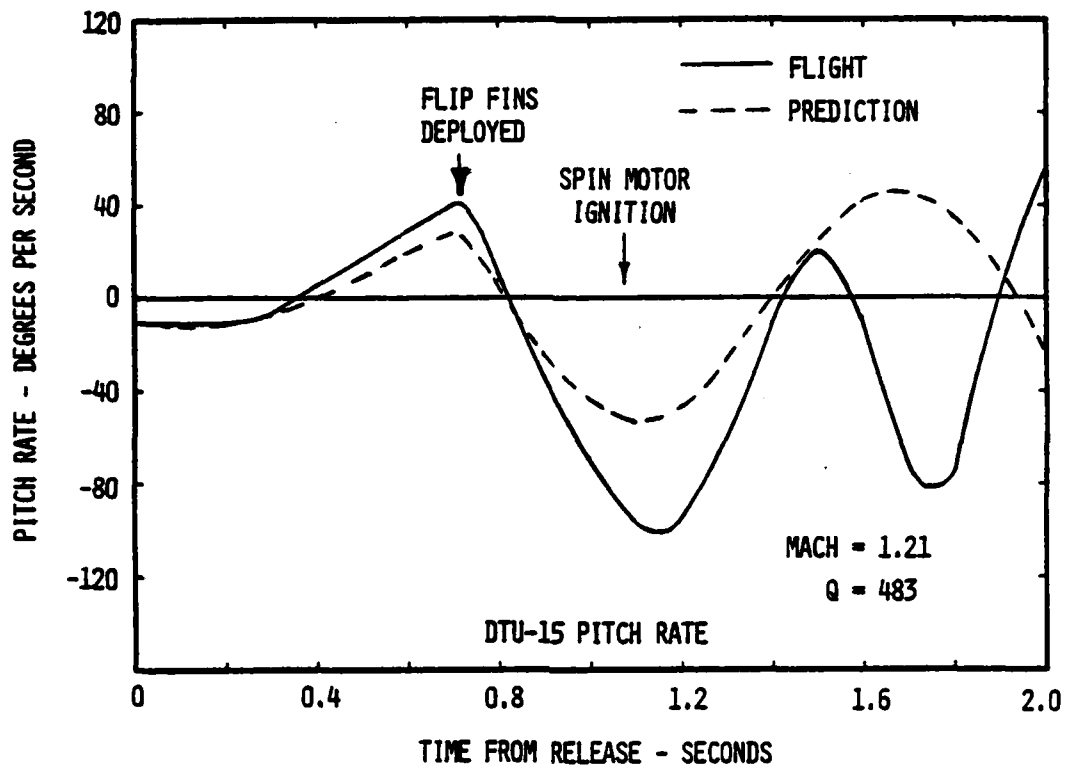
FIGURE 15 - DTU-15 PITCH MOTION
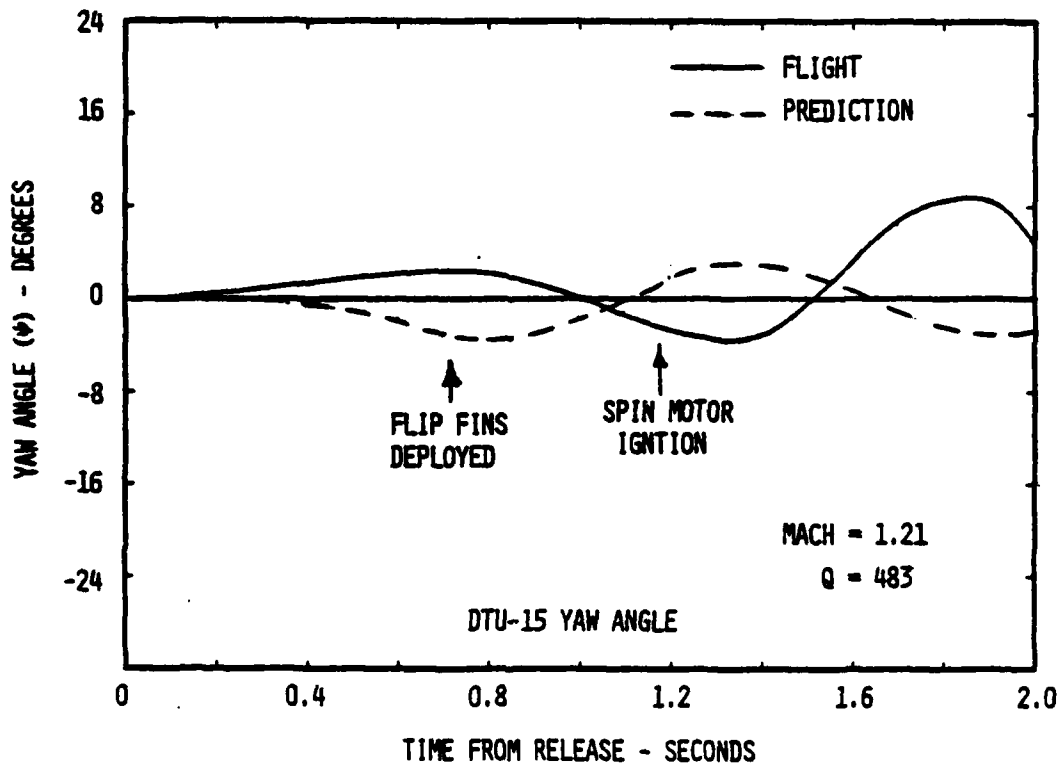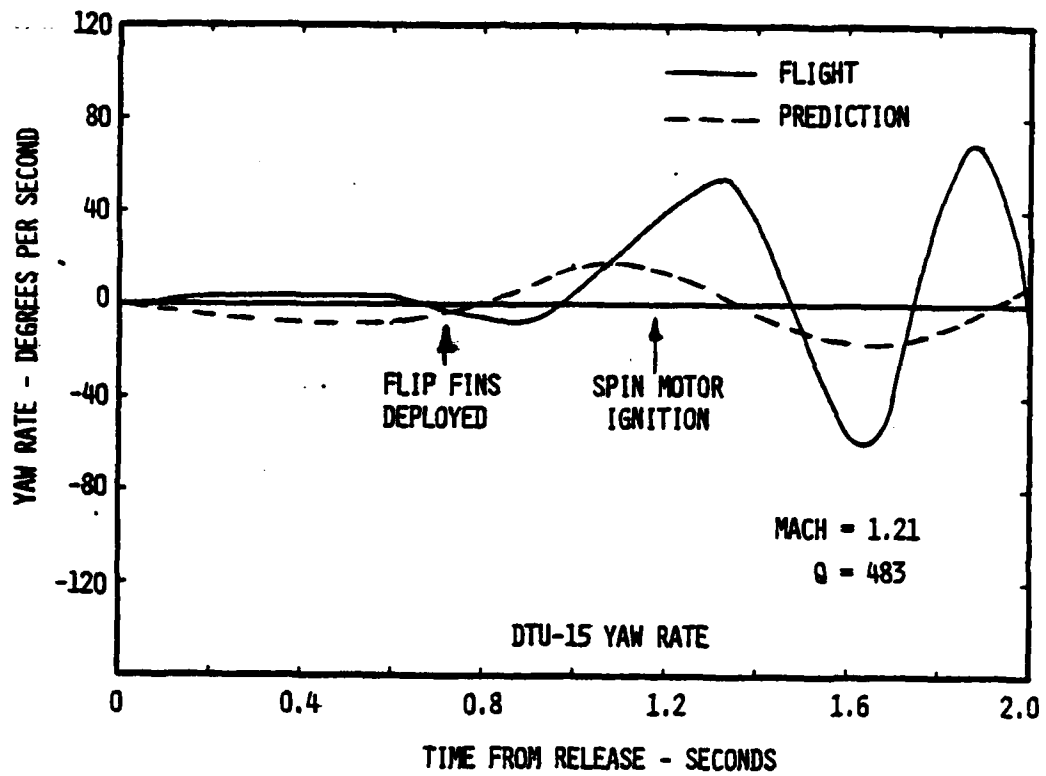
FIGURE 16 - DTU-15 YAW MOTION

References

1. "Wind-Tunnel Test to Determine the Captive Separation Characteristics of a 0.05 Scale Store Model From the F-4C and F-111D/E/F Aircraft in the Mach Range 0.8 to 1.4," LTV Test Report HSWT-540, LTV Aerospace Corporation, Dallas, Texas, September 1975.

2. "Wind-Tunnel Test to Determine the Captive Separation Characteristics of a 0.05 Scale Store Model From the F-4C and F-111D/E/F Aircraft in the Mach Range 1.8 to 2.2 and From the A-7 Aircraft in the Mach Range 0.6 to 0.9," LTV Test Report HSWT-560, LTV Aerospace Corporation, Dallas, Texas, March 1976.

3. "VSD Wind Tunnel Test to Obtain Five Component Force and Moment Data on a 0.05 Scale Store Model in the Mach Range of 0.95 to 1.2", Vought Test Report HSWT-525/557, Vought Systems Division, Dallas, Texas, November 1975.

4. "Captive Loads Test of a 0.05 Scale Store Model in a F-111 Weapons Bay in the Vought Corporation High Speed Wind Tunnel at Mach Numbers of 0.8 to 1.8", Vought Test Report HSWT-591, Vought Systems Division, Dallas, Texas, April 1977.

5. Vought Wind Tunnel Test to Determine the Separation Characteristics of a 0.05 Scale Store Model from the F-111 Aircraft Model in the Mach Range of 0.8 to 2.2", Vought Test Report HSWT-592, Vought Systems Division, Dallas, Texas, April 1977.

6. Wolfe, J. A., "A Computer Controlled Wind Tunnel Testing System for Investigation of Aircraft or Booster Separation Problems," Aircraft/Stores Compatibility Symposium Proceedings, Vol. 3, Joint Technical Coordinating Group/Air Launched Non-nuclear Ordnance, August 1972, pp. 312-338.

7. Spahr, H. R., Everett, R. N., and Kryvoruka, J. K.," A Multifaceted Store Separation Analysis," Proceedings of the AIAA 9th Aerodynamic Testing Conference, June 7-9, 1976.

8. Little, R. E., "A Parametric Method of Aerodynamic Flow Field Presentation," Aircraft/Stores Compatibility Symposium Proceedings, Vol. 3, Joint Technical Coordinating Group/Air Launched Non-nuclear Ordnance, January 1974, pp. 183-229.

9. Jones, D. A. III, "Some Aspects of the Aircraft Store Separation Problem," NWL TR-2206, Naval Weapons Laboratory, Dahlgren, Virginia, September 1965.

10. Schindel, L. H., "Store Separation," AGARDograph No. 202, Advisory Group for Aerospace Research and Development, Neuilly-Sur-Seine, France, June 1975.

11. Everett, R. N., "SIX DOF - A computer Program for Trajectory Simulation and Accuracy Analysis," Sandia Laboratories Report, Sandia Laboratories, Livermore, California, to be published.

AUTOBIOGRAPHY

Roger N. Everett

Sandia Laboratory

Livermore, California

Mr. Everett is a member of the technical staff at Sandia Laboratories, Livermore, California. His professional experience includes the areas of reentry vehicle flight dynamics, projectile ballistics, store separation, flight dynamics, and over fifteen years in wind tunnel testing. He is currently in charge of test planning and flight data analysis of all ballistic drop units on a major Sandia weapons program. This includes store separation calculations from eight Air Force and Navy aircraft as well as a dispersion assessment for all delivery modes. He has also provided analytical and test support for the lifting parachute used in the same system. He holds a MSME (1964) from the University of New Mexico and a BAE (1962) from Georgia Institute of Technology. Mr. Everett has served on the AIAA Membership Committee and the technical committee on Application of Aerospace Technology to Society.

EFFECTS OF EXTERNAL STORES ON THE AIR COMBAT
CAPABILITY OF A DELTA WING FIGHTER
(U)
(Article UNCLASSIFIED)

by

M. LEROY SPEARMAN AND WALLACE C. SAWYER
NASA Langley Research Center
Hampton, Virginia 23665

ABSTRACT. (U) Delta wing point-design fighters with two pylon
mounted missiles and aft tail controls (similar to several Soviet
designs) have been investigated for a Mach number range from about
0.6 to 2.0. Whereas minimum drag penalties that are expected with
the addition of external stores do occur, the effects at higher lifts,
corresponding to maneuvering flight, are less severe and often favor-
able. The drag-due-to-lift factor is less with stores on although the
lift curve slope is unaffected. The longitudinal stability level is
reduced by the addition of stores while the pitch control effectiveness
is unchanged. The directional stability was generally reduced at
subsonic speeds and increased at supersonic speeds by the addition of
stores but sufficiently high stability levels are obtainable that are
compatible with the longitudinal maneuvering limits. Some examples of
the potential maneuvering capability in terms of normal acceleration
and turn radius are included.

LIST OF FIGURES

SYMBOLS

The longitudinal results are referred to the stability axis system and the lateral results are referred to the body axis system. The coefficients and symbols are defined as follows:

a_n normal acceleration in g units

b wing span

$\bar{c}$ wing mean aerodynamic chord

C_D drag coefficient, $\dfrac{\text{Drag}}{qS}$

$C_{D,o}$ drag coefficient at zero lift

C_ℓ rolling-moment coefficient, $\dfrac{\text{Rolling moment}}{qSb}$

C_{ℓ_β} effective dihedral parameter, per degree

C_L lift coefficient, $\dfrac{\text{Lift}}{qS}$

C_m pitching-moment coefficient, $\dfrac{\text{Pitching moment}}{qS\bar{c}}$

$\dfrac{\partial C_m}{\partial \delta_h}$ horizontal tail effectiveness

$\dfrac{\partial C_m}{\partial C_L}$ longitudinal stability parameter

C_{n_β} directional stability parameter, per degree

C_{Y_β} side-force parameter, per degree

h altitude

L/D lift-drag ratio

843

SYMBOLS (continued)

M	free-stream Mach number
q	free-stream dynamic pressure
R	turn radius
S	reference wing area including fuselage intercept
W	weight
W/S	wing loading
α	angle of attack, degrees
β	angle of sideslip, degrees
δ_h	horizontal tail deflection (positive trailing edge down), degrees

INTRODUCTION

Since the advent of air-to-air missiles for air combat fighters, the integration of the weapon carriage with the airplane has been a problem that must be considered. With the obvious exception of airplanes designed with an internal weapons bay (such as the F-101 and the F-106), missiles have typically been carried externally on pylons. The aerodynamic effects that may be associated with this type of external carriage include the effects on lift and drag; control effectiveness; longitudinal and lateral stability; and mutual interference.

Many fighters originally designed with gun systems were adapted to accept pylon-mounted missiles. With the proliferation of pylons and missiles, many newer fighters have also been required to accommodate a wide variety of existing standard pylon and store arrangements. In some cases such adaptation can be reasonably acceptable, whereas in other cases some performance limitation may result.

The objective of the paper will be to make some observations on the case for simplifying the fighter/missile configuration so that adverse effects are minimized and the air combat capability maximized in the Mach number range from 0.60 to about 2.0. Delta wing configurations with two pylon mounted missiles and aft tail controls were considered. The arrangements were similar to several Soviet concepts such as Fishbed, Fishpot, and Flagon, and are illustrative of an approach to point-design air combat fighters. Some examples of the potential maneuvering capability in terms of normal acceleration and turn radius for various speeds and/or altitude will be shown. Previous NASA-Langley fighter/stores summary papers are contained in references 1 and 2. Results for the delta wing configurations used in the present paper are, as yet, unpublished.

DISCUSSION

A lightweight type fighter concept, similar to a Mig-21 Fishbed, with two underwing pylon-mounted missiles is shown in figure 1. Longitudinal characteristics for this concept (fig. 2) for M = 0.60 and 1.20 indicate a progressive reduction in the stability level as the pylon and missile are added with no change in the total lift. This characteristic of decreasing values of C_m with no change in C_L was observed over the Mach number range from 0.60 to 2.00 and is apparently caused by a redistribution of lifting pressure on the underside of the wing that occurs primarily from the presence of the pylon. The effect was more noticeable in the speed range up to M = 1.20 and was somewhat reduced in magnitude at higher supersonic Mach numbers.

The drag characteristics for the delta wing fighter at M = 0.60 and 1.20 (fig. 3) indicate an expected increase in C_D at lower lifts but a reduction in the drag-due-to-lift as the pylon and missile are added. The net result is only a small reduction in maximum L/D and essentially no effect of stores on L/D at the higher lifts that are associated with maneuvering flight.

A summary of some of the longitudinal characteristics for the delta wing fighter (fig. 4) indicate the progressive decrease in stability level and increase in $C_{D,0}$ as the pylon and missile are added, and also show that no measurable change occurred in the horizontal tail control effectiveness. Hence, despite the increased $C_{D,0}$ due to the stores, the results indicated no degradation in maneuvering capability because of the reduced stability level, the reduced drag-due-to-lift, and the unchanged lift and control effectiveness.

Lateral stability characteristics for the fighter at M = 0.60 and 1.20 (fig. 5) indicate an increase in the magnitude of C_{Y_β} that might be expected due to the addition of the stores. This was translated into a decrement in C_{n_β} that was fairly large in the transonic range only (about M = 0.90 to 1.20) but still permitted positive C_{n_β} to sufficiently high angles of attack for good maneuvering capability (about 16° to 18°) because of the inherently higher values of C_{n_β} that exist in the transonic range for the basic configuration. At higher supersonic Mach numbers the adverse effect of stores on C_{n_β} disappears and may even become favorable.

846
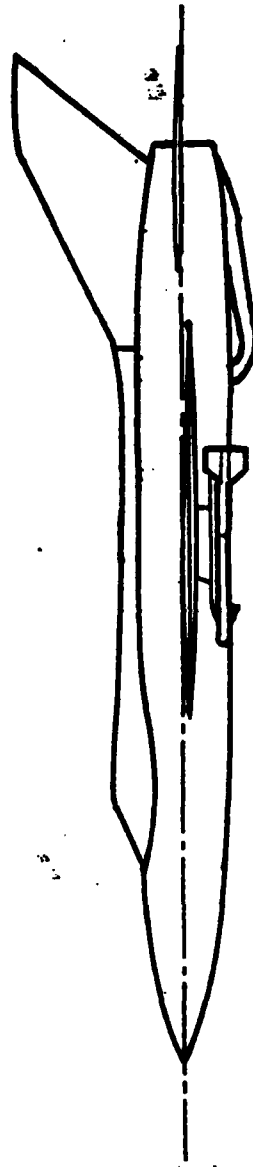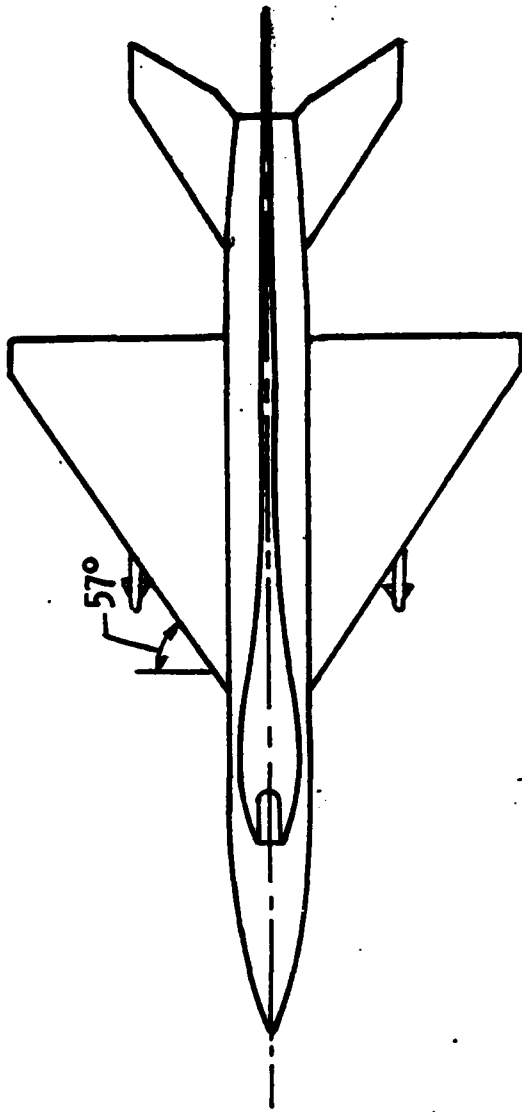
Figure 1. - Delta wing fighter configuration.

57°
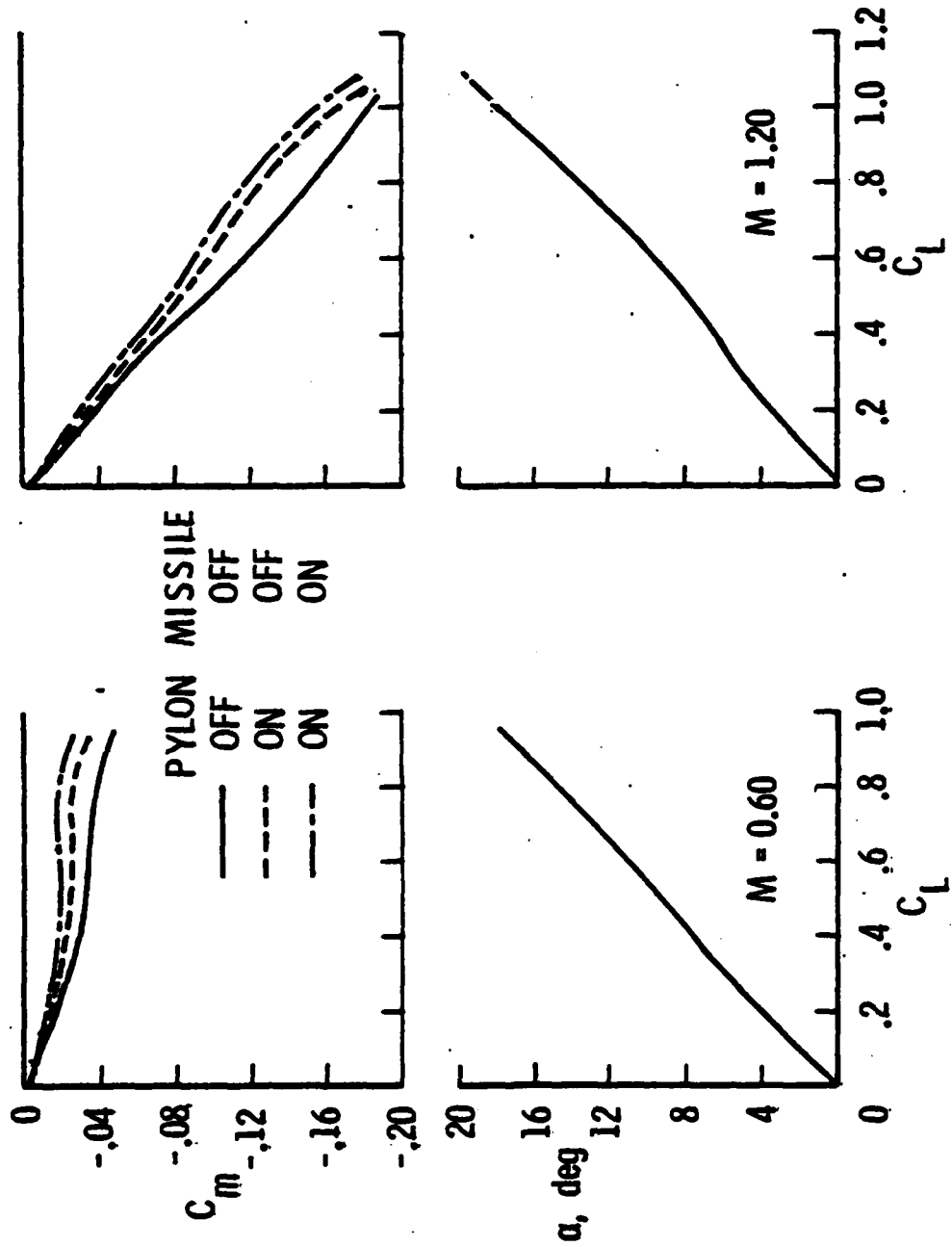
Figure 2. - Longitudinal characteristics for delta wing fighter at M = 0.60 and 1.20.
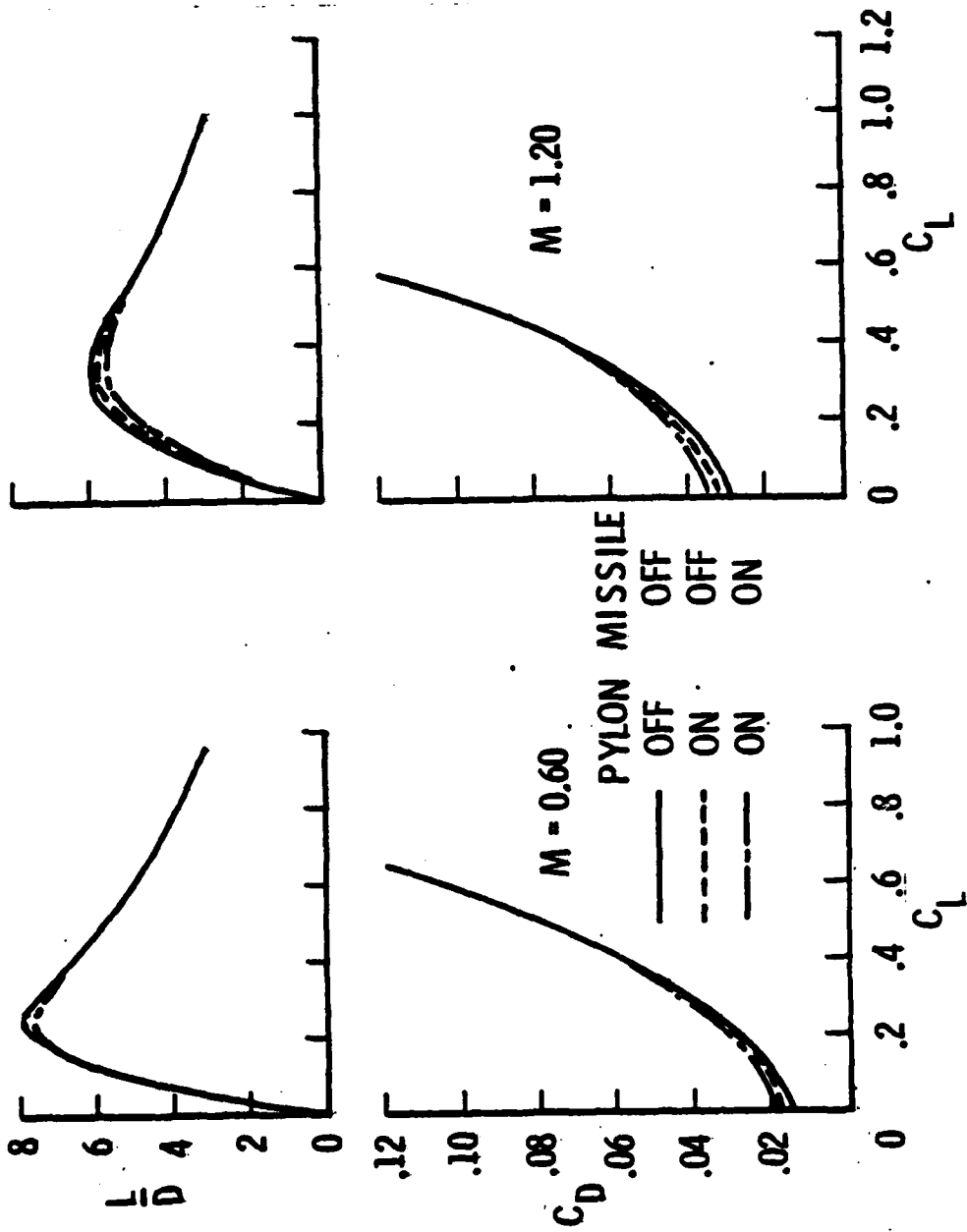
Figure 3. - Drag characteristics for delta wing fighter at M = 0.60 and 1.20.
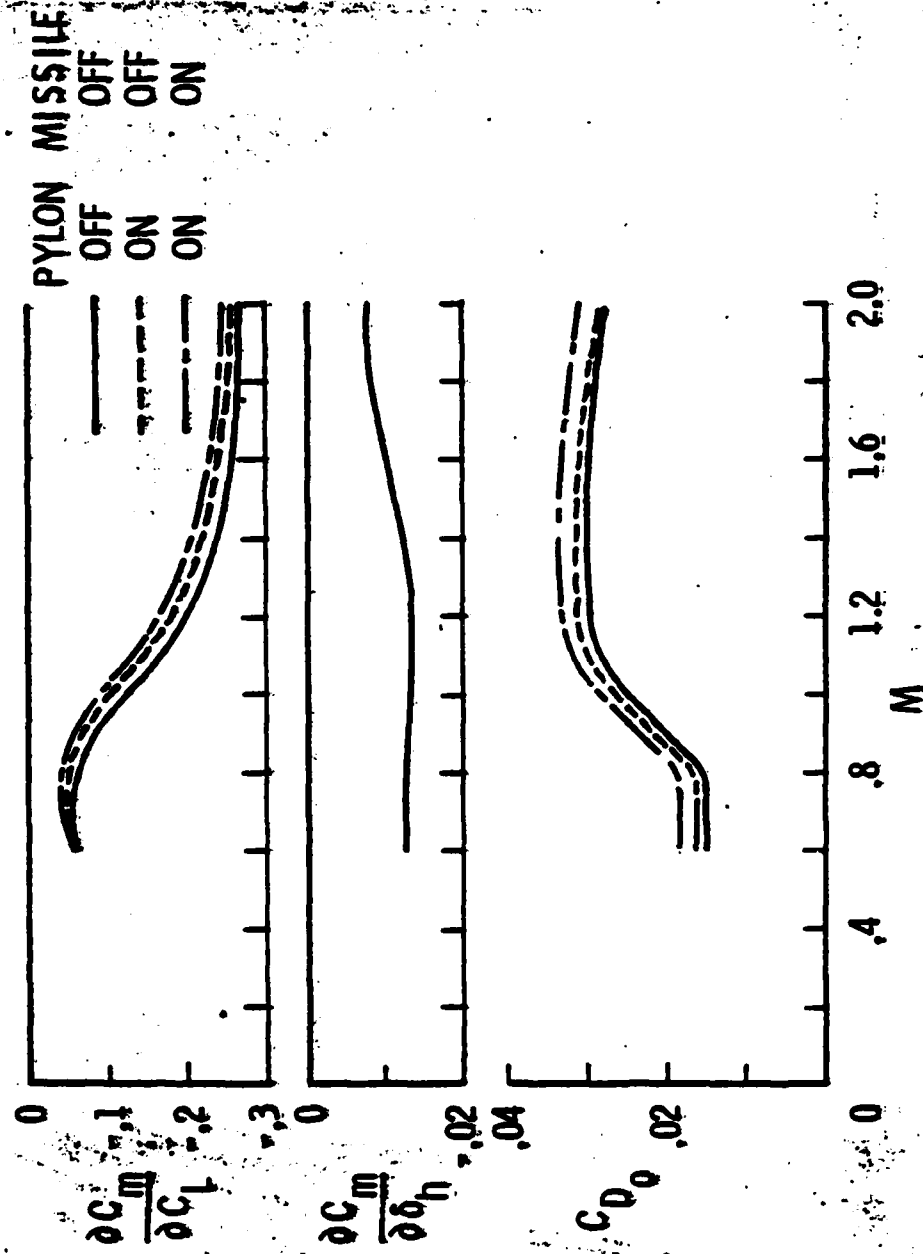
Figure 4. - Longitudinal summary for delta wing fighter.
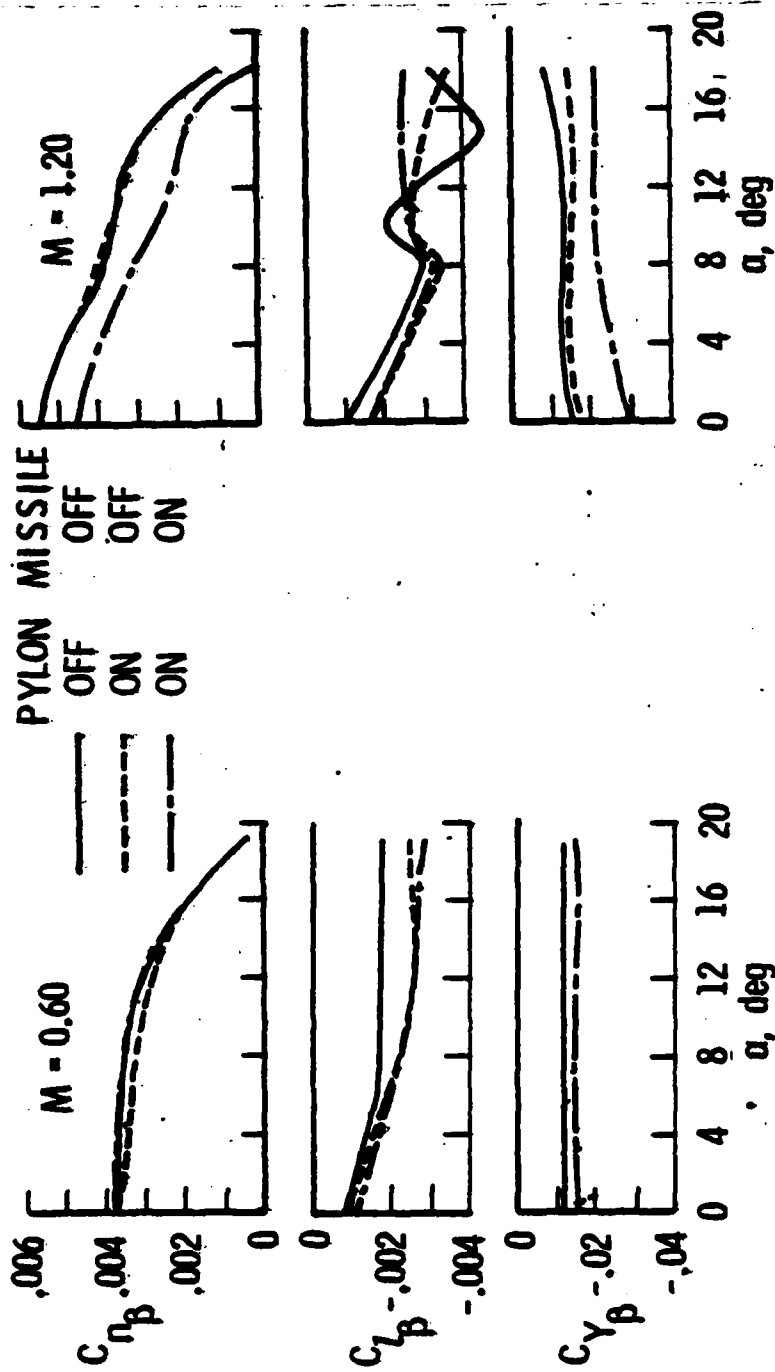
Figure 5. – Lateral characteristics for delta wing fighter at M = 0.60 and 1.20.

Some of these higher Mach number effects can be better illustrated with some results from an investigation of a delta wing interceptor configuration. The interceptor configuration (fig. 6) is similar to the fighter configuration in general geometry but is representative of a slightly larger airplane and missile such as the SU-11 Fishpot or the SU-15 Flagon. The longitudinal characteristics for the interceptor at $M = 1.60$ (fig. 7) indicate little effect of the pylon and missile on the control effectiveness and show a slight increase in lift at higher α's and a small decrease in stability. The increase in lift shown for this Mach number probably results from the fairly large pylon inducing an increase in local dynamic pressure over a large portion of the underside of the wing. The increase in C_D

and decrease in L/D at low to moderate lifts would have some detrimental effect on acceleration and cruise flight regimes. However, if maneuvering requirements should occur, the drag and L/D at angles of attack of about 16° to 18° are essentially unaffected by the stores because of the decrease in drag-due-to-lift.

The lateral characteristics for the interceptor at $M = 1.60$ (fig. 8) indicate a substantial increase in C_{n_β} due to the stores which

would be of special benefit if maneuvering requirements to high angles of attack should occur. The effective dihedral is reduced by the addition of the stores resulting in a favorable reduction in the roll-to-yaw ratio. The reduction in $-C_{\ell_\beta}$, as has been noted in other investi-

gations in the supersonic speed range, is apparently caused by an interference flow field from the store installation that, in sideslip, results in a reduction of lift on the inboard section of the windward wing and an increase in lift on the inboard section of the downwind wing.

Some indication of the resultant maneuvering potential is indicated by the next two figures. The normal acceleration for a wing loading of 50 lb/ft^2 and with the maximum C_L limited to 0.8 ($\alpha = 16^o$ to 18°) is shown in figure 9 for $M = 0.60$, 1.20, and 1.60 at various altitudes. Sustained a_n's shown at $M = 0.60$ and 1.20 are for a hypothetical engine

of about 13,000 lbs. static sea-level thrust with no afterburning. These results are included to show the greater detrimental effects on sustained a_n's at supersonic speeds due to the difference in drag

level from subsonic speeds. The effects of sustained maneuver can be improved, of course, through the use of higher thrust engines or through afterburning. The expected trends are apparent - the increase in a_n with decreasing altitude and with increasing speed - both due to an increase in dynamic pressure that results in lower lift required for level flight and greater excess lift available for maneuvering. It is

852
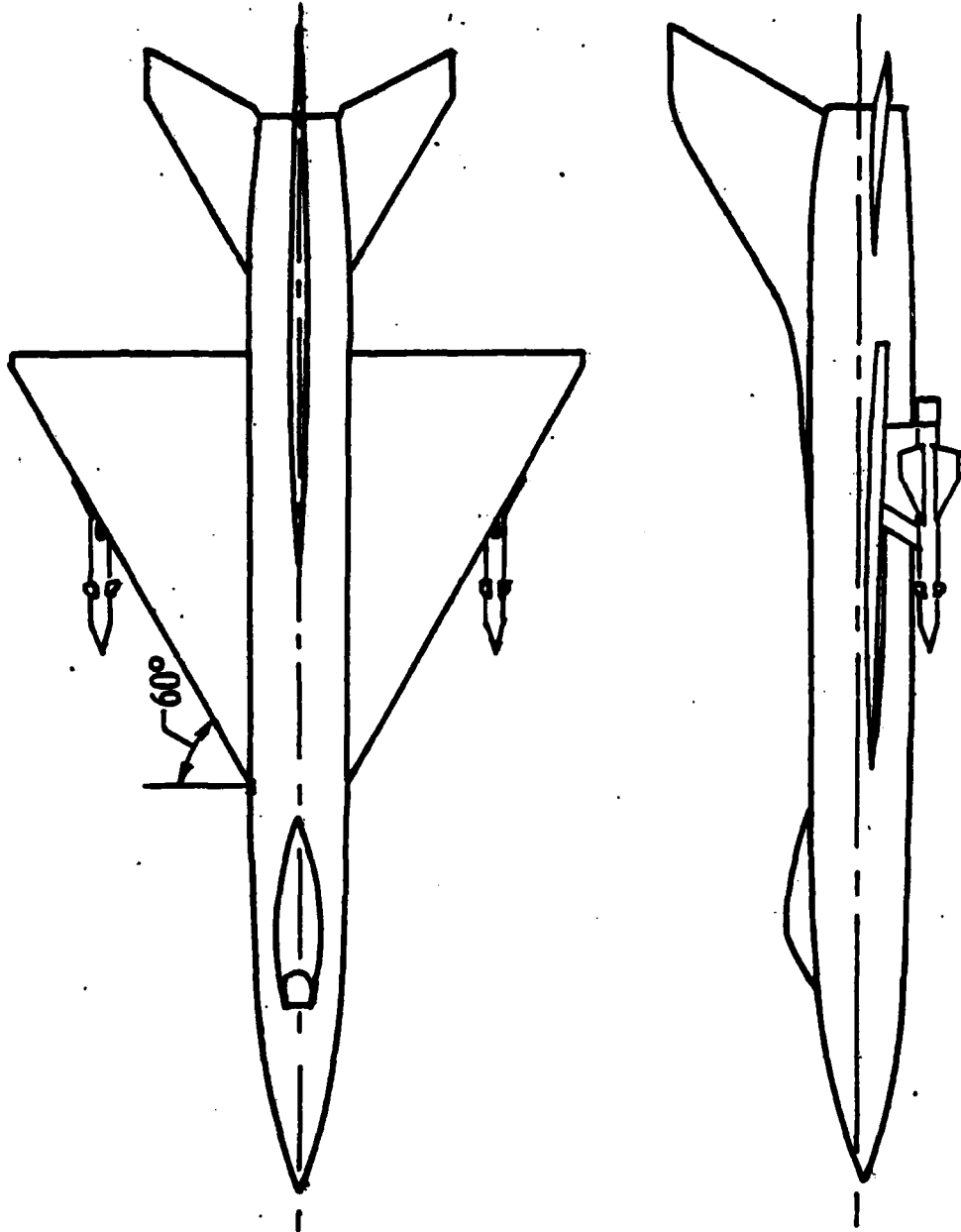
Figure 6. - Delta wing interceptor configuration.
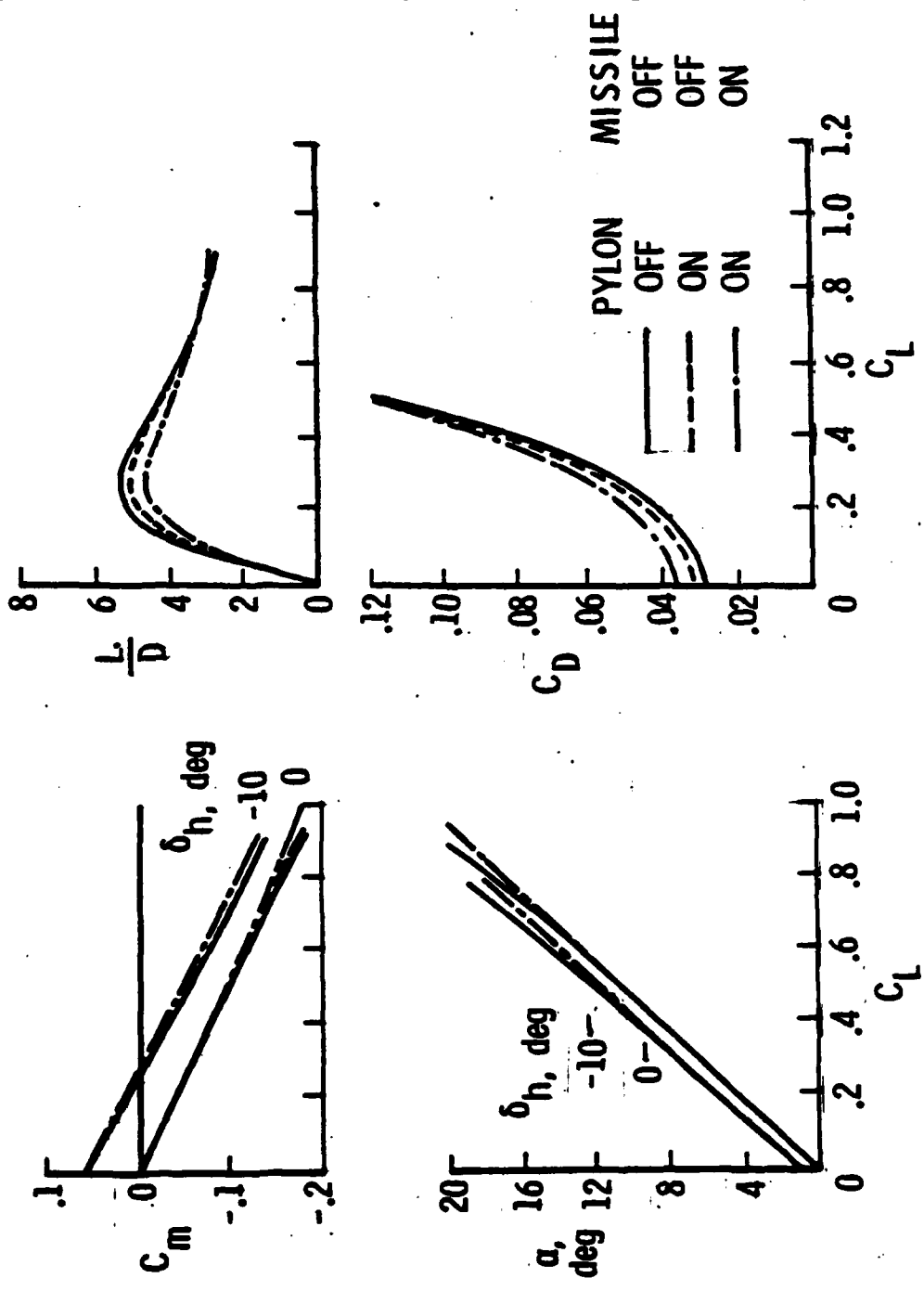
Figure 7. - Longitudinal characteristics for delta wing interceptor at M = 1.60.
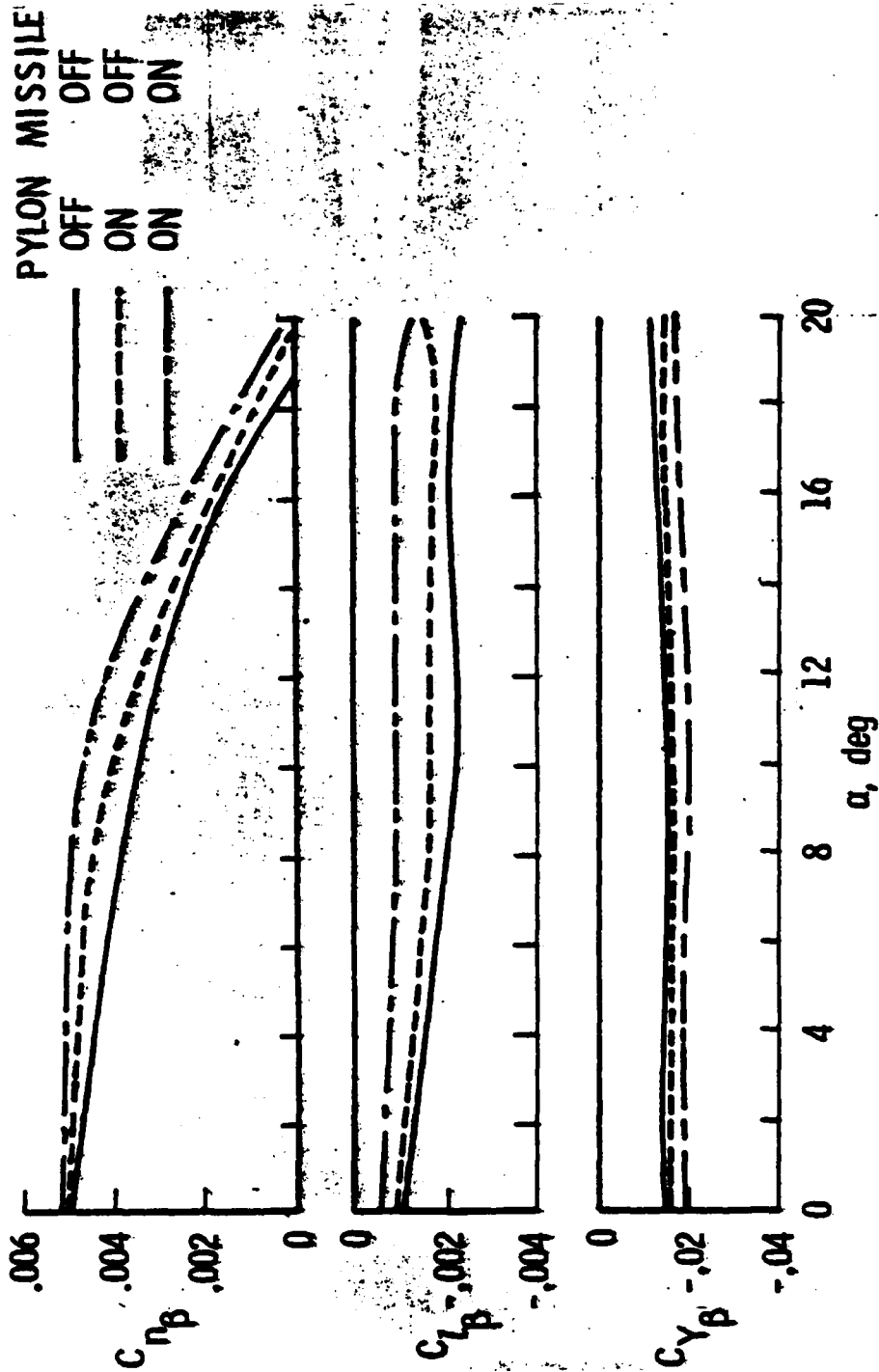
Figure 8. - Lateral characteristics for delta wing interceptor at M = 1.60.

855
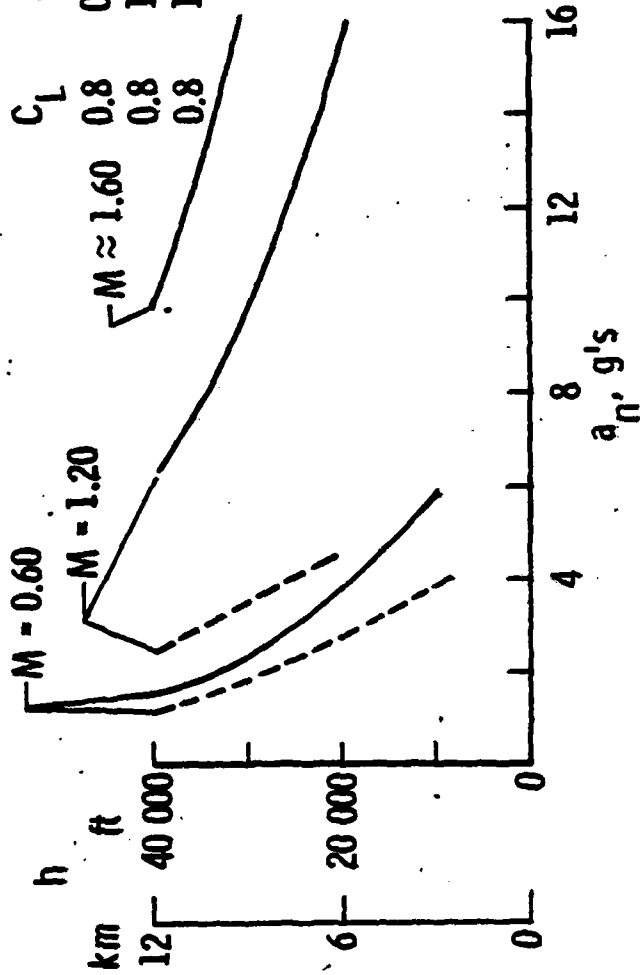
Figure 9. – Normal acceleration characteristics.

more or less obvious that the slower flying fighter would want to descend to low altitudes in order to achieve higher values of a_n.

The supersonic fighter would obviously suffer while maneuvering at lower altitudes due to structural limitations and one-on-one air-to-air combat would eventually tend to degenerate to subsonic speeds even though the combatants may be flying supersonic fighters. These effects can also be translated in terms of turn radius where the combat advantage would generally go to the airplane capable of sustaining a tighter turn. Figure 10 illustrates the effects of a_n and M on the turn radius. The obvious is readily apparent in this nomograph - that is, turn radius can be reduced by increasing a_n for a constant M or by decreasing M for a constant a_n. The illustration shows that, for $a_n = 4$, the M = 0.6 airplane has a turn radius about 3/8 that of the M = 1.2 airplane. For the M = 1.2 airplane to achieve an equivalent radius it would be necessary to increase a_n to about 10. The turn radius for the M = 1.6 airplane would be about 4 times that of the M = 0.6 airplane and the equivalent a_n is completely unrealistic. Also for $a_n = 4$, the M = 1.2 airplane can turn well within the capability of the M = 1.6 airplane and the M = 1.6 airplane would require an a_n of about 6 to become equivalent. It thus appears that air-to-air combat suffers little penalty from store installations at high lift, and that higher speed flight might be reserved for interceptors with long-range missiles where the weapon carriage penalty at low angles of attack are of prime importance.

REFERENCES

1. Spearman, M. Leroy: Some Effects of External Stores on the Static Stability of Fighter Airplanes. NASA TN D-6775, April 1972.

2. Spearman, M. Leroy; and Sawyer, Wallace C.: External Store Effects on the Stability of Fighter and Interceptor Airplanes. NASA TM X-71935, March 1974.
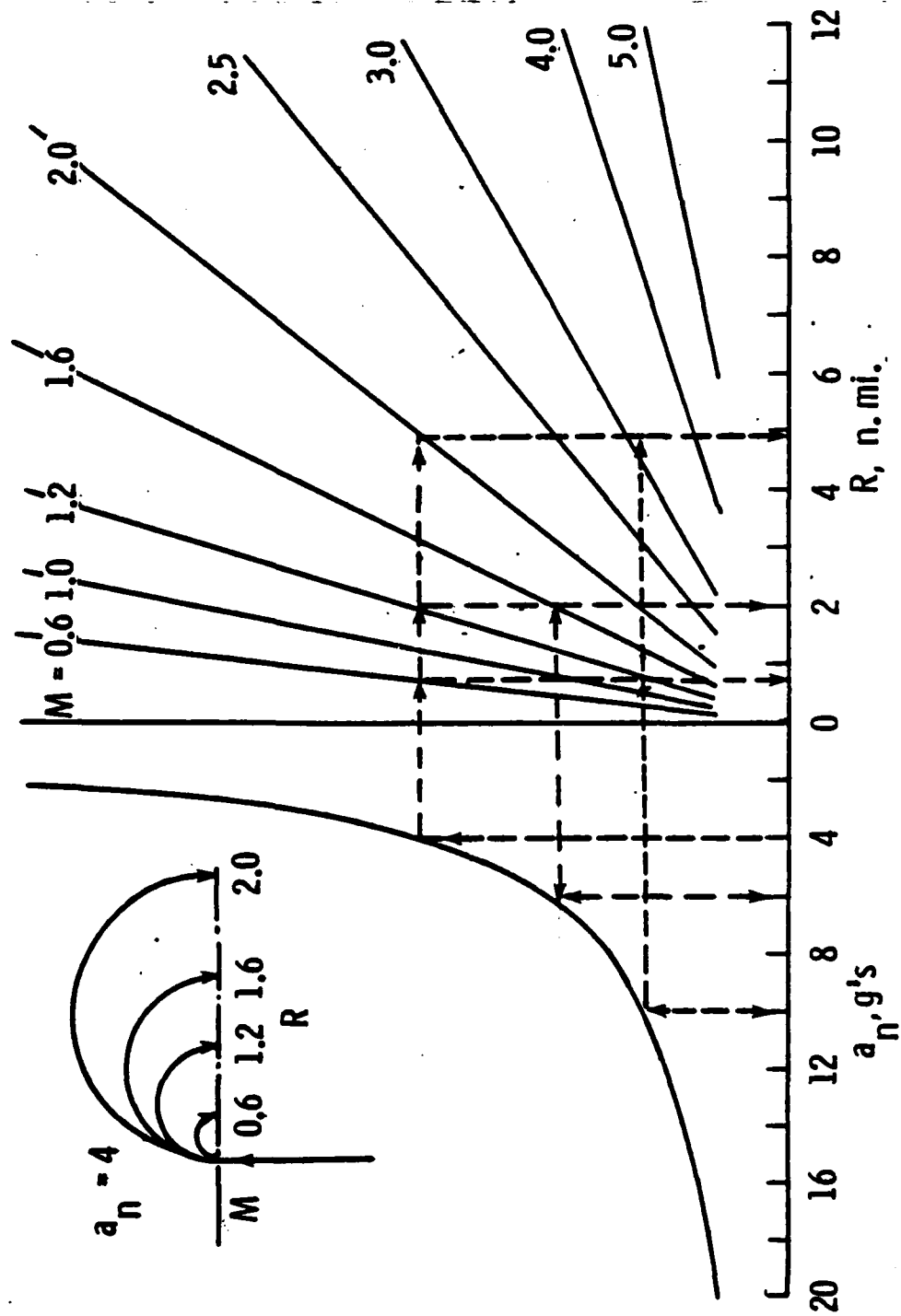
Figure 10. - Turn radius characteristics.

AUTOBIOGRAPHY

M. LEROY SPEARMAN

Graduated from Auburn University in 1943 with a degree in Aeronautical Engineering. Employed for 33 years at the Langley Research Center of the National Aeronautics and Space Administration in the fields of aerodynamics, stability, control, and performance of aircraft, spacecraft, and missiles. Author of 121 NASA technical publications.

Conducted early research studies on the use of sweptback wings for high-speed aircraft; early studies of canard missiles and aircraft; research studies of virtually all U.S. supersonic military airplanes; first supersonic studies of the variable wing sweep concept; investigations of commercial transport aircraft, advanced fighters, missiles, spacecraft, and launch vehicle systems.

Member of the American Institute of Aeronautics and Astronautics, American Defense Preparedness Association, Air Force Association, Engineer's Club of the Virginia Peninsula, American Security Council, and Auburn University Alumni Engineering Council.

Currently Chief Scientist for Military and Foreign Technology, NASA-Langley High-Speed Aerodynamics Division.

WALLACE C. SAWYER

Graduated from Elon College in 1960 with a degree in Physics. Graduate Study at the College of William and Mary and George Washington University Center. Employed for 12 years at the Langley Research Center of the National Aeronautics and Space Administration in Hampton, Virginia. Presently Head of the Concepts Analysis Group in the Supersonic Aerodynamics Branch of the High-Speed Aerodynamics Division. Author of 14 NASA technical publications and developer of analytic computer programs used in predicting characteristics of missile configurations.

Member of the American Institute for Aeronautics and Astronautics; the AIAA Technical Committee for Missile Systems; and the Navy Aeroballistics Committee.

859

(The reverse of this page is blank)

PRESSURE AND HEAT-TRANSFER MEASUREMENTS ON SEVERAL PYLON-MOUNTED STORE CONFIGURATIONS[1]
(U)
(Article UNCLASSIFIED)

by

R. K. Matthews and G. D. Spencer
ARO, Inc., AEDC Division
A Sverdrup Corporation Company
Arnold Air Force Station, Tennessee 37389

and

Maj. J. C. Key, Jr.
Armament Development and Test Center
Air Force Armament Laboratory
Eglin Air Force Base, Florida 32542

ABSTRACT. (U) Wind tunnel pressure and heat-transfer measurements were obtained on several pylon-mounted store configurations in the 40-inch Supersonic Tunnel at AEDC. The test techniques used demonstrated the versatility of scale model testing and provided a comprehensive look at the effects of complex flow fields on store pressure and heat-transfer distributions. The distributions showed that the heating amplification effects of the interference flow field were generally less than might be expected. Correlation of pressure and heat-transfer data are presented, and the significance of outside air temperature is briefly discussed.

LIST OF ILLUSTRATIONS

TABLE

NOMENCLATURE

A_0, A_1 Constants in linear curve fit equation

h Heat-transfer coefficients, $\dot{q}/(T_r - T_w)$, Btu/ft^2-sec-$^{\circ}R$ (or as noted)

L Model length, in.

M_∞ Free-stream Mach number

p Measured surface pressure, psia

p_∞ Free-stream static pressure, psia

$\dot{q}$ Heat-transfer rate, Btu/ft^2-sec

Re_∞/ft Free-stream unit Reynolds number, ft^{-1}

T_0 Tunnel stilling chamber temperature, $^{\circ}R$

T_r Recovery temperature, $^{\circ}R$ (or as noted)

T_w Model wall temperature, $^{\circ}R$

T_∞ Free-stream temperature, $^{\circ}R$ (or as noted)

X Axial distance from store nose, in.

α F-111 model angle of attack, deg

ϕ_{inst} Model instrumentation circumferential location, deg (see Fig. 8)

SUBSCRIPTS

e Conditions at edge of boundary layer

u Conditions in undisturbed (interference-free) flow field

INTRODUCTION

The need for supersonic carriage of stores has been discussed by Epstein (1) and Hume (2). At the 1971 Store Compatibility Symposium, Epstein discussed the somewhat arbitrary restrictions of aircraft performance envelopes with external stores because of temperature constraints. He also elaborated on the complexity of the heating caused by shock impingement and on the need for flight testing because of inadequate ground test techniques. Flight test pressure distributions on a store have been measured (3) and were used to calculate heat distributions; however, this type of testing is very costly.

In 1973, Matthews, et al., documented (4 and 5) the results of wind tunnel test on a 0.05-scale model of a store mounted on an F-4 aircraft. The test technique utilized temperature sensitive thermographic phosphor paint, and produced very vivid thermal mappings of the store heating patterns. Typical photographs from this test are presented in Fig. 1. In addition to these photographs quantitative data were also produced as shown in Fig. 2. The experimental data fairing in this figure is compared to a theoretical heating distribution based on interference-free flow-field calculations. It is common practice to compare undisturbed (interference-free) and disturbed (interference) data since reliable theoretical techniques are not available for complex flow fields. In Fig. 2 the 100-percent increase in heating at $X/L = 0.5$ was attributed to shock impingement from a simulated fuel tank mounted on the outboard pylon. This shock impingement can be seen in the shadowgraph picture presented in Fig. 3 which was also obtained from (4).

The wind tunnel test techniques documented in (4) clearly showed that flight testing was not the only tool available to the engineer responsible for defining store thermal environments. However, this test had several major deficiencies:

1. The photographic technique of defining heating distributions (Fig. 1) was limited to those areas in camera view.

2. The uncertainty of the thermographic phosphor data (±39%) was greater than desired.

3. Existing models were utilized, resulting in configurations which were unrealistic (i.e., F-4 with MK-84's and fuel tanks at $M_\infty = 2.0$).

The test described in this paper circumvented these problems by utilizing heat gages on a model of a store configuration which had previously been flight tested on the F-111 up to Mach 2.5. This flight test was described in (6), and a comparison of wind tunnel and flight test data was presented in (7). This work was part of a project sponsored by the Aircraft Compatibility Branch of AFATL to develop techniques and procedures for defining the thermal environment of stores. The
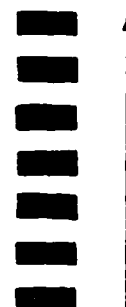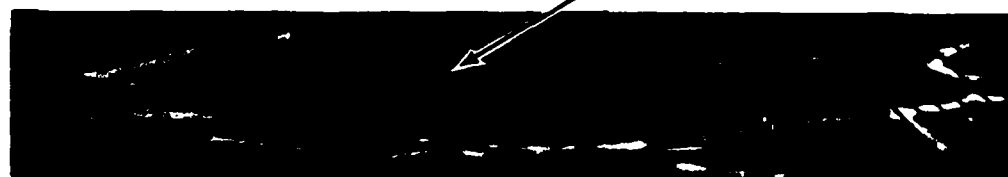
Figure 1 Examples of heating data obtained by thermal
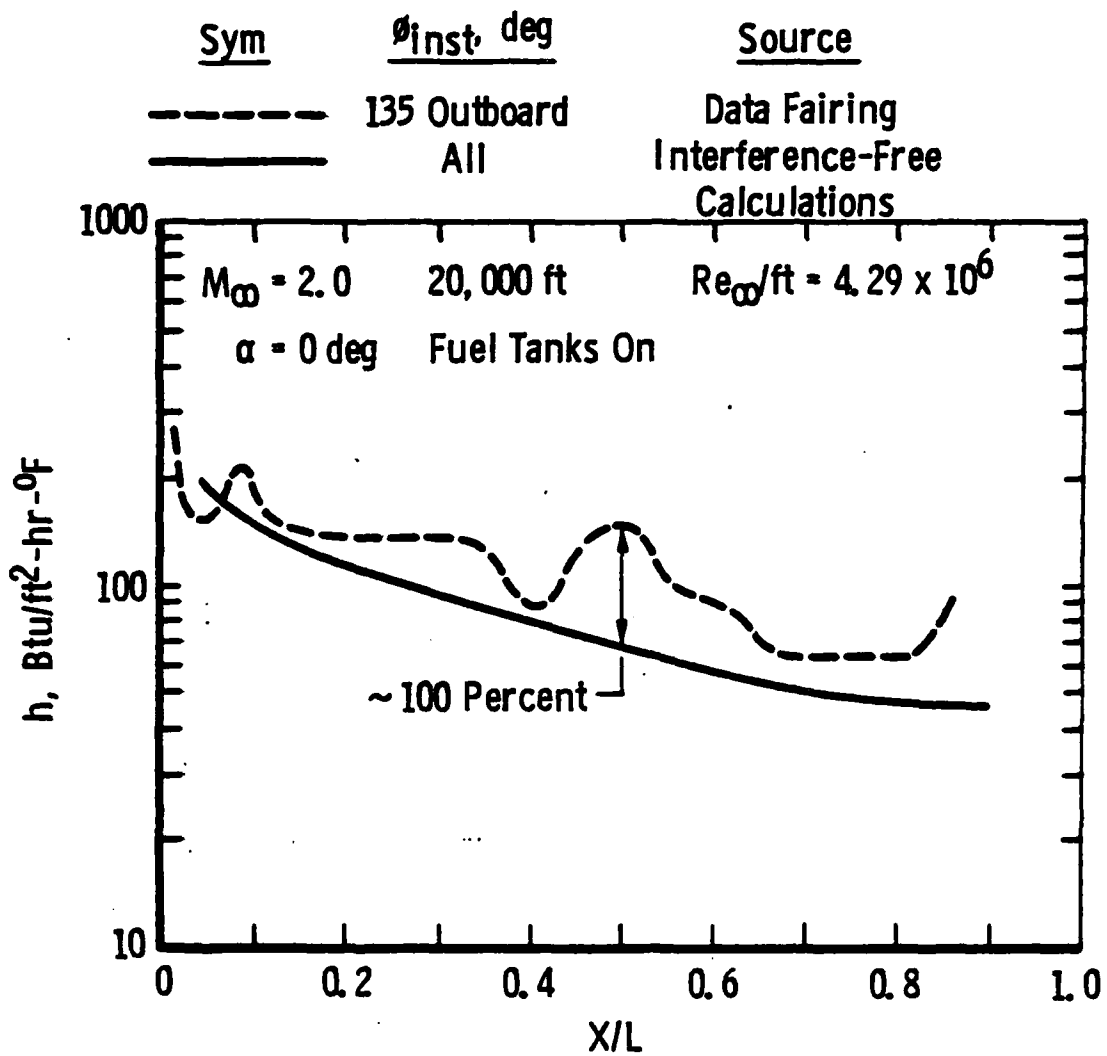mapping techniques (from Ref. 4)

Figure 2 Comparison of data fairing with interference-free calculations (from Ref. 4)

Figure 3 Shadowgraph illustrating shock
impingement (from Ref. 4)

present paper will describe the test techniques and the major results of the wind tunnel phase of this project.

APPARATUS

WIND TUNNEL

Tunnel A (Fig. 4) is a continuous, closed-circuit, variable density wind tunnel with an automatically driven flexible-plate-type nozzle and a 40- by 40-in. test section. The tunnel can be operated at Mach numbers from 1.5 to 6 at maximum stagnation pressures from 29 to 200 psia, respectively, and stagnation temperatures up to 750°R (M_∞ = 6). Minimum operating pressures range from about one-tenth to one-twentieth of the maximum at each Mach number. The tunnel is equipped with a model injection system which allows removal of the model from the test section while the tunnel remains in operation. A description of the tunnel and airflow calibration information may be found in (8).

MODELS

The parent aircraft used for this wind tunnel test program was a 1/15th-scale model of the F-111 which was provided by General Dynamics, Fort Worth. This model was originally intended for side wall mounting (i.e., half-span model); however, for the current test it was important to sting mount the model and utilize the model injection system described above. To provide sting mounting and to better duplicate the F-111 flow a model support and nose section were fabricated to simulate the right side of the fuselage. Figure 5 shows the model injected into the Tunnel A test section. The store mounted on the inboard pylon is a 1/15th-scale model of the BDU-12. A close-up picture of this store (Fig. 6) clearly shows the heat gages along the model axis and inspection of the nose region shows the grit distributed around the nose. This type of grit is commonly used in wind tunnel testing to produce a turbulent boundary layer. A unique feature of the BDU models used during this test was the capability to roll the models 360 deg about their axis while mounted to the pylon. This feature was incorporated in the design so that the heat gages could be rolled into any position. With this capability, data could be obtained on the inboard side of the store, thereby circumventing the shortcoming of the photographic test technique previously used (i.e., deficiency No. 1 in the Introduction).

In addition to the BDU model shown in Fig. 6, three other store models were fabricated:

1. Second BDU heat gage model
2. BDU pressure model
3. GBU-8 heat gage model

A photograph of the two heat gage models mounted on the F-111 is presented in Fig. 7. Because of its geometry the GBU-8 model was limited to the discrete roll positions of 0 and 180 deg. However, heat gages
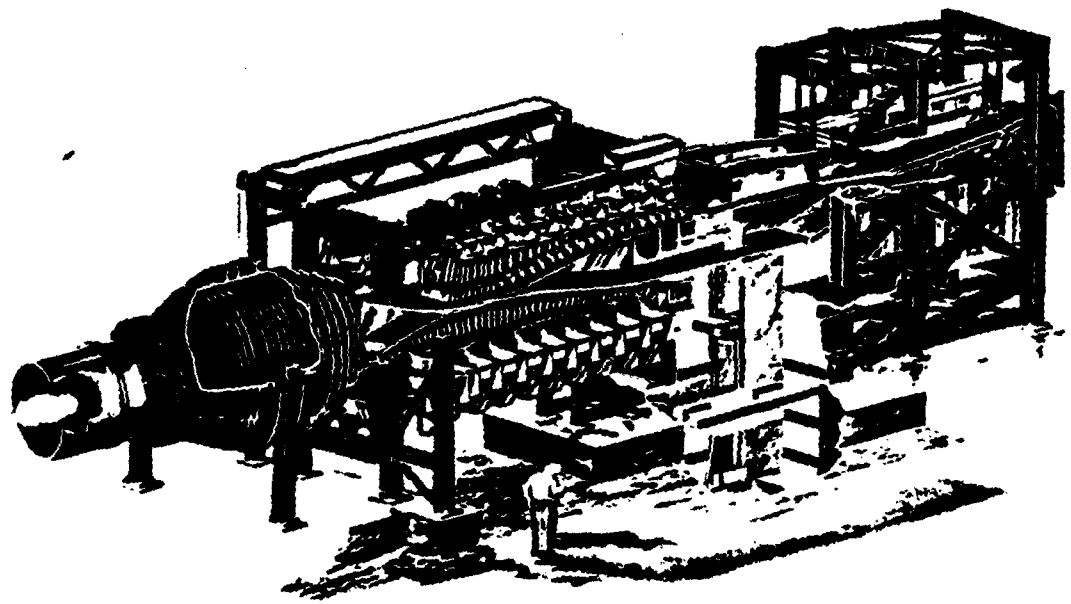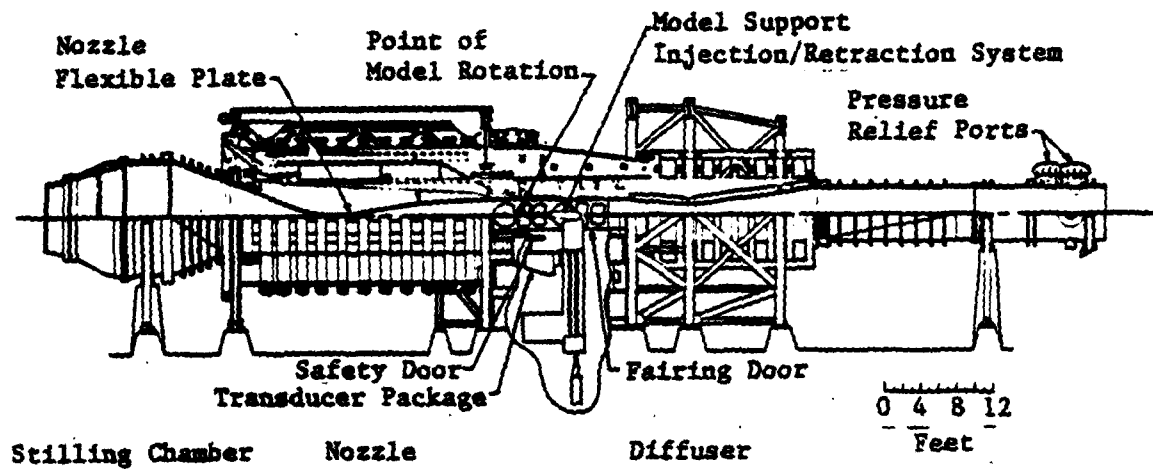
868

Figure 4 Tunnel A assembly

869

Figure 5 Photograph of 1/15 scale model of F-111 and BDU-12 in Tunnel A test section
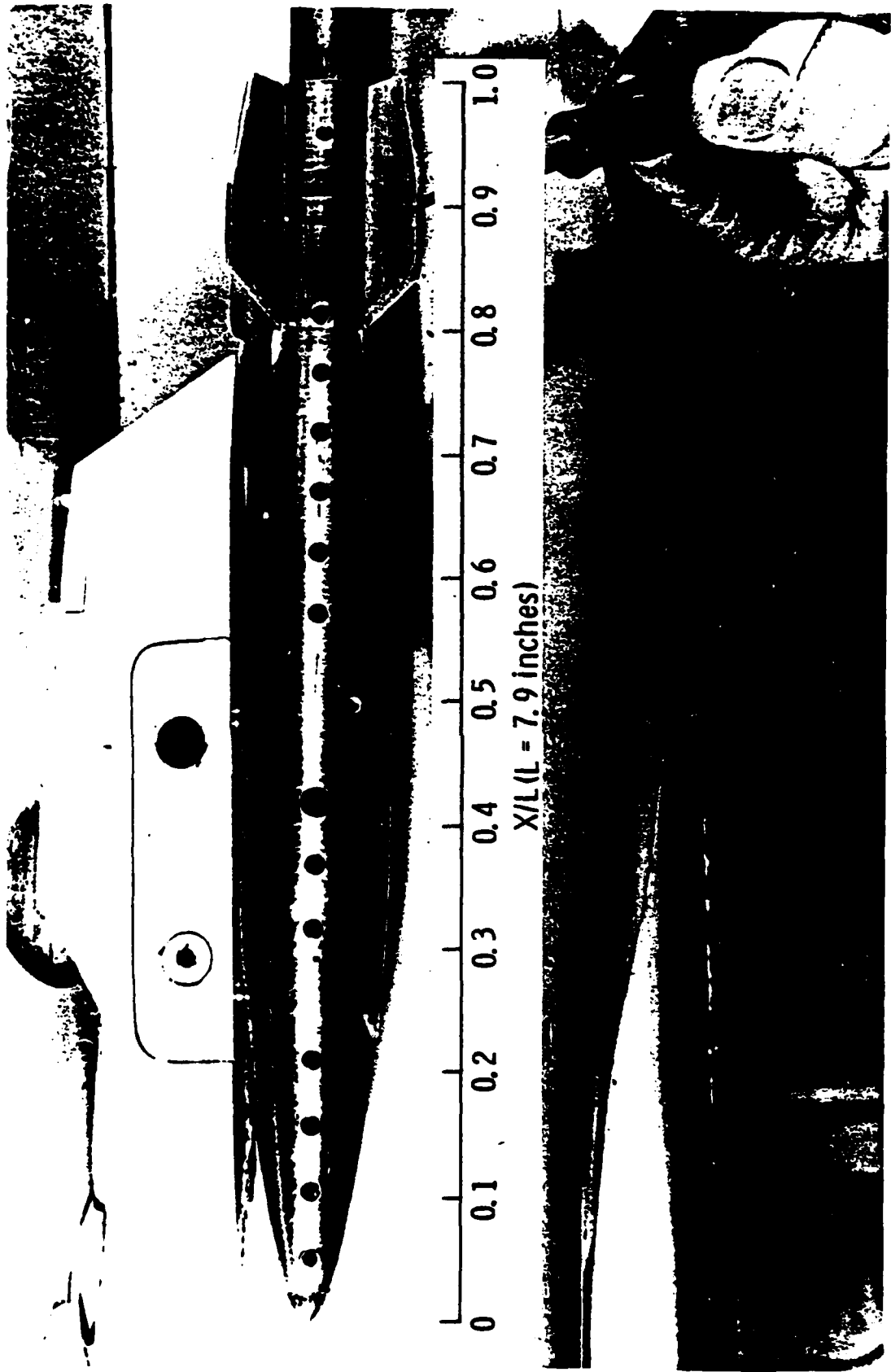
X/L (L = 7.9 inches)

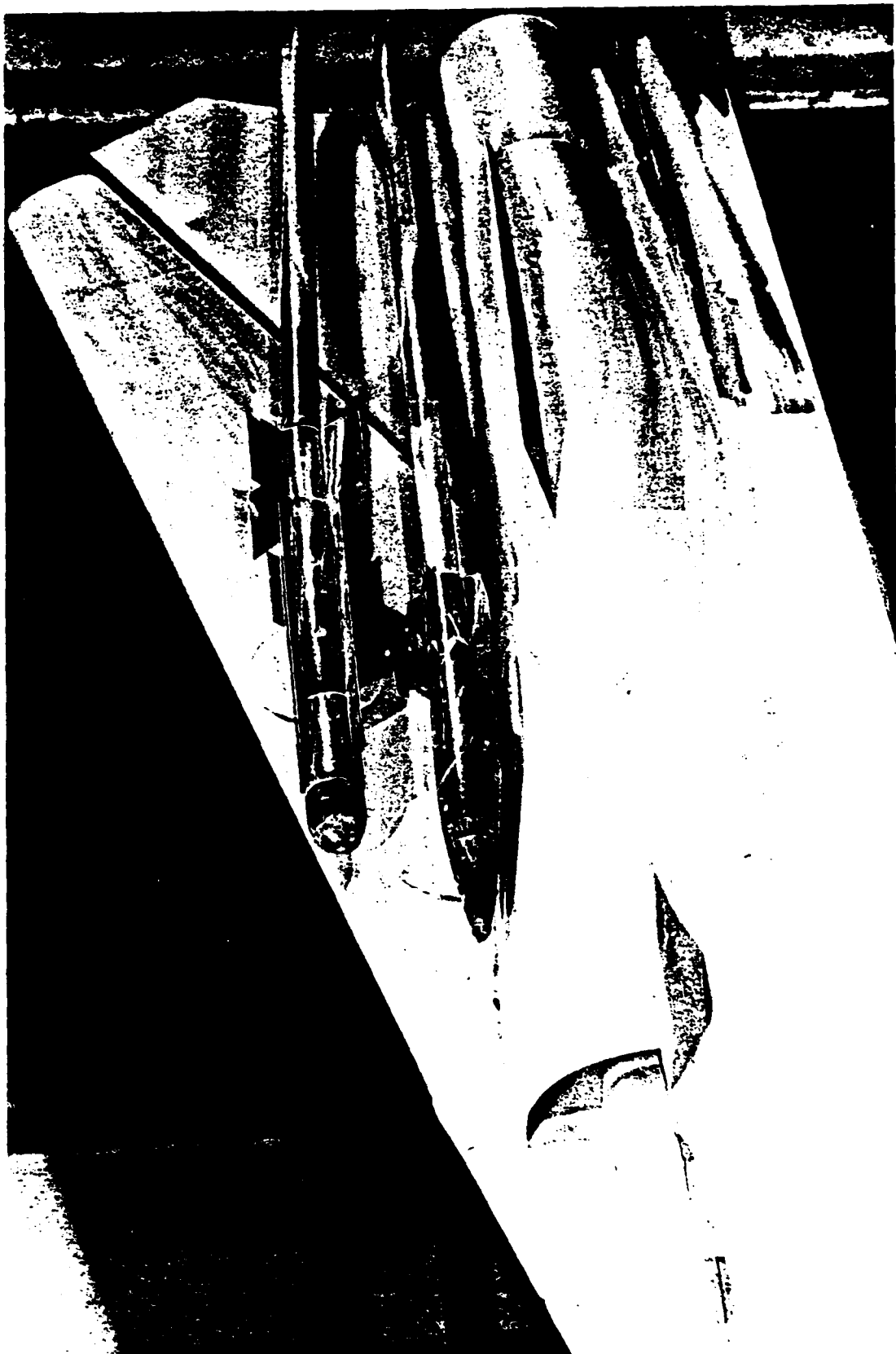Figure 6 Photograph of heat gage BDU model

Figure 7 Photograph of GBU (outboard) and BDU (inboard) in carriage position on F-111 model

were installed at three circumferential positions (ϕ_{inst} = 22.5, 90, and 157.5 deg). Thus, by rolling the model 180 deg the gages were positioned at three more locations (ϕ_{inst} = 202.5, 270, and 337.5 deg).

By utilizing the store roll capability just described and by interchanging the store-mounting position, a large amount of store interference data was obtained. The specific configurations tested are illustrated in Fig. 8.

PROCEDURES

The test was conducted at Mach numbers of 1.76, 2.0, and 2.5. The free-stream unit Reynolds number ranged from 2.7 to 5.2 million per foot. A summary of the specific test conditions for each configuration is presented in Table I.

The tunnel stilling chamber conditions and the BDU pressure data were measured with the standard Tunnel A pressure system which is described in (8). The heat-transfer data were obtained with gages designed, fabricated, and calibrated at AEDC.

During a typical heat-transfer run the model was injected into the airstream at a relatively cool initial temperature and held at a fixed position while the store was heated. Each gage measured both a heating rate, $\dot{q}$, and a "wall" temperature (T_w) during the heating cycle. An example illustrating the repeatability of these basic measurements is presented in Fig. 9. To convert these measurements from heating rate, $\dot{q}$, to heat-transfer coefficient, h, the definition of heat-transfer coefficient was used as illustrated below:

$$h \equiv \frac{\dot{q}}{T_r - T_w}$$
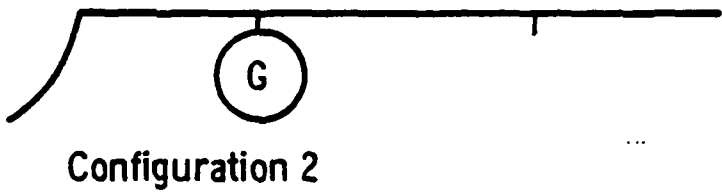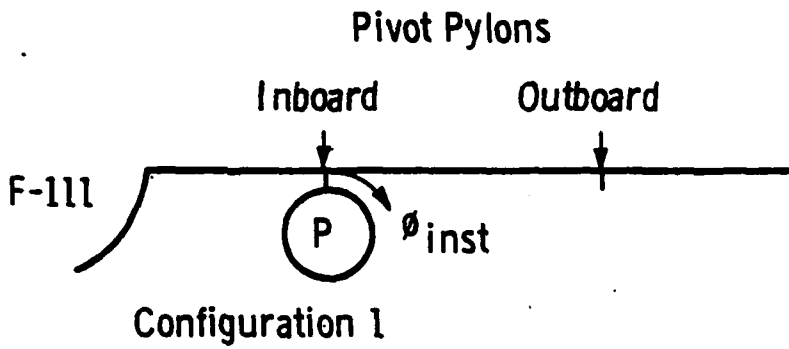
or rearranging,

$$\dot{q} = hT_r - hT_w$$

But since h and T_r are approximately constant for a given gage we have an equation of the form

$$\dot{q} = A_0 + A_1 T_w$$

where

$$A_0 \equiv hT_r \text{ and } A_1 \equiv -h.$$

Therefore the slope of the data presented in Fig. 9 is identical to the negative of the heat-transfer coefficient. This same technique was used in the data reduction of the flight test data (6).
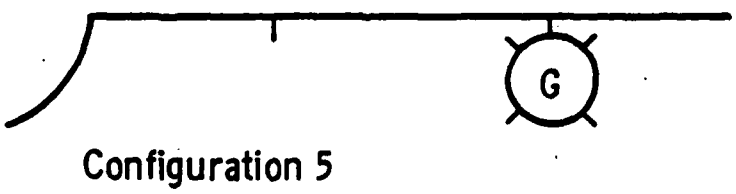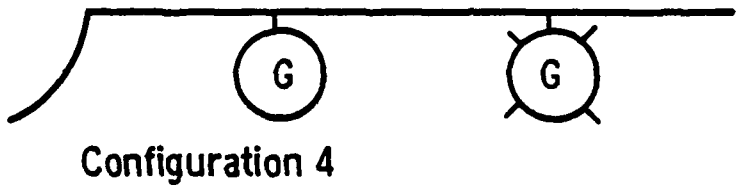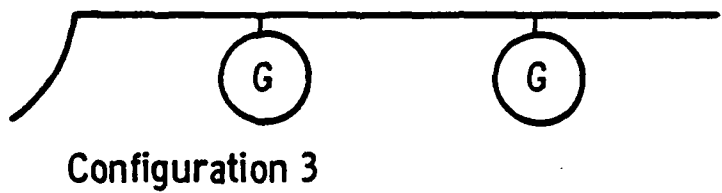
873

Figure 8 Configurations tested

Table I Test Summary

Configuration	Type Data	Mach	$Re_\infty/\text{ft} \times 10^{-6}$	Pitch, α, deg	ϕ_{inst}, deg
BDU (un-disturbed)	Heat-Transfer	1.75	3.8	0	N/A
		2.0	1.5, 2.8, 4.2	0, 2, 4, 6	
		2.5	5.0	0	
GBU (un-disturbed)	Heat-Transfer	1.75	3.9	0	0 → 360
		2.0	1.4, 2.3, 4.2	0	
		2.5	5.1	0	
1	Pressure	1.75	3.8	0, 1, 2, 4, 6	0 → 360
		2.0	4.3	0, 1, 2, 4, 6	
		2.5	5.2	4	
2	Heat-Transfer, Oil Flow*	1.75	3.8	1, 4	0 → 360
		2.0	2.8, 4.2	0, 1, 2, 4, 6	
		2.5	5.1	0, 4	
3	Heat-Transfer	2.0	1.4, 2.4, 4.2	0, 4	
4		2.0	1.4, 4.2	0, 4	
		2.5	5.1	0, 4	
5		2.0	4.1	0, 4	
		2.5	5.1	0, 4	

*Tested at each Mach number with α = 4 deg and ϕ = 105 deg only
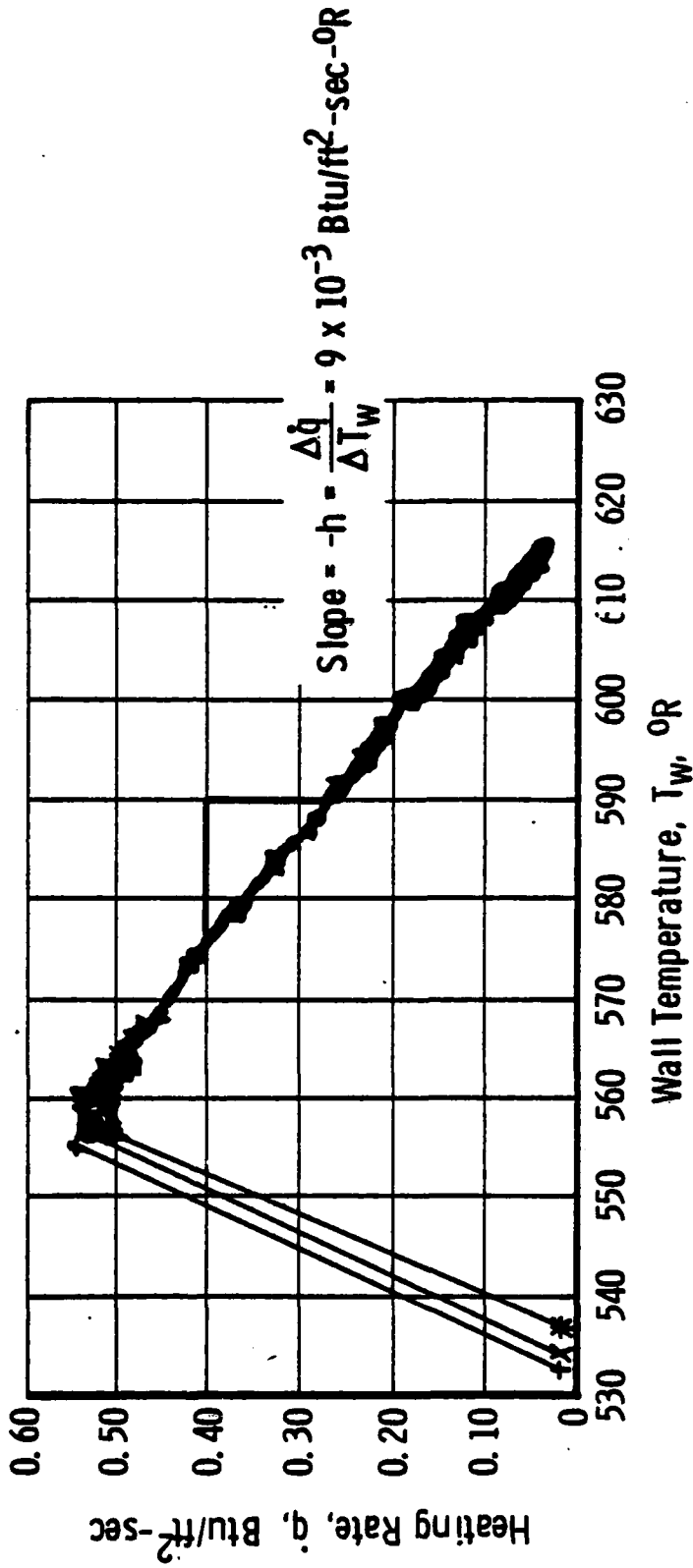
Figure 9 Illustration of heat gage data reduction technique

RESULTS AND DISCUSSION

As noted in the test summary (Table I), a very large volume of data was obtained during these tests. In this paper, only selected results will be presented; however, a more comprehensive report will be published in the near future.

Before presenting the interference heating data it is important to establish reference heating distributions. The reference level normally used is an undisturbed or interference-free value and can be based on theoretical calculations or experimental measurements. In the present case experimental measurements were used. An illustration of the $\alpha = 0$, "undisturbed" data used for the BDU is presented in Fig. 10. These data were obtained with the same model that was used for the "disturbed" data obtained with the model mounted in the interference flow field of the F-111. For X/L > 0.3 the data fairing shows good agreement with turbulent theoretical calculations based on the method of Spalding and Chi. For X/L < 0.3 the data fairing exhibited the "classical overshoot" of a transitional boundary layer. This figure demonstrates that the grit affixed to the BDU nose (see Fig. 6) was indeed effective in producing a turbulent boundary layer on this relatively small model (1/15th scale). In addition to substantiating that the grit produced a turbulent boundary layer, this figure also indicated the general data quality. Although the data quality may not be as good as desired, it is significantly better than the ±39% obtained with the thermal mapping technique (Ref. 4).

It is also important to note that the data and theory of Fig. 10 are for an angle of attack of 0 deg, whereas the remainder of the data in this paper correspond to a 4-deg angle of attack. This was done to simplify the theoretical computations[2] and to provide one reference value for the interference data at any angle of attack. Similar undisturbed reference data were also obtained for the GBU model.

Comparison of the measurements from the F-111 pylon-mounted stores with those of the undisturbed case provides an "amplification factor" which quantifies the increase (or decrease) in heating caused by the severe interference generated by the parent aircraft and the pylon. These amplification factors are simply the ratio of the heating rates at a given model location. That is,

$$AF \equiv h/h_u = \left(\frac{\text{heating measured with pylon mounting}}{\text{heating measured in undisturbed flow}}\right)_{\text{each gage}}$$

Typical data showing the magnitude and circumferential distribution of the amplification factors (h/h_u) for the various configurations

---

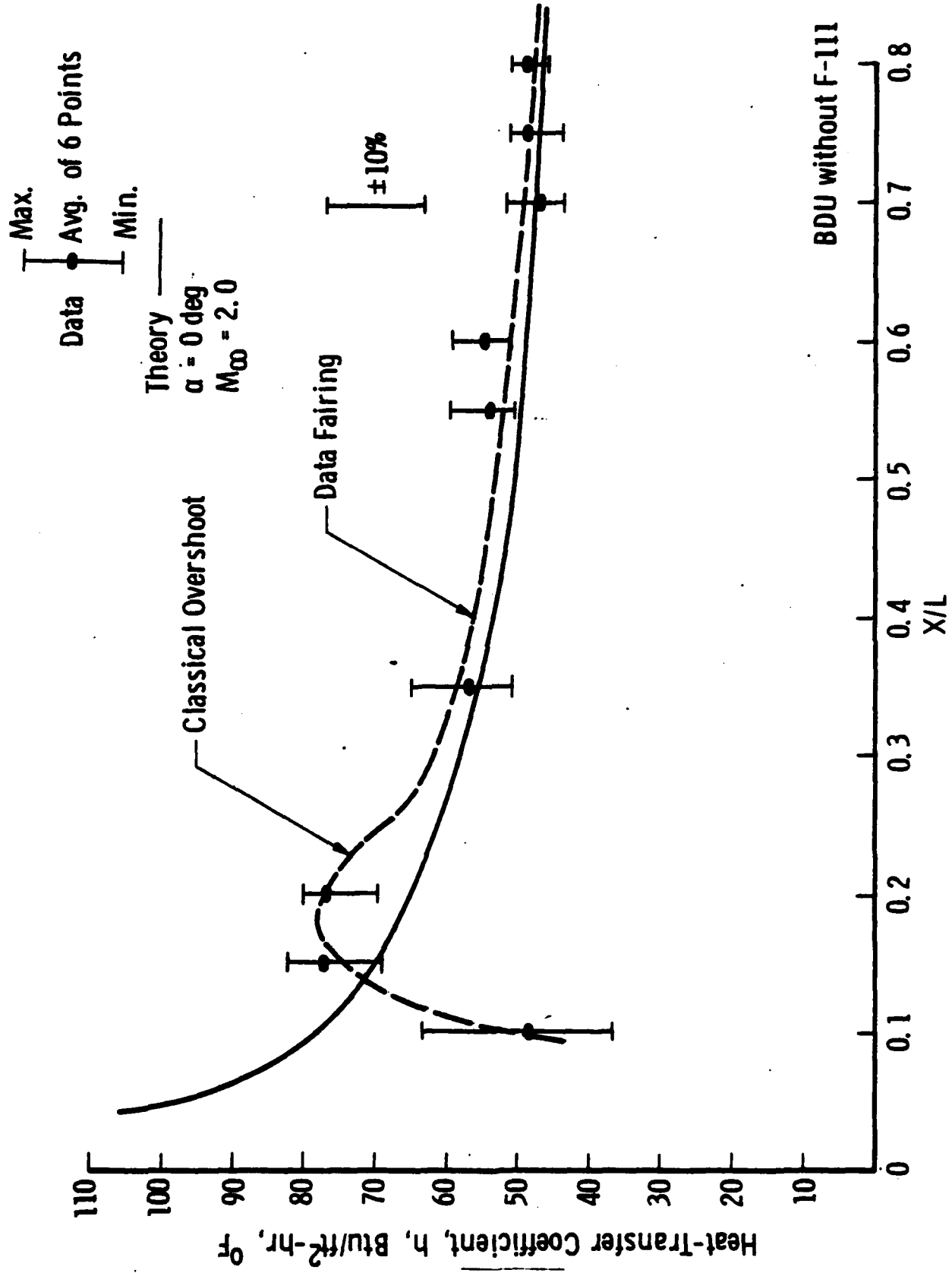[2]Theoretical calculation for $\alpha \neq 0$ are more complex and are less precise.

Figure 10 Undisturbed (interference-free) heat distribution on BDU model

tested are presented in Figs. 11a through f. The solid symbols in Fig. 11 illustrate the good data repeatability.

It is important to notice that almost all the data are below 1.5 and that a large percentage of the data are below 1.0. This statement is true for all the data obtained during this test and is not limited to the relatively small amount present in this paper. In the past there has been a general fear that interfering flow fields produced large amplification factors, and this may still be true for small localized areas. However, the present data show that the interference heating at $\alpha = 4$ deg was within $\pm 50\%$ of that for an undisturbed flow field at zero angle of attack. This means that, for engineering purposes, store thermal environments can be estimated based on undisturbed flow-field calculations at zero angle of attack.

Circumferential pressure distributions for Configuration 1 are presented in Fig. 12. This was the only configuration on which pressure measurements were obtained. The number of instrumented locations was limited[3] because of the relatively larger size of pressure tubing as compared to the electrical wires for the heat gages. Figure 12 also shows theoretical levels based on the method of characteristics for an undisturbed flow field. It is interesting to note that the experimental pressure data at $X/L = 0.15$ are above the theoretical value (1.14), whereas at $X/L = 0.35$ the experimental data are below the undisturbed value (0.92).
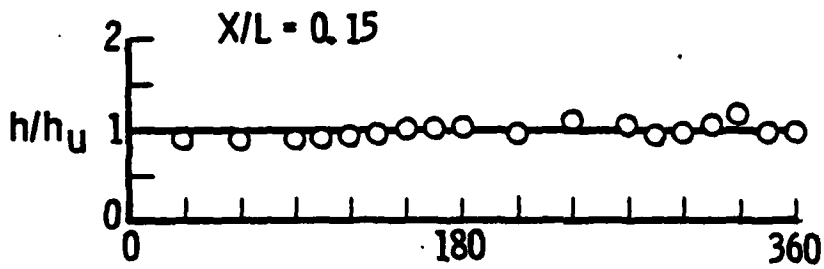
In (3) Van Aken and Markarian used pressure data to predict heating distributions by applying a correlation equation of the form

$$ h/h_u = \left[\frac{(p/p_\infty)}{(p/p_{\infty_u})} \right]^{0.85} $$

The pressure distributions presented in Fig. 12 were substituted into this equation to give the interference heating predictions shown in Fig. 13. These predicted heating distributions are compared to the present experimental heat-transfer measurements and in general the data correlation was within 20%.

This paper has been directed toward defining aerodynamic heat-transfer coefficients for pylon-mounted stores since this parameter is fundamental in the analyses of store transient heating. However,

---

[3]This 1/15th scale pressure model had a total of eight tubes installed as opposed to 26 heat gages in the same size heat model.
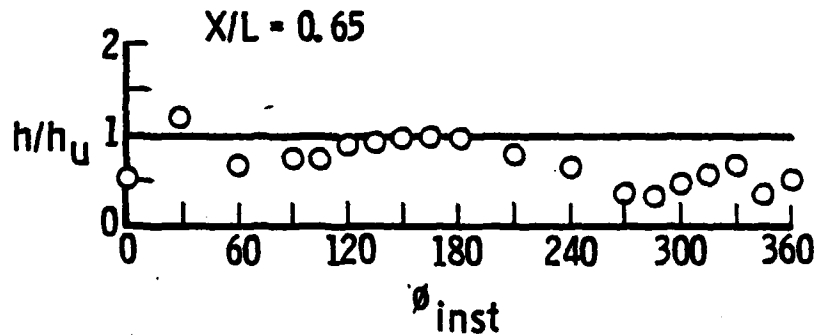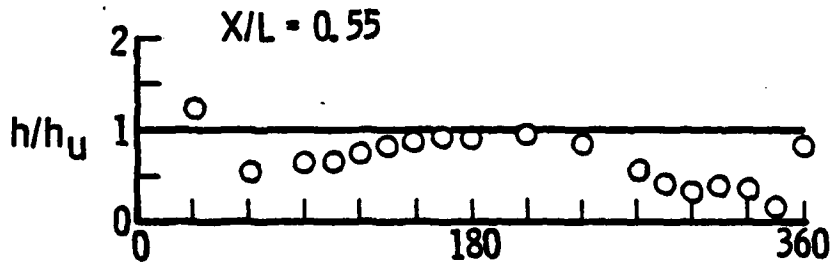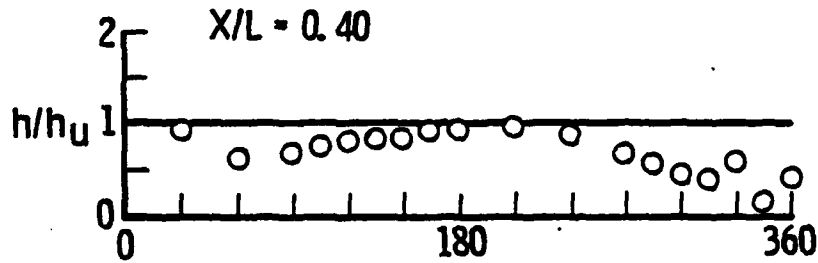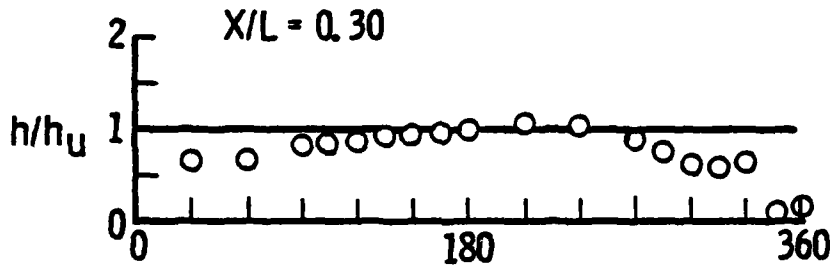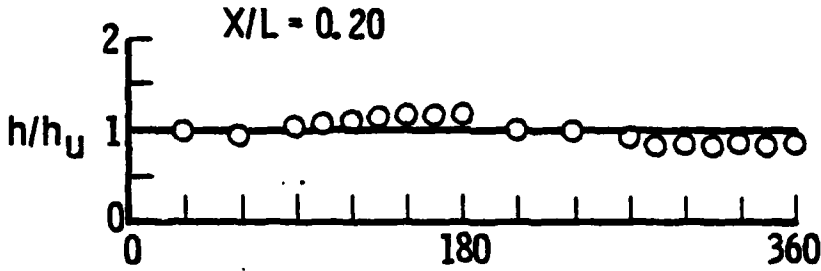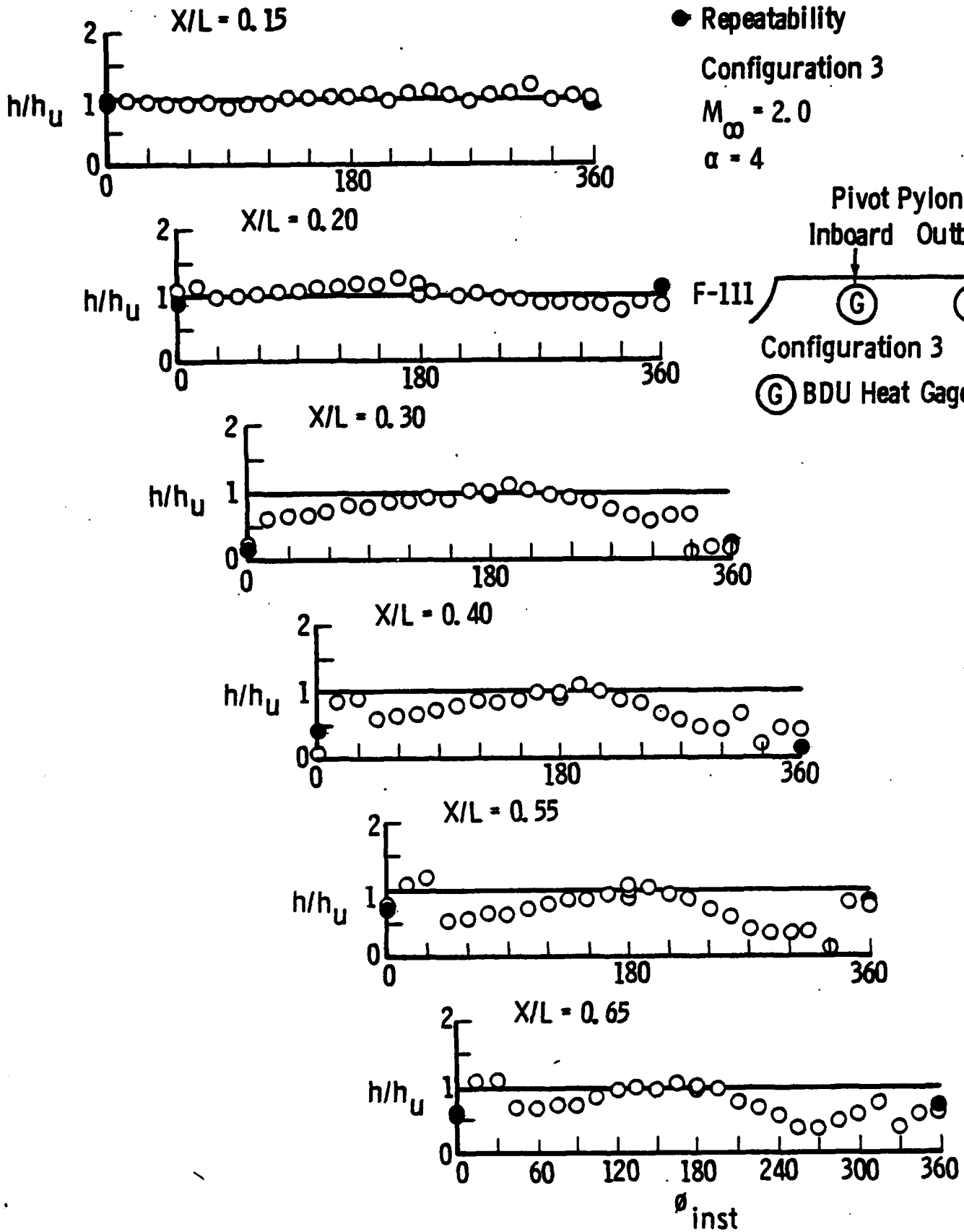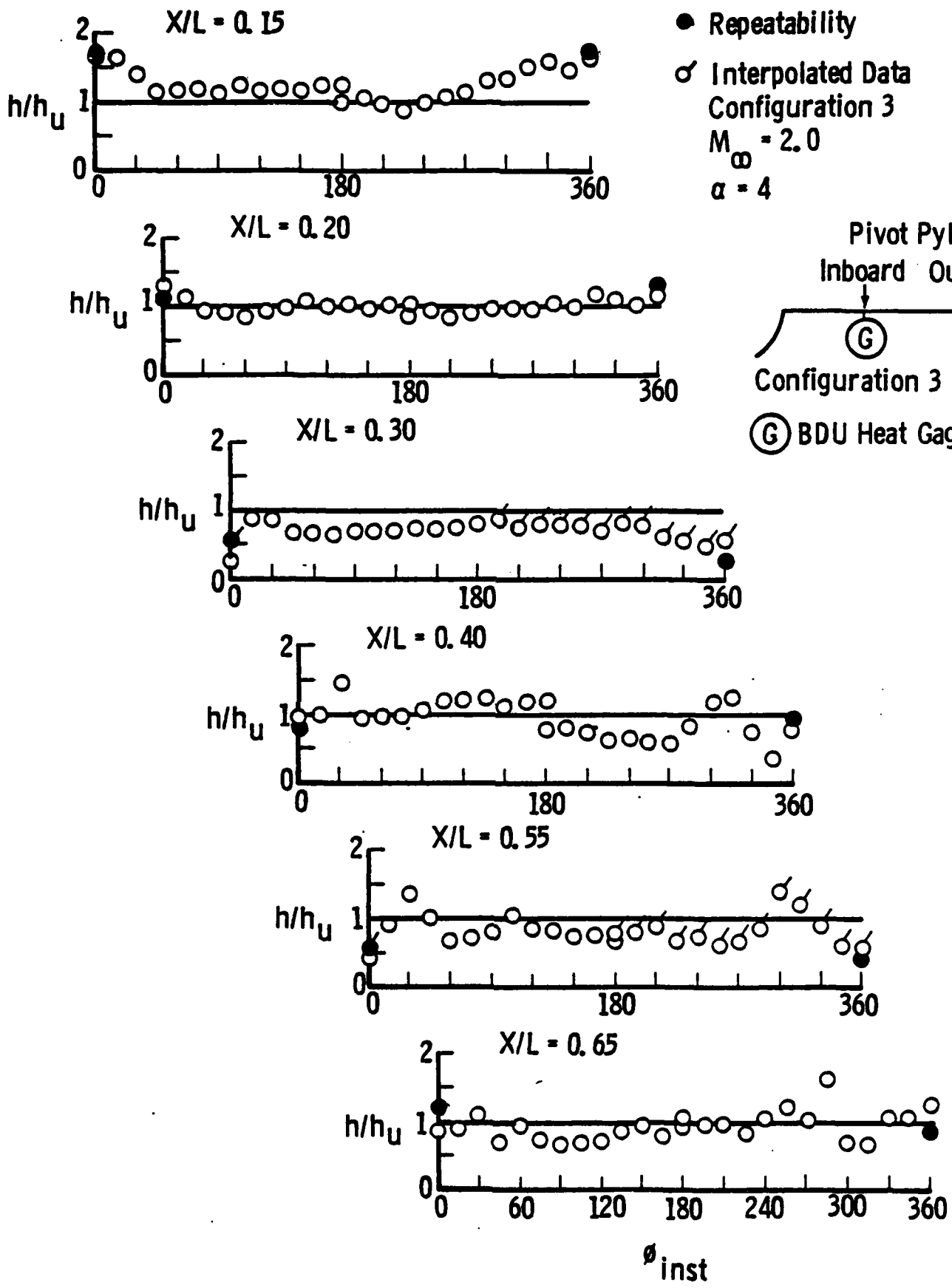
a. Inboard BDU

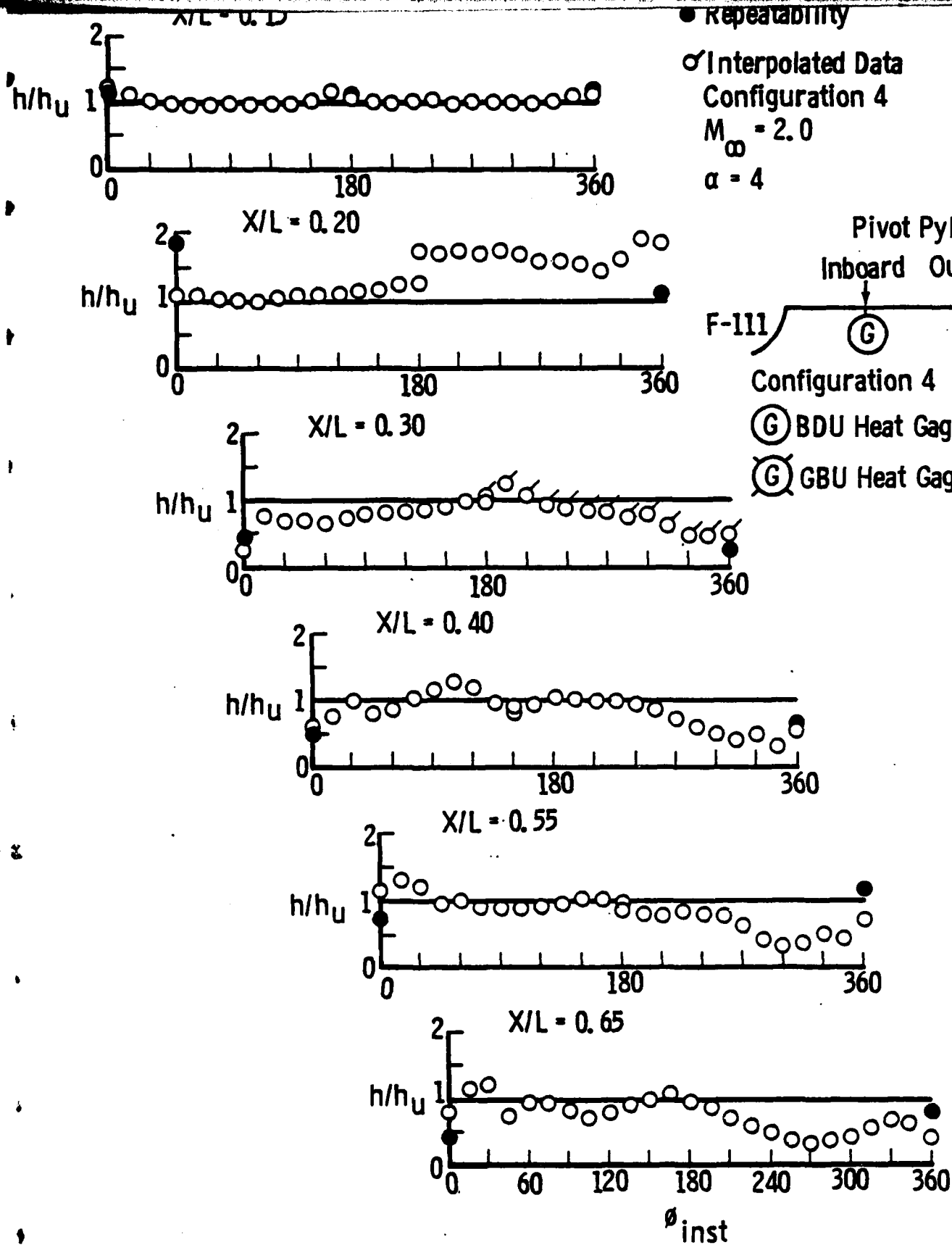Figure 11 Circumferential heating distributions on store models

b. Inboard BDU with BDU on outboard pylon
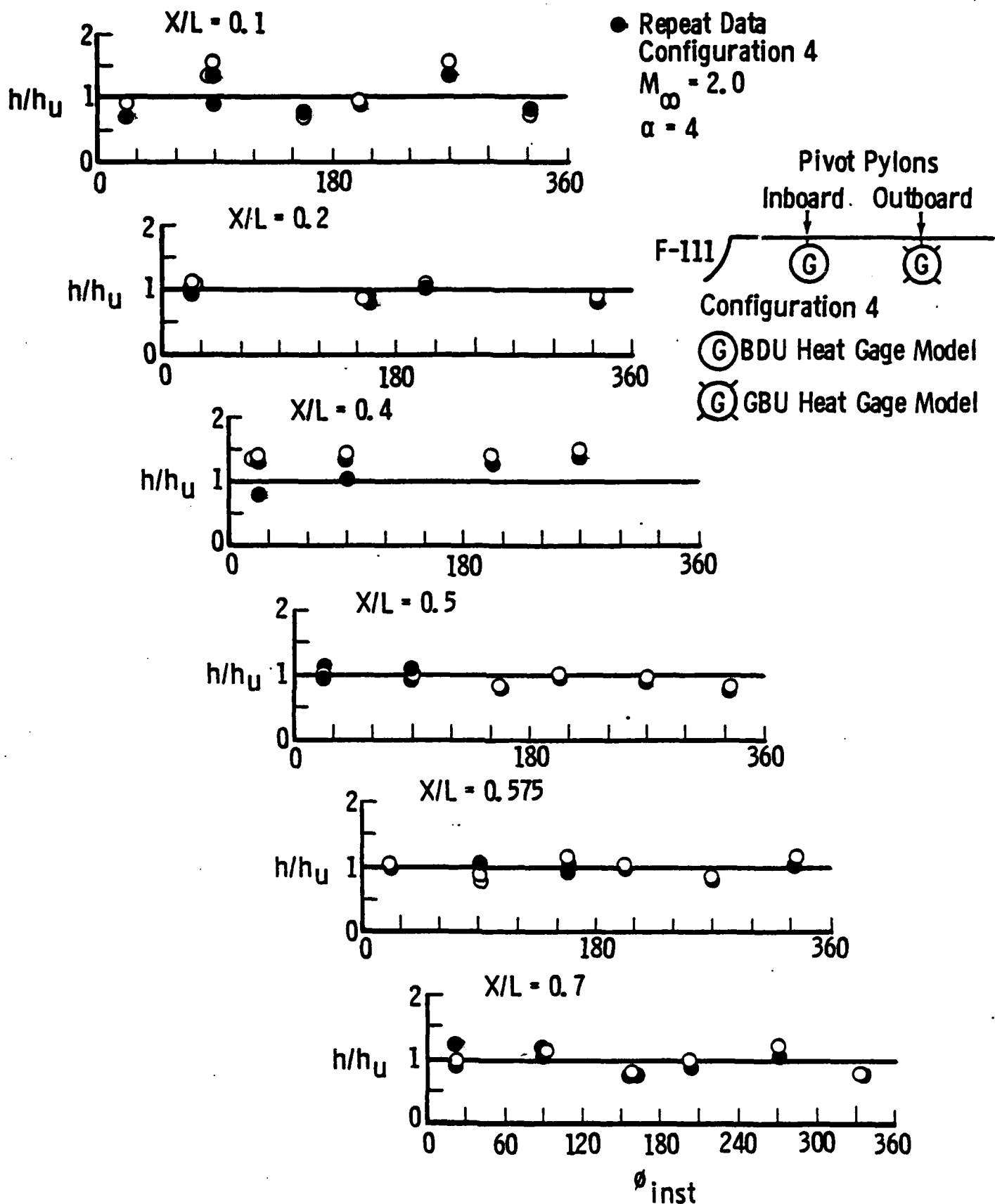
Figure 11 Continued

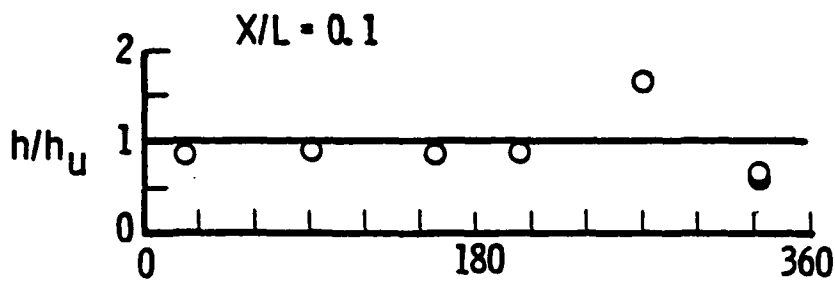c. Outboard BDU with BDU on inboard pylon

Figure 11 Continued

d. Inboard BDU with GBU on outboard pylon

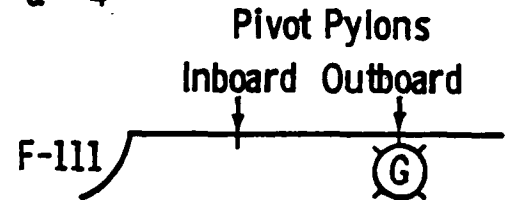Figure 11 Continued

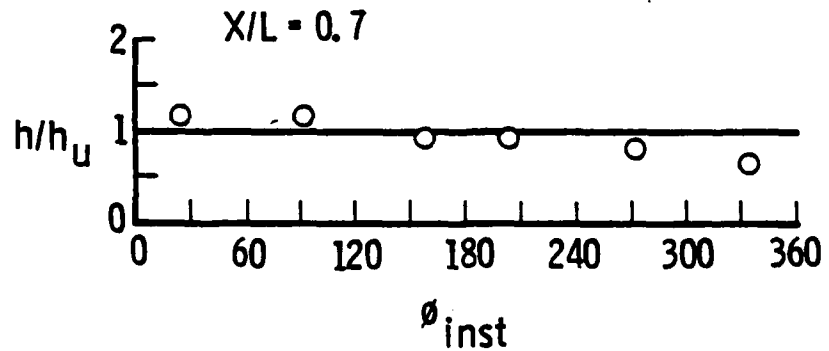e. Outboard GBU with BDU on inboard pylon

Figure 11 Continued
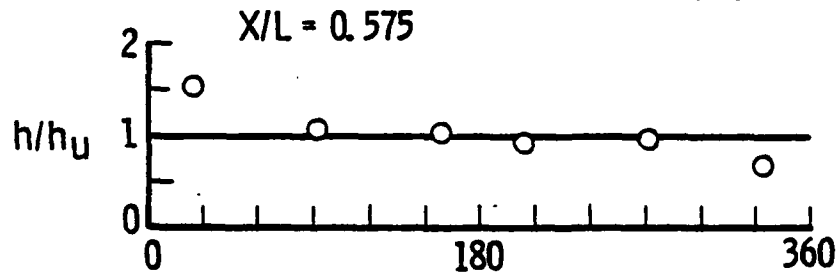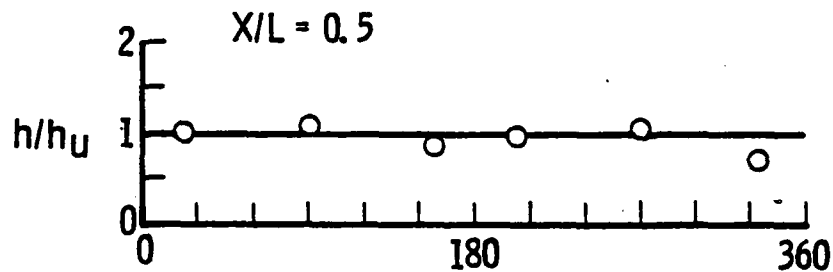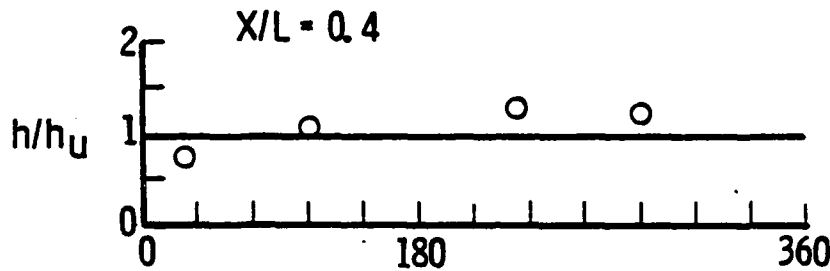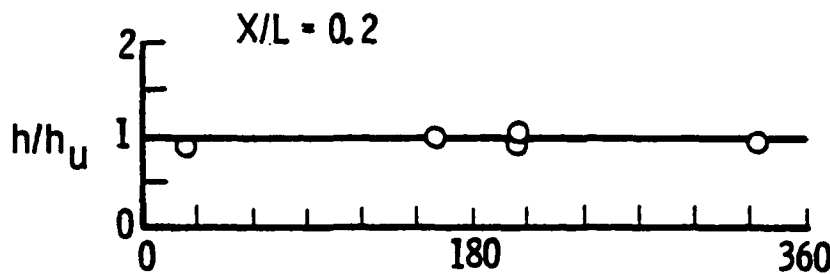
f. GBU on outboard pylon

Figure 11 Concluded
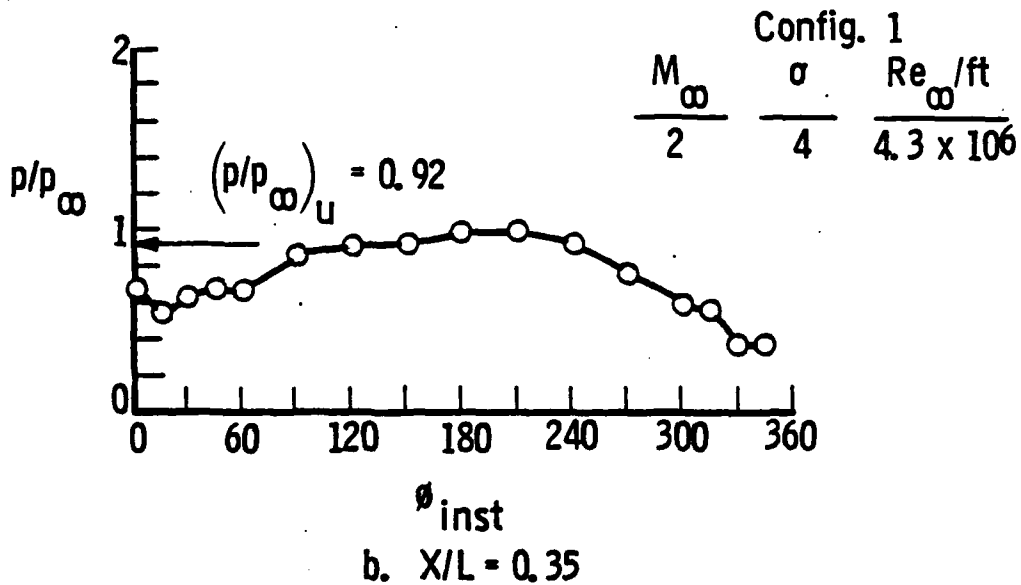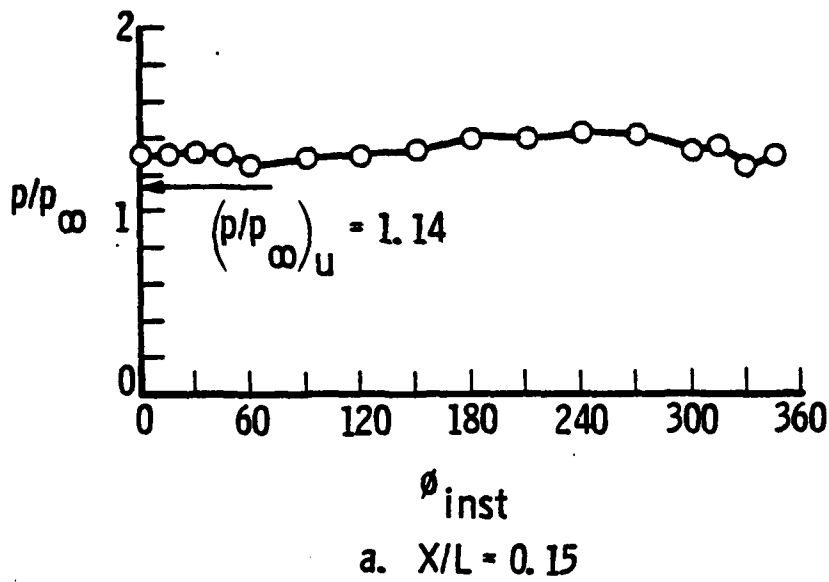
a. X/L = 0.15

b. X/L = 0.35

Figure 12 Circumferential pressure distributions on BDU model
mounted on inboard pylon

Config.	M_∞	α	$Re_\infty \times 10^{-6}$
2	2.0	4	4.1

Sym	Source
—☐—	Present Heat-Transfer Data
– – –	Correlation Equation

$$h/h_u = \left[(p/p_\infty) \middle/ (p/p_\infty)_u \right]^{0.85}$$

(Fig. 12 Pressure Data)
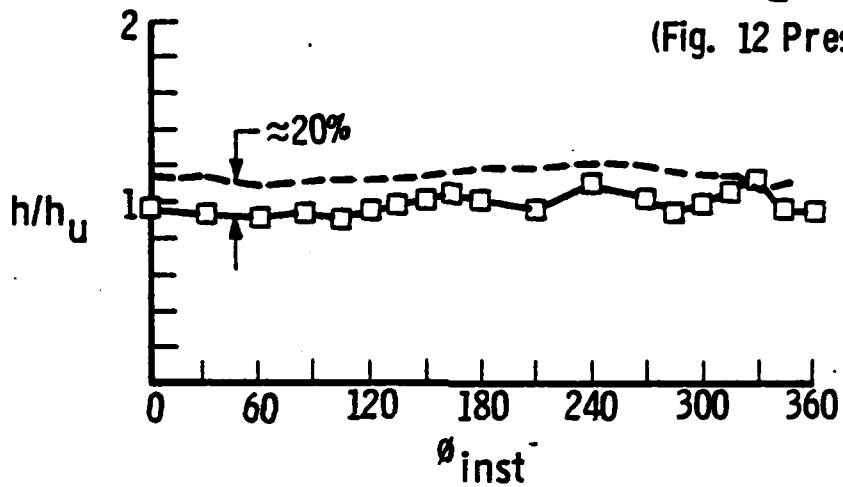
a. X/L = 0.15
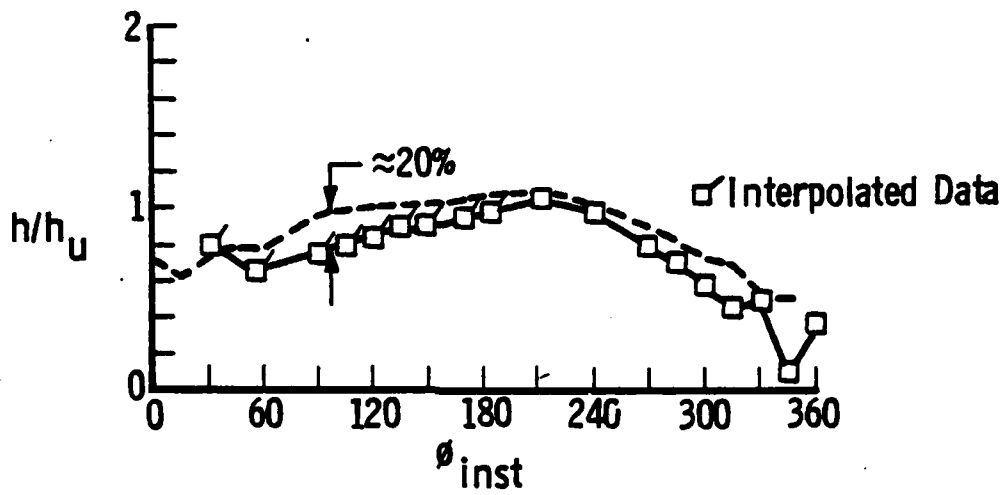
b. X/L = 0.35

Figure 13 Comparison of measured and calculated interference heating
distributions on BDU model mounted on inboard pylon

another parameter also plays a major part in determining store component temperatures. This parameter is recovery temperature, T_r, and it can be estimated by the simple equation

$$T_r = T_e \ (1 + 0.18 \ M_e^2)$$

where $T_e \gtrsim T_\infty \equiv$ ambient air temperature and $M_e \gtrsim M_\infty$. Recovery temperature is an upper temperature limit which could be encountered during extremely long flight times. A plot of this parameter for various temperatures and Mach numbers is presented in Fig. 14. Also shown in Fig. 14 is a nominal limiting component temperature level of 165°F. Note that if the ambient temperature is -70°F unlimited operation is possible up to Mach 1.8. On the other extreme, if the ambient temperature is 130°F limited flight times are required for all Mach numbers above 0.6. The intent of this figure is to illustrate that ambient air temperature (as well as aerodynamic heating) is an extremely important parameter in the analyses of store thermal environments.

CONCLUSIONS

Wind tunnel pressure and heat-transfer tests were conducted on several pylon-mounted store configurations in the 40-inch supersonic tunnel at AEDC. The major results of these tests are:

1. The test techniques demonstrated the versatility of scale model testing and illustrated refinements in the application of wind tunnel testing to define store pressure and thermal environments.

2. In general, the heating amplification factors were less than 1.5 which means, that for engineering purposes, store thermal environments can be estimated based on undisturbed flow-field calculations at zero angle of attack.

3. The pressure data were correlated within 20 percent of the heat-transfer data by use of a simple equation.

4. Ambient air temperature was shown to be a very important parameter in the analyses of store thermal environments.

REFERENCES

1. Epstein, Charles S. "Supersonic Delivery of Conventional Weapons – Facts or Fancy?" Aircraft/Stores Compatibility Symposium, AFFDL-TR-72-67, Volume 1, August 1972, pp. 51-72.

2. Hume, Robert A., Jr. "Supersonic Delivery of Selected Conventional Munitions from F-4 and F-111 Aircraft," AFATL-TR-75-69, May 1975.
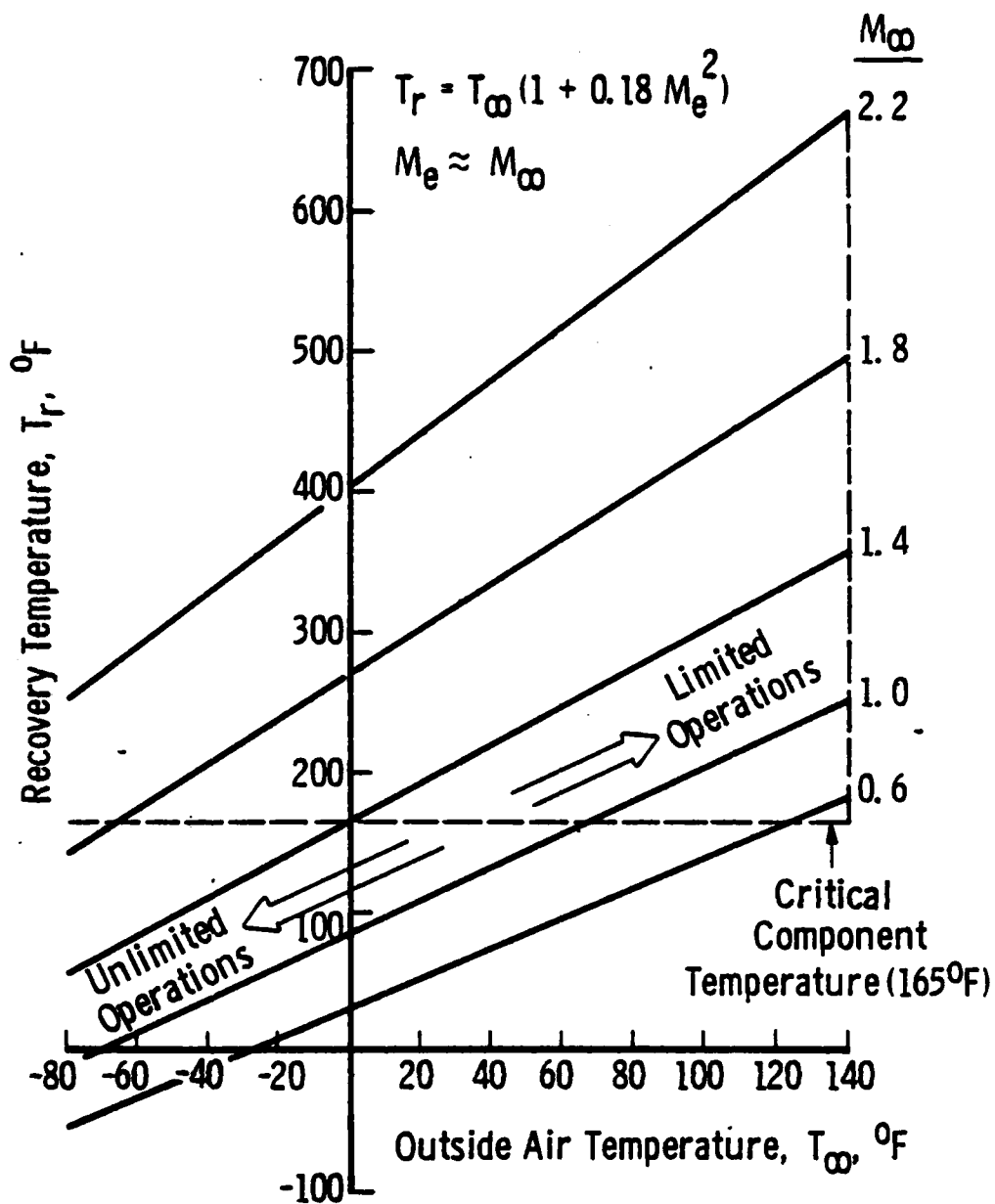
Figure 14 Illustration showing the importance of ambient temperatures on maximum possible store temperatures

3. Van Aken, Ray W. and Markarian, C. F. "Thermal Considerations of Stores in Captive Flight," Aircraft/Stores Compatibility Symposium Proceedings, JTCG/ALNNO WP-12-2, Vol. 4, September 1973.

4. Baker, S. S. and Matthews, R. K. "Demonstration of the Thermographic Phosphor Heat-Transfer Technique as Applied to Aerodynamic Heating of External Stores," Arnold Engineering Development Center, Arnold AFS, Tenn., AEDC-TR-73-128 (AD769306), August 1973.

5. Matthews, R. K., Baker, S. S., and Key, J. C., Jr. "Wind Tunnel Heating Test of Aircraft Stores," Aircraft Stores Compatibility Symposium Proceedings, JTCG/ALNNO WP-12-2, Vol. 4, September 1973.

6. Matthews, R. K. and Key, J. C., Jr. "Flight Test Heat Transfer Measurements on a Pylon Mounted Store," Aircraft/Stores Compatibility Symposium Proceedings, JTCG/MD WP-12, Vol. 2, September 1975.

7. Matthews, R. K. and Key, J. C., Jr. "Comparison of Wind Tunnel and Flight-Test Heat-Transfer Measurements on a Pylon-Mounted Store," Journal of Aircraft, Vol. 14, No. 6, June 1977.

8. Test Facilities Handbook (Tenth Edition). "Von Kármán Gas Dynamics Facility, Vol. 4." Arnold Engineering Development Center, May 1974.

AUTOBIOGRAPHY

R. K. MATTHEWS

Mr. Matthews has over 15 years experience as a project engineer in
the Aerodynamics Projects Branch of the von Kármán Gas Dynamics Facility
(VKF) of the Arnold Engineering Development Center (AEDC). In recent
years he has been the principal investigator on research directed toward
aircraft/store capability and has also conducted extensive aerodynamic
heating tests on space shuttle configurations and published numerous re-
ports and papers analyzing the results of these tests. He is a member
of the AIAA and has experience in all fields of aerodynamic wind tunnel
testing at both supersonic and hypersonic speeds. In 1967, he was
awarded an M.S. degree from the University of Tennessee Space Institute.
His undergraduate work was done at Parks College of St. Louis University,
where he also received a commission in the Air Force. He served three
years as an aircraft maintenance officer and has taught basic engineering
courses at several colleges.

AUTOBIOGRAPHY

GEORGE D. SPENCER

Mr. Spencer graduated in 1960 from the University of Tennessee with a Bachelor of Science degree in Mechanical Engineering and has continued part-time graduate studies in aerodynamic heating at the University of Tennessee. In 1960, he was employed as a project engineer with Pratt and Whitney Aircraft, West Palm Beach, Florida. His assignments involved development testing of turbojet hardware, aerodynamic heating studies, and durability testing of engine burners, turbine, and afterburner hardware. He served as Pratt and Whitney's flight test engineer at the aircraft manufacturer's test site. In 1967, he joined The Boeing Company as a staff engineer on the flight evaluation of the Saturn V Launch Vehicle. His assignment involved the flight analysis and evaluation of the Launch Vehicle Systems for NASA/MSFC. In 1971, he joined Martin-Marietta of Denver Division as a Section supervisor in Systems Engineering which evaluated the performance of the Skylab Systems. In 1974, he joined ARO, Inc. as a project engineer. His assignments involved infra-red sensor testing/performance evaluation and aerodynamic heating testing/evaluation of user supplied models. He is a Registered Professional Engineer.

AUTOBIOGRAPHY

JAMES C. KEY, JR.

Major Key graduated from the University of Florida with a BME degree in 1963. He entered the USAF the same year and was assigned to ASD (AFSC) at Wright-Patterson AFB, Ohio, as a propulsion and power engineer. He was selected for graduate studies in aerospace engineering at the U. S. Air Force Institute of Technology, entering in 1967 and graduating in 1969 with an MSAE. He was then assigned to AFLC units at McClellan AFB, California (aircraft modification and design engineer) and Bangkok, Thailand (depot-level aeronautical engineering support to PACAF operational units).

He is now assigned to the Air Force Armament Laboratory (AFSC) at Eglin AFB, Florida, as a project engineer for Aircraft/Weapons Aerodynamic Heating.

(The reverse of this page is blank)

THE EFFECTS OF WEAPONS BAY TURBULENCE SUPPRESSION
DEVICES ON WEAPONS CARRIAGE AND SEPARATION

(U)
(Article UNCLASSIFIED)

by

Rodney L. Clark
Air Force Flight Dynamics Laboratory
Wright Patterson Air Force Base, Ohio   45433

John W. Doran
Air Force Weapons Laboratory
Kirtland Air Force Base, N. M.   87117

ABSTRACT.   (U)   The internal weapons bay environment immediately
before and during weapons realese continues to present severe aircraft
and weapon design, structural and operational problems. The Air Force
Flight Dynamics Laboratory (AFFDL) and the Air Force Weapons Labora-
tory (AFWL) are engaged in a joint program to demonstrate an improved
F-111 bay aeroacoustic environment and the associated expanded inter-
nal release envelope for the B-43 weapon.

A 1/15 scale F-111 weapons bay equipped model has been tested in
the AEDC 16T wind tunnel with and without turbulence suppression
devices. The most promising devices were also tested to determine
their effects on the separation characteristics of the B-43 and B-57
weapons. Significant turbulence reductions within the bay were demon-
strated with a spoiler device mounted at the bay leading edge. Separa-
tion characteristics were also improved with this spoiler.

LIST OF FIGURES

INTRODUCTION

A joint in-house research program of the Air Force Flight Dynamics and Weapons Laboratories has been in progress since 1973. The objectives of this program have been to develop a detailed definition of the internal weapons bay aero-acoustic environment of the F-111 aircraft and experimentally evaluate techniques to improve this environment. Specifically, the program was directed toward the environment associated with the B-43 weapon. In flight test, this weapon received structural damage to the "tail can" assembly which resulted in establishment of weapon bay delivery limits for this weapon below the delivery capabilities of the F-111 and FB-111 aircraft. Demonstration of an improved environment within the weapon bay could result in an expanded delivery envelope for the B-43 weapon.

DISCUSSION OF PROGRAM HISTORY

At the request of and with principle funding from the AFWL, the AFFDL undertook the series of tests described below. The culmination of which was a contracted design study of potential modifications to the F-111 performed by General Dynamics - Fort Worth Division. The most promising of these modifications have been tested to determine the effects on the weapon bay environment and on the weapon separation characteristics from the modified bay.

There have been five (5) tests conducted by the AFFDL directly related to the F-111 weapon system. The fourth test in this series was conducted in the Arnold Engineering Development Center (AEDC) Propulsion Wind Tunnel Facility - 16T. This test which is the principle subject of this paper consisted of both turbulence suppressor evaluations and weapon separation tests with and without suppressors installed.

WIND TUNNEL MODEL AND INSTRUMENTATION

The 1/15 scale F-111 model, Figure 1, selected for the test program in the AEDC 16T wind tunnel has been previously tested by the AFFDL in the 4T wind tunnel. The latter facility was determined to be unsuitable for separation tests due to the large size of the model relative to the four (4) ft. cross section of this tunnel. The instrumentation systems previously used had been removed from the model; however, new instrumentation was necessary in any case due to the added model hardware associated with the weapon separation ejectors.

General Dynamics originally designed the wind tunnel model and was therefore the logical choice to prepare the model for this test program. As previously mentioned, GD-FW had performed a preliminary design study to define candidate suppression devices and/or modifications to the F-111 weapon bay. Model hardware was fabricated by the contractor representing four (4) of the most promising suppressor candidates.

The instrumentation system included fifteen (15) Kulite solid state

22.00

18.19

57.03

WEAPONS BAY
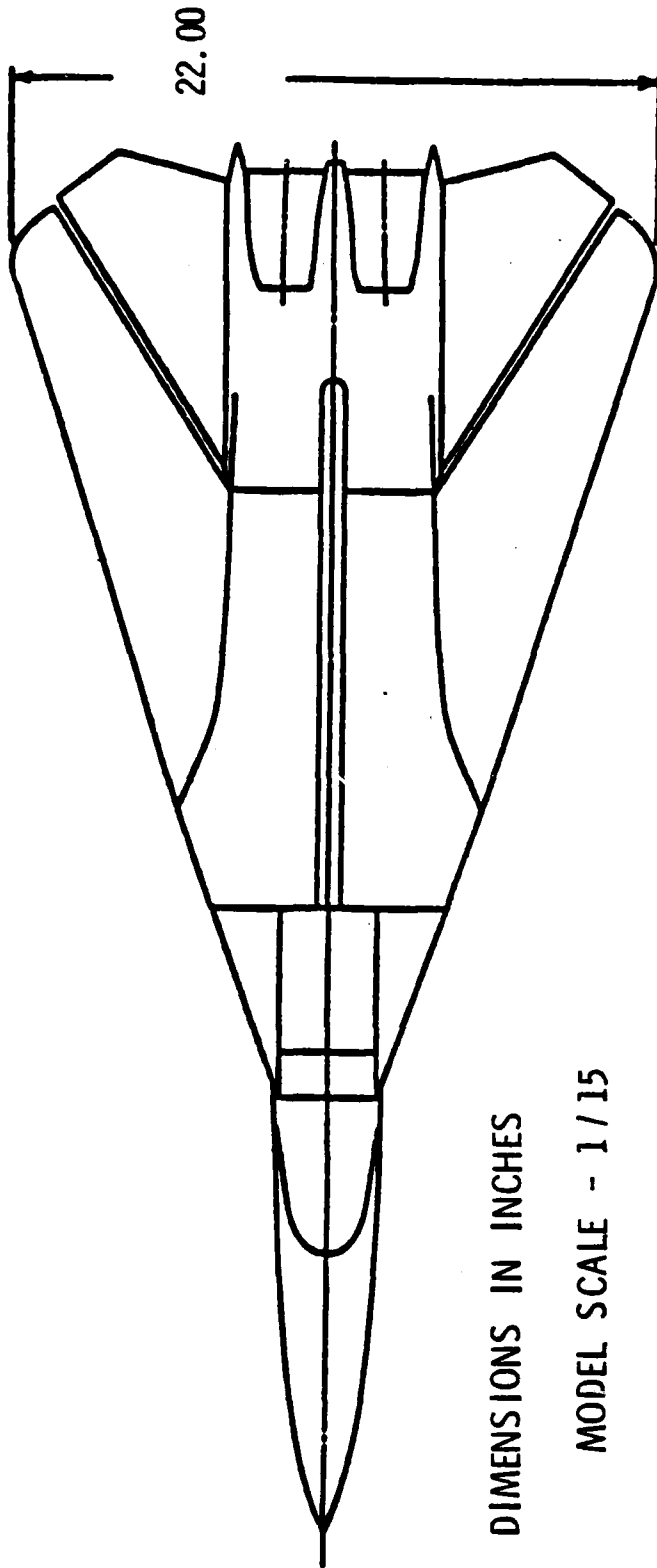
DIMENSIONS IN INCHES

MODEL SCALE - 1 / 15
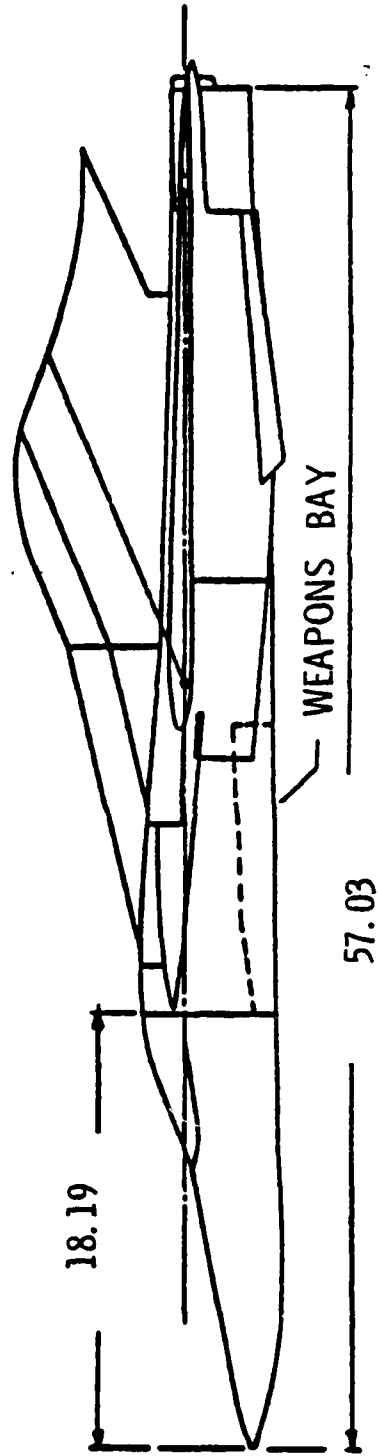
FIG. 1   F-111 WEAPON BAY MODEL

pressure transducers with screened crystal diaphrams. (This type transducer has proven to be significantly more reliable than the unscreened transducers used in the previous test in the 4T tunnel). Sixteen (16) steady state pressure taps and three (3) thermocouples were also installed in and around the bay. The locations of these are indicated in Figure 2. One transducer was located in the nose of the model to monitor the tunnel dynamic pressure (noise) level. The left engine inlet was also instrumented with twelve (12) total pressure taps.

Figures 3 and 4 show the B-43 and B-57 weapons geometry as installed in the model bay. The black dots indicate the centerline and left wall locations of the pressure transducers relative to the stores. Both single and double B-43 bay loadings were investigated; however, only single B-57 loadings were investigated. In addition, this test program included configurations with a gun plus ECM Pod mounted on the right side of the bay with a B-43 mounted on the left hand side.

The turbulence level (dynamic pressure) data in this paper is presented as a ratio of PRMS/Q. "PRMS" is the root mean square of the non-steady pressure level as measured with the high frequency response Kulite (25 psid range) differential pressure transducers. "Q" is the freestream tunnel dynamic pressure. (Note: Turbulence level or dynamic pressure as used in this paper refers to the non-steady or acoustic (oscillatory) component of the pressure at a point normalized by Q. See Table I.) The PRMS level is obtained using a root mean square volt meter to process the transducer output signal. The transducer output signal was also recorded on magnetic tape for further analysis off line. Power spectral density narrowband analysis was performed to evaluate the frequency content and resonance characteristics of each configuration.

SUMMARY OF TEST PROGRAMS

FLIGHT TEST (1973)

The initial test in this series consisted of a flight test of an instrumented BDU-8 (inert practice version of the B-43) in an F-111. The BDU-8 was instrumented to acquire both steady state pressure and acoustic (dynamic pressure) data. This test was reported in Reference 1. Structural failure of the nose cone of the BDU-8 and problems with the instrumentation systems limited the data acquired. Some comparisons of these data with wind tunnel data are presented later.

CAVITY TURBULENCE REDUCTION TEST (JULY 1974)

A generic weapon bay wind tunnel model was acquired for test in the Air Force Flight Dynamics Laboratory (AFFDL) Trisonic Gas Dynamics Facility. The test was conducted in the transonic section of this wind tunnel and results are presented in Reference 2. Significant aero-acoustic turbulence reductions were demonstrated with various fences or spoilers mounted at the leading edge of the cavity. The design of the spoiler

TABLE I

FREESTREAM TUNNEL DYNAMIC PRESSURE (Q) VERSUS MACH NUMBER FOR UNIT REYNOLDS NUMBER OF APPROXIMATELY THREE MILLION PER FOOT

Mach	Q(psf)	See note below
.7	430	
.85	475	
.95	530	
1.20	595	
1.30	615	
1.50	640	

NOTE: These values of "Q" are representative of the values used to normalize the PRMS (non-steady) turbulence data acquired during this test program.

FIG. 2   LOCATION OF INSTRUMENTATION

BAY ROOF

LEFT WALL

L = 12.1

X/L   .5   .35   .5   .8   .95
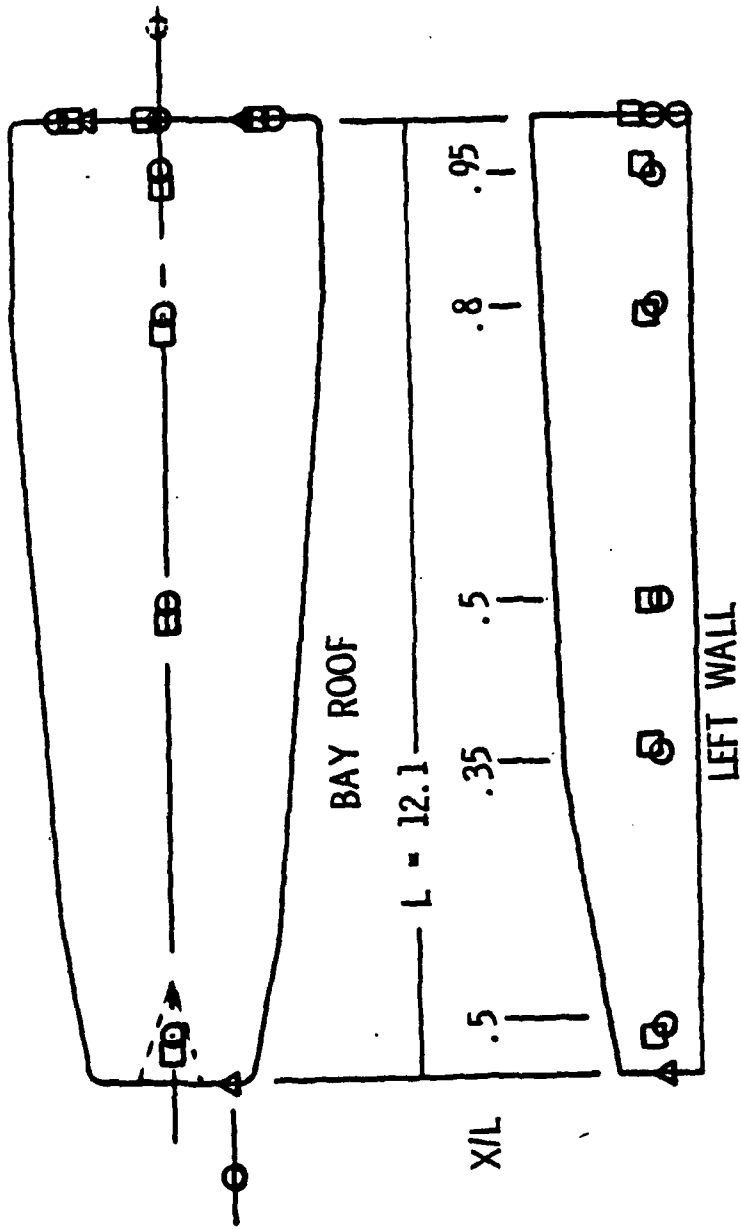
○ DYNAMIC PRESSURE TRANSDUCER
□ STEADY STATE PRESSURE TAP
△ THERMOCOUPLE
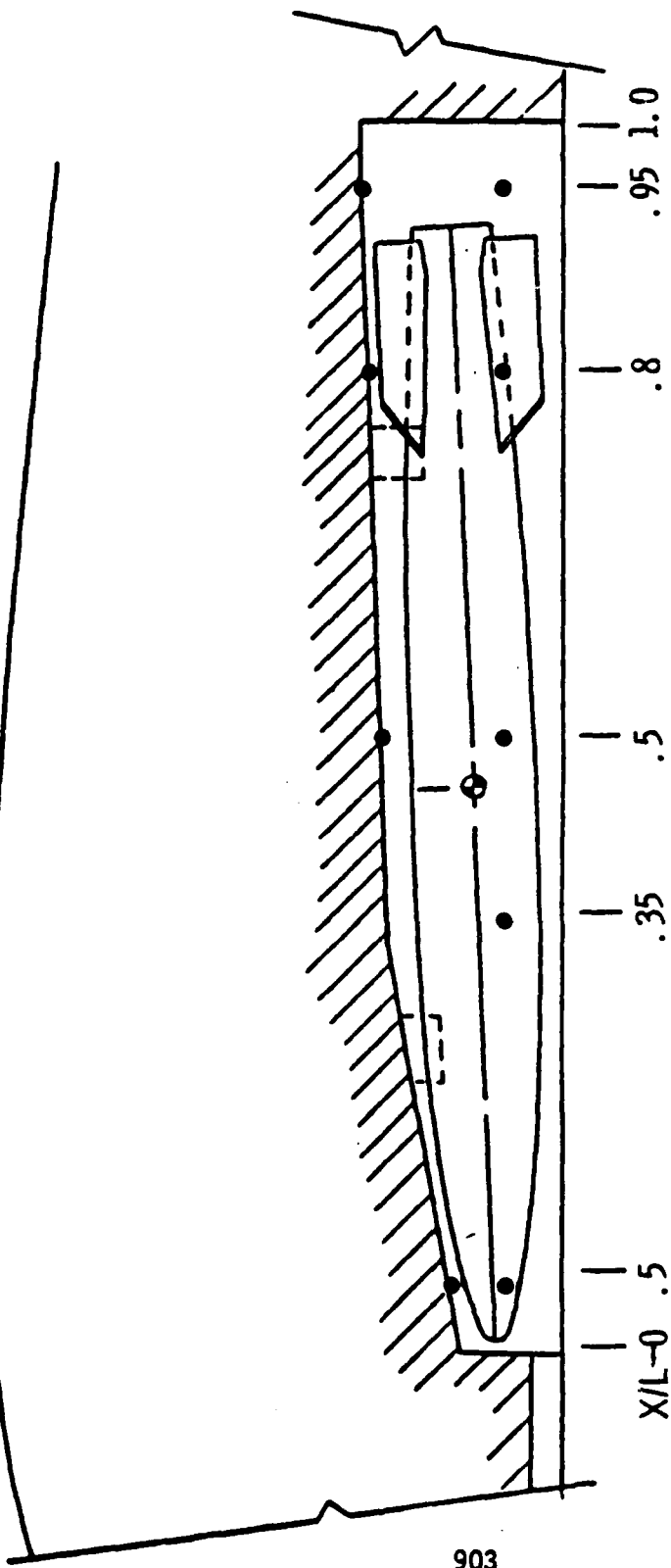
FIG. 3 B-43 WEAPON IN BAY

X/L=0 .5 .35 .5 .8 .95 1.0

903
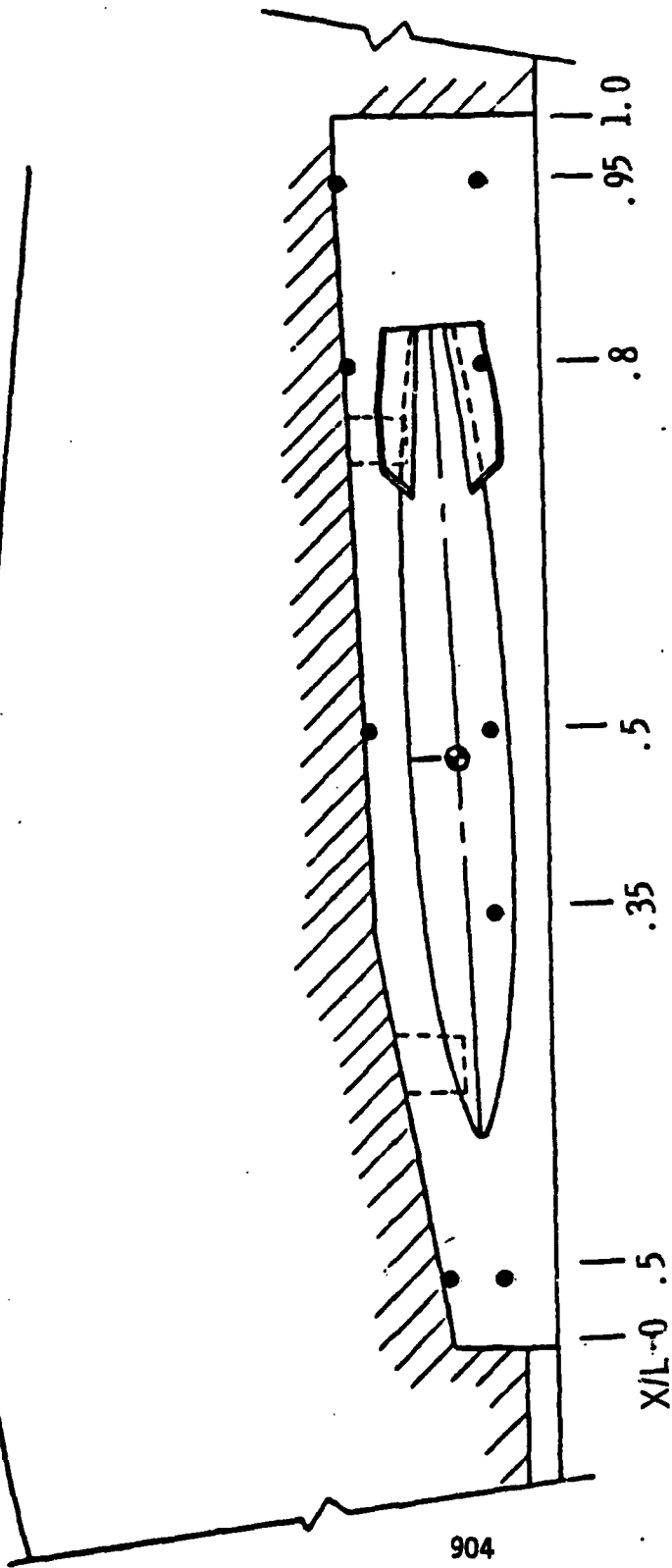
FIG. 4 . B-57 WEAPON IN BAY

X/L-0 .5 .35 .5 .8 .95 1.0

evaluated on the F-111 wind tunnel model discussed above was based upon these results.

F-111 WIND TUNNEL MODEL - 4T TEST (AUGUST 1974)

The 1/15 scale F-111 model (Figure 1) on loan from General Dynamics/ FW was instrumented and tested in the Arnold Engineering Development Center (AEDC) Propulsion Wind Tunnel - 4T Facility. In this test reported in Reference 3, the model was extensively instrumented to acquire temperature steady state and dynamic pressure data to define the aero-acoustic environment of the F-111 weapon bay and for correlation with the BDU-8 flight test results. To accomplish the latter, a model BDU-8 (B-43 aerodynamic shape) was instrumented to acquire data on the surface of the model bomb. Other instrumentation was placed on the walls, roof, and adjacent fuselage surfaces of the model. Boundary layer profiles were also obtained.

Figures 5A and B compare dynamic pressure data from the surface of the BDU-8 measured in flight and in the 4T wind tunnel. Generally good correlation is observed at the 10,000 ft altitude in the transonic region. In Figure 5B, correlation improves for the 30,000 ft altitude condition above Mach 1. While the data were acquired at the same unit Reynolds number at each Mach number obviously full scale Reynolds number could not be achieved in the wind tunnel. Figure 6 compares data on the left side of the BDU-8 which was installed on the left side of F-111 weapon bay. The data in this figure were not acquired at identical locations due to failure of pressure transducers at these locations. Similar trends are observed in this figure with a significant drop in level near Mach 1 observed in the wind tunnel data. The flight test data show a smaller reduction near Mach 1 with the turbulence levels increasing slowly above Mach 1.1.

F-111 WIND TUNNEL MODEL - 16T TEST (APRIL 1977)

This test which was conducted during April 1977 will be discussed in detail below. Both aero-acoustic turbulence in the bay and weapon separation studies were performed with and without suppression devices installed. This test used the same 1/15 scale model previously tested in the 4T wind tunnel; however, the model had completely new instrumentation and was modified to be as close as possible to the operational weapon bay configuration of the F-111 aircraft.

F-111 WIND TUNNEL MODEL - 4T TEST (AUGUST 1977)

Again the same model was tested and, the configuration and instrumentation were unchanged from the previous 16T test. This test had the objective of more fully defining the angle of attack and yaw effects on the turbulence in the F-111 weapon bay with and without a suppression device (saw tooth) spoiler mounted at the leading edge of the bay. Also the geometry, height and width, of the spoiler were varied to fully define the turbulence levels which can be achieved with such a device.

905

FIG 5A WIND TUNNEL TO FLIGHT DATA CORRELATION, BOTTOM OR
AIRSTREAM SURFACE OF WEAPON

SYM X/L   SUPPR.
□   .86 BOTTOM NONE   4T TUNNEL DATA
X   .86 BOTTOM NONE   FLIGHT DATA
                  ALTITUDE - 30,000 FT

PRMS / Q

MACH NUMBER
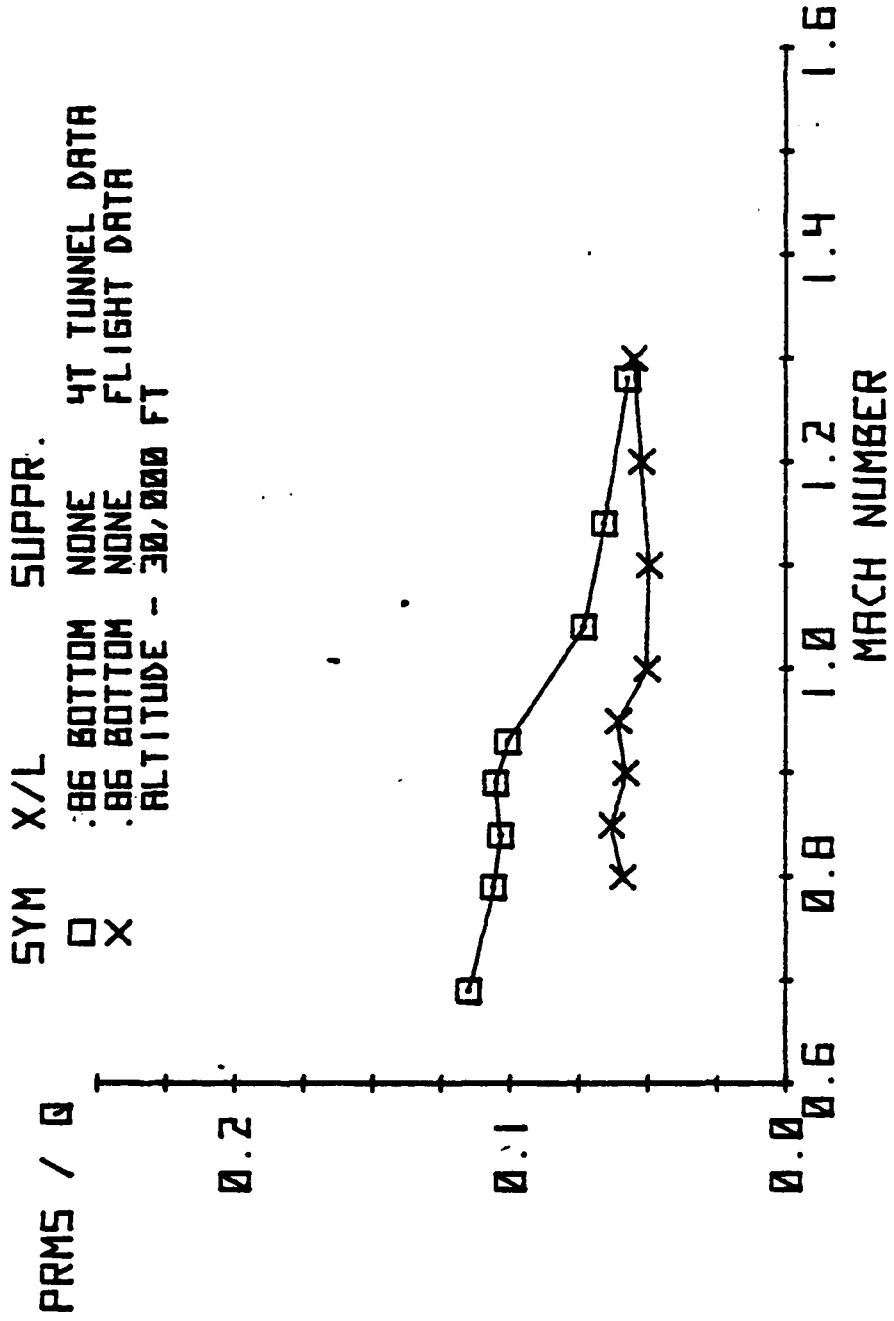
FIG 5B WIND TUNNEL TO FLIGHT DATA CORRELATION, BOTTOM OR
AIRSTREAM SURFACE OF WEAPON

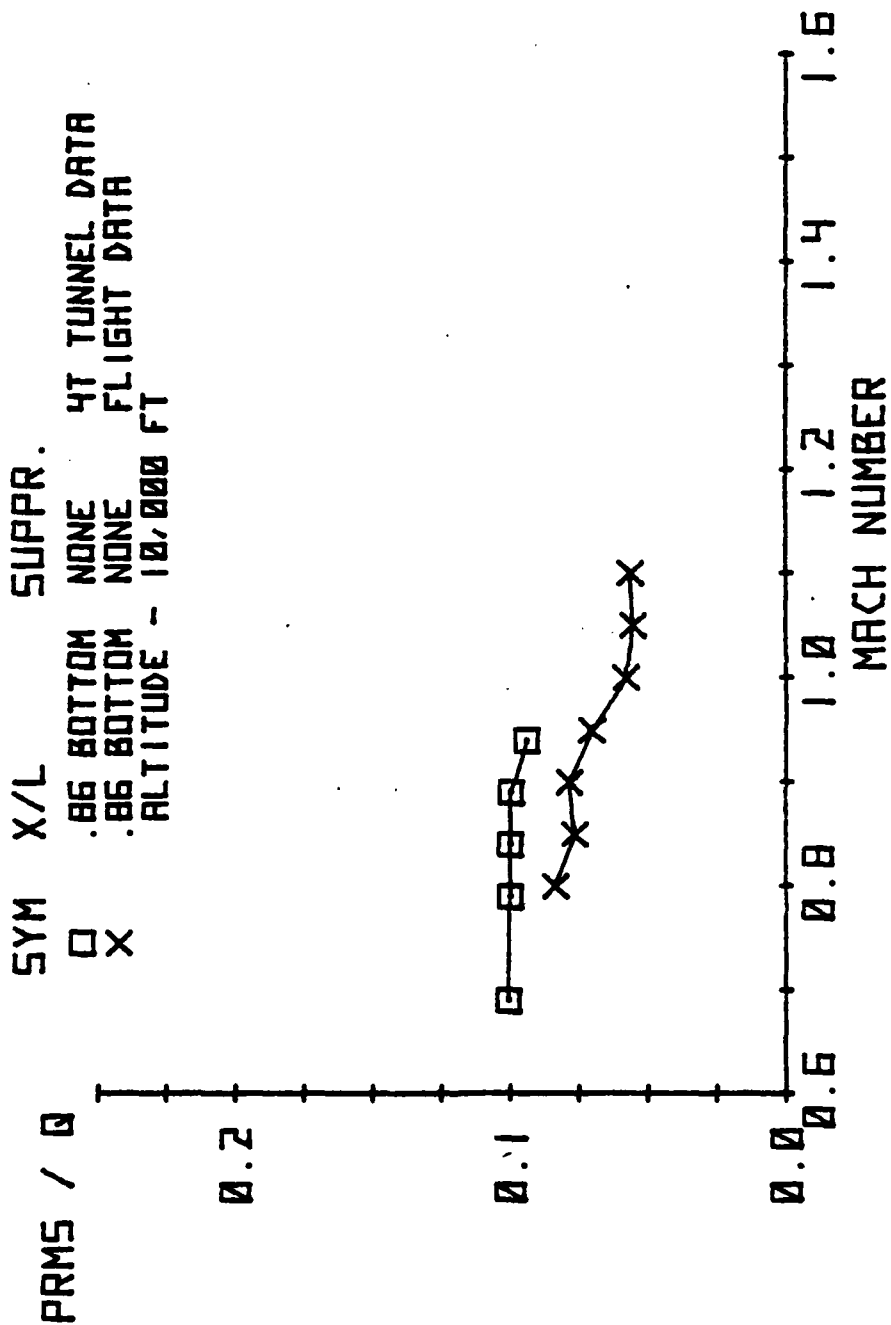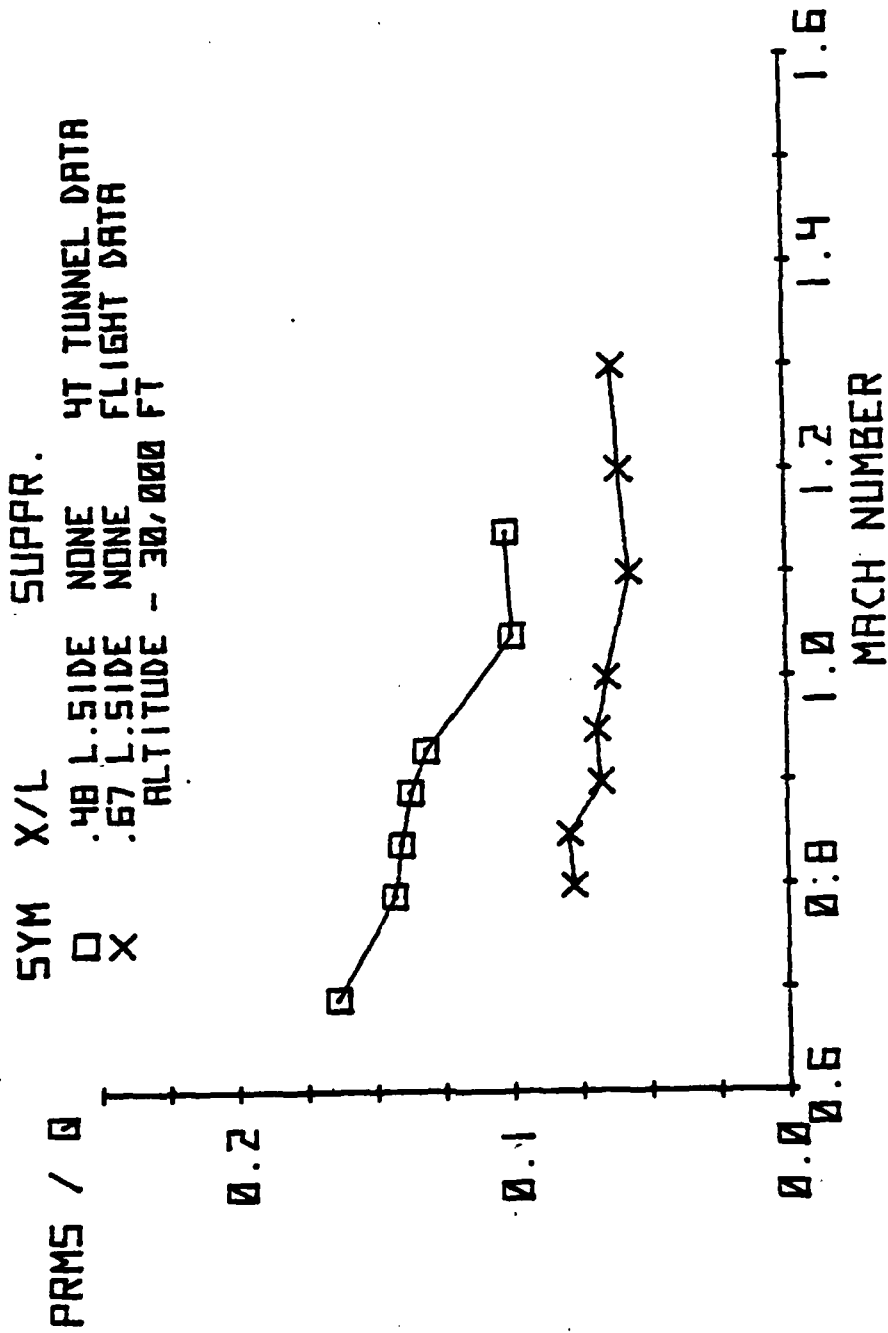FIG 6   WIND TUNNEL TO FLIGHT DATA COMPARISON, LEFT
         SIDE OF WEAPON ADJACENT TO BAY WALL

Since this test was conducted in August 1977, only preliminary data are available.

RESULTS OF 16T TEST

CORRELATION WITH FLIGHT TEST AND 4T DATA

Figure 7 shows PRMS/Q versus Mach number data from 16T and the above F-111 flight test. The wind tunnel data were acquired at a unit Reynolds number of three (3) million per foot while the flight test data were acquired during 10,000 ft level flight with unit Reynolds number varying from about four (4) to approximately six (6) million per foot. The flight test data were on the surface of the B-43 store between the lower tail fins while the wind tunnel data were acquired on the left wall of the bay adjacent to the tail cone assembly. The turbulence levels observed in the wind tunnel are consistently higher than the comparable flight test data; however, the same general trend with Mach number was observed. Reynolds number was not a primary test variable during this wind tunnel test program. Reynolds number varied from approximately 2.5 to 3.5 million per foot during the drop test phase. Most other data were acquired at a constant 3 million per foot because of tunnel limits.

Figure 8 presents data from the 4T and 16T wind tunnel tests. The data correlation is generally excellent in the transonic Mach range. The supersonic data from the 4T test do not follow the trend observed in both the 16T and the flight test, that is a slow increase in PRMS/Q versus Mach number in the supersonic region. The better correlation between the flight and 16T data is attributable at least in part to the fact that the 16T model geometry is more representative of the actual F-111 weapons bay in two areas. The first being the "island" between the inward folding doors at the bay leading edge is included in the 16T model, and secondly, this model has more accurately represented weapon bay doors in the aft attachment region.

BASELINE CONFIGURATION DATA

Figures 9 and 10 are representative of the dynamic pressure distribution at Mach .95 and 1.3, respectively for the basic or unmodified F-111 weapon bay. Data are presented for the empty; single and double B-43; and single B57 store loading configurations. Figures 9A and 10A present the bay centerline distribution while Figures 9B and 10B show the left side wall distribution.

The centerline distributions are relatively consistent with turbulence levels increasing from the fully loaded (double B-43's) to the empty bay configuration. The PRMS/Q levels increase from the front of the bay ($X/L = 0$) to the rear ($X/L = 1.0$). This trend is much stronger at Mach .95 than at the supersonic, Mach 1.3 condition.

Significantly different effects of bay loading are observed along the left side wall, Figures 9B and 10B. Higher levels were observed for

909
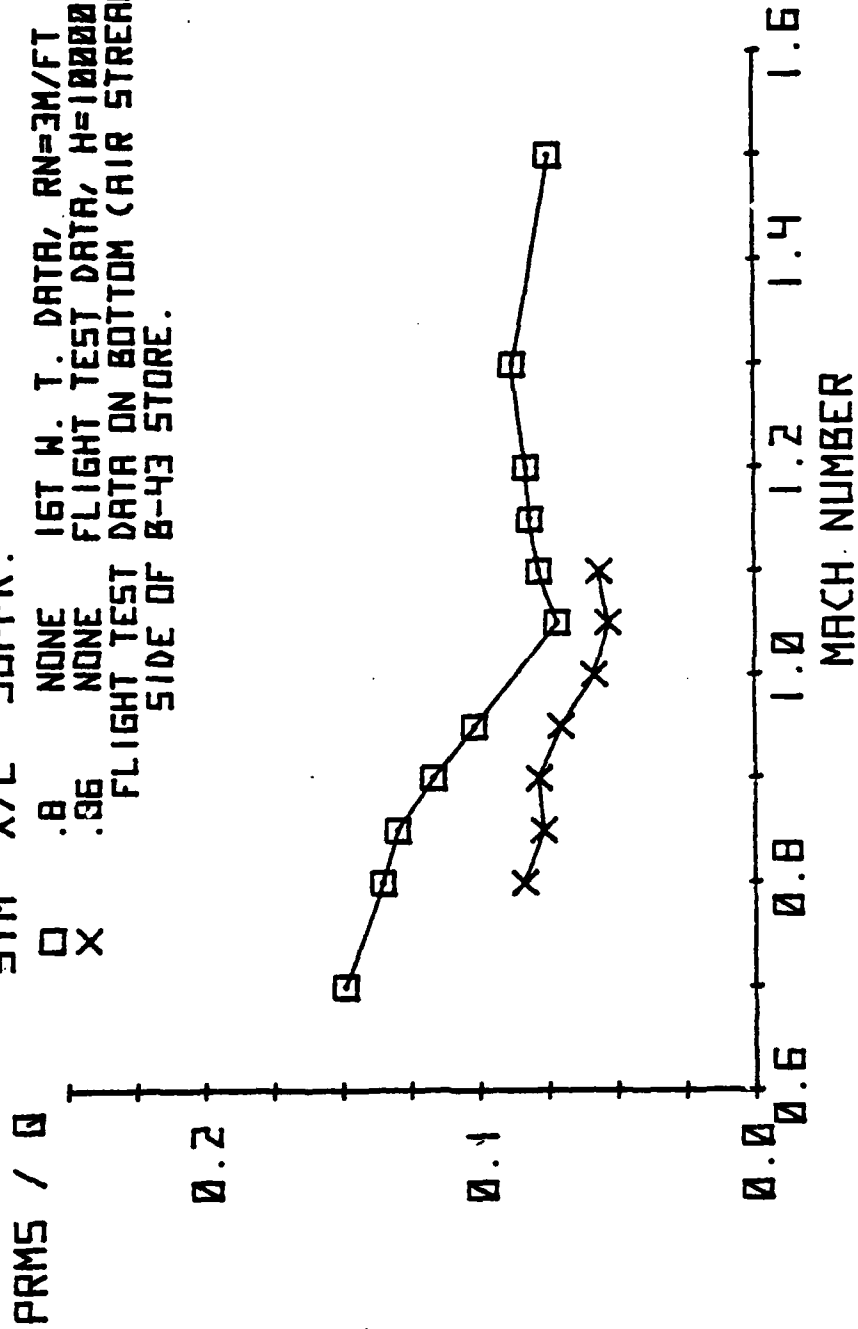
FIG 7   COMPARISON OF FLIGHT TEST DATA WITH
PWT-16T TUNNEL DATA
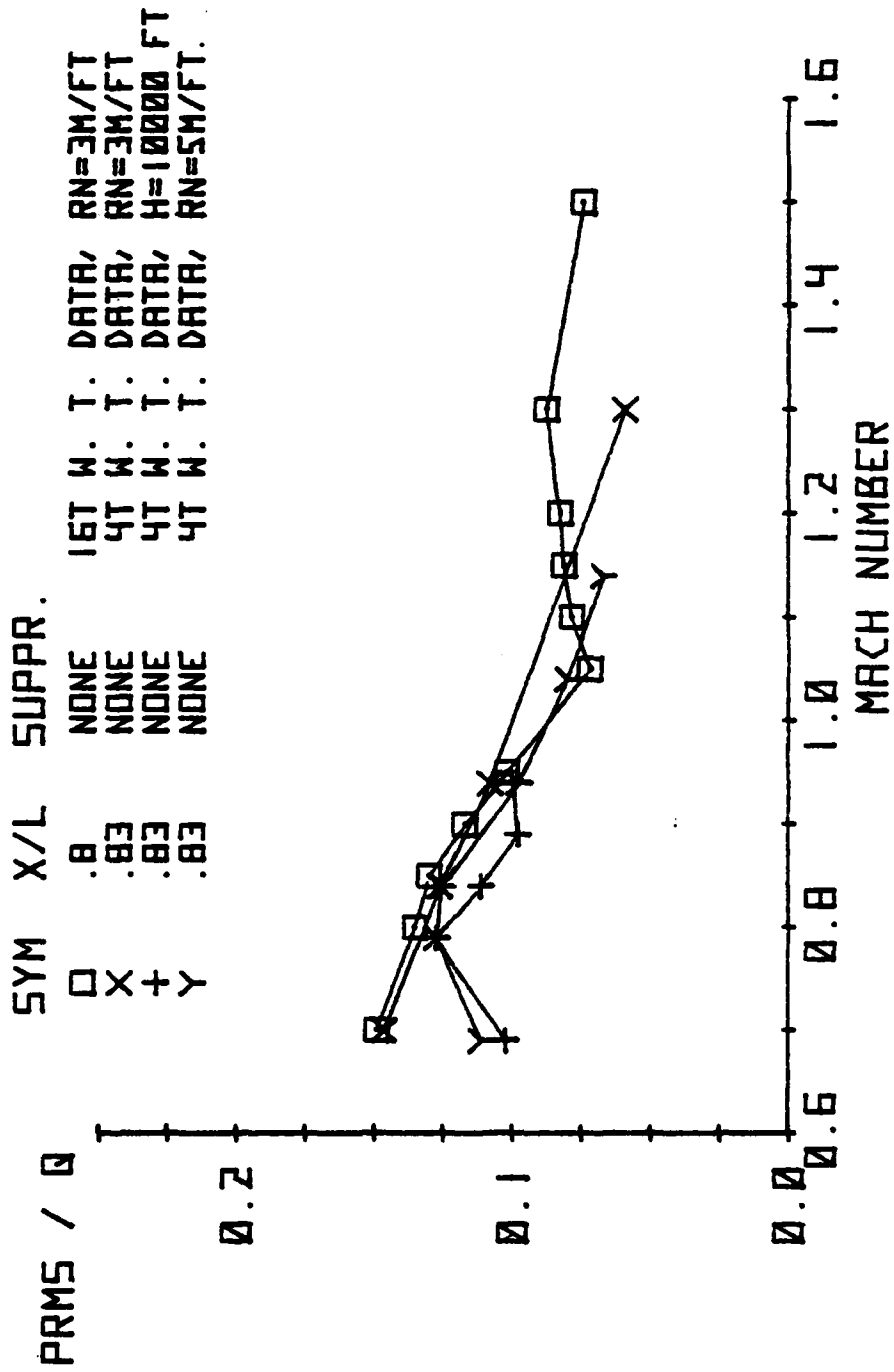
FIG 8 COMPARISON OF PWT-4T WITH PWT-16T TUNNEL DATA
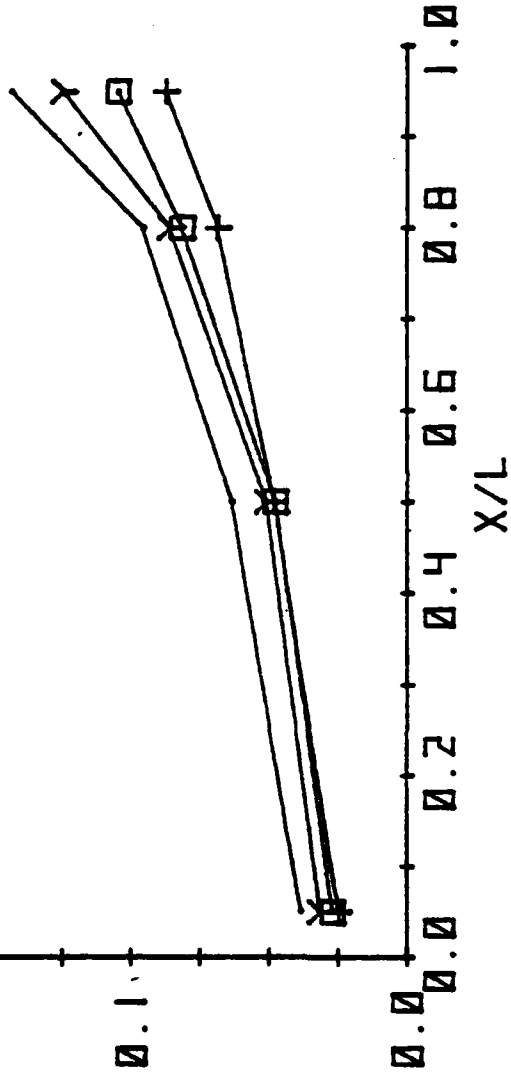
FIG 9A   TRANSONIC DYNAMIC PRESSURE DISTRIBUTION FOR

BASIC F-111 BAY LOADING CENTERLINE

912

SYM MACH LEFT BAY RIGHT BAY BAY SUPPR.

SYM	MACH	LEFT BAY	RIGHT BAY	BAY SUPPR.
—	.95	EMPTY	EMPTY	NONE
□	.95	B-43	EMPTY	NONE
+	.95	B-43	B-43	NONE
Y	.95	B-57	EMPTY	NONE

FIG 9B   TRANSONIC DYNAMIC PRESSURE DISTRIBUTION FOR

BASIC F-111 BAY LOADINGS, LEFT BAY WALL

913
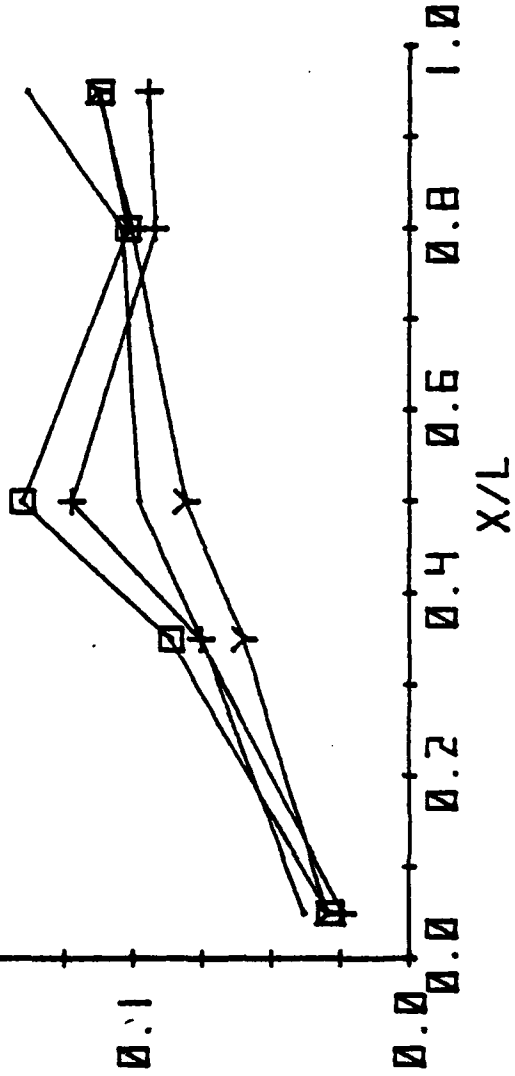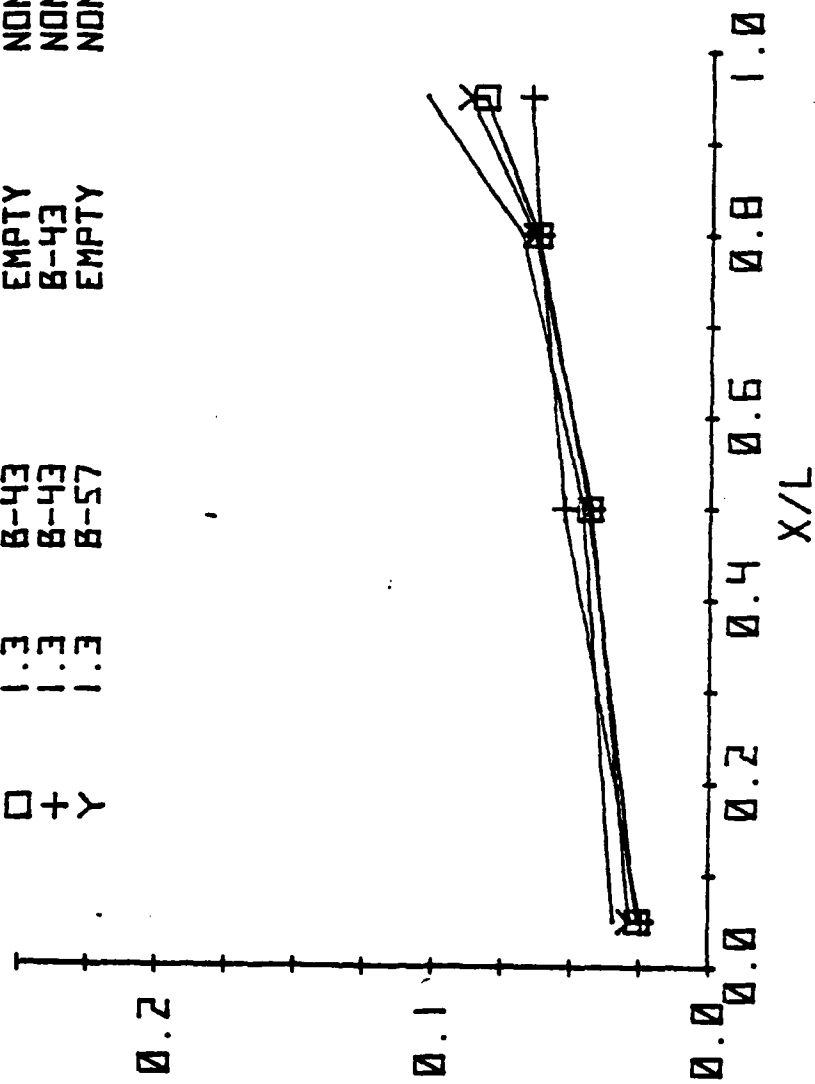
FIG 10A SUPERSONIC DYNAMIC PRESSURE DISTRIBUTION FOR
BASIC F-111 BAY LOADINGS, CENTERLINE
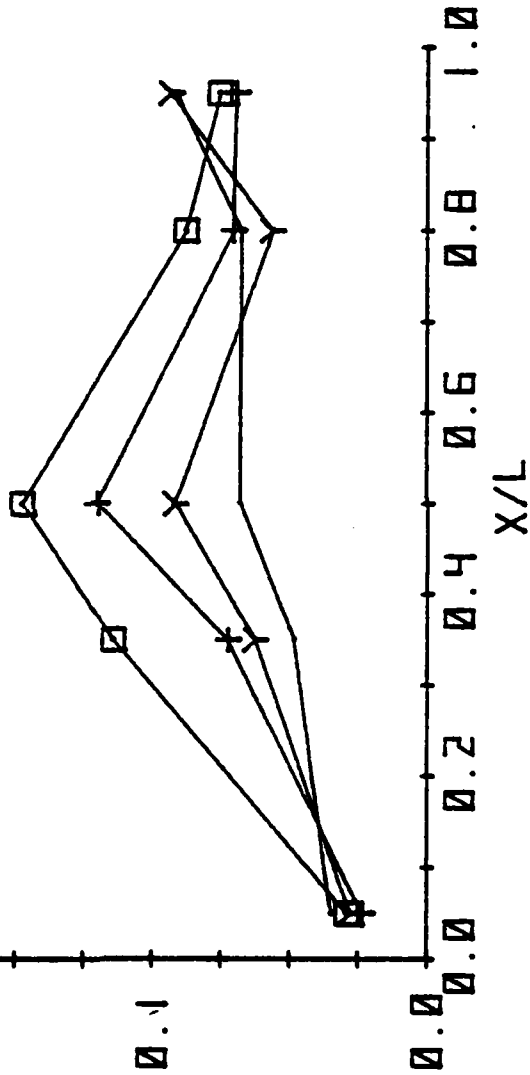
FIG 10B   SUPERSONIC DYNAMIC PRESSURE DISTRIBUTION FOR

BASIC F-111 BAY LOADINGS, LEFT BAY WALL

the B-43 versus empty configurations with the highest level occurring with the single B-43 at an X/L of .5. The empty configuration again peaks at the rear of the bay. The same trends were observed at Mach .95 and 1.3: however, the single B-57 is seen to have a lower turbulence level at Mach .95 than the empty bay while at Mach 1.3 the reverse is observed.

Figure 11 presents data at Mach .95 showing the effect of angle of attack on the turbulence distribution along the centerline of the empty bay. Turbulence level is seen to increase with angle of attack. The data presented below was acquired at a wing angle of attack of three degrees.

EFFECTIVENESS OF THE TURBULENCE SUPPRESSOR DEVICES

Figures 12 through 15 show the suppression devices evaluated during this test program. Figure 13 depicts the installation of vortex generators on the F-111 aircraft while the other drawings are model scale parts. Suppressors A, B, and C are mounted at the leading edge or ahead of the bay. Suppressor D is attached to the aft bulkhead inside the bay. Suppressors A and C would be raised into position as the bay doors open. Devices A, B, and C are sized to be approximately one local boundary layer height (.2 to .35 inches).

Figure 16 compares the peak turbulence level on the left wall of the bay without a suppressor to that with each of the four suppressors. This comparison clearly shows the superiority of Suppressor A, the saw tooth spoiler, at all Mach numbers evaluated. This comparison is for the single B-43 installed on the left side of the bay. This bay loading produced the highest turbulence level of all of the baseline configurations on the left wall of the bay. This mid wall (X/L = .5) location produced turbulence levels that were only exceeded on the aft bulkhead. The aft bulkhead levels were not used for comparison of the suppressors because the stores are mounted sufficiently ahead of the bulkhead so as to reduce the effect of turbulence at this location on the stores. Also, Suppressor D shields two (2) of the three (3) aft bulkhead transducers and affects the flow approaching the transducer located on the aft lip of the bay. The Vortex Generators, Suppressor B, produced only a small reduction in the turbulence level while the Rear Facing Step, Suppressor C, increased the turbulence level slightly at Mach .95 and above.

Similar results were observed at other locations in the bay. In all cases, the Saw Tooth Spoiler is the most effective suppressor. The other suppressors are significantly less effective with no consistent ranking of the other suppressors. Suppressor D was the second most effective at the supersonic Mach numbers and essentially as effective as Suppressors B and C at the lower Mach numbers at most locations in the bay.

Figure 17 presents similar comparisons of the three forward mounted suppressors used in combination with the Rear Ramp Deflector. The combination of the Saw Tooth (A) with the Rear Ramp Deflector (D) was

SYM ALPHA WING

SYM	ALPHA	WING
□	0	
X	3	
+	6	

MACH = .95; EMPTY BAY

PRMS / 0

X/L
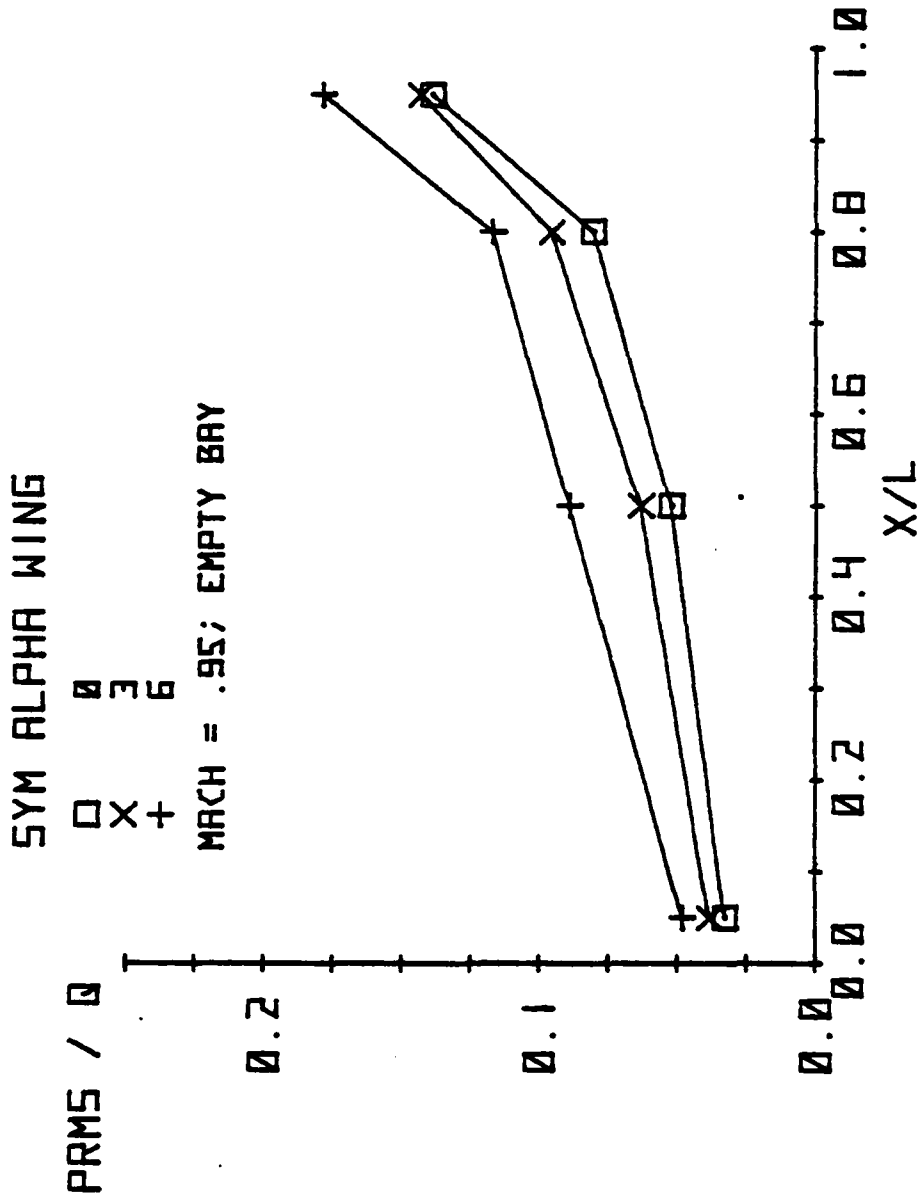
FIG 11   EFFECT OF ANGLE OF ATTACK ON THE BAY CENTERLINE
DYNAMIC PRESSURE DISTRIBUTION

DIMENSIONS IN INCHES

.23

1.27

BL 0.0

SECTION A-A

A

A
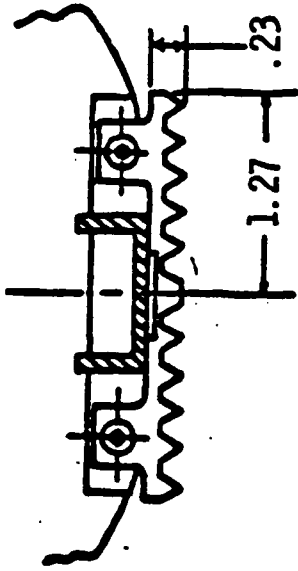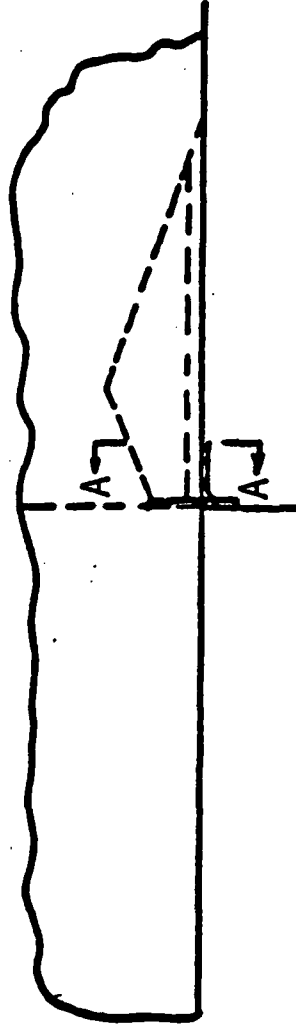
BAY LEADING EDGE

FIG. 12 SUPPRESSOR "A" – SAW TOOTH SPOILER

918

PLAN VIEW
OF
VORTEX GENERATOR

FIXED
VORTEX GENERATORS

BAY LEADING EDGE
F.S. 278.5

WEAPONS
BAY

NOSE GEAR DOORS

3.00

3.00

15°

20°

20°

5.00

15.00

~60

FLOW

DIMENSIONS IN INCHES
(FULL SCALE)

BOTTOM VIEW
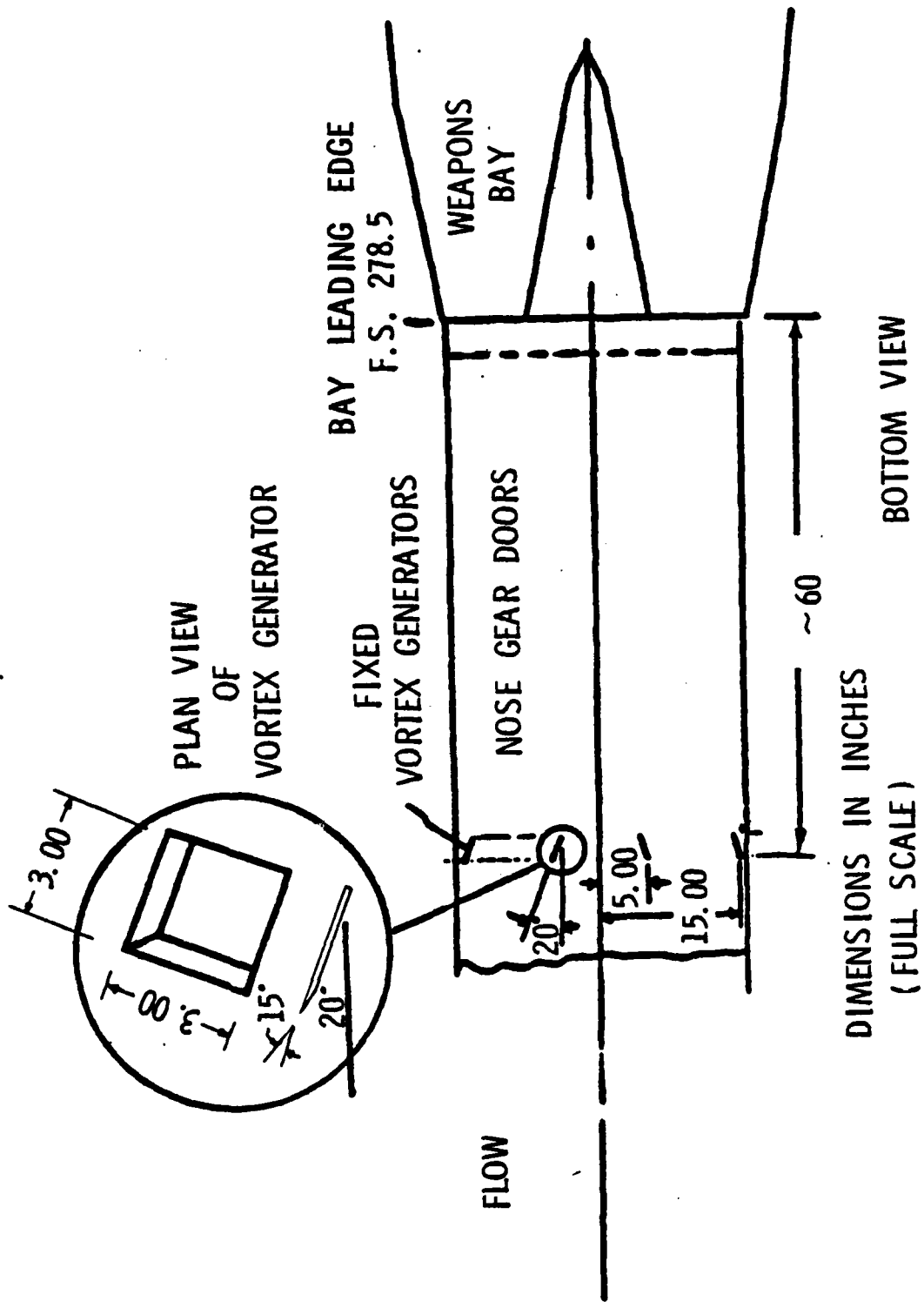
FIG. 13 SUPPRESSOR B – VORTEX GENERATORS

919

DIMENSIONS IN INCHES

FS 18.567

0.24

1.21

1.00

16°

0.35
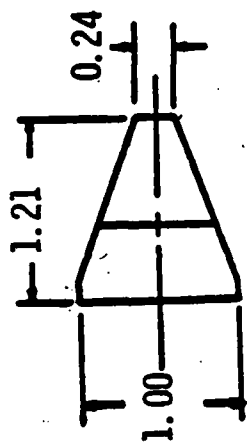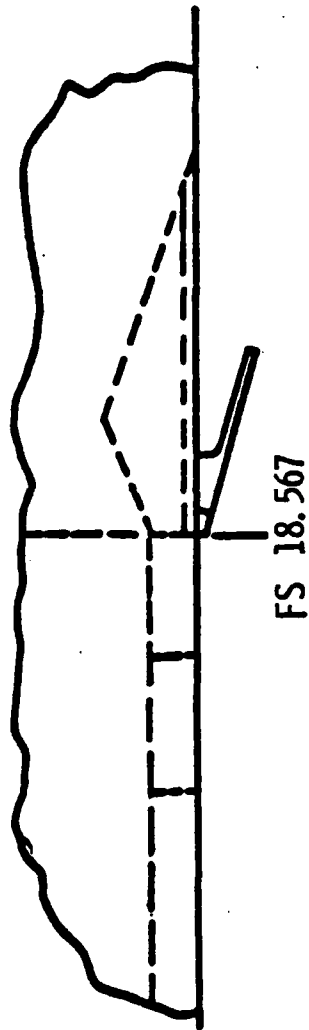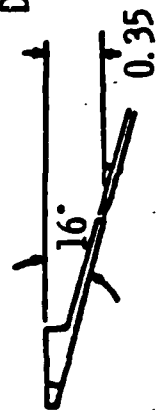
FIG. 14 SUPPRESSOR C - REAR FACING STEP
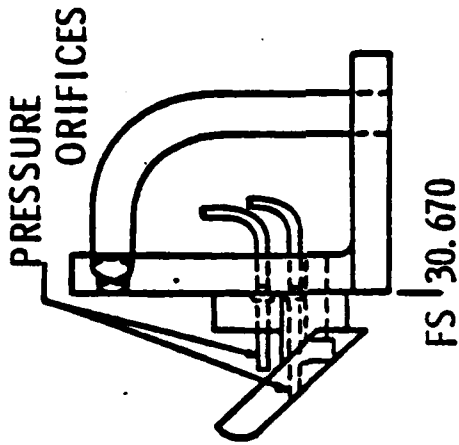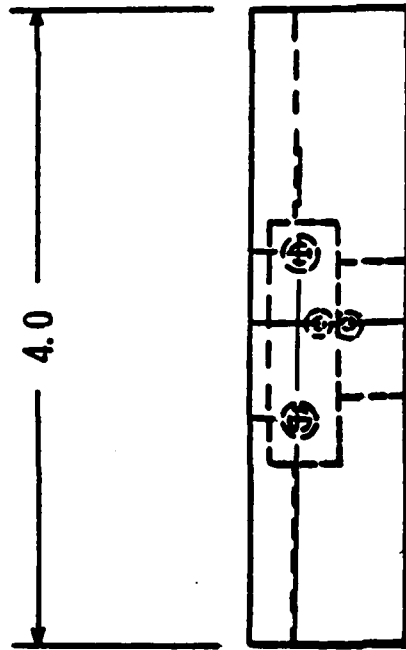
FIG. 15 SUPPRESSOR "D" REAR RAMP DEFLECTOR
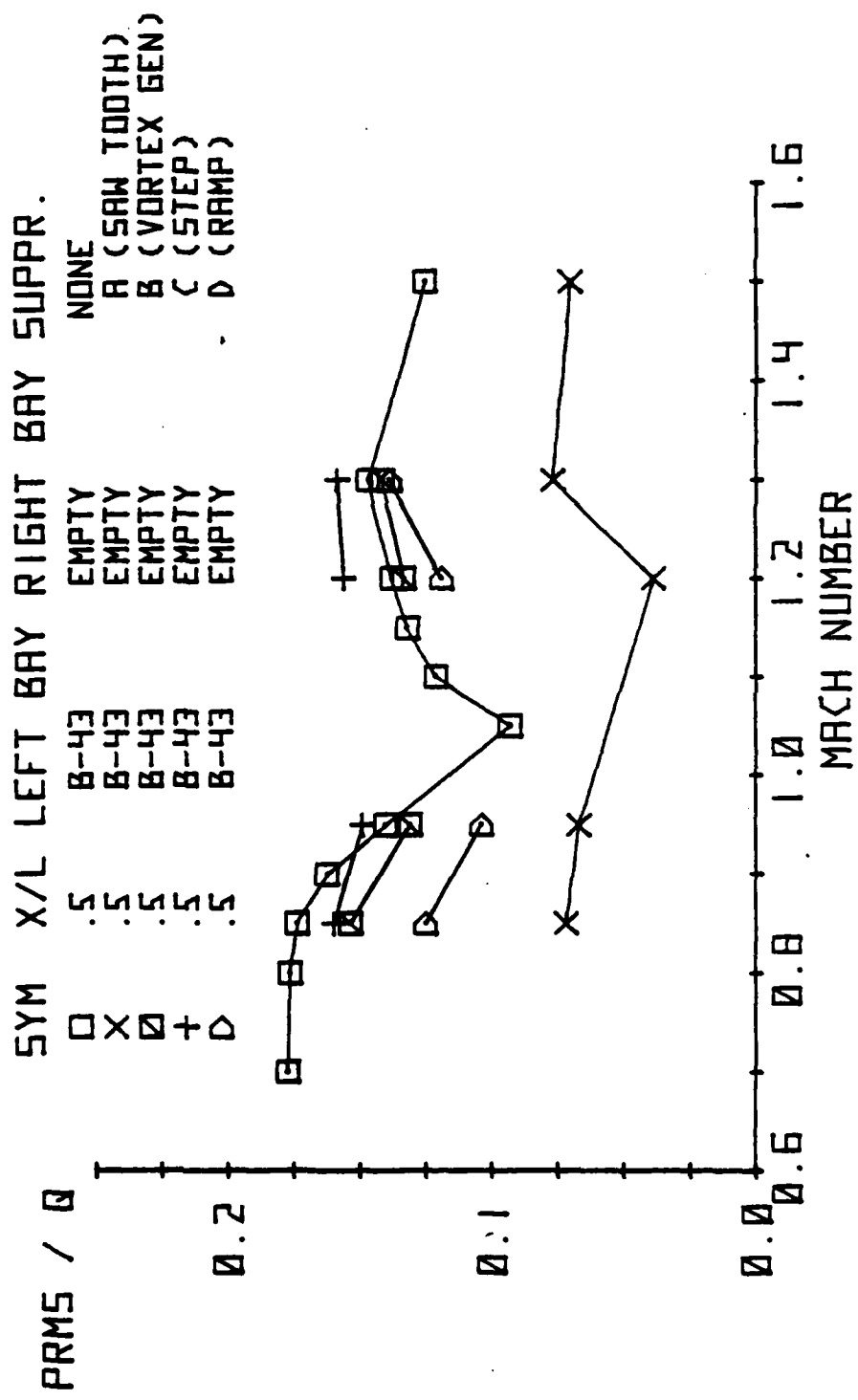
FIG 16   COMPARISON OF DYNAMIC PRESSURES WITH AND WITHOUT

SUPPRESSORS, LEFT WALL OF BAY
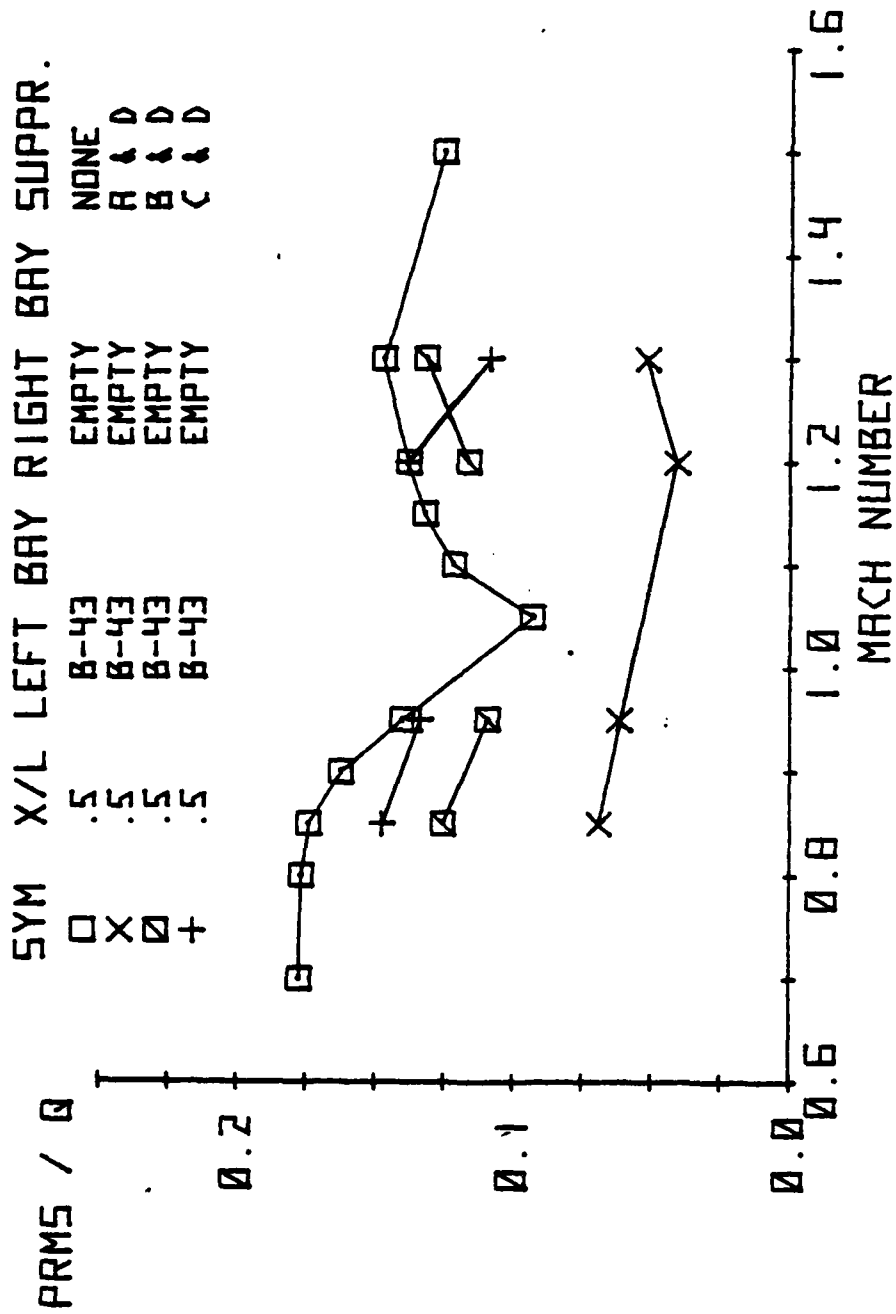
FIG 17   COMPARISON OF DYNAMIC PRESSURES WITH AND
WITHOUT THE COMBINATION SUPPRESSORS, LEFT WALL OF BAY

substantially superior to the other two combinations.

Figure 18 is a more detailed comparison of the turbulence suppression produced by Suppressor A and the combination of Suppressors A and D. Figure 18A shows that at Mach .85, the centerline distribution produced by the combination is slightly superior to the Saw Tooth Spoiler alone. Figure 18B is the same comparison of the distribution along the left side wall. At the X/L .95 location, the combination of A and D spikes above the turbulence level of the baseline configuration. This is possibly due to the physical relationship of the ramp and the transducer. The ramp forms a corner with the wall at this location and partially covers the transducer. The turbulence in such a corner may be concentrated locally and therefore, not representative of turbulence that a store located away from the wall would experience.

Figure 19 presents very similar results at Mach 1.3. Again the combination of Suppressors A and D are slightly superior to the Saw Tooth Spoiler (A) alone.

Figure 20 presents data comparing various B-43 loading configurations to the empty bay and also shows the effect of the saw Tooth Spoiler on the double B-43 loading configuration. Figure 20A is the centerline distribution and Figure 20B is the left wall distribution. The spoiler is effective at all locations; however, it is least effective at the X/L .95 position on the left wall. The peak level of turbulence for the double B-43 configuration is approximately .12 without the spoiler and approximately .9 with the spoiler. The location of the peak level is shifted from the mid wall to the X/L .95 position on the left wall with the spoiler in place.

Figure 21 presents data for the single B-57 loading configuration at Mach .95. The B-57 is a much smaller store than the B-43, and as seen in Figures 9 and 10, the turbulence distribution for this loading is very similar to that for the empty bay. The X/L .8 position is near the rear of the B-57; therefore, the turbulence levels aft of this station are not considered to significantly affect the store. Figure 21A, the centerline distribution, shows that the spoiler (Suppressor A) reduces the turbulence levels only slightly. The left wall distribution, Figure 21B, shows similar results except aft of the store where the turbulence is actually increased significantly.

Suppressor A was found to be more effective at the higher Mach numbers investigated. Figures 22 and 23 present data which compares the B-57 loading with and without the Saw Tooth Spoiler at Mach 1.2 and 1.3 respectively. The spoiler is seen to effectively reduce the turbulence at all locations on the left wall at these Mach numbers. Similar results were observed along the bay centerline at these Mach numbers.
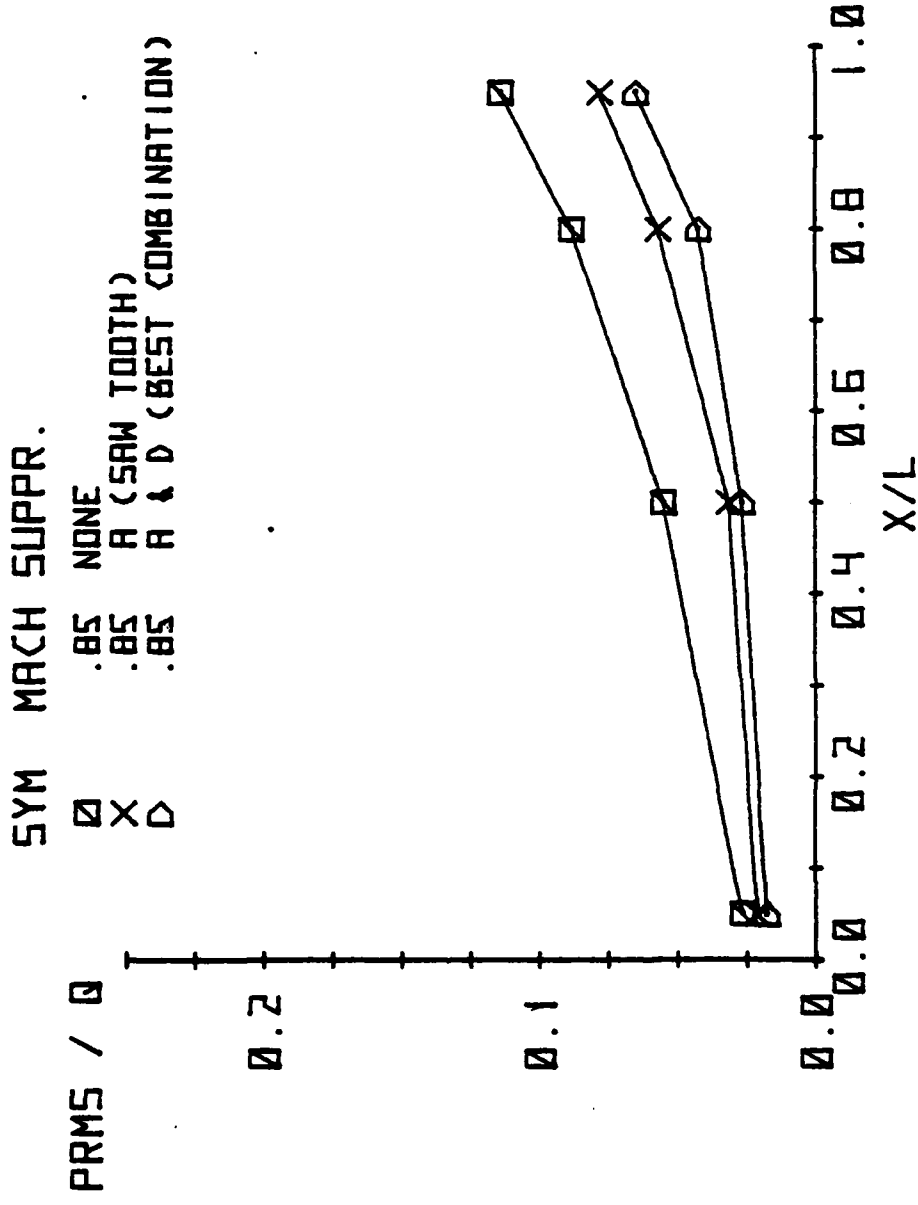
FIG 18A COMPARISON OF CENTERLINE DYNAMIC PRESSURE DISTRIBUTIONS WITH BEST SUPPRESSORS TO THE BASIC BAY AT MACH .85.

925
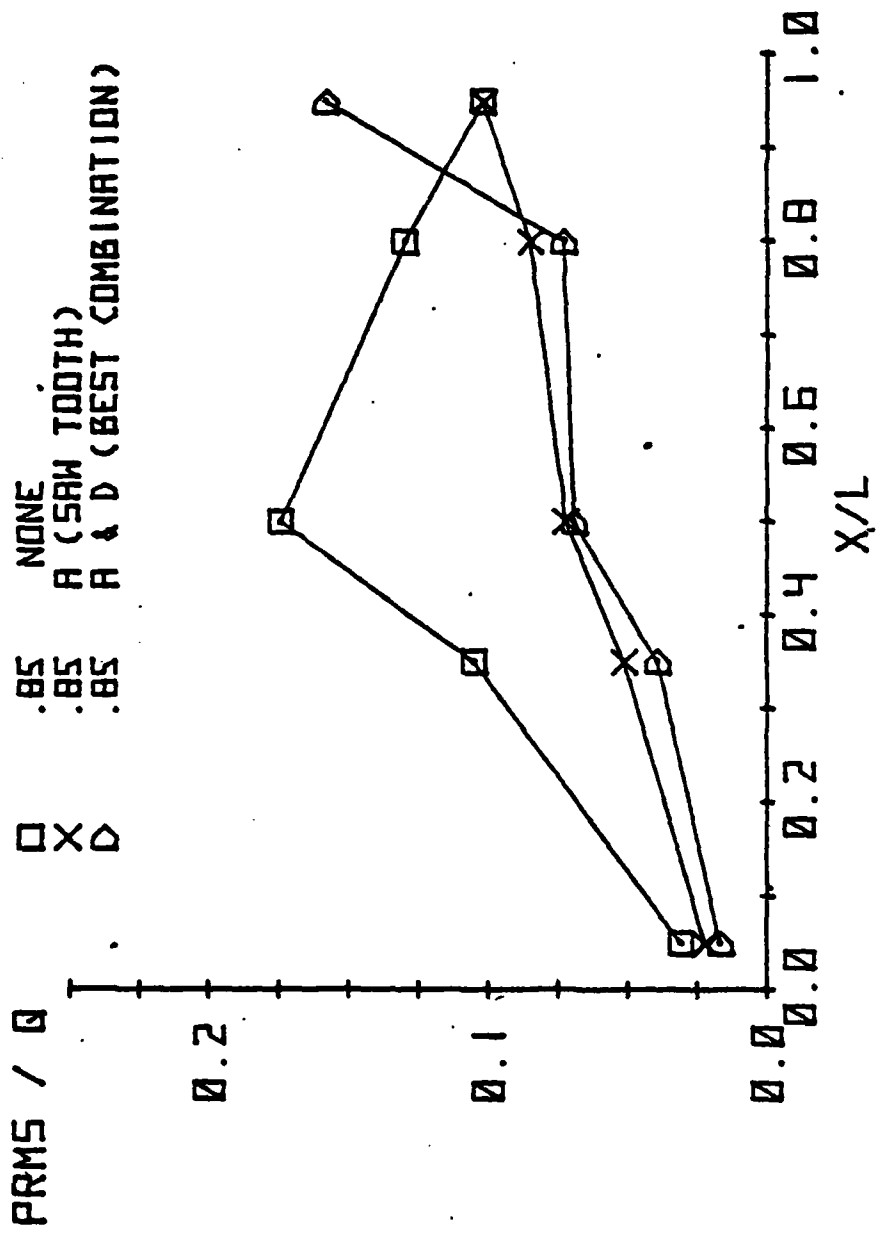
FIG 18B COMPARISON OF LEFT BAY WALL DYNAMIC PRESSURE
DISTRIBUTIONS WITH BEST SUPPRESSORS TO THE
BASIC BAY AT MACH .85.

926

FIG 19A COMPARISON OF CENTERLINE DYNAMIC PRESSURE DISTRIBUTIONS
WITH BEST SUPPRESSORS TO THE BASIC BAY AT MACH 1.3.

FIG 19B   COMPARISON OF LEFT WALL DYNAMIC PRESSURE DISTRIBUTIONS
WITH BEST SUPPRESSORS TO THE BASIC BAY AT MACH 1.3.

FIG 20A   COMPARISON OF CENTERLINE DYNAMIC PRESSURE
DISTRIBUTIONS FOR VARIOUS BAY LOADINGS TO THE EMPTY BAY

FIG 29B COMPARISON OF LEFT WALL DYNAMIC PRESSURE DISTRIBUTIONS FOR VARIOUS BAY LOADINGS TO EMPTY BAY

930

FIG 21A   SINGLE B-57 LOADING WITH AND WITHOUT SUPPRESSOR A, CENTERLINE DISTRIBUTION AT MACH .95.

931
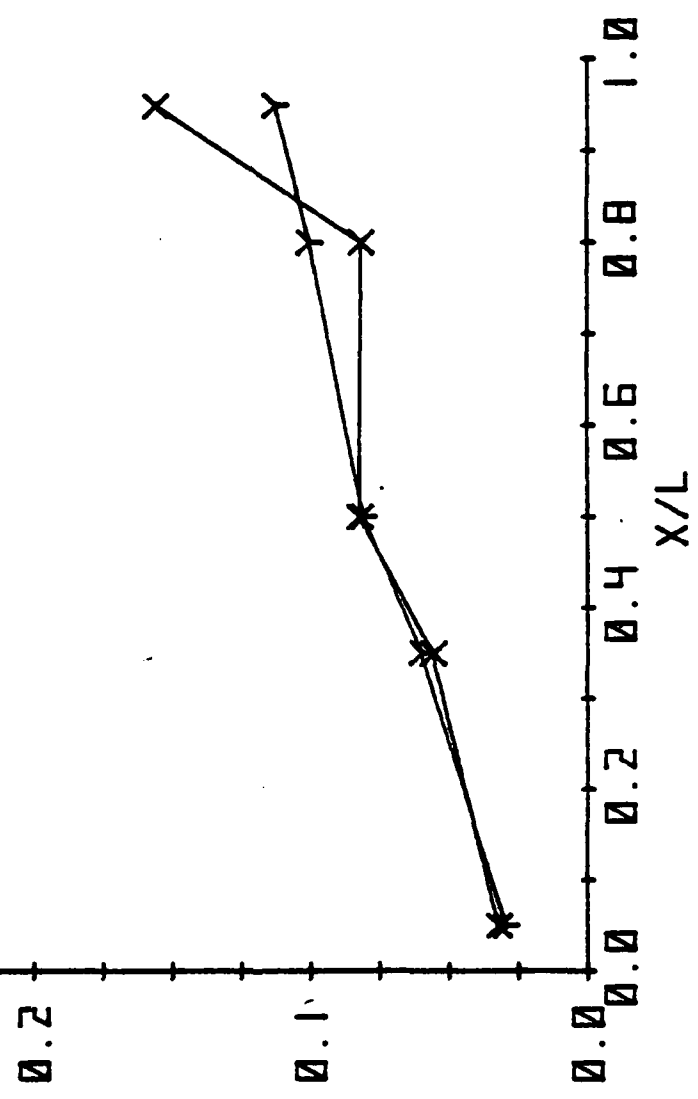
FIG 21B   SINGLE B-57 LOADING WITH AND WITHOUT SUPPRESSOR A,
LEFT BAY WALL DISTRIBUTION AT MACH .95.

932

SYM MACH LEFT BAY. RIGHT BAY. BAY SUPPR.

Y   1.2   B-57   EMPTY   NONE
X   1.2   B-57   EMPTY   A (SAW TOOTH)

PRMS / Q

0.2

0.1

0.0

0.0   0.2   0.4   0.6   0.8   1.0

X/L
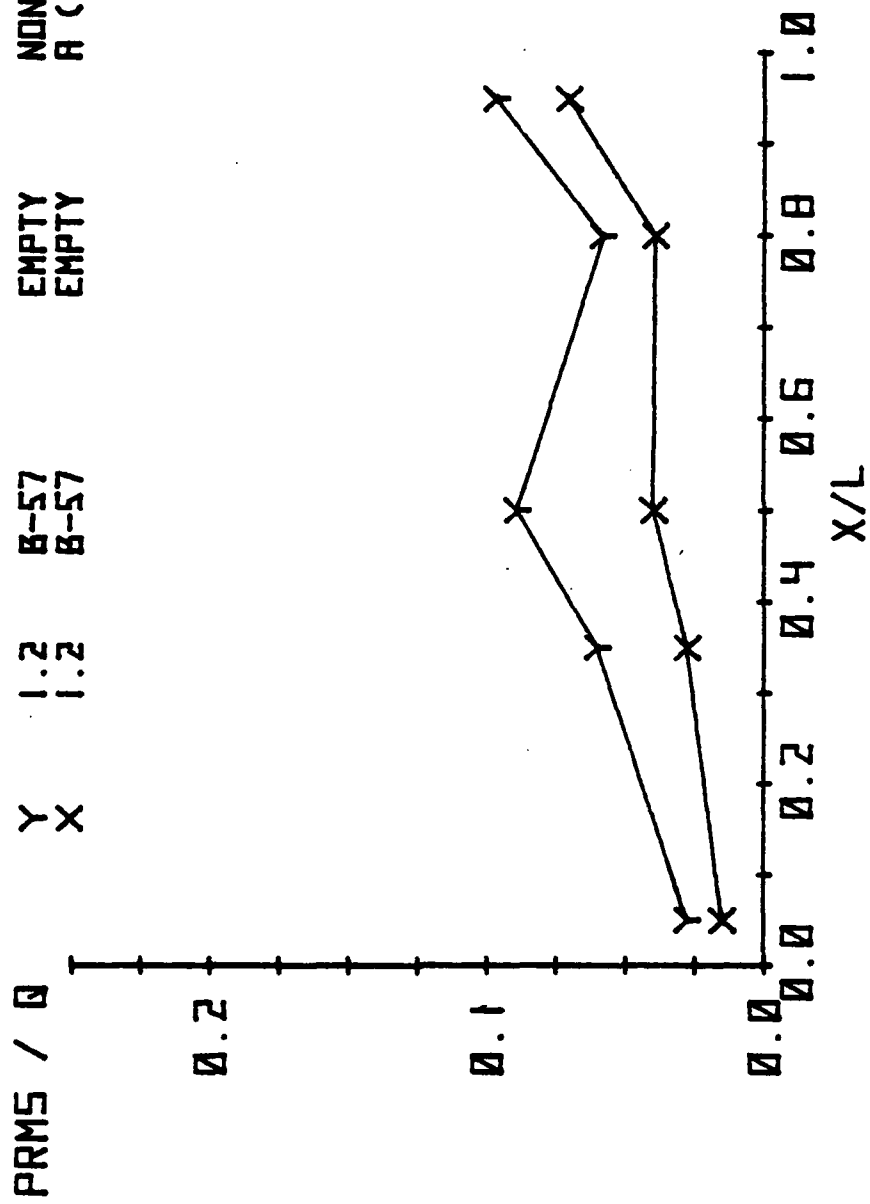
FIG 22   SINGLE B-57 LOADING WITH AND WITHOUT SUPPRESSOR A, LEFT BAY WALL DISTRIBUTION AT MACH 1.2.

933
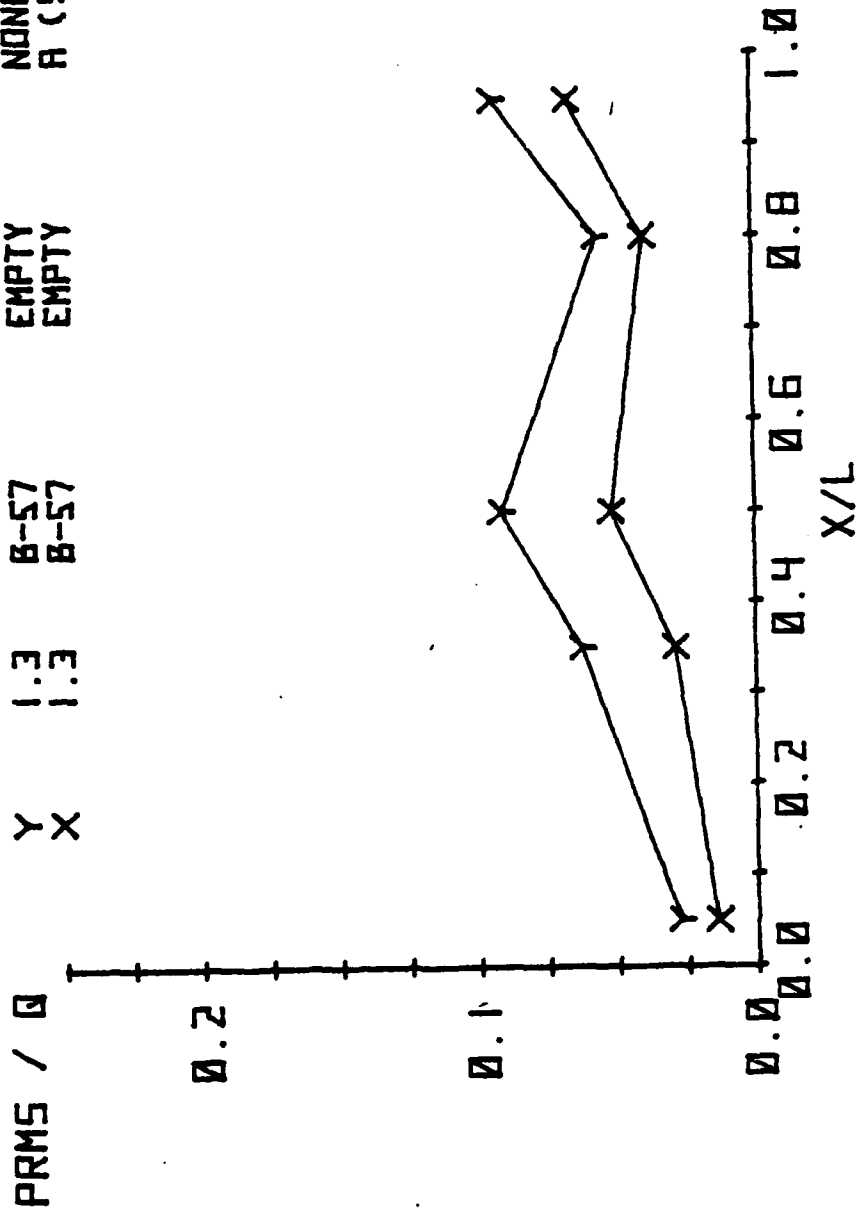
FIG 23   SINGLE B-57 LOADING WITH AND WITHOUT SUPPRESSOR A, LEFT WALL DISTRIBUTION AT MACH 1.3.

EFFECT OF SAW TOOTH SPOILER SUPPRESSOR ON WEAPON SEPARATION

Figure 24 shows the details of the model weapon ejection system with a scaled B-43 store installed. The heavy model scaling laws (Reference 4) were used to design the B-43 and B-57 drop models fabricated by General Dynamics for this test program. This reference also describes the data acquisition and analysis procedures used by AEDC. Wind tunnel conditions were adjusted to provide the proper simulated altitude for heavy model scaling.

Figures 25 and 26 show the favorable effect of the spoiler on the pitch attitude, theta of the B-43 store at Mach .95 and 1.3 respectively. Theta is the angle between the centerline of the tunnel and the centerline of the store during the store separation. Since the store separation data is obtained by analysis of high speed 16mm film of the drop, the store while inside the bay is not visible from the side. The store becomes viewable from the side camera approximately .2 seconds into the trajectory. The data presented in these figures is presented in full scale and not model scale form. Reference 4 contains the appropriate conversion equations.

The standard F-111 ejection parameters scaled in accordance with Reference 4 were used for all of the separation tests. The full scale launch parameters for the two stores tested are as follows:

Launch	B-43	B-57
Ejection Velocity (fps)	10.5	16.6
Pitch Rate (Positive nose up, degs/sec)	-16.6	-92.8

Figures 25 and 26 clearly indicate that there is a strong nose up moment applied to store by the flow field without the spoiler which overcomes the nose down moment applied by the ejector. The Saw Tooth Spoiler (Suppressor A) significantly reduces the maximum pitch angle of the store and delays the occurrence of this maximum angle to a later point in the trajectory. The separation trajectory at Mach 1.3, Figure 26, represents the worst case for either the single B-43 or double B-43 loadings. The spoiler reduces the maximum pitch angle to approximately one half that of the standard F-111 configuration.

Separation tests were conducted for the single B-57, double B-43, B-43/gun and B-43/gun plus ECM pod configurations with and without Suppressor A. For the latter two configurations, the suppressor was modified by removing the portion of the right half of the spoiler which would block the gun port. All of the trajectories were improved by addition of the suppressor. The improvements were particularly significant for the B-43/gun and B-43/gun plus ECM pod configurations at Mach 1.3.

935
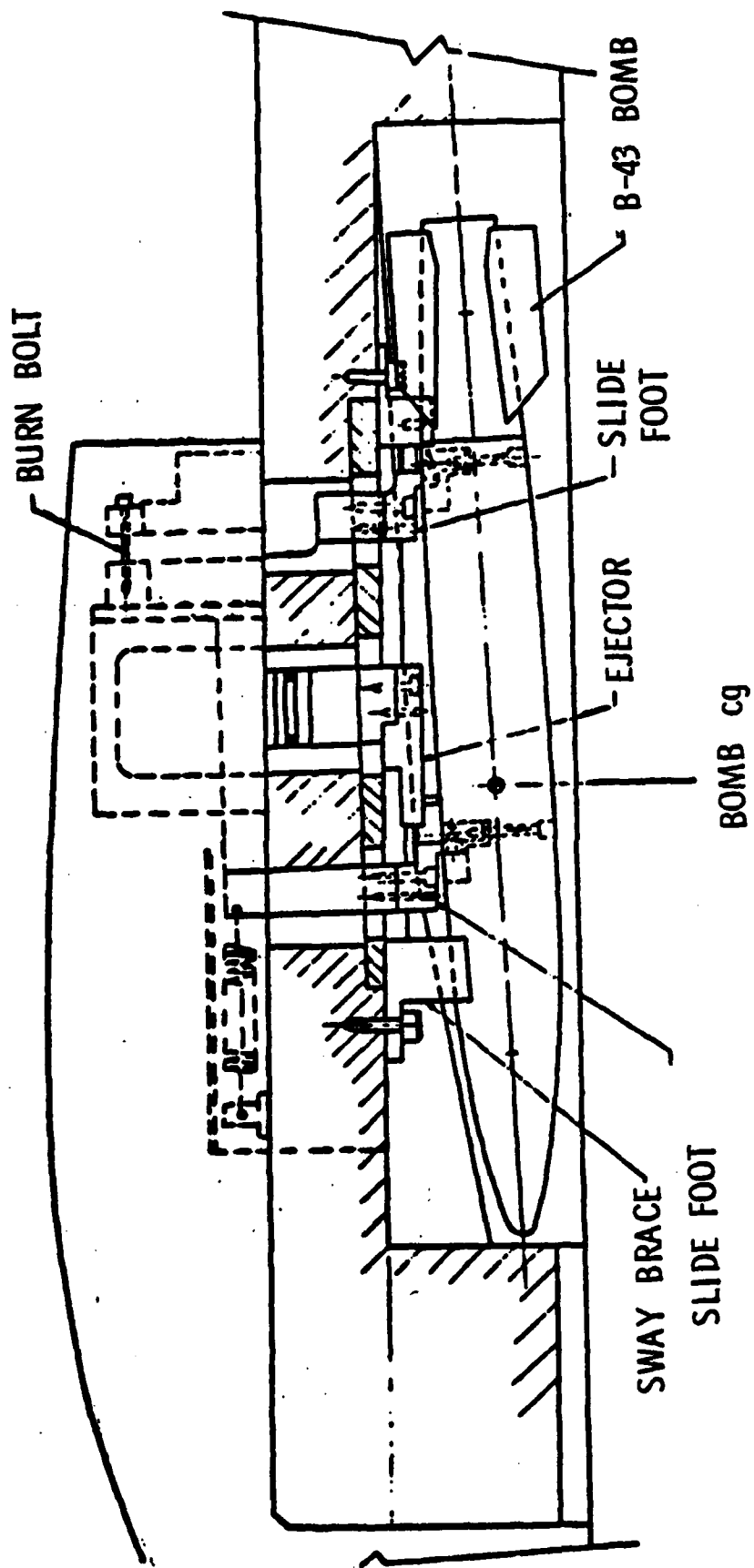
FIG. 24 MODEL STORE EJECTION SYSTEM
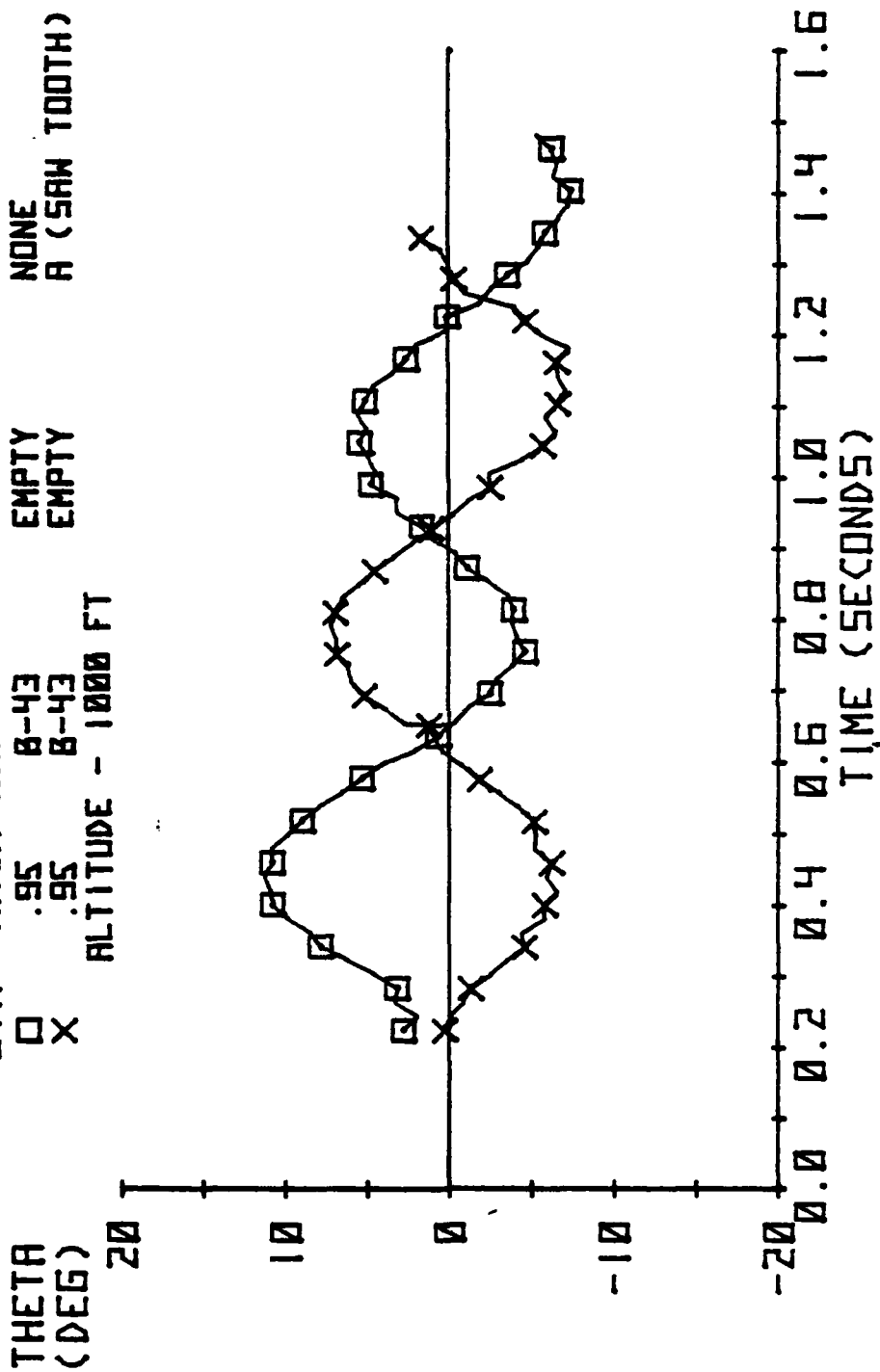
FIG 25   B-43 PITCH ATTITUDE DURING SEPARATION AT

MACH .95 WITH AND WITHOUT SUPPRESSOR A.
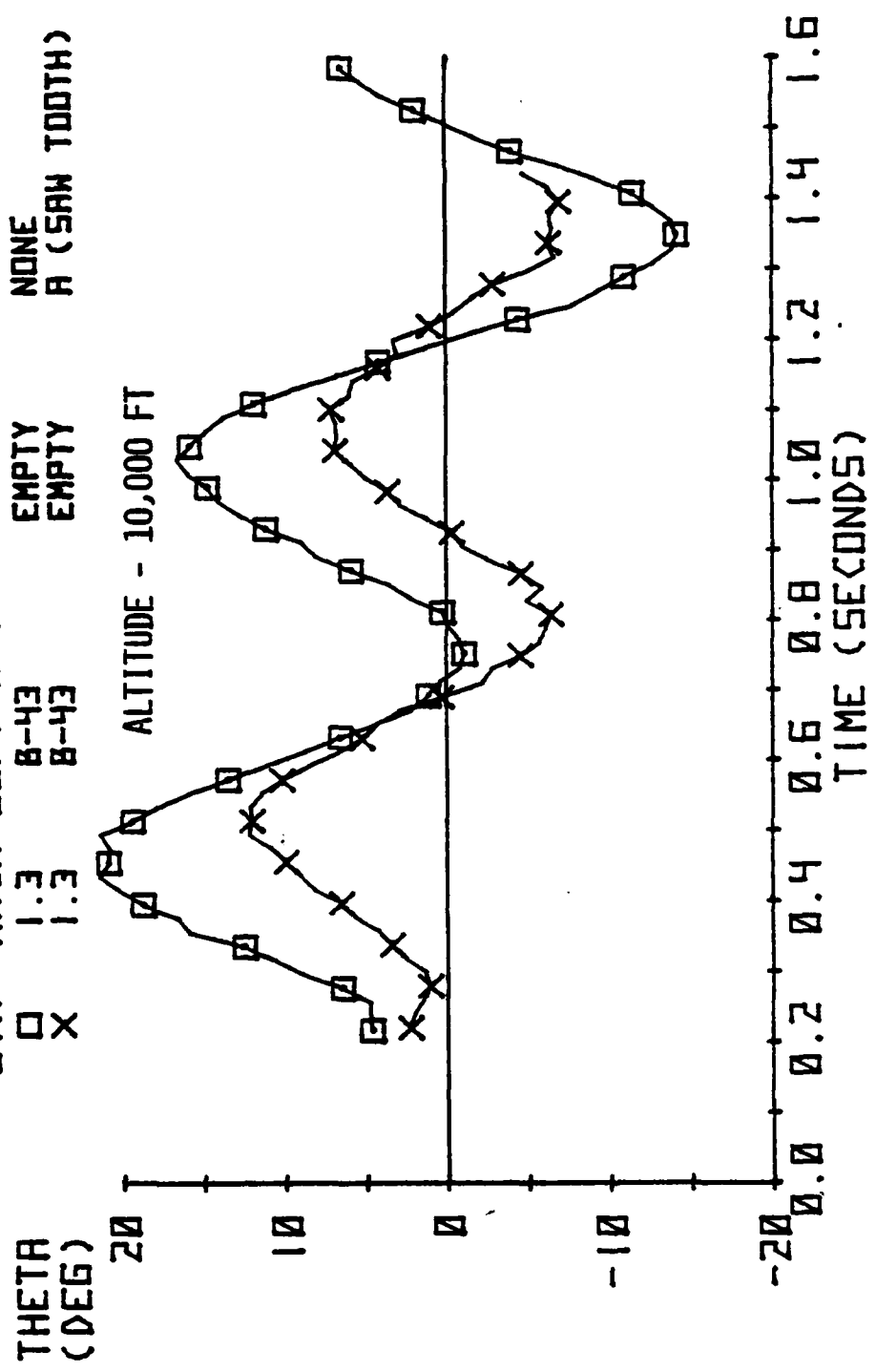
FIG 26 B-43 PITCH ATTITUDE DURING SEPARATION AT MACH 1.3 WITH AND WITHOUT SUPPRESSOR A.

Limited separation tests were also performed to evaluate the best combination of suppressors, the saw tooth (A) with the rear ramp deflector (D).

CONCLUSIONS

1. The turbulence levels in the F-111 internal weapons bay can be significantly reduced during weapon delivery (bay open) operations.

2. The saw tooth spoiler type aero-acoustic (turbulence) suppression device mounted at the bay leading edge is the most effective single modification investigated to date.

3. The saw tooth spoiler investigated produced favorable separation effects for all test conditions and configurations investigated.

4. Modifications to the aft bulkhead of an internal weapons bay can improve the internal bay environment, and these improvements will complement those produced by a bay leading edge mounted spoiler.

5. Mach 1.3 and 10,000 ft was determined to be the most severe separation condition investigated during this test program.

6. Significant potential improvements in the F-111 weapon bay have been demonstrated during wind tunnel investigations of a scaled F-111 wind tunnel model. Full scale flight investigations will be required to confirm the expected operational improvements.

REFERENCES

1.   Shaw, L.L. and Smith, D.L., "Aeroacoustic Environment of a Store in an Aircraft Weapons Bay," AFFDL-TR-77-18, March 1977.

2.   Clark, R.L., "Weapons Bay Turbulence Reduction Techniques," AFFDL-TM-75-147-FXM, December 1975.

3.   Anderson, C.F., "Static and Fluctuating Pressures in the Weapons Bay of a 1/15-Scale F-111F Model at Transonic Speeds," AEDC-TR-75-113, August 1975.

4.   Kukainis, Janis, "Free Drop Trajectory Characteristics of Bluff-Shaped Bombs Released From the F-111 Aircraft Weapons Bay at Mach Numbers From 0.70 to 1.30," AEDC-TR-103, May 1971.

Rodney L. Clark

Mr. Clark is currently assigned to the Aeromechanics Division of
the Air Force Flight Dynamics Laboratory, Wright-Patterson AFB, Ohio.
He graduated from Texas Technological University in 1961 with a B.S. de-
gree in Mechanical Engineering. He initially worked in the Aeronautical
Systems Division in the V/STOL Propulsion Branch. Reassigned to the Air
Force Flight Dynamics Laboratory in 1966, he continued work in the area
of V/STOL propulsion aerodynamics (powered lift) until 1973. For the
past four years, he has been working in the area of internal and exter-
nal weapons carriage and separation. He has conducted in-house research
experiments on turbulence reduction techniques which can be applied to
internal weapons bays. He is presently responsible for the technical
direction of the AFFDL/AFWL F-111 Weapons Bay Program.

John Doran

Mr. John Doran attended Rutgers University, New York University, and the University of New Mexico. He now resides in Alburquerque, New Mexico. He has a Bachelor of Science Degree in Education and has done graduate work in nuclear engineering. He is presently an aerospace engineer for the Systems Branch, Nuclear Systems Division, Air Force Weapons Laboratory at Kirtland AFB, New Mexico. While in the USAF he attended radar officers school at Keesler AFB and the Atomic Weapons School at Sandia Base. In 1957 he entered Civil Service and joined the organization which later became the Air Force Weapons Laboratory. He has attended several schools including Systems Engineering/Configuration Management, AFIT/AFWL Vulnerability/Survivability, and Management of Scientists & Engineers. Early in his career he managed the Defense Atomic Support Agency now Defense Nuclear Agency Nuclear Weapons Fire and Impace Test Program at Nevada Test Site and Edwards AFB. Later, he gained experience in the internal carriage and separation of AIR-2A/F-101 & F-106, AIM-47-YF-12, and F-111/B43, 57, 61 Weapons Systems.

Recently Mr. Doran has been active in Working Party 12 of the Joint Technical Coordinating Group for Munitions Development and for the last ten years has been engaged in aerodynamic theoretical studies, wind tunnel, and fullscale flight tests with other AF Laboratories and contractors.

943

(The reverse of this page is blank)

A SIMPLIFIED TECHNIQUE FOR THE SOLUTION OF SUBSONIC
FLOWS USING SURFACE SINGULARITIES
(U)
(Article UNCLASSIFIED)

by

Fred W. Martin
and
John E. Burkhalter
Aerospace Engineering
Auburn University
Auburn, Alabama   36830

ABSTRACT. (U) A technique is proposed for determining the span-
wise and chordwise distribution of load on thin finite wings in com-
pressible subsonic flow. The method is based on the application of
planar lifting surface theory with a simple technique for evaluating
the kernel function integral. A somewhat similar method is presented
for the solution of axisymmetric bodies using the method of source
panels. Excellent correlation with experimental results is shown for
both cases.

945

LIST OF FIGURES

946

LIST OF FIGURES (CONCLUDED)

INTRODUCTION

The mutual aerodynamic interference problem for external stores has received considerable attention during the past few years. The authors, among others, have studied this problem for some time using the Rankine method. While this technique has proved most useful, it is quite difficult to apply this method to arbitrary body shapes. A more appealing approach to the problem, at least in regard to arbitrary shapes, is to use distributed surface singularities such as in the methods of vortex-lattice and source panels. These techniques have some serious drawbacks, however, such as requiring large computer storage and computational times as well as mathematical discontinuities which must also be properly handled.

A technique which circumvents many of the classical problems has been applied to thin wings by Purvis, Reference 1. The method is based on the application of the planar lifting surface theory. Classical theoretical results are used to define stable, low-order functions for the pressure coefficient distribution, and a new technique is presented for evaluating the kernel function integral.

A somewhat similar method has been applied to axisymmetric bodies by Baker, Reference 2. The surface source density distribution is determined in a simplified manner by formulating a general functional form for the distribution.

The general techniques presented by Purvis and Baker are outlined in the following Sections. Liberal use has been made of passages and figures from their theses.

SUBSONIC LIFTING SURFACE

INTRODUCTION

A method is presented for using the lifting surface theory which retains the advantages of the theory while eliminating or minimizing some of the inherent problems. In this connection results of lifting line, thin airfoil, and slender wing theories are used to develop a general functional form for the ΔC_p distribution, and the basic integral equation is expressed in terms of vorticity (vortex strength distribution).

Additionally, evaluation of the integral is done in a closed form-finite summation manner, which eliminates the need for numerical integration, reduces the order of the singularity (and hence the sensitivity of the solution near control points), and eliminates the need for using the Mangler technique.

The governing equation is the usual Prandtl-Glauert equation

$$\beta \phi_{xx} + \phi_{yy} + \phi_{zz} = 0 \tag{1}$$

where β is the Mach number parameter expressed as

$$\beta = \sqrt{1-M_\infty^2} \tag{2}$$

The body boundary condition is expressed as

$$\vec{v} \cdot \text{grad } f = 0 \tag{3}$$

where
$$f(x,y,z) = 0 \tag{4}$$

is the equation of the body.

ANALYSIS

The plane of the wing is represented mathematically as a finite sheet of elemental horseshoe vortices with a variable strength distribution over the surface. The resulting kernel function which satisfies the potential equation for compressible flow, equation (1), can be expressed as

$$\phi(x,y,z) = \frac{1}{4\pi} \iint_S \frac{\gamma(x_o,y_o)}{(y-y_o)^2+z^2} \; z \left[1 + \frac{(x-x_o)}{\sqrt{(x-x_o)^2+\beta^2(y-y_o)^2+\beta^2z^2}} \right] dx_o dy_o$$

(5)

which is the non-dimensional perturbation velocity potential for a thin planar lifting surface in compressible subsonic flow. The following analysis is quoted (with appropriate changes in numbering) from Reference 1:

The variables of integration x_o, y_o are defined over the planform surface S, and $\gamma(x_o,y_o)$ is the unknown distribution of vorticity. The relation between the pressure loading coefficient ΔC_p and the vorticity is found by applying the Kutta-Joukowski Theorem, or more rigorously, Stokes' Theorem, at a point on the surface (See Reference 3),

$$\gamma(x_o,y_o) = \frac{\Delta C_p(x_o,y_o)}{2}$$

(6)

The non-dimensional perturbation velocity w, or downwash, which the lifting surface induces normal to itself is found by differentiating equation (5) with respect to z and taking the limit as $z \to 0$. Defining the dimensionless spanwise and chordwise variables ξ and η as

$$\xi = \frac{x-x_{LE}(y)}{c(y)}, \quad \eta = \frac{y}{b/2}$$

(7)

the differentiation and limit evaluation results in

$$w(x,y) = \frac{1}{8\pi} \iint_S \frac{\Delta C_p(\xi,\eta)}{(y-y_o)^2} \left[1 + \frac{(x-x_o)}{\sqrt{(x-x_o)^2 + \beta^2(y-y_o)^2}} \right] dx_o dy_o$$

(8)

By expressing ΔC_p as the proper combination of spanwise and chordwise variables, the behavior along a chord line or across the span can be examined independently. Since the loading along each chord line should behave in the classical two-dimensional manner at the leading and trailing edges, thin airfoil theory results can be used to define ΔC_p as

$$\Delta C_p(\xi,\eta) = \sqrt{\frac{1-\xi}{\xi}} \; \sum_{n=0}^{N} A_n(\eta)\xi^n$$

(9)

950

The first term in equation (9) has the required leading edge singularity and each term satisfies the Kutta condition at the trailing edge, as shown in Figure 1. Lifting line theory indicates that the spanwise coefficients $A_n(\eta)$ should be elliptic in nature for finite values of taper ratio, and for zero taper ratio the required behavior is that of slender wing theory. A functional form found to satisfy both of these requirements is

$$A_n(\eta) = \left[\frac{\sqrt{1-\eta^2}}{1-\eta(1-\lambda)} \right] \sum_{m=0}^{M} B_{nm}\eta^m \qquad (10)$$

The B_{nm}'s are constant coefficients, and the denominator in brackets is the equation for a local chord based on a unit root chord. For zero taper ratio, the bracketed term reduces to $\sqrt{1+\eta}/\sqrt{1-\eta}$, which has the required slender wing behavior near the wing tips. For a taper ratio of 1.0, the classical elliptic loading term $\sqrt{1-\eta^2}$ is obtained. These properties are illustrated in Figure 2. Combining equations (9) and (10) the complete expression for the pressure loading coefficient becomes:

$$\Delta C_p(\xi,\eta) = \sqrt{\frac{1-\xi}{\xi}} \left[\frac{\sqrt{1-\eta^2}}{1-\eta(1-\lambda)} \right] \sum_{n=0}^{N} \left\{ \sum_{m=0}^{M} B_{nm}\eta^m \right\} \xi^n \qquad (11)$$

Returning to the evaluation of the downwash, note that over a sufficiently small element of the planform surface ΔC_p is approximately constant and so can be taken outside the integral. The downwash due to this small element then becomes

$$\Delta w(x,y) = \frac{\Delta C_p(\bar{\xi},\bar{\eta})}{8\pi} \int_{y_1}^{y_2} \int_{x_1}^{x_2} \frac{1}{(y-y_0)^2} \left[1 + \frac{(x-x_0)}{\sqrt{(x-x_0)^2+\beta^2(y-y_0)^2}} \right] dx_0\,dy_0 \qquad (12)$$

where $\Delta C_p(\bar{\xi},\bar{\eta})$ is evaluated at the centroid of the element. The integral thus obtained can be evaluated in closed form with the result:

$$\Delta w(x,y) = \frac{\Delta C_p(\bar{\xi},\bar{\eta})}{8\pi} \left[K(x_2,y_2) - K(x_2,y_1) - K(x_1,y_2) + K(x_1,y_1) \right] \qquad (13a)$$

951

$$\Delta C_p(\xi, \eta) = \sqrt{\frac{1-\xi}{\xi}} \sum_{n=0}^{N} A_n(\eta) \xi^n$$
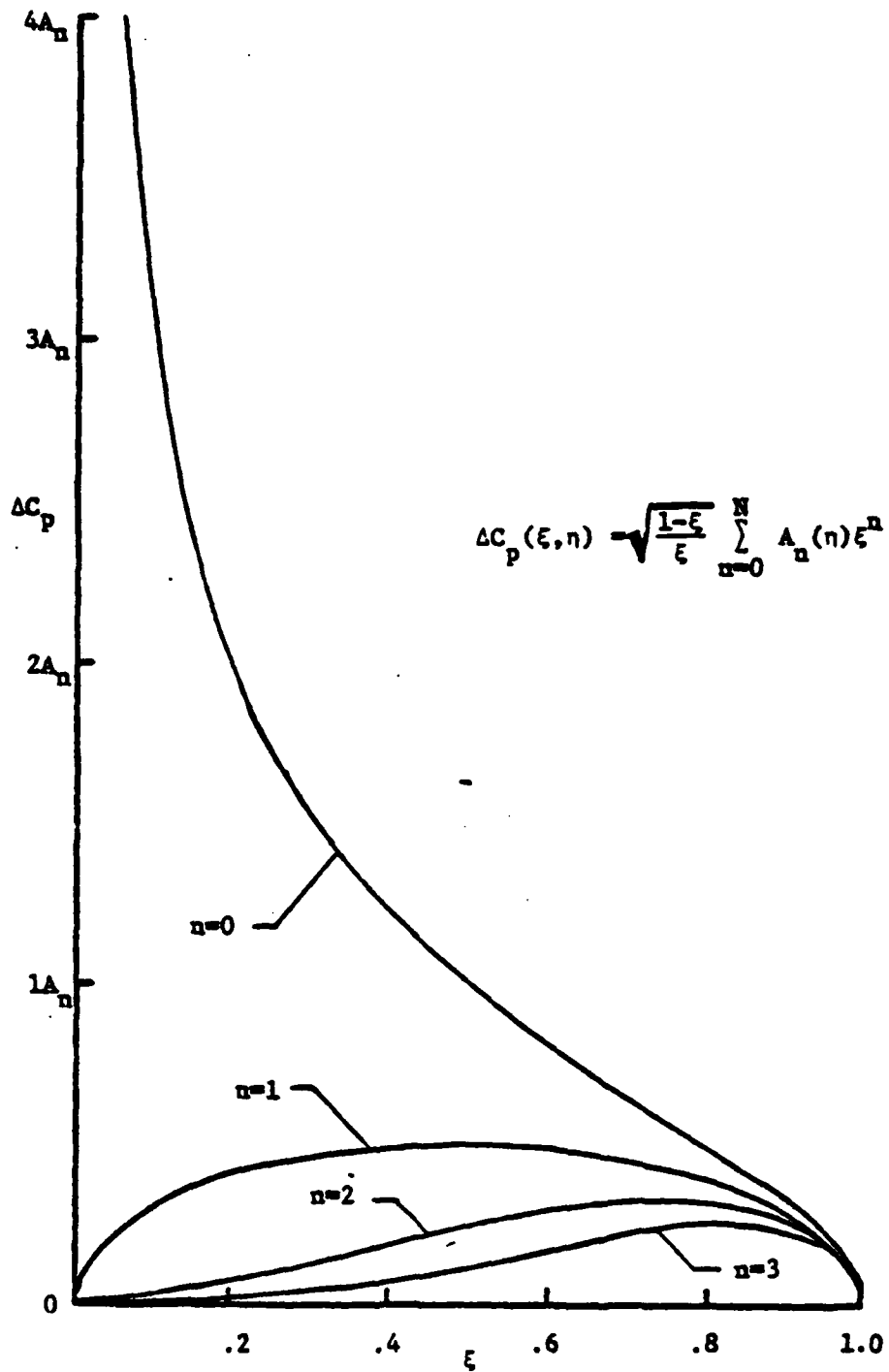
Figure 1. Chordwise Loading Showing the Effect of the Higher Order Corrections.

952

$$A_n(\eta) = \left[\frac{1-\eta^2}{1-\eta(1-\lambda)}\right]\sum_{m=0}^{M} B_{nm}\eta^m$$
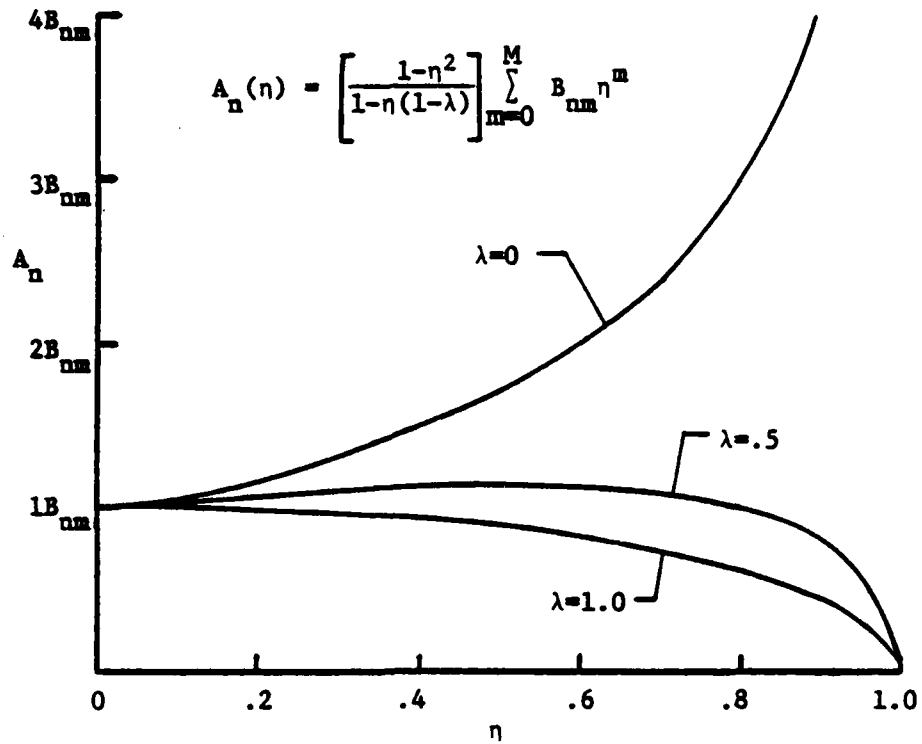
a. Schematic Showing Effect of Taper Ratio, d(m=0)
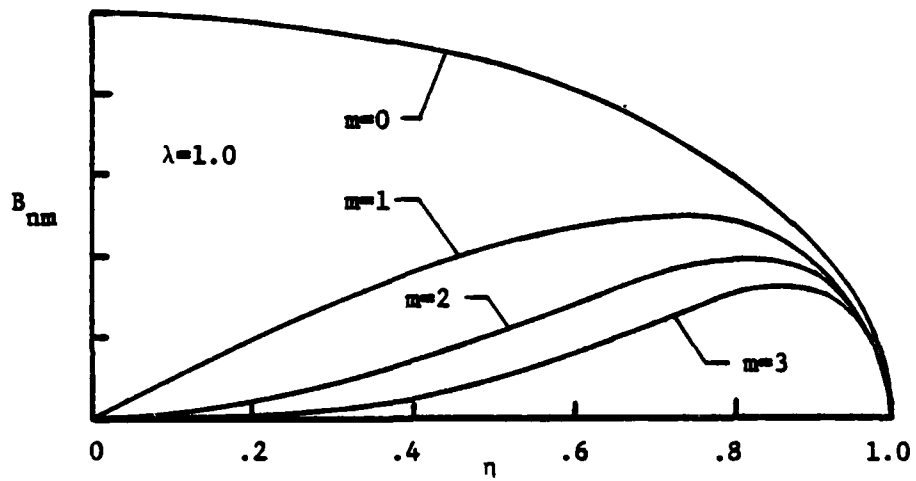
b. Schematic Showing Effect of the Index, m.

Figure 2. Spanwise Loading Showing the Effect of
the Higher Order Corrections.

953

where

$$K(x,y) = -\frac{(x-x_o) + \sqrt{(x-x_o)^2 + \beta^2(y-y_o)^2}}{(y-y_o)}$$

$$+ \beta \log_e\left[\beta(y-y_o) + \sqrt{(x-x_o)^2 + \beta^2(y-y_o)^2}\right] \qquad (13b)$$

If the entire planform is divided into similar small elements, the total downwash at any point on the wing surface may be written as

$$w(x,y) = \sum_S \Delta w(x,y) \qquad (14)$$

where equations (11) and (13) are used to evaluate each Δw. Limiting the analysis to small angles of attack, the freestream velocity component normal to the wing is $V_\infty \tan \alpha \approx V_\infty \alpha$ and the non-dimensional tangency condition is then

$$w(x,y) + \alpha(x,y) = 0 \qquad (15)$$

Introducing this tangency condition into equation (14) defines the load distribution in terms of the physical requirement of no flow through the wing. Choosing spanwise and chordwise control points according to

$$x_i = x_{LE}(y_j) + \frac{c(y_j)}{2}\left[1 - \cos\left(\frac{\pi i}{N+1}\right)\right] , \quad i=1,2,\ldots,N+1$$

$$y_j = \frac{b}{2} \cos\left(\frac{\pi i}{2M+2}\right) , \quad j=1,2,\ldots,M+1 \qquad (16)$$

and evaluating equation (15) at each control point gives:

$$\alpha(x_i,y_j) + \sum_S \Delta w(x_i,y_j) = 0 \qquad (17)$$

Equation (17), together with the defining relations (11) and (13), constitutes a set of simultaneous algebraic equations for the NxM unknown loading coefficients B_{nm}. The reasons for the particular choice of control point locations is discussed in the following section.

As long as each (x_i,y_j) control point is centered spanwise in an element for the Δw calculations, there are no "y" singularity problems. However, if $(y-y_1)$ or $(y-y_2)$ is negative, and $(x-x_1)^2$ or $x-x_2)^2$ is

954

close to zero, computer difficulties in evaluating the logarithm term may be avoided by using the relation

$$\log_e\left[\frac{-y + \sqrt{x_1^2 + y^2}}{-y + \sqrt{x_2^2 + y^2}}\right] = \log_e\left[\frac{y + \sqrt{x_2^2 + y^2}}{y + \sqrt{x_1^2 + y^2}}\right] \tag{18}$$

Once the B_{nm} coefficients have been found by matrix inversion, the pressure coefficient at any point on the wing is available from equation (11).

The spanwise section loading is given by (See Reference 4),

$$cc_\ell\Big|_{y=y_o} = c \int_0^1 \Delta C_p(\xi, \eta_o)d\xi \tag{19}$$

This integration can be done in closed form. Defining

$$I_n = \int_0^1 \xi^n \sqrt{\frac{1-\xi}{\xi}} \, d\xi, \quad n=0,1,2,\ldots,N \tag{20}$$

and integrating yields

$$I_n = \frac{\pi}{2} , \text{ for } n = 0$$

$$I_n = \left(\frac{2n-1}{2n+2}\right) I_{n-1} , \text{ for } n=1,2,\ldots,N \tag{21}$$

which reduces equation (19) to

$$cc_\ell\Big|_{y=y_o} = c\left[\frac{\sqrt{1-\eta_o^2}}{1-\eta_o(1-\lambda)}\right] \sum_{n=0}^{N}\left\{\sum_{m=0}^{M} B_{nm}\eta_o^m\right\} I_n \tag{22}$$

The total lift coefficient can then be found in the standard manner (See Reference 4),

$$C_L = \frac{1}{S} \int_{-b/2}^{b/2} cc_\ell \, dy_o \tag{23}$$

955

The section pitching moment coefficient and chordwise center of pressure can be found with an equation similar to (22):

$$cc_m\Big|_{y=y_o} = c^2 \left[\frac{\sqrt{1-\eta_o^2}}{1-\eta_o(1-\lambda)}\right] \sum_{n=0}^{N} \left\{\sum_{m=0}^{M} B_{nm}\eta^m\right\} I_{n+1} \tag{24}$$

and from Reference 4,

$$x_{cp} = \frac{cc_m}{cc_l} \tag{25}$$

The total pitching moment coefficient from Reference 4 is

$$c_m = \frac{1}{S\bar{c}} \int_{-b/2}^{b/2} cc_m dy_o \tag{26}$$

If $\alpha(x,y)$ is not a constant, or if the planform is not symmetric, the rolling and yawing moment coefficients may also be evaluated using standard integrals.

RESULTS AND CONCLUSIONS

Comparison of the present theory with experimental results for a low AR delta wing is shown in Figure 3, which gives the chordwise distribution of ΔC_p at three spanwise locations. The agreement is excellent except near the leading edges and wing tips, where ΔC_p theoretically becomes infinite. There seems to be a noticeable improvement over results obtained from a computer program given by Chadwick (Reference 5) which solves the lifting surface integral in the standard manner (i.e., by numerical integration). For comparison, both analytical methods used twelve tangency points; three along each chord at four spanwise locations; requiring the solution of a 12 by 12 matrix.

The theoretical and experimental spanwise distribution of lift on two swept, tapered wings of moderate aspect ratio (AR = 4.5) is shown in Figure 4. The theoretical section coefficients are the chordwise integrals of ΔC_p found from equations (22). The maximum deviation between experiment and theory is 5.65 percent, occurring near the center of the semispan on the $\lambda=1.0$ wing. Note that the well known loss of lift near the center span of swept wings is accurately predicted. The calculations for spanwise centers of pressure, and hence the section pitching moment, also show good agreement.

The measured and predicted C_{L_α}'s for low aspect ratio delta wings are shown in Figure 5. The theoretical curves properly approach the slender wing theory result for very small aspect ratios, and tend toward 2π as AR $\rightarrow \infty$. The present method shows a slight improvement over results from the method of Reference 5.

Figure 6 shows the effect of Mach number on the theoretical and experimental lift curve slopes of two thin wings. The agreement between theory and experiment is excellent for Mach numbers less than approximately 0.85.

Figure 7 shows the distribution of $\alpha-w$ over the surface of a delta wing. From the present analysis, less than two percent deviation is obtained except near the leading edge.

In conclusion, the method retains the inherent advantages of lifting surface theory; i.e., providing a continuous and realistic load distribution over the surface, satisfying the tangency conditions over most of the wing, and requiring a solution for relatively few unknowns. In addition, the resulting mathematical form is easy to program and computationally fast (other techniques require more than four times as much core and twice the execution time). Wing load distribution solutions compare extremely well with experiment, even for low aspect ratio delta wings, and show better agreement with experimental data than standard numerical integration solutions. If the airfoil section is sufficiently thin, accurate results are obtained at Mach numbers up to 0.85.

a. Spanwise Station, y/b/2 = 0.0

b. Spanwise Station, y/b/2 = 0.5

DELTA WING AR=2.5

⊙   EXPERIMENT
—   PRESENT METHOD
--   NUMERICAL INTEGRATION

y/b/2=.9
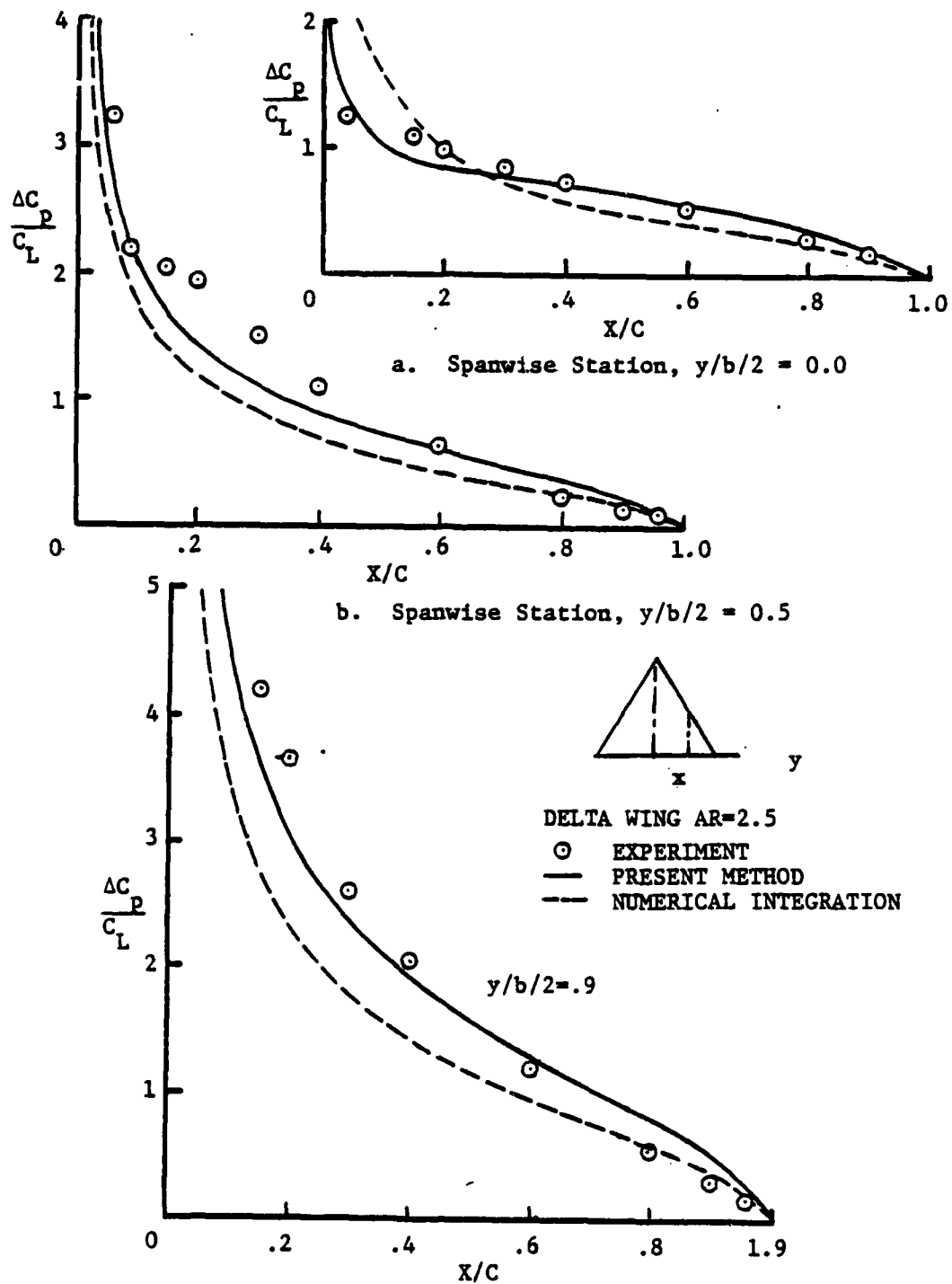
Figure 3.   Comparison of Theoretical and Experimental
Results for a Delta Wing.

a. AR=4.5, Λ=40°, λ=0.5

b. AR=4.5, Λ=40°, λ=1.0
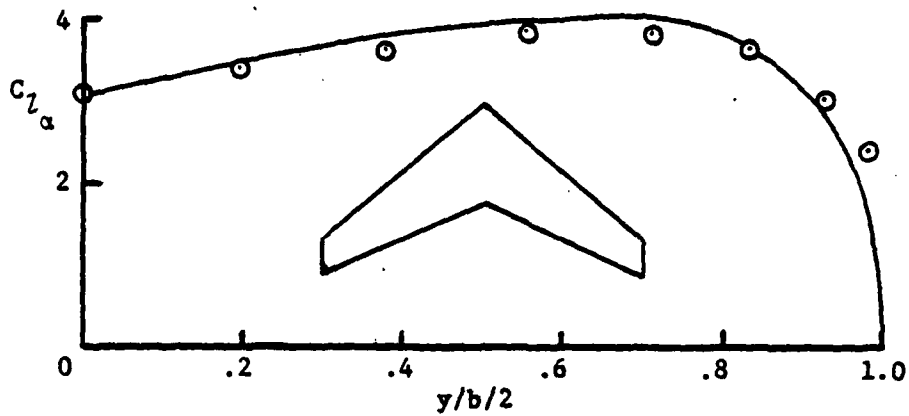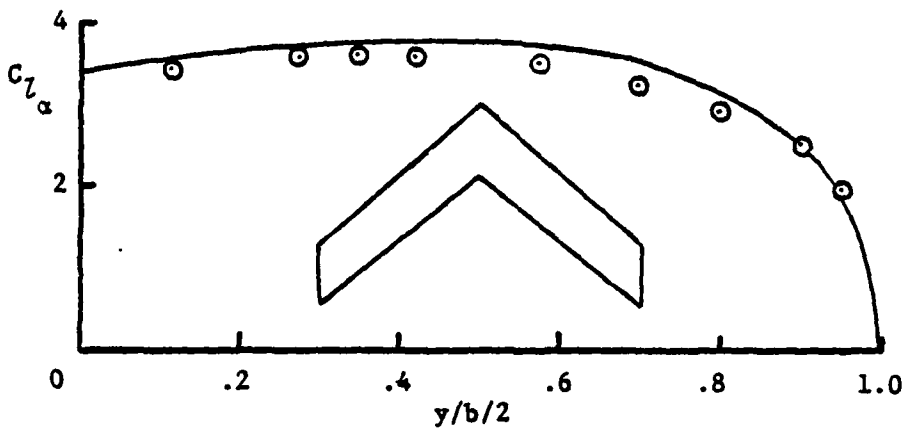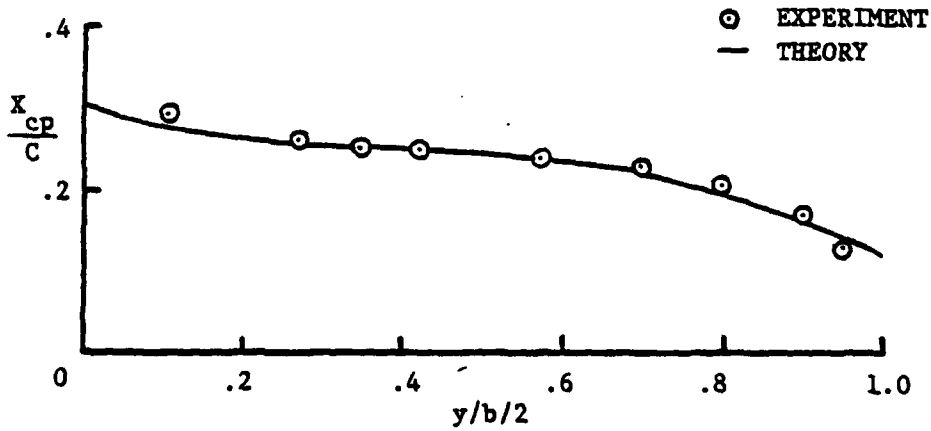
c. AR=4.5, Λ=40°, λ=1.0

Figure 4. Comparison of Theoretical and Experimental
Results for Two Swept Wings.

959

Figure 5. Comparison of Theoretical and Experimental
Results for Delta Wings.
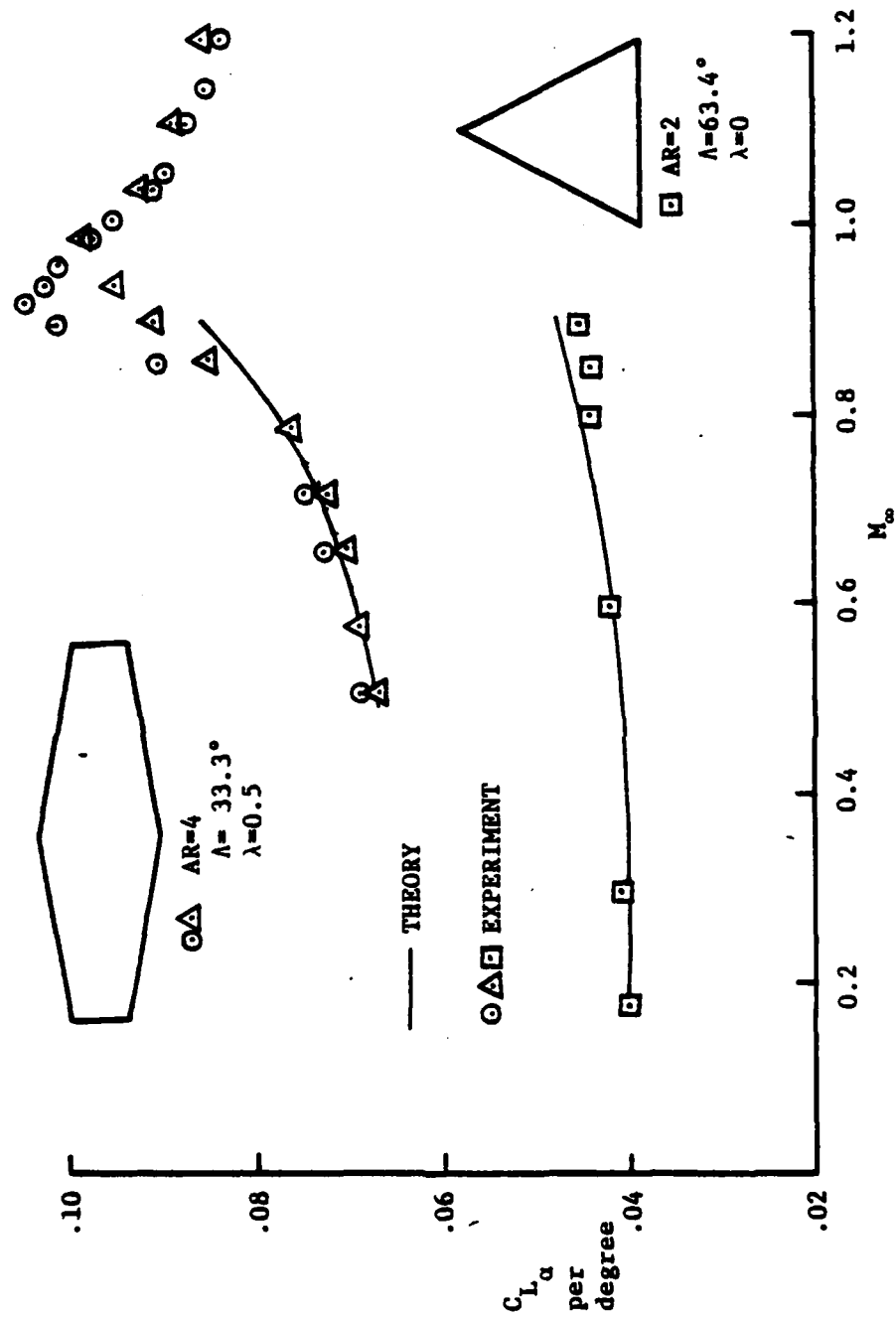
Figure 6. Comparison of Theoretical and Experimental Results as a Function Mach Number for Two Thin Wings.

Figure 7. Schematic Showing Error in Flow Tangency Conditions in the Plane of the Wing.

SUBSONIC AXISYMMETRIC BODIES

INTRODUCTION

A technique has been developed by Baker (Reference 2) which minimizes the disadvantages of the method of source panels for axisymmetric bodies while retaining its inherent accuracy and simplicity. The principal means of the technique was to derive a general functional form for the source density distribution which eliminates the need for large matrix inversion.

The approach taken in this effort was to separate the axial and crossflow solutions so that a functional form could be derived for each.

The axial distribution for the surface source density is determined by aligning the body in the flow with $\alpha = 0°$. Slender body theory is used to find the axial dependence of the source density, which is then corrected by a polynomial to fit the body in question. Similarly, the crossflow solution involves the circumferential dependence of the crossflow source density distribution, which may also be simplified through a functional form. The two functions are added together in the same way the conventional axial and crossflow solutions are added to produce an angle-of-attack solution.

The governing equations and the body boundary condition are as previously given by equations (1) through (4).

The following analysis is a condensation of the work by Baker (Reference 2).

ANALYSIS

The body is represented mathematically by assuming that the entire body surface can be replaced by source panels of constant density. The resulting expression for the velocity potential due to the source panels is the sum of the potentials for each panel and can be expressed as

$$\phi = \sum_{j=1}^{N} \sigma_j \iint_{S_j} \frac{dS}{r} \tag{27}$$

where N is the number of panels over the body surface, and r is the stretched radius given as

$$r = [(x-\xi)^2 + \beta^2(y-\eta)^2 + \beta^2(z-\zeta)^2]^{\frac{1}{2}} \tag{28}$$

Since each panel is oriented tangent to the body surface as shown in Figure 8, integration over a panel with respect to the body coordinate system is rather difficult and awkward. Consequently, appropriate coordinate transformations are made to permit integration over a panel with respect to a coordinate system attached to the respective panel. In this manner the integration problems are minimized and the algebra appears much less complicated. After integration, transformation back to the body coordinate system must be made in order to finally add solutions from each of the panels.

The derivatives of the potential equation provide the velocity components which, along with the boundary condition given by Equation (3), form a system of linear algebraic equations with the source densities as the unknowns.

The velocity components for an arbitrary source panel have been derived and when formulated for the arbitrary source panel shown in Figure 9 are as follows:

$$
V_x = \frac{n_1-n_2}{d_{12}} \ln\left(\frac{r_1+r_2+d_{12}}{r_1+r_2-d_{12}} \right) + \frac{n_2-n_3}{d_{23}} \ln\left(\frac{r_2+r_3+d_{23}}{r_2+r_3-d_{23}} \right) \tag{29}
$$
$$
+ \frac{n_3-n_4}{d_{34}} \ln\left(\frac{r_3+r_4+d_{34}}{r_3+r_4-d_{34}} \right) + \frac{n_4-n_1}{d_{41}} \ln\left(\frac{r_4+r_1+d_{41}}{r_4+r_1-d_{41}} \right)
$$
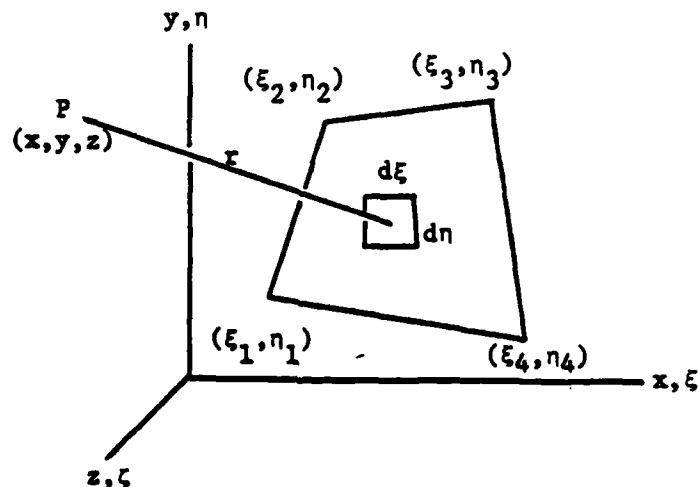
Figure 9. A Planar Quadrilateral Source Element.
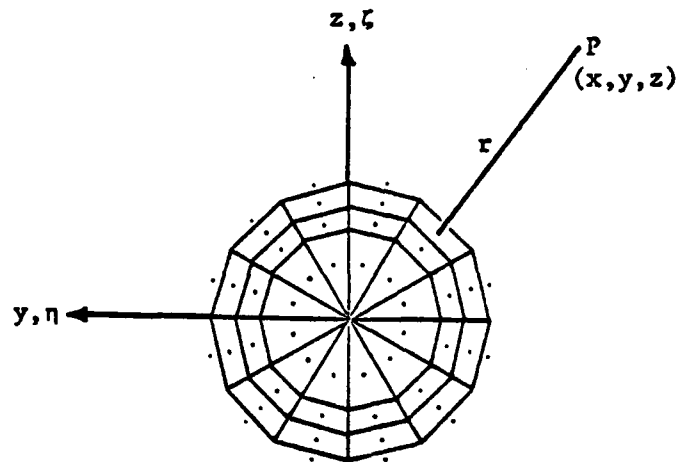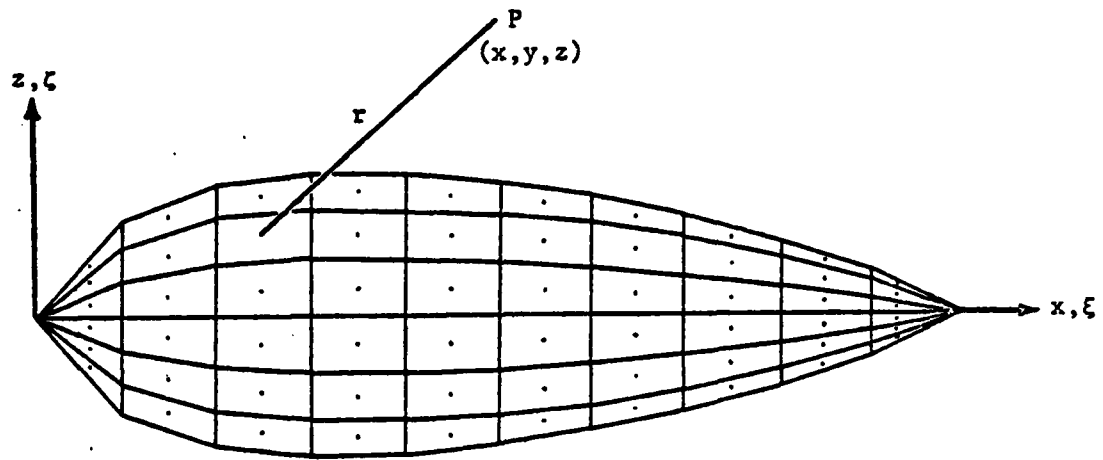
Fig. 8. Influence of a Source Panel on an Axisymmetric Body at a Point in Space.

$$V_y = \frac{\xi_2 - \xi_1}{d_{12}} \, \ln\left(\frac{r_1 + r_2 + d_{12}}{r_1 + r_2 - d_{12}} \right) + \frac{\xi_3 - \xi_2}{d_{23}} \, \ln\left(\frac{r_2 + r_3 + d_{23}}{r_2 + r_3 - d_{23}} \right)$$

$$+ \frac{\xi_4 - \xi_3}{d_{34}} \, \ln\left(\frac{r_3 + r_4 + d_{34}}{r_3 + r_4 - d_{34}} \right) + \frac{\xi_1 - \xi_4}{d_{41}} \, \ln\left(\frac{r_4 + r_1 + d_{41}}{r_4 + r_1 - d_{41}} \right) \tag{30}$$

$$V_z = \tan^{-1}\left(\frac{p_2 - m_{12} e_2}{z r_2} \right) - \tan^{-1}\left(\frac{p_1 - m_{12} e_1}{z r_1} \right) + \tan^{-1}\left(\frac{p_3 - m_{23} e_3}{z r_3} \right)$$

$$- \tan^{-1}\left(\frac{p_2 - m_{23} e_2}{z r_2} \right) + \tan^{-1}\left(\frac{p_4 - m_{34} e_4}{z r_4} \right) - \tan^{-1}\left(\frac{p_3 - m_{34} e_3}{z r_3} \right)$$

$$+ \tan^{-1}\left(\frac{p_1 - m_{41} e_1}{z r_1} \right) - \tan^{-1}\left(\frac{p_4 - m_{41} e_4}{z r_4} \right) \tag{31}$$

where

$$d_{12} = \sqrt{(\xi_2 - \xi_1)^2 + \beta^2 (n_2 - n_1)^2}$$

$$d_{23} = \sqrt{(\xi_3 - \xi_2)^2 + \beta^2 (n_3 - n_2)^2}$$

$$d_{34} = \sqrt{(\xi_4 - \xi_3)^2 + \beta^2 (n_4 - n_3)^2}$$

$$d_{41} = \sqrt{(\xi_1 - \xi_4)^2 + \beta^2 (n_1 - n_4)^2}$$

$$r_j = \sqrt{(x - \xi_j)^2 + \beta^2 (y - n_j)^2 + \beta^2 z^2} \, , \quad j = 1,2,3,4$$

$$e_j = (x - \xi_j)^2 + \beta^2 z^2 , \quad j = 1,2,3,4$$

$$p_j = (y - n_j)(x - \xi_j) \, , \quad j = 1,2,3,4$$

and

$$m_{12} = \frac{n_2 - n_1}{\xi_2 - \xi_1} \, , \quad m_{23} = \frac{n_3 - n_2}{\xi_3 - \xi_2} \, , \quad m_{34} = \frac{n_4 - n_3}{\xi_4 - \xi_3} \, , \quad m_{41} = \frac{n_1 - n_4}{\xi_1 - \xi_4}$$

It should be noted that the quadrilateral source element shown in Figure 9 lies in the x-y plane so that ζ in equation (28) will be zero.

For an arbitrary body, the number of unknown densities which must be determined is equal to the number of source panels on the body. However, the number of unknowns for an axisymmetric body is greatly reduced because of the linearity of the governing equations and because of symmetry. As mentioned earlier, the angle-of-attack solution for such a body is determined by adding the axial ($\alpha = 0°$) and pure crossflow ($\alpha = 90°$). Hence, for an axial flow solution, the number of panel densities which must be solved is equal to the number of frustrums used to model the body.

A similar reduction in the number of unknowns in the pure crossflow solution ($\alpha = 90°$) results from the circumferential variation of the crossflow source density being known. The variation was shown by Hess (Reference 5) to be a product of the cosine of the circumferential angle and the value of the crossflow source density on the top of the body ($\theta = 0°$). The problem thus reduces to determining the source density on the top of each frustrum along the body. Hence, the conventional source paneling solution for an axisymmetric body involves the inversion of two matrices, each equal in size to the number of frustrums used to model the body. The number of frustrums along the body is commonly referred to as the number of points in the solution. For example, a 60-point solution would require a 60 x 60 array to be solved twice. As shown by Hess, in typical source paneling solutions, anywhere from 50 to 150 points are required.

The technique presented herein by Baker was developed by examining the nature of the axial and circumferential dependences of the surface source density and a simplified solution was formulated.

Axisymmetric Solutions

The axial dependence was examined by aligning the body axis in the direction of the flow, which, because of symmetry, required the surface source density to be constant in the circumferenial direction. An approximate solution for the source density for axisymmetric bodies is derived from slender body theory in the following manner:

A tube whose surface is covered with an infinite number of point sources is enclosed in a cylindrical control volume, as shown in Figure 10. The combined density of all the sources on the tube is designated as Λ, which by the continuity equation is equal to the total volumetric flow rate from the source tube, so that

$$\Lambda = \iint\limits_{A} V_r \, dA \qquad (32)$$

967

where A is the surface area of the control volume and V_r is the radial component of the velocity. The total density of the source tube may also be written as

$$\Lambda = \iint\limits_{A_t} \sigma_a \, dA_t \tag{33}$$

where A_t is the surface area of the source tube and σ_a is the axial
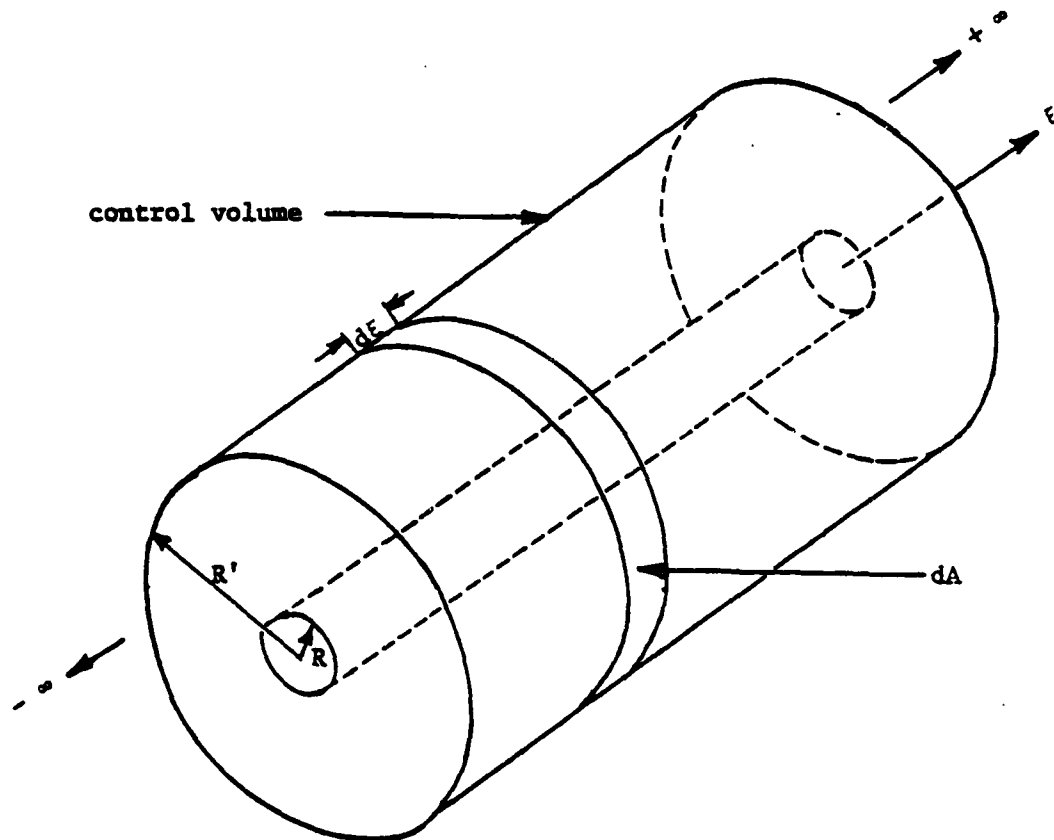
Figure 10. A Source Panel Tube Enclosed in a Cylindrical Control Volume.

968

surface source density per unit area. The differential area of the source tube is

$$dA_t = R \, d\theta \, d\xi \qquad (34)$$

so that Equation (33) becomes

$$\Lambda = \int_{\xi_1}^{\xi_2} \int_0^{2\pi} \sigma_a R d\theta \, d\xi = \int_{\xi_1}^{\xi_2} \sigma_a 2\pi R d\xi \qquad (35)$$

Equation (32) may be evaluated over the surface of the control volume, yielding

$$\Lambda = \int_{\xi_1}^{\xi_2} \int_0^{2\pi} V_r R' \, d\theta \, d\xi = \int_{\xi_1}^{\xi_2} V_r 2 R' \, d\xi$$

which may be equated with Equation (35):

$$\int_{\xi_1}^{\xi_2} V_r 2\pi R' \, d\xi = \int_{\xi_1}^{\xi_2} \sigma_a 2\pi R \, d\xi$$

or

$$\int_{\xi_1}^{\xi_2} 2\pi (R'V_r - \sigma_a R) \, d\xi = 0 \qquad (36)$$

If Equation (35) is to be satisfied, then

$$R'V_r = \sigma_a R$$

and in the limit as $R' \to R$,

$$V_r \doteq \sigma_a \qquad (37)$$

The boundary condition on the surface of a slender body in terms of nondimensional velocity components is

$$\frac{dR}{d\xi} = \frac{V_r}{1+V_x} \doteq V_r \tag{38}$$

Hence, Equation (37) may be written as

$$\sigma_a = \frac{dR}{d\xi} \tag{39}$$

As previously discussed, this expression must be corrected near the ends of the body and near discontinuities in the body slope. Writing the correction in the form of a convergent power series, the axial dependence of the surface source density for an axisymmetric body becomes

$$\sigma_a(\xi) = \frac{dR}{d\xi} \sum_{n=0}^{N} A_n \xi^n \tag{40}$$

Crossflow Solution

The circumferential dependence of the crossflow source density for an axisymmetric body in pure crossflow ($\alpha = 90°$) was derived by Hess (See Reference 6) and can be expressed as

$$\sigma_c(\xi,\theta) = \sigma_c(\xi) \cos \theta \tag{41}$$

where $\sigma_c(\xi)$ is the fundamental value of the crossflow source density for a given axial location, and θ is the circumferential angle measured from the top of the body, as shown in Figure 11.

The approach taken by Hess was to imagine the surface source distribution on an axisymmetric body as an infinite number of ring sources distributed along the body. The circumferential variation of the density of each ring source is proportional to the cosine of the circumferential angle, as given in equation (41). It may be shown that the equation for the velocity induced by a ring source of this nature contains an elliptic integral, and the presence of an elliptic integral precludes an analytic solution for the fundamental value distribution. However, conventional crossflow solutions revealed that for a large number of slender bodies, the fundamental values were nearly constant, $\frac{1}{2\pi}$. Hence, an approximate crossflow solution may be obtained by letting

970
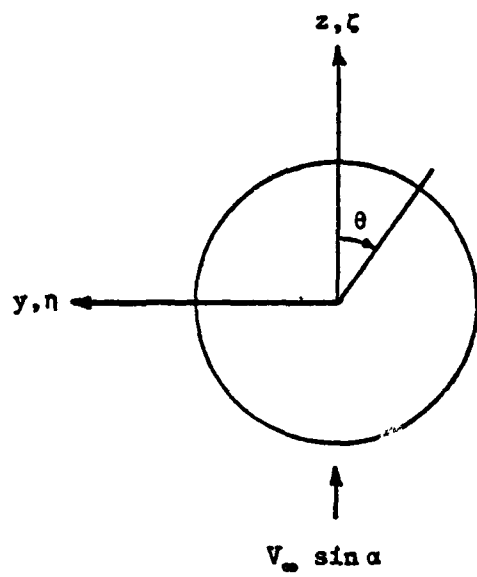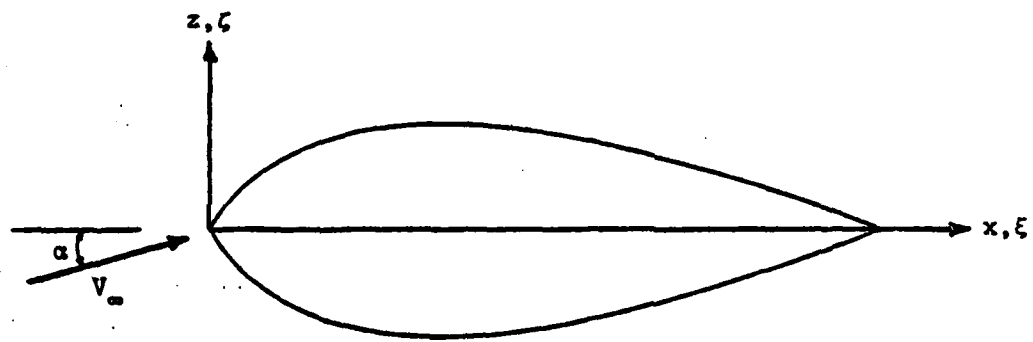
Fig. 11. Angles Used to Define the Axial and Circumferential Dependence
of the Surface Source Density.

$$\sigma_c(\xi) = \frac{1}{2\pi} \tag{42}$$

This expression may be corrected by a power series, as was the axial dependence given in Equation (40). However, this is unnecessary for most bodies, as will be shown later. Hence, from equations (41) and (42) the circumferential dependence of the source density becomes

$$\sigma_c(\xi,\theta) = \frac{1}{2\pi} \cos\theta \tag{43}$$

Thus, a crossflow solution by matrix inversion may be completely avoided.

Combined Axisymmetric and Crossflow Solution

The density of any source panel on a body at an angle of attack is found by combining the axial and circumferential dependences in a manner where the circumferential dependence will vanish at zero angle of attack, and the axial dependence will vanish at 90° angle of attack. These conditions lead to

$$\sigma(\xi,\theta) = \sigma_a(\xi) \cos\alpha - \sigma_c(\xi,\theta) \sin\alpha \tag{44}$$

or with the substitution of equations (40) and (43)

$$\sigma(\xi,\theta) = \frac{dR}{d\xi} \sum_{n=0}^{N} A_n \xi^n \cos\alpha - \frac{1}{2\pi} \cos\theta \sin\alpha \tag{45}$$

Equation (45) defines the density of any source panel on the body. It should be reemphasized here that the axial solution is obtained independent of the crossflow solution. This is done by aligning the body in the flow at zero angle of attack and solving for the A_n's, the power series coefficients. As there are N+1 coefficients, there must also be N+1 control points at which the boundary condition specified in equation (3) is satisfied. An unevenly-spaced control point distribution was chosen, so that

$$\xi_i = \frac{i}{N+1} - \frac{1}{2(N+1)} \quad , \quad i = 1,2,\ldots,N+1 \tag{46}$$

where all the body coordinates are expressed in nondimensionalized terms with respect to the length of the body.

972

RESULTS

The simplified analytic solution presented in this paper was compared with experimental pressure distributions for the three axisymmetric bodies shown in Figure 12. Two of the bodies have continuous slopes, while the third body, the M117 bomb, is made up of three distinct sections: an ogive nose, a cylindrical mid-section, and a straight-taper tail section.

The simplified solution was also compared to an equivalent conventional solution. The conventional solution utilized a Gauss-Seidel iteration scheme to solve the system of equations for the axial and crossflow source density distributions. Double-precision arithmetic was used in the conventional solution to minimize round-off error, while single-precision calculations were sufficient for the simplified solution. There were no discernible differences in the pressure distributions calculated by the two solutions.

A conventional 60-point solution of the axial source density distribution was obtained for each of the bodies shown in Figure 12. From examining equation (40) one may isolate the correction power series by dividing the axial density distribution ($\sigma_a(\xi)$) by the local body slope ($dR/d\xi$). This quotient will provide a measure of the order of the power series needed in equation (40). If the quotient was found to be constant over the entire body, then only a correction by a constant would be necessary, and the axial density solution would be independent of axial location. The results for the 60-point solution are shown in Figure 13, which indicate low-order corrections are required for the prolate spheroid and the transonic body. A third-order power series was found to be sufficient for both bodies.

One would expect the M117 bomb to be a much more difficult problem because of the two discontinuities in the body's slope. The conventional axial density distribution for this body revealed very marked discontinuities corresponding to its slope discontinuities. Also, the conventionally-determined source density over the body's mid-section could not be divided by $dR/d\xi$ as the body slope was zero. Instead, the densities over that section were divided by unity. The discontinuities in the source distribution are quite evident in Figure 13. These discontinuities were accounted for by using a different power series over each section of the M117 bomb. The shape of the curve over the nose indicates that at least a second-order equation would be required as a correction factor, but a third-order equation appears to be more likely. Similarly, first-order and second-order equations would correct the mid- and tail-sections, respectively. Again, equation (40) is utilized over the mid-section by setting $dR/d\xi$ equal to unity instead of the actual body slope of zero.

973

Prolate Spheroid of Fineness Ratio 6
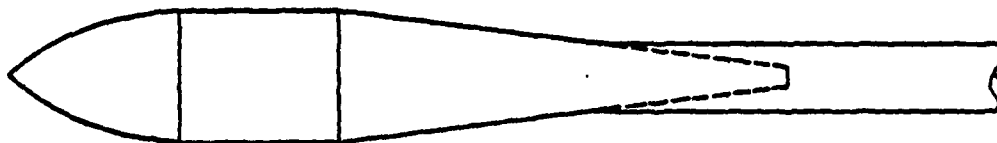
M117 Bomb (without fins)

Transonic Body of Fineness Ratio 12

Fig. 12. Profiles of Three Axisymmetric Bodies
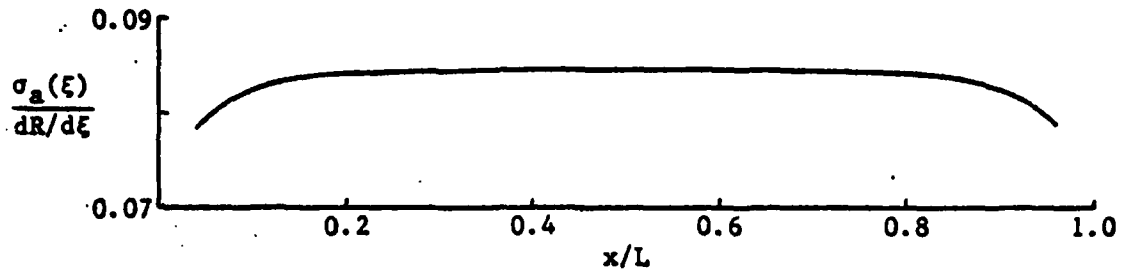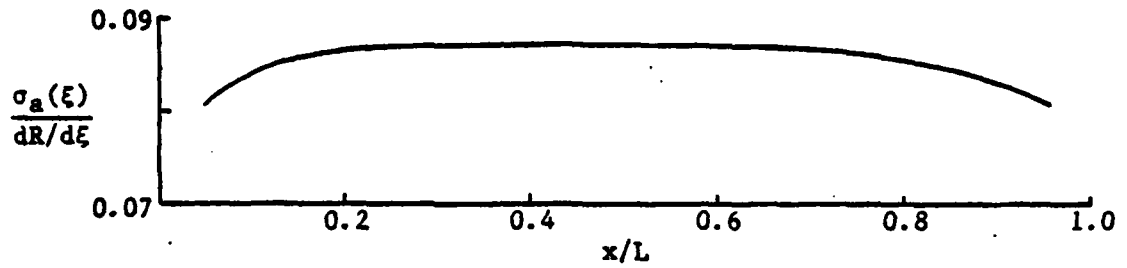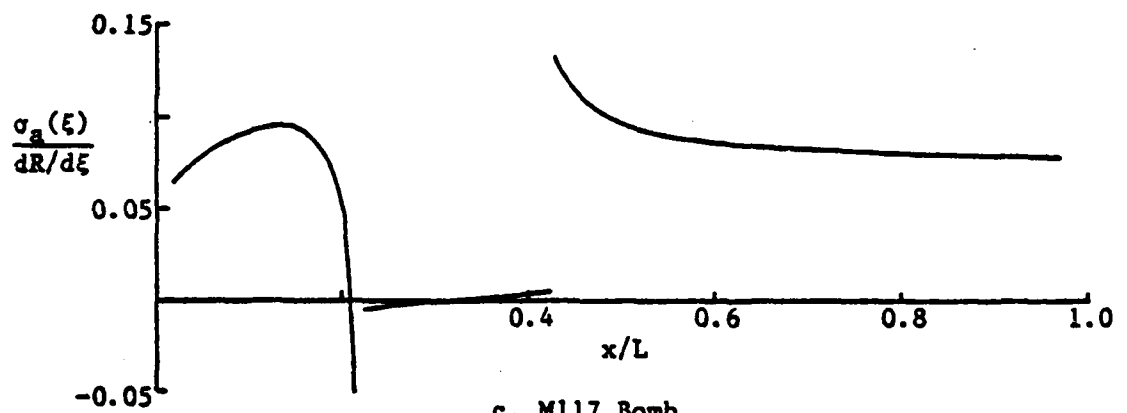
Fig. 13. Comparison of Conventional Axial Source Density Distributions to Theory.

975

These conventional solutions for the axial source density distribution, along with others, led to a general rule for the order of the power series need in equation (40). The order of the power series should be one order higher than the equation of the body surface. Hence, third-order power series were used for the entire length of the prolate spheroid and the transonic body, as both had continuous normal vectors.

The accuracy of the pure crossflow fundamental value distribution assumed in equation (42) was tested by comparing it to conventional 60-point pure crossflow solutions. The results are presented in Figure 14. The data for the prolate spheroid and the transonic body shows excellent agreement over nearly the entire body length. The fundamental values for the M117 bomb exhibit some deviation from the assumed value of $\frac{1}{2\pi}$, but the simplicity of the solution compensates for the loss in accuracy.

The pressure distributions for a prolate spheroid at zero angle of attack are presented in Figure 15. The results are for a 60-point solution, with each frustrum divided into 36 equal-sized panels in the circumferential direction. A 60-point solution was used for all the numerical examples presented here. The experimental data for the prolate spheroid was obtained from Reference 7, and the simplified solution showed very good agreement with experiment at Mach numbers of 0.0 and 0.6.

The results for an M117 bomb at zero angle of attack are presented in Figure 16. The incompressible data came from Reference 8, while the compressible data was obtained from Reference 9. In both cases, the simplified solution showed excellent agreement with experiment.

Pressure distributions were calculated for the prolate spheroid at the largest angle of attack (7.7°) for which experimental data was available. Figure 17 shows the pressure distributions on the top of the body ($\theta=0°$). The incompressible solution does not match the experimental data nearly as well as the compressible solution does. This discrepancy is due to the manner in which the zero Mach number data was obtained. As stated in Reference 6, the zero Mach number data was determined by the extrapolation of data for Mach numbers greater than 0.5 down to 0.0. The solution for a Mach number of 0.6 shows excellent correlation with the experimental data.

The pressure distributions on the side and bottom of the prolate spheroid ($\theta=90°$ and ($\theta=180°$) are shown in Figures 18 and 19, respectively. The simplified solution exhibited excellent agreement with the experimental data for all cases.

Experimental data for the transonic body was given in Reference 10 for several circumferential angles. Figure 20 shows the pressure distribution around the body at a fixed axial location of $x/L = 0.0333$.
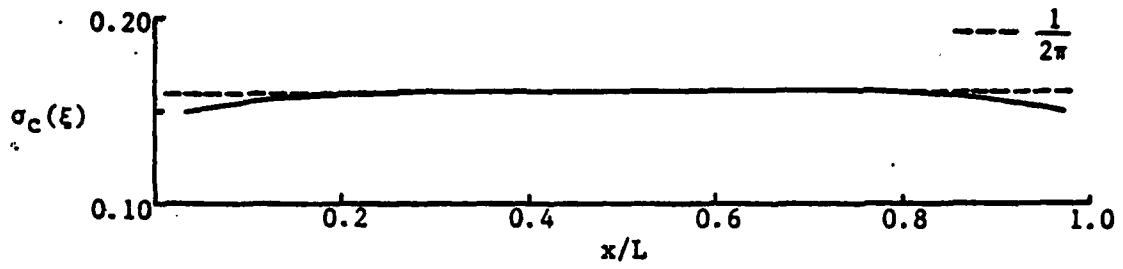
a. Prolate Spheroid
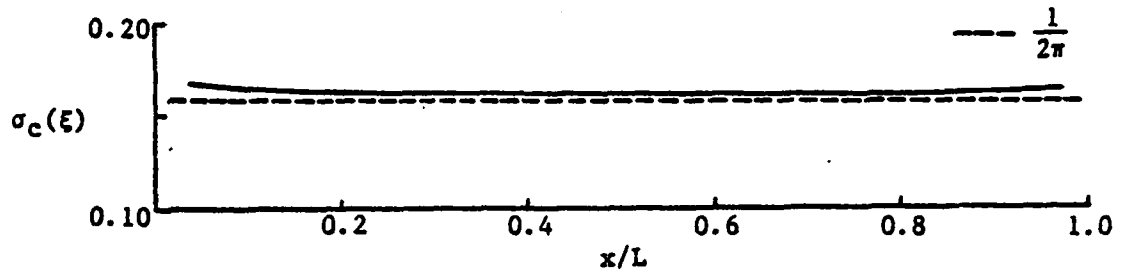
b. Transonic Body
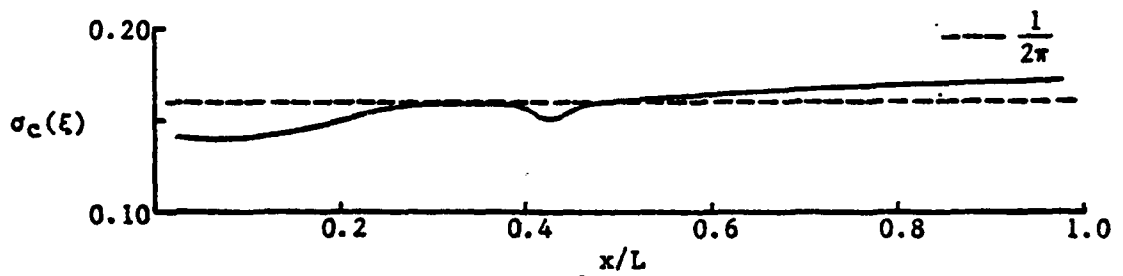
c. M117 Bomb

Fig. 14. Comparison of Conventional Pure Crossflow Fundamental Value
Distributions to Theory.

977
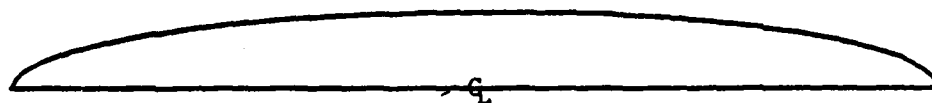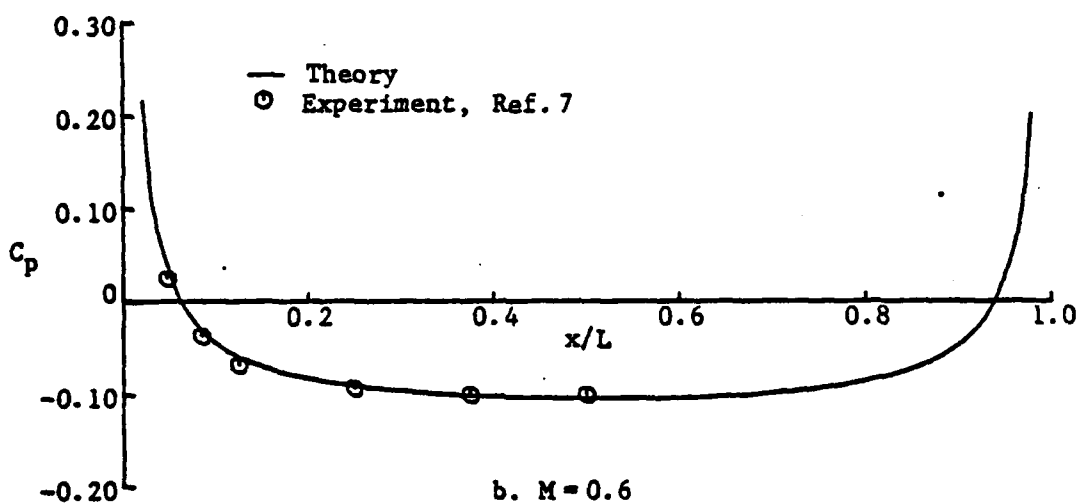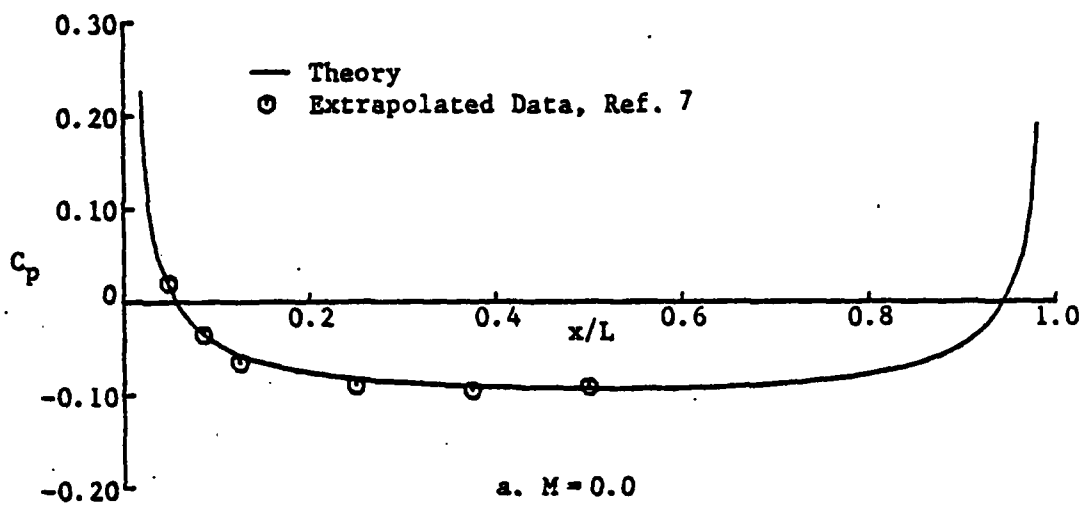
Fig. 15. Pressure Distributions over a Prolate Spheroid at Zero Angle of Attack.

a. M = 0.0

b. M = 0.5
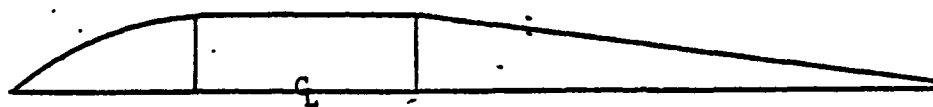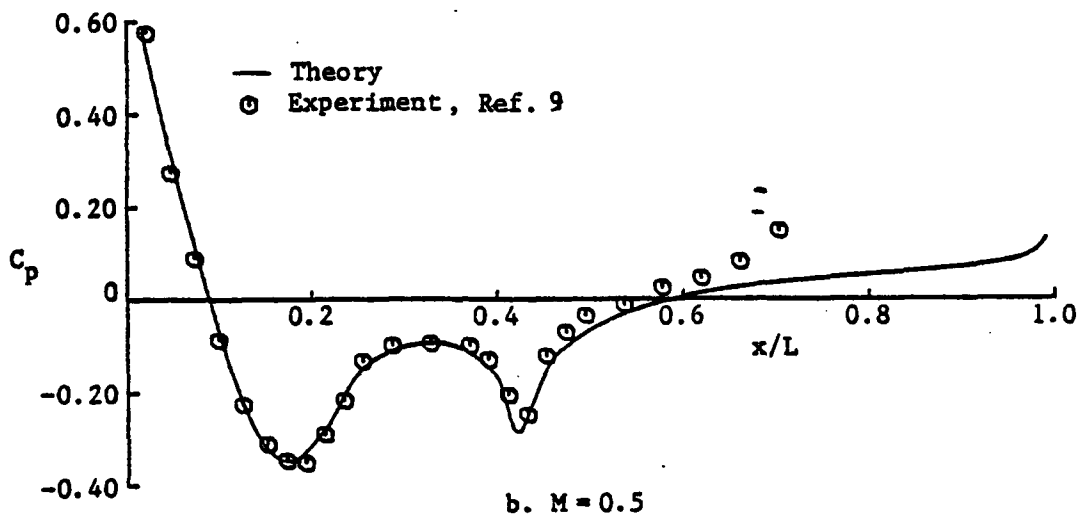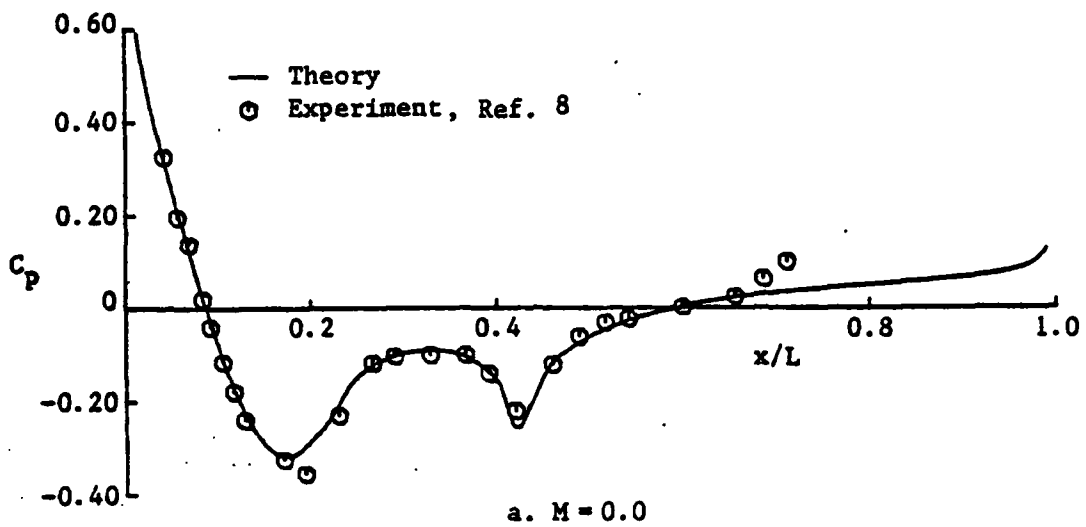
c. Body Profile

Fig. 16. Pressure Distributions over an M117 Bomb at Zero Angle of Attack.
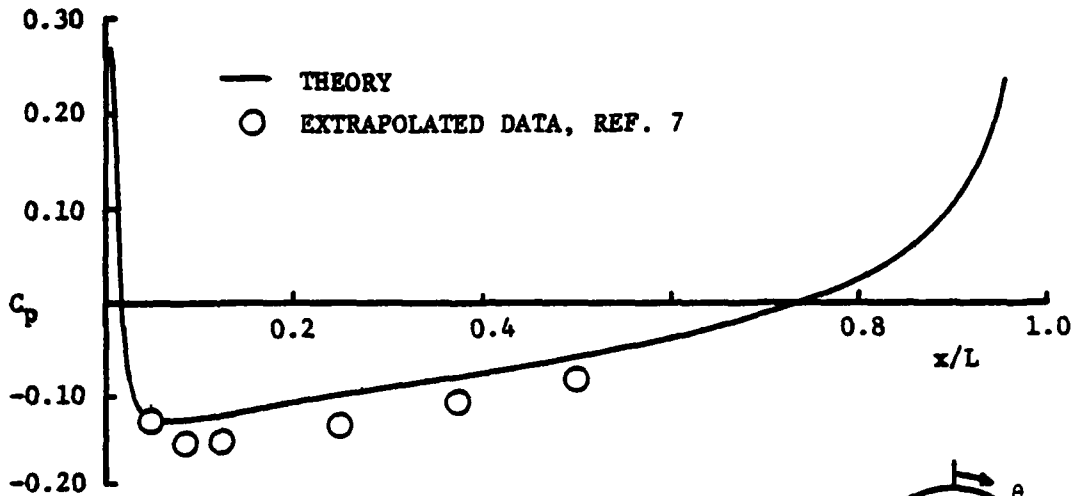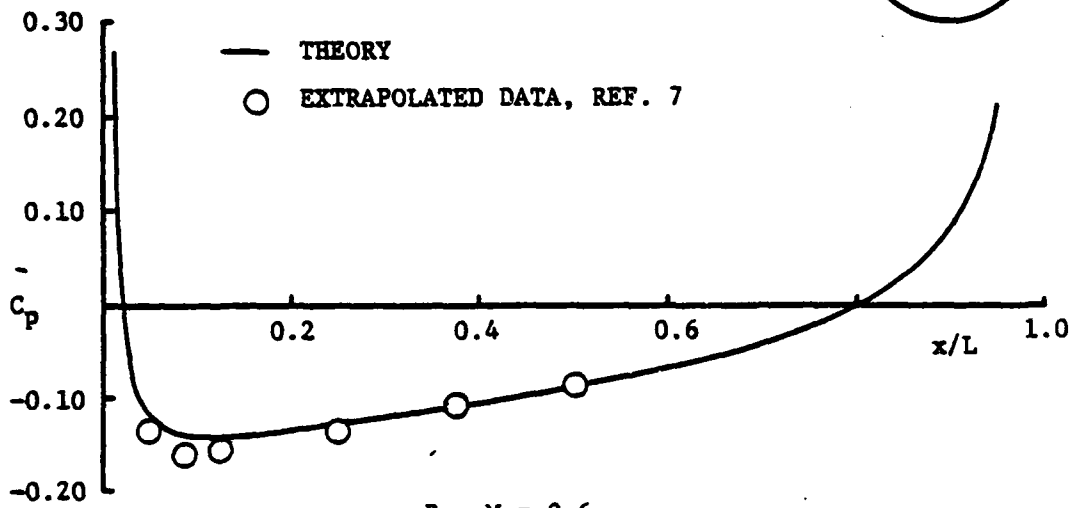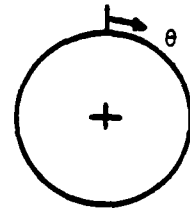
Figure 17. Pressure Distributions over a Prolate Spheroid at 7.7° Angle of Attack, $\theta = 0°$.
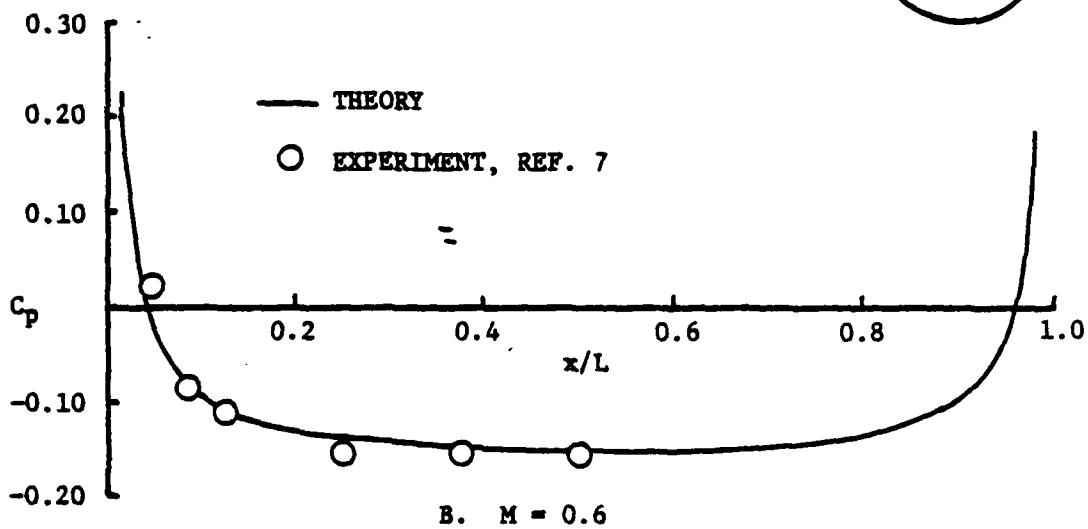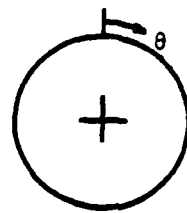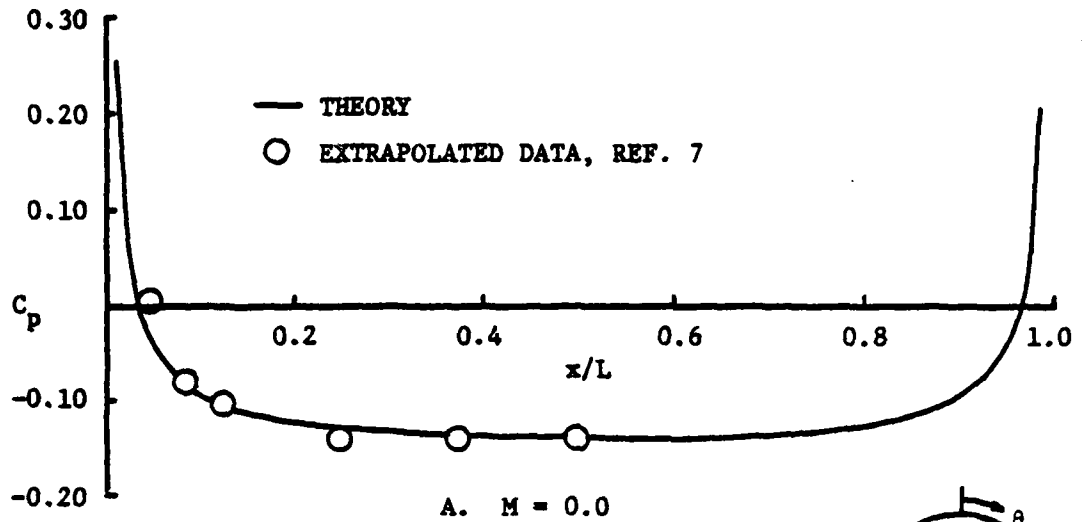
Figure 18. Pressure Distributions over a Prolate Spheroid at 7.7° Angle of Attack, θ = 90°.
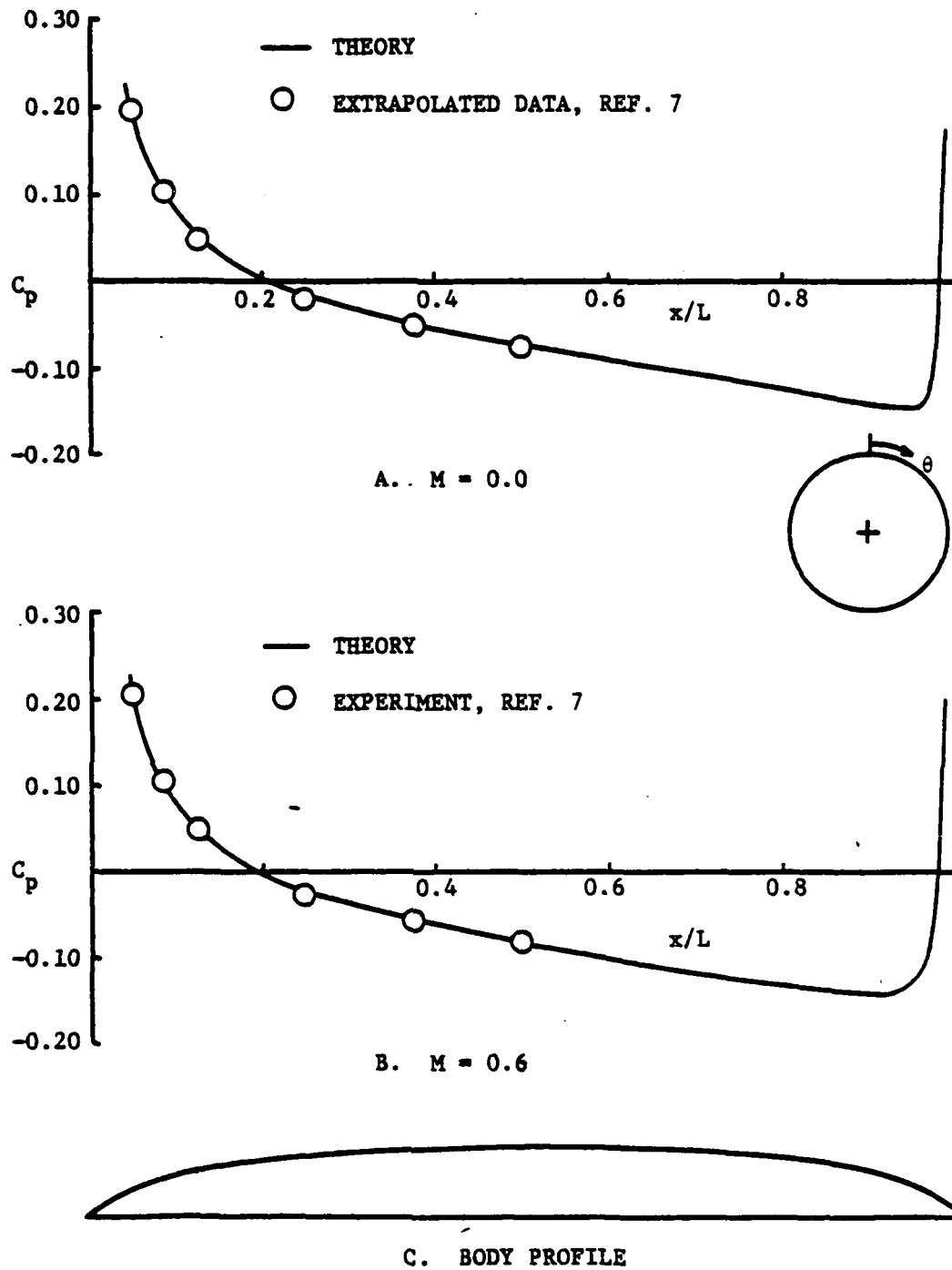
Figure 19. Pressure Distributions over a Prolate Spheroid at 7.7° Angle of Attack, θ = 180°.
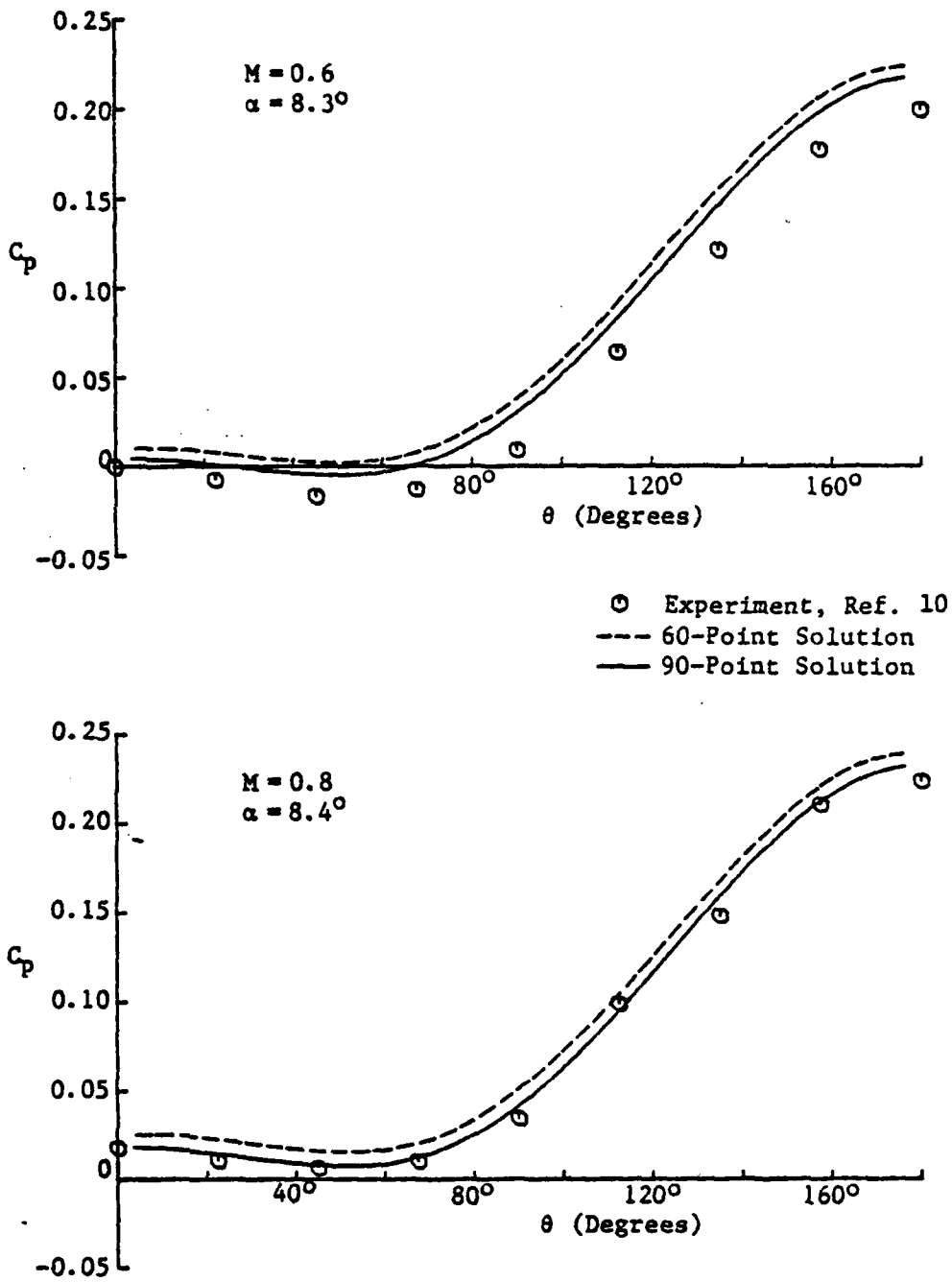
Fig. 20. Pressure Distributions around a Transonic Body at an Angle of Attack, x/L = .0333.

This location was chosen because the local crossflow Reynolds number was below the critical value, and because a location very near the body nose is a good test of the assumed crossflow fundamental value of $\frac{1}{2\pi}$.

Several simplified solutions were obtained for the transonic body, including 60-, 90-, and 120-point solutions. The 120-point solution was nearly identical to the 90-point, so it was not plotted. The increase in the number of points in the simplified solution affected only the axial source density distribution, as the crossflow density distribution given in equation (42) is independent of the number of points in the solution. In Figure 20, both the 60- and 90-point solution pressure distributions are shown. The 90-point solution matches the experimental data better than the 60-point solution because of a better axial density solution. However, both pressure distributions have identical curve shapes, which is due to the crossflow solution. The shape of the pressure curves also matches that of the experimental data, showing the accuracy of the assumed crossflow density distribution.

A few comments are in order on some of the characteristics of the simplified solution. First, the technique is essentially independent of the size of the source panels used to model the body. The question of how many points to use in the solution is largely one of what accuracy is acceptable. The results given here are all 60-point solutions, with the additional 90-point solution included in Figure 20. Hess used 90- and 150-point solutions, but the gain in accuracy rarely warrants such solutions.

The control point distribution given by equation 46 was obtained after several other trial-and-error solutions. For example, a cosine distribution for the control points caused the pressure distribution to oscillate instead of producing a smooth curve. On the other hand, evenly-spaced control points did produce a smooth pressure distribution, leading to the formulation of equation (46).

CONCLUSIONS

The accuracy of the method of source panels for axisymmetric bodies and the validity of slender body theory have been well established. The technique presented here combines both slender body theory and the method of source panels in developing a functional form for the surface source distribution over an axisymmetric body at an angle of attack. The advantages of the method of source panels are preserved while its inherent disadvantages of excessive computer storage and execution time are minimized. For example, a simplified 60-point solution for the M117 bomb at an angle of attack required less than one-third time of an equivalent conventional solution at zero angle of attack. Also, the conventional solution required a 60 x 60 array,

while the simplified solution required only a 9 x 9 array. This emphasizes the major advantage of the simplified solution: the number of points in the solution may be increased without altering its storage requirements, as the computer storage depends solely on the order of the power series needed in the solution.

LIST OF REFERENCES

1. Purvis, James W., "Simplified Solution of the Compressible Sub-
   sonic Lifting Surface Problem," M.S. Thesis, Auburn University,
   Auburn, Alabama, June 30, 1975.

2. Baker, G. M., "Simplified Compressible Solution of the Method of
   Source Panels for Axisymmetric Bodies," M.S. Thesis, Auburn
   University, Auburn, Alabama, June 7, 1977.

3. Ashley, H., and Landall, M., Aerodynamics of Wings and Bodies,
   Addison-Wesley, Mass., 1965.

4. Kuethe, A., and Schetzer, J., Foundations of Aerodynamics, John
   Wiley & Sons, New York, 1959.

5. Chadwick, W., "The Application of Non-Planar Lifting Surface Theory
   to the Calculation of External Store Loads," U.S. Naval Weapons
   Laboratory TR-2696, 1971.

6. Hess, J. L., "Calculation of Potential Flow About Bodies of
   Revolution Having Axes Perpendicular to the Free-Stream Direction,"
   Journal of the Aerospace Sciences, Vol. 29, No. 6, June, 1962.

7. Matthews, C. W., "A Comparison of the Experimental Subsonic Pres-
   sure Distributions About Several Bodies of Revolution with Pres-
   sure Distributions Computed by Means of the Linearized Theory,"
   NACA TN 2519, February, 1952.

8. Smith, C. J., "Mutual Aerodynamic Interference Effects for Two
   Similar Bodies," M.S. Thesis, Aerospace Engineering Department,
   Auburn University, Auburn, Alabama, December 1972.

9. Mattasits, G. R., "Aerodynamic Interference Effects on Various
   Weapon Shapes in the Flow Field of a Transonic Wing Configuration
   at Mach Numbers from 0.5 to 1.3," AFATL-TR-75-88, July 1975.

10. Swihart, J. M., and Whitcomb, C. F., "Pressure Distributions on
    Three Bodies of Revolution to Determine the Effects of Reynolds
    Number up to and Including the Transonic Speed Range," NACA RM
    L53H04, October 1953.

AUTOBIOGRAPHY

DR. FRED W. MARTIN

The author was born in portsmouth, VA, on February 26, 1926. He attended the public schools in Portsmouth and Norfolk, VA, until he was employed as a mechanic learner at the United States Naval Air Station, Norfolk, VA, in March 1942. He served in the United States Army Air Corps from March 1944 until he was honorably discharged as a private first class in November 1945. He returned to the Naval Air Station, Norfolk, VA, as an apprentice aircraft mechanic. From this position, he entered the Virginia Polytechnic Institute from which he received a B.S. degree, 1952; M.S. degree, 1954; and the Ph.D. degree, 1969. He also held a teaching position at V.P.I. from September 1952 to June 1955. He has held his present position as Professor, Aerospace Engineering, Auburn University, Auburn, Alabama, since 1956 which he accepted after working in an engineering position in aerodynamics with the North American Aviation Company, Downey, CA. Other industrial experience has been obtained during summer employment at the Langley Research Center (two summers); George C. Marshall Space Flight Center; Thiokol Chemical Company, Space Booster Division; and the Air Force Armament Laboratory (AFATL), Eglin AFB, FL. His principal responsibility at Auburn University is in aerodynamics and in developing and directing the aerodynamics laboratory. He has served as the project director on several Air Force contracts.

AUTOBIOGRAPHY

JOHN E. BURKHALTER

Mr. John E. Burkhalter was born on Jan 23, 1940, in Chilton County, Alabama. He graduated from public high school and entered Auburn University in the fall of 1958. He completed his Bachelor's degree in Aerospace Engineering in June 1963 and his Master's degree in December 1964. In 1967, he pursued a year of graduate work at the University of Tennessee Space Institute, Tullahoma, TN. In 1970, he entered the graduate school at the University of Texas at Austin and received his Ph.D. degree in August 1972. While in school at Auburn, he was employed as a Co-op with the Lockheed Georgia Company, Marietta, GA, and did both manual labor and theoretical work. As a graduate student at the University of Tennessee Space Institute, he was chief designer of a supersonic combustor and also performed work in boundary layer analysis. During his graduate work in Texas, he performed extensive experimental work on inertial instability of viscous fluids and also served as Engineer on an artificial heart project. His work since returning to Auburn in the Aerospace Engineering Department has centered around mathematical modeling of flow fields, both in subsonic and supersonic flow. Considerable emphasis has been placed on multi-body interference problems as well as surface paneling solution for thin wings. He has written and presented papers on instability in fluids and aerodynamic interference problems. He has also served as an engineering consultant to the U.S. Army Missile Command, Huntsville, Alabama.

GRUMMAN STORE SEPARATION PHOTOGRAMMETRY TECHNIQUES
(U)
(Article UNCLASSIFIED)

by

THOMAS J. REILLY
Vehicle Flight Test Department
Grumman Aerospace Corporation
PMTC, Pt. Mugu, Calif. 93042

ABSTRACT. (U) This paper describes the photogrammetric techniques used by the Flight Test Department of Grumman Aerospace Corporation during the last several years to obtain in-flight store separation trajectory data. In particular, the refined computerized techniques used successfully during the F-14A Tomcat Separation Test Program at PMTC, Pt. Mugu, California, are reviewed in detail.

Grumman reviewed various photogrammetric techniques involving chase camera only, single camera on-board, and multiple cameras on-board. A two camera space triangulation procedure was selected on the basis of accuracy and data validation check capability not available with other methods.

The F-14A Flight Test effort was divided into four major categories:

1.   Camera locations and orientations selected along with the desired wide angle lens size using the Camera/Lens Installation Definition Computer Program. This program eliminated the guesswork prevalent during camera placement attempts on previous programs.

2.   Lens calibration to correct for wide angle spherical (barrel) distortion.

3.   On-board calibration to determine exact locations and orientations of each camera/lens after installation.

4.   Trajectory calculation using all calibration information plus on-board recorded timing and film data. Six degree-of-freedom data is output along with store length, sight-line intersection, and mated position for error monitoring.

989

TABLE OF CONTENTS

LIST OF FIGURES

TABLE OF CONTENTS (Continued)

LIST OF REFERENCES

Reference	Description
1	"The Use of An Interactive Computer To Optimize A Photographic Data Acquisition System"
2	American Society of Photogrammetry "Manual of Photogrammetry"

1.0 INTRODUCTION

The major aerospace contractors and military weapons testing centers are faced with the challenge of developing sophisticated analytical techniques and safe, productive flight test methods to clear ever increasing weapon release envelopes for today's complex airborne weapon systems. The high cost of air-launched guided missiles makes it virtually impossible to demonstrate release characteristics for every combination of aircraft angle-of-attack, release mode, normal load factor, flight path angle, and carriage location throughout the entire aircraft mach-altitude release envelope. For this reason, current practices call for wind tunnel based predicted trajectories to be compared with actual in-flight separation characteristics at predetermined buildup and demonstration flight conditions with the intent of validating the aerodynamic analytical technique. If satisfactory correlation is obtained at critical demonstration conditions, non-critical flight regimes can be cleared by less expensive computer analysis. If, however, correlation is not satisfactory, it then becomes necessary to perform sufficient drops for comparison with the analysis until an acceptable confidence level is achieved through the update and refinement process based upon actual in-flight data. Inherent in this procedure is the requirement for an accurate store trajectory determination flight test capability. The success of the entire procedure is contingent upon the accuracy and reliability of both the aerodynamic prediction technique and the flight test data reduction process to minimize the number of drops and flights required in establishing safe and operational clearance envelopes. Grumman believes that its Aerodynamic and Flight Test capabilities are among the best in the industry.

2.0 TEST PHILOSOPHY AND METHODS

Prior to discussing photogrammetric techniques, a review of background information is provided to acquaint the reader with procedures that have been followed by Grumman to produce separation clearances.

The objective of any store separation test program is to establish a maximum release envelope which generally is based just upon safety considerations but can, in addition, be a function of such operational characteristics as release attitude, angular rates, space positioning or delivery accuracy. A separation can be either a jettison or employment. Jettison tests are store releases during which the designed function of the store is not utilized; for example, emergency jettison (safety) to decrease aircraft weight and drag in the event of engine power loss on takeoff. Examples of employment releases are live missile firings (launches), air-to-ground weapon releases with deployed fins, and investigation of tactical release intervals. The highly competitive nature of the aerospace industry makes it necessary to satisfy separation requirements with minimum cost while assuring adequate safety. To meet this objective, it is necessary to tailor separation procedures to the specific requirements of each release program. Grumman utilizes the "Predict and Verify" approach, with wide variations in scope ranging from greatly simplified to highly sophisticated.

2.1 Grumman separation test experience can be divided into the following general categories:

° Minimum Requirements Program -

In a case where the effects of a minor aircraft modification on store release characteristics are desired, and trajectories of the same or similar type stores from the basic unmodified aircraft are available, the entire separation program may consist merely of a single "spot check" release from an uninstrumented aircraft using chase photography to verify gross store motions after release. A visual comparison can be sufficient if no unusual store motions are apparent and if the release speed is at or near the maximum to be cleared so that no engineering measurements are required to project release characteristics at higher speeds. Prior aerodynamic investigation may consist of cursory inspection of "tuft" photographs, review of aerodynamic data, and/or reliance on basic engineering judgment. In some cases a separation may not even be warranted if high confidence exists in the predicted aerodynamic effect.

° Moderate Complexity -

This situation calls for more aerodynamic analysis along with the acquisition of some in-flight trajectory data for comparison to predicted trajectories. In the case of the A-6A Intruder D-704 In-Flight Refueling Buddy Tank jettison program, separation data had already existed for the 300 gallon tank which is similar in shape to the buddy tank. However, the significant change in store mass properties and the presence of some changes in aerodynamic properties warranted a fairly detailed prediction effort. In order to achieve an acceptable balance between funding, safety and productivity, a single drop was authorized at 1g level flight conditions with chase film being analyzed to determine longitudinal, vertical and pitch motions of the store after release with the assumption that lateral, yaw and roll motions would be negligible. The X and Z motions for the nose and tail of the store were established through the use of a Bensen-Lehner 29E film reader, with data referenced to nose and tail points on the aircraft as shown in Figure 1. Pitch motion was calculated simply as Arctan (Y/X) referenced to the aircraft nose-tail axis on a frame by frame basis. Monitoring the store and aircraft length in film counts provided assurance that store lateral and yaw motions were negligible and provided a scale factor for each frame. With actual store motion primarily in the X-Z plane and with the store motion generally parallel to the chase camera film plane, satisfactory data was obtained for correlation with the predicted motion and a full release envelope was cleared.
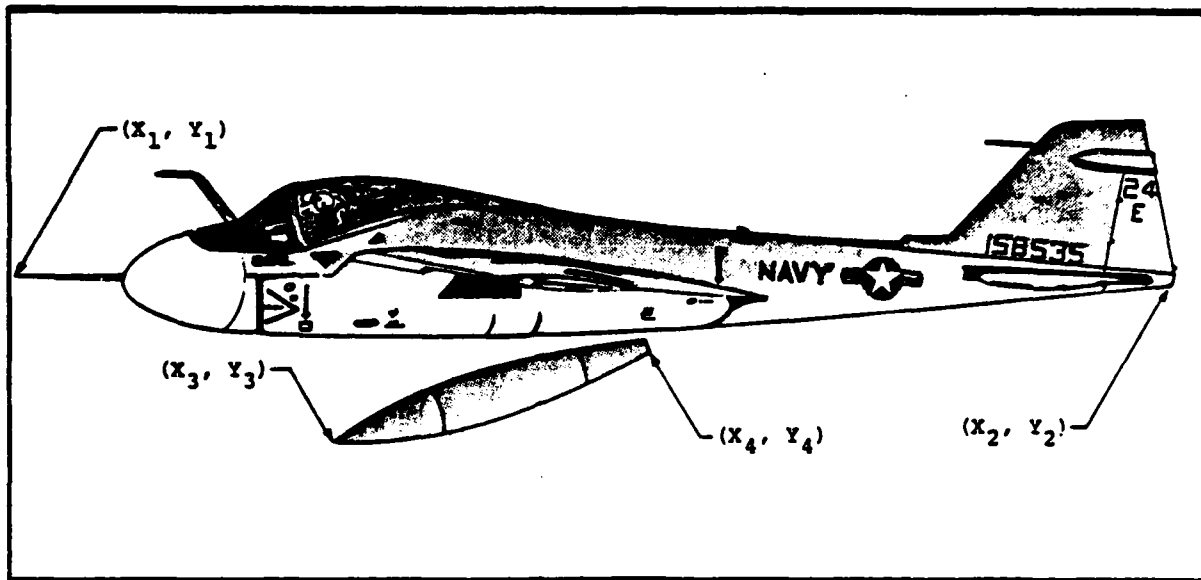
FIGURE 1. D-704 BUDDY TANK DROP FROM A-6A INTRUDER

Equations (1) and (2) establish filmreader scale factors for each data frame based upon the known aircraft and store dimensions, while equation (3) provides the best first order approximation for the average scale factor that should be utilized for the trajectory calculation.

$$S_1 = \sqrt{(X_2-X_1)^2 + (Y_2-Y_1)^2 + (Z_2-Z_1)^2} \Big/ \text{AIRCRAFT LENGTH} \tag{1}$$

$$S_2 = \sqrt{(X_4-X_3)^2 + (Y_4-Y_3)^2 + (Z_4-Z_3)^2} \Big/ \text{STORE LENGTH} \tag{2}$$

$$S_{\text{AVERAGE}} = (S_1+S_2)/2 \tag{3}$$

Optimum data accuracy is available when the chase camera is oriented such that the lens field of view is centered on the mid-trajectory point, and the chase aircraft to separation aircraft distance is a constant during the release $(Z_1 = Z_2)$.

• Highly Complex -

The F-14A Separation Program is the most recent and most demonstrative example of the situation where much effort is expended in both the aerodynamic prediction and flight test verification phases.

Analysis of predicted trajectories based upon numerous wind
tunnel tests provided the ground work for planning the Flight
Demonstration Program by identifying potential problem areas
in the flight envelope for each test store from each release
station. Wind tunnel tests consisted of installed loads
measurements on the various stations, flow field mapping,
and captive trajectory traverses to obtain an aerodynamic
representation of the interference flow field environment
through which released stores would have to pass prior to
reaching the free airstream flow field. The above data was
placed into a computer compatible format for recall as re-
quired by the Aerodynamic Engineering six degree-of-freedom
trajectory prediction computer program which uses all appli-
cable data (including autopilot response, thrust character-
istics, etc. for missiles) to compute trajectories which are
primarily a function of Mach, dynamic pressure and angle-of-
attack. With predictions available throughout the required
F-14A flight envelope the Flight Test Demonstration Program
was prepared and submitted to the Technical Branch of the
Naval Air Systems Command for approval. The program was
designed to provide clearance for the largest possible
envelope with a minimum number of drops and flights while
still permitting safe build-up and investigation of potential
trouble areas. The number of planned build-up drops reflected
the degree of concern for safety, such as when flight regimes
would be investigated where minimum miss distances or violent
store motions were predicted. The number of planned drops
also reflected the degree of confidence in the predictions,
as when conflicts in wind tunnel data existed or where store
stability data was unavailable for extreme attitudes and
had to be theoretically determined. Conservatism was built
into the program by following the established Grumman prac-
tice that requires utilization of wind tunnel data which
would place the store trajectory closest to the aircraft
whenever scatter or conflict existed in the input data to
the prediction program.

During the Air-to-Air Missile Separation Test Program,
initial drops were conducted at subcritical speeds to pro-
vide a comparison with predictions at conditions where
errors in trajectory predictions would be of least conse-
quence regarding aircraft safety. Quantitative six degree-
of-freedom trajectory data parameters were obtained from a
space calibrated time correlated camera system featuring
high speed 16mm DBM-20A Milliken movie cameras located on
the test aircraft. When correlation was within predeter-
mined limits, more critical test conditions were approved
for the next drop. For those instances where correlation
was not immediately obtained, predicted trajectories were

995

modified to agree with actual ones by altering aerodynamic input data such as flow field, installed loads, or aerodynamic coefficient representations. This information was then used to repredict trajectories at more critical conditions in order to establish the next drop in the sequence. This iterative procedure was continued until safe separation characteristics had been demonstrated at the most critical points which were not always the end points of the store envelope. Full envelope clearance was therefore obtained by a combination of flight demonstrations and validated or updated aerodynamic analysis. The greater the accuracy of both predictive analysis and inflight trajectories, the fewer iterations required to complete the procedure and effect maximum time and cost savings. Since the convergence rate is in part a function of confidence in the system, it was necessary for Grumman to thoroughly acquaint the Navy with Aerodynamic and Flight Test capabilities to gain acceptance of the procedure.

Determination of how many drops constituted program completion was a matter of judgment and required submittal of convincing data to substantiate the Grumman position. Figure 2 is a schematic of the entire procedure. The locations, orientations and lens size for these on-board cameras were determined by analysis of the Camera Simulation Computer Program outputs which consisted of plots indicating the field of view (aircraft contours, store trajectory, drop zone planes) coverage of a camera at a given location/orientation. Trajectory data was obtained by a two camera space triangulation procedure, requiring at least two cameras to view the store at any given point of the trajectory. Usually two or more sets of two-camera combinations were required to complete a full trajectory.

Wide angle lenses (110° and 165°) were selected to optimize the field of view coverage. However, these lenses produce a distorted view (spherical or "barrel" distortion) which must be eliminated mathematically through a lens distortion calibration procedure. A computer program accepts film data of grid board points and outputs a lens distortion curve, focal length, and distortion center. Once cameras were installed on the aircraft, the on-board Camera Calibration Procedure was used to determine exact lens principle point locations and camera/lens orientations with respect to the aircraft axis system. All the above inputs were utilized as constant data for the Store Trajectory Computer Program (STRAJ). Film coordinates of the store and on-board recorded timing data provided the complete information required for the definition of quantitative trajectory data for each drop. All test stores were painted with a scheme designed to facilitate accurate film reading of desired store coordinates.
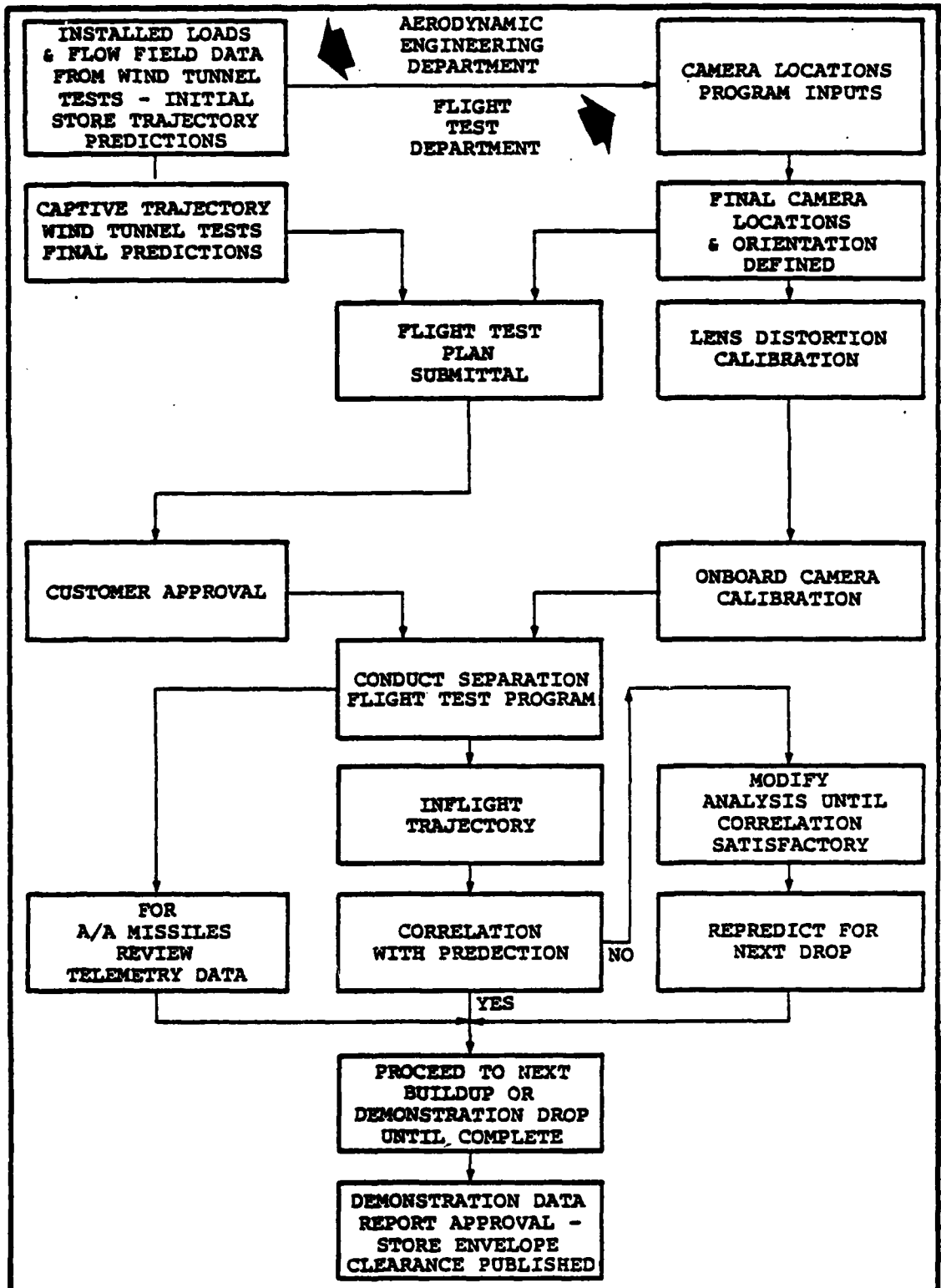
FIGURE 2. GRUMMAN WEAPON SEPARATION METHODOLOGY FOR F-14A

- **New Store Comparison -**

  One of the major benefits to be derived from the highly complex procedure is that at the conclusion of testing, a data bank of validated flow field characteristics is available throughout the flight envelope for each store carriage position. For any new store subsequently added to the aircraft inventory, prediction of release characteristics using this stored data enables definition of flight programs requiring a minimum number of drops in order to clear a desired envelope, thus effecting considerable time and cost savings. This analysis may also indicate which stores should not be carried on a particular aircraft, or define modifications to ejector hardware needed to achieve a desired envelope.

The above examples serve primarily to point out that it is not always necessary to provide inflight trajectory data, but that when data is necessary, the degree of accuracy required is a function of the use of such data.

2.2 The above techniques have been utilized during the following Grumman Separation Programs:

- MK-4 Gun Pod, Standard Arm Missile and D-704 Buddy Tank from A-6A Intruder (1968)

- 150 gallon fuel tank, LS-59 flasher pod, ALQ-80 ECM Pod from OV-1D Mohawk (1969)

- ALQ-99 Tracker - Jammer Pod from EA-6B (1970)

- AIM-54A Phoenix, AIM-7E-2/F Sparrow, AIM-9 Sidewinder, 267 gallon external supersonic fuel tank from F-14A Tomcat (1972 - 1975)

- MK-82, 83, 84 general purpose bombs, MK-20 Rockeye II, CBU-59/B APAM, MK-45 Flare, MK-76 Practice Bomb from F-14A Tomcat (1974 - 1975)

- AIM-7F Autopilot Separation Program from F-14A (1977)

3.0 CAMERA/LENS INSTALLATION DEFINITION COMPUTER PROGRAM

The placement of movie cameras on a test aircraft has traditionally received minimum technical effort and has generally been accomplished through relatively brief review of front, side and planform views of the aircraft with heavy reliance on personal judgement. This was essentially the Grumman procedure until 1969 when an attempt was made on the OV-1D Mohawk Separation Program to optimize the field of view coverage of two Milliken DBM-4C movie cameras by establishing the desired locations,

orientations and lens angular coverage using a procedure graphically described
in Figure 3. Predicted store trajectory data, along with mated position coor-
dinates were input to a desk top computer. Also input were various camera yaw,
pitch and roll (in the event of a rectangular film format) angles for candidate
locations. A three axis transformation was performed in the calculations to
reference selected store points to the film axis system. Normalizing the new
coordinations by simulating a unity focal length provides a camera format numer-
ically representative of the tangent of half angle coverage for each direction
from the lens center. By reviewing the above data, design information was made
available to the Instrumentation Department well in advance of the program with
no concern for last minute modifications to hardware as had occurred during
prior programs when final refinements to camera hardmount angles were based
upon the use of a boresight attachment (prism which enables the viewer to ob-
serve the lens coverage) to the camera to establish final look angles.

$$X' = X \cos\psi - Y \sin\psi$$
$$Y' = X \sin\psi + Y \cos\psi$$
REPEAT FOR θ AND ϕ
TRANSFORMATIONS

FILM POSITION
OF POINT IN
SPACE

FILM
PLANE $f=1$

LENS FORWARD NODE OR PRINCIPLE POINT -
FIRST CROSSING POINT OF ALL LIGHT RAYS
GATHERED BY LENS

AFT LENS NODAL POINT (LAST CROSSING
POINT OF LIGHT RAYS PRIOR TO REACHING
FILM PLANE)

• POINT IN SPACE WITH
AIRCRAFT COORDINATES
(X, Y) AND TRANSFORMED
COORDINATES (X', Y')
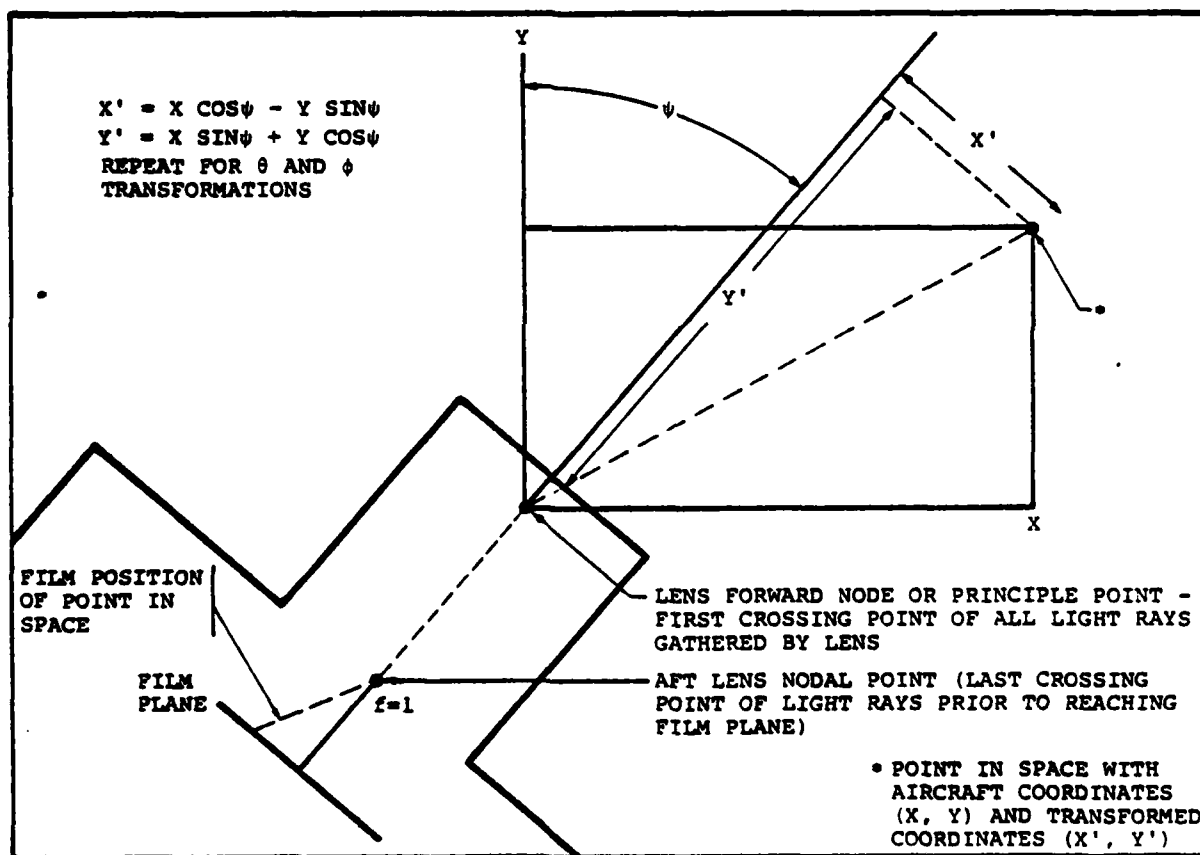
FIGURE 3. AIRCRAFT TO FILM COORDINATE TRANSFORMATION

3.1 In preparation for the F-14A Separation Test Program, an attempt was made to gain a thorough understanding of all aspects of the two camera trajectory calculation system in order to exploit its capabilities to the fullest. An analysis of every step of the separation calculation procedure was undertaken to determine where improvements could be made. It had been noted during prior separation programs that under certain ideal conditions, data accuracies to within several inches for space positioning of a store 30 feet radially from the mated position were being experienced. A consistent two inch space positioning accuracy throughout the first 30 feet of store travel was established as the goal for F-14A tests. The first place to start, and the one that would remain fixed as a constraining factor during the entire program, was in determination of camera locations, orientations, and lens size. To more fully appreciate the familiar process of triangulation insofar as it is applied to the separation problem, a brief acquaintance with the Grumman process is provided here with a more detailed review following in a later section. Figure 4 illustrates a representative situation where a fuel tank nose and aft band are the targets for filmreader crosshairs. Dotted lines indicate the two-dimensional sightlines depicting the calibrated lens optical axis for each camera, while the solid lines indicate the sightlines emanating from the lens principle point and passing through the crosshair position on the film to the point on the store serving as the target. Distance between camera principle points is calculated using equation (4).

$$D = \sqrt{(X_2-X_1)^2 + (Y_2-Y_1)^2 + (Z_2-Z_1)^2} \qquad (4)$$

DOTTED LINES REPRESENT CALIBRATED LENS CENTERLINE ORIENTATIONS

CAMERA NO. 1

CAMERA NO. 2
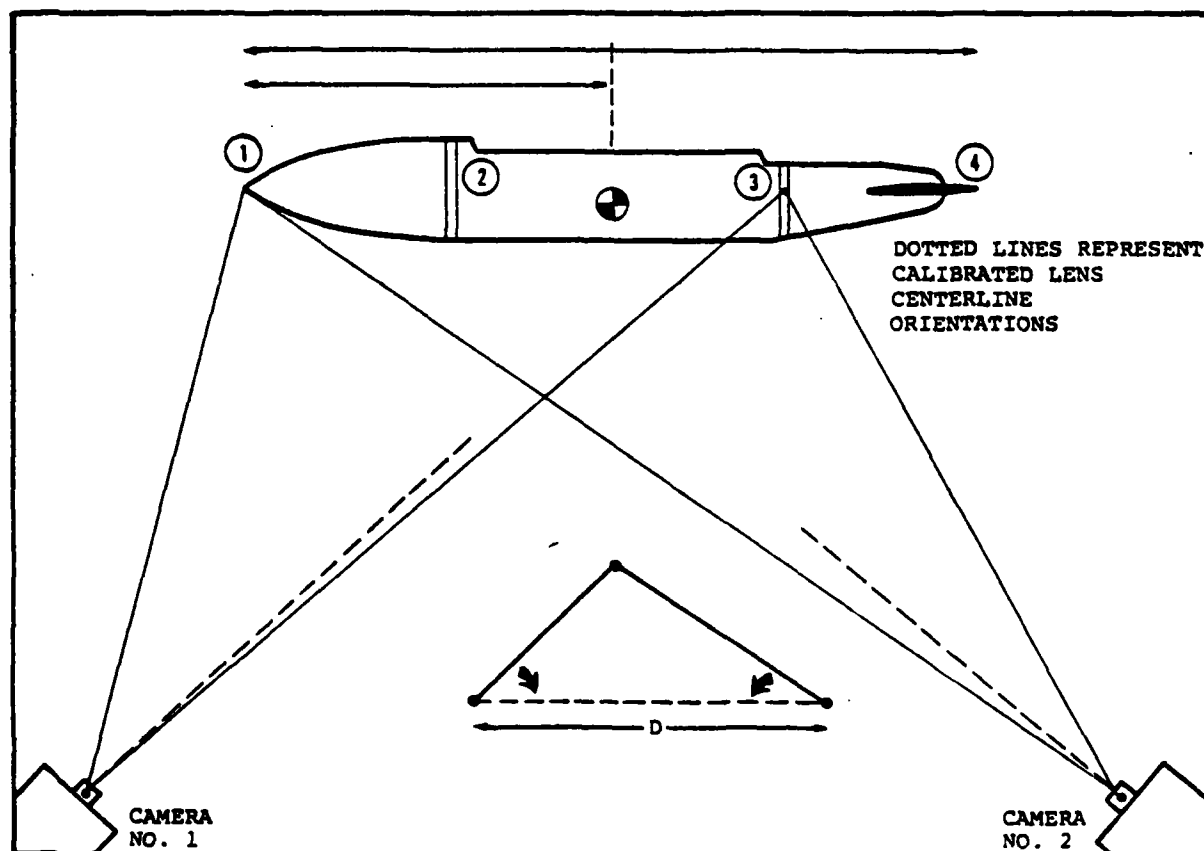
FIGURE 4. BASIC TRIANGULATION DIAGRAM

1000
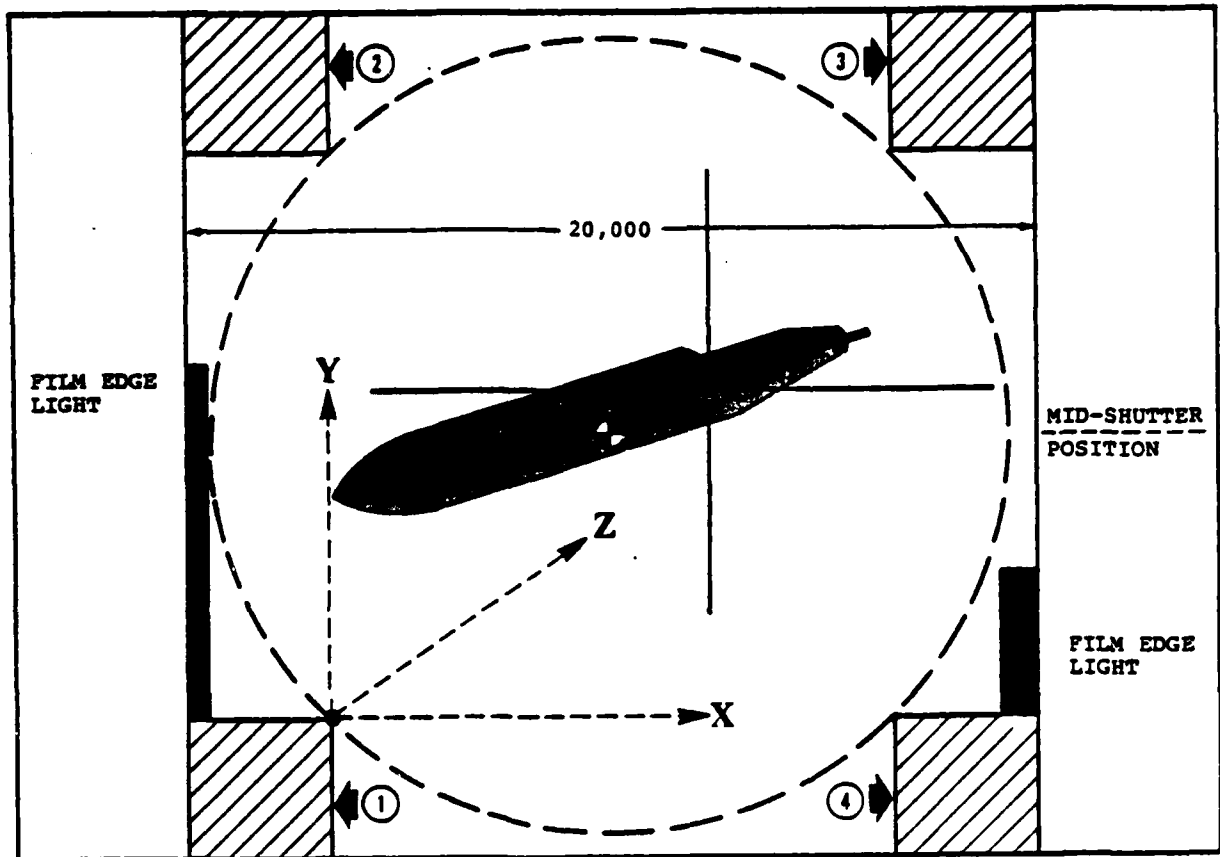
FIGURE 5. CAMERA VIEW OF STORE

Figure 5 shows this view as seen from the film in one camera. In a nutshell, the triangulation procedure requires one side (baseline) and two angles of a triangle to be known in order to calculate the length of the remaining sides. Calibration data provides the aircraft coordinates of each camera's effective location, and filmreading provides the angles. Expanding this procedure to three dimensions and applying the principles of solid analytical geometry to effect a least squares solution to describe the "best fit" intersection of two sightlines in space represent the heart of the Grumman procedure. Sightlines are described by a direction cosine matrix relating them to aircraft and film axes, with the least squares solution being required since the chances of any two sightlines in space actually intersecting at a single point are essentially zero. For a given point in space, the angle between two sightlines is a function of the origination of those sightlines; namely, cameras in our case. When the intersection angle approaches either 0° or 180°, a small angular error can result in a relatively large trajectory computation error, with minimum errors experienced when sightlines approach 90° intersections. As a result of a sensitivity analysis performed by Grumman using an allowable error based upon prior experience of ± 5 filmreader counts (out of 20,000 between the outside edges of the horizontal sprockets) for a store 30 feet from both cameras, it was determined that with all other system errors held to a reasonable minimum, a sightline

1001

variation corresponding to +5 counts at intersection angles less than 20° and greater than 160° would result in trajectory calculation errors in excess of the two inches allowed. Final camera location decisions would have to take this factor into account. Total camera coverage requirements for the F-14A Program are listed below:

- Coverage by at least one set of two cameras for the entire set of drops zones defined on the basis of preliminary trajectory predictions by the Aerodynamic Engineering Group.

- Coverage for multiple drops per flight, any station, jettison or launch to permit desired flexibility in program planning/efficiency.

- Submerge cameras/lenses into aircraft structure wherever possible to minimize disturbances to the flow field – this requires submittal of Mach 2+ hardmount/fairing design criteria far in advance of actual flying with no capability for last minute shimming or modifying; also provides easy access for loading/installation.

- Provide one wing tip orientation for coverage from 20° to 68° wingsweep.

- Select best compromise wide angle lens to satisfy coverage requirements, eliminate excess coverage by maximizing the simultaneous field of view of the various camera combinations, and minimize optical distortion and number of cameras.

- Maintain sightline intersections between 20° and 160° as discussed above by judicious selection of camera locations.

- Attempt, whenever possible, to permit the expected trajectory to pass through the lens center to obtain maximum accuracy at the lens area that produces minimum distortion.

- Provide desired view of non-trajectory related items such as operation of arming devices, rocket motor plume impingement, installed fin to fin clearances at high speed, retarding devices, motor ignition, etc.

- Monitor location of missiles relative to radar illumination field.

In order to meet the above objectives, the simplified camera placement program used with the desk top computer for the OV-1D Mohawk Program was expanded for use with the CDC 6400.[1] The program computes a simulation of any desired camera view for any lens size, orientation and location. A sample wing tip view of a Phoenix and related drop zone is shown in Figure 6.

SPARROW-PHOENIX LAUNCH ZONE FROM LEFT GLOVE PYLON   CAMERA NO. 7 LEFT WING TIP
FS=620   WL=150   BL=343   EL=330   AZ=100   SF=1.5   WS=20 DEGREES
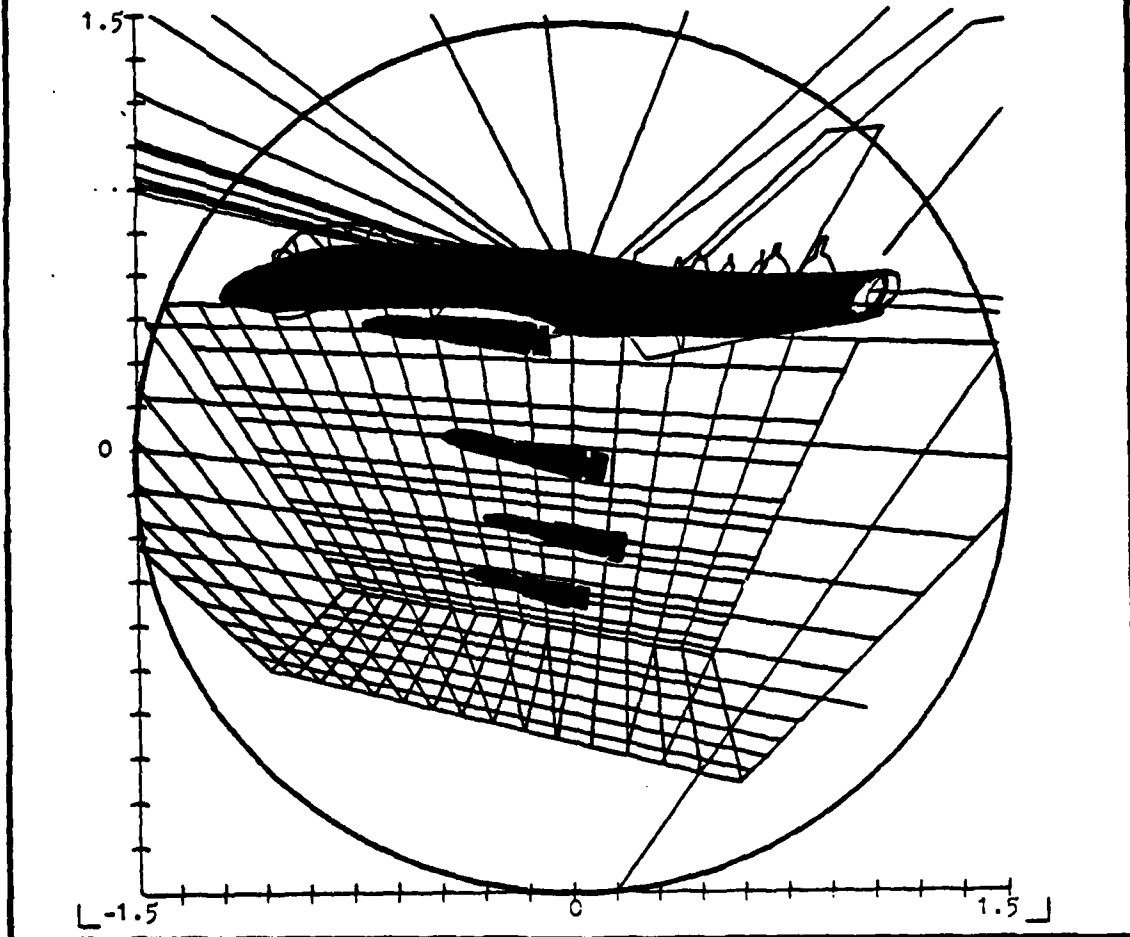
FIGURE 6.   SIMULATED WING TIP CAMERA VIEW OF A PYLON PHOENIX JETTISON

An overview of the procedure is provided below:

* All aircraft and store contour data (X, Y, Z) coded in computer
  card format using televised optical target orthomat machine.
  This was a one day effort for the F-14A Program.

* Expected trajectories, store mate position data and desired drop
  zones also coded onto computer cards.

* Potential submergible locations obtained from Structural Engi-
  neering and Instrumentation Installation Groups.

* Variable input data consisting of lens principle point, orien-
  tation angles of lens centerline axis and plot scale factors
  coded.

1003

- Angles defined in order - yaw in waterline plane, pitch from waterline, roll about lens axis (useful only in non-circular format picture).

- Computations - distance between each input point and camera principle point; double or triple axis rotation; data normalized to unity focal length (divide X, Y of film value by Z distance radially from camera); distance from lens center presented as tangent of angular coverage in each direction; angular intersections between various two-camera combinations at selected drop zone points computed.

As a result of the above procedures, locations/orientations chosen were as shown in Figure 7. Guesswork was entirely eliminated and a firm basis upon which other improvements in the system could be made was established. A side benefit of this information was to permit Navy and Hughes Aircraft Company personnel to quickly establish camera orientations for viewing their weapon compatibility releases from the F-14A.

- NINE CAMERA HARDMOUNT POSITIONS

- 15 ORIENTATIONS AVAILABLE

- UP TO SEVEN CAMERAS ON ONE FLIGHT

- ALL LENSES 110° WITH THE EXCEPTION OF 165° WIDE ANGLE LENSES FOR THE TWO OUTBOARD NACELLE CAMERAS
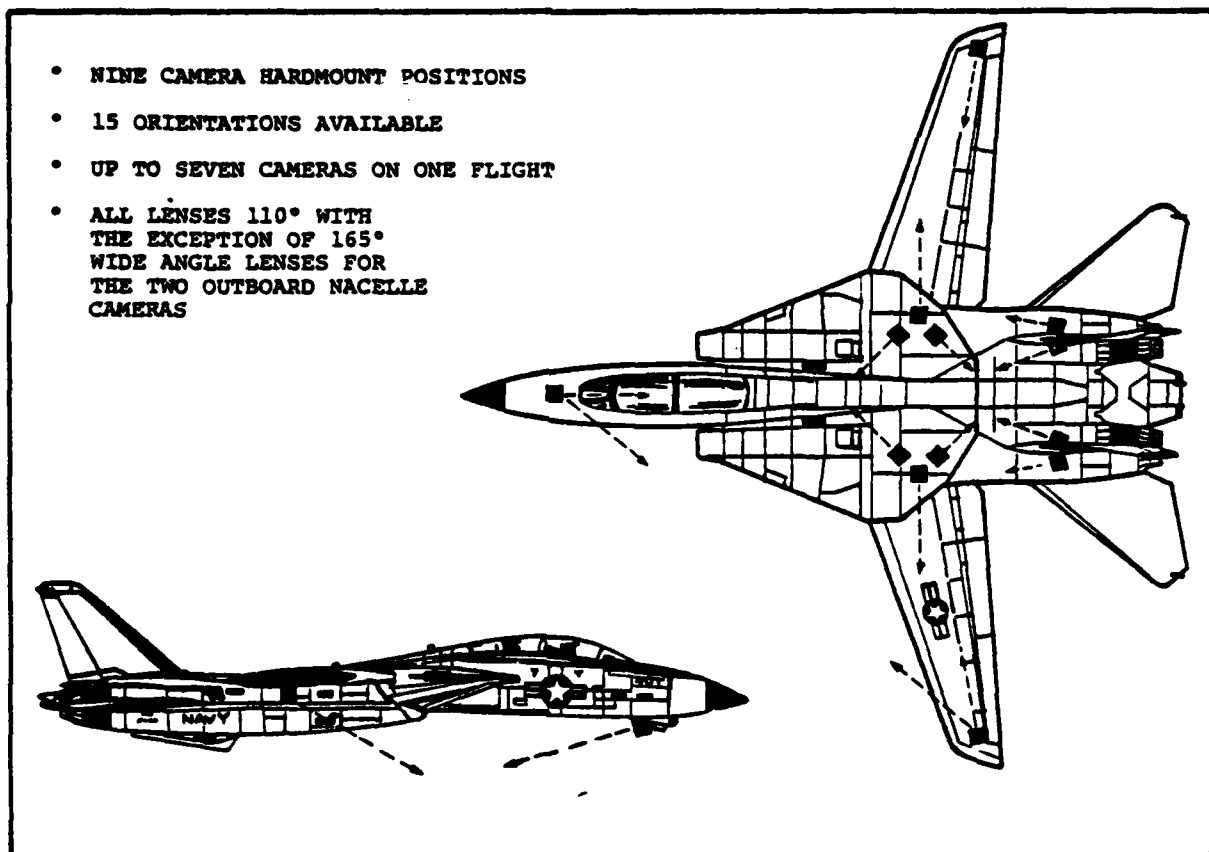
FIGURE 7. CAMERA LOCATIONS/ORIENTATIONS CHOSEN FOR F-14A PROGRAM

4.0 LENS DISTORTION CALIBRATION PROGRAM·

The Grumman use of wide angle lenses for documentation of separation char-
acteristics dates back to the Standard Arm Program on the A-6A Intruder in 1968
when 84° wide angle lenses were used with three Milliken DBM-4C movie cameras
mounted on the aircraft. Since the acquisition of on-board trajectory data en-
tails conversion of linear film information to aircraft coordinate values, the
distortion produced by wide angle (Fisheye) lenses must be eliminated. This
distortion, as depicted in Figure 8, is alternately referred to as barrel (posi-
tive), pin cushion (negative), radial or spherical, and should not be confused
with f-stop distortion, a characteristic of narrow angle lenses which decreases
in significance as angular coverage increases.

The basic effect of radial distortion is a shrinkage of film images toward
the center of the lens, with an increasing effect as the radial distance from
the lens optical axis is increased. This can also be described as a non-linear
film plane representation of equal angles in the field-of-view coverage which
must be rectified prior to use with a linear calculation system. The Lens Dis-
tortion Calibration Procedure enables a purely mathematical correction to be
applied to the raw film reading data such that the average deviation of the
image points from their correct positions will be a minimum. Calibrations are
always accomplished with a camera and lens combined as a unit.
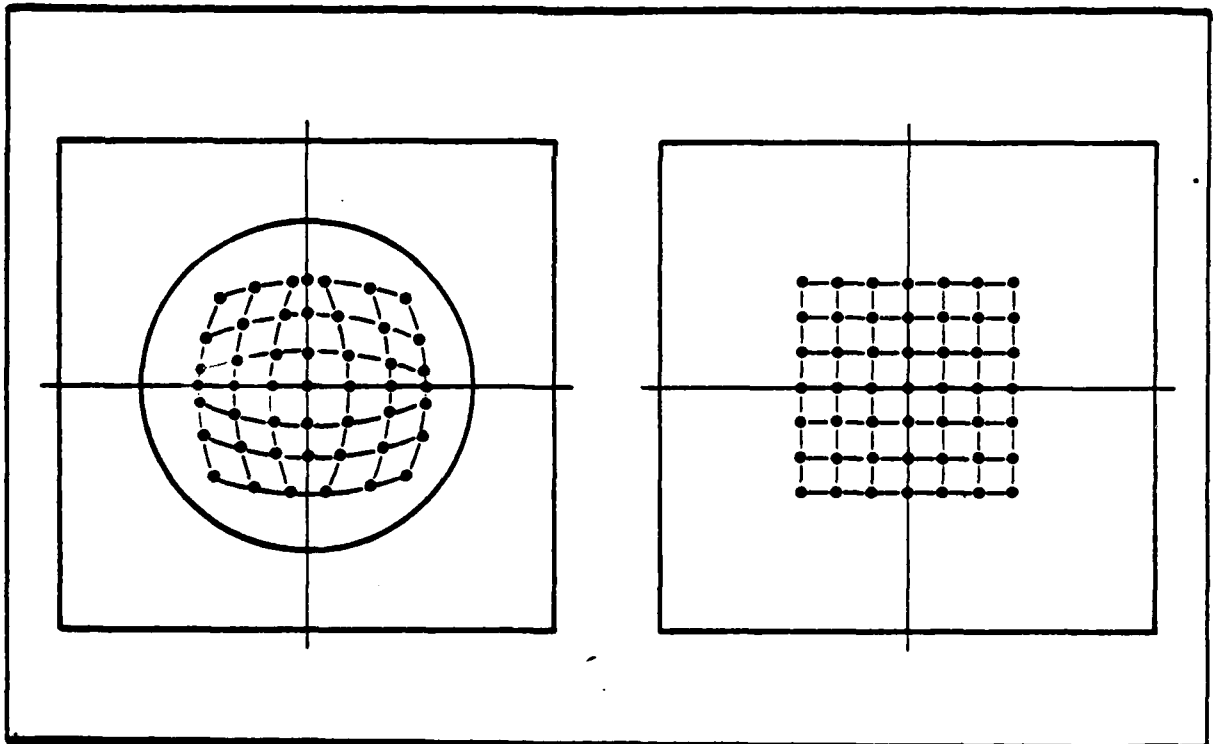
FIGURE 8. DISTORTED AND UNDISTORTED VIEW OF A SQUARE GRID

All of the Grumman procedures utilized for elimination of distortion since 1968 have involved photography of a square grid board with a black background and a 13 by 13 pattern of uniform white dots machined with centers 2.0 $\pm$ .001 inches apart in the vertical and horizontal directions. A two inch diameter circle surrounding the center dot is removable to permit viewing through the center of the board while it is being positioned for the calibration. A structure on the aft side of the board with a metal face machined as nearly as possible parallel to the dotted front face of the grid serves as an optical target holder and first surface optical mirror support. This enables accurate positioning of the grid pattern centered on and perpendicular to the lens optical axis as established by an auto-collimator linescope. With the board in position, the center plug is carefully replaced and movie films of the grid pattern are taken.

Prior to the development of specialized techniques for the F-14A Program, the board was positioned only once with the grid close to the lens to fill the entire field-of-view. A linescope was used to establish the lens optical axis through an iterative process of collimation, autocollimation, and auto-reflection. Three separate heavy (but stable) optical tripods as shown in Figure 9 were used to support the camera, grid board and linescope with six degree-of-freedom adjustments available for each. The basic procedure consisted of the following steps:
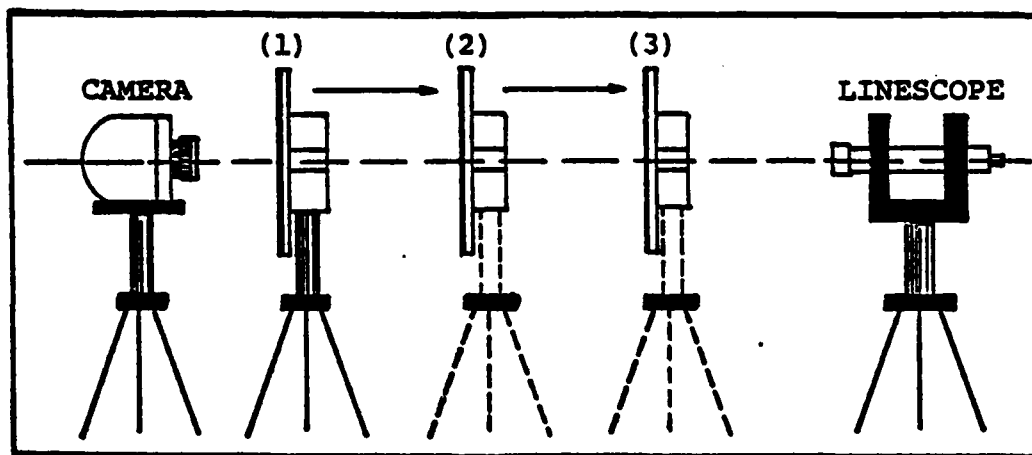
FIGURE 9.   DISTORTION CALIBRATION SETUP FOR PRE-F-14A PROGRAMS

1.   Roughly align the camera, grid board and linescope as per Figure 9 with the dotted grid facing the camera.

2.   With a small first surface mirror placed behind and firmly against the camera film plane to optically establish the orientation of a movie film frame, with the grid board center plug removed and with the lens removed from the camera, adjust the positions and orientations of the camera and linescope until a line, perpendicular to the film plane mirror and centered approximately at the mechanical center of the frame, is established.

1006

3. With the lens firmly installed and f-stop set to the smallest aperture opening, initiate an iterative process by adjusting the camera and linescope until the following conditions are satisfied:

° In the telescope (transit) mode, and focused on the lens Iris, the linescope crosshairs are positioned on the Iris center - collimation.

° With the linescope focused at infinity, the lighted projected crosshair return (very faint after passing through multiple lens elements) from the film plane mirror is superimposed upon the reticle crosshair - autocollimation.

° With the linescope focused upon the reflected image of the linescope bullseye pattern from the front lens element, the center bullseye is aligned with the reticle crosshair - auto-reflection.

4. Simultaneously satisfying the above criteria assures optimum accuracy in determination of the lens optical axis within the design tolerances of the lens. The next step calls for alignment of the grid board to this optical axis. A circular transparent optical target is placed in the hole vacated by the center dot, and a magnetic machined base first surface optical mirror representing the grid plane is placed on the aft structure whose surface is parallel to the grid. The position and orientation of the grid is varied until the center of the board is aligned with, and square to, the lens axis. With the grid pattern set the proper distance from the lens and the center dot replaced, filming can begin. ·

Data analysis of the above film was accomplished by obtaining the film coordinates of each of the 169 grid points with respect to either the film sprockets or the intersection of small mechanical marks called fiducials located at the center of each frame edge in the camera and therefore photographed on each frame. Comparison of the radial distance in film counts of each dot from the center dot enables calculation of a distortion curve as shown in Figure 10. Since the center of the lens is essentially undistorted, a film scale factor can be obtained by averaging the counts of the four axial dots surrounding the center. The correct position for every other dot is a multiple of this factor. Comparison of compressed or distorted film values to linearized or corrected locations for each of the remaining 164 grid points permits generation of a ratio multiplier or additive factor curve relating distorted to non-distorted film values. The film coordinates of the center dot represent the intersection of the lens optical axis with the camera film plane. Only by coincidence would this be the exact mechanical center of the aperture, a situation which rarely occurs. Use of the three tripods resulted in a cumbersome and time consuming setup which would have been unsatisfactory for the F-14A Program considering the number of cameras to be calibrated. For previous programs, the distortion correction curve was first established using a desk top computer, and then tabulated for input to a computer table lookup routine in the form of a series of ratio multipliers versus distorted radii.

VERTICAL AXIS CAN BE:

R_L LINEARIZED RADIUS, OR

R_L R_D RADIO MULTIPLIER, OR

DELTA RADIUS

DISTORTED RADIUS IN FILM COUNTS R_D
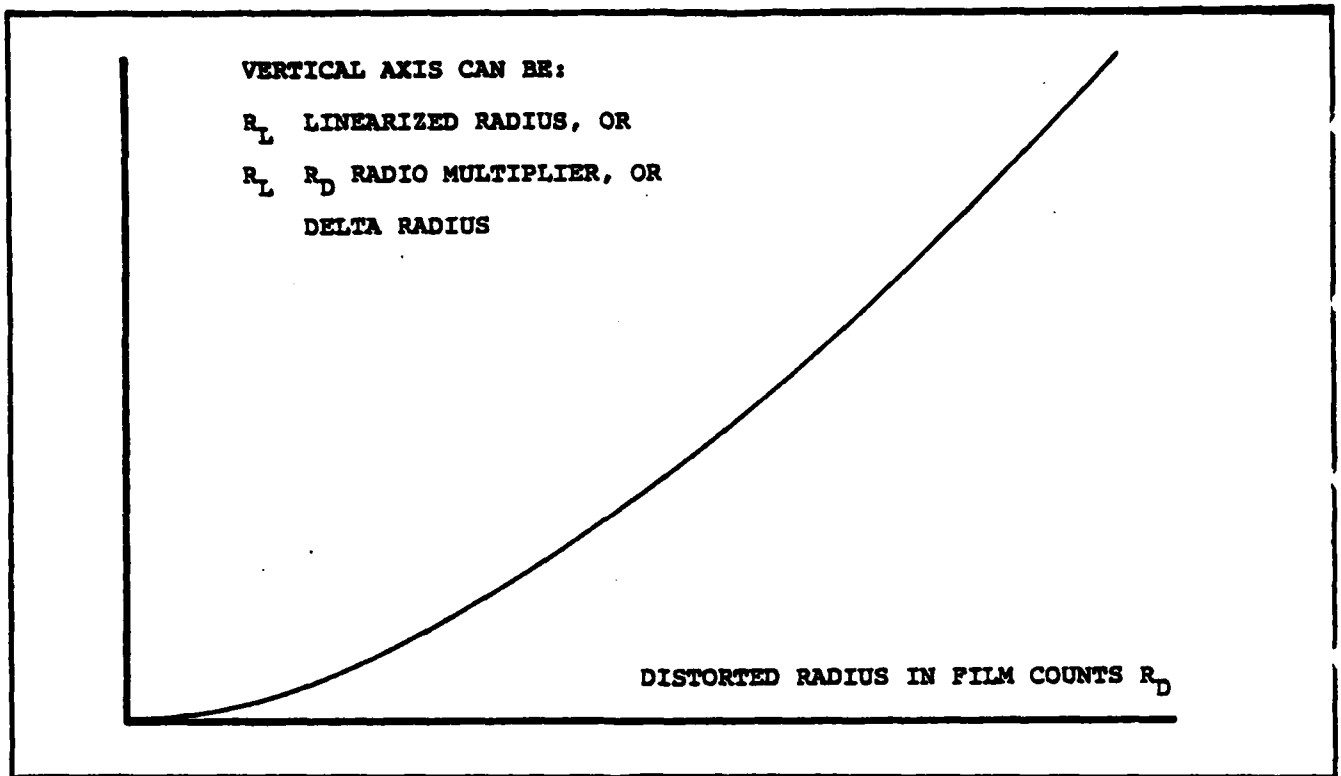
FIGURE 10.   DISTORTION CURVE

For the F-14A Program, several modifications and improvements were made
to the lens distortion calibration procedures to streamline the effort.   Fore-
most among these were use of an optical tooling bar to facilitate the align-
ment process, design of a six degree-of-freedom adjustment mount for the camera,
lighting adapters for the grid board and incorporation of a lens focal length
calculation which is discussed in a later section of this paper.   Streamlining
the lens calibration process enabled calibration of ten seven element 110° and
two 165° wide angle lenses to be completed in less than one week of a two man
operation including setup, familiarization and repeatability checks.   The last
several cameras required less than an hour each to calibrate once a smoothly
coordinated procedure was established using the highly sensitive optical equip-
ment.   In addition to the above changes to physical calibration techniques, a
computer program compatible with an IBM 360-67 time sharing remote terminal
system was developed to more rapidly and accurately handle the large volume of
data from the many lenses to be calibrated in addition to incorporating the
focal length calculation and several other features discussed in the following
paragraphs.

Figure 11 is a schematic of the fixture used for F-14A lens calibrations.
Alignment procedures were essentially the same as those used previously with
the tripod arrangement.   The tooling bar provides a rough alignment and a track
for forward and aft motion of the grid board.   The closest position is used for
calculation of the distortion curve as before, and the two other grid board
positions are used for calculation of the focal length as shown in Figure 12.

1008
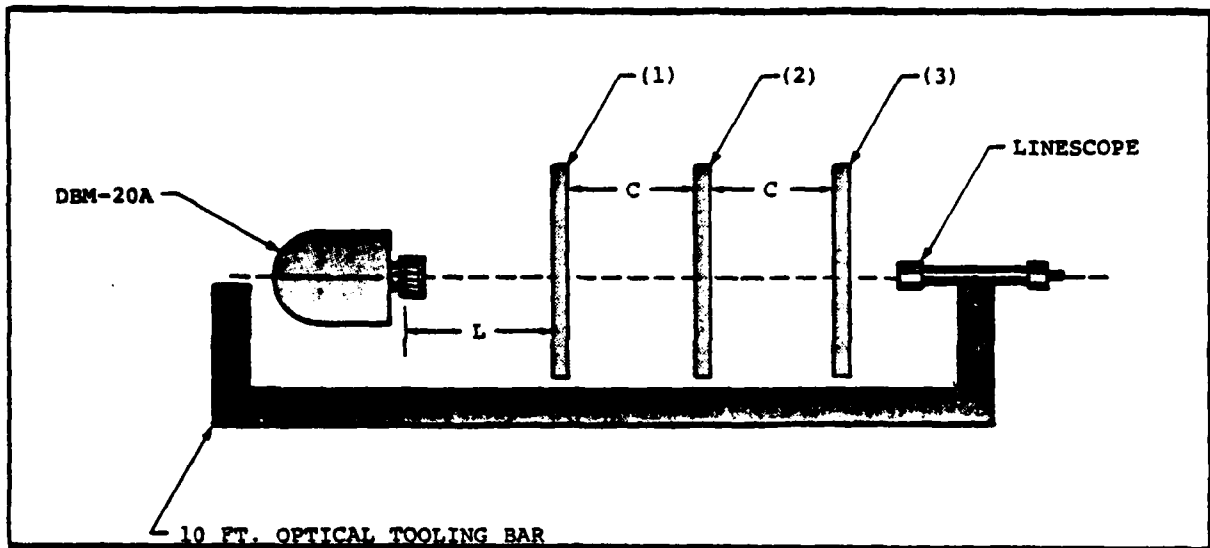
FIGURE 11.   F-14A DISTORTION CALIBRATION SETUP

For each grid position, the alignment procedure must be repeated to center the board on the lens optical axis and assure that the grid is parallel to the film plane.

$$\frac{R_1}{f} = \frac{R}{L} \qquad \frac{R_2}{f} = \frac{R}{L+C}$$

$$f = \frac{(R_1)\ (R_2)\ (C)}{R\ (R_1 - R_2)}$$
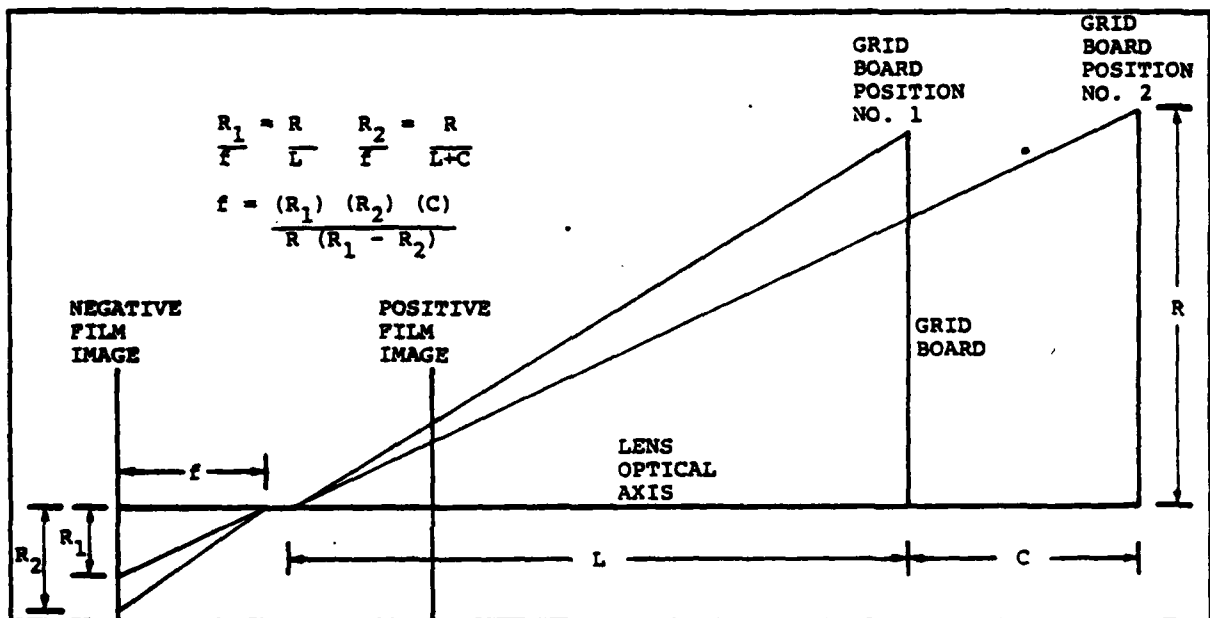
FIGURE 12.   FOCAL LENGTH CALIBRATION SETUP

The computer program was modified to normalize all film input data as a function of percentage of film sprocket distances instead of using raw film reader counts in order to eliminate differences in scale from different film reader machines and also avoid potential errors due to film shrinkage during processing or expansion at elevated temperatures. All output data is computed in terms of normalized counts to enable reading on any film reader. The distortion curve was calculated with the least squares technique in two stages using odd powers (vertical axis symmetry) of a fifth order polynomial. The first curve utilized the center dot coordinates as the assumed distortion center which had been determined optically using the calibration linescope.

An iterative process using the first curve to linearize distorted film images is accomplished to "fine tune" the best mathematical fit for the distortion center to which the normalized film counts are then referenced for calculation of a "fine tuned" distortion correction curve which converts distorted film counts to corrected values.

Summary of lens distortion correction procedure:

° Mathematically eliminates radial or spherical distortion inherent in a wide angle or fisheye lens.

° Calculates lens distortion center, distortion curve and focal length in terms of normalized film reader counts.

° Above data used as constant data for input to the trajectory calculation computer program.

Due to the requirement for Mach 2+ releases with associated high airstream temperatures, the lens support structure was specified as stainless steel which has a thermal coefficient of expansion similar to that of optical glass. This minimizes any possibility of thermal distortion at elevated temperatures. Insulating glass over the outside of the lens is not permitted since relative movement of the glass window and the lens would introduce random refraction errors that could not be corrected. As a result, the lenses are exposed to the flow field.

5.0 ON-BOARD CAMERA CALIBRATION

The on-board camera calibration is a relatively simple procedure that establishes the actual position and orientation of cameras to within close tolerances once they have been installed on the test aircraft in accordance with camera location program instructions. In addition, the aircraft coordinates of targets called reference points used for monitoring and updating camera locations/orientations due to inflight aero-elastic motion are established during this procedure. All of the above data are input to the trajectory calculation program as constant data.

For the previous programs, the calibration was accomplished using three grid board positions and some rather esoteric solid analytic geometry techniques to calculate the space position of the forward nodal point (principle point) of the wide angle lens in addition to the lens focal length in filmreader counts and the transformation matrix relating the film axes to the aircraft axes. The procedure consisted of aligning the grid board along an optically determined aircraft axis, establishing the aircraft coordinates of a known point on the grid board at the closest board position and then photographing the board at three positions along the aircraft axis. Cameras were attached to hardmounts using standard dovetail mounts. Using the principles of vanishing point theory (depicted in Figure 13) the desired camera data can be calculated.

1010
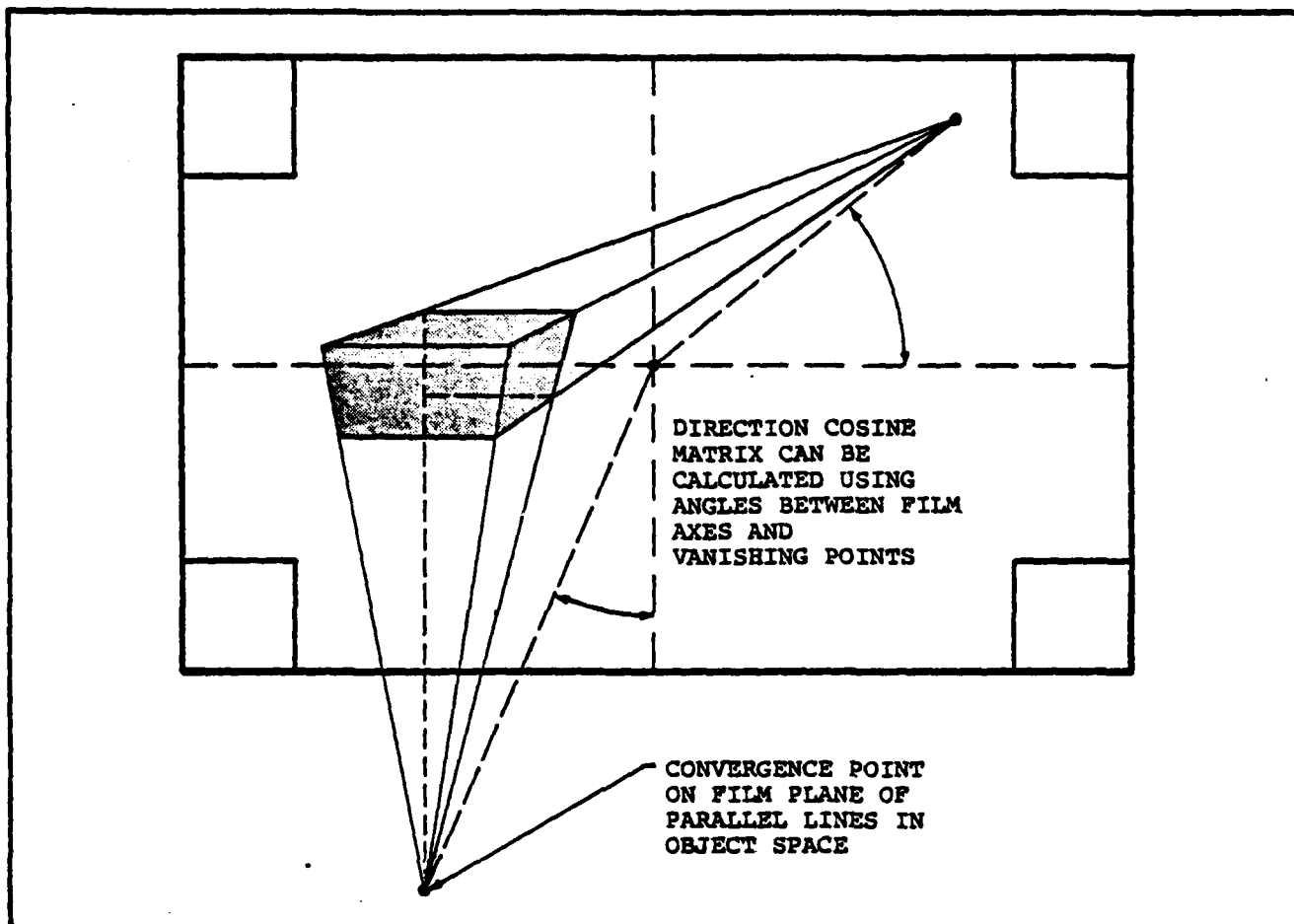
FIGURE 13. VANISHING POINT SCHEMATIC

The above procedure was considered to be too time consuming, and since the focal length calculation was being incorporated into the distortion calibration procedure, an alternative method of physically measuring the required locations and orientations of the installed cameras was devised with the aid of Grumman Optical Engineering and Metrology (OE&M) personnel and used on a non-interference basis during the EA-6B calibration for comparison with the previously established method. The new method entailed use of optical transit squares or theodolites to obtain the required data in only a fraction of the previous time and with comparable or greater accuracy.

A brief review at this time of basic camera and wide angle lens features, and of camera preparations made for the F-14A Program, will enable greater understanding and appreciation of the Grumman techniques developed for acquisition of on-board trajectory data. Two views of the Milliken DBM-20A 16mm movie camera with attached Pacific Optical 110° wide angle lens are presented in Figure 14.

1011
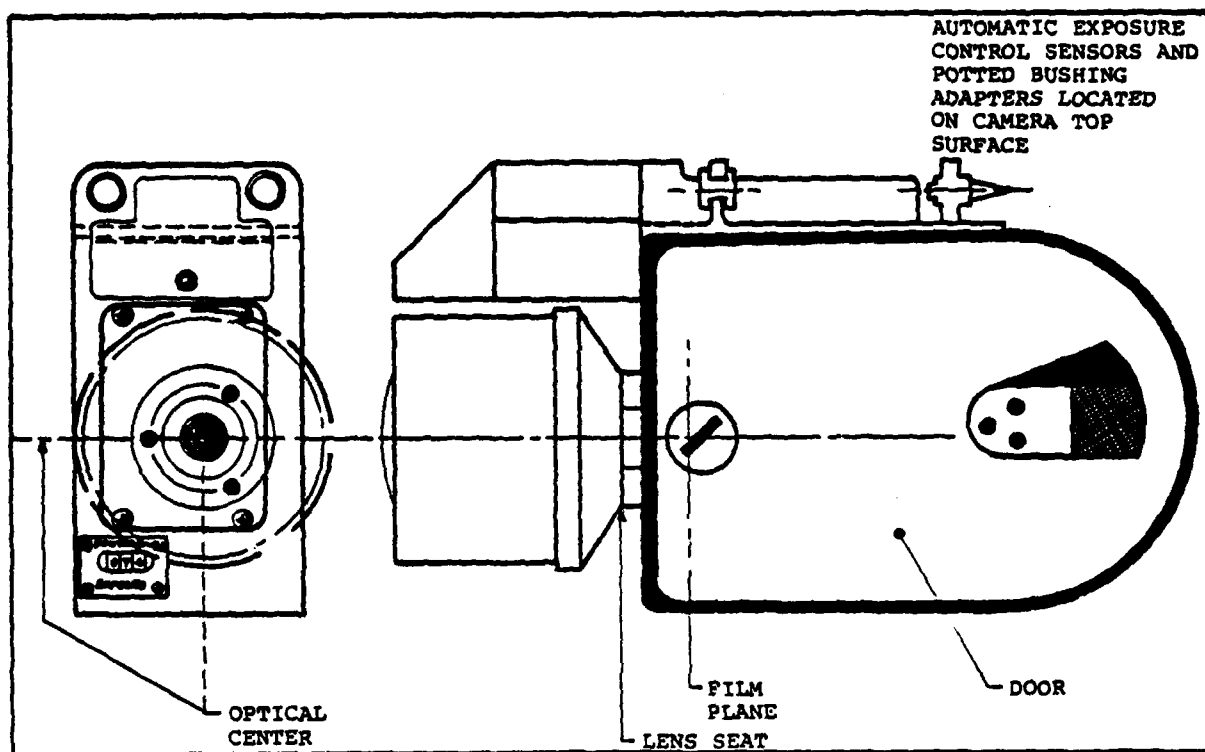
FIGURE 14. DBM-20A CAMERA WITH SPECIAL ADAPTERS FOR F-14A PROGRAM

In order to provide complete interchangeability of all cameras on all hard-mount locations, a capability not available during prior programs, a universal adapter was designed by the Grumman Instrumentation Department in conjunction with the OE&M Department. Design requirements for the adapter included structural integrity for attachment of the camera to the aircraft throughout the flight envelope, easy loading and unloading, and repeatability of calibrated parameters. The OE&M Department designed and manufactured a camera fixture to properly mate the universal adapter to each camera using adjustable potted bushings with the face surface aligned using the same fixture to provide a proper mating surface. The bushings were located such that the vertical, lateral and longitudinal distances of the bushing centers to the mechanical center of the film aperture would be the same for all cameras. With this location established, a high temperature and high strength epoxy resin, such as Epon 934 and Aerobond 2143, was injected into the bushing support to maintain this setting. With interchangeability and repeatability requirements thus satisfied, it became necessary only to calibrate each hardmount position rather than each hardmount/camera combination. Special adapters were built by OE&M to enable precise and efficient optical determination of desired parameters for the F-14A calibration which was being conducted in conjunction with an optical alignment layup of the test aircraft which required that the aircraft be leveled on jacks. A weapon system alignment fixture was used to define the aircraft axes and locate tooling bars parallel to the aircraft lateral and longitudinal axes. Strategically placed transit squares and theodolites referencing the optical alignment fixture enabled the yaw and pitch orientation of each hardmount to be established using a lens adapter whose first surface mirror had been set parallel to the film

1012

plane of the particular camera being used. The optical return of a mirror behind the camera film plane was unsatisfactory and necessitated fabrication of an adapter to provide more surface area return. To obtain the space position at which all rays cross after entering the front face of lens, another lens adapter was fabricated (Figure 15) with a plumb bob line support located at the simulated forward node. Location of the forward nodal point is shown in Figure 15 along with a view of the adapter used to simulate this point.
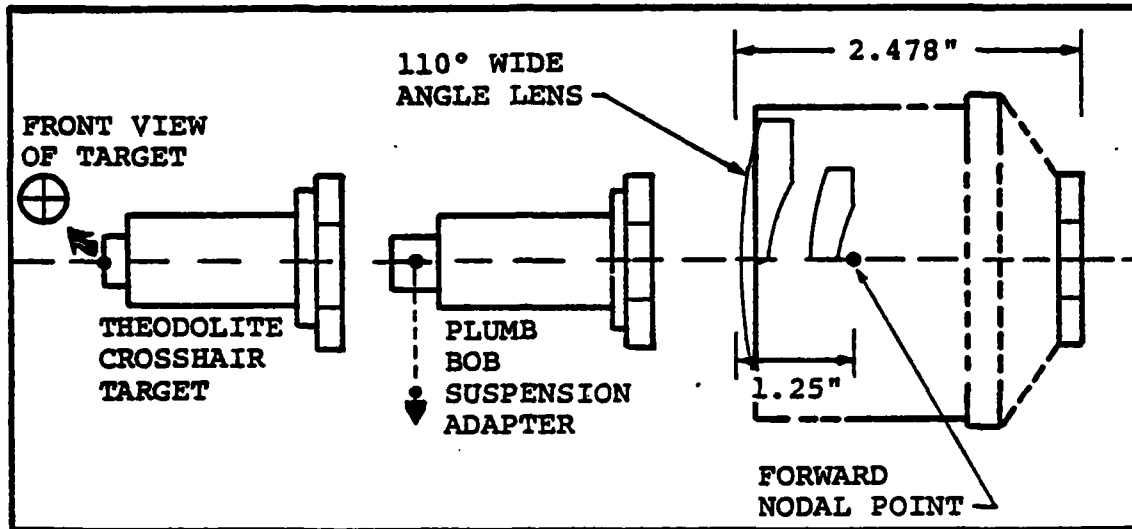
FIGURE 15. LENS SCHEMATIC AND ADAPTER

Lateral and longitudinal coordinates of the line were then determined using transit squares, with the vertical measurement read directly on the adapter. Transits were also utilized to accurately determine the space position of the center of target bullseyes painted on the aircraft used to update camera positions/orientations from aircraft inflight flexing. Only the roll orientation remained to be determined. This parameter was specified to be zero for all cameras since a circular presentation of the coverage provided by the wide angle lenses eliminated any advantage of rolling the lens. To obtain this parameter which is required for data calculation, a series of plumb bobs were photographed across the field of view of the lens using any camera with a mated, distortion calibrated lens. As shown to the left of Figure 16a with all plumb lines stabilized and aligned with the gravity vector, the vanishing point formed by the intersection of the linearized lines on the film plane establishes a vector to the lens center. The angle between the vertical film axis and this vector is the camera roll angle. Usually five plumb lines were utilized to establish the vanishing point location. An alternate method to accomplish the same objective by using vanishing point theory is shown to the right of Figure 16a, and in Figure 16b. Only one plumb line is required and, with knowledge of the camera pitch angle and calibrated focal length, the vanishing point can be determined through the intersection of a circle of radius $f/\text{Tan } \theta$ and the plumb line. This method proved to be of equal accuracy as the multiple plumb line intersection method and much less time consuming from a setup and film reading standpoint. In conjunction with roll shots, the film coordinates of all targets in the field of view of each position were obtained.

1013
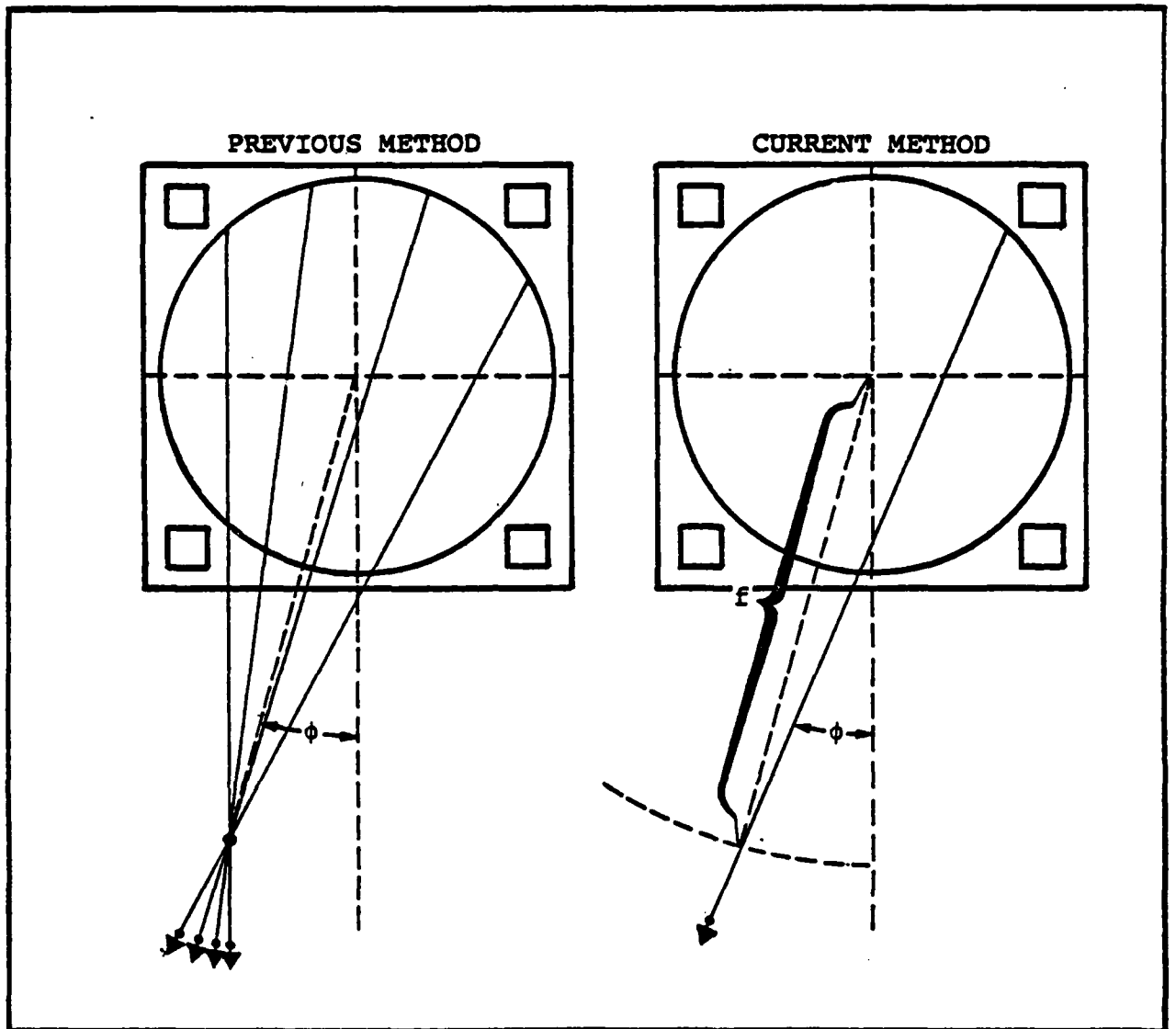
FIGURE 16a.   ROLL CALCULATION PROCEDURE COMPARISON

LENS
OPTICAL
AXIS

SINGLE
PLUMB
BOB

VANISHING
POINT

X = f/TAN θ
f = LENS FOCAL LENGTH
θ = LENS PITCH ANGLE
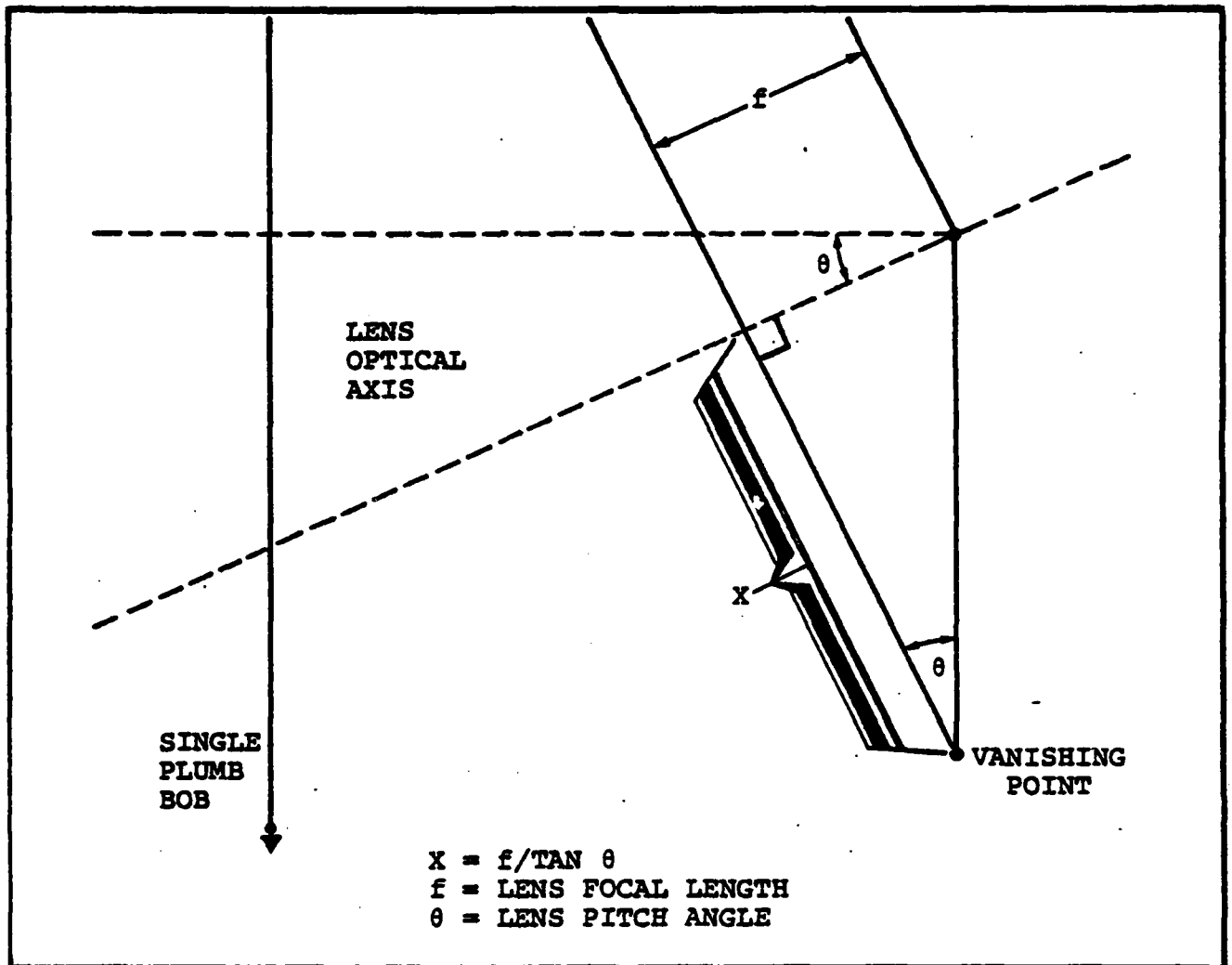
FIGURE 16b.   ROLL CALCULATION PROCEDURE COMPARISON

Prior to disassembly of the optical setup, several checks were made to pro-
vide assurance that no errors in the calibration were made, and also to validate
the accuracy of the wing tip reorientation technique and the basic system accu-
racy under ideal controlled conditions. Ping pong balls were placed at various
precisely known locations under the aircraft and photographed by cameras at each
hardmount position and orientation. Since the ping pong ball represents a small
well defined target, the lighting ideal, and flexing/timing errors non-existent,
any significant errors in the calculation of the ball positions using the many
combinations of two camera solutions would indicate a position or orientation
error. The average error in establishing the location of the ball centers were
approximately .25 inches for all three coordinates. As a check on the wing tip
reorientation technique, more fully reviewed in the following section, the wing
cameras were calibrated at five positions varying between 20° (maximum forward)
and 68° (maximum aft) wing sweep angles. The Church Resection technique using
combinations of three targets on the aircraft also calculated the camera posi-
tion and orientation at each wing position. Comparison of the two values indi-
cated generally good agreement under such ideal conditions to establish full

confidence in the system. Using target based locations/orientations for the wing tips, ping pong ball location calculation errors averaged .50 inches compared to .25 inches using calibrated values. However, this was considered to be excellent agreement in comparison to prior update methods. Traditionally, due to the large amount of structural flexing, wing tip cameras produce the largest trajectory calculation errors, and this was expected in the F-14A program. With non-coplanar points of known coordinates on the fuselage spaced widely apart in the field of view, Church Resection provided the best technique to correct for inflight camera motions which can vary significantly at any wing angle due to load factor and dynamic pressure.

In summary, the on-board camera calibration program determines the following:

* Aircraft coordinates of lens forward nodal or principle point to within ± .05 inches.

* Yaw and pitch orientation of lens centerline axis with respect to aircraft axes to within several minutes of arc. Roll orientation of frame sprockets is also established to the aircraft.

6.0   STORE TRAJECTORY PROGRAM

The current Store Trajectory (STRAJ) Program computes six degree of freedom trajectory parameters and error check parameters based on inputs derived from on-board high speed motion picture cameras, measured store data, on-board recorded instrumentation measurements, and prior distortion and camera location/orientation calibrations. The program utilizes a two (or more) camera photogrammetric technique to obtain the space position of known points on the store. From this information, the space position of the store nose, C.G and tail are calculated along with the store yaw, pitch and roll (body axis) attitudes with respect to the aircraft axis system. An indication of the relative data accuracy is obtained by calculation of the distance between measured points on the store and comparison of the calculated to the known value. In addition, a parameter called sightline miss distance (SLMD) is calculated to indicate the three dimensional distance between two sightlines (one from each camera observing the store at a given time) at their point of closest proximity. This information can be used to evaluate the quality of filmreading for a particular drop. Currently all filmreading is accomplished manually using a Benson-Lehrner 29E Telereadex machine.

As with any other system, the accuracy of data output is a function of input data quality. For an average store, space position accuracy to within two inches for a radial distance of 30 feet from mate position is not uncommon using this sytem, with angular accuracies of one degree for pitch and yaw and five degrees for roll.

1016

6.1 The basic mathematics of the store trajectory calculation program have remained unchanged since the introduction of the two camera space triangulation procedure to the Grumman Store Separation Flight Test Capabilities during the A-6A Intruder Standard Arm and MK-4 Gun Pod Programs in 1968. General data inputs to the program are:

* Calibration information from lens distortion and on-board camera computer programs, store physical properties, desired output format (control cards)

* On-board recorded/telemetered data such as camera speeds, hook open time

* Film data for released store, bullseye reference targets and film timing marks

General program outputs are:

* Space position in aircraft coordinates of any desired point(s) on the store - usually nose, C.G. and tail

* Store yaw and pitch angles - usually output as projected angles in aircraft X-Y and X-Z planes, respectively (store body axis roll angle was added as a program output during the EA-6B Prowler TJ Pod Program.)

* Data check parameters for determination of relative data accuracy: store length, sightline miss distance and mated position

6.2 Background - The A-6A Program in 1968 marked the first utilization of the two camera technique, with only five degree-of-freedom data being output (roll was absent). Frame speeds for each of the three on-board cameras were determined by counting the number of mid-shutter pulses on visicorder paper that occurred during the one second time period for which trajectory data was desired. Each pulse represents a voltage spike that is generated when a magnet attached to the shutter gear train passes an inductor coil in the camera. This signal was then telemetered for monitoring of camera operation, prior to the drop, and recorded using an on-board analog instrumentation system for backup. Milliken DBM-4C 16mm movie cameras equipped with 84° (5.3 mm) lenses were operated at 128 frames per second with 72° shutters and f-stops of either 2.8 or 4.0. Ektachrome EF color film on an acetate base with an ASA rating of 125 was utilized for all tests. Stores were painted in a yellow-orange scheme to take advantage of the spectral response characteristics of the film for greatest contrast in reading desired store points. Store readings were referenced to target bullseye coordinates which, in turn, were referenced to camera fiducial marks on the aperture as shown in Figure 17. This two dimensional correction of camera motions due to aeroelastic flexing is most useful when the plane of motion of the camera is parallel to the film plane of camera.

1017
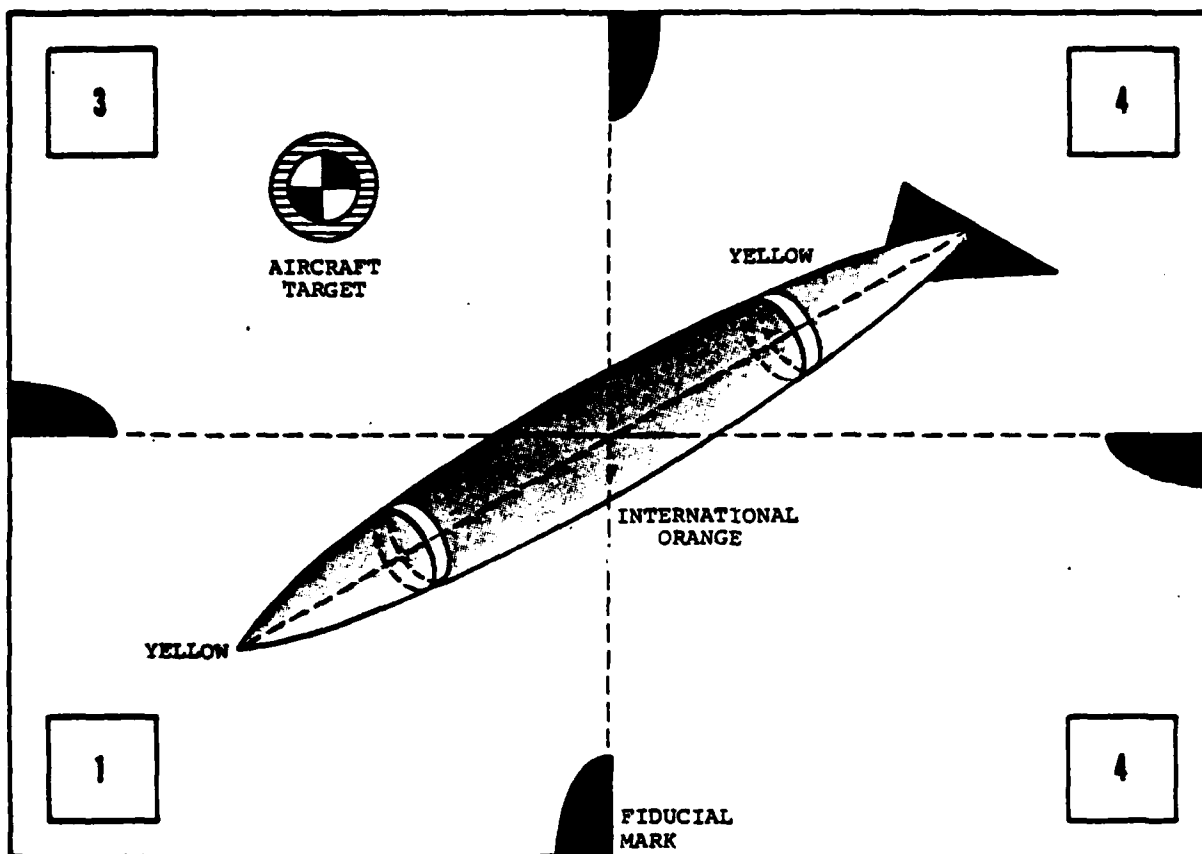
FIGURE 17. TYPICAL DATA FRAME FOR A-6A PROGRAM

Cameras were run asynchronously then, as now, with timing correlation provided by a neon edge light activated simultaneously in all cameras by a hook pulse which was also recorded on the visicorder. The store paint scheme shown in Figure 17 was utilized to obtain coordinates of the intersection of the color difference planes and the spin axis of the store. As shown additionally in Figure 17, the film image of this point on the store must be estimated as the center of an ellipse unless the store attitude provides a direct side or head-on view. From knowledge of the store physical properties in relation to the color scheme, nose, tail and C.G positions in space can be calculated. Nose and tail points were not read on the film due to the fact that typical store motions will temporarily remove these points from the field of view of each camera. The Store Trajectory (STRAJ) Computer Program run on an IBM 360-30 computer require less than five minutes to output three sets of data, one for each set of two camera combinations. Analysis of data validity parameters was used for weighted averaging during the manual smoothing process before sending final data to the Aerodynamic Engineering Group for trajectory correlation. Pertinent aircraft parameters such as airspeed, altitude, Mach, normal load factor, angles of attack and sideslip (test noseboom installed), and pitch/roll attitude were also provided in a time history format. Final data output after the availability of processed film ranged from several hours to as many as 24 hours depending upon priorities, amount of data required and number of filmreaders employed, not to mention pressure and harassment provided by impatient flight test personnel.

1018

Only two cameras were utilized during the OV-1D Mohawk Program to reduce trajectory data for the 21 drops performed. A switch to ektachrome EF color film on a Mylar base (estar film) eliminated film breakage occurrences that had been experienced with acetate based film at high frame speeds during prior programs. Milliken DBM-4C's equipped with 110° wide angle lenses were run at 128 fps. Clearance requirements included free fall release of an empty fuel tank from the inboard starboard wing station with the adjacent engine being operated at maximum power and the port engine feathered to simulate the single engine out minimum control speed sideslip condition. Predicted trajectories based upon theoretical propeller slipstream calculations indicated that store impact with the propeller would occur at speeds above the minimum control point. Yaw and lateral motions as calculated by the two camera technique were not as large in the direction of the engine as predicted during initial buildups, and as a result, a minimum control speed demonstration was safely performed. Based upon visual film reviews it is doubtful that any lower accuracy trajectory calculation system would have provided the necessary confidence to attempt the more critical conditions and clear the full envelope. With limited film to be read, five trajectories were computed during one 24 hour period beginning with film development. Only minor changes were made to the STRAJ Program prior to the major modifications geared to the F-14A requirements. These minor changes included use of film sprockets instead of fiducial marks for reference since the sprockets were already being used to properly align the frame in the filmreader, and a division of the sightline miss distance into its X, Y and Z components to aid in identifying the primary source of error.

Modifications to the STRAJ Computer Program for the F-14A Tomcat Separation effort are outlined below:

°   Normalization of all data to sprocket distances

°   Distortion correction with fifth order polynomial equation

°   Expansion of program options to include up to a total of
    six store points, two of which would be utilized for a
    store roll angle calculation, and up to four to calculate
    the remaining five degrees-of-freedom. The four points
    are the nose and tail, and if the store is painted, the
    forward and aft band. Any combination of a minimum of two
    of these points can be utilized for input to the program.

°   Correction of fuselage camera motions using two reference
    points to update camera angles with the position assumed
    to be the calibrated value.

°   Correction of wing camera locations and orientations using
    sets of three targets (up to six can be input to the rou-
    tine) and the Church Resection technique.

°   Input of timing information in ten frame increments to
    eliminate low amplitude data cycling due to prior tech-
    nique of averaging frame rate over one second.

1019

- Division of program into four phases to meet data storage restrictions of the SEL-840 computer system utilized at Pt Mugu.

- Output of up to twelve sets of two camera combinations with all data check parameters. A program option is provided to manually establish which sets of data will be mathematically smoothed to produce final output. Translation and angular rates are also output as final smoothed data.

- Inclusion of automatic plot routines for use with microfilm plotter to handle large data volumes.

The camera change from the DBM-4C to the newer and smaller Milliken DBM-20A was primarily dictated by the limited space available for nacelle camera placement. Other characteristics included an improved pin registration system for frame locking in the film gate, use of light emitting diodes in place of neon film edge lights for quicker solid state response, use of automatic exposure control and a speed control infinitely variable between one and 200 frames per second.

Aircraft flight conditions were recorded/telemetered using a PCM instrumentation system capable of monitoring several hundred parameters with a basic commutation rate of 200 data frames per sec. An engineering units computer program containing all necessary scaling data was utilized to produce time history plots of desired aircraft parameters. Computer cards containing all requested aircraft flight condition and trajectory data time histories were rapidly transmitted from the flight test facility at Pt Mugu to the Aerodynamic Engineering Analysis section in Bethpage, N.Y. for correlation using an IBM 1056 teleprocessing cardreader.

In order to correct for wing camera flexing, a technique known as Church Resection was utilized to update the calibrated position and orientation of the lens principle point and axis for both wing tip cameras. Resection is defined as "the graphical or analytical determination of a position as the intersection of at least three lines of known direction to corresponding points of known positions". [2]

The mathematically rigorous procedure involving solution of six simultaneous equations consists first of an iteration of successive approximations seeking the location of a principle point in space such that the three target bullseyes whose aircraft coordinates are known subtend the same apex angles in space as their film coordinates do to the principle point in the film axis system. Figure 18 depicts this situation graphically.

Since the number of iterations required to effect a solution are a function of the initial estimation, the wing sweep angle was input to the program to provide the best estimation available and minimize computer time. Due to the potential for excessive wing camera motion during maneuvering flight compared to nacelle camera installations, a detailed on-board calibration

1020

MATHEMATICAL PROCEDURE

1) TRIANGLE FACE ANGLES CALCULATED FROM FILM COORDINATES OF AIRCRAFT TARGET BULLSEYES. A/C ONBOARD CAMERA CALIBRATION HAS ALREADY ESTABLISHED A/C COORDINATES OF BULLSEYES.

2) BEST "FIT" DETERMINED FOR LENS PRINCIPLE POINT LOCATION AND LENS ORIENTATION TO MAINTAIN SAME TRIANGLE FACE ANGLES FOR FILM AND AIRCRAFT COORDINATES OF TARGETS.

LENS PRINCIPLE POINT LOCATION IN SPACE - AIRCRAFT COORDINATE SYSTEM

POSITIVE FILM IMAGE

TARGET BULLSEYES PAINTED ON SIDE OF AIRCRAFT NACELLE
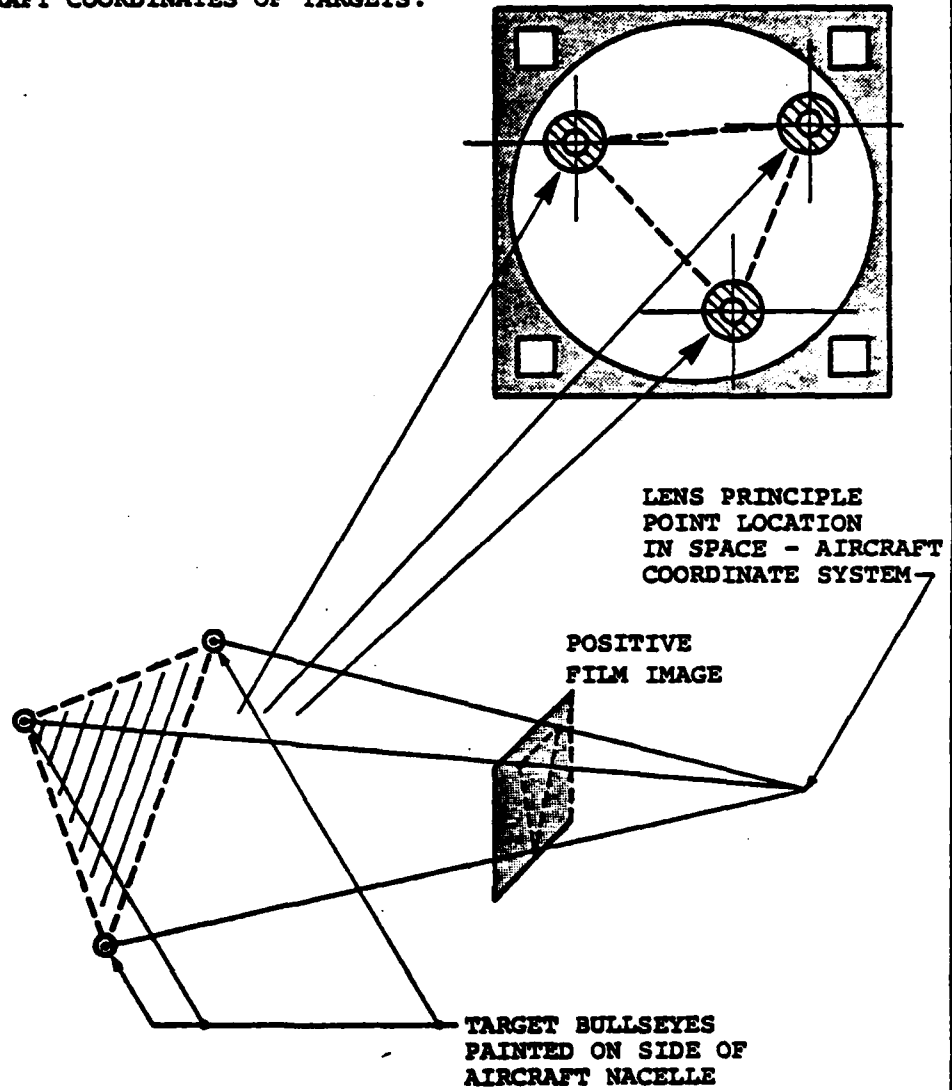
FIGURE 18.   CHURCH RESECTION SCHEMATIC

for wing tip cameras need not always take place, thus minimizing aircraft layup time. Although this technique could be utilized in place of a ground calibration for all cameras, and could in fact be utilized to calculate trajectories, experience has shown that the extra computation created random errors in excess of the allowable for F-14A tests and was therefore unacceptable. In the case of wing tip cameras, no better alternative method was available to reorient the cameras.

As previously discussed, cameras are run asynchronously and must be precisely time correlated for computation of accurate trajectory parameters.

New techniques were required to accomplish this for the F-14A Program since a PCM system without analog capability formed the heart of the onboard instrumentation package. A camera pulse logic box was designed to meet the requirements by digitally gating the PCM time from the IRIG time code generator between every tenth mid-shutter pulse for up to seven cameras at a time. Eleven BITS of Binary Coded Decimal (BCD) record the time of occurrence to within .1 ms. Pilot command release (trigger or button depression) was used to synchronize all cameras to the PCM system by the simultaneous activation of a film edge light in each camera and advancement of the seven divide-by-ten counters, such that the next succeeding mid-shutter pulse from each of the seven cameras would prematurely gate eleven BITS of BCD time into the PCM unit with the system thereafter reverting back to the normal ten pulse time. In this manner the relationship between the mid-shutters of each camera can be established, along with any cycling of camera speeds. Figure 19 is a schematic of the timing procedure. According to the Instrumentation Digital Design magicians, the logic box was simple to design and fabricate and was similar in cost to an analog system while providing a more convenient, automatic and accurate method of timing correlation. A one per second timing light located on the opposite film edge and keyed to the IRIG time provided a backup correlation capability. PCM time for hook opening was utilized to establish zero time for trajectory data.
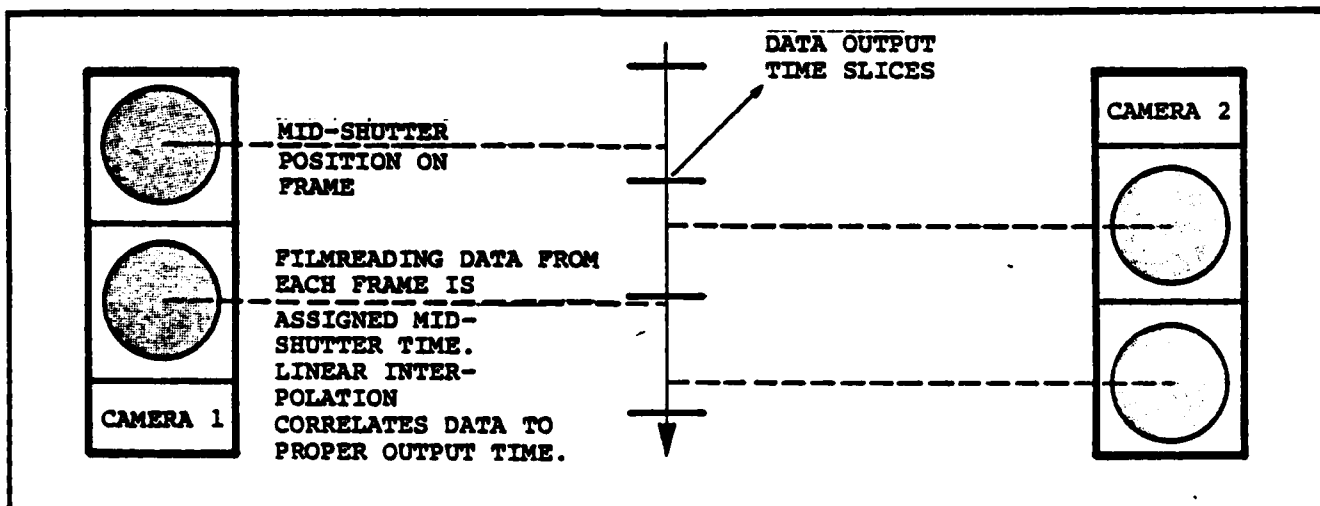
FIGURE 19.   TIMING SCHEMATIC

1022

PCM updated output from the logic box was monitored by Flight Test personnel immediately prior to separation "Clear-to-Fire" to assure proper camera operation. As shown in Figure 20, the film edge light is located at a position between 13 and 14 frames prior to the exposed frame. This also must be accounted for in timing calculations. The end result of the timing procedure is to assign aircraft time to the mid-shutter position of each frame of each camera for which data is available. With the desired data output time identified in the STRAJ control cards, a linear interpolation of camera data (which is already matched with mid-shutter times) is performed to establish data values which correspond to the desired output time for trajectory data. Using this procedure, cameras need not even be run at the same speed.
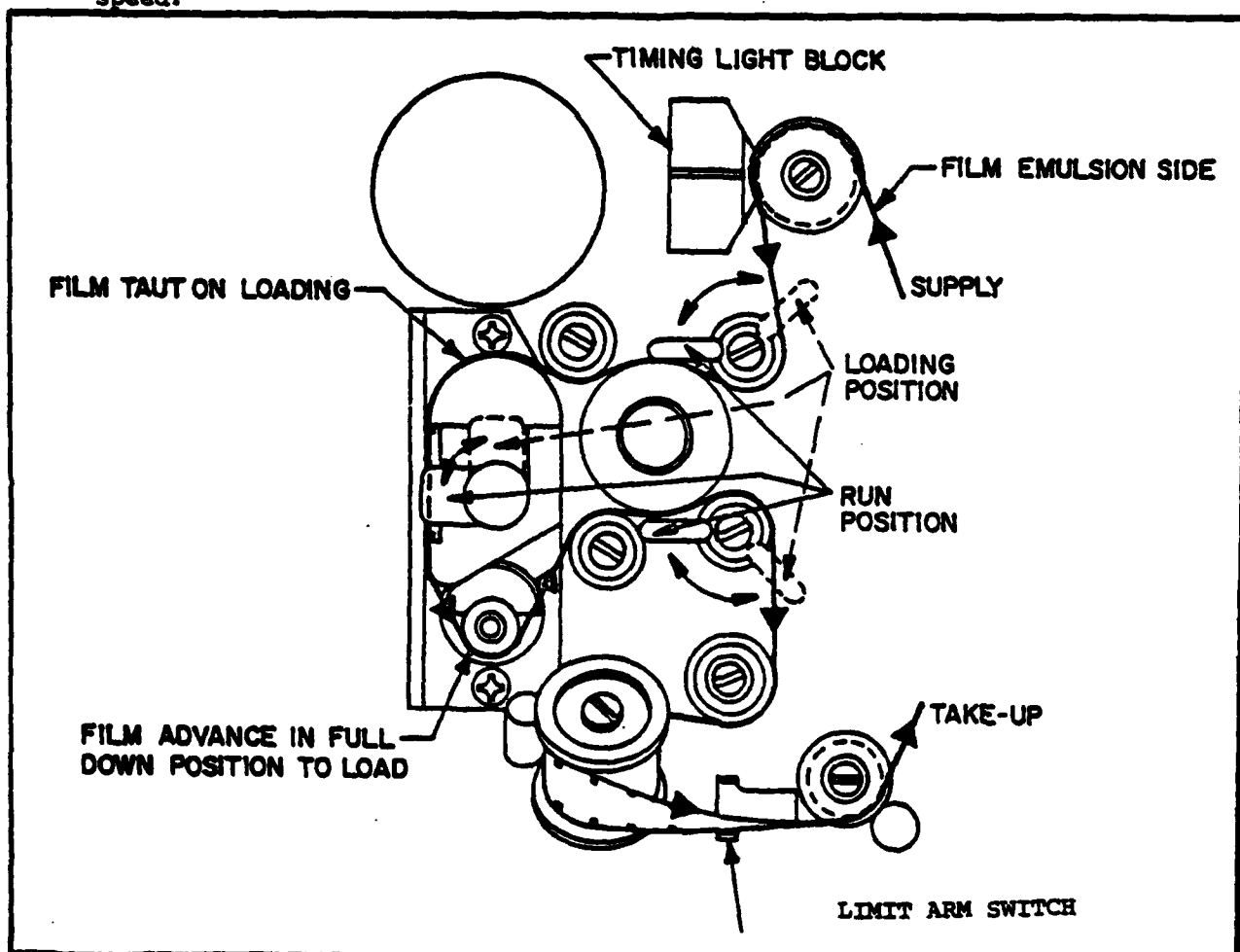
FIGURE 20. CAMERA INTERNAL CONFIGURATION

Figure 21 depicts two views of the angle calculation method for triangulation. Raw film reading coordinates corrected for distortion are used to calculate direction numbers on the film referenced to the lens optical axis. The direction cosine of this sightline in space is calculated after inflight flexing corrections are applied to the calibrated optical axis, and timing interpolations are applied to the direction numbers.
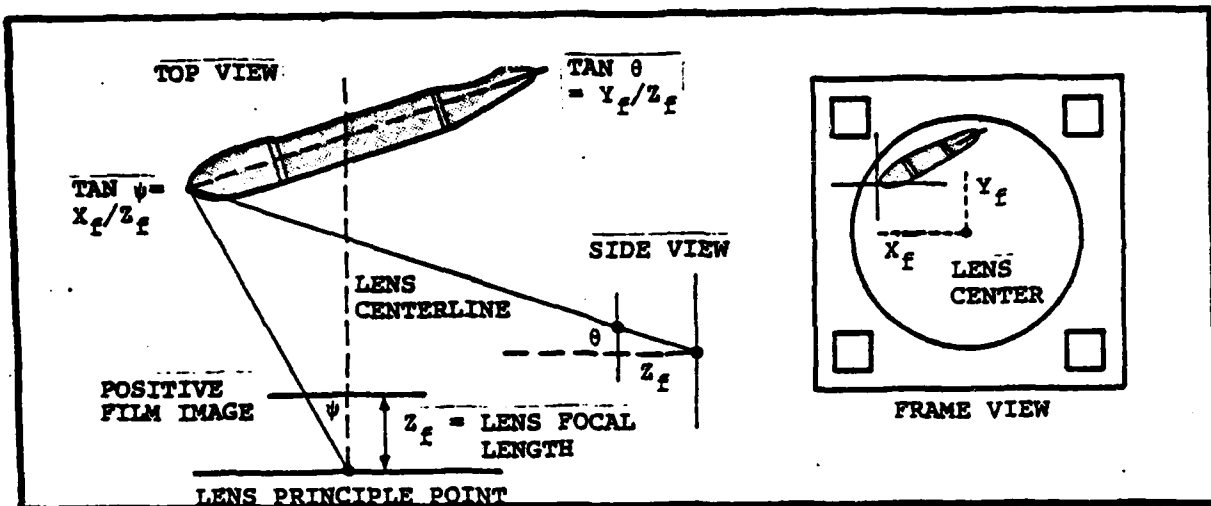
FIGURE 21. ANGLE CALCULATION FROM FILM DATA

Using a nine element updated direction cosine matrix to convert film image
points to directed line segments in the aircraft coordinate system, the
intersection equations are applied to calculate desired store points in
space, and sightline miss distances (SLMD) for each point read on the store
are determined along with distances between these points. Comparison of
these values to measured store parameters, and comparison of mated posi-
tion calculations to known values, in addition to review of SLMD parameters
enable determination of data quality. Poor quality data can be eliminated
from the data smoothing merge routine or, if the film clarity indicates
that data could be improved, steps can be taken such as review of all in-
puts and possibly re-reading of film. Aircraft roll and pitch data can be
used to correct small amplitude apparent motions. No limitations are im-
posed on this system by odd store shapes.

Future improvements to the STRAJ Program will include automatic elimi-
nation of data in a least squares merge when SLMD or store length cri-
teria exceed a predetermined value. In addition, an automatic iteration
to determine optimum timing inputs based upon error monitoring routines
can be programmed into STRAJ.

7.0 F-14A SEPARATION PROGRAM RESULTS

Both the Air-to-Air and Air-to-Ground Separation Test Programs for the F-14A
Tomcat were conducted entirely by GAC at PMTC, Pt.Mugu, California. Jettison and
launch clearances were provided for the AIM-9 Sidewinder, AIM-7E-2/F Sparrow, and
AIM-54A Phoenix missiles, with a total of 78 separations performed to establish a
full ACM envelope. A total of 20 external fuel tank separations were accomplished
to develop a supersonic ACM release envelope for the full, empty and partially
filled tank.

A total of 312 separations during 55 flights were required to establish employment, normal jettison and auxiliary (free fall backup) jettison release envelopes for the following A/G stores:

° MK-82, 500 lbs, General Purpose Bomb with Snakeye fins (both opened and closed), and with low drag conical fins

° MK-83, 1,000 lbs, General Purpose Bomb with low drag conical fins

° MK-84, 2,000 lbs, General Purpose Bomb with conical fins

° MK-40 Destructor with fins (both opened and closed)

° MK-20 Mod II Rockeye II

° CBU-59/B APAM

° MK-45 Parachute Flare

° MK-76 Practice Bomb

Loading densities for the A/G bombs, as exemplified by the MK-82 configuration shown in Figure 22, required careful visual examination of the film to detect minor bomb-to-bomb contact during initial release, while full data reduction procedures were required to substantiate predictions throughout the trajectory. The availability of accurate data eliminated unnecessary drops in the build-up program for such specialized concerns as high drag fin clearance relative to the external fuel tanks, and establishment of safe release intervals for ripple bomb modes.

NOTE: MK-82'S NOT CARRIED ON STATION 4D & 5A DUE TO INTERFERENCE WITH ARRESTING HOOK FAIRING.

MK-82 CONFIGURATION IN CHANNEL
MK-82 LOADING

STATIONS 5 AND 6 — STATIONS 3 AND 4
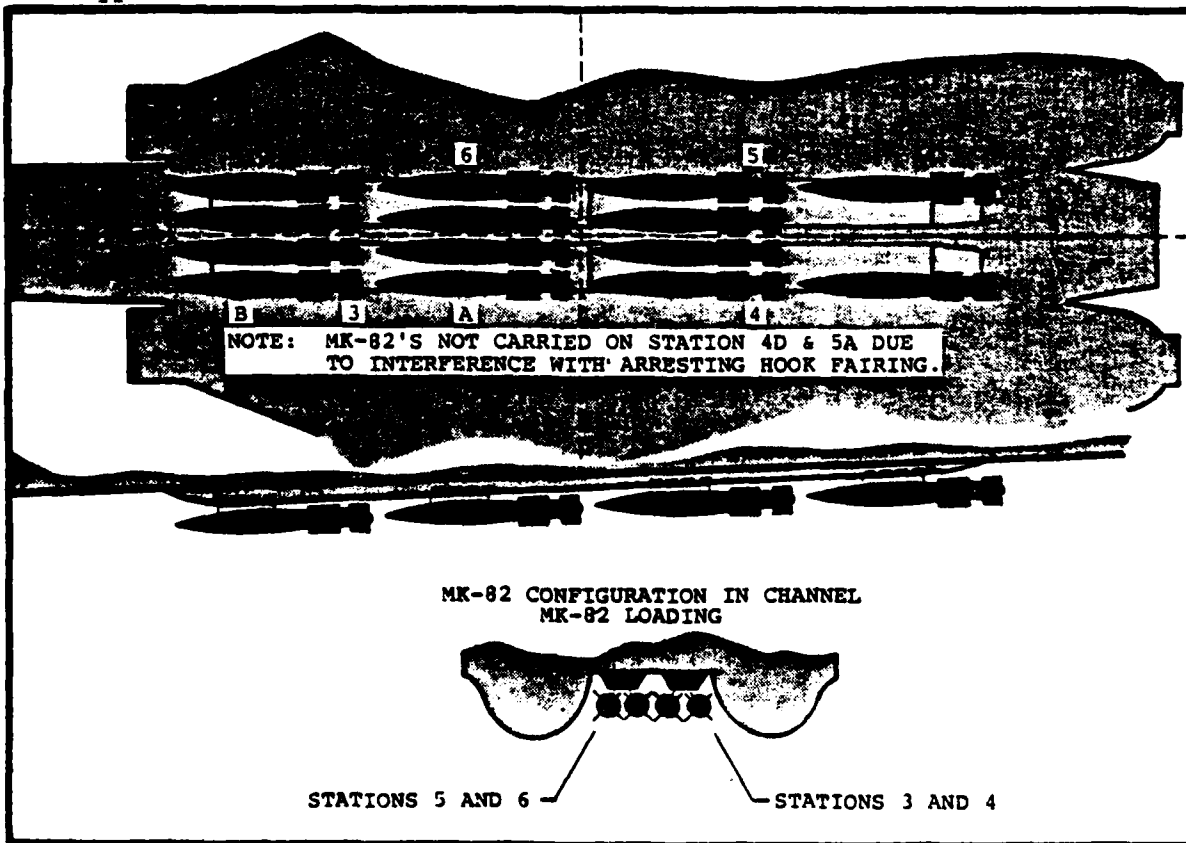
FIGURE 22. MK-82 AIR-TO-GROUND CONFIGURATION

Data reduction was not a constraint during either the A/A or A/G programs since releases of all stores in each program were fully integrated to minimize dependence upon data turnaround.

8.0 COMPARISON TO OTHER PHOTOGRAMMETRIC TECHNIQUES

Prior to selection of the two camera space triangulation system for F-14A tests, several alternate methods of trajectory data calculations were investigated, including non-photographic means. Single and multi-camera chase, single and multi-camera onboard, laser, radar and photocell arrays were all considered, along with a cost and schedule analysis using the older "March Around the Envelope" procedure without any calculated trajectory data. Reliance on chase coverage was quickly rejected in light of the maneuvering envelope to be cleared, and low probability of adequate chase photography during maneuvering releases based upon prior experience. The wisdom of this decision became apparent early in the test program. Consideration of the many variables to be evaluated during the A/A Separation Program also led quickly to the decision to provide accurate trajectory data, based upon both cost and schedule estimates. The five and six figure dollar costs for missiles, added to flight and range support costs for a "March Around" program, proved to be prohibitive and eliminated this option as a viable alternative. Laser, radar and photocell techniques all seemed to indicate some promise, but the research and development costs and schedule, plus the lack of prior experience with these techniques, eliminated them from contention and narrowed the possible selections to on-board cameras. Use of a single camera for trajectory calculations was desirable from many aspects, including number of cameras required, amount of film to be analyzed, data turnaround time and elimination of requirement for a complete on-board calibration. The lens distortion calibration would still have been required if wide angle lenses were utilized, and a target calibration on the aircraft would have been required for a Church Resection or similar type of calculation procedure. Due to the requirement for simple visual observation of release related occurrences, the difference in number of cameras required for either single or multi-camera solutions became minimal. The clincher, however, in selection of the two-camera solution, was the accuracy requirement. Prior experience showed that the two-camera method would satisfy F-14A requirements. Analysis of the situation (shown in Figure 23) where a side view of the store is presented to a camera located 30 feet away, demonstrates a limitation of any single camera technique. Simple geometrical analysis of a two-inch store motion radially away from the camera, combined with knowledge of typical filmreader errors for placement of crosshair cursors on desired store targets (nose, color bands, tail, etc.), indicates that this motion may not be detectable in terms of filmreader counts. Use of narrow angle lenses would improve the accuracy, but extra cameras would be required to compensate. Analysis of the combined yaw/lateral motion, with respect to the camera film plane, further exemplified the inability of the single camera technique to meet F-14A requirements. However, use of the single camera technique is certainly a possibility for separation programs where tight accuracies are not mandatory and/or where non-recurring calibration costs are judged to be too large in comparison to recurring flight costs. For a multi-year program as the F-14A, the off-aircraft lens calibration and on-aircraft camera calibration efforts
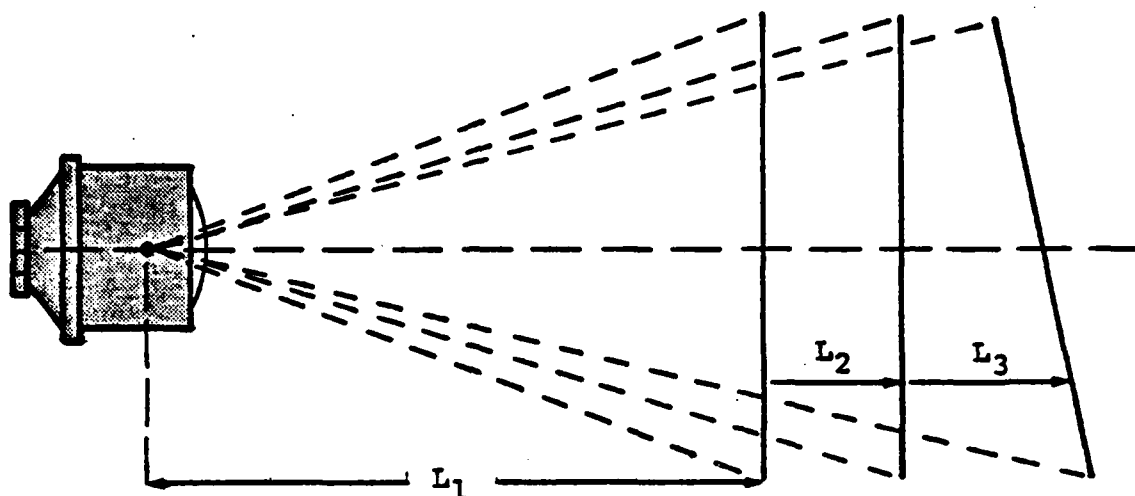
AS L_1 INCREASES, ANGLE SUBTENDED
AT CAMERA DECREASES FOR CONSTANT
L_2 or L_3

FIGURE 23.   LIMITATION OF THE SINGLE CAMERA TECHNIQUE

did not logically consititute a valid reason to avoid the multi-camera approach.
Likewise, the additional time for data turnaround due to increased filmreading
requirements did not degrade flight productivity since the entire process of
correlation and acquisition of aircraft flight conditions (and sometimes missile
parameters) also had to be conisdered. Careful flight test planning was the key
to permitting a high degree of efficiency throughout the program.

9.0   CONCLUSION

A detailed knowledge of all facets of a separation program is a prerequisite
to determination of data requirements and associated data reduction procedures.
Photogrammetric techniques spanning the full range from eyeball only to a complex
multi-camera solution for calculation of separation trajectories may be employed
dependent upon the intended use of such data. Grumman analysis indicates that
the most consistently accurate method of trajectory calculation is provided by
the multi-camera triangulation approach. Determination of the optimum technique
for any given program requires evaluation of the many factors relating safety,
economics, schedule and technical usage of the data.

REFERENCES

1.   "The Use of An Interactive Computer To Optimize A Photographic Data
     Acquisition System" by Sam Whiting - Presented at October 1970 SFTE
     Symposium in New York.

2.   American Society of Photogrammetry "Manual Of Photogrammetry", Third
     Edition, Volumes I and II, 1965.

AUTHOR BIOGRAPHY

Thomas J. Reilly graduated from the State University of New York at Stony Brook, College of Engineering, in 1968 with a Bachelor Degree in Engineering Science. Undergraduate studies included an emphasis on physics, mathematics and materials science.

Work experience prior to graduation included two summers at Grumman Aerospace Corporation, one of which was in the Optical Engineering and Metrology Department assisting in the development and testing of a laser autocollimator for rapid alignment of aircraft avionics and armament systems.

Upon graduation, Tom joined the Grumman Flight Test Division and assisted in separation programs involving the A-6A Intruder, EA-6B Prowler, and OV-1D Mohawk. During this time several optical techniques for determination of in-flight trajectories were developed along with an increasing reliance upon computer technology.

In 1970, Tom was designated Group Leader of the Weapon Separation Flight Test Section and headed the F-14A effort at Pt. Mugu between 1972 and 1975. Weapons cleared included such Air-to-Air missiles as Phoenix, Sparrow and Sidewinder and Air-to-Ground Stores such as the MK-80 series, practice bombs, rockeye, etc.

Tom currently is assigned to NAS, Pt.-Mugu with Grumman Flight Test as a Vehicle Test Engineer responsible for various tasks such as Test Conductor, Planning and Reporting, and proposal writing for all categories of flight testing.

AIM-9E & J MISSILES
STATIC AND DYNAMIC STRUCTURAL CHARACTERISTICS AND CAPABILITIES
DETERMINATION AND IMPROVEMENT PROGRAM
FOR
WARNER ROBINS AIR LOGISTICS CENTER
(U)
(Article UNCLASSIFIED)

By

Robert G. Fusco
Dayton T. Brown, Inc., Church St., Bohemia, NY   11716

ABSTRACT. (U) Since its entry into the inventory in the mid
1950's, a number of modifications have been made to the AIM-9 series of
missiles. With the advent of newer and more highly maneuverable air-
craft, it became necessary to reassess the structural characteristics
and capabilities of the versions of the AIM-9 in service. In 1975 the
USAF initiated such a program for the AIM-9E and J missiles. The pur-
pose of this paper is to present USAF/Dayton T. Brown, Inc. program
objectives, test and analysis methods, and results. The primary objec-
tives of the program were as follows:

1. Determine the weight, C.G., and moments of inertia of the vari-
    ous missile components and the resultant values for fully assem-
    bled missiles.

2. Evaluate proposed missile changes to the guidance control unit,
    warhead, and rocket motor.

3. Determine the static strength of the AIM-9E and J missiles in
    a fashion that would allow relatively quick determination of
    the capability of the missile under various static loading con-
    ditions, its compatibility with existing or proposed aircraft,

the effect of proposed modification on static strength, and which regions of the missile to strengthen if increased capability becomes necessary.

4. Determine the dynamic characteristics of the missiles in various aircraft mounting configurations, particularly the F-15A and F-16A. The primary purpose here was to determine the effect of the configuration on missile response and the suitability of relatively simple fixturing for vibration qualification type testing.

5. Determine missile structural capabilities with respect to vibration in a manner that would facilitate its extrapolation to environments and mounting configurations other than the precise environment and configuration tested.

6. Determine the missile structural capabilities with respect to transient loads, again in a manner allowing for mounting configuration variation.

Due to the nature of the AIM-9E and J missiles, the above objectives required a departure from the "normal" methods of determining structural strength capabilities in several respects.

1. Rather than a "paper" stress analysis based on the item drawings followed by limited testing of the fully assembled item, component strengths were determined by individual tests, followed by limited analysis and fully assembled missile tests.

2. Rather than a vibration endurance test based on a particular aircraft environment and time compression via increased test levels, real time levels were combined with resonance dwells to compress test time and minimize errors due to the highly nonlinear system being tested.

LIST OF FIGURES

LIST OF TABLES

APPENDICES

INTRODUCTION

The AIM-9, or Sidewinder, missile is an air launched heat seeking intercept missile carried on numerous Air Force and Navy fighter/attack aircraft. The missiles are carried in various attitudes and aircraft locations (wing tips, pylons, fuselage) using two basic launcher systems to meet the varying requirements of the services. The Air Force uses the Aero 3B launcher and its derivatives, and the Navy uses the LAU-7. To give an idea of scale, the AIM-9E and J each have basically a 5 inch case diameter, and weigh approximately 170 lbs. The AIM-9E and AIM-9J are approximately 118 and 122 inches in overall length, respectively. Each missile consists of seven primary components as follows and as shown in Figure 1:

1. rocket motor
2. wing & rolleron assemblies (4)
3. influence fuze
4. warhead
5. contact fuze
6. guidance control unit
7. canards (4)

The first five items are identical on both the AIM-9E and J. Externally the AIM-9J guidance control unit is longer than the AIM-9E, and the canards have a different planform.

WING

ROCKET MOTOR

HANGERS

INFLUENCE
FUZE

CONTACT FUZE (NOT SHOWN,
INSIDE GUIDANCE CONTROL
UNIT & WARHEAD)

WARHEAD

CANARDS

SEEKER

GUIDANCE CONTROL UNIT
(INCLUDES SEEKER, HOMING SET,
AND SERVO HOUSING (S))
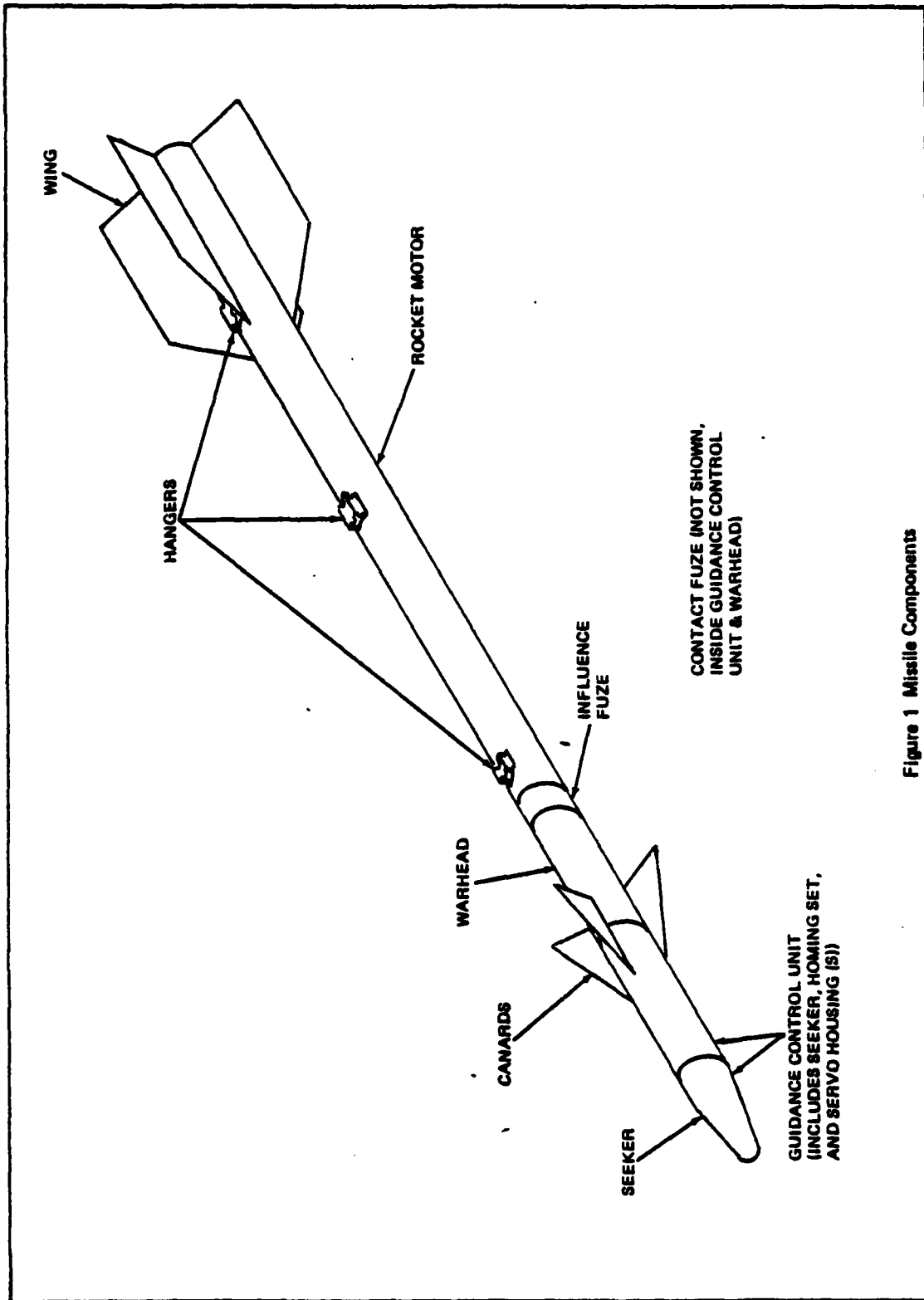
Figure 1 Missile Components

1033

WEIGHT, C.G., AND MOMENTS OF INERTIA

The weight, center of gravity, and moments of inertia were determined for both live and inert AIM-9E and AIM-9J missiles and missile components. The Air Force was concerned that since there were no weight, C.G., and moment of inertia requirements for the various missile components, there might be a wide variation in these parameters for the components and fully assembled missiles in the inventory. Additionally, the information was necessary for structral analysis. Accordingly, the weight, C.G., and moments of inertia were determined for 16 to 20 of each of the components making up the AIM-9E and J. The components initially measured were all live and the most current configuration. Later, 10 each of two earlier types of wing and rolleron assemblies and several inert rocket motors and warheads were measured.

Weights were measured via either calibrated scales or load cells.

Depending on geometry, one of several methods were used for C.G. location. C.G.'s were assumed to lie along the cylindrical axis of cylindrical items such as rocket motors, warheads, and guidance control units. This was verified for several such items and assumed for the rest. For the wing and rolleron assemblies and canards, the C.G. was assumed to lie in the item's mid-plane. C.G. location along the cylindrical axis was determined either by balancing on a rolling pin or through the use of an inclinometer, with the item held in a clamp suspended by a wire. C.G. location in the plane of the wing or canard was determined by suspension from different locations and noting the intersection of the marked plumb lines.

Moments of inertia were determined by either of two well known methods. The torsional pendulum method was used for the contact fuzes, canards, and wing and rolleron assemblies. In the torsional pendulum method, the item being measured is attached to a torsional spring with a known stiffness. The system is set oscillating and the period is measured. Total inertia is then calculated and tare inertias, which must be kept small to maintain accuracy, are subtracted to result in the test item inertia. The bifilar pendulum method was used for all other inertia measurements. In this method the item is suspended by two vertical wires equidistant to its C.G. The system is oscillated through a small angle and the period measured. Knowing the period, wire length, and distance to the C.G., the total inertia can then be calculated. Holding clamp and wire inertias and transfer terms are then subtracted to result in the test item inertia.

Using a computer with a random number generator, measured missile components were randomly chosen, and a total of 3200 live AIM-9E and AIM-9J missiles were constructed and their weights, centers of gravity, and moments of inertia were computed. The 3200 missiles consisted of 800 missiles each of four basic live missile configurations. Two of the three types of wing and rolleron assemblies had virtually identical mass

properties. Therefore, two sets of data were computed for the AIM-9E and two sets for the AIM-9J. An AIM-9E and AIM-9J with specific components were also constructed by the computer and their mass properties calculated. These missiles were then physically assembled and their weights, centers of gravity, and moments of inertia were measured similarly to the components. The results compared well with the computer generated missiles. Additionally, using the mean values for inert warheads and rocket motors and the most current wing and rolleron assembly, an inert AIM-9E and AIM-9J were generated.

The resultant mass properties for the components and computer generated missiles are summarized in Tables I, II, and III. Figure 2 shows the missile reference frame. Review of the calculated and measured data shows the standard deviation, σ, to be well under 1 percent of the mean for all the data for a given missile configuration. Inert missile mass properties were within 2 percent of live missile mean values, except for roll inertia (I_{xx}), which was within 7 percent.
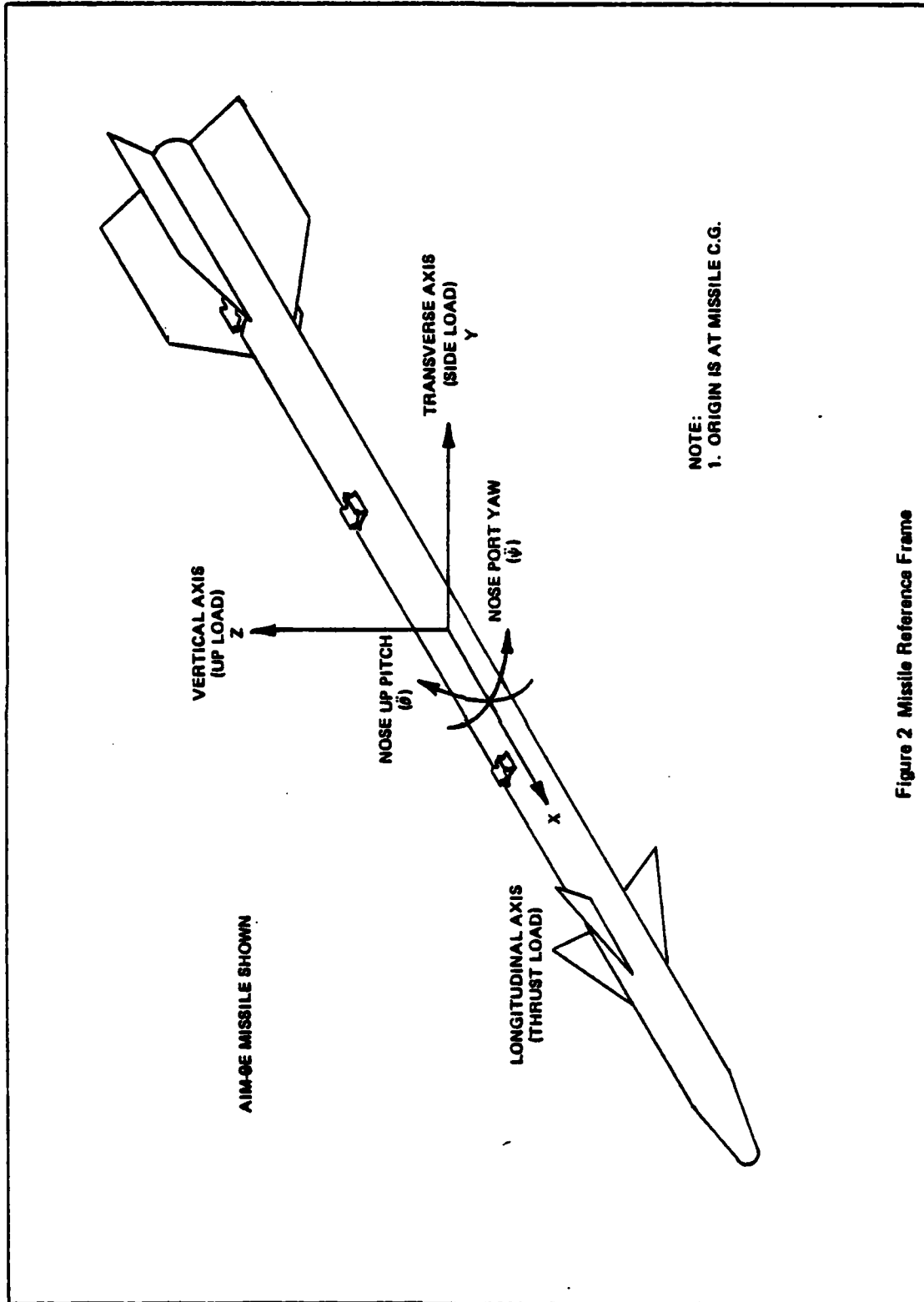
Figure 2 Missile Reference Frame

TABLE I - AIM-9E & J MISSILE CYLINDRICAL COMPONENTS MASS PROPERTIES

Component	Mean or σ	Weight (pounds)	X Axis C.G. (inches)	Moments of Inertia		
				I_{xx} (lbin²)	I_{yy} (lbin²)	I_{zz} (lbin²)
Rocket Motor						
Live	Mean	75.97	32.98	337.54	33,835	33,887
	σ	.23	.10	7.60	334	332
Inert	Mean	72.05	33.44	233.12	38,745	38,745
	σ	N/A	N/A	N/A	N/A	N/A
Influence Fuze	Mean	6.71	75.48	30.30	34	34
	σ	.04	.01	.82	1	1
Warhead						
Live	Mean	25.33	84.63	137.01	479	480
	σ	.09	.04	3.19	13	12
Inert	Mean	25.39	84.73	117.31	459	461
	σ	N/A	N/A	N/A	N/A	N/A
Contact Fuze	Mean	1.38	88.86	.38	5	5
	σ	.01	.04	.00	0	0
Guidance Control Unit						
AIM-9E	Mean	33.72	101.46	127.84	1,260	1,256
	σ	.28	.07	8.48	56	53
AIM-9J	Mean	36.84	103.98	139.69	1,980	1,988
	σ	.25	.07	5.79	57	62

Note: Components are live except as indicated.

TABLE II - <u>AIM-9E & J MISSILE CANARD & WING & ROLLERON ASSY. MASS PROPERTIES</u>

Component	Mean or σ	Weight (pounds)	C.G. Location X Axis (Inches)	C.G. Location Y' Axis (Inches)	Moments of Inertia Ixx' (lbin²)	Moments of Inertia Iyy' (lbin²)	Moments of Inertia Izz' (lbin²)
Wing & Rolleron Assy.							
P/N 69E33005	Mean	5.28	6.81	7.28	25.76	136.41	161.01
	σ	.03	.06	.04	.69	1.39	1.37
P/N 657458	Mean	4.70	7.20	7.11	25.85	127.88	150.40
	σ	.04	.07	.03	.78	.86	1.91
P/N 1568339	Mean	4.65	7.18	7.10	25.36	127.27	148.79
	σ	.02	.05	.02	.43	1.15	.83
Canard							
AIM-9E	Mean	1.39	91.59	4.02	1.98	7.01	8.82
	σ	.04	.05	.02	.18	.20	.26
AIM-9J	Mean	.79	100.35	4.64	2.39	4.73	6.87
	σ	.02	.03	.02	.15	.16	.24

Notes:

1. The X' axis is parallel to the X axis and passes through the component C.G.
2. The Y' and Z' axes are rotated about the X' axis such that the Y' axis lies in the plane of the canard or wing & rolleron assembly.

TABLE III - AIM-9E & J MISSILE MASS PROPERTIES

Missile	Wing & Rolleron Assembly Part Number	Mean or σ	Weight (pounds)	X Axis C.G. (inches)	Moments of Inertia		
					Ixx (lbin²)	Iyy (lbin²)	Izz (lbin²)
Live AIM-9E	69E33005	Mean	169.50	55.06	1,940	229,005	229,096
		σ	.33	.09	11	767	865
Live AIM-9E	1568339/657458	Mean	166.99	55.82	1,759	222,309	222,355
		σ	.33	.09	11	766	851
Inert AIM-9E	69E33005	Mean	165.92	55.82	1,824	231,180	231,178
		σ	N/A	N/A	N/A	N/A	N/A
Live AIM-9J	69E33005	Mean	170.25	56.10	1,934	244,215	244,263
		σ	.30	.09	10	757	860
Live AIM-9J	1568339/657458	Mean	167.74	56.88	1,753	237,206	237,254
		σ	.31	.09	9	768	862
Inert AIM-9J	69E33005	Mean	166.65	56.89	1,818	246,068	246,078
		σ	N/A	N/A	N/A	N/A	N/A

Note: Inert missile data based on component mean values.

1039

MISSILE MODIFICATION EVALUATION

Three proposed types of missile modifications were evaluated. These were:

1. New guidance control unit bolts to improve resistance to loosening under vibration.

2. Increasing the number of warhead clamps from four to eight to increase the strength of the guidance control unit to warhead and warhead to influence fuze joints.

3. Increasing the number of aft hanger mounting bolts from four to eight to increase aft hanger strength.

FASTENER VIBRATION RESISTANCE

The first was evaluated by first establishing vibration loosening criteria for the existing configuration and then verifying that the new bolts would not loosen when subjected to the same condition.

For these tests the setup was basically as shown in Figure 3. Testing was conducted in the missile Z axis only. Inert rocket motors, warheads, influence fuzes, and contact fuzes were used. Both the AIM-9E and AIM-9J were surveyed from 2 to 2,000 Hz with an input of 0.10 inch D.A. below 10 Hz and ± 0.5 g above 10 Hz and all resonances determined. Dwells, each 5 minutes long, were then performed at each of the resonances which yielded high responses near the fasteners in question and observed for bolt loosening. If no loosening was observed, the level was increased in half g increments up to a maximum of 0.60 inch D.A. below 11 Hz and ± 5 g's above 11 Hz. Alternately, the maximum permitted input level was further constrained such that the maximum missile response (except on the canards or wings) was not to exceed 0.60 inch D.A. below 18 Hz and ± 10 g's above 18 Hz. The ± 5 g dwells were performed for 1 hour each as the last effort at inducing fastener loosening. At the time, these were considered to be the maximum real time sinusoidal vibration levels which might be encountered by the AIM-9.

It was intended that a vibration induced bolt loosening "map" would be developed for each missile, with both types of fasteners. In actuality, only a resonance at 42 Hz on the AIM-9E produced bolt loosening, and this after 50 minutes of vibration at ± 3.0 g's. The new bolts were then installed in the AIM-9E guidance control unit with the intent to dwell at 42 Hz with ± 3.0 g's until the new bolts loosened. Changing the bolts shifted the resonance upward to 49 Hz. After 4.5 hours of dwelling the test was halted with no loosening of the fasteners.

VERTICAL

TRANSVERSE

LONG.

SHAKER

AERO 3B-30 LAUNCHER

CONTROL FROM HARD FIXTURE

HYDROPAD SUPPORTS

AIM-9 MISSILE
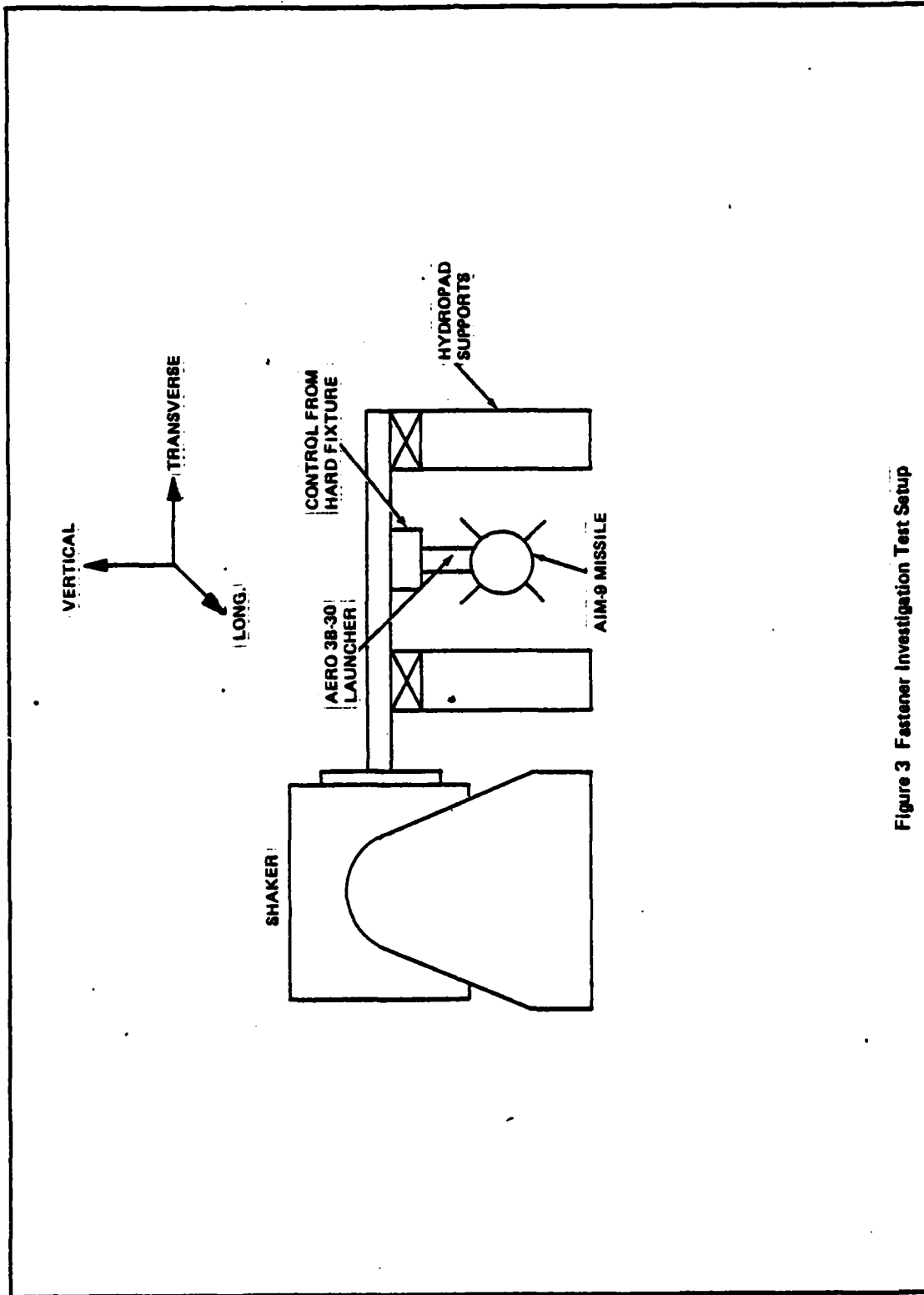
Figure 3 Fastener Investigation Test Setup

The new, "Dynathread", fasteners were clearly superior to the existing bolts, and were used for all further testing involving the guidance control unit.

EIGHT VERSUS FOUR CLAMP WARHEAD

The MK-8 Mod 0 warhead used on the AIM-9E and AIM-9J utilizes four "C" clamps at each end for attachment to the guidance control unit and influence fuze. The approximate mating interface cross section is shown for the warhead/influence fuze interface in Figure 4. A total of eight proposed warhead clamp and influence fuze configurations were statically tested for comparison with the standard four clamp configuration. Inert MK-8 Mod 0 warheads were used for all tests, modified as necessary to accept additional or differing clamps. Shortly after completion of the tests it was determined that the special 80° clamps used for four of the configurations had not been heat treated by the manufacturer as required. The remainder of the configurations, to which the discussion will be limited, are listed in Table IV.

TABLE IV - WARHEAD/INFLUENCE FUZE INTERFACE CONFIGURATIONS

Case	Influence Fuze Housing	Number of Clamps	Clamp Arc (degrees)	Clamp Thickness (inches)
1	MK-303	4	45	0.156
2	MK-303	8	38	0.178
3	MK-303	8	38	0.156
4	MK-303	8	38	0.218
5	DSU-21	8	38	0.156

Static loads were applied to the warhead such that a bending moment was produced at the warhead/influence fuze joint. Loads were increased incrementally and deflections measured in an attempt to determine yield and ultimate strengths.

Figures 1 through 5 of Appendix A show the bending moment and load versus deflection plots for cases 1 through 5, which were typical of other test results. Note that there was no single yield point in the classical sense, rather a series of inflection points. For cases 1 through 4 the load was reduced to zero to verify yield had occurred prior to continuing to ultimate load. Although the test setup was not disturbed, the ultimate strengths obtained when loads were re-applied were in some cases as much as twice as great as expected based on the deflection data. This and the series of inflection points were apparently due to the warhead housing, clamps, and influence fuze housing sliding and shifting with respect to one another. Therefore, ultimate loads based on projection of the deflection curves to zero slope points are considered a more valid method of comparison. The actual and projected ultimate loads are summarized in Table V.

1042
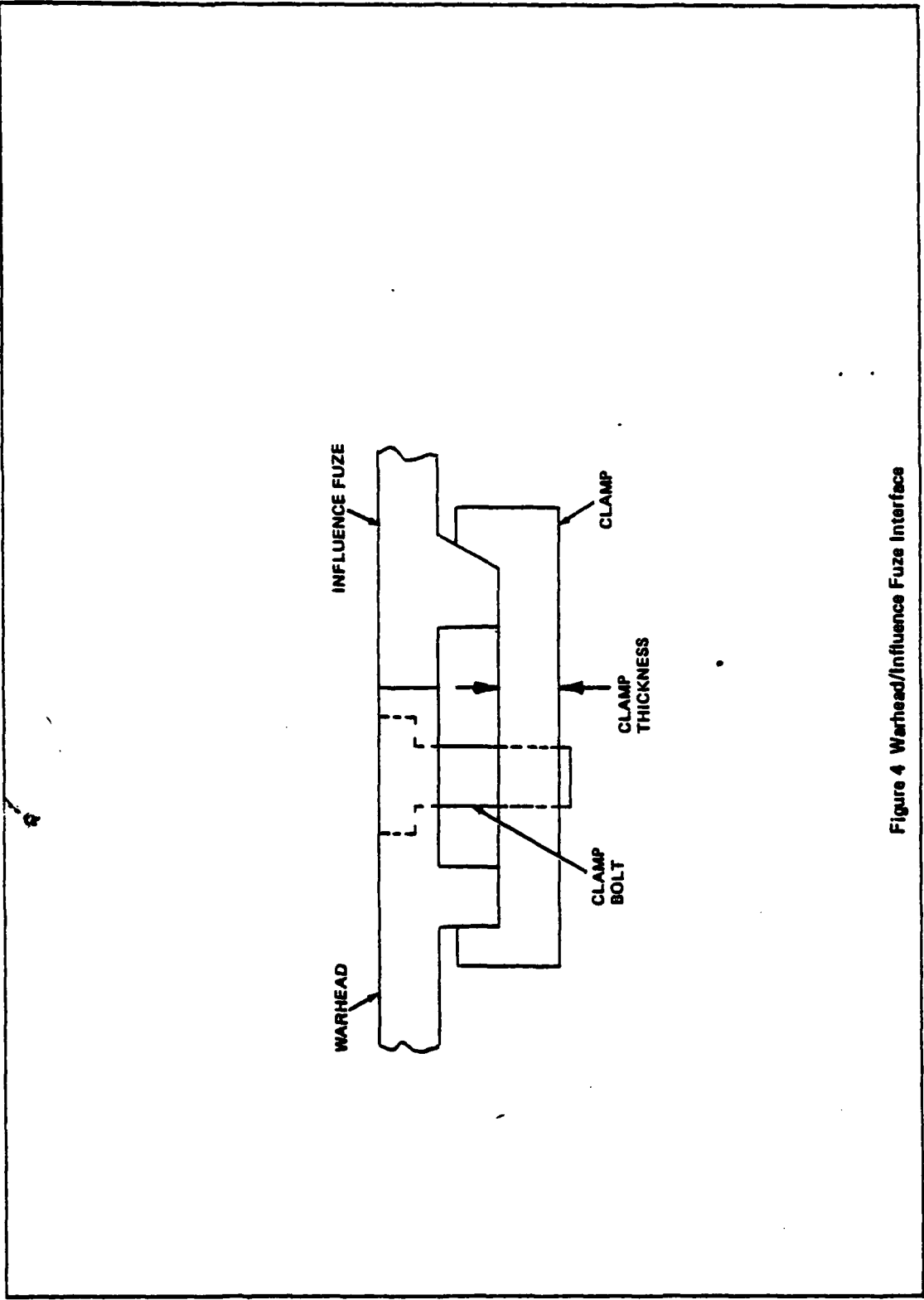
Figure 4 Warhead/Influence Fuze Interface

INFLUENCE FUZE

CLAMP

CLAMP THICKNESS

CLAMP BOLT

WARHEAD

TABLE V - WARHEAD/INFLUENCE FUZE INTERFACE ULTIMATE STRENGTH

Ultimate Strength (inch-pounds)

Case	Actual	Projected
1	57,000	28,000
2	77,900	62-67,000
3	71,900	62,000
4	100,900	67,000
5	66,500	N/A

Based on the projected ultimate strengths, the following conclusions can be made.

1. The four configurations of eight 38° clamps are at least twice as strong as the standard four 45° clamp configuration, using either the MK-303 or DSU-21 housing.

2. Increasing the clamp thickness does not significantly increase joint strength.

Accordingly, the eight 38°, 0.156 inch thick clamp configuration was used for all further testing involving the warhead except component static tests, where additional comparison data was desired.

AFT HANGER MODIFICATION

The standard MK-71 Mod 0 rocket motor, used for both the AIM-9E and AIM-9J, has three hangers by which it attaches to the launcher rail. The aft hanger is held to the rocket motor case by only four bolts, and with limited thread engagement. In order to increase missile aft hanger strength it was suggested that the number of bolts be increased from four to eight.

Several inert rocket motors were modified to the eight bolt configuration and static side and down load tests comparing the relative strengths of the two configurations were performed. It was anticipated that doubling the number of bolts would double the static strength, and this was the approximate result as shown in Table VI.

TABLE VI - EIGHT VS. FOUR BOLT AFT HANGER ULTIMATE STRENGTH

Direction	Percent Ultimate Strength Increased
Down (-Z)	83
Side (Y)	94

As a result of the above, the eight bolt aft hanger configuration was used for all further testing involving the rocket motor.

MISSILE STATIC STRENGTH DETERMINATION

Generally, to determine the static strength of a structure, a stress analysis is first performed, calculating margins of safety for various loading conditions. Depending on the criticality of the system and the confidence in the analysis, a varying number of static tests would then be preformed to verify the analysis. This is usually the best approach for a system whose structure is both well defined and well behaved; well defined in the sense that all structural component characteristics are known, and well behaved in the sense that slipping and load path changes are minimal.

For the AIM-9E and AIM-9J it had been anticipated that the structure might not be well behaved, as was later demonstrated during the warhead joint tests. Therefore, it had been intended from the inception of the program that the static strength of missile components would be determined by testing the individual components. Component test results and a limited analysis to calculate missile hanger reaction loads and equivalent inertia loads would then be combined to predict overall missile strength under almost unlimited loading configurations. An inert missile, minus canards and wings, would then be statically tested to destruction for an arbitrary load condition and the results compared to those predicted. If there were any critical predictions, with respect to prediction accuracy, the most critical of these was to be used for the comparison test.

COMPONENT TESTS

The component tests consisted of static tests conducted on five basic portions of the missile, plus secondary tests on the wings and canards, as listed below:

1. seeker to homing set joint (both parts of the guidance control unit)
2. guidance control unit to warhead joint
3. warhead to influence fuze joint
4. influence fuze to rocket motor joint
5. rocket motor hangers to launcher rail
6. canards to guidance control unit
7. wings to rocket motor

Test setups are shown in Figures 1 through 9 of Appendix B. Deflection data plots are shown in Figures 1 through 10 of Appendix C and the results are summarized in Table III of Appendix D.

Seeker to homing set joint tests were conducted with loads applied to the seeker, perpendicularly to the missile longitudinal axis. The homing set was clamped at the guidance control unit C.G. Tests

1046

were conducted on both AIM-9E and AIM-9J guidance control units. In all cases failure occurred in the bulkhead at the threaded holes holding the four fasteners on the homing set side of the seeker to homing set joint. The ultimate strength of this joint is therefore dependent on the load direction. Due to the fastener orientation, the joint is strongest when subjected to pure side (Y) or vertical (Z) loads, as was the case during the actual tests, and weakest when the side and vertical components are equal. Deflections were measured during each test in an effort to determine the joint yield strength. Two test methods were used. In the first method, loads were incrementally increased to the Nth increment, returned to no load, and then incrementally increased to the (N + 1)th increment, etc., until failure. In the second method, the loads were increased incrementally directly to failure. The results showed the strength to be extremely load time history dependent, probably due primarily to plastic flow of potting compound within the unit. The second method resulted in shorter test durations and less plastic flow, and are closer to the loading histories that would be encountered in service. Therefore, static strengths resulting from the quicker test method were used for strengh predictions.

Bending moment and force versus deflection plots for the quicker tests are shown in Figure 1 of Appendix C. As can be seen from the data, yield points could not be determined with any degree of confidence. It had been anticipated that the aluminum bulkhead of the AIM-9J would be stronger than the phenolic one of the AIM-9E, but the differing results for the two AIM-9J tests could not be accounted for. Therefore, the lower AIM-9J value was used for predictions.

Guidance control unit to warhead joint tests were conducted using both test methods (not in all cases), as during the seeker tests. Data for the quicker, increasing only, tests is plotted in Figure 3 of Appendix C. The plots were similar to those obtained during the eight versus four clamp warhead tests. Again, it was decided that only the strengths resulting from tests using the quicker loading method would be used for predictions. Tests were conducted on both the AIM-9E and AIM-9J guidance control units, with both four and eight clamp warheads. For the AIM-9E, failure was always at the forward servo housing to aft servo housing joint of the guidance control unit. For the AIM-9J, the guidance control unit always pulled out of the warhead. Since warhead orientation is not controlled in service, testing was conducted with the four clamp warhead loaded in its weakest direction. Eight clamp warhead results did not appear to be significantly affected by orientation, since it is clamped at 84 percent of its circumference. Due to clamp shifting, the AIM-9J guidance control unit to warhead joint was found to be affected by prior loading history, but not to the same degree as had been the case with the seeker. As seen from the plotted data, accurate yield loads could not be determined from the data.

Only one warhead to influence fuze test was conducted at this time, using the eight 38°, 0.156 inch thick clamp warhead. The test was conducted primarily to determine the effect of allowing influence fuze deformation. The influence fuze housing had been restrained during the earlier tests. The effect was to decrease the ultimate strength by approximately 15 percent when influence fuze housing deformation was allowed. Curiously, the data plot was essentially linear up to approximately 58,000 inlbs, at which point yield was apparent. It had not been possible to be certain of yield during the earlier tests. Apparently there was less slipping and shifting during this particular test. Although the results of this test were used for predictions for the eight clamp warhead to influence fuze joint strength, it was felt that the 28,000 inlb ultimate strength allowable from the earlier four clamp test was sufficiently conservative to preclude further reduction.

Influence fuze to rocket motor tests were used only to verify that the rocket motor forward hanger would fail before the influence fuze itself. Rocket motor hangers were then tested individually for side and vertical strength.

As an aside, a wings to rocket motor test was performed to determine the wing bending load capability. Failure actually occurs in the rocket motor casing. Similarly, the AIM-9E canards were tested to show that failure would occur at the mounting bolts.

STATIC STRENGTH PREDICTION

Using the previously determined component mean weights and centers of gravity, bending moments at each critical joint and hanger reaction loads were then determined for vertical and side inertia loads, and for pitch and yaw accelerations about the missile C.G. The Aero 3B-30 launcher, used by the USAF, is constructed such that the forward and aft missile hangers are restrained in both vertical directions and both sideward directions. The center hanger is restrained in both sideward directions, but vertically it is only restrained downward. The snubbers take out upward loads at the forward and aft hangers, and the launcher rail takes out down loads at all three hangers. There are no snubbers at the center hanger. Longitudinal loads are reacted at the forward hanger only. Simple supports were assumed in all cases and the missile was treated as a bending beam of unknown stiffness. The launcher rail was assumed to be rigid so that deflections could be assumed to be zero at the supports in the cases where all three hangers were loaded. Rocket motor mass was assumed to act only aft of the forward hanger centerline, and was distributed varying linearly such that inertia loads due to the rocket motor acted at its C.G. Wing and rolleron assembly mass was distributed in a similar fashion, but restricted such that it acted only aft of the aft hanger. The three moment method was used to calculate reactions for redundant cases. The unit hanger reactions (pounds per g and pounds per radian/second^2)

were then calculated for side, down, and up inertial loads, and for nose up pitch, nose down pitch, and yaw angular accelerations. Unit joint bending moments (inch-pounds per g and inch-pounds per radian/second^2) were also calculated. Dividing the ultimate joint bending moments or ultimate hanger loads by the unit reactions gives the equivalent ultimate g load or angular acceleration. These results are summarized in Table II of Appendix D. Table I of Appendix D, generated from Table II, summarizes the predicted static strengths of the versions of the AIM-9E and AIM-9J in service and compares them with proposed versions of these missiles..

The assumption of no deflection at the supports was known to be invalid for side loads and yaw accelerations since one side of the center hanger would try to lift off the launcher rail. It was not known how significantly this would affect reaction loads calculated by the three moment method. Since the missile is very strong in yaw, it was decided that a side load test should be used for prediction verification. The AIM-9J was selected for test, for which the predicted failure is at just under 34 g's. When the test was conducted, the failure occurred at just over 38 g's, at the forward hanger as predicted. This result was approximately 13 percent greater then predicted. When the possible variation in ultimate strength from one hanger to the next is considered, this result is good and the prediction method is considered to be sufficiently accurate for its intended purpose.

The purposes of these tests were to obtain a rough idea of the dynamic characteristics of various service configurations, the dependence of missile response on those configurations, the suitability of relatively simple fixturing for vibration qualification type testing, and to develop a vibration qualification test method for the AIM-9. These tests were not intended to be destructive, nor were they intended to be the rigorous modal surveys necessary for flutter analysis verification.

Dynamic characteristics were to be determined for three configurations, pylon mounted on the F-15A aircraft, wing tip mounted on the F-16A aircraft, and mounted to a hard mounted Aero 3B-30 launcher. It was hoped that the missile response on the last configuration would be similar to the response in the aircraft configurations, at least at the more structurally significant lower frequencies. If this were the case, the only "special" fixturing that would be required for a valid qualification test would be an Aero 3B-30 launcher, which is used by the USAF on such aircraft as the F-4 and F-15A. The Aero 3B-30 launcher is not used on the F-16A. It uses a launcher that has the same basic rail and missile attachment configuration, but is structurally modified to meet F-16A requirements. Unfortunately, it was not possible to obtain an F-16A launcher for the time period required due to scheduling conflicts in spite of the cooperative efforts of both the manufacturer and the F-16A S.P.O.

Testing was therefore limited to the F-15A and hard mounted configurations. Since the AIM-9E was not to be in service on the F-15A, tests in the F-15A configuration were conducted with only the AIM-9J. Both the AIM-9E and AIM-9J were used for tests in the hard mounted Aero 3B-30 configuration. The latter configuration was the same as for the fastener investigation test setup, shown in Figure 3. The F-15A configuration setup is shown in Figure 5.

PROCEDURE

The tests were divided into two portions: surveys to obtain accelerometer data, and mode identification for the lowest frequency modes. The surveys were further divided into two overlapping parts, from 2 to 20 Hz and from 10 to 2,000 Hz.

During surveys, control accelerometer tracking filter bandwidths were 2 and 10 Hz for the low and high frequency parts, respectively. For mode identification attempts, which were below 50 Hz, a 2 Hz bandwidth was used. In the F-15A configuration, only the forward pylon to beam fitting carries load in all three axes. The middle fitting carries only transverse load, and the aft fitting only vertical load. Control was averaged or single point, as appropriate for the input axis, with control accelerometers mounted on the fittings. In the

a Side View

VERTICAL

LONGITUDINAL

ADAPTER BEAM

BEAM TO PYLON FITTINGS

AIM-9

PYLON

SHAKER

NOTE: HYDROPAD SUPPORTS NOT SHOWN

b Plan View

TRANSVERSE

LONGITUDINAL

MISSILE

LAUNCHERS

MISSILE

PYLON

ADAPTERS
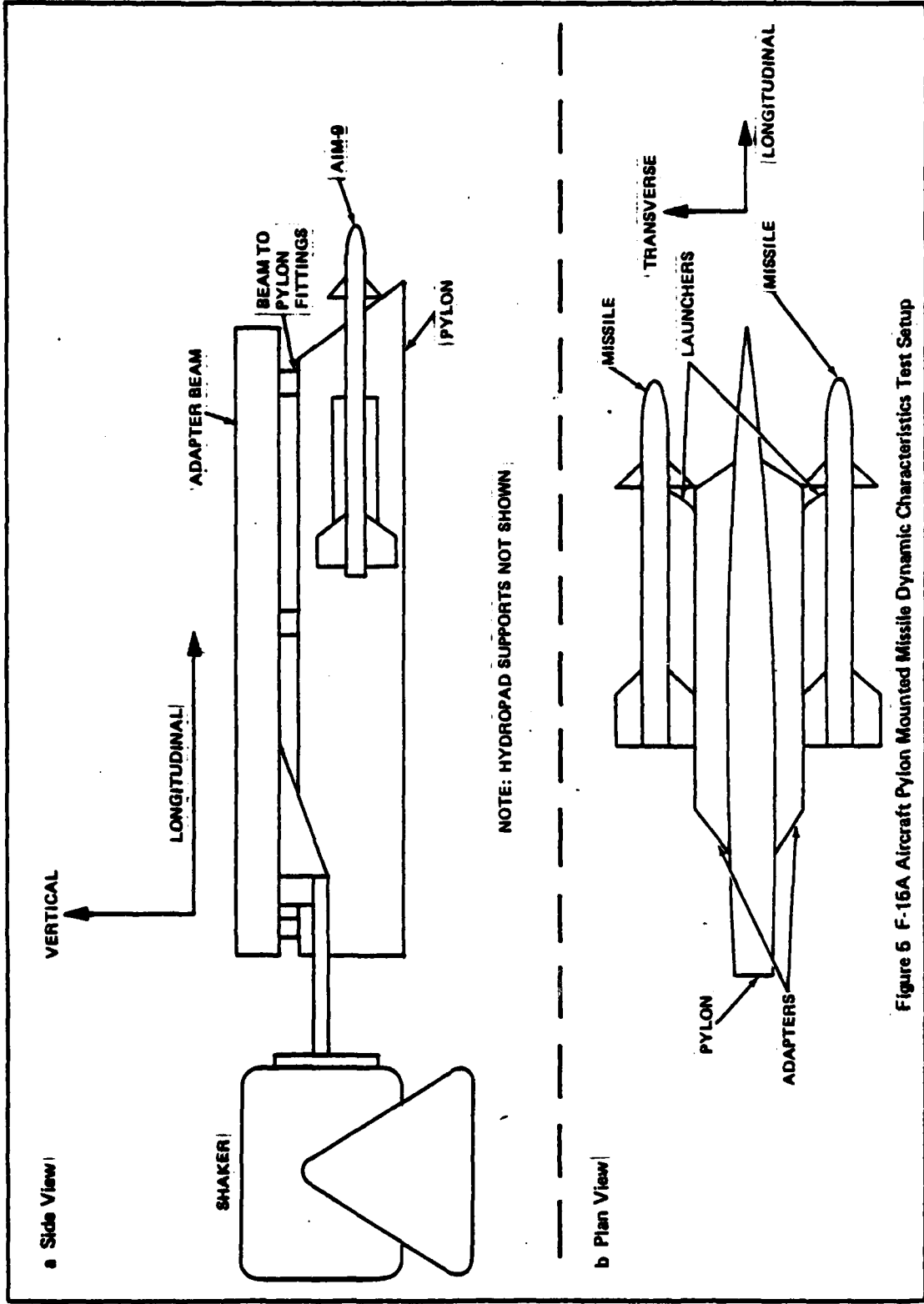
Figure 6 F-16A Aircraft Pylon Mounted Missile Dynamic Characteristics Test Setup

hard mounted Aero 3B-30 configuration, control was by the average of
the inputs as measured on the "hard" fixture near the two launcher
mounting bolts.

Input vibration levels for the surveys were as shown in Table VII,
and varied during mode identification attempts.

TABLE VII - SURVEY INPUT VIBRATION LEVELS

Survey Portion	Frequency Range (Hz)	Input Amplitude
A	2 to 5	0.20 inch D.A.
A	5 to 20	± 0.25 g's
B	10 to 2,000	± 1.0 g's

RESULTS

Including F-15A configuration surveys with dummy masses in place
of inert missiles, a total of 467 accelerometer plots were generated.
None of the configurations showed structurally signficant missile re-
sponse in the longitudinal axis. Above approximately 60 Hz, missile
response of the hard mounted and F-15A configurations varied signifi-
cantly. Below 60 Hz, noting that vertical in one configuration was
equivalent to transverse in the other, resonances at approximately 8,
11, 15 and 19-20 Hz with the F-15A pylon all showed up in the data for
the hard mounted Aero 3B-30, but at reduced levels in some cases. The
8 and 11 Hz resonances were two weak to be well excited in the hard
mounted configuration, the 15 Hz mode became 17 Hz, and the 19-20 Hz
mode was at 20.5 Hz. When vibrated from the pylon fittings, as in
these tests, vertical or transverse inputs induce a good deal of cross
axis missile response. This effect is negligible in the hard mounted
configuration. Therefore, modes which show up strongly with either
vertical or transverse inputs with the pylon only show up in one axis
with the hard mounted launcher. Comparison of data at both ± 0.25 g
and ± 1.0 g showed downward frequency shifts on the order of 10 to
15 percent as well as transmissibility decreases as high as 50 per-
cent as the input level increases.

VIBRATION ENDURANCE

The purpose of these tests was to determine missile structural capabilities with respect to vibration in a manner that would facilitate its extrapolation to environments and mounting configurations other than the precise environment and configuration tested. The tests were only partly successful in achieving these goals, partly because a component in a dynamic system can never be treated completely independently of the system of which it is a part, and partly due to the perversity of nonlinear mechanical systems.

From the results of the dynamic characteristics tests, it was concluded that the hard mounted Aero 3B-30 launcher configuration could be used for these tests. From static test and analysis results it was known that in this configuration transverse axis static strength was 30 percent less than vertical axis static strength. Although this was not certain to be true dynamically, it was probable. Furthermore, missile response had been greatest in the transverse axis. In view of the above and the proposed test method, it was decided to test in only the transverse axis.

Since the system was known to be nonlinear, test time compression by increased test levels, whether random or sinusoidal vibration was used, could not be employed. Therefore, it was decided that test levels would be representative of the worst case real time vibration levels anticipated for the AIM-9. This would have meant imposing levels based on the F-16A. However, at the low end of the spectrum these requirements appeared to be overly conservative for an endurance type test. It was felt that the worst case real time level in the low frequency range (7 to 50 Hz) was more likely to be on the order of $\pm$ 1 g sinusoidal. The random requirements for the rest of the spectrum were based on the F-16A. Input levels are given in Table VIII.

TABLE VIII - VIBRATION ENDURANCE TEST INPUT LEVELS

Description	Frequency Range (Hz)	Input Vibration Levels
Sinusoidal	7 to 50	$\pm$ 1.0 g $\pm$ 10%, 2 Hz Tracking Filter
Random, overall level	50 to 117	0.04 g^2/Hz $\pm$ 1.5 dB
	117 to 300	Increase at 4 dB/octave $\pm$ 1.5 dB
13.2 g's r.m.s.	300 to 1000	0.14 g^2/Hz $\pm$ 3 dB
$\pm$ 10%	1000 to 2000	Decreasing at 6 dB/ octave $\pm$ 3 dB

The tests conducted consisted of repeating cycles of 10 minute resonance dwells at each significant resonance between 7 and 50 Hz and 10 minutes of random vibration. The total test time per cycle is thus dependent on the number of resonances. The cycles were repeated until failure occurred.

RESULTS

AIM-9E and AIM-9J results are summarized in Tables IX and X, respectively. The total test time to failure was 2 hours 10 minutes for the AIM-9E and 7 hours 30 minutes for the AIM-9J.

TABLE IX - AIM-9E VIBRATION ENDURANCE TEST RESULTS

Maximum Response at Resonances Indicated Below

Cycle	Resonance 1 Frequency (Hz)	Resonance 1 Ampl. (± g's)	Resonance 2 Frequency (Hz)	Resonance 2 Ampl. (± g's)	Resonance 3 Frequency (Hz)	Resonance 3 Ampl. (± g's)
1	34.9	3.6	16.7	9.8	-	-
2	34.3	4.0	15.4	13.0	-	-
3	34.0	4.3	14.4	9.4	13.3	11.7
4	34.0	3.5	-	-	12.8 - 11.8	9.2

TABLE X - AIM-9J VIBRATION ENDURANCE TEST RESULTS

Maximum Response at Resonances Indicated Below

Cycle	Resonance 1 Freq. (Hz)	Resonance 1 Ampl. (± g's)	Resonance 2 Freq. (Hz)	Resonance 2 Ampl. (± g's)	Resonance 3 Freq. (Hz)	Resonance 3 Ampl. (± g's)	Resonance 4 Freq. (Hz)	Resonance 4 Ampl. (± g's)
1	40.0	2.6	36.3	5.0	17.8	5.6	14.8	10.6
2	40.0	2.3	36.3	3.9	17.8	3.4	14.8	8.7
3	40.0	1.6	36.3	2.8	17.8	2.1	14.8	5.8
4	40.0	1.7	36.3	2.7	17.8	2.3	14.8	6.1
5	40.0	1.8	36.3	2.9	17.8	2.1	14.8	5.5
6	40.0	1.7	36.3	2.6	17.8	1.9	14.8	4.9
7	40.0	1.6	36.3	2.4	17.8	1.9	14.8	6.0
8	40.0	1.5	36.3	3.2	17.8	2.2	13.6	11.2
9	39.0	2.4	33.2	4.1	18.2	1.8	11.1	6.8

The tests of the AIM-9E and AIM-9J essentially produced the same result – failure of the Aero 3B-30 launcher. The launcher rail fails at the aftmost hole for the forward snubber guide. This in turn will cause failure of the forward missile hanger. In summary, the results of these tests showed the missile/launcher system to be launcher limited.

However, during a later vibration test conducted as part of an evaluation of a proposed wing and rolleron restraint kit, the missile failed instead of the launcher. This later test was conducted using a similarly configured AIM-9E except that there was no wing and rolleron restraint kit or string fix. The test setup was the same except that an Aero 3B-10 was used instead of an Aero 3B-30. The vibration consisted basically of downsweeps from 50 to 5 Hz at a sweep rate of 0.5 octave/minute. The initial sweep was made with an input level of $\pm$ 1 g with the input level increasing by $\pm$ 0.5 g for each succeeding sweep. The prime concern was to determine what input level and frequency would cause uncaging of the rollerons. Therefore, only the wing and rolleron assemblies were being observed critically during each sweep.

During the latter part of the fourth downsweep, at $\pm$ 2.5 g's the AIM-9E missile guidance control unit failed in two places. The screws had loosened and backed out at both the seeker/homing set and forward servo housing/aft servo housing joints. No structural failures of either the missile or launcher were found, but the guidance control unit components were so loose that structural failure would be inevitable in flight. Note that the screws which loosened were the original missile screws; dynathread screws were not used in these locations.

TRANSIENT LOADS

The purpose of these was to determine AIM-9 missile strength under transient load conditions such as could be encountered from store ejections, hard landings, sharp edged gusts, etc.

TEST METHODS

Store ejections were considered to be the worst case cause of transient loads. Since aircraft measured data showed missile response to be similar to what might be expected from sine-beat transients, that test method was chosen. A typical sine-beat transient is shown in Figure 6. It can be shown analytically that the maximum sine-beat response for a given resonance is close to the resonance obtained when the number of cycles of the resonant frequency per beat is equal to the resonant frequency. For example, for a 20 Hz resonant frequency there would be 20 cycles per beat. The applied transient pulse would have a total duration of one beat (1 second). The same test setup was used as for vibration endurance, but with modified instrumentation such that relative acceleration of each hanger with respect to the launcher was measured directly, as well as overall missile C.G. and nose acceleration.

For the AIM-9E and AIM-9J, the resonances below 20 Hz were the only ones considered structurally significant. For the AIM-9E, the test would be limited to 16.7 Hz. For the AIM-9J, comparison of the response with 1.0 g peak at the missile C.G. at both 14.8 and 17.8 Hz showed that the response was greater using 14.8 Hz. Only the AIM-9J was tested, since only one useable Aero 3B-30 launcher remained at this point in the program. The AIM-9J was chosen since with its longer length it would have higher forward hanger reaction loads, which was where failure was anticipated. Sine-beat tests were then to be conducted, increasing the peak g level incrementally until failure occurred.

RESULTS

A total of 20 sine-beat tests were performed, up to the maximum output of the test equipment, at which point the test was halted. The only discrepancy noted was that the aft snubbers of the Aero 3B-30 launcher were no longer tight at the completion of the test. The maximum missile C.G. peak acceleration was approximately 25 g's. Therefore, the AIM-9J missile itself is structurally capable of transient loads of at least 25 g's, and the AIM-9E would be expected to be stronger, assuming eight clamp warheads in both cases.

1057
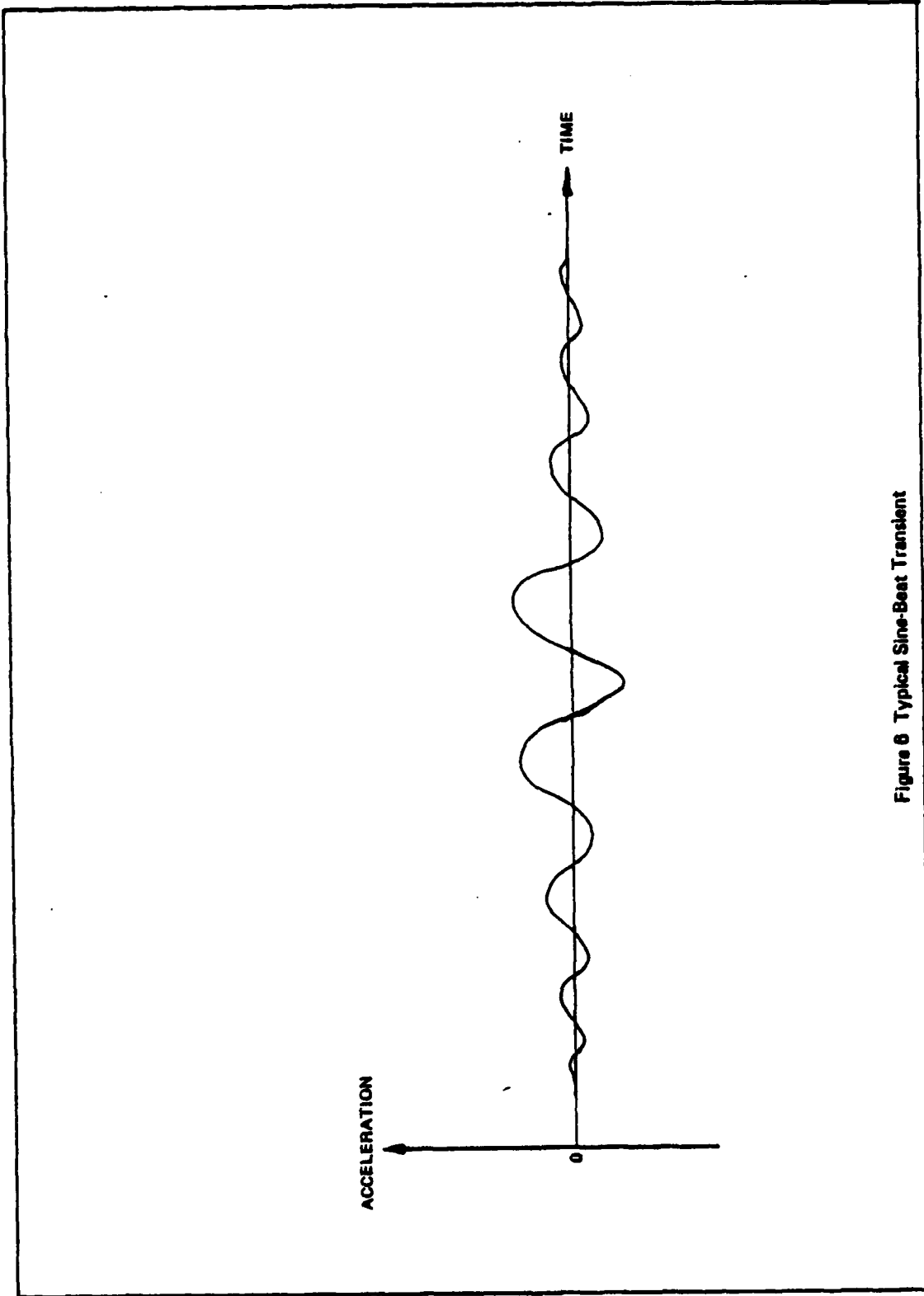
Figure 8 Typical Sine-Beat Transient

CONCLUSIONS

1. The three missile modifications reviewed, the new guidance control unit fasteners, eight vs. four clamp warhead, and eight vs. four screw aft hanger, all offer significant improvements of missile capabilities.

2. Static strength, predicted semi-empirically based on component static tests and analytically predicted load distributions, is in good agreement with full-up missile test results.

3. Use of the actual missile launcher (in this case the Aero 3B-30) is sufficient to obtain a satisfactory representation of the missile vibration response characteristics for qualification testing.

4. Due to the nonlinearities of the AIM-9E/Aero 3B-30 and AIM-9J/Aero 3B-30 systems, only limited predictions with respect to dynamic strength can be made. These are as follows:

    a. Low level ($\pm$ 1.0 g or less), low frequency (50 Hz or less) vibration will result in Aero 3B-30 launcher rail fatigue failures at high cycle numbers. This will occur for both the AIM-9E and AIM-9J missiles.

    b. High level ($\pm$ 2.5 g's or more), low frequency (20 Hz or less) vibration will result in loosened screws on the AIM-9E guidance control unit in a very short time, probably less than 1 minute. The loosened joints would be extremely susceptible to inertia and/or air load induced failures. The applicability of this to the AIM-9J would require further investigation for verification.

    c. Transient loads similar to what would be expected to result from store ejections, hard landings, sharp edged gusts, etc. producing missile C.G. accelerations up to at least 25 g's should not cause structural failure of either the AIM-9E or AIM-9J. However, the effectiveness of the Aero 3B-30 launcher snubbers may be reduced after repetitive 25 g transient loads.

Appendix A

Eight Versus Four Clamp Warhead Data Plots

CASE 1: FOUR STANDARD 45°, 0.156" THICK CLAMPS, 12-28 BOLTS, & MK-303 INFLUENCE FUZE

BENDING MOMENT AT FAILURE: 56,970 IN. LBS.

BENDING MOMENT (1,000 IN. LBS.)

DEFLECTION (INCHES)
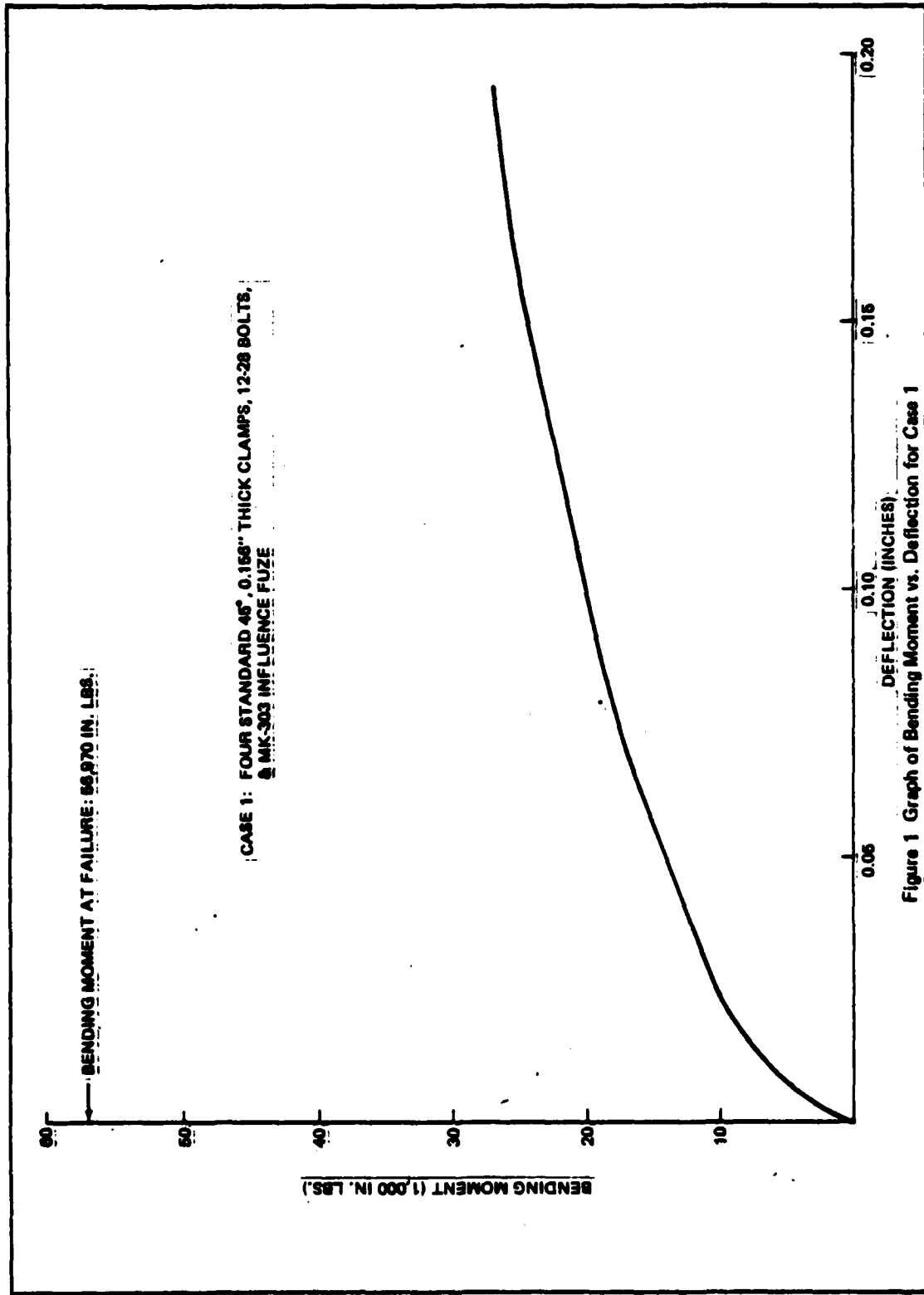
Figure 1 Graph of Bending Moment vs. Deflection for Case 1

CASE 2: EIGHT 38°, 0.178" THICK CLAMPS, 12-28 BOLTS, & MK-303 INFLUENCE FUZE
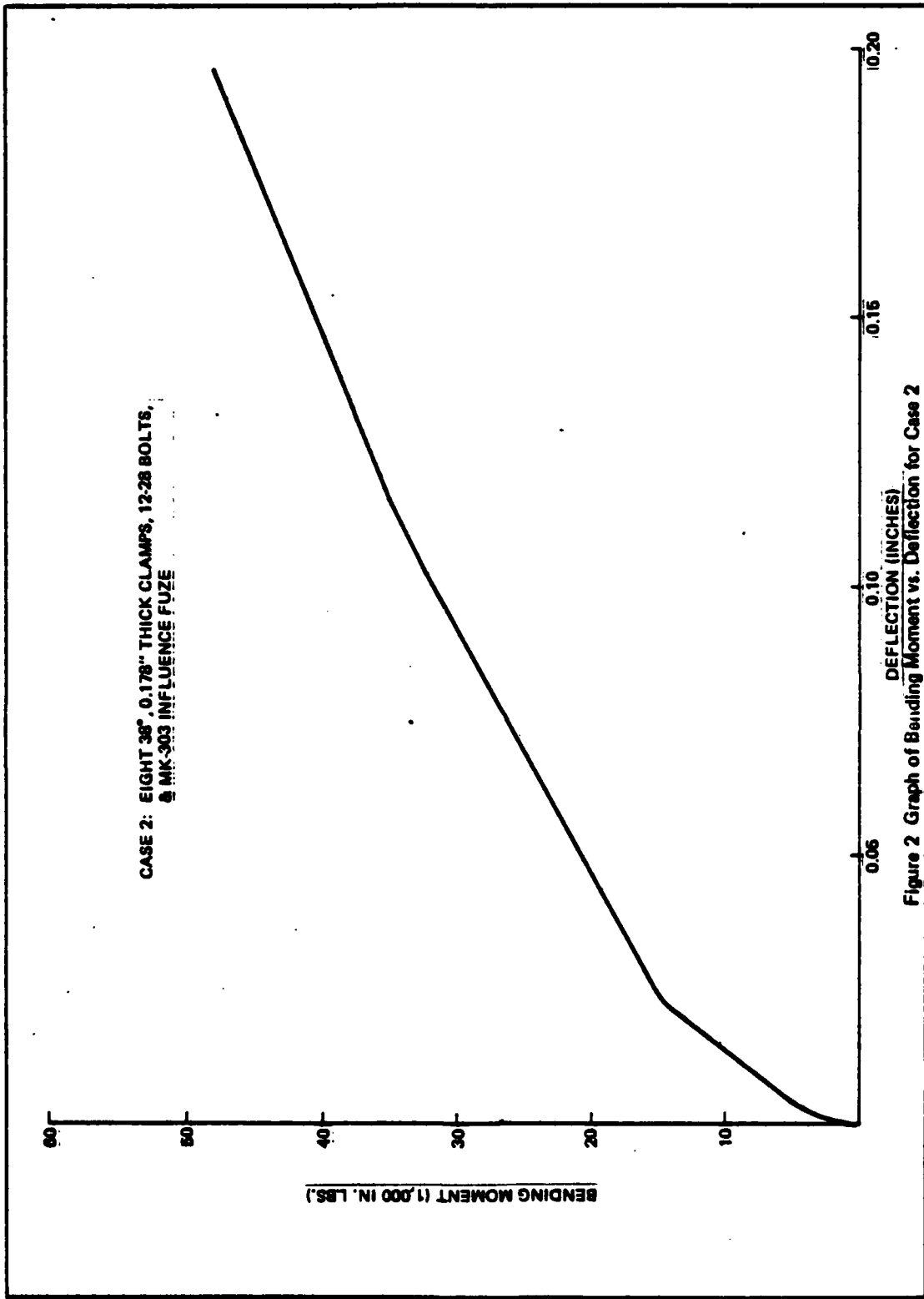
Figure 2 Graph of Bending Moment vs. Deflection for Case 2

CASE 3: EIGHT 38°, 0.158" THICK CLAMPS, 12-28 BOLTS, & MK-303 INFLUENCE FUZE

BENDING MOMENT (1,000) IN. LBS.)

DEFLECTION (INCHES)
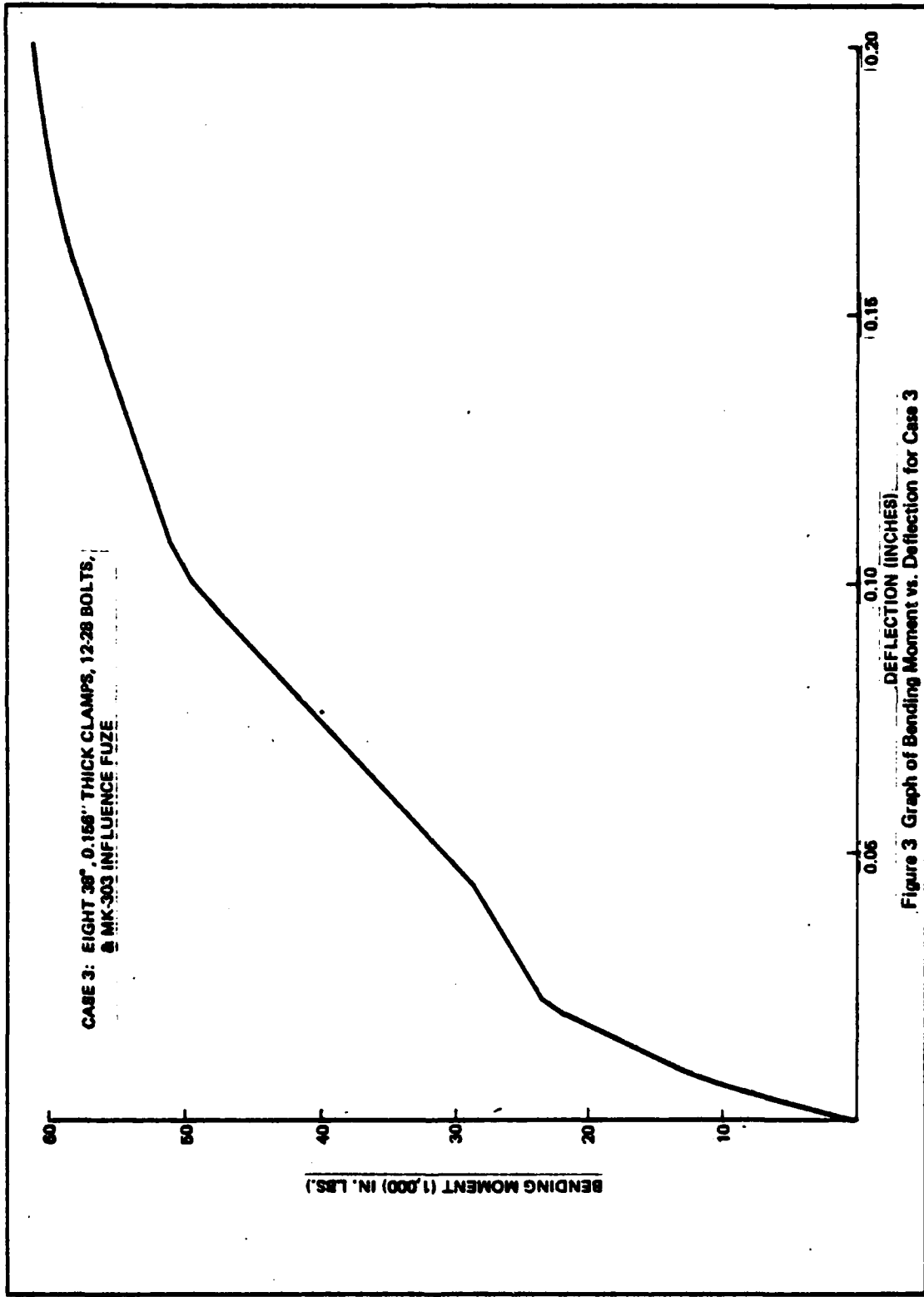
Figure 3 Graph of Bending Moment vs. Deflection for Case 3
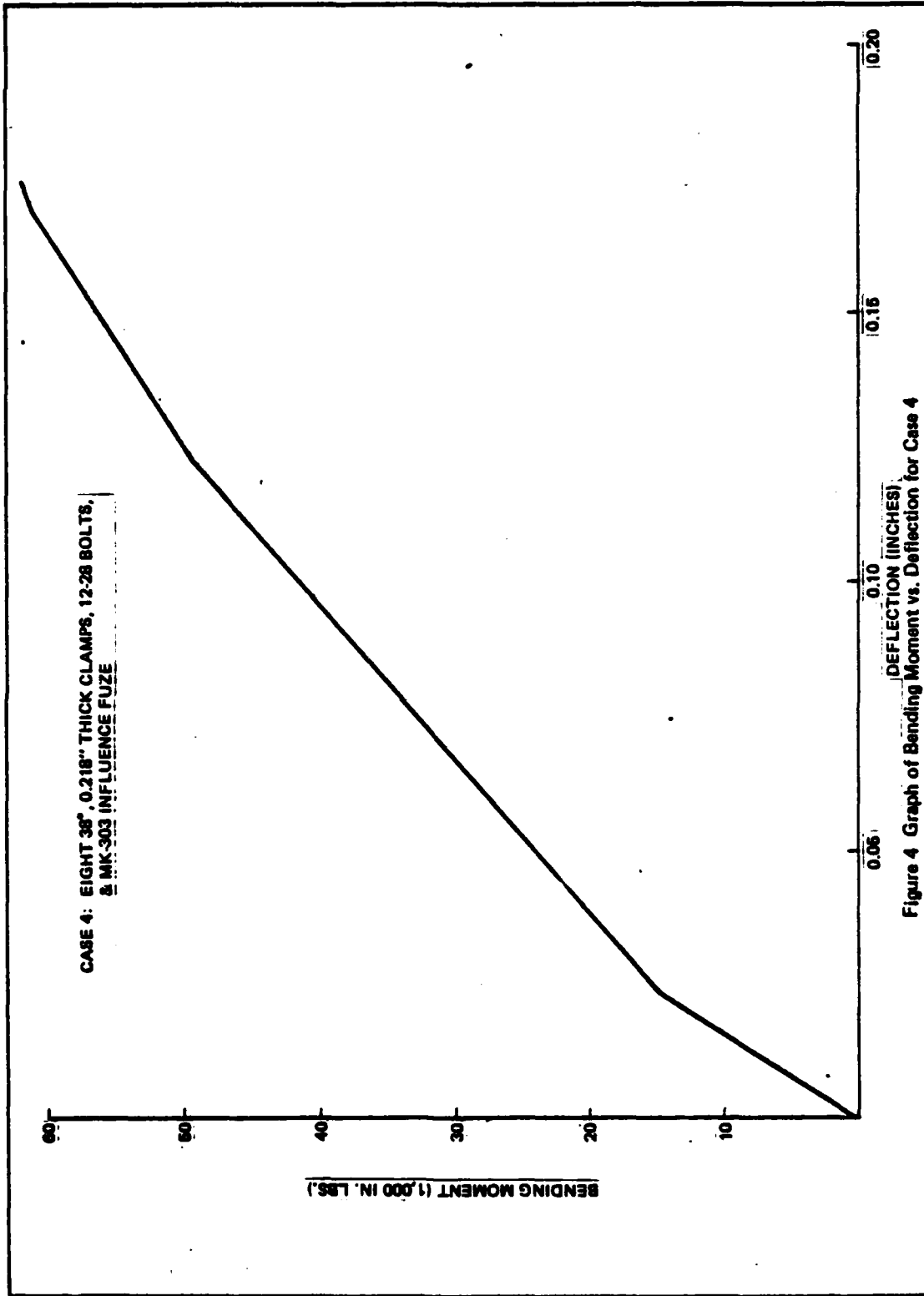
Figure 4 Graph of Bending Moment vs. Deflection for Case 4

CASE 4: EIGHT 36°, 0.218″ THICK CLAMPS, 12-28 BOLTS, & MK-303 INFLUENCE FUZE

DEFLECTION (INCHES)

BENDING MOMENT (1,000 IN. LBS.)

CASE 5: EIGHT MODIFIED 36° 0.156" THICK CLAMPS, 12-28 BOLTS, & DSU-21 HOUSING
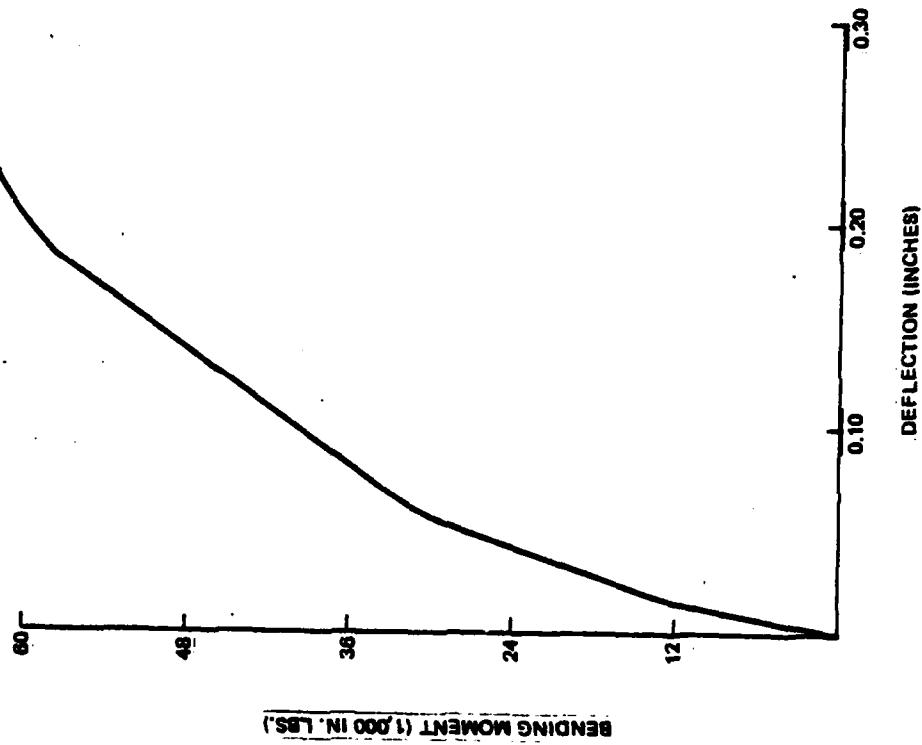
Figure 5 Graph of Bending Moment vs. Deflection for Case 5

Appendix B

Component Static Test Setups
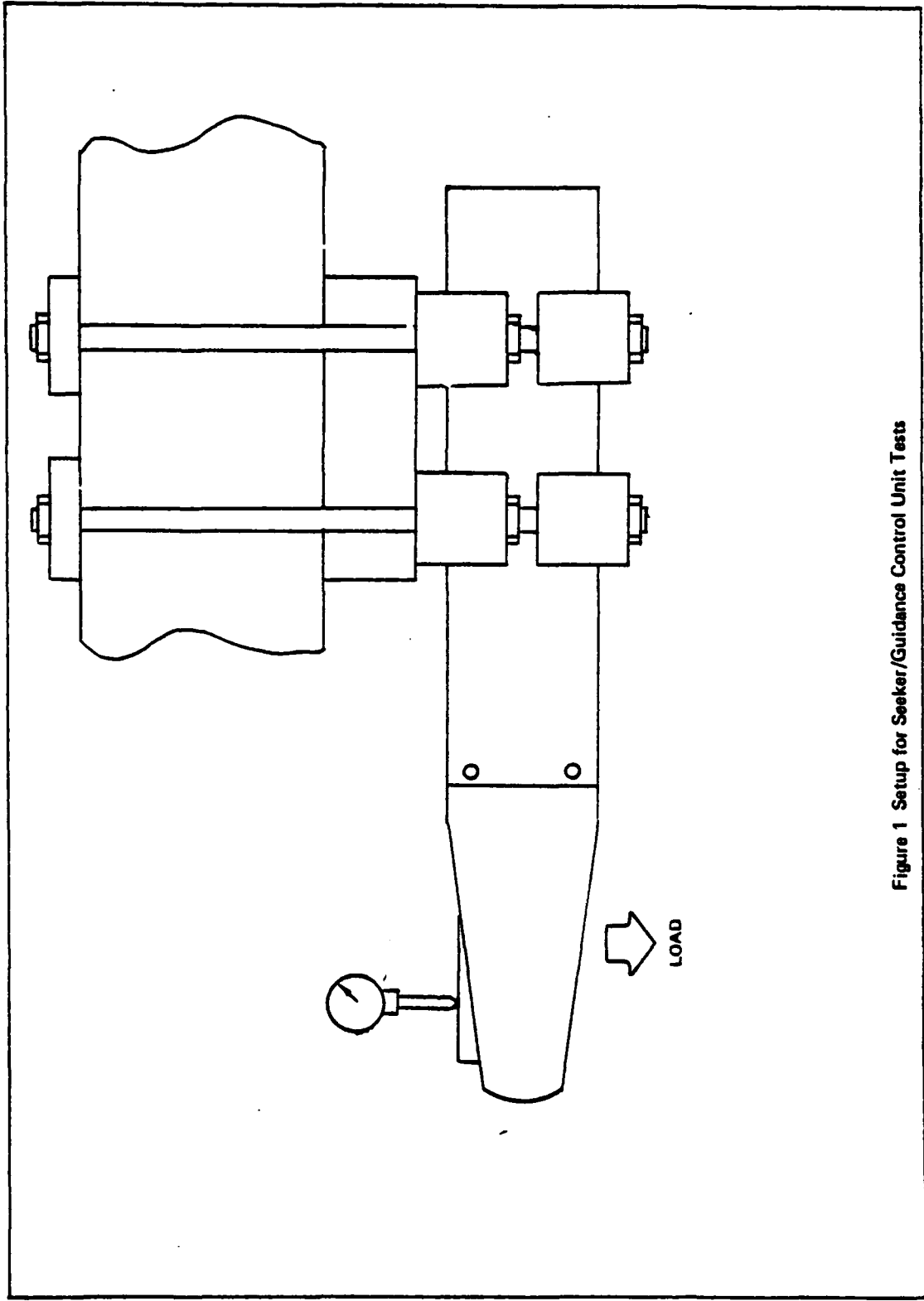
Figure 1 Setup for Seeker/Guidance Control Unit Tests
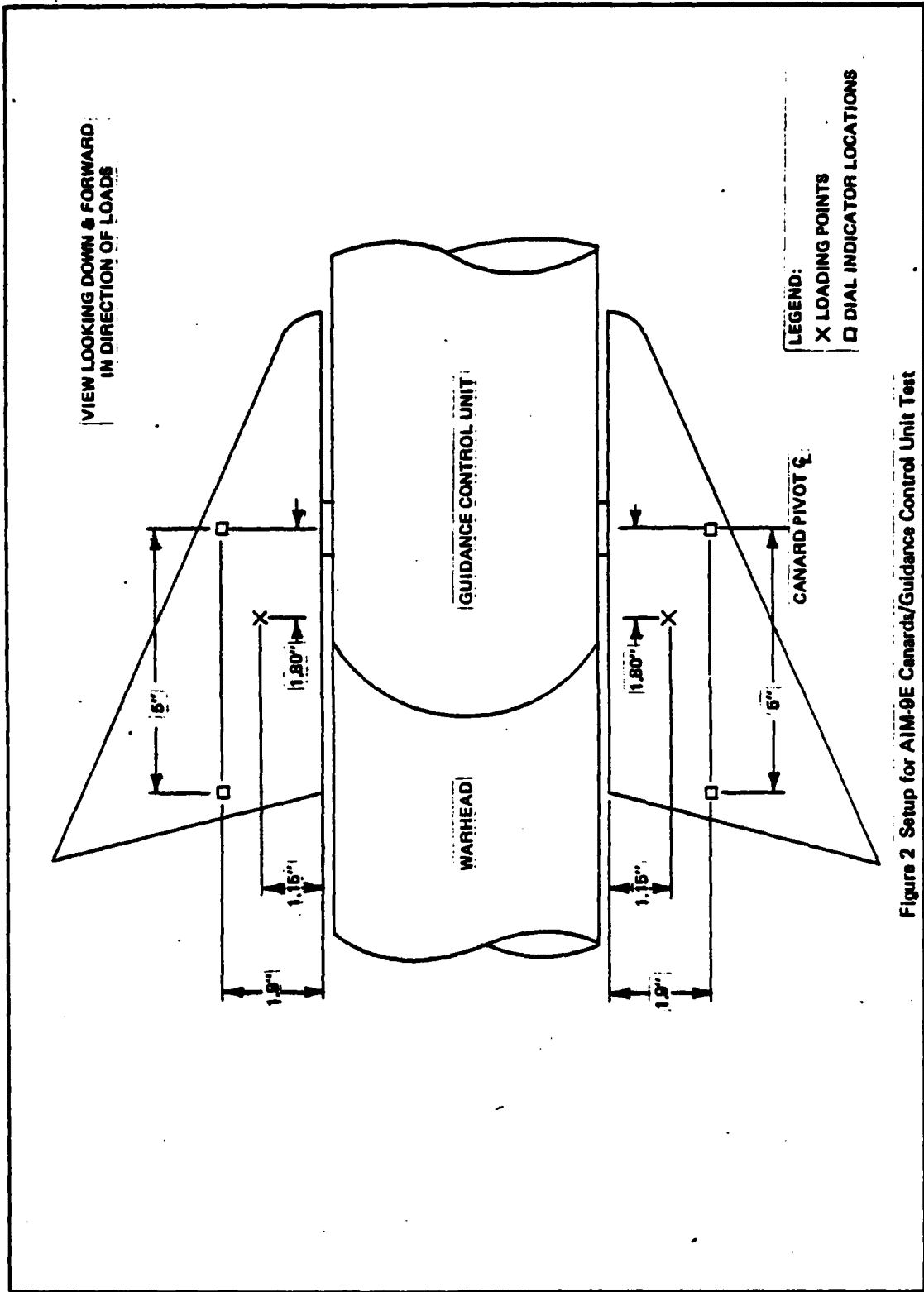
Figure 2 Setup for AIM-9E Canards/Guidance Control Unit Test

WARHEAD

GUIDANCE
CONTROL
UNIT
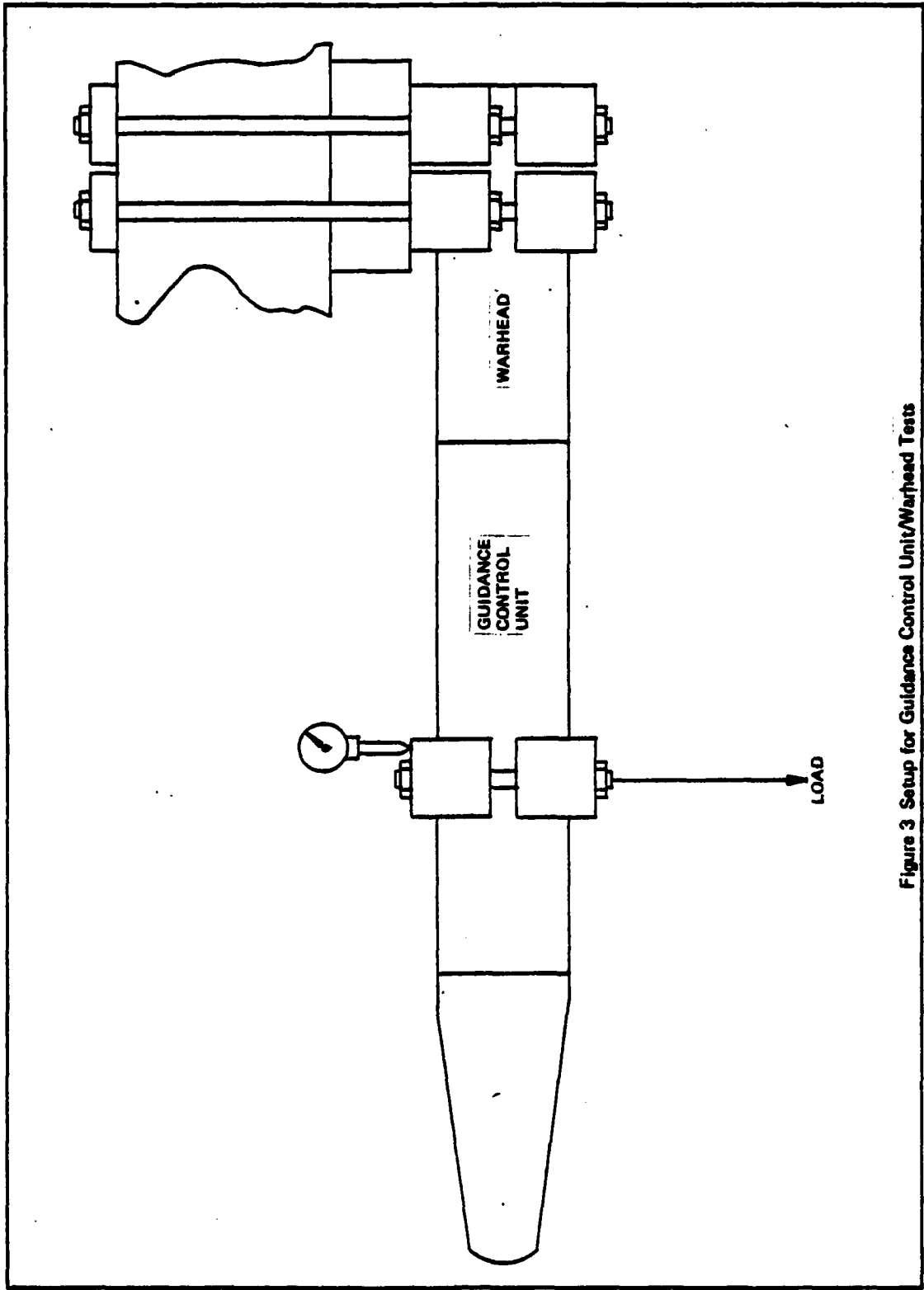
LOAD

Figure 3 Setup for Guidance Control Unit/Warhead Tests
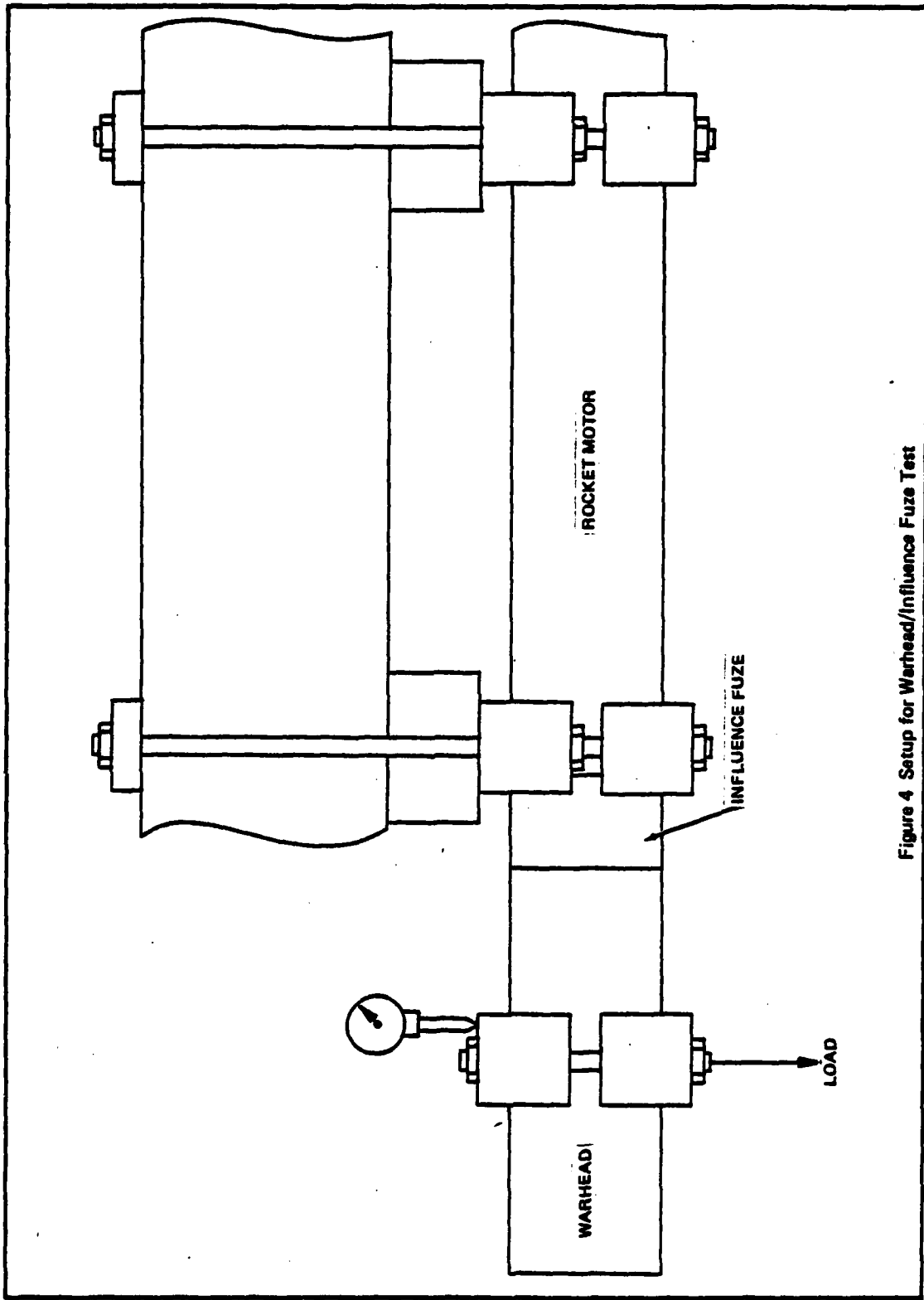
Figure 4 Setup for Warhead/Influence Fuze Test

ROCKET MOTOR

INFLUENCE FUZE

WARHEAD
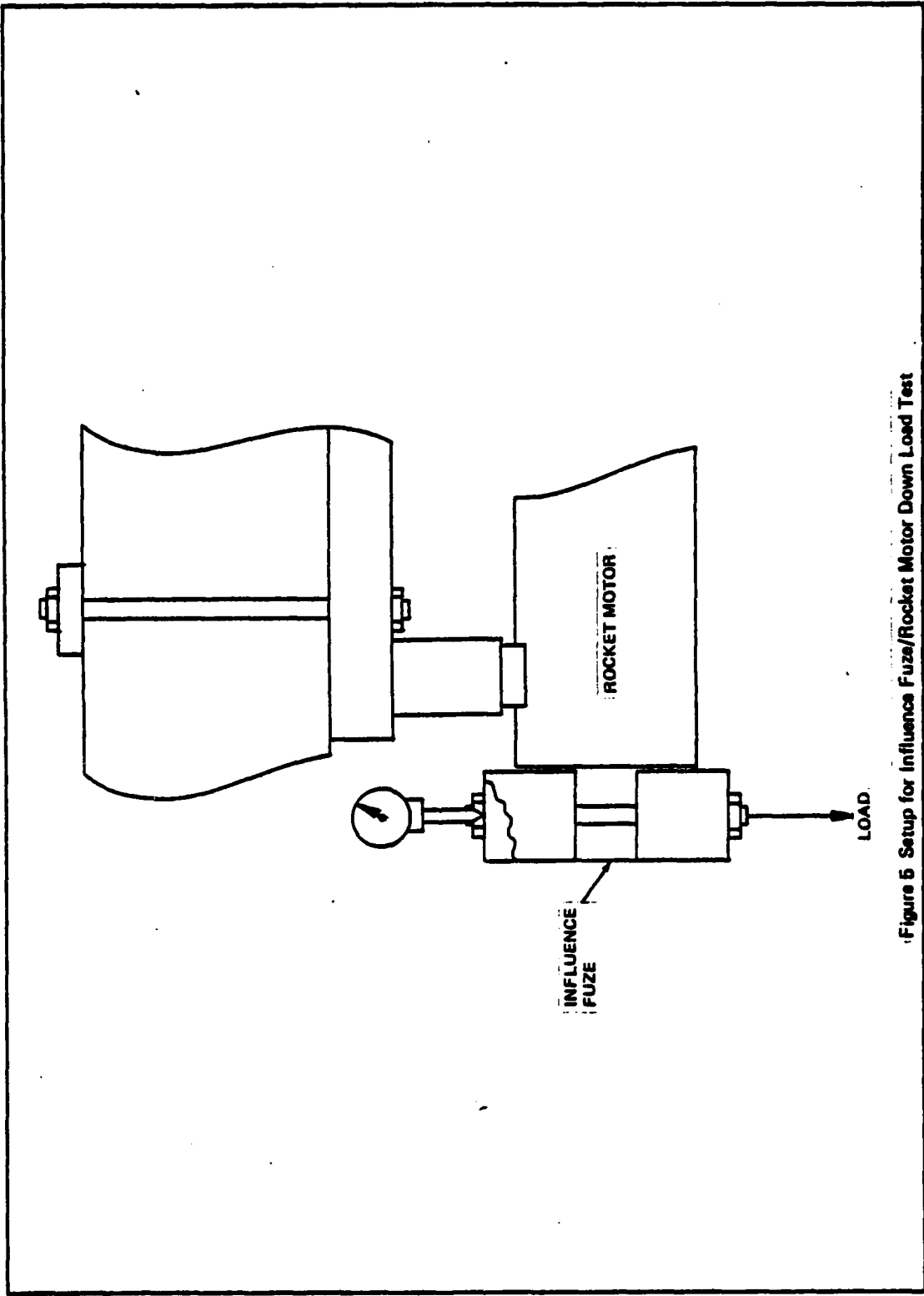
LOAD

Figure 5 Setup for Influence Fuze/Rocket Motor Down Load Test

LOAD

VIEW LOOKING AFT
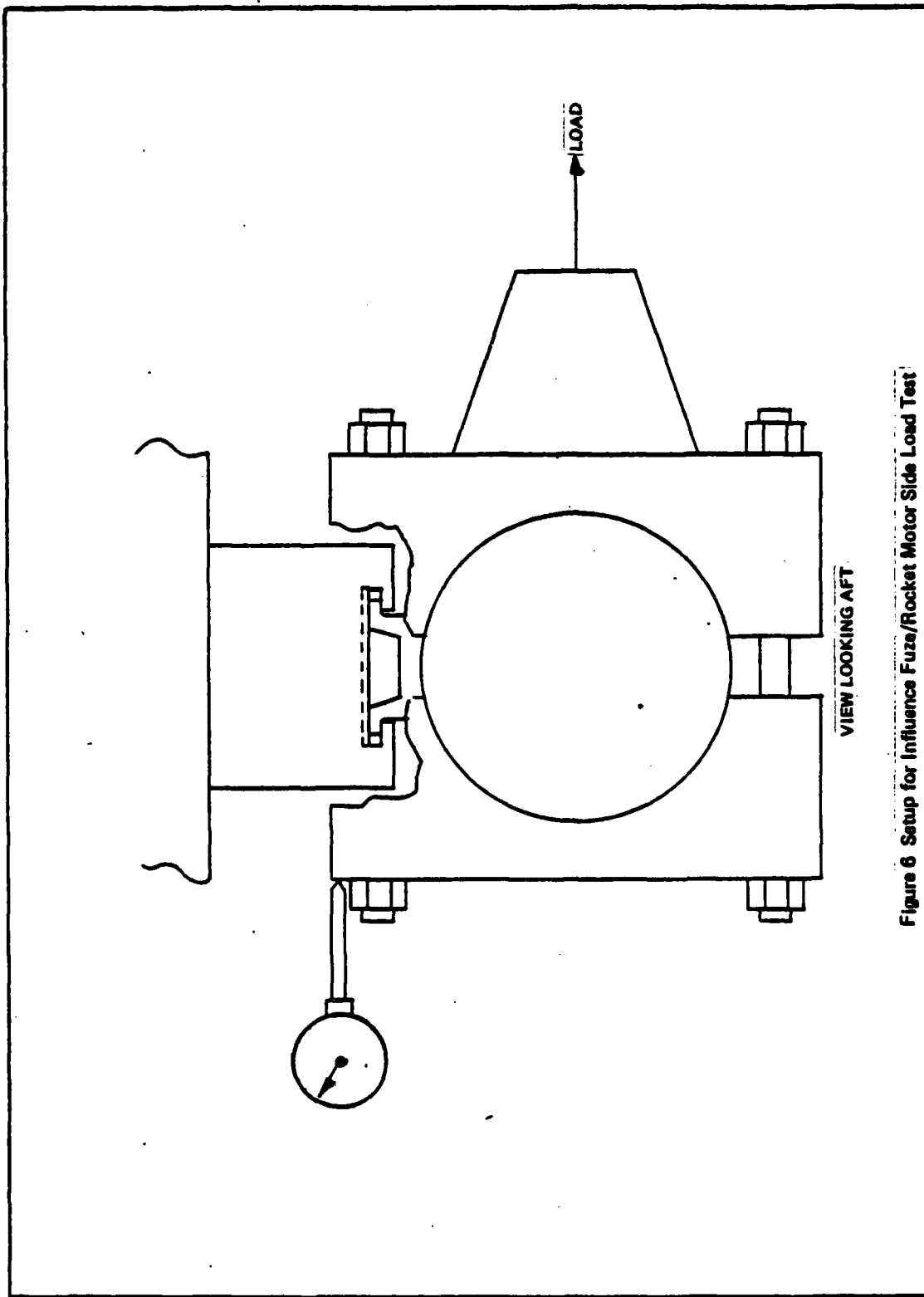
Figure 6 Setup for Influence Fuze/Rocket Motor Side Load Test

VIEW LOOKING DOWN

LEGEND:
X LOADING POINTS
□ DIAL INDICATOR LOCATIONS
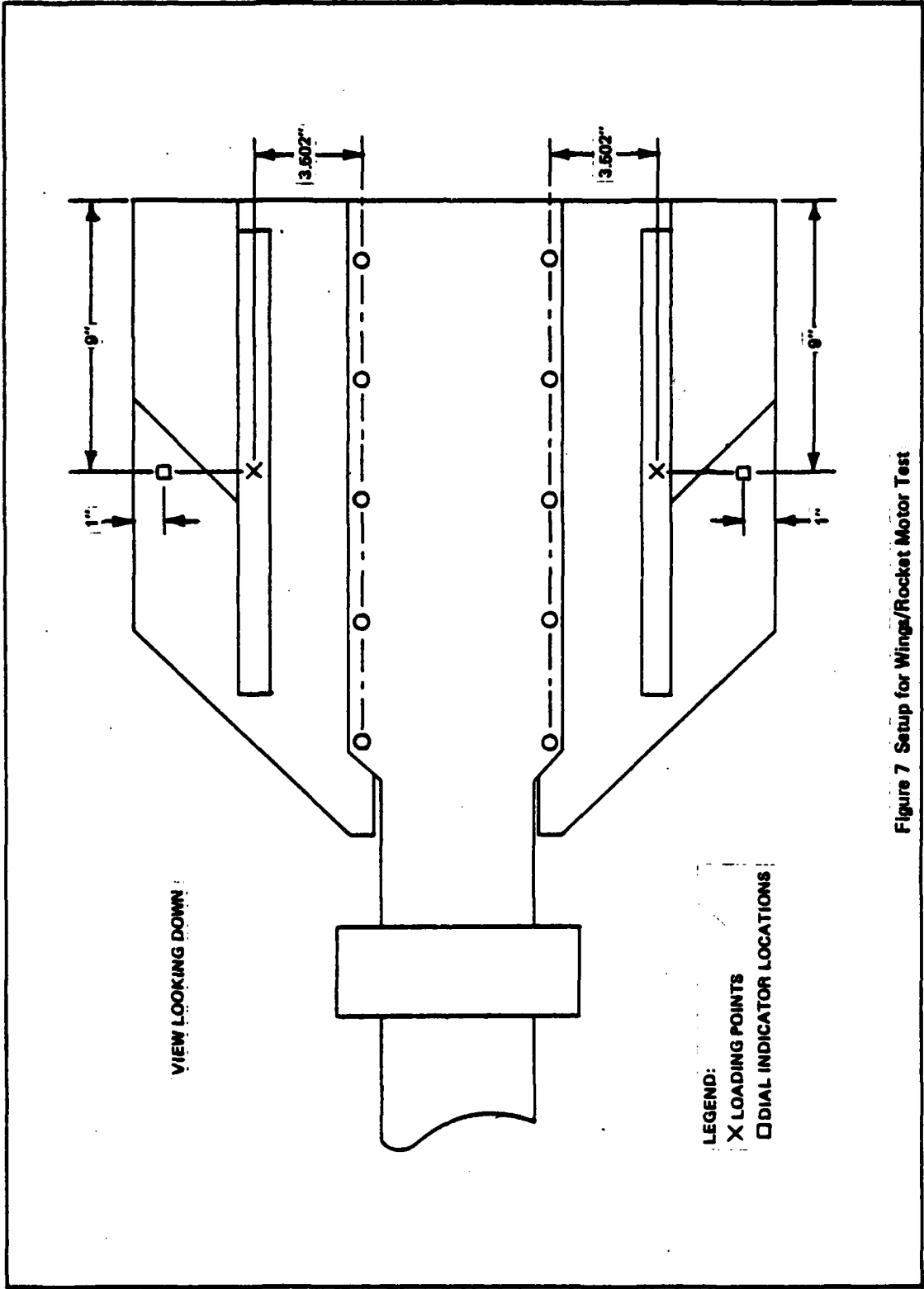
Figure 7 Setup for Wings/Rocket Motor Test

VIEW LOOKING AFT

CENTER
HANGER
FIXTURE
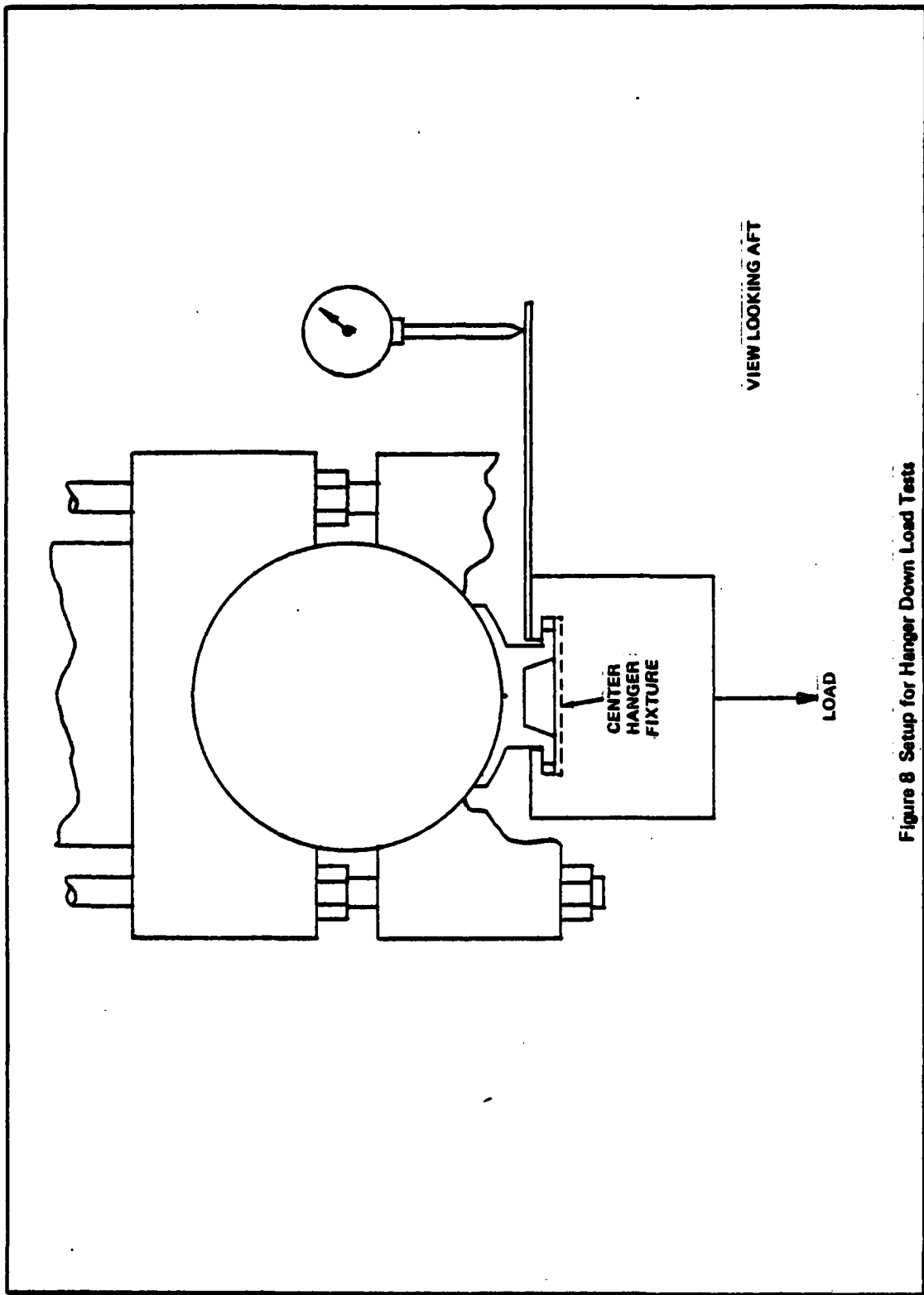
LOAD

Figure 8 Setup for Hanger Down Load Tests

CENTER HANGER FIXTURE

LOAD

VIEW LOOKING AFT
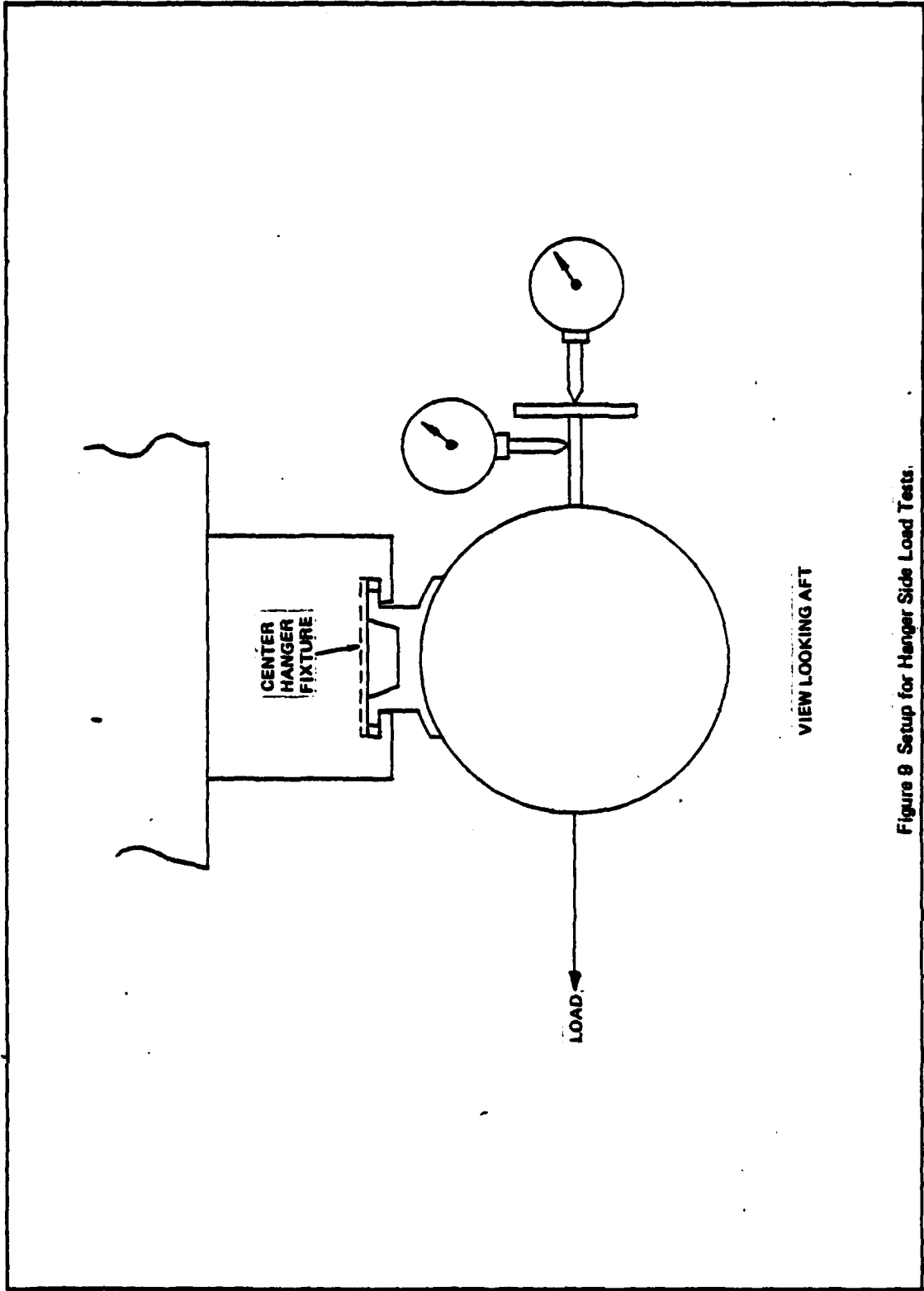
Figure 8 Setup for Hanger Side Load Tests.

Appendix C

Component Static Test Data Plots
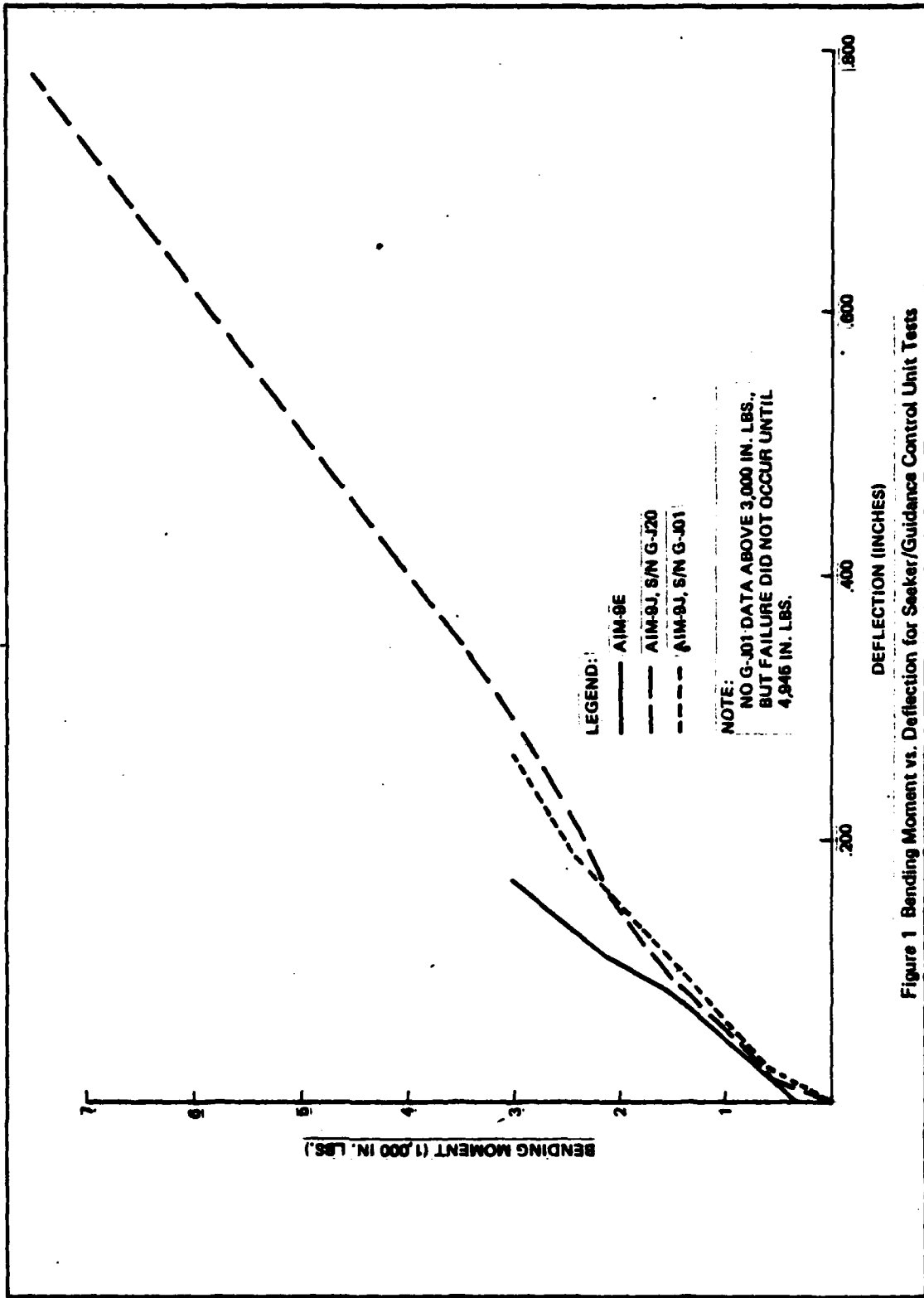
Figure 1 Bending Moment vs. Deflection for Seeker/Guidance Control Unit Tests

LEGEND:

———— AIM-9E

— — — AIM-9J, S/N G-J20

- - - - AIM-9J, S/N G-J01

NOTE:
NO G-J01 DATA ABOVE 3,000 IN. LBS.,
BUT FAILURE DID NOT OCCUR UNTIL
4,946 IN. LBS.

BENDING MOMENT (1,000 IN. LBS.)

DEFLECTION (INCHES)
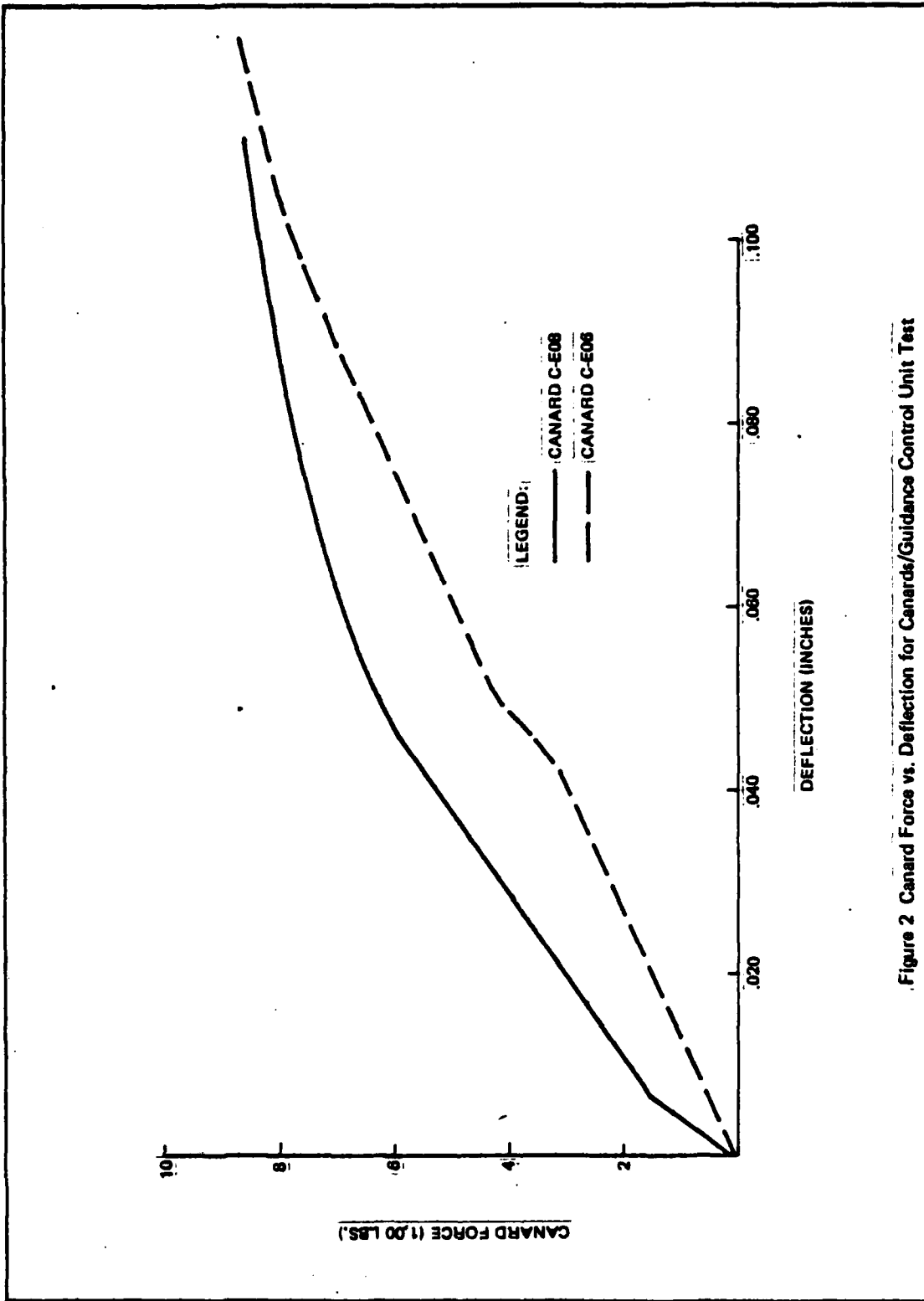
Figure 2 Canard Force vs. Deflection for Canards/Guidance Control Unit Test
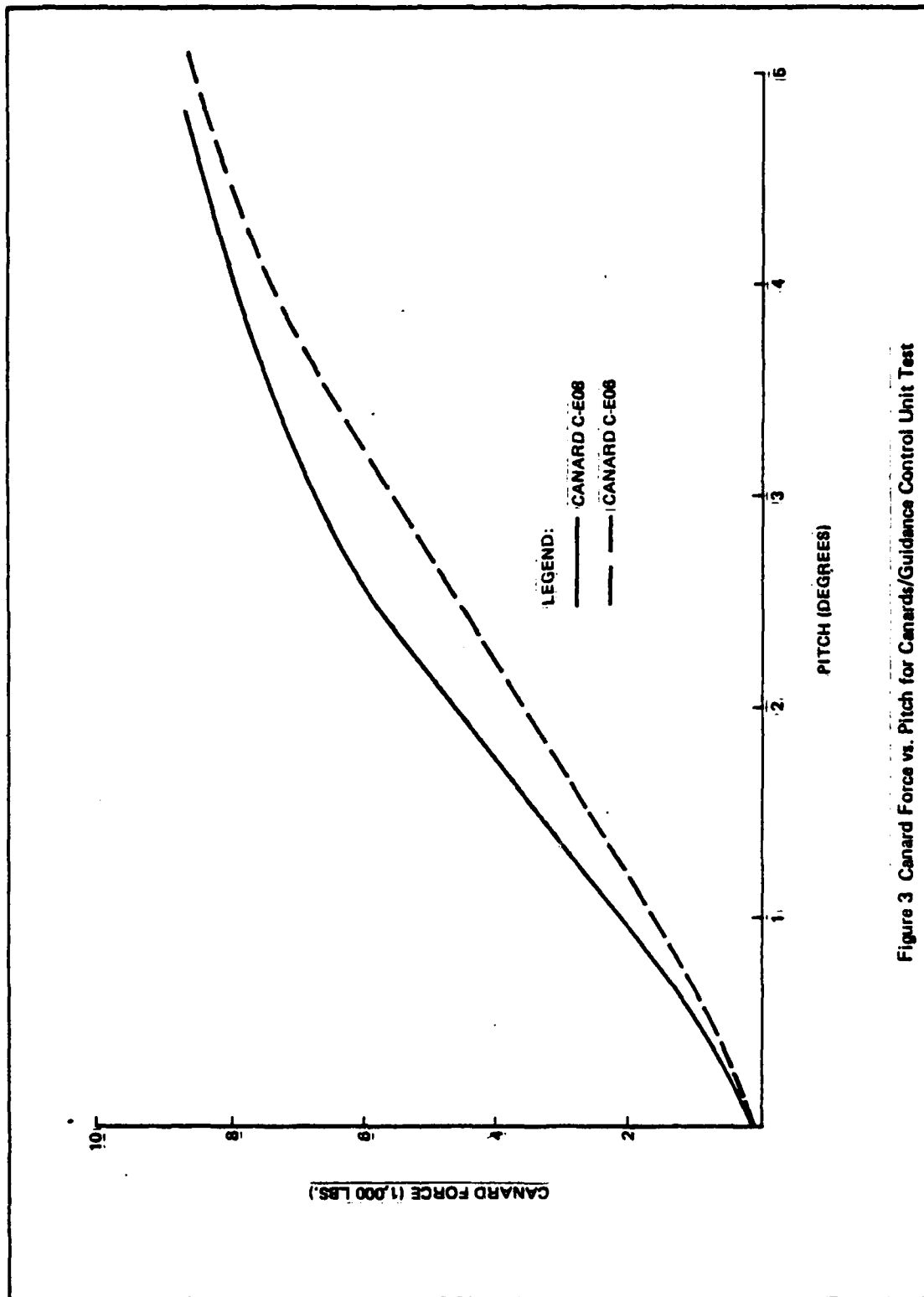
Figure 3 Canard Force vs. Pitch for Canards/Guidance Control Unit Test
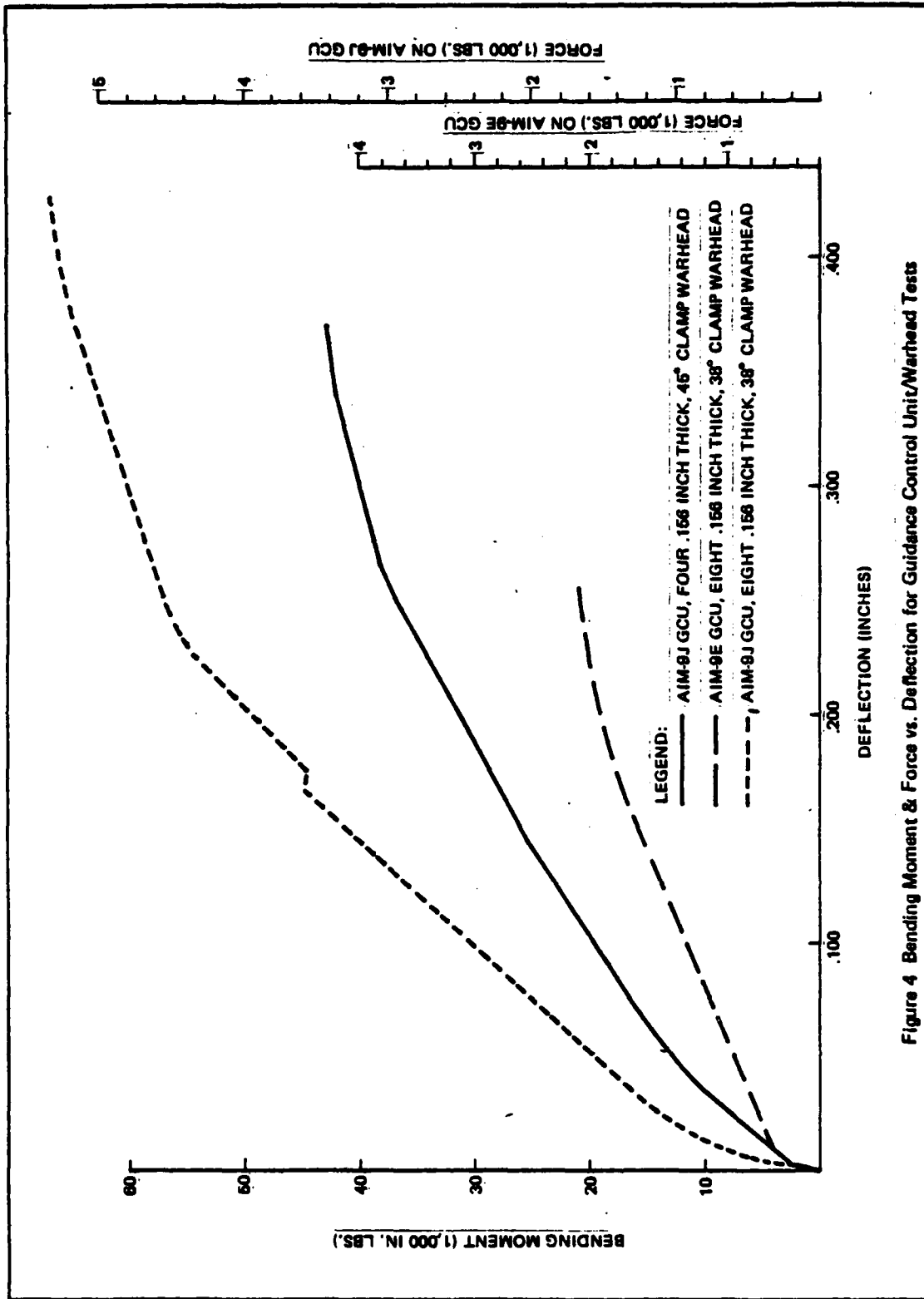
Figure 4 Bending Moment & Force vs. Deflection for Guidance Control Unit/Warhead Tests
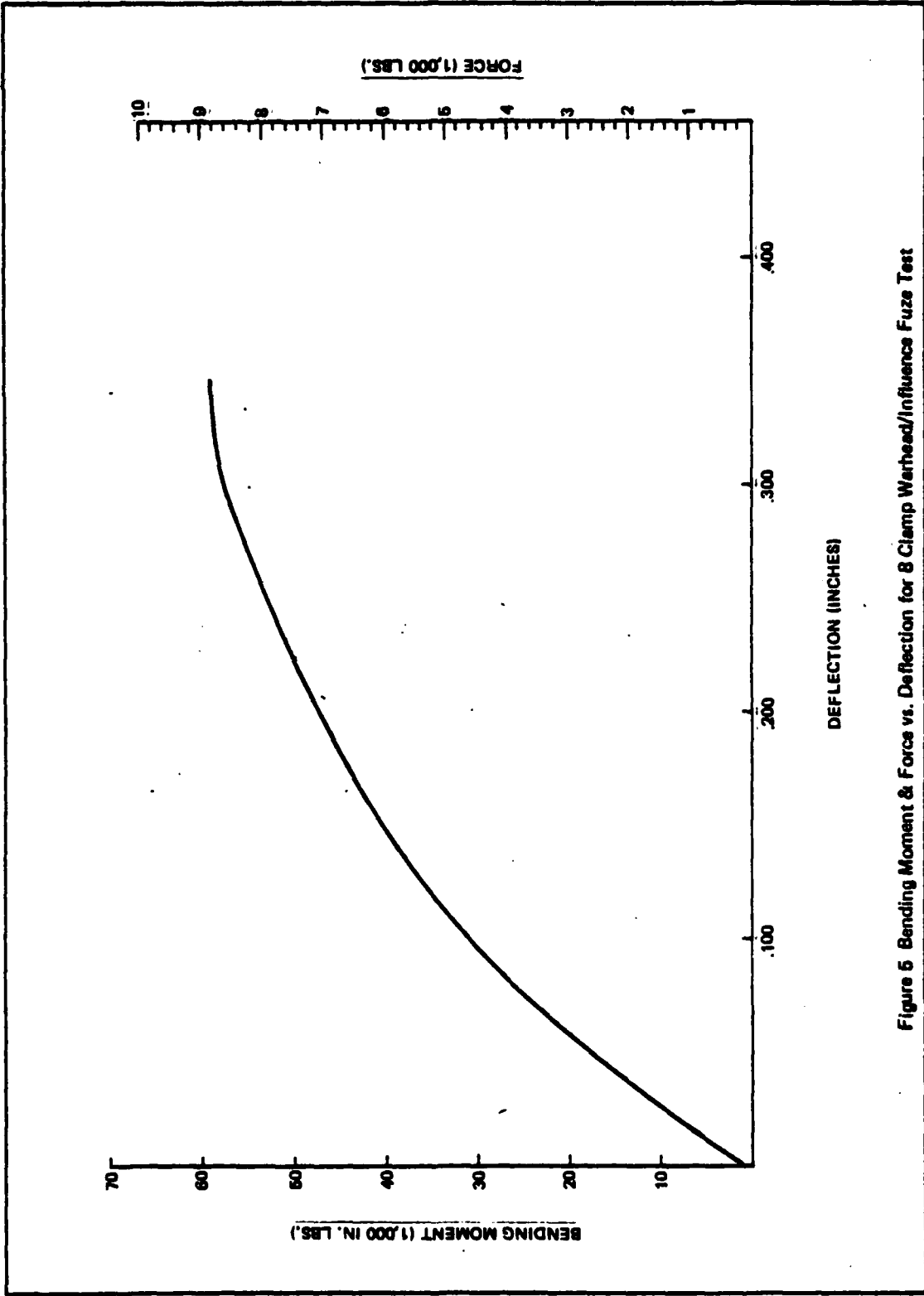
Figure 5 Bending Moment & Force vs. Deflection for 8 Clamp Warhead/Influence Fuze Test
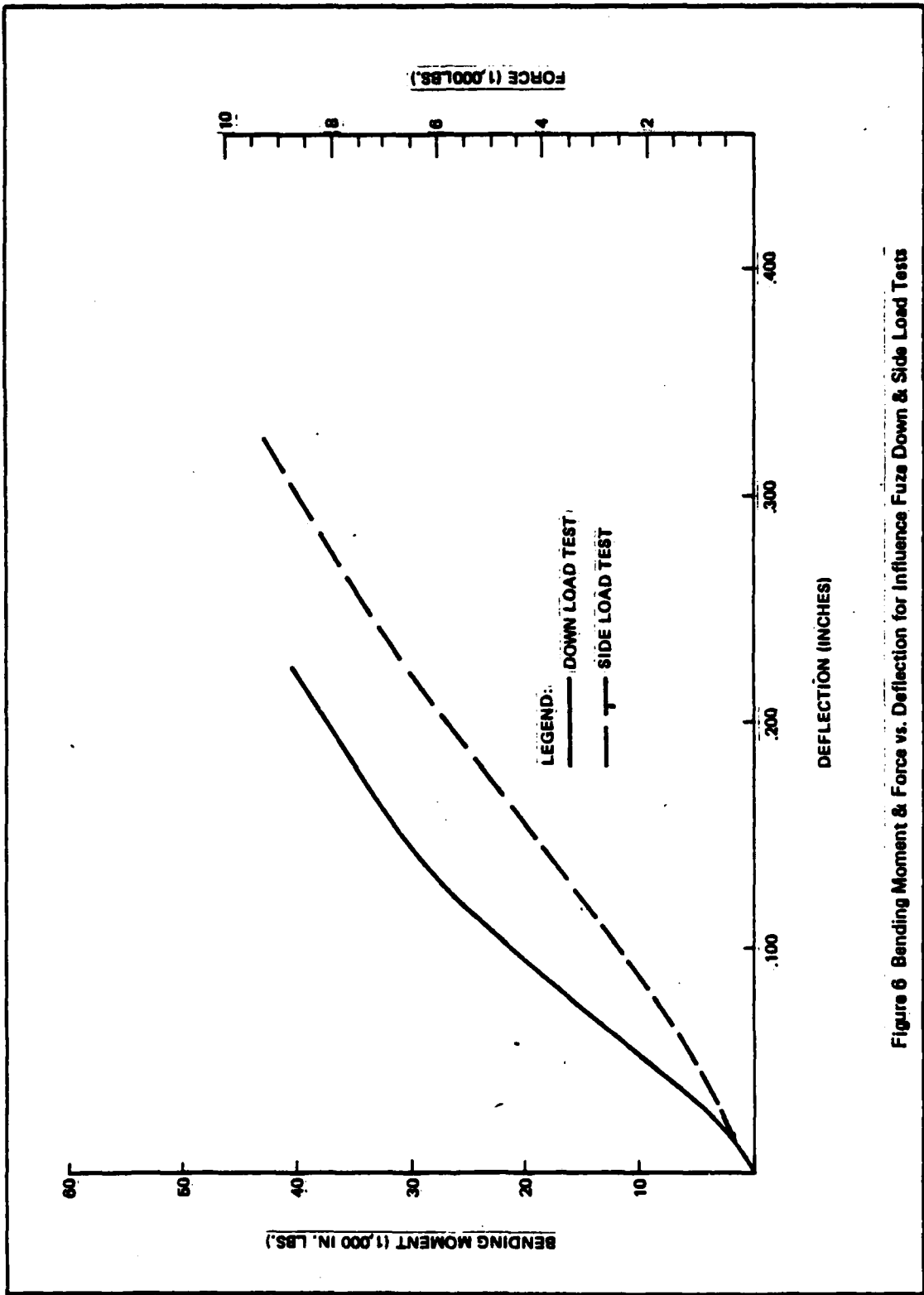
Figure 6 Bending Moment & Force vs. Deflection for Influence Fuze Down & Side Load Tests
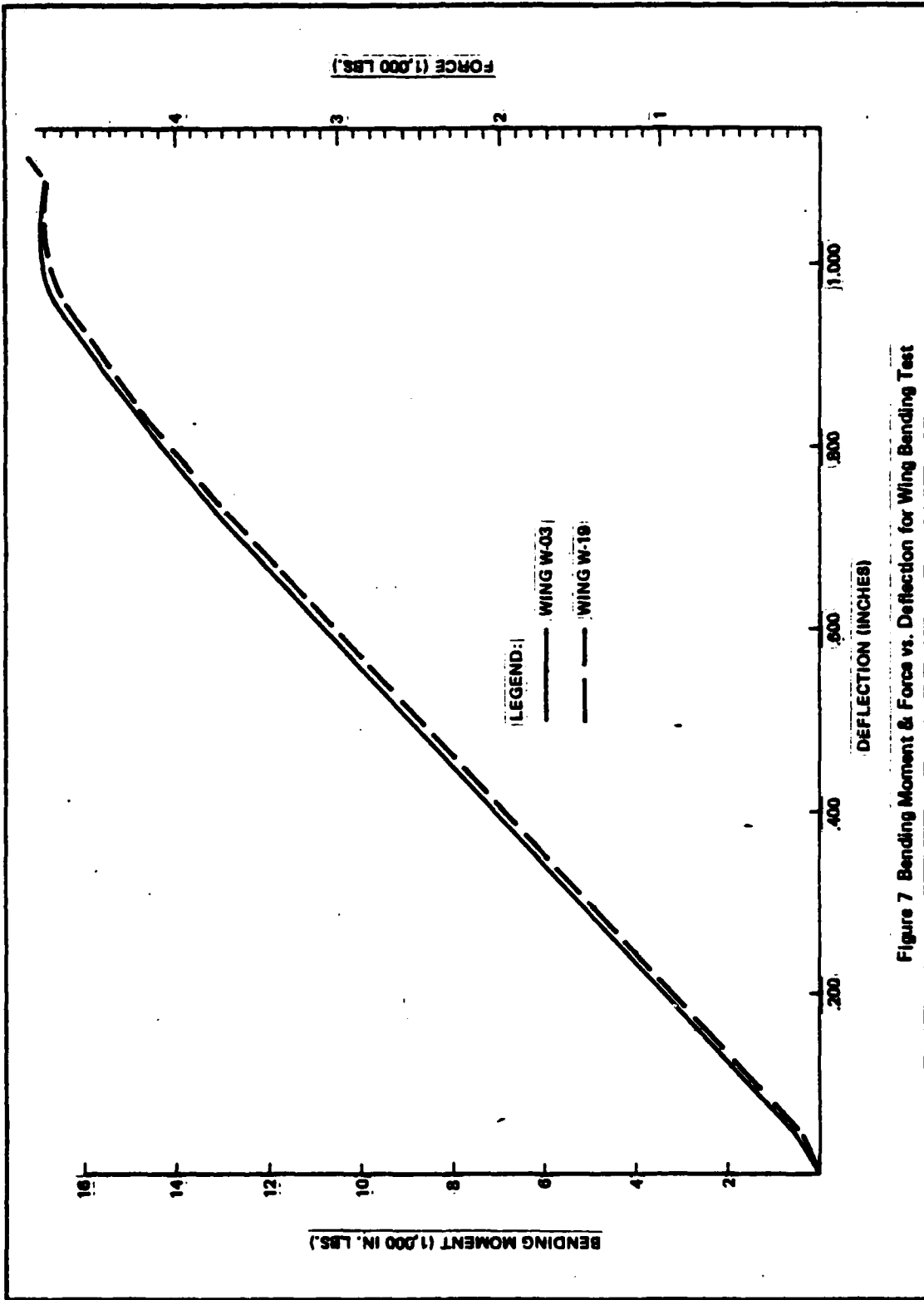
Figure 7 Bending Moment & Force vs. Deflection for Wing Bending Test
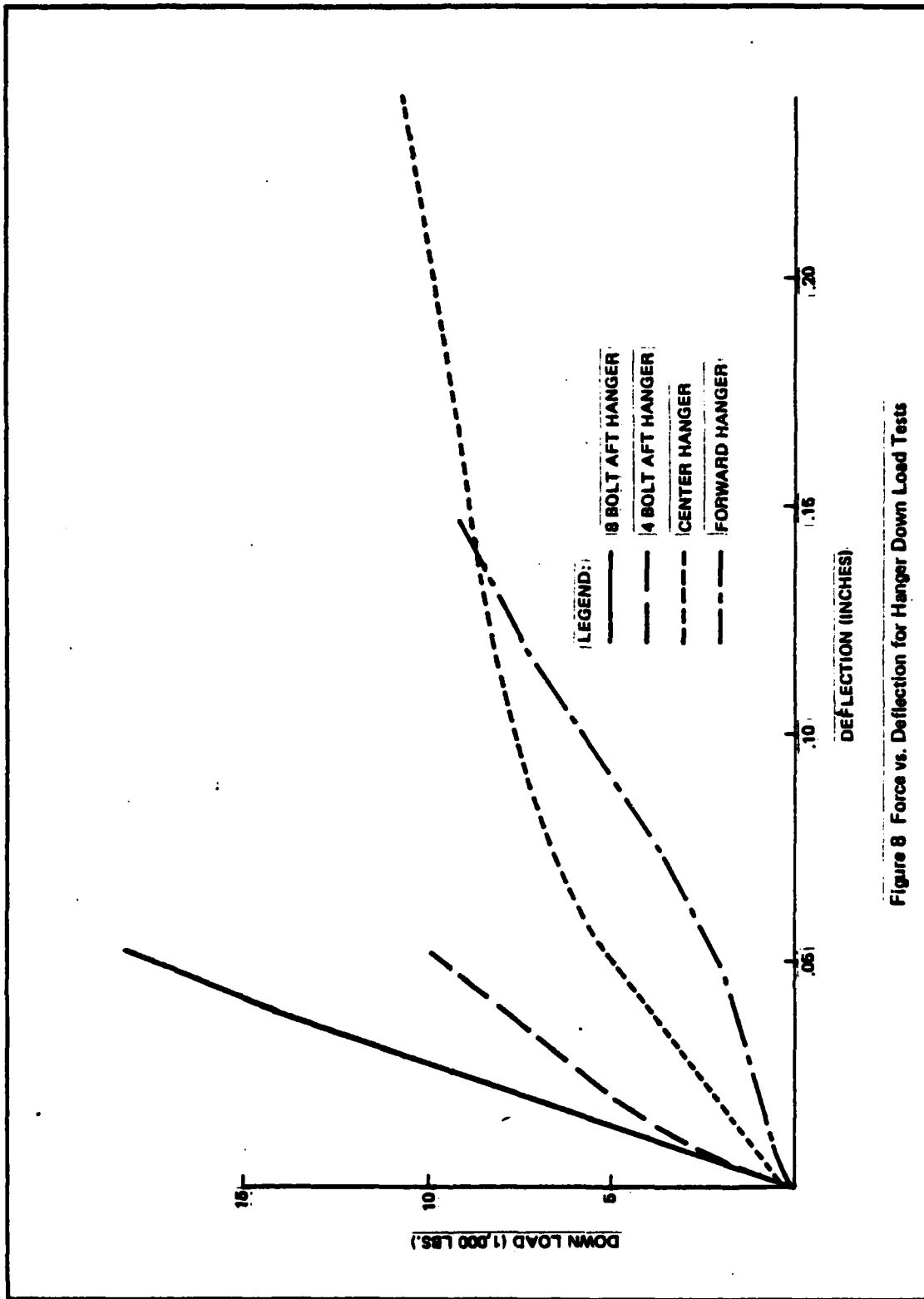
Figure 8 Force vs. Deflection for Hanger Down Load Tests

LEGEND:
8 BOLT AFT HANGER
4 BOLT AFT HANGER
CENTER HANGER
FORWARD HANGER

DEFLECTION (INCHES)

DOWN LOAD (1,000 LBS.)

Figure 9 Roll Moment & Side Load vs. Sideward Deflection for Hanger Side Load Tests
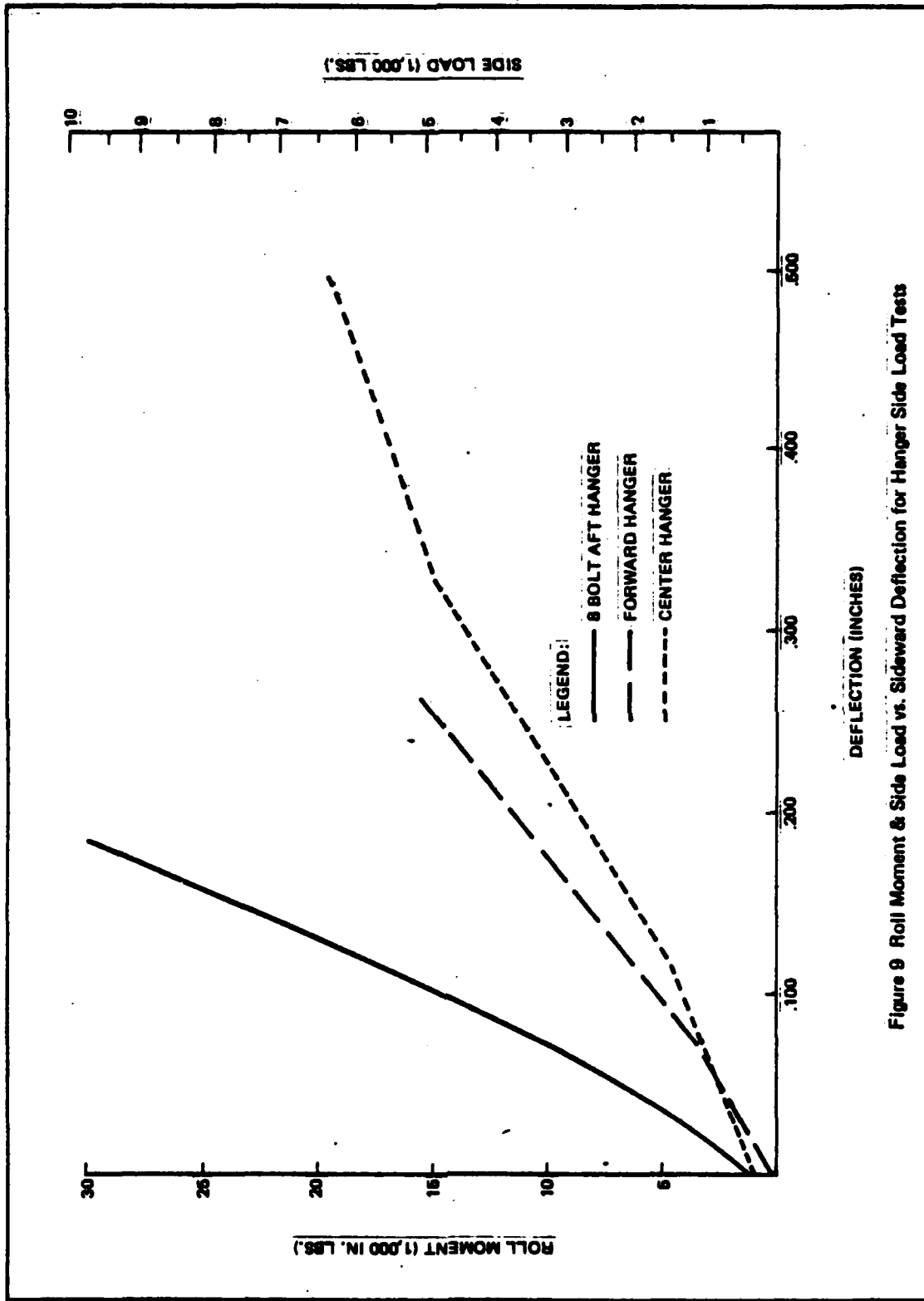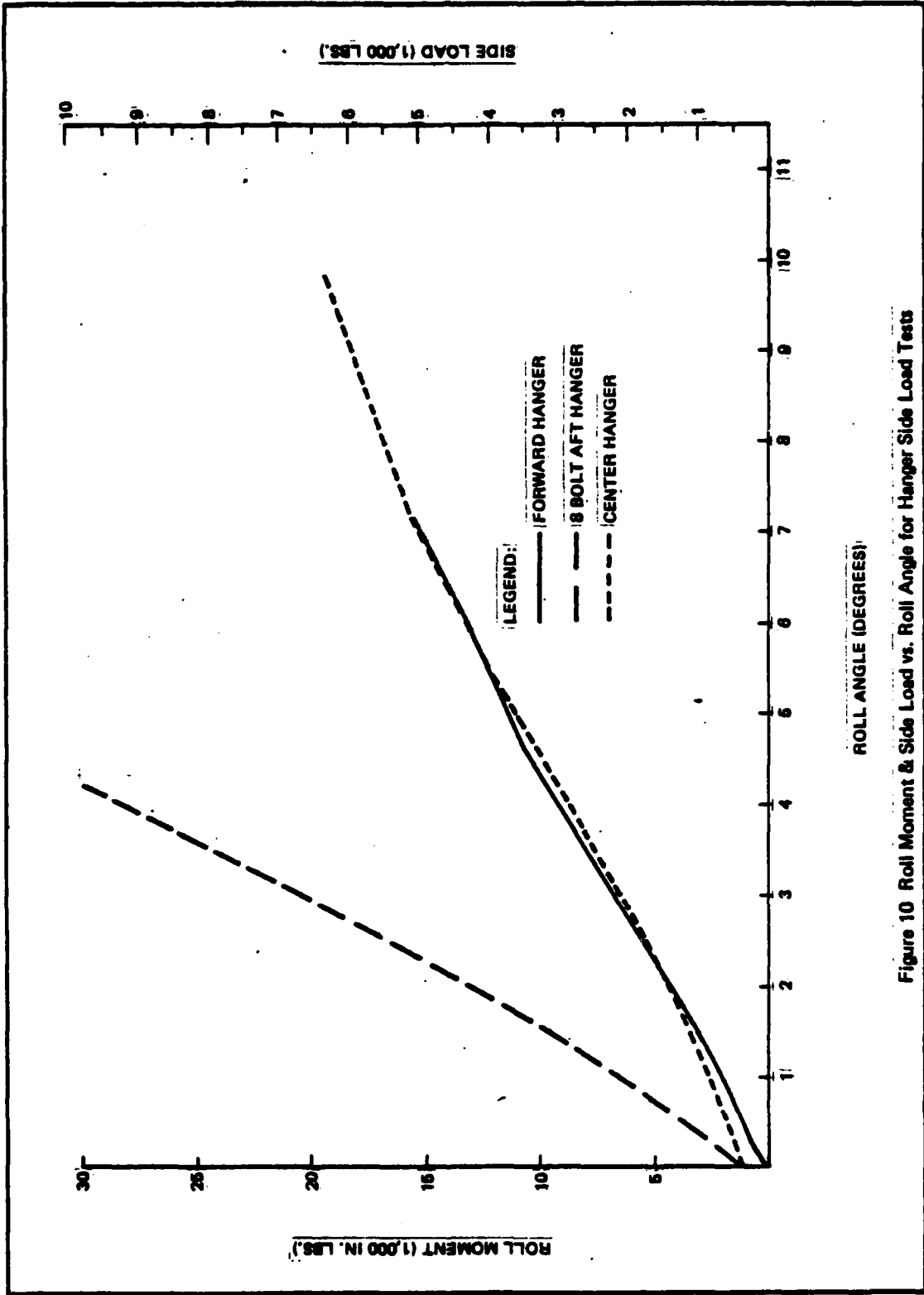
Figure 10 Roll Moment & Side Load vs. Roll Angle for Hanger Side Load Tests

Appendix D

Static Test Results Summary Tables

TABLE 1 - AIM-9E AND AIM-9J MISSILE ULTIMATE STRENGTH UNDER VARIOUS INERTIA LOADS

MISSILE	NUMBER OF WARHEAD CLAMPS	NUMBER OF AFT HANGER BOLTS	ULTIMATE STRENGTH UNDER INDICATED INERTIA LOAD					
			LOAD (2g's)			ANGULAR ACCELERATION (RAD/SEC²)		
			VERTICAL	SIDE	EQUAL SIDE & VERTICAL	PITCH	YAW	EQUAL YAW & PITCH
AIM-9E	4	4	27	27	27 D,U	240	240	240 D,U
	4	0	27	27	27 D,U	240	240	240 D,U
	0	4	50	36	35 D	493	386	377 D
	0	0	60	36	35 D	493	386	377 D
AIM-9J	4	4	23	23	23 D,U	199	199	199 D,U
	4	0	23	23	23 D,U	199	199	199 D,U
	0	4	50	31	33 D	433	352	347 D
	0	0	60	31	33 D	433	352	347 D

NOTES:

1. ALL TRANSLATIONAL INERTIA LOADS ACT AT THE MISSILE C.G. AND ARE GIVEN AS TOTAL VECTOR MAGNITUDES.
2. ALL ANGULAR ACCELERATIONS ACT ABOUT THE MISSILE C.G. AND ARE GIVEN AS TOTAL VECTOR MAGNITUDES.
3. REFER TO FIGURE 2 IN THE TEXT FOR DEFINITION OF LOAD AND ANGULAR ACCELERATION DIRECTIONS.
4. D = DOWN LOAD OR NOSE DOWN PITCH ONLY; U = UP LOAD OR NOSE UP PITCH ONLY; D,U = EITHER DOWN OR UP LOAD, OR EITHER NOSE DOWN OR NOSE UP PITCH.

TABLE II - AIM-9X AND AIM-9X MISSILE COMPONENTS: ULTIMATE STRENGTH UNDER VARIOUS INERTIA LOADS

MISSILE	FAILURE MODE	PREDICTED ULTIMATE STRENGTH UNDER INDICATED INERTIA LOAD(S)							
		LOAD (LB'S)				ANGULAR ACCELERATION (RAD/SEC)			
		UP	DOWN	SIDE	EQUAL SIDE & VERTICAL	NOSE UP PITCH	NOSE DOWN PITCH	YAW	EQUAL YAW & PITCH
	SEEKER/HOMING SET	74	74	74	52 D,U	493	493	493	347 D,U
	4CU/WARHEAD								
	FOUR CLAMP WARHEAD	84	84	84	84 D,U	499	499	499	499 D,U
	EIGHT CLAMP WARHEAD	84	84	84	84 D,U	499	499	499	499 D,U
AIM-9X	WARHEAD/INFLUENCE FUZE								
	FOUR CLAMP WARHEAD	27	27	27	27 D,U	240	240	240	240 D,U
	EIGHT CLAMP WARHEAD	50	50	50	58 D,U	523	523	523	523 D,U
	ROCKET MOTOR								
	FORWARD HANGER	-	71	36	35 D	-	866	866	377 D
	CENTER HANGER	159	-	102	88 U	1,667	-	1,078	730 U
	FOUR BOLT AFT HANGER	-	193	66	61 D	1,466	-	722	678 U
	EIGHT BOLT AFT HANGER	-	352	109	116 D	2,607	-	1,391	1,608 U
	SEEKER/HOMING SET	114	114	114	61 D,U	729	729	729	615 D,U
	4CU/WARHEAD								
	FOUR CLAMP WARHEAD	90	90	90	90 D,U	728	728	728	728 D,U
	EIGHT CLAMP WARHEAD	142	142	142	142 D,U	1,147	1,147	1,147	1,147 D,U
AIM-93	WARHEAD/INFLUENCE FUZE								
	FOUR CLAMP WARHEAD	23	23	23	23 D,U	199	199	199	199 D,U
	EIGHT CLAMP WARHEAD	50	50	50	50 D,U	433	433	433	433 D,U
	ROCKET MOTOR								
	FORWARD HANGER	141	77	34	33 D	-	613	352	347 D
	CENTER HANGER	-	-	90	78 U	1,397	-	866	742 U
	FOUR BOLT AFT HANGER	-	206	55	61 D	1,449	-	732	680 U
	EIGHT BOLT AFT HANGER	-	373	107	117 D	2,645	-	1,420	1,306 U

NOTES:

1. D = DOWN LOAD OR NOSE DOWN PITCH ONLY; U = UP LOAD OR NOSE UP PITCH ONLY; D,U = EITHER DOWN OR UP LOAD, OR EITHER NOSE DOWN OR NOSE UP PITCH.

2. ALL LOADS AND ANGULAR ACCELERATIONS GIVEN ARE TOTAL VECTOR MAGNITUDES. SEE ALSO FIGURE 2 IN TEXT AND TABLE 1 OF APPENDIX D.

TABLE III - AIM-95 AND AIM-93 MISSILE COMPONENTS' ULTIMATE LOADS AND BENDING MOMENTS

FAILURE MODE	ULTIMATE STRENGTH		COMMENTS
	LOAD (POUNDS)	BENDING MOMENT (INCH-POUNDS)	
SEEKER/HOMING SET			BENDING MOMENTS ABOUT HOMING SET BOLT CENTERLINE
AIM-95	721/510	3,183/2,251	PHENOLIC BULKHEAD FAILS (ALL FOUR BOLTS LOADED/TWO BOLTS LOADED)
AIM-93	1,413/999	4,945/2,417	ALUMINUM BULKHEAD FAILS (ALL FOUR BOLTS LOADED/TWO BOLTS LOADED)
GCU/WARHEAD			BENDING MOMENTS ABOUT GCU/WARHEAD JOINT, WORST DIRECTION
AIM-95			
FOUR CLAMP WARHEAD	3,850	20,300	} FORWARD SERVO HOUSING/AFT SERVO HOUSING JOINT FAILS
EIGHT CLAMP WARHEAD	2,840	20,300	
AIM-93			
FOUR CLAMP WARHEAD	3,530	43,910	} GUIDANCE CONTROL UNIT PULLS OUT OF WARHEAD
EIGHT CLAMP WARHEAD	6,540	69,230	
WARHEAD/INFLUENCE FUZE			BENDING MOMENTS ABOUT WARHEAD/INFLUENCE FUZE JOINT, WORST DIRECTION
FOUR CLAMP WARHEAD	4,130	20,900	} WARHEAD PULLS OUT OF INFLUENCE FUZE
EIGHT CLAMP WARHEAD	9,110	60,860	
ROCKET MOTOR			LOADS ACT AT ROCKET MOTOR TUBE CENTERLINE
BODY LOADS			
FORWARD HANGER	9,260	0	HANGER SPLITS IN HALF LONGITUDINALLY
CENTER HANGER	10,970	0	BOLT HEAD PULLS THROUGH CENTER HANGER BAND
FOUR BOLT AFT HANGER	10,100	0	} THREADED HOLES IN ROCKET MOTOR TUBE FAIL
EIGHT BOLT AFT HANGER	18,440	0	
SIDE LOADS			
FORWARD HANGER	5,240	0	HANGER SPLITS IN HALF LONGITUDINALLY
CENTER HANGER	7,007	0	HANGER BREAKS AWAY FROM CENTER HANGER BAND
FOUR BOLT AFT HANGER	5,105	0	} THREADED HOLES IN ROCKET MOTOR TUBE FAIL
EIGHT BOLT AFT HANGER	9,900	0	
WINGS/ROCKET MOTOR	4,907	17,190	BENDING MOMENT ABOUT WING/ROCKET MOTOR BOLTS, WHICH FAIL
CANARDS/GCU			LOAD AT CANARD CENTER OF AREA
AIM-95	930	1,896	CANARD/GUIDANCE CONTROL UNIT BOLTS FAIL
AIM-93	-	-	NOT DETERMINED, USE CANARD/GCU BOLT STRENGTH FOR FAILURE CRITERION

NOTE: UNDERLINED VALUES ARE EXTRAPOLATED OR ESTIMATED BASED ON SIMILAR TESTS.

ROBERT G. FUSCO

Mr. Fusco received a Bachelor of Aeronautical Engineering from
Rensselaer Polytechnic Institute in 1967. He continued his studies
part time at the Polytechnic Institute of Brooklyn from 1967 through
1968 while working for Grumman Aerospace Corporation. At Grumman,
he was employed as an aeronautical engineer in the experimental dynam-
ics group of the loads and dynamics section and worked on such pro-
grams as A-6, F-14, and LM. He was primarily responsible for predic-
tion and determination of vibration environments, establishing
qualification test requirements, and review of vendor qualification
tests. Mr Fusco joined Dayton T. Brown, Inc. in 1971 as a project
engineer in the Engineering and Test Division. Since joining the
laboratory, he has been responsible for development, qualification,
and acceptance test programs of both aircraft and non-aircraft mechan-
ical, electromechanical, and explosively activated equipment and mater-
ial, development of aircraft armament military specifications, and the
design and development of special test equipment.

(The reverse of this page is blank)

LIST OF ATTENDEES

Addison, Edward	Lockheed	Huntsville AL
Alders, Gerard	National Aerospace Lab	Amsterdam, Neth.
Allen, Frank, Capt	ASD/AERS	Wright-Patterson AFB OH
Anderson, Howard	Fairchild Republic	Farmingdale NY
Andrews, Randolph	Northrop	Hawthorne CA
Armstrong, Odis	AFATL/DLJC	Eglin AFB FL
Arnold, Robert	AFATL/DLJC	Eglin AFB FL
Arthurs, T. Desmond	Northrop	Hawthorne CA
Atkinson, Frank, Lt	3246TW/TETF	Eglin AFB FL
Ausman, John	Litton	Woodland Hills CA
Baker, Hugh	Hunting	Ampthill, Bedford, UK
Baker, William	ARO	Arnold AFS TN
Baldwin, William	RAE	Farnborough, Hants, UK
Balian, Roxy	ASD/ENFSR	Wright-Patterson AFB OH
Ballard, Duel	NASC/AIR-5321	Washington DC
Bartholomew, Francis	Hunting	Ampthill, Bedford, UK
Bartlett, Robert	BAC	Filton, Bristol, UK
Baullinger, Norman	Boeing	Seattle WA
Beaumont, Kenneth	Hunting	Ampthill, Bedford, UK
Bensinger, Charles	General Dynamics	Fort Worth TX
Benton, Richard	Brunswick	Costa Mesa CA
Berke, Laszlo	AFFDL/FBR	Wright-Patterson AFB OH
Betts, Morgan	Veeder-Root	Hartford CT
Bitterle, Heiner, LTC	MoD/FRG	Koln, FRG
Blose, Terry	Rockwell	Columbus OH
Boan, Roger	Dayton T. Brown	Warner Robins GA
Boillot, Pierre	Dassault	Vaueresson, France
Boosa, J. David	Vought	Dallas TX
Bore, Clifford	Hawker Siddeley	Kingston-upon-Thames, Surrey, UK
Bott, Hans	GAF	Koblenz, FRG
Bouffard, Michael	ADTC/SD15	Eglin AFB FL
Boulet, Ronald	AFATL/DLJA	Eglin AFB FL
Bowers, B. Robert	AFATL/DLJC	Eglin AFB FL
Bradley, Edward	ADTC/SD7E	Eglin AFB FL
Brennan, David, Maj (CF)	AFATL/DLJC	Eglin AFB FL
Brick, Ted	Allied Intl	New York NY
Brooks, Donald	General Dynamics	Fort Worth TX
Brown, David	Martin Marietta	Orlando FL
Bunton, Robert	AFATL/DLJC	Eglin AFB FL
Burich, Joseph	Teledyne Ryan	San Diego CA
Burnside, Randy, LTC	3246TW/TEO	Eglin AFB FL
Burt, Robert	ARO	Arnold AFS TN
Bush, Donald	AFWL/NSCA	Kirtland AFB NM

Calano, Richard	NASC/PMA-265	Washington DC
Calfee, Dewey	ADTC/SD20E	Eglin AFB FL
Cannella, Sam	AFATL/DLJA	Eglin AFB FL
Campbell, Richard	ADTC/SD20M	Eglin AFB FL
Carmichael, John	Martin Marietta	Orlando FL
Carroll, Michael, Cmdr	NASC/AIR-530	Washington DC
Carroll, Terry, Capt	AFATL/DLJC	Eglin AFB FL
Chandler, Kenneth, Maj	AETE Cold Lake	Medley, Alta., Can.
Childs, Joseph	Grumman	Bethpage NY
Chung, Jung	Fairchild Republic	Farmingdale NY
Clark, Rodney	AFFDL/FXM	Wright-Patterson AFB OH
Clarke, Donald	Raytheon	Shalimar FL
Clarke, Michael, LTC	ADTC/SEF	Eglin AFB FL
Clelland, Alexander	ASD/ENFSL	Wright-Patterson AFB OH
Clifton, Joe	3246TW/TEEAD	Eglin AFB FL
Colburn, Laurence	AFFTC/DOEES	Edwards AFB CA
Connell, Robert	General Dynamics	Pomona CA
Conrad, Allen, Capt	AETE Cold Lake	Medley, Alta., Can.
Conyers, William	ADTC/SD20E	Eglin AFB FL
Cooley, Dale	AFFDL/FBR	Wright-Patterson AFB OH
Coon, Richard, Capt	ADTC/SD3C	Eglin AFB FL
Cooper, Guy	PMTC	Pt Mugu CA
Coste, Jacques	ONERA	Chatillon sous Bagneux, France
Craigie, Samuel	M L Aviation	Maidenhead, Berkshire, UK
Crain, William	ARO	Arnold AFS TN
Crockett, David, Lt	3246TW/TETF	Eglin AFB FL
Crouch, Billy	Martin Marietta	Orlando FL
Cunningham, Dean	Oklahoma City ALC/MMSRHB	Tinker AFB OK
Curry, David	ADTC	Eglin AFB FL
Dalley, Edward	Hawker Siddeley	Kingston-on-Thames, Surrey, UK
Dalzell, Donald, Sqd Ldr	RNZAF	Ohakea, NZ
Dankievitch, Edward	Dayton T. Brown	Bohemia NY
Dat, Rolland	ONERA	Chatillion, France
Davis, Duane	ADTC/SD9E	Eglin AFB FL
Delaney, Roland, Capt	AETE Cold Lake	Medley, Alta., Can.
Demos, George	Western Gear	Jamestown ND
Desha, Ernest, Lcdr	PMTC/2140	Pt Mugu CA
Dick, Samual, Lt	ADTC/SD9E	Eglin AFB FL
Dix, Richard	ARO	Arnold AFS TN
Donavin, Matthew	ADTC/SD20E	Eglin AFB FL
Doran, John	AFWL/NSSA	Kirtland AFB NM
Dougherty, Kevin, Lt	AFATL/DLJC	Eglin AFB FL
Doyle, Lawrence	AVRADCOM-ORDAV-EQA	St Louis MO
Dragowitz, Charles	Grumman	Shalimar FL
Dreadin, William	AFATL/DLJC	Eglin AFB FL
Duncan, John	Sandia Lab	Albuquerque NM
Dunshee, Robert, Capt	3246TW/TEOF	Eglin AFB FL
Durrenberger, Thomas	AFATL/DLJC	Eglin AFB FL
Dyess, William	AFATL/DLJC	Eglin AFB FL

Dyer, Calvin	AFFDL	Wright-Patterson AFB OH
Dyer, Richard	AFFDL/FXM	Wright-Patterson AFB OH
Eaton, Christopher	Hunting	Ampthill, Bedford, UK
Edwards, Kenneth, Lt	AFATL/DLJA	Eglin AFB FL
Ehlers, Harry	Dayton T. Brown	Bohemia NY
Ellis, Larry	Western Gear	Jamestown ND
Ellis, Richard, Capt	USAF	Washington DC
Epstein, Charles	AFATL/DLJC	Eglin AFB FL
Evans, James	3246TW/TEEAD	Eglin AFB FL
Everett, Roger	Sandia Lab	Livermore CA
Fields, William	ADTC/SD9E	Eglin AFB FL
Filbin, Richard	Raytheon	Bedford MA
Fontana, Samuel	NAFI	Indianapolis, IN
Forsching, Hans	DFVLR	Gottingen, FRG
Fortier, Michel	DND/DREV	Courcelette, Que., Can.
Foss, Herbert	Douglas	Long Beach CA
Foughner, Jerome	NASA Langley	Hampton VA
Frank, Robert	AVRADCOM-ORDAV-EVW	St Louis MO
Frazier, Dillis	ADTC/SD7E	Eglin AFB FL
Fredrick, Mark, Capt	ADTC/SD3	Eglin AFB FL
Froberg, Ken	Bell Helicopter	Ft Worth TX
Fuller, Glenn	Martin Marietta	Orlando FL
Furlong, Chester	AEDC	Arnold AFS TN
Fusco, Robert	Dayton T. Brown	Bohemia NY
Gardner, David	BAC	Preston, Lancashire, UK
Garner, Carlton	AEDC/XRRX	Arnold AFS TN
Gilroy, Kenneth	Lockheed	Sunneyvale CA
Goldsmith, N. Kent	Alkan, USA	Hurst TX
Gooch, Stanford	SAC/XPHN	Offutt AFB NE
Goodey, John	Canadair	Montreal, Ont., Can.
Gormley, Owen, Capt	ASD/YFEFF	Wright-Patterson AFB OH
Greenway, Milford, Capt	ADTC/SD3E	Eglin AFB FL
Gregory, Nigel	DRDS (Brit Def Staff)	Washington DC
Grow, Robert, Capt	AFATL/DLJC	Eglin AFB FL
Haidl, Gunther	Messerschmitt	Munchen, FRG
Hartley, William	ASD/ENFEA	Wright-Patterson AFB OH
Henderson, Martin	Ogden ALC	Hill AFB UT
Herbert, Raymond	AETE Cold Lake	Medley, Alta., Can.
Herleikson, Arne	PMTC (1155)	Pt Mugu, CA
Hermans, A.G.M., Maj	Airstaff, RNAF	The Hague, Netherlands
Hester, Jerry	Veeder-Root	Alexandria VA
Himes, Thomas	Westinghouse	Baltimore MD
Hixon, Eugene	ASD/SD30EF	Wright-Patterson AFB OH
Hodges, Roy	Beech	Wichita KS
Holden, Donald	Western Gear	Jamestown ND
Hornbuckle, Jerry	ADTC/SD7E	Eglin AFB FL
Howells, Frederick	Systems Research Labs	Dayton OH
Hoyle, Charles	Sandia Labs	Livermore CA
Hume, Robert	AFATL/DLJC	Eglin AFB FL
Ingram, C. Wayne	AFATL/DLJC	Eglin AFB FL
Irwin, W. George	Northrop	Anaheim CA

Jesse, Rudolf	Messerschmitt	Munchen, FRG
Jewell, Bernard, Gr. Capt	MoD, AD/AIR ARM 2	London, UK
Johnson, Ralph	AFATL/DLJC	Eglin AFB FL
Junko, John	Honeywell	Hopkins MN
Karipides, Samuel	Goodyear	Akron OH
Kaufman, Louis	Grumman	Bethpage NY
Keeling, William	General Dynamics	Pomona CA
Kellar, Robert, Maj	3246TW/TETT	Eglin AFB FL
Key, James, Maj	AFATL/DLJC	Eglin AFB FL
Kidd, Calvin	ADTC/ADPA	Eglin AFB FL
Kidd, Edwin	General Dynamics	Ft Worth TX
Kietzman, Robert	Douglas	Long Beach CA
Killeen, Roger, Wg Cmdr	DoD/AF Office	Canberra, Aus.
Kimber, Ken	Canadair	Montreal, Ont., Can.
King, Howard	BAC	Filton, Bristol, UK
King, Roger	Alkan, USA	Hurst TX
Kirby, Jack	General Dynamics	Shalimar FL
Koomen, Nelis	Tally Indust.	Mesa AZ
Korn, Stephen	AFATL/DLJC	Eglin AFB FL
Kratzert, Keith, Capt	ADTC/SD3T	Eglin AFB FL
Kropenick, John	Alkan, USA	Shalimar FL
Krull, Larry	ADTC/SD20	Eglin AFB FL
Kuhnold, Georg	FRG	Koblenz, FRG
Kundrat, W.	Hughes	Tuscon AZ
Kurz, Wolfgang	Messerschmitt	Muchen, FRG
Kyle, Robert	Acft, Hydro-Forming	Gardena CA
Lacerenza, Mark, Lt	AFATL/DLJC	Eglin AFB FL
Lanterman, Benny	McDonnell Douglas	St Louis MO
Laudeman, Ernest	General Dynamics	San Diego CA
Lauro, Michael	Pyrotech Data	Monroe CT
Lemacon, Jacques	Dassault	Base de Cavaux, France
Lembertas, Vitalis	Hughes	Culver City CA
Liebenberg, John	Sandia Labs	Livermore CA
Ligon, Johnnie, Capt	3246TW/TETT	Eglin AFB FL
Lijewski, Larry	AFATL/DLJC	Eglin AFB FL
Linnen, Don, Capt	AFATL/DLJC	Eglin AFB FL
Little, Ray	Rockwell	Los Angeles CA
Lockhart, Jess	Douglas	Long Beach CA
Lohmeyer, Arthur	ASD	Wright-Patterson AFB OH
Long, Jeff	AFATL/DLJC	Eglin AFB FL
Loria, Joseph	General Dynamics	Shalimar FL
MacDonald, John, LTC	Can. Def. Liaison Staff	Washington DC
Maples, Dupree	LSU (AFATL/DLJC)	Eglin AFB FL
Marrin, Al	AFATL/DLJC	Eglin AFB FL
Marshall, John	ARO	Arnold AFS TN
Martin, Fred	Auburn Univ.	Auburn AL
Martin, Robert	Sandia Labs	Albuquerque NM
Mathews, Charles	AFATL/DLJC	Eglin AFB FL
Matthews, Richard	ARO	Arnold AFS TN
May, James	Emerson Elec.	St Louis MO
McEwen, Dan, LTC	AFATL/DLJA	Eglin AFB FL
McGee, James, Lt	AEDC/DOOP	Arnold AFS TN

McGivern, Dennis	Honeywell	Lexington MA
McNally, David	Northrop	Hawthorne CA
McNeece, Robert	Douglas	Long Beach CA
Meyer, Ray	Honeywell	Hopkins MN
Meyer, Stanley	Sandia	Albuquerque NM
Miko, Richard	EDO	College Point NY
Milhous, Thomas	NADC/3044	Warminster PA
Miller, Virgil	AFATL/DLDG	Eglin AFB FL
Monaghan, Charles	AFATL/DLJC	Eglin AFB FL
Money, Alexander	AEDC/DOTR	Arnold AFS TN
Moore, T. Walter	General Dynamics	Ft Worth TX
Morel, Charles	Hughes	Culver City CA
Morin, Serge, Maj	DOND	Ottawa, Ont., Can.
Mullikin, Vernon	McDonnell Douglas	St Louis MO
Murray, William	Ogden ALC/MMSRW	Hill AFB UT
Nankey, Ralph	General Electric	Utica NY
Nielsen, Harvey, LTC	Nat. Def. Hdqtrs/DASSE 5	Ottawa, Ont., Can.
Neimeier, Byron	General Dynamics	Pomona CA
Northey, Geoffrey, Wg Cdr	Australia Embassy (RAAF)	Washington DC
O'Neill, Edward	Boeing	Seattle WA
Pace, William	Rockwell	Los Angeles CA
Paez, Thomas	Univ. of New Mexico	Albuquerque NM
Paisley, Eric	Westland	Winston-Salem NC
Papa, James	AFFTC/DOEEP	Edwards AFB CA
Parker, Daniel	AFIT/ENA	Wright-Patterson AFB OH
Passi, Henry, Col	ADTC/SD3	Eglin AFB FL
Peck, William	NOTS	Indianhead MD
Peters, Spence, Lt	AFATL/DLJC	Eglin AFB FL
Pettis, Wiley		
Pierce, Fredrick	NASC/AIR-530113	Washington, DC
Pollard, Ben M., Col	USAF Prep School	USAF Academy CO
Pollock, Samuel	AFFDL/FBR	Wright-Patterson AFB OH
Pinney, Chuck, Lt	AFATL/DLJC	Eglin AFB FL
Poole, Ronald	Hughes	Canoga Park CA
Powell Dudley	Western Gear	Atlanta GA
Powers, Stephen	ASD/YXEF	Wright-Patterson AFB OH
Rabiansky, Ronald	4751ADS	Hurlburt Fld FL
Ramachandra, S.	Hindustan	Bangalore, India
Reilley, Thomas	Grumman	Pt Mugu CA
Richter, Bernard	Lockheed	Sunnyvale CA
Riley, Aaron B.	General Dynamics	Ft Worth TX
Rivera, Joseph	Grumman	Calverton NY
Robertson, Charles	AFATL/DLJC	Eglin AFB FL
Robinson, W. James	AFATL/DLJC	Eglin AFB FL
Roos, Rudolf	National Aerospace Lab	Amsterdam, Neth.
Sanky, George	Allied Intl	New York NY
Santini, Richard	AFATL/DLD	Eglin AFB FL
Schmidt, Edward	US Army Ballistics Res Lab	Aberdeen Prov. Gnd MD
Schmidt, Wolfgang	Dornier	Friedrichshafen, FRG
Schnacke, Richard	General Dynamics	Ft Worth TX
Schoelerman, Duane	Vought	Dallas TX
Seal, Lynn	Dayton T. Brown	Bohemia NY

Shafer, W. Mack	General Dynamics	Ft Worth TX
Sharp, James	Warner Robins ALC/MMIRDB	Robins AFB GA
Shelton, Jerry	McDonnell Douglas	St Louis MO
Shifrar, Frank	Ogden ALC/MMWRAE	Hill AFB UT
Shirley, Benjamin	3246TW/TEEAO	Eglin AFB FL
Short, Claude, Maj	AFSC/SDZ	Andrews AFB MD
Sierra, Celestino	General Dynamics	Ft Worth TX
Smith, Keith	Hunting	Ampthill, Bedford, UK
Smith, Lee	Vought	Dallas TX
Smith, Reynard	NWC/3163	China Lake CA
Spahr, Harold	Sandia Labs	Albuquerque NM
Spearman, M. Leroy	NASA Langley	Hampton VA
Speer, Thomas, Lt	AFATL/DLJC	Eglin AFB FL
Stahara, Stephen	Nielsen	Mountain View CA
Steeper, William	NASA/AIR-5302	Washington DC
Stein, Berthold	AURADCOM/DRDAV-EVW	St Louis MO
Stitt, Graylin	AFATL/DLJC	Eglin AFB FL
Stone, Leland	Sandia Labs	Albuquerque NM
Stowe, William	ASD/YXEF	Wright-Patterson AFB OH
Strickland, Ed	AFATL/DLJC	Eglin AFB FL
Taussig, Barrett	Emerson Elec	St Louis MO
Taylor, Jack, LTC	AFATL/DLJC	Eglin AFB FL
Tessitore, Frank	Grumman	Bethpage NY
Theibert, L. Scott	AFML/MXE	Wright-Patterson AFB OH
Tilley, James, Capt	3246TW/TEOF	Eglin AFB FL
Turner, Charles	AFATL/DLJC	Eglin AFB FL
Turner, Malford	Raytheon	Bedford MA
Twigger, Michael	RAE	Farnborough, Hants, UK
Uter, Fritz	BWB-ML (FRG)	Muchen, FRG
Van Aken, Ray	NWC/316	China Lake CA
Van Der Kramer, M.	Air Staff, RNAF	The Hague, Netherlands
Van Putte, Ronald, Maj	AFATL/DLJC	Eglin AFB FL
Venables, David	Hunting	Eglin AFB FL
Viel, Maurice	Dassault	St Cloud, France
Volz, William	NASC/AIR-530C	Washington DC
Vore, Donald, Capt	AFATL/DLJC	Eglin AFB FL
Wade, William, Lt	ADTC/SD20	Eglin AFB FL
Walker, Neil	AFATL/DLJC	Eglin AFB FL
Walter, Fritz	German Liaison Off	Wright-Patterson AFB OH
Washmuth, Harold	PMTC/1243	Pt Mugu CA
Welch, Byron	Lockheed	Sunnyvale CA
Williams, Robert	NAFI/921	Indianapolis IN
Williams, Larry, Maj	AFATL/DLJC	Eglin AFB FL
Wilson, Ronald	NATC/SY-91	Patuxent River MD
Wolf, Jack, Maj	AFATL/DLJK	Eglin AFB FL
Workman, Theodore, LTC	3246TW/TETF	Eglin AFB FL
Wright, Jefferson	Allied Intl	New York NY
Young, John	Aircraft Hydro-Forming	Gardena CA
Zinke, Henry	3246TW/TETE	Eglin AFB FL